Reactions of Functionalized Fluoroalkenes: Ni Fluorometallacycles and Cu Fluoroalkyls for R^F Transfer to Organic Electrophiles

By

Luana Leticia Teixeira Nunes Porto

Thesis submitted in partial fulfilment of the requirements for the

Doctorate in Philosophy degree in Chemistry

Faculty of Science

Department of Chemistry and Biomolecular Sciences

University of Ottawa

Abstract

The more we learn about fluorine, the more we understand why this fascinating element has been extensively explored for use in polymers, surfactants, refrigerants, agrochemicals, pharmaceuticals, and PET imaging. Switching chlorine to fluorine and adding a double bond drastically decreases fluorocarbons' atmospheric half-lives and pushes the development of new routes to hydrofluoroolefins (HFOs) as 4th generation refrigerants. In another application, the inclusion of fluorine into drugs improves their pharmacokinetic and pharmacodynamic properties. Since the first fluorinated drugs were introduced in the 1960s, the use of organoflruoine compounds has greatly expanded in both the pharmaceutical and agrochemical markets. However, there is still a need for improved synthetic methodologies for late-stage fluoroalkylation of bioactive compounds. Moreover, moving beyond -CF_3 and -CF_2H, the use of additional R^F groups like -CF_2CF_2H that increase lipophilicity while also allowing for H-bonding may also lead to the identification of improved bioactivity over a broad spectrum.

Previous work in the Baker group demonstrated that regioselective insertion of hexafluoropropene, CF_2=$CF(CF_3)$ into a Cu-F bond generated the hexafluoroisopropyl group that could be efficiently transferred to aroyl chlorides. Moreover, the insertion of tetrafluoroethylene (TFE) into Cu-H gave a stable Cu-CF_2CF_2H complex that could also transfer its R^F group to aryl iodides in the presence of catalytic CuCl(NHC) (NHC = N-heterocyclic carbene). In this thesis we expand the regioselective Cu-H insertion strategy to include chlorotrifluoroethylene, CTFE, CF_2=CFCl, and perfluoro(methyl vinyl ether), PMVE, CF_2=$CF(OCF_3)$. With the former, we showed the importance of ancillary ligands in stabilizing the Cu complex and enabling the successful transfer of the -$CFClCF_2H$ group to aroyl chlorides (aryl iodides gave only biaryls). In contrast, we found that stable Cu[$CF(OCF_3)(CF_2H)$] complexes could be prepared using a variety of ligands spanning 2- to 4-coord Cu, and we showed that DMSO serves as a 'privileged' ligand for transfer of this R^F group to organic electrophiles. With the help of a computational chemistry collaborator, we identified the importance of pre-equilibria that hampered the aryl iodide addition step, leading us to develop a 'ligandless' polar solvent-stabilized Cu-R^F strategy, using added CuBr to trap the phosphine ligands for efficient transfer of the novel -$CF(OCF_3)(CF_2H)$ group. Further calculations showed that rate-limiting product elimination for R^F transfer to aroyl chloride involves an asynchronous transition state occurring at a single Cu coordination site. Finally, adding the

'ligandless' Cu-R^F strategy with our previously reported Cu-CF_2CF_2H complexes, derived from the stable 1:1 TFE: CO_2 mixture, allowed for the successful tetrafluoroethylation of alkenyl iodide nucleobases, nucleosides and glycals with potential biological activity. In another collaboration, we report the results of preliminary molecular docking studies of fluorinated-carboxamides as potential fungicide targets.

In an effort to expand the range of readily available fluoroalkenes using the Baker group's Ni-catalyzed homologation approach, we first collaborated with another computational chemistry to investigate the mechanism of fluoronickelacyclopentane formation. This work showed that the NiL_2 fragment often led to reduced activation barriers (*vs.* NiL) and that the transition state involves a wide L-Ni-L angle of ca. 150°. Using the wide bite-angle bis(phosphine) DPEPhos, we were able to characterize a model for the initially formed pseudotetrahedral metallacycle. We then expanded the range of isolated fluoronickelacycles to include those derived from PMVE and CTFE. While the former gave regio- and stereoselective formation of stable metallacycles with *trans* -OCF_3 groups on Cα, the stability and regioselectivity of the latter depended on the ancillary ligands. Preliminary reactivity of these metallacycles with Lewis and Brønsted acids is also reported.

In summary, using two functionalized fluoroalkenes, we have advanced our understanding of the stabilization of Cu-R^F complexes and their ability to transfer their R^F group to organic electrophiles. In addition, we assessed the synthesis, stability, and reactivity of new fluoronickelacycles to provide additional insight into the Baker group's Ni-catalyzed fluoroalkene homologation strategy.

Acknowledgments

First and foremost, I want to thank God for making all this possible and providing me with the protection and guidance I needed to complete this research work successfully. I would like to express my deep gratitude to my supervisor, Prof. R. Tom Baker. Thank you for allowing me to be part of your group, for being patient, optimistic and motivating me when something did not go as expected, and for encouraging me to have fun while working hard. Thanks for teaching me, listening to me and always being open to new projects out of your field. Your friendship, empathy, guidance, and great sense of humour made me always feel at home.

I also want to thank Baker lab members for all their assistance in introducing me to the routine inorganic chemistry lab. Thanks to Drs. Nicholas Andrella and Alexandre Sicard for all their support and guidance during my first weeks. I cannot express in words my gratitude to Nick and his wife for all they have done for my family. To Dr. Fernanda Mendonca, who came to the group and became part of my family, a special thanks to you and your husband, Dr. Walace do Pim, who have helped me with chemistry and given a lot of advice throughout my Ph.D. journey. It means the world to me. To Dr. Loïc Mangin and Dr. Behnaz Ghaffari, thank you for all your assistance and for always being there to help; I have learned a lot from you. Thanks to my excellent students, Nicole, Amena and Moutasem, for teaching me to be a good mentor; I wish them the best in their future. To my Arabian friend Bakr Barnawi, thanks for all the good times (the best cook!).

Thank you to my committee members Profs. Jennifer Love, Jeffrey Manthorpe, Steven Newman and Darrin Richeson and to all staff, technicians, and administration at uOttawa, especially Annik St-Jean, Peter Pallister, and Chloé Lagacé. Thanks to all my collaborators, Dr. Christian Ehm, Dr. Russell Hughes, Dr. Michele Loewen, Dr. Antony St-Jacques, and especially to Dr. Omar Boutureira, Dr. Jordi Mestre and Isabel Bascuas for all their support and reception during my visit and the teamwork in making our project successful. I am so grateful that I had the opportunity to do research in your lab. To all Sintcarb group members that made my time in Spain more than special, thank you all for our moments together and for showing me the best ‘tapas’ in Tarragona. Finally, thanks to all my TA supervisors, on top of all Dr. Loewen, Dr. Beaulieu, Dr. Campbell-Valois, and Dr. Musende, who inspired me to be a better teacher and scientist.

To all my friends, my besties Hemylen and Thaisi, throughout more than 20 years of friendship, thanks for making part of this even from so far away. Carulini for your endless support. Daliane, I cannot imagine these four intensive years without you; thanks for staying with me and sharing all the hard/good times, from science to life, to become part of my family. To my craziest girl, Nayara, thank you for making my first years funnier.

My Father, Teomar, thanks for all your rational and pragmatic advice and presence in my life. My Mother, Lucia, you have taught me far more than I could have ever learned through my studies. It is incredible what you have done, being a poor Brazilian woman without education and raising a girl to pursue a Ph.D. degree in Canada. You made me believe in myself and my dreams. Your extreme love, sacrifices, and prayers guided me through this journey. To my siblings Henrique and Lucelia for their unwavering support and belief in me. To my niece, Livya, thanks for always being there for me, for fielding my phone calls and calming me down anytime.

To the most special man, my husband. Raphael, this thesis could never exist without your hard work and endless support. You always stood behind me, calming me down and telling me that I was awesome even when I didn`t feel that way. Thanks for your patience when I put the work first, your love, and for constantly reminding me of the end goal. To the most important person in my life, my daughter Laura. Thanks for understanding that moms need to work, even on the weekends. You teach me every day to be a better person. I love you so much, and I hope you will be proud of me and everything I did for us one day.

I enjoyed working on this thesis; fluorine chemistry is fascinating. I am so proud and thankful for all the work I`ve done. This Ph.D. thesis increased my appetite for learning and discovery but also showed me how hard it is to work on this and how much we need support from others. Being an international Ph.D. student and a mother was the hardest experience I could have ever imagined, with more challenges through the COVID-19 pandemic. There is a lack of recognition of graduate student mothers in academia, which makes it more challenging. We are heavily dependent on our supervisor and partner support, and this is okay; here, even with a great team (all support from my supervisor and husband), it was not easy. We need a tribe to make this happen. When we become mothers, we change our view of life/work and our plans, but not our goals. Every woman deserves it, we cannot close the science door for mothers.

Table of Contents

Abstract ii

Acknowledgments iv

Abbreviations x

List of Schemes xii

List of Figures xiv

List of Tables xxix

List of New Compounds xxx

CHAPTER 1. INTRODUCTION 1

1. The Power of Fluorine 1

1.1 Properties of fluorine 1

1.2 Application of fluorine in industry: Fluorocarbon refrigerants 2

1.3 Metal organofluorine chemistry 4

1.3.1 Perfluoroalkyl metal complexes 4

1.3.2 Perfluorometallacycles: 3- vs. 5-membered ring 6

1.3.3 Reactivity of nickel fluorometallacyclopentanes 8

1.4 Fluorine in medicinal chemistry 12

1.4.1 Fluorine in pharmaceutical compounds 12

1.4.2 Fluorine in nucleoside analogs: Anticancer and antiviral activity 13

1.4.3 Fluorine in drugs for COVID-19 treatment 14

1.4.4 Fluorine in agrochemicals 15

1.5 Late-stage fluorination 17

1.5.1 Incorporation of fluorine 17

1.5.2 Fluoroalkylation 22

1.5.3 Transition-metal catalyzed trifluoromethythiolation, trifluoromethoxylation and difluoromethylation. 26

1.5.4 Copper-mediated fluoroalkylation 32

1.6 Summary and thesis outline 37

Chapter 2. Generation of Copper Fluoroalkyl Complexes (CuR^FLn) from Chlorotrifluoroethylene and $-R^F$ Transfer to Benzoyl Chloride 59

2.1 INTRODUCTION 59

2.2 RESULTS AND DISCUSSION 60

2.2.1 Synthesis of $Cu(CFClCF_2H)Ln$ complexes: 60

2.2.2 Reactivity of **2-3** with aroyl chlorides: 62
2.2.3. Reactivity of **2-3** with aryl iodides: 64
2.3 CONCLUSION 64
2.4 EXPERIMENTAL SECTION 65
2.4.1. General Procedures 65
2.4.2. Synthesis of copper complexes: 66
2.4.3. General experimental procedure for fluoroalkylation of aroyl chlorides, NMR scale: 67
2.5 REFERENCES 68
Chapter 3. Copper-Mediated -$CF(OCF_3)CF_2H$ Transfer to Organic Electrophiles 70
3.1 INTRODUCTION 70
3.2 RESULTS AND DISCUSSION 71
3.2.1 Synthesis and characterization of $Cu[CF(OCF_3)CF_2H]Ln$: 71
3.2.2 Reactivity of **3-1** with aroyl chlorides: 73
3.2.3 Influence of ancillary ligands on fluoroalkylation efficiency: 73
3.2.4 Fluoroalkylation of aryl iodides: 75
3.2.5 Aryl iodide substrate scope: 77
3.2.6 Computational insights into the role of DMSO: 78
3.3 CONCLUSIONS 84
3.4 EXPERIMENTAL SECTION 84
3.4.1 General Procedures: 84
3.4.2 Synthesis of Copper Complexes 85
3.4.3 R^F Transfer Reactions: 86
3.5 REFERENCES 90
Chapter 4. Copper-mediated Tetrafluoroethylation of Bioactive Compounds 97
4.1 INTRODUCTION 97
4.2 RESULTS AND DISCUSSION 100
4.2.1 Ligand effects in -CH_2CH_2F transfer to aryl iodides: 100
4.2.2 DFT studies of Cu-mediated R^F transfer to organic electrophiles: 101
4.2.2 Tetrafluoroethylation of bioactive compounds using 'ligandless' CuR^F strategy: 107
4.2.3 Synthesis and molecular docking studies of potential succinate dehydrogenase inhibitors (SDHi): 110
4.2.3.1 In silico molecular docking results: 111
4.2.3.2 Docking simulations of known SDHi: 112

4.2.3.2 Docking of fluoroalkylated SDHi analogues 114
4.3 CONCLUSIONS 115
4.4 EXPERIMENTAL SECTION 116
4.4.1 General Procedures: 116
4.4.2 Synthesis of Cu(CF_2CF_2H)(Xantphos (**4-2**): 116
4.4.3 Procedures for R^F transfer using **4-2**: 117
4.4.4 General procedure for 'ligandless' R^F transfer using **4-1** / CuBr: 117
4.4.5 Computational details 119
4.4.6 Molecular docking studies: 119
4.5 REFERENCES 120
Chapter 5: Mechanism of Perfluoronickelacyclopentane Formation from Tetrafluoroethylene 127
5.1 INTRODUCTION 127
5.2 RESULTS AND DISCUSSION 129
5.2.1 Computational studies 129
5.2.1.1 Pathways for metallacycle formation: 129
5.2.1.3 Monodentate ligands (Table 5-1; entries 1-6): 133
5.2.1.4 Bidentate ligands (**Table 5-1**; entries 7-16): 137
5.2.2 Experimental Studies: 140
5.3 CONCLUSIONS 145
5.4 EXPERIMENTAL SECTION 146
5.4.1 General procedures: 146
5.4.2 X-ray crystallography: 146
5.4.3 Computational Methods: 147
5.4.4 Synthesis: 147
5.5 REFERENCES 149
Chapter 6: Synthesis and Reactivity of Functionalized Fluoro-Nickelacyclopentanes 156
6.1 INTRODUCTION 156
6.2 RESULTS AND DISCUSSION 160
6.2.1 Synthesis of functionalized nickelacyclopentanes and nickel alkene complexes from perfluoro(methyl vinyl ether) (PMVE) 160
6.2.2 Synthesis of functionalized nickelacyclopentanes, nickel alkene, and -vinyl complexes from chlorotrifluoroethylene (CTFE) 164
6.2.3 Reactions of nickelacycles with Lewis and Brønsted acids 166
6.3 CONCLUSION 168

6.4 EXPERIMENTAL SECTION 169
6.3.1 General procedures: 169
6.3.2 Generation of nickelacycles from PMVE- NMR Scale: 170
6.3.3 Generation of electron-rich PMVE-derived nickelacycles: 171
6.3.4 Synthesis of nickelacycles from PMVE: 171
6.3.5 Generation of nickelacycles from CTFE- NMR scale: 172
6.3.6 Generation of electron-rich CTFE-derived nickelacycles: 172
6.3.7 Synthesis of nickel complexes from CTFE: 173
6.3.8 Reactions of CTFE-derived nickelacycles with Lewis and Brønsted acids 174
6.5. REFERENCES 174
Chapter 7. Conclusions and Future Work 177
7.1 REFERENCES 181
Appendix for 182
Reactions of Functionalized Fluoroalkenes: Ni Fluorometallacycles and Cu Fluoroalkyls for R^F Transfer to Organic Electrophiles 182
Chapter 2: Generation of Copper Fluoroalkyl Complexes (CuR^FL_n) from Chlorotrifluoroethylene and -R^F Transfer to Aroyl Chlorides 182
Chapter 3: Copper-Mediated -$CF(OCF_3)CF_2H$ Transfer to Organic Electrophiles 216
Chapter 4: Copper-mediated Tetrafluoroethylation of Bioactive Compounds 269
Chapter 5: Mechanism of Fluoronickelacyclopentane Formation from Fluoroalkenes 301
Chapter 6: Designing and synthesis of stable perfluoronickelacyclopentane from PMVE and CTFE 312

Abbreviations

ADME – Absorption, distribution, metabolization and excretion
Ar – Aryl
Arg - Arginine
Atm – Atmosphere
Bisbi - 2,2'-Bis(diphenylphosphinomethyl)-1,1'-biphenyl
Bpy – 2,2’-bipyridine
Bpy-Cl_2 – 4,4-dichloro-2,2’-bipyridine
Ca. – Circa, approximately
Cf. - Compare
CFC – Chlorofluorocarbon
C_6H_6 – Benzene
CH_3CN – Acetonitrile
Cod – 1,5-Cyclooctadiene
Cp - Cyclopentadienyl
CPME – Cyclopentyl methyl ether
CTFE – Chlorotrifluoroethylene
DEE – Diethyl ether
DCE – 1,2-Dichloroethane
DCM - Dichloromethane
DFT - Density functional theory
DMAP – 4-(N,N-Dimethylamino)pyridine
DME - 1,2-Dimethoxyethane
DMF - Dimethylformamide
DMSO – Dimethylsulfoxide
Dppe - 1,2-Bis(diphenylphosphino)ethane
Dppp - 1,3-Bis(diphenylphosphino)propane
DPEPhos – Bis(2-diphenylphosphino)phenyl ether
Dppf - 1,1’-Bis(diphenylphosphino)ferrocene
EI-MS – Electron ionization mass spectrometry
ESI-MS - Electrospray ionization mass spectrometry
Et – Ethyl
Et_2O – Diethyl ether
Equiv – Equivalents
F - Phenylalanine
FC – Fluorocarbon
fgSDH - *Fusarium graminearum* succinate dehydrogenase
H – Hour(s)
HF – Hydrofluoric acid
HFO – Hydrofluoroolefin
HFP – Hexafluoropropene
His - Histidine
Hz – Hertz
IAd – 1,3-Bis(adamantyl)imidazol-2-ylidene
IBO – Intrinsic bond orbital theory

Ille – Isoleucine
IMes - 1,3-Bis(2,4,6-trimethylphenyl)imidazol-2-ylidene
i-Pr – Isopropyl
IPr – 1,3-Bis(2,6-diisopropylphenyl)imidazol-2-ylidene)
L – Ligand
LA – Lewis acid
Me – Methyl
NAQ - N-[(4-Tert-butylphenyl)methyl]-2-(trifluoromethyl)benzamide
NHC – N-Heterocyclic carbene
NMR – Nuclear magnetic resonance
NRT – Natural resonance theory
OTf – Trifluoromethanesulfonate
Ph – Phenyl
Phen – 1,10-Phenanthroline
PMDTA - N,N,N′,N″,N″-Pentamethyldiethylenetriamine
PMVE – Perfluoro(methyl vinyl ether)
PTFE – Polytetrafluoroethylene
Pyr – Pyridine
R – Arginine
R^F – Fluoroalkyl group
RT – Room temperature
SDH – Succinate dehydrogenase
SDHi – Succinate dehydrogenase inhibitor
SIMes - 1,3-Bis(2,3,6-trimethylphenyl)imidazolidin-2-ylidene
SIPr - 1,3-Bis(2,6-diisopropylphenyl)imidazolidin-2-ylidene
Terpy - 2,2’;6’,2”-Terpyridine
TFE – Tetrafluoroethylene
TFT – Trifluorotoluene
THF – Tetrahydrofuran
THT – Tetrahydrothiophene
TMSOtf - Trimethylsilyl trifluoromethanesulfonate
Tol - Toluene
Trp - Tryptophan
TrFE – Trifluoroethylene
Tripod - 1,1,1-Tris(diphenylphosphinomethyl)ethane
Triphos - Bis(2-diphenylphosphinoethyl)phenyl phosphine
Ttfet – 1-Trifluoromethyl-1,2,2-trifluoromethoxy-ethyl
Tyr – Tyrosine
VDF - Vinylidene difluoride
W - Tryptophan
Xantphos - (9,9-Dimethyl-9H-xanthene-4,5-diyl)bis(diphenylphosphine)

List of Schemes

Scheme 1.1 (**A**) Incorporation of fluorine in organic molecules; (**B**) PTFE synthesis. 1
Scheme 1.2 Synthesis of CFC-12 (**A**), HCFC-21 and HCFC-22 (**B**, **C** and **D**). 3
Scheme 1.3 Synthesis of HFC-134a. 4
Scheme 1.4 Synthesis of HFO-1234yf 4
Scheme 1.5 Synthesis of transition metal perfluoro-alkyl and -alkenyl complexes. 5
Scheme 1.6 Oxidative addition of R^FI to form perfluoroalkyl metal iodides. 5
Scheme 1.7 $Pt(cod)_2$ reaction with tetrafluoroethylene. 7
Scheme 1.8 Nickel-complex catalyzed TFE hydrodimerization to generate octafluorobutane. 9
Scheme 1.9 Reactivity of perfluoronickelacycle with Lewis acid. 9
Scheme 1.10 Reactivity of 3-coordinate perfluoronickelacycle with Lewis acid. 9
Scheme 1.11 Cα-F abstraction and phosphine migration to C_α. 10
Scheme 1.12 C-F bond activation of metallacyclopentanes derived from Ni^0 and TrFe. 11
Scheme 1.13 Reactivity of Ni^0 with VDF. 12
Scheme 1.14 Metabolic reactions of capecitabine to afford 5-FU. 14
Scheme 1.15 a. Reactivity of fluorine with nucleophile using quaternary salt reagents and **b**. SET pathway. 18
Scheme 1.16 α-Fluorination of carboxylic acids (**a**,**b,e**), styrene (**c**), and decarboxylative fluorination (**d**). 20
Scheme 1.17 The proposed mechanism by Doyle et al. uses a nucleophilic source (**A**), while Lectka et al. use an electrophilic source (**B**). 21
Scheme 1.18 Fluorination of acyl chloride catalyzed by perfluorinated metal (M = Rh, Ir, or Co). 22
Scheme 1.19 Trifluomethylation using nucleophilic sources. 23
Scheme 1.20 Copper-catalyzed trifluoromethylation. 24
Scheme 1.21 Trifluomethylation employed by Togni`s reagent. 24
Scheme 1.22 Trifluoromethylation using radical source. 25
Scheme 1.23 a. Trifluoromethylation of alcohols; **b**. Pentafluoroethylation of alcohols and phenols. 25
Scheme 1.24 Trifluoromethylthiolation of aryl halides using $AgSCF_3$. 26
Scheme 1.25 Trifluoromethylthiolation of aryl halides using Me_4NSCF_3. 27
Scheme 1.26 Trifluoromethylthiolation of hetero(aryl) C-H bonds. 28
Scheme 1.27 Trifluoromethoxylation using nucleophilic sources. 29
Scheme 1.28 Metal-catalyzed difluoromethylation of aryl halides. 30
Scheme 1.29 Metal-catalyzed difluoromethylation of bioactive compounds. 31
Scheme 1.30 Iron-catalyzed difluoromethylation of diaryl zinc. 31
Scheme 1.31 Copper-mediated trifluoromethylation of aryl iodides using fluoroalkanes. 32
Scheme 1.32 Trifluoromethylation of aryl iodides using $Zn(R^F)Br$. 33
Scheme 1.33 Copper-mediated trifluoromethylation of aryl iodides using $TMSCF_3$ reagent. 34
Scheme 1.34 Copper-mediated pentafluoroethylation of aryl iodide and boronate using $TMSCF_3$. 35
Scheme 1.35 Copper-mediated difluoromethylation using $TMSCF_2H$ as the fluorinated source. 36
Scheme 1.36 Perfluoroalkylation of aryl iodides using CF_3H (**a**) and HFP (**b**). 37
Scheme 2.1 Synthesis of $Cu(hfip)(PPh_3)_2$ from HFP + Cu-F generated from Cu-H + HFP 60
Scheme 2.2 Generation of Cu-$CFClCF_2H$ complexes **2-1,2**. 61
Scheme 2.3 Synthesis of $[Cu(CFClCF_2H)(\mu\text{-}\kappa^1,\kappa^2\text{-triphos})]_2$ (**2-3**). 61

Scheme 2.4 Perfluoroalkylation of aroyl chlorides. 63
Scheme 3.1 Synthesis of Cu[CF(OCF_3)CF_2H](PPh_3)$_2$ (**3-1**)..... 72
Scheme 3.2 Synthesis of additional Cu-ttfet complexes. 75
Scheme 3.3 Substrate scope for –[CF(OCF_3)CF_2H] transfer to aryl iodides..... 77
Scheme 3.4 Potential energy surface for the reaction of **3-1** with benzoyl chloride. Black trace without coordinated solvent, green trace with coordinated DMSO. Insert shows relative energies of key species for different solvents with respect to **3-1** (L_2Cu-R^F). T = 298 K. 79
Scheme 4.1 Several arene tetrafluoroethylation strategies…..... 98
Scheme 4.2 Synthesis of **4-1** and tetrafluoroethylation of aroyl chlorides and aryl iodides. 99
Scheme 4.3 Hu's fluoroalkyl-trimethylsilane routes to arene tetrafluoroethylation. 99
Scheme 4.4 Tetrafluoroethylation of electron-rich heterocyclic alkenyl iodides..... 108
Scheme 4.5 Tetrafluoroethylation of electron-rich iodoglycols. 109
Scheme 4.6 Tetrafluoroethylation of electron-rich heterocyclic alkenyl iodides using 1.5 equiv. of substrate. 110
Scheme 5.1 First synthesis and reactivity demonstration of nickelacyclopentanes……128
Scheme 5.2 Nature of decomposition products derived from PPh_3 nickelacycles depends on P:Ni ratio……128
Scheme 5.3 Reaction of Ni(cod)(DPEphos) with TFE in THF. 143
Scheme 6.1 Reactivity of perfluoronickelacyclopentanes with Lewis acids…..... 157
Scheme 6.2 Controlling fluoronickelacycle regioselectivity with ancillary ligands. 158
Scheme 6.3 Reactions of Ni TrFE metallacycle with Lewis acids. 159
Scheme 6.4 Reactions of Ni(C_4F_8)(SIPr) with carboxylic acids 159
Scheme 6.5 Ni-catalyzed hydrodefluorodimerization of VDF 159
Scheme 6.6 Synthesis of complexes **6-1a** and **6-2a** from Ni(0), P(O^iPr)$_3$ and PMVE. 160
Scheme 6.7 Synthesis of complex **6-1b** from Ni(0), P(O-*o*-tol)$_3$ and PMVE..... 162
Scheme 6.8 Synthesis of complexes **6-2c** and **6-3** from reaction of **6-1a/6-2a** with dppe. 163
Scheme 6.9 Synthesis of **6-4a, 6-5** and **6-6a** from Ni(cod)$_2$, P(O^iPr)$_3$ and CTFE. 165
Scheme 6.10 Synthesis of stable CTFE-derived nickelacycles. 165
Scheme 6.11 Synthesis of Xantphos alkene complex **6-4e**, metallacycles **6-5d** and **6-8a,b** and vinyl complex **6-6e.**..... 167
Scheme 6.12 Reaction of nickelacycle **6-5d** with TMSOTf..... 167
Scheme 6.13 Reaction of nickelacycle mixture **6-5b** / **6-7b** with trifluoroacetic acid. 167
Scheme 6.14 ^{19}F NMR (282 MHz, C_6D_6) spectrum of Ni[$C_4Cl_2F_6$](dppp) (**6-5b**) and Ni[C_2ClF_3](dppp)-[(P(O^iPr)$_3$] (**6-7c**) (green line) plus trifluoroacetic acid after 7 h (black line) and 16 h (red line). 168

List of Figures

Figure 1.1 Perhalo-organoplatinum products from PtL_4 and fluoro-olefins. 7
Figure 1.2 Structures of rhodium fluorometallacycles derived from fluoroolefins and $Rh(acac)(PPh_2Me)_2$. 7
Figure 1.3 Structures of Group 10 metallacycles derived from fluorinated ketone and imine. 8
Figure 1.4 Reactivity of Ni^0 with TrFE. 11
Figure 1.5 (**A**) Structures of fludrocortisone, 5-FU, trifluridine, thalidomide, fluorothalidomide, fluorastrol, monastrol, and (**B**) BACE-1 inhibitor. RE = Efflux ratios. 13
Figure 1.6 Structures of Paxlovid active ingredients. 15
Figure 1.7 Examples of agrochemicals containing fluoroalkyl groups. 15
Figure 1.8 Structures of Ag chemicals Pydiflumetofen, Isoflucypram (**A**), and Carboxin (**B**). 17
Figure 1.9 Structures of Selectfluor®, NFSI, and NFPy. 18
Figure 1.10 Four categories of trifluoromethylation sources. 23
Figure 2.1 ^{19}F NMR spectra of complex **2-3** in benzene (**A**), with 8 eq. of DMSO (**B**), 8 eq. of THT (**C**), and THT as solvent (**D**). 62
Figure 2.2 Variation of reaction color in DMSO after addition of substrate. 63
Figure 2.3 ^{19}F NMR spectra of **2-3** (**A**) and aroyl-R^F (**B**). 64
Figure 3.1 Bioactive compounds containing $-OCF_3$ and $-CF_2H$ groups. 71
Figure 3.2 Molecular diagram representation of the molecular structure of **3-1**. Thermal ellipsoid probabilities are set at 50%, and hydrogens atoms and alternate conformations of disordered ttfet group are omitted. Selected bond distances (Å) and angles (deg): Cu-C 2.012(18)-2.062(16) Cu-P1 2.271(2) Cu-P2 2.286(2) P1-Cu-C1 118.50(4)-120.5(5), P1-Cu-P2 114.50(9), P2-Cu-C1 121.2(4)-126.7(4). 72
Figure 3.3 Molecular diagram representation of the molecular structures of **3-4b** (**A**) and **3-5** (**B**). Thermal ellipsoid probabilities are set to 50%, with hydrogen atoms and alternate conformations for disordered ttfet group omitted for clarity. Selected bond distances (Å) and angles (deg) for **3-4b**: Cu-C1 1.99(2)-2.02(2), C1-F1 1.42(2)-1.44(2), C1-Cu-P1 123(1)-133(1) and for **3-5**: Cu-C31 1.976(5)-2.033(7), Cu-C13 1.920(2), C31-F3 1.414(9)-1.436(7), C31-Cu-C13 165.1(2). 75
Figure 3.4 Yield of 4-iodoanisole fluoroalkylation product as a function of added DMSO in benzene after 24 h at 50 °C with a substrate/**3-1** ratio of 1.5/1. 77
Figure 3.5 Metal-ligand IBOs, frontier molecular orbitals and NRT structures for the key intermediate. 81
Figure 3.6 IBO bond composition at the TS stage, key metric parameters, charges and WBIs. 82
Figure 3.7 Electron flow along the intrinsic reaction coordinate (IRC) during reductive elimination. Hydrogen atoms omitted for clarity. The two IBOs with the largest changes along the reaction pathway are depicted. 83
Figure 4.1 ^{19}F NMR spectrum of $[CuH(PPh_3)]_6$ + Xantphos + tetramethyldisiloxane + TFE:CO_2 + methyl-4-iodobenzoate in DMF after 7 h at 50 °C. 100
Figure 4.2 ^{19}F NMR spectrum of $Cu(CF_2CF_2H)$(Xantphos) (**4-2**) + 4-nitro-iodobenzene + 10 mol% CuCl(SIMes) in toluene at 90 °C after 12 h. I = internal standard $PhCF_3$. 101
Figure 4.3 Calculated reaction coordinate for R^F transfer from $Cu(CF_2CF_2H)(PPh_3)$ to iodobenzene in toluene (energies are in kcal/mol). 103
Figure 4.4 R^F- and halo-bridged copper dimers. 106
Figure 4.5 Fluoroalkylated carboxamide analogues proposed for molecular docking studies. 112
Figure 4.6 (a) Structure of N-[(4-tert-butylphenyl)methyl]-2-(trifluoromethyl)benzamide (NAQ). (b) NAQ (green) binding mode with Sus scrofa SDH (PDB ID: 4YTP). The heme group is shown in cyan.

The binding site residues are labelled with a 1-letter amino acid code, and the chain letter near the Cα shown as spheres. 112
Figure 4.7 Chemical structures of known SDH inhibitors. 113
Figure 4.8 Simulation results of known SDHis docked into the binding site of fgSDH homology model 1. (**a**) isoflucypram, (**b**) thifluzamide, (**c**) (S)-pydiflumetofen, (**d**) pyflubimide and (**e**) flubendiamide. The SDHIs and heme groups are shown as green and cyan sticks, respectively. Chlorine and fluorine atoms are shown in pink and light green, respectively. 113
Figure 4.9 Simulation results of known SDHIs docked into the binding site of fgSDH homology model 2. (**a**) isoflucypram, (**b**) thifluzamide, (**c**) (S)-pydiflumetofen, (**d**) pyflubimide and (**e**) flubendiamide. The SDHIs and heme groups are shown as green and cyan sticks, respectively. Chlorine and fluorine atoms are shown in pink and light green, respectively. 114
Figure 4.10 Simulation results of fluoroalkylated-carboxamides (**4-5b**,**c**,**f**,**g** and **4-6a**,**b**,**c**) docked into the binding site of fgSDH homology model 2. 115
Figure 5.1 Calculated relative free energy landscape (not to scale) for Ni-metallacycle formation from two molecules of C_2F_4 using monodentate ancillary ligands. G values are relative to G[$L_2Ni(C_2F_4)$ + free C_2F_4] = 0.0 kcal/mol. 131
Figure 5.2 Calculated structures for Ni-C_2F_4 complexes **A-I** (Figure 5.1) using PMe_3 as the ancillary ligand. Hydrogen atoms are omitted for clarity. 132
Figure 5.3 Calculated relative free energy landscapes (not to scale) for Ni-metallacycle formation from two molecules of C_2F_4 using the P^iPr_3 ligand. 134
Figure 5.4 Calculated relative free energy landscapes (not to scale) for Ni-metallacycle formation from two molecules of C_2F_4 using bipy and tmeda chelate ligands. Structures for the bipy complexes are shown, with hydrogen atoms omitted for clarity. 137
Figure 5.5 Calculated free energy landscape for metallacycle formation using DPEphos. H-atoms omitted for clarity. 140
Figure 5.6 Alternative views of the computed structures of the **E** isomers in the DPEphos and Xantphos cyclization reactions, with H-atoms omitted for clarity. 141
Figure 5.7 ^{19}F (**A**) and $^{31}P\{^1H\}$ (**B**) NMR spectra of $Ni(cod)_2$ + dppf + 3 equiv TFE in C_6D_6. 142
Figure 5.8 Molecular diagram representation of the molecular structure of Ni(h^2-C_2F_4)(dppf) (**5-1b**). Thermal ellipsoid probabilities are set to 30% with hydrogen atoms and co-crystallized solvent omitted for clarity. Selected bond distances (Å) and angles (deg): Ni-P1 2.2003(4); Ni-C1 1.8839(14); C1-C1' 1.409(3); Ni-Centroid(C1,C1') 1.7471(10); Ni-Fe 4.1955(4); P1-Ni-P1' 106.6(1); C1-Ni-P1 104.95(5); C1-Ni-P1' 148.2(1); P1-Ni-Centroid(C1,C1') 126.7(1). 142
Figure 5.9 ^{19}F (**A**) and $^{31}P\{^1H\}$ (**B**) NMR spectra of $Ni(cod)_2$ + DPEphos + 3 equiv TFE in C_6D_6. 143
Figure 5.10 Variable temperature ^{19}F NMR spectra of metallacycle **5-3.** 143
Figure 5.11 Molecular diagram representation of molecular structure of **5-2c**. Thermal ellipsoid probabilities are set to 30% with hydrogen atoms, co-crystallized solvent and alternate conformations of the disordered nickelacyclopentane ring are omitted for clarity. Selected bond distances (Å) and angles (deg): Ni-C1 1.956(3); Ni-C4 1.948(3); Ni-P1 2.2403(8); Ni-P2 2.2512(9); Ni----O 2.947(2); C1-Ni-P1 153.01(10); C4-Ni-P2 157.29(10); C1-Ni-C4 84.32(13); P1-Ni-P2 100.43(3); C1-Ni-P2 91.44(10); C4-Ni-P4 93.13(9). 144
Figure 5.12 ^{19}F (**A**) and $^{31}P\{^1H\}$ (**B**) NMR spectra of Ni(cod)(Bisbi) + 3 equiv TFE in benzene. 145
Figure 5.13 Molecular diagram representation of molecular structure of **5-5**. Thermal ellipsoid probabilities are set to 30% with hydrogen atoms, co-crystallized solvent and alternate conformations of disordered nickelacyclopentane ring are omitted for clarity. Selected bond distances (Å) and angles (deg): Ni-C1 1.898(3)-1.899(3); Ni-C2 1.940(3)-1.943(4); Ni-P1 2.2589(9)-2.2734(8); Ni-N1 1.885(3)-1.897(3); C1-Ni-N1 175.12(13)-175.27(11); C2-Ni-P1 174.29(11)-175.01(14); C1-Ni-C4 85.68(13)-85.92(16); C1-Ni-P1 92.91(10)-93.23(9); C4-Ni-N1 89.20(15)-89.95(12); P1-Ni-N1 90.95(7)-91.98(9) 145
Figure 6.1 ^{19}F (**A**) and $^{31}P\{^1H\}$ NMR spectra (**B**) of **6-1a** and **6-2a**. 161

Figure 6.2 Molecular diagram representation of molecular structure of **6-1a**. Thermal ellipsoid probabilities are set to 30% with hydrogen atoms, disordered OCF_3 and terminal Me of i-Pr are omitted. Selected bond distances (Å) and angles (deg): Ni-P1: 2.2085(5) Ni-P2 2.2108(4) Ni-C2: 1.9416(17) NiC5: 1.9448(18) P1-Ni-P2: 95.41(2) P1-Ni-C2: 92.36(6) P1-Ni-C5: 159.35(7) P2-Ni-C5: 91.90(6) P2-Ni-C2: 159.00(6), C1-Ni-C5: 87.54(8). 161
Figure 6.3 ^{19}F (**A**) and $^{31}P\{^{1}H\}$ NMR spectra (**B**) of **6-2** 162
Figure 6.4 ^{19}F (**A**) and $^{31}P\{^{1}H\}$ NMR spectra (**B**) of **6-2c** and **6-3**. 163
Figure 6.5 Molecular diagram representation of the molecular structure of **6-3**. Thermal ellipsoid probabilities are set to 50% with hydrogen atoms omitted. Selected bond distances (Å) and angles (deg): Ni-P1 2.2185(4) Ni-P2 2.2895(4) Ni-P3 2.1827(4) Ni-C1 1.868(6)-1.892(2) Ni-C2 1.926(2)-1.948(5) P1-Ni-P2 86.453(14) P1-Ni-P3 102.166(15) Ni-$C_{1,2centroid}$ 1.775(1) P1-Ni-$C_{1,2centroid}$ 120.5(1)-121.8(1) P2-Ni-P3 101.995(15) P2-Ni-$C_{1,2centroid}$ 124.4(1)-125.7(1) P3-Ni- $C_{1,2centroid}$ 114.7(1)..... 164
Figure 6.6 Molecular diagram representation of the molecular structure of **6-7c**. Thermal ellipsoid probabilities are set to 50% with hydrogen atoms omitted. Selected bond distances (Å) and angles (deg): Ni-P1 2.3219(4) Ni-P2 2.2074(4) Ni-P3 2.1582(4) Ni-C1 1.8970(15) Ni-C2 1.9197(16) P1-Ni-P2 88.132(14) P1-Ni-P3 107.754(15) Ni-$C_{1,2centroid}$ 1.771(2) P1-Ni-$C_{1,2centroid}$ 116.6(1) P2-Ni-P3 97.493(15) P2-Ni-$C_{1,2centroid}$ 123.5(1) P3-Ni- $C_{1,2centroid}$ 118.3(1). 166
Figure A2.1 ^{19}F NMR spectrum (282 MHz) of $[CuH(PPh_3)]_6$ + 3 equiv/Cu of $P(O^iPr)_3$ + CTFE in benzene.…..... 182
Figure A2 2 ^{19}F NMR spectrum (282 MHz) of $[CuH(PPh_3)]_6$ + 3 equiv/Cu of $P(OEt)_3$ + CTFE in benzene. 182
Figure A2.3 ^{19}F (**A**) and $^{19}F\{^{1}H\}$ (**B**) NMR spectra (282 MHz) of $Cu(CFClCF_2H)[(POEt)_3]_n$ (**2-2**) in benzene. 183
Figure A2.4 $^{31}P\{^{1}H\}$ NMR spectrum (121 MHz) of $[CuH(PPh_3)]_6$ + 3 equiv/Cu of $(POEt)_3$ + CTFE in benzene. 183
Figure A2.5 ^{19}F NMR spectrum (282 MHz) of $[CuH(PPh_3)]_6$ + 3 equiv/Cu of triethylphosphite + CTFE in benzene after removal of solvent. SP = uncharacterized side-product(s). 184
Figure A2.6 ^{19}F NMR spectrum (282 MHz) of $[CuH(PPh_3)]_6$ + 2 equiv/Cu of PPh_2Me + CTFE in benzene. 184
Figure A2.7 ^{19}F NMR spectrum (282 MHz) of $[CuH(PPh_3)]_6$ + 2 equiv/Cu of PPh_3 + CTFE in benzene. 185
Figure A2.8 ^{19}F NMR spectrum (282 MHz) of $[CuH(PPh_3)]_6$ + 2 equiv/Cu of PPh_3 + CTFE in benzene after removal of solvent. SP = uncharacterized side-products 185
Figure A2.9 ^{19}F NMR (282 MHz) of $[CuH(PPh_3)]_6$ + 1 equiv/Cu of phen + CTFE in benzene. 186
Figure A2.10 ^{19}F NMR spectrum (282 MHz) of $[CuH(PPh_3)]_6$ + 1 equiv/Cu of terpyridine + CTFE in benzene. 186
Figure A2.11 ^{19}F NMR spectrum (282 MHz) of $[CuH(PPh_3)]_6$ + 1 equiv/Cu of PMDTA+ CTFE in benzene. 187
Figure A2.12 ^{19}F NMR spectrum (282 MHz) of $[CuH(PPh_3)]_6$ + 1 equiv/Cu of PMDTA + CTFE in DMF. 187
Figure A2.13 ^{19}F NMR spectrum (282 MHz) of $[CuH(PPh_3)]_6$ + 1 equiv/Cu of tripod + CTFE in benzene. 188
Figure A2.14 ^{19}F NMR spectrum (282 MHz) of $[CuH(PPh_3)]_6$ + 1 equiv/Cu of triphos + CTFE in benzene. 188
Figure A2.15 $^{19}F\{^{1}H\}$ NMR spectrum (282 MHz) of $[CuH(PPh_3)]_6$ + 1 equiv/Cu of triphos + CTFE in benzene. 189

Figure A2.16 ^{19}F NMR spectrum (282 MHz, C_6D_6) of complex **2-3**. 189
Figure A2.17 $^{19}F\{^1H\}$ NMR spectrum (282 MHz, C_6D_6) of complex **2-3**. 190
Figure A2.18 $^{31}P\{^1H\}$ NMR (121 MHz, C_6D_6) of complex **2-3**. 190
Figure A2.19 ^1H NMR spectrum (300 MHz, C_6D_6) of complex **2-3**. 190
Figure A2.20 ESI-MS (positive mode) spectrum of complex **2-3**. 191
Figure A2.21 ^{19}F NMR spectrum (282 MHz) of complex **2-3** + 8 eq. of DMSO in benzene. 191
Figure A2.22 $^{19}F\{H\}$ NMR spectrum (282 MHz) of Complex **2-3** + 8 eq. of DMSO in benzene. 192
Figure A2.23 ^{19}F NMR spectrum (282 MHz) of complex **2-3** with 8 eq. of tetrahydrothiophene (THT) in benzene. 192
Figure A2.24 $^{31}P\{H\}$ NMR spectrum (282 MHz) of Complex **2-3** with 8 eq. of THT in benzene. 192
Figure A2.25 ^{19}F NMR spectrum (282 MHz) of complex **2-3** in THT. 193
Figure A2.26 $^{19}F\{H\}$ NMR spectrum (282 MHz) of complex **2-3** in THT. 193
Figure A2.27 ^{19}F NMR spectrum (282 MHz) of complex **2-3** in THT at -40 °C. 193
Figure A2.28 $^{31}P\{^1H\}$ NMR spectrum (121 MHz) of complex **2-3** in THT. 193
Figure A2.29 $^{31}P\{^1H\}$ NMR spectrum (121 MHz) of complex **2-3** in THT at -40 °C. 194
Figure A2.30 $^{31}P\{^1H\}$ NMR spectrum (121 MHz) of $[CuH(PPh_3)]_6$ + 2 equiv/Cu of PPh_3 + 1 equiv/Cu of triphos in benzene. 194
Figure A2.31 $^{31}P\{^1H\}$ NMR spectra (121 MHz) of reaction of $[CuH(PPh_3)]_6$ + 1 equiv/Cu of PPh_3 + 0.5 equiv/Cu of triphos (**A**) and 1 eq. of triphos (**C**) in benzene. 195
Figure A2.32 $^{31}P\{^1H\}$ NMR (121 MHz) of $[CuH(PPh_3)]_6$ + 1 equiv/Cu of triphos in benzene after 22 h at 50 ºC. 195
Figure A2.33 ^{19}F NMR spectrum (282 MHz) of $[CuH(PPh_3)]_6$ + 0.5 equiv/Cu of triphos + CTFE in benzene. 196
Figure A2.34 ^{19}F NMR spectrum (282 MHz) of $[CuH(PPh_3)]_6$ + 2 equiv/Cu of PPh_3 + 0.5 equiv/Cu of triphos + CTFE in benzene. 196
Figure A2.35 ^{19}F NMR spectrum (282 MHz) of $[CuH(PPh_3)]_6$ + 1 equiv/Cu of PPh_3 + 1 equiv/Cu of triphos + CTFE. 197
Figure A2.36 ^{19}F NMR spectrum (282 MHz) of complex **2-2** in DMSO with benzoyl chloride. 197
Figure A2.37 ^{19}F NMR spectrum (282 MHz) of complex **2-2** in DMF with 1 equiv of benzoyl chloride and 1 equiv of phen. 198
Figure A2.38 ^{19}F NMR (282 MHz) of Complex **2-3** with benzoyl chloride in benzene. SM = Starting material **2-3**. 198
Figure A2.39 ^{19}F NMR spectrum (282 MHz) of complex **2-3** with 1.5 eq. of benzoyl chloride (**2-4a**) in DMSO at 25 ºC after 12 h. 198
Figure A2.40 $^{19}F\{^1H\}$ NMR spectrum (282 MHz) of Complex **2-3** with 1.5 eq. of benzoyl chloride (**2-4a**) in DMSO at 25 ºC after 12 h. 199
Figure A2.41 ^{19}F NMR spectrum (282 MHz) of complex **2-3** with 1.5 eq. of toluoyl chloride (**2-4b**) in DMSO at 25 ºC after 12 h. 199
Figure A2.42 $^{19}F\{^1H\}$ NMR spectrum (282 MHz) of complex **2-3** with 1.5 eq. of p-toluoyl chloride (**2-4b**) in DMSO at 25 ºC after 12 h. 199
Figure A2.43 Selected GC-MS peak from reaction mixture of complex **2-3** with 1.5 eq. of toluoyl chloride (**2-4b**) in DMSO at 25 ºC after 12 h (after filtration through alumina). 200
Figure A2. 44 ^{19}F NMR spectrum (282 MHz) of complex **2-3** with 1.5 eq. of 4-fluoro-benzoyl chloride (**2-4c**) in DMSO at 25 ºC after 12 h. 200

Figure A2.45 ^{19}F NMR spectrum (282 MHz) of Complex **2-3** with 1.5 eq. of 4-fluoro-benzoyl chloride (**2-4c**) and 8 eq. of DMSO in benzene at 50 ºC after 12 h. S = substrate 201
Figure A2.46 ^{19}F NMR spectrum (282 MHz) of Complex **2-3** with 1.5 eq. of 1-naphthoyl chloride (**2-4d**) in DMSO at 25 ºC after 12 h. 201
Figure A2.47 ^{19}F{^{1}H} NMR spectrum (282 MHz) of complex **2-3** with 1.5 eq. of 1-naphthoyl chloride (**2-4d**) in DMSO at 25 ºC after 12 h. 202
Figure A2.48 ^{19}F NMR spectrum (282 MHz) of complex **2-3** with 1.5 eq. of 2-thiophenecarbonyl chloride (**2-4e**) in DMSO at 25 ºC after 12 h. 202
Figure A2.49 ^{19}F{^{1}H} NMR spectrum (282 MHz) of complex **2-3** with 1.5 eq. of 2-thiophenecarbonyl chloride (**2-4e**) in DMSO at 25 ºC after 12 h. 203
Figure A2.50 ^{19}F NMR spectrum (282 MHz) of Complex **2-3** with 1.5 eq. of m-Br-benzoyl chloride (**2-4f**) in DMSO at 25 ºC after 12 h 203
Figure A2.51 ^{19}F{^{1}H} NMR spectrum (282 MHz) of Complex **2-3** with 1.5 eq. of m-Br-benzoyl chloride (**2-4f**) in DMSO at 25 ºC after 12 h. 204
Figure A2.52 ^{19}F NMR spectrum (282 MHz) of Complex **2-3** with 1.5 eq. of 4-cyano-benzoyl chloride (**2-4g**) in DMSO at 25 ºC after 12 h. 204
Figure A2.53 ^{19}F{^{1}H} NMR spectrum (282 MHz) of Complex **2-3** with 1.5 eq. of 4-cyano-benzoyl chloride (**2-4g**) in DMSO at 25 ºC after 12h. 204
Figure A2.54 ^{19}F NMR spectrum (282 MHz) of Complex **2-3** with 1.5 eq. of 2-nitro-benzoyl chloride (**2-4h**) in DMSO at 25 ºC after 12 h. 205
Figure A2.55 ^{19}F{^{1}H} NMR spectrum (282 MHz) of Complex **2-3** with 1.5 eq. of 2-nitro-benzoyl chloride (**2-4h**) in DMSO at 25 ºC after 12 h. 205
Figure A2.56 ^{19}F NMR spectrum (282 MHz) of Complex **2-3** with 1.5 eq. of 2,4,6-trichloro-benzoyl chloride (**2-4i**) in DMSO at 25 ºC after12 h. 205
Figure A2.57 ^{19}F{^{1}H} NMR spectrum (282 MHz) of complex **2-3** with 1.5 eq. of 2,4,6-trichloro-benzoyl chloride (**2-4i**) in DMSO at 25 ºC after 12 h. 206
Figure A2.58 ^{19}F NMR spectrum (282 MHz) of complex **2-3** with p-F-benzyl bromide (**6**) in benzene. S = substrate. 206
Figure A2.59 ^{19}F NMR spectrum (282 MHz) of complex **2-3** with 4-fluoro-iodobenzene in benzene. SM = starting material **2-3**, S = substrate. 206
Figure A2.60 ^{19}F NMR spectrum (282 MHz) of complex **2-3** with methyl-2-iodobenzoate in DMSO at room temperature. 207
Figure A2.61 ^{19}F NMR spectrum (282 MHz) of complex **2-3** with 4-iodo-benzonitrile and 8 equiv. of DMF in benzene at 50 ºC 207
Figure A2.62 ^{19}F NMR spectrum (282 MHz) of complex 2-3 with methyl-2-iodobenzoate and 8 eq. of DMSO in benzene at 50 ºC. 207
Figure A2.63 ^{19}F NMR spectrum (282 MHz) of complex **2-3** with 4-iodo-benzonitrile in benzene at 35 ºC overnight. 208
Figure A2.64 ^{19}F NMR spectrum (282 MHz) of complex **2-3** with methyl 2-iodo-benzoate in benzene at 35 ºC overnight. 208
Figure A2.65 ^{19}F NMR spectrum (282 MHz) of complex **2-3** with 4-fluoro-iodobenzene and 8 eq. of DMSO in benzene at 35 ºC overnight. 208
Figure A2.66 ^{19}F NMR spectrum (282 MHz) of complex **2-3** with 4-fluoro-iodobenzene in DMF diluted 2x. 209
Figure A2.67 ^{19}F NMR spectrum (282 MHz) of complex **2-3** with 4-fluoro-iodobenzene in benzene diluted 2x. 209

Figure A2.68 ^{19}F NMR spectrum (282 MHz) of complex **2-3** in DMSO. 210
Figure A2.69 ^{19}F NMR spectrum (282 MHz) of complex **2-3** in DMF. 210
Figure A2.70 ^{19}F NMR spectrum (282 MHz) of complex **2-3** in DMPU. 210
Figure A2.71 ^{19}F NMR spectrum (282 MHz) of complex **2-3** in CPME after 30 min (**A**), addition of 8 eq. of DMSO and 1.5 eq. of 4-fluoro-iodobenzene (**B**), after heating at 50 °C overnight (**C**). 211
Figure A2.72 ^{19}F NMR spectrum (282 MHz) of complex **2-3** with 4- fluoro-iodobenzene + 8 eq. of DMPU in benzene diluted. 211
Figure A2.73 ^{19}F NMR spectrum (282 MHz) of complex **2-3** with 4-fluoro-iodobenzene in benzene diluted at 40 °C. 212
Figure A2.74 ^{19}F NMR spectrum (282 MHz) of complex **2-3** in 1,4-dioxane after 24 h. 212
Figure A2.75 ^{19}F NMR spectrum (282 MHz) of complex **2-3** with 4-fluoro-iodobenzene in DMSO at 50 °C. 212
Figure A2.76 ^{19}F NMR spectrum (282 MHz) of complex **2-3** with 4-iodo-benzonitrile in benzene at 50 °C. 213
Figure A2.77 ^{19}F NMR spectrum (282 MHz) of complex **2-3** with 4-fluoro-iodobenzene in CPME at 50 °C. S = substrate. 213
Figure A2.78 ^{19}F NMR spectrum (282 MHz) of complex **2-3** with 4-iodobenzonitrile in CPME at 100 °C. 213
Figure A2.79 ^{19}F NMR spectrum (282 MHz) of complex **2-3** with methyl-2-iodobenzoate in benzene at 50 °C. 214
Figure A2.80 ^{19}F NMR spectrum (282 MHz) of complex **2-3** with iodo-benzonitrile in ACN at room temperature. 214
Figure A2.81 ^{19}F NMR spectrum (282 MHz) of complex **2-3** with iodo-nitrobenzene in DMSO/ benzene 1:1 at 50 °C. 214
Figure A2.82 ^{19}F NMR spectrum (282 MHz) of complex **2-3** + 4-fluoro-iodobenzene + 8 equiv. of pyridine in benzene. S = substrate. 215
Figure A2.83 ^{19}F NMR spectrum (282 MHz) of complex **2-3** +2-methyliodo benzoate + 2 equiv. of CuBr + 28 equiv. of DMSO in benzene. I = internal standard, $PhCF_3$. 215
Figure A3.1 ^{19}F NMR spectrum (282 MHz, C_6D_6) of complex **3-1**. 217
Figure A3.2 $^{19}F\{^1H\}$ NMR spectrum (282 MHz, C_6D_6) of complex **3-1**. 217
Figure A3.3 ^{31}P NMR spectrum (121 MHz, C_6D_6) of complex **3-1**. 218
Figure A3.4 ^1H NMR spectrum (300 MHz, C_6D_6) of complex **3-1**. 218
Figure A3.5 EI-MS spectrum of complex **3-1**. 219
Figure A3.6 ESI-MS (positive mode) spectrum of complex **3-1**. 219
Figure A3.7 Mass spectrum of complex **3-1**. 220
Figure A3.8 ^{19}F NMR spectrum (282 MHz, C_6D_6) of complex **3-1** and $PMePh_2$ in benzene. 220
Figure A3.9 ^{19}F NMR spectrum (282 MHz, C_6D_6) of complex **3-1** and IMes in benzene. 221
Figure A3.10 ^{19}F NMR spectra (282 MHz, C_6D_6) of complex **3-1** with 1 equiv of benzoyl chloride in THF and after heating at 40 °C. $CF_2HCHF(OCF_3)$: -56.6 (s, OCF_3), -134 (dmult, $^2J_{FH}$ = 55 Hz, CF_2H) and -144.9 ppm (dmult, $^2J_{FH}$ = 54 Hz, CF). SP = uncharacterized side product 221
Figure A3.11 ^{19}F NMR spectrum (282 MHz, C_6D_6) of complex **3-1** with 1 equiv of benzoyl chloride in Et_2O and after heating at 40 °C. 222
Figure A3.12 ^{19}F NMR spectrum (282 MHz, C_6D_6) of complex **3-1** with 1 equiv of benzoyl chloride in N,N-dimethylacetamide after 7 h. SP = uncharacterized side products. 222

Figure A3.13 ^{19}F NMR spectrum (282 MHz, C_6D_6) of complex **3-1** with 1 equiv of benzoyl chloride in acetonitrile. 223
Figure A3.14 ^{19}F NMR spectrum (282 MHz, C_6D_6) of complex **3-1** with 1 equiv of benzoyl chloride in cyclopentyl methyl ether. 223
Figure A3.15 ^{19}F NMR spectrum (282 MHz, C_6D_6) of complex **3-1** with 1 equiv of benzoyl chloride in toluene. 224
Figure A3.16 ^{19}F NMR spectrum (282 MHz, C_6D_6) of product fluorinated ketone **3-3a**, after complex **3-1** reacted with 1 equiv of benzoyl chloride in DMSO. SP = side product and I = Internal Standard ($PhCF_3$). 224
Figure A3.17 ^{19}F NMR spectrum (282 MHz, C_6D_6) of **3-3b**, after complex **3-1** reacted with 1 equiv of 4-toluoyl chloride in DMSO. I = Internal Standard ($PhCF_3$). 225
Figure A3.18 ^{19}F NMR spectrum (282 MHz, C_6D_6) of **3-3c**, after complex **3-1** reacted with 1 equiv of 2,4,6-trichlorobenzoyl chloride in DMSO. I = Internal Standard ($PhCF_3$). 225
Figure A3.19 ^{19}F NMR spectrum (282 MHz, C_6D_6) of **3-3d**, after complex **3-1** reacted with 1 equiv of 4-cyanobenzoyl chloride in DMSO. I = Internal Standard ($PhCF_3$). 226
Figure A3.20 ^{19}F NMR spectrum (282 MHz, C_6D_6) of **3-3e**, after complex **3-1** reacted with 1 equiv of 2-furoyl chloride in DMSO. I = Internal Standard ($PhCF_3$). 226
Figure A3.21 ^{19}F NMR spectrum (282 MHz, C_6D_6) of **3-3f**, after complex **3-1** reacted with 1 equiv of naphthoyl chloride in DMSO. SP = side products and I = Internal Standard ($PhCF_3$). 227
Figure A3.22 ^{19}F NMR spectrum (282 MHz, C_6D_6) of **3-3g**, after complex **3-1** reacted with 1 equiv of 2-nitrobenzoyl-chloride in DMSO. SP = side product and I = Internal Standard ($PhCF_3$). 227
Figure A3.23 ^{19}F NMR spectrum (282 MHz, C_6D_6) of **3-3h**, after complex **3-1** reacted with 1 equiv of 4-nitrobenzoyl chloride in DMSO. SP = side product and I = Internal Standard ($PhCF_3$). 228
Figure A3.24 ^{19}F NMR spectrum (282 MHz, C_6D_6) of **3-3i**, after complex **3-1** reacted with 1 equiv of 2-thiophenylcarbonyl chloride in DMSO. SP = side product and I = Internal Standard ($PhCF_3$). 228
Figure A3.25 ^{19}F NMR (282 MHz, C_6D_6; **A**) and $^{31}P\{^1H\}$ NMR (121 MHz; **B**) spectra of complex **3-4a**. 229
Figure A3. 26 ^{19}F NMR (282 MHz, C_6D_6; **A**) and $^{31}P\{^1H\}$ NMR (121 MHz; **B**) of complex **3-4b.** 229
Figure A3.27 ^1H NMR spectrum (282 MHz, C_6D_6) of complex **3-4b.** 230
Figure A3.28 ESI-MS (positive mode) spectrum of complex **3-4b** showing $[Na\text{-}MR_{F(}Cl_2\text{-bipy})]^+$ 230
Figure A3.29 ^{19}F NMR spectrum (282 MHz, C_6D_6) of complex **3-5**. 231
Figure A3.30 ^1H NMR spectrum (282 MHz, C_6D_6) of complex **3-5**. 231
Figure A3.31 ESI-MS (positive mode) spectrum of complex **3-5**. 232
Figure A3.32 ^{19}F NMR spectrum (282 MHz, C_6D_6) after complex **3-4a** reacted with 1.5 equiv of 4-fluorobenzoyl chloride in benzene. SP = side product, SM = start material, S= substrate. 232
Figure A3.33 ^{19}F NMR spectrum (282 MHz, C_6D_6) after complex **3-4a** reacted with 1.5 equiv of benzoyl chloride in benzene. SM = starting material. 233
Figure A3.34 ^{19}F NMR spectrum (282 MHz, C_6D_6) after complex **3-5** reacted with 1.5 equiv of 4-benzoyl chloride in benzene. SP = side products, SM = starting material. 233
Figure A3.35 ^{19}F NMR spectrum (282 MHz, C_6D_6) after complex **3-5** reacted with 1.5 equiv of 4-CF_3-benzoyl chloride in benzene. SP = side products, SM = starting material. 234
Figure A3.36 ^{19}F NMR spectrum (282 MHz, C_6D_6) after complex **3-5** reacted with 1.5 equiv of 4-fluorobenzoyl chloride in benzene. SP = side product, SM = starting material. 234
Figure A3.37 ^{19}F NMR spectrum (282 MHz, C_6D_6) after complex **3-5** reacted with 1.5 equiv of naphthoyl chloride in benzene. SP = side product, SM = starting material. 235

Figure A3.38 ^{19}F NMR spectrum (282 MHz, C_6D_6) after complex **3-5** reacted with 1.5 equiv of o-toluoyl chloride in benzene. P = product, SP = side product, SM = starting material. 235
Figure A3.39 ^{19}F NMR spectrum (282 MHz) of complex **3-1** in DMSO-d_6..... 236
Figure A3.40 $^{19}F\{^1H\}$ NMR spectrum (282 MHz) of complex **3-1** in DMSO-d_6..... 236
Figure A3.41 ^1H NMR spectrum (300 MHz) of complex **3-1** in DMSO-d_6. 237
Figure A3.42 ^{19}F NMR spectrum (282 MHz, C_6D_6) after complex **3-1** reacted with DMSO (8 eq.) and methyl-2-iodobenzoate (1.5 eq.) in benzene at 50 ^oC. SM = starting material, I = internal standard ($PhCF_3$). 237
Figure A3.43 ^{19}F NMR spectrum (282 MHz, C_6D_6) after complex **3-1** reacted with DMSO (8 eq.) and 4-fluoroiodobenzene (1.5 eq.) in benzene at 50 ^oC. SM = starting material, S = substrate..... 238
Figure A3.44 ^{19}F NMR spectrum (282 MHz, C_6D_6) after complex **3-1** reacted with DMSO (8 eq.) and 4-iodo-nitrobenzene (1.5 eq.) in benzene at 50 ^oC. SM = starting material, I = internal standard ($PhCF_3$). 238
Figure A3.45 ^{19}F NMR spectrum (282 MHz, C_6D_6) after complex **3-1** reacted with DMSO (8 eq.) and 3-iodobenzonitrile (1.5 eq.) in benzene at 50 ^oC. SP = side product, I = internal standard ($PhCF_3$)..... 239
Figure A3.46 ^{19}F NMR spectrum (282 MHz, C_6D_6) after complex **3-1** reacted with DMSO (8 eq.) and 2-iodo-pyridine (1.5 eq.) in benzene at 50 ^oC. SM = starting material, SP = side product, I = internal standard ($PhCF_3$). 239
Figure A3.47 ^{19}F NMR spectrum (282 MHz, C_6D_6) after complex **3-1** reacted with DMSO (10 eq.) and 4-iodo-nitrobenzene (1.5 eq.) in benzene at 50 ^oC. SM = starting material, SP = side product. 240
Figure A3.48 ^{19}F NMR spectrum (282 MHz, C_6D_6) after complex **3-4b** reacted with 1.5 equiv of iodobenzonitrile in benzene. P = product..... 240
Figure A3.49 ^{19}F NMR spectrum (282 MHz, C_6D_6) after complex **3-4b** reacted with 1.5 equiv of 4-fluoro-iodobenzene in benzene. P = product, SM = starting material, S = substrate. 241
Figure A3.50 ^{19}F NMR spectrum (282 MHz, C_6D_6) after complex **3-4b** reacted with 1.5 equiv of 4-iodo-nitrobenzene in benzene. P = product, SM = starting material. 241
Figure A3.51 ^{19}F NMR spectrum (282 MHz, C_6D_6) after complex **3-1** reacted with CuCl/ DMSO (1.5 eq.) and 4-benzonitrile (1.5 eq) in benzene. P = product, SP = side product, I = internal standard ($PhCF_3$). 242
Figure A3.52 ^{19}F NMR spectrum (282 MHz, C_6D_6) after complex **3-1** reacted with CuCl/DMSO (2 eq.) and 4-benzonitrile (1.5 eq.) in benzene. P = product, I = internal standard ($PhCF_3$). 242
Figure A3.53 ^{19}F NMR spectrum (282 MHz, C_6D_6) after complex **3-1** reacted with CuCl/DMF (2 eq.) and 4-benzonitrile (1 eq.) in benzene. P = product, I = internal standard ($PhCF_3$). 243
Figure A3.54 ^{19}F NMR spectrum (282 MHz, C_6D_6) after complex **3-1** reacted with CuCl/DMSO (2 eq.) and 4-benzonitrile (1 eq.) in benzene. P = product, I = internal standard ($PhCF_3$). 243
Figure A3.55 ^{19}F NMR spectrum (282 MHz, C_6D_6) after complex **3-1** reacted with CuI/DMSO (1.5 eq.) and 4-benzonitrile (1.5 eq.) in benzene. P = product, I = internal standard ($PhCF_3$). 244
Figure A3.56 ^{19}F NMR spectrum (282 MHz, C_6D_6) after complex **3-1** reacted with CuI/DMSO (2 eq.) and 4-benzonitrile (1.5 eq.) in benzene. P = product, I = internal standard ($PhCF_3$). 244
Figure A3.57 ^{19}F NMR spectrum (282 MHz, C_6D_6) after complex **3-1** reacted with CuI/DMSO (2 eq.) and 4-benzonitrile (1 eq.) in benzene. P = product, I = internal standard ($PhCF_3$). 245
Figure A3.58 ^{19}F NMR spectrum (282 MHz, C_6D_6) after complex **3-1** reacted with CuI/DMF (2 eq.) and 4-benzonitrile (1 eq.) in benzene..... 245
Figure A3.59 ^{19}F NMR spectrum (282 MHz, C_6D_6) after complex **3-1** reacted with CuBr/DMSO (1.5 eq.) and 4-iodo-benzonitrile (1.5 eq.) in benzene. P = product, I = internal standard ($PhCF_3$). 245
Figure A3. 60 ^{19}F NMR spectrum (282 MHz, C_6D_6) after complex **3-1** reacted with CuBr/DMSO (2 eq.) and 4-iodobenzonitrile (1.5 eq.) in benzene. P = product, I = internal standard ($PhCF_3$). 246

Figure A3.61 ^{19}F NMR spectrum (282 MHz, C_6D_6) after complex **3-1** reacted with CuBr/DMSO (2 eq.) and 4-iodobenzonitrile (1 eq.) in benzene. P = product, I = internal standard ($PhCF_3$). 246
Figure A3.62 ^{19}F NMR spectrum (282 MHz, C_6D_6) after complex **3-1** reacted with CuBr/DMF (2 eq.) and 4-iodo-benzonitrile (1 eq.) in benzene. P = product, I = internal standard ($PhCF_3$)..... 247
Figure A3.63 ^{19}F NMR spectrum (282 MHz, C_6D_6) after complex **3-1** reacted with CuBr/DMF (2 eq.) in 20 eq. of DMSO and 4-iodoanisole (1 eq.) in 0.5 mL of benzene at 50 °C. P = product, I = internal standard ($PhCF_3$). 247
Figure A3.64 ^{19}F NMR spectrum (282 MHz, C_6D_6) after complex **3-1** reacted with CuBr/DMF (2 eq.) in 25 eq. of DMSO and 4-iodoanisole (1 eq.) in 0.5 mL of benzene at 50 °C. I = internal standard ($PhCF_3$). 248
Figure A3.65 ^{19}F NMR spectrum (282 MHz, C_6D_6) after complex **3-1** reacted with CuBr/DMF (2 eq.) in 35 eq. of DMSO and 4-iodoanisole (1 eq.) in 0.5 mL of benzene at 50 °C. I = internal standard ($PhCF_3$), SP = side product. 248
Figure A3.66 ^{19}F NMR spectrum (282 MHz, C_6D_6) after complex **3-1** reacted with CuBr/DMF (2 eq.) in 45 eq. of DMSO and 4-iodoanisole (1 eq.) in 0.5 mL of benzene at 50 °C. I = internal standard ($PhCF_3$). 249
Figure A3.67 ^{19}F NMR spectrum (282 MHz, C_6D_6) after complex **3-** reacted with CuBr/DMF (2 eq.) in 55 eq. of DMSO and 4-iodoanisole (1 eq.) in 0.5 mL of benzene at 50 °C. I = internal standard ($PhCF_3$). 249
Figure A3.68 ^{19}F NMR spectrum (282 MHz, C_6D_6) after complex **3-1** reacted with CuBr/DMF (2 eq.) in 65 eq. of DMSO and 4-iodoanisole (1 eq.) in 0.5 mL of benzene at 50 °C. I = internal standard ($PhCF_3$), SP = side product. 250
Figure A3.69 ^{19}F NMR spectrum (282 MHz, C_6D_6) of **3-7a**, after complex **3-1** reacted with CuBr (2 eq) DMSO (28 eq.) and methyl-2-iodobenzoate (1 eq.) in benzene at 50 °C. I = internal standard ($PhCF_3$). 250
Figure A3.70 ^{1}H NMR spectrum (300 MHz, C_6D_6) of **3-7a**, after complex **3-1** reacted with CuBr (2 eq) DMSO (28 eq.) and methyl-2-iodobenzoate (1 eq.) in benzene at 50 °C. 251
Figure A3.71 GC-MS of **3-7a**, after complex **3-1** reacted with CuBr (2 eq) DMSO (28 eq.) and 4-iodobenzonitrile (1 eq.) in benzene at 50 °C. Retention time 12.483 min, expected 302.17 m/z (100%), found 302.1 m/z (20%) and 251 m/z (99%)..... 251
Figure A3.72 ^{19}F NMR spectrum (282 MHz, C_6D_6) of **3-7b**, after complex **3-1** reacted with CuBr (2 eq) DMSO (28 eq.) and 4-iodo-benzonitrile (1 eq.) in benzene at 50 °C. I = internal standard ($PhCF_3$). 252
Figure A3.73 ^{1}H NMR spectrum (300 MHz, C_6D_6) of **3-7b**, after complex **3-1** reacted with CuBr (2 eq) DMSO (28 eq.) and 4-iodobenzonitrile (1 eq.) in benzene at 50 °C. 252
Figure A3.74 GC-MS of **3-7b**, after complex **3-1** reacted with CuBr (2 eq) DMSO (28 eq.) and 4-iodobenzonitrile (1 eq.) in benzene at 50 °C. Retention time 6.791 min, expected 269.15 m/z and found 269 m/z. 253
Figure A3.75 ^{19}F NMR spectrum (282 MHz, C_6D_6) of **3-7c**, after complex **3-1** reacted with CuBr (2 eq) DMSO (28 eq.) and 4-nitroiodobenzene (1 eq.) in benzene at 50 °C. I = internal standard ($PhCF_3$). 253
Figure A3.76 GC-MS of **3-7c**, after complex **3-1** reacted with CuBr (2 eq) DMSO (28 eq.) and 4-iodonitrobenzene (1 eq.) in benzene at 50 °C. Retention time 12.357 min, expected 289.13 m/z (100%), found 289 m/z (20%) and 238 m/z (99%)..... 254
Figure A3.77 ^{19}F NMR spectrum (282 MHz, C_6D_6) of **3-7d**, after complex **3-1** reacted with CuBr (2 eq) DMSO (28 eq.) and 4-fluoroiodobenzene (1 eq.) in benzene at 50 °C. S = substrate, I = internal standard ($PhCF_3$). 254
Figure A3.78 ^{19}F NMR spectrum (282 MHz, C_6D_6) of **3-7e**, after complex **3-1** reacted with CuBr (2 eq) DMSO (28 eq.) and 1-iodonaphthalene (1 eq.) in benzene at 50 °C. I = internal standard ($PhCF_3$)..... 255

Figure A3.79 ^{19}F NMR spectrum (282 MHz, C_6D_6) of **3-7f**, after complex **3-1** reacted with CuBr (2 eq) DMSO (28 eq.) and 2-iodobenzonitrile (1 eq.) in benzene at 50 °C. I = internal standard ($PhCF_3$)..... 255
Figure A3. 80 ^{19}F NMR spectrum (282 MHz, C_6D_6) of **3-7g**, after complex **3-1** reacted with CuBr (2 eq) DMSO (28 eq.) and (1 eq.) of biphenyl iodobenzene in benzene at 50 °C. I = internal standard ($PhCF_3$). 256
Figure A3.81 ^{19}F NMR spectrum (282 MHz, C_6D_6) of **3-7h**, after complex **3-1** reacted with CuBr (2 eq) DMSO (28 eq.) and 2-iodoanisole (1 eq.) in benzene at 50 °C. I = internal standard ($PhCF_3$)..... 256
Figure A3.82 ^{1}H NMR spectrum (282 MHz, C_6D_6) of **3-7h**, after complex **3-1** reacted with CuBr (2 eq) DMSO (28 eq.) and 2-iodoanisole (1 eq.) in benzene at 50 °C..... 257
Figure A3.83 ^{19}F NMR spectrum (282 MHz, C_6D_6) of **3-7i**, after complex **3-1** reacted with CuBr (2 eq) DMSO (28 eq.) and 4-trifluoromethyliodobenzene (1 eq.) in benzene at 50 °C. P = product, I = internal standard ($PhCF_3$)..... 257
Figure A3.84 ^{19}F NMR spectrum (282 MHz, C_6D_6) of **3-7j**, after complex **3-1** reacted with CuBr (2 eq) DMSO (28 eq.) and 3-trifluoromethyl-iodobenzene (1 eq.) in benzene at 50 °C. I = internal standard ($PhCF_3$). 258
Figure A3.85 ^{19}F NMR spectrum (282 MHz, C_6D_6) of **3-7k**, after complex **3-1** reacted with CuBr (2 eq) DMSO (28 eq.) and 3-iodopyridine (1 eq.) in benzene at 50 °C. I = internal standard ($PhCF_3$)..... 258
Figure A3.86 ^{1}H NMR spectrum (282 MHz, C_6D_6) of **3-7k**, after complex **3-1** reacted with CuBr (2 eq) DMSO (28 eq.) and 3-iodopyridine (1 eq.) in benzene at 50 °C..... 259
Figure A3. 87 ^{19}F NMR spectrum (282 MHz, C_6D_6) of **3-7l**, after complex **3-1** reacted with CuBr (2 eq) DMSO (28 eq.) and 2-iodopyridine (1 eq.) in benzene at 50 °C. I = internal standard ($PhCF_3$)..... 259
Figure A3.88 ^{1}H NMR spectrum (282 MHz, C_6D_6) of **3-7l**, after complex **3-1** reacted with CuBr (2 eq) DMSO (28 eq.) and 2-iodopyridine (1 eq.) in benzene at 50 °C..... 260
Figure A3.89 ^{19}F NMR spectrum (282 MHz, C_6D_6) of **3-7m**, after complex **3-1** reacted with CuBr (2 eq) DMSO (28 eq.) and 4-iodobenzaldehyde (1 eq.) in benzene at 50 °C. I = internal standard ($PhCF_3$)..... 260
Figure A3.90 ^{19}F NMR spectrum (282 MHz, C_6D_6) of **3-7n**, after complex **3-1** reacted with CuBr (2 eq) DMSO (28 eq.) and 4-iodoacetophenone (1 eq.) in benzene at 50 °C. I = internal standard ($PhCF_3$)..... 261
Figure A3.91 ^{19}F NMR spectrum (282 MHz, C_6D_6) of **3-7n**, after complex **3-1** reacted with CuBr (2 eq) DMSO (28 eq.) and 4-iodoacetophenone (1 eq.) in benzene at 50 °C..... 261
Figure A3.92 ^{19}F NMR spectrum (282 MHz, C_6D_6) of **3-7o**, after complex **3-1** reacted with CuBr (2 eq), DMSO (28 eq.) and t-butyl-4-iodobenzene (1 eq.) in benzene at 50 °C. I = internal standard ($PhCF_3$)... 262
Figure A3.93 ^{19}F NMR spectrum (282 MHz, C_6D_6) of complex **3-1** reacted with CuBr (2 eq), DMSO (28 eq.) in benzene 5 min after addition of 4-benzonitrile at 50 °C. I = internal standard ($PhCF_3$)..... 262
Figure A3.94 ^{19}F NMR spectrum (282 MHz, C_6D_6) of complex **3-1** reacted with CuBr (2 eq), DMSO (28 eq.) in benzene 10 min after addition of 4-benzonitrile at 50 °C. I = internal standard ($PhCF_3$)..... 263
Figure A3.95 ^{19}F NMR spectrum (282 MHz, C_6D_6) of complex **3-1** reacted with CuBr (2 eq), DMSO (28 eq.) in benzene 20 min after addition of 4-benzonitrile at 50 °C. I = internal standard ($PhCF_3$)..... 263
Figure A3.96 ^{19}F NMR spectrum (282 MHz, C_6D_6) of complex **3-1** reacted with CuBr (2 eq), DMSO (28 eq.) in benzene 30 min after addition of 4-benzonitrile at 50 °C. I = internal standard ($PhCF_3$)..... 264
Figure A3.97 ^{19}F NMR spectrum (282 MHz, C_6D_6) of complex **3-1** reacted with CuBr (2 eq), DMSO (28 eq.) in benzene 40 min after addition of 4-benzonitrile at 50 °C. I = internal standard ($PhCF_3$)..... 264
Figure A3.98 ^{19}F NMR spectrum (282 MHz, C_6D_6) of complex **3-1** reacted with CuBr (2 eq), DMSO (28 eq.) in benzene 50 min after addition of 4-benzonitrile at 50 °C. I = internal standard ($PhCF_3$)..... 265
Figure A3.99 ^{19}F NMR spectrum (282 MHz, C_6D_6) of complex **3-1** reacted with CuBr (2 eq), DMSO (10 eq.) in benzene at 25 °C. A, B, and C are different species of CF_2H. 265

Figure A3.100 ^{1}H NMR spectrum (282 MHz, C_6D_6) of complex **3-1** reacted with CuBr (2 eq), DMSO (10 eq.) in benzene at 25 °C. 266
Figure A3.101 ^{19}F NMR spectrum (282 MHz, C_6D_6) of complex **3-1** reacted with CuBr (2 eq), DMSO (10 eq.) in benzene at 40 °C. 266
Figure A3.102 Selected peak (7.33 min) from GC-MS of Cu(hfip)$(PPh_3)_2$ after reacting with CuBr (2 eq) DMSO (28 eq.) and methyl-2-iodobenzoate (1 eq.) in benzene at 50 °C. Expected 304.16 m/z (100%), found 302.1 m/z (20%) and 251 m/z (99%). 267
Figure A3.103 ^{19}F NMR of Cu(hfip)$(PPh_3)_2$ after reacting with CuBr (2 eq) DMSO (28 eq.) and methyl-2-iodobenzoate (1 eq.) in benzene at 50 °C after 2 and 12 h. SM = starting material, I = internal standard ($PhCF_3$). 267
Figure A3.104 Time course reaction of complex **3-1** with CuBr/DMSO and 1 equiv. of 4-iodo-benzonitrile in benzene at 50 °C monitored by ^{19}F NMR using the internal standard ($PhCF_3$) to calculate the concentration of product and starting material. 268
Figure A4.1 ^{19}F NMR spectrum (282 MHz) of [CuH(PPh_3)] + Xantphos + TMDSO + TFE:CO_2 in DMF after 7 h at RT… 269
Figure A4.2 ^{19}F NMR spectrum (282 MHz) of Cu(CF_2CF_2H)(Xantphos) (**4-2**) in DMF. 269
Figure A4.3 ^{19}F NMR spectrum (282 MHz) of Cu(CF_2CF_2H)(Xantphos) (**4-2**) in C_6D_6. 270
Figure A4.4 ^{19}F{^{1}H} NMR spectrum (282 MHz) of Cu(CF_2CF_2H)(Xantphos) (**4-2**) in C_6D_6. 270
Figure A4.5 ^{31}P{^{1}H} NMR spectrum (121 MHz, C_6D_6) of Cu(CF_2CF_2H)(Xantphos) (**4-2**). 271
Figure A4.6 ^{1}H NMR spectrum (300 MHz) of Cu(CF_2CF_2H)(Xantphos) **4-2**) in C_6D_6. 271
Figure A4.7 EI-MS of **4-2** showing $[Cu(Xantphos)]^+$ ion at m/s = 642. 272
Figure A4.8 ^{19}F NMR spectrum (282 MHz) of **4-2** + 2-methyl-4-iodobenzoate in DMF at 50 °C after 16 h. SP = side product, SM = **4-2**, P = Product and I = Internal standard ($PhCF_3$). 272
Figure A4.9 ^{19}F NMR spectrum (282 MHz) of **4-2** + 4-iodo-benzonitrile in DMF at 50 °C after 16. SP = side product, SM = **4-2**, P = Product and I = Internal standard ($PhCF_3$). 273
Figure A4.10 ^{19}F NMR spectrum (282 MHz) of **4-2** in DMF at 50 °C. After 15 min (**A**) and upon addition of 4-iodo-methyl-2-benzoate after 5 min (**B**), 2 h (**C**), 12 h (**D**) and 22 h (**E**). 273
Figure A4.11 ^{19}F NMR spectrum (282 MHz) of **4-2** + 4-iodo-methyl-2-benzoate + 10 mol% CuCl(SIMes) in DMF at 90 °C after 12 h. 274
Figure A4.12 ^{19}F NMR Cu(CF_2CF_2H)(Xantphos) + 4-iodo-ethyl-2-benzoate + CuCl(SIMes) in DMF at 90 °C after 12 h. ^{19}F NMR -113.4 ppm (m, CF_2), and – 137.0 ppm (dt, J^{FF} 10 Hz and J^{FH} 54 Hz). 274
Figure A4.13 ^{19}F NMR (**A**) and ^{31}P{^{1}H} NMR (**B**) spectra of Complex **4-1** and 2 eq. of CuCl after 72 h in DMF. 275
Figure A4.14 ^{19}F NMR (**A**) and ^{31}P{^{1}H} NMR (**B**) spectra of Complex **4-1** and 2 eq. of CuCl after 96 h in DMF. 275
Figure A4.15 ^{19}F NMR (**A**) and ^{31}P{^{1}H} NMR (**B**) (spectra of Complex **4-1** and 2 eq. of CuCl after 2 weeks in DMF. 275
Figure A4.16 ^{19}F NMR (**A**) and ^{31}P{^{1}H} NMR (**B**) (spectra of Complex **4-1** and 2 eq. of CuCl after 4 months in DMF. 276
Figure A4.17 ^{19}F NMR (**A**) and ^{31}P{^{1}H} NMR (**B**) spectra of Complex **4-1** and 2 eq. of CuBr after 72 h in DMF. 276
Figure A4.18 ^{19}F NMR (**A**) and ^{31}P{^{1}H} NMR (**B**) spectra of Complex **4-1** and 2 eq. of CuBr after 96 h in DMF. 276
Figure A4.19 ^{19}F NMR (**A**) and ^{31}P{^{1}H} NMR (**B**) spectra of Complex **4-1** and 2 eq. of CuBr after 2 weeks in DMF. 277

Figure A4.20 ^{19}F NMR (**A**) and $^{31}P\{^{1}H\}$ NMR (**B**) spectra of Complex **4-1** and 2 eq. of CuBr after 4 months in DMF. 277
Figure A4.21 ^{19}F NMR (**A**) and $^{31}P\{^{1}H\}$ NMR (**B**) spectra of Complex **4-1** and 2 eq. of CuI after 72 h in DMF. 277
Figure A4.22 ^{19}F NMR (**A**) and ^{31}P NMR (**B**) spectra of Complex **4-1** and 2 eq. of CuI after 96 h in DMF. 278
Figure A4.23 ^{19}F NMR (**A**) and ^{31}P NMR (**B**) spectra of Complex **4-1** and 2 eq. of CuI after 2 weeks in DMF. 278
Figure A4.24 ^{19}F NMR (**A**) and ^{31}P NMR (**B**) spectra of Complex **4-1** and 2 eq. of CuI after 4 months in DMF. 279
Figure A4.25 ^{19}F NMR (**A**) (282 MHz, C_6D_6) of Complex **4-1**, 1.5 eq. of CuI, 25 eq. of DMSO and 1 equiv. of 4-iodobenzonitrile after 7 h. I = internal standard ($PhCF_3$). 9% yield. 279
Figure A4.26 ^{19}F NMR (**A**) (282 MHz, C_6D_6) of Complex **4-1**, 1.5 eq. of CuBr, 25 eq. of DMSO and 1 equiv. of 4-iodo-benzonitrile after 7 h. I = internal standard ($PhCF_3$), SM = Starting material. 11% yield. 280
Figure A4.27 ^{19}F NMR (**A**) (282 MHz, C_6D_6) of Complex **4-1**, 1.5 eq. of CuCl, 25 eq. of DMSO and 1 equiv. of 4-iodobenzonitrile after 7 h. I = internal standard ($PhCF_3$). 16% yield. 280
Figure A4.28 ^{19}F NMR (282 MHz, C_6D_6) of **4-3a**. The reaction of **4-1**, 2 eq. of CuBr, and 1 equiv. of 2'-deoxy-5-iodo-uridine in DMF after 12 h at 50 °C. I = internal standard ($PhCF_3$). 281
Figure A4.29 ^{19}F NMR (282 MHz, C_6D_6) of **4-3b**. The reaction of **4-1**, 2 eq. of CuBr, and 1 equiv. of 2'-deoxy-5-iodo-cytidine in DMF after 12 h at 50 °C. I = internal standard ($PhCF_3$). 281
Figure A4.30 ^{19}F NMR (282 MHz, C_6D_6) of **4-3c**. The reaction of **4-1**, 2 eq. of CuBr, and 1 equiv. of 5-iodouridine in DMF after 12 h at 50 °C. I = internal standard ($PhCF_3$). 282
Figure A4.31 ^{19}F NMR (282 MHz, C_6D_6) of **4-3d**. The reaction of **4-1**, 2 eq. of CuBr, and 1 equiv. of 2'-5 o acetyl-5-iodo-uridine in DMF after 12 h at 50 °C. I = internal standard ($PhCF_3$). 282
Figure A4.32 ^{19}F NMR (282 MHz, C_6D_6) of **4-3e**. The reaction of **4-1**, 2 eq. of CuBr, and 1 equiv. of 5-iodo-2',3',5'-triacetate uridine in DMF after 12 h at 50 °C. I = internal standard ($PhCF_3$). 283
Figure A4.33 ^{19}F NMR (282 MHz, C_6D_6) of **4-3f**. The reaction of **4-1**, 2 eq. of CuBr, and 1 equiv. of 4-iodo uracil in DMF after 12 h at 50 °C. I = internal standard ($PhCF_3$). 283
Figure A4.34 ^{19}F NMR (282 MHz, C_6D_6) of **4-3g**. The reaction of **4-1**, 2 eq. of CuBr, and 1 equiv. 6-Fluoro-3-iodochromone in DMF after 12 h at 50 °C. I = internal standard ($PhCF_3$). 284
Figure A4.35 ^{19}F NMR (282 MHz, C_6D_6) of **4-3h**. The reaction of **4-1**, 2 eq. of CuBr, and 1 equiv. of t-butyl 5-fluoro-3-iodo-1H-indole-1-carboxylate in DMF after 12 h at 50 °C. I = internal standard ($PhCF_3$). 284
Figure A4.36 ^{19}F NMR (282 MHz, C_6D_6) of **4-3i**. The reaction of **4-1**, 2 eq. of CuBr, and 1 equiv. of 1,5-anhydro-3,4,6-tri-O-benzyl-2-deoxy-2-iodo-D- lyxo-hex-1-enitol in DMF after 12 h at 50 °C. I = internal standard ($PhCF_3$). 285
Figure A4.37 ^{19}F NMR (282 MHz, C_6D_6) of **4-3j**. The reaction of **4-1**, 2 eq. of CuBr, and 1 equiv. of 1,5-anhydro-3,4,6-tri-O-acetyl-2-deoxy-2-iodo-D- lyxo-hex-1-enitol in DMF after 12 h at 50 °C. I = internal standard ($PhCF_3$). 285
Figure A4.38 ^{19}F NMR (282 MHz, C_6D_6) of **4-3k**. The reaction of **4-1**, 2 eq. of CuBr, and 1 equiv. of methyl 5-acetamido-4,7,8,9-tetra-O-acetyl-2,6-anhydro-3,5-dideoxy-3-iodo-D-glycero-D-galacto-non-2-enonate in DMF after 12 h at 50 °C. I = internal standard ($PhCF_3$). 286
Figure A4.39 ^{19}F NMR (282 MHz, C_6D_6) of **4-3l**. The reaction of **4-1**, 2 eq. of CuBr, and 1 equiv. of methyl 5-acetamido-4,7,8,9-tetra-O-acetyl-2,6-anhydro-3,5-dideoxy-3-iodo-D-glycero-D-galacto-non-2-enonate in DMF after 12 h at 50 °C. I = internal standard ($PhCF_3$). 286

Figure A4.40 ^{19}F NMR (282 MHz, C_6D_6) of **4-3m**. The reaction of **4-1**, 2 eq. of CuBr, and 1 equiv. of 1,5-Anhydro-3,4,6-tri-O-pivaloyl-2-deoxy-2-iodo-D-arabino-hex-1-enitol in DMF after 12 h at 50 ºC. I = internal standard ($PhCF_3$). 287
Figure A4.41 ^{19}F NMR (282 MHz, C_6D_6) of **4-3n**. The reaction of **4-1**, 2 eq. of CuBr, and 1 equiv. of 1,5-anhydro-3,6-di-O-acetyl-2-deoxy-4-O-(2,3,4,6-tetra-O-acetyl-β-D-galactopyranosyl)-2-iodo-D-arabino-hex-1-enitol in DMF after 12 h at 50 ºC. I = internal standard ($PhCF_3$). 287
Figure A4.42 ^{19}F NMR (282 MHz, C_6D_6) of **4-3a**. The reaction of **4-1**, 2 eq. of CuBr, and 1.5 equiv. of 2'-deoxy-5-iodo-uridine in DMF after 12 h at 50 ºC. I = internal standard ($PhCF_3$). 288
Figure A4.43 ^{19}F NMR (282 MHz, C_6D_6) of **4-3d**. The reaction of **4-1**, 2 eq. of CuBr, and 1.5 equiv. of 2'-5 o acetyl-5-iodo-uridine in DMF after 12 h at 50 ºC. I = internal standard ($PhCF_3$). 288
Figure A4.44 ^{19}F NMR (282 MHz, C_6D_6) of **4-3e**. The reaction of **4-1**, 2 eq. of CuBr, and 1 equiv. of 5-iodo-2',3',5'-triacetate uridine in DMF after 12 h at 50 ºC. I = internal standard ($PhCF_3$). 289
Figure A4.45 ^{19}F NMR (282 MHz, C_6D_6) of **4-3f**. The reaction of **4-1**, 2 eq. of CuBr, and 1 equiv. of 4-iodo uracil in DMF after 12 h at 50 ºC. I = internal standard ($PhCF_3$). 289
Figure A4.46 ^{19}F NMR (282 MHz, C_6D_6) of **4-3i**. The reaction of **4-1**, 2 eq. of CuBr, and 1.5 equiv. of 1,5-Anhydro-3,4,6-tri-O-benzyl-2-deoxy-2-iodo-D- lyxo-hex-1-enitol in DMF after 12 h at 50 ºC. I = internal standard ($PhCF_3$). 290
Figure A4.47 ^{19}F NMR (282 MHz, C_6D_6) of **4-3j**. The reaction of **4-1**, 2 eq. of CuBr, and 1 equiv. of 1,5-anhydro-3,4,6-tri-O-acetyl-2-deoxy-2-iodo-D-lyxo-hex-1-enitol in DMF after 12 h at 50 ºC. I = internal standard ($PhCF_3$). 290
Figure A4.48 ^{19}F NMR (282 MHz, C_6D_6) of reaction 1.5 equiv. of **4-1**, 0.5 equiv. of CuBr, and 1 equiv. of 4-iodouracil in DMF after 12 h at 50 ºC. I = internal standard ($PhCF_3$). 291
Figure A4.49 ^{19}F NMR (282 MHz, C_6D_6) of reaction 1 equiv. of **4-1**, 1 equiv. of CuBr, and 1 equiv. of 4-iodouracil in DMF after 12 h at 50 ºC. I = internal standard ($PhCF_3$). 291
Figure A4.50 ^{19}F NMR (282 MHz, C_6D_6) of reaction 1 equiv. of **4-1**, 1 equiv. of CuBr, and 1.5 equiv. of 4-iodouracil in DMF after 12 h at 50 ºC. I = internal standard ($PhCF_3$). 292
Figure A4.51 ^{19}F NMR (282 MHz, C_6D_6) of reaction 1 equiv. of **4-1**, 2 equiv. of CuCl, and 1.5 equiv. of 4-iodouracil in DMF after 12 h at 50 ºC. I = internal standard ($PhCF_3$). 292
Figure A4.52 ^{19}F NMR (282 MHz, C_6D_6) of reaction 1 equiv. of **4-1**, 2 equiv. of CuBr, and 1.5 equiv. of 4-iodouracil in Et_2O/ DMF (1:0.005) after 12 h at 50 ºC. I = internal standard ($PhCF_3$). 293
Figure A4.53 ^{19}F NMR (282 MHz, C_6D_6) of reaction 1 equiv. of **4-1**, 2 equiv. of CuBr, and 1 equiv. of 4-iodouracil in Toluene/DMF (1:0.005) after 12 h at 50 ºC. I = internal standard ($PhCF_3$). 293
Figure A4.54 ^{19}F NMR (282 MHz, C_6D_6) of reaction 1 equiv. of **4-1**, 3 equiv. of CuBr, and 1 equiv. of 4-iodouracil in Toluene/DMF (1:0.005) after 12 h at 50 ºC. I = internal standard ($PhCF_3$). 294
Figure A4.55 ^{19}F NMR (282 MHz, C_6D_6) of reaction 1 equiv. of **4-1**, 3 equiv. of CuBr, and 1 equiv. of 4-iodouracil in Toluene/DMF (1:0.005) after 12 h at 50 ºC. I = internal standard ($PhCF_3$). 294
Figure A4.56 Binding modes of chemical analogues **4-4a-c.** 295
Figure A4.57 Binding modes of chemical analogues **4-4d-f.** 296
Figure A4.58 Binding modes of chemical analogues **4-4g-i.** 297
Figure A4.59 Binding modes of chemical analogues **4-5a-c**. 298
Figure A4.60 Binding modes of chemical analogues **4-5d-f**. 299
Figure A4.61 Binding modes of chemical analogues **4-5g-i** 300
Figure A5.1 ^{19}F NMR spectra of $Ni(cod)_2$ + DPPE + 3 equiv of TFE in C_6D_6 after 5m, 1h and 2h….302
Figure A5.2 Selected peaks from the EI mass spectrum of complex **5-2a**. 302
Figure A5.3 ^{19}F NMR of $Ni(cod)_2$ + dppf + TFE in benzene, 5 min (a), 2 h (b) and 12 h (c) after TFE addition. **M** = metallacyclopentane; **O** = olefin complex. 303

Figure A5.4 ^{31}P NMR of $Ni(cod)_2$ + dppf + TFE in benzene, 5 min (a), 2 h (b) and 12 h (c) after TFE addition. **M** = metallacyclopentane; **O** = olefin complex. 303
Figure A5.5 ^{19}F NMR (A) and $^{31}P\{^1H\}$ NMR (B) of $Ni(\eta^2\text{-}C_2F_4)(dppf)$ (**5-1b**) in benzene (**a**), addition of TFE after 5 min (**b**), after 3 h (**c**) and after pumping off the solvent (**d**). **M** = metallacyclopentane; **O** = olefin complex. 304
Figure A5.6 ^{19}F NMR (**A**) and $^{31}P\{^1H\}$ NMR (**B**) of $Ni(cod)_2$ + dppf + TFE in acetone, before TFE (a), 5 min (b), 2 h (c) and 12 h (d) after TFE addition. **M** = metallacyclopentane; **O** = olefin complex. 304
Figure A5.7 ^{19}F NMR of $Ni(cod)_2$ + dppf + TFE in THF, 5 min (a), 2 h (b) and 12 h (c) after TFE addition. **M** = metallacyclopentane; **O** = olefin complex. 305
Figure A5.8 ^{31}P NMR of $Ni(cod)_2$ + dppf + TFE in THF, 5 min (a), 2 h (b) and 12 h (c) after TFE addition. **M** = metallacyclopentane; **O** = olefin complex. 305
Figure A5.9 ^{19}F NMR of $Ni(cod)_2$ + dppf + TFE in benzene, acetone and THF after 5 min, 2 h and 12 h after TFE addition. Acetone line shifted to right for clarity. 306
Figure A5.10 Selected peaks from the EI mass spectrum of complex **5-2c**..... 306
Figure A5.11 ^{19}F (**A**) and $^{31}P\{^1H\}$ (**B**) NMR spectra of $Ni(cod)_2$ + Xantphos + 3 equiv TFE in benzene C_6D_6 307
Figure A5.12 ^{19}F (**A**) and $^{31}P\{^1H\}$ (**B**) NMR spectra of $Ni(cod)_2$ + Bisbi + 3 equiv TFE in benzene C_6D_6. Star = $Ni(cod)(C_4F_8)$. 307
Figure A5.13 ^{19}F NMR of $Ni(cod)_2$ + TMEDA + TFE in THF, after 7 h at 50 °C. 308
Figure A5.14 ^{19}F NMR of $Ni(cod)_2$ + TMEDA + TFE in acetone, after 30 m (**1a**), 7 h (**1c**) at 21 °C, 30 m (**1b**) and 7 h (**1d**) at 50 °C. 308
Figure A5.15 ^{19}F NMR of $Ni(cod)_2$ + TMEDA + TFE in acetonitrile, after 7 h at 50 °C..... 309
Figure A5.16 ^{19}F NMR spectrum of $Ni(cod)_2$ + TMEDA + TFE in 2,5-dimethyldihydrofuran, after 4 h at 25 °C..... 309
Figure A5.17 ^{19}F NMR spectra of $Ni(COD)_2$ + TMEDA + TFE in 2,5-dimethyldihydrofuran, after 21 h at 25 °C (**A**) and 7 h at 50 °C (**B**). 310
Figure A5.18 ^{19}F NMR spectrum of $Ni(cod)_2$ + bipyridine + TFE in acetone, after 7 h at 50 °C..... 310
Figure A5.19 ^{19}F NMR spectrum of $Ni(cod)_2$ + bipyridine + TFE in THF, after 7 h at 50 °C. 311
Figure A5.20 ^{19}F NMR of $Ni(cod)_2$ + 2 Pyridine + TFE in acetone, after 30 min at 50 °C. 311
Figure A6.1 ^{19}F NMR spectrum (282 MHz, C_6D_6) of $Ni(cod)_2$, 2 equiv. of $P(OiPr)_3$ and PMVE…..... 313
Figure A6.2 Selected peaks from the ESI mass spectrum (positive mode, CH_3CN) of complex **6-2a**.... 313
Figure A6.3 ^{19}F NMR (282 MHz, C_6D_6, **A**) and $^{31}P\{^1H\}$ NMR spectra (121 MHz, C_6D_6, **B**) of $Ni(cod)_2$, 2 equiv. of tri-o-tolyl phosphite and PMVE. 314
Figure A6.4 ^{19}F NMR spectrum (282 MHz, C_6D_6) of $Ni(cod)_2$, 2 equiv. of PPh_3 and PMVE. 314
Figure A6.5 ^{19}F NMR spectrum (282 MHz, C_6D_6) of $Ni(cod)_2$, 2 equiv. of $PMePh_2$ and PMVE. 315
Figure A6.6 ^{19}F NMR (282 MHz, C_6D_6) spectrum of $Ni(cod)_2$, PCy_3 and PMVE. 315
Figure A6.7 ^{19}F NMR (282 MHz, C_6D_6) spectrum of $Ni(cod)_2$, IPr and PMVE. 316
Figure A6.8 ^{19}F NMR (282 MHz, C_6D_6) spectrum of IPr and PMVE, without $Ni(cod)_2$. 316
Figure A6.9 ^{19}F NMR (282 MHz, C_6D_6) of IAd and PMVE, without $Ni(cod)_2$. 317
Figure A6.10 ^{19}F NMR spectrum (282 MHz, C_6D_6) of $Ni(cod)_2$, 1 equiv. of dppp and PMVE. 317
Figure A6.11 ^{19}F NMR (282 MHz, C_6D_6, **A**) and $^{31}P\{^1H\}$ NMR (121 MHz, C_6D_6, **B**) spectra of $Ni(Xantphos)_2$ and PMVE. 318
Figure A6.12 ^{19}F NMR (282 MHz, C_6D_6, **A**) and $^{31}P\{^1H\}$ NMR (121 MHz, C_6D_6, **B**) spectra of **6-2c** and **6-3** from addition of 1 equiv. of dppe to **6-1a,b.**..... 318

Figure A6.13 ^{19}F NMR (282 MHz, C_6D_6) spectrum of Ni[$C_2(OCF_3)F_3$][P(O-o-tolyl)$_3$] with IMes and excess PMVE. 319
Figure A6.14 ^{19}F NMR (282 MHz, C_6D_6) spectrum of addition of 2 equiv. of P^iPr_3 to the reaction containing Ni(cod)$_2$, 2 equiv. of tri-o-tolyl phosphite and PMVE. 319
Figure A6.15 ^{19}F NMR (282 MHz, C_6D_6) spectrum of Ni(cod)$_2$, 2 equiv. of P(OiPr)$_3$ and CTFE. 320
Figure A6.16 ^{31}P NMR (121 MHz, C_6D_6) of Ni(COD)$_2$, 2 equiv. of P(OiPr)$_3$ and CTFE. 320
Figure A6.17 ^{19}F NMR (282 MHz, C_6D_6, **A**) and $^{31}P\{^1H\}$ NMR (121 MHz, C_6D_6, **B**) spectra of Ni(cod)$_2$, P(O-o-tolyl)$_3$ and CTFE after 4 h. 321
Figure A6.18 ^{19}F NMR (282 MHz, C_6D_6) spectrum of Ni(cod)$_2$, P(O-o-tolyl)$_3$ and CTFE after 12 h. 321
Figure A6.19 ^{19}F NMR (282 MHz, C_6D_6, **A**) and $^{31}P\{^1H\}$ NMR (121 MHz, C_6D_6, **B**) spectra of Ni(cod)$_2$, PPh_3 and CTFE. 322
Figure A6.20 Selected peaks from the EI mass spectrum (positive mode, CH_3CN) of NiCl(h^1-$CF=CF_2$)(PPh_3)$_2$. 322
Figure A6.21 ^{19}F NMR (282 MHz, C_6D_6, **A**) and $^{31}P\{^1H\}$ NMR (121 MHz, C_6D_6, **B**) spectra of Ni(cod)$_2$, DPEphos and CTFE. 323
Figure A6.22 ^{19}F NMR (282 MHz, C_6D_6, **A**) and $^{31}P\{^1H\}$ NMR (121 MHz, C_6D_6, **B**) spectra of Ni(cod)$_2$, DPEphos and CTFE after 6 and 24 h, showing conversion of olefin into vinyl complex. 323
Figure A6.23 ^{19}F NMR (282 MHz, C_6D_6) spectrum of Ni(cod)$_2$, BINAP and CTFE after 7 h. 324
Figure A6.24 ^{19}F NMR (282 MHz, C_6D_6) spectrum after phen addition to the reaction of Ni(cod)$_2$, tri-isopropylphosphite and CTFE. 324
Figure A6.25 ^{19}F NMR (282 MHz, C_6D_6, **A**) and $^{31}P\{^1H\}$ NMR (121 MHz, C_6D_6, B) spectra of Ni[C_2ClF_3](dppe)[(P(OiPr)$_3$]. 325
Figure A6.26 Selected peaks from the ESI mass spectrum (positive mode, CH_3CN) of complex Ni(C_2ClF_3)(dppe)[(P(OiPr)]. 325
Figure A6.27 Selected peaks from the ESI mass spectrum (positive mode, CH_3CN) of complex Ni(C_2ClF_3)(dppp)[(P(OiPr)]. 326
Figure A6.28 ^{19}F NMR (282 MHz, C_6D_6, **A**) and $^{31}P\{^1H\}$ NMR (121 MHz, C_6D_6, **B**) spectra of Ni(Xantphos)$_2$ + CTFE in benzene after 4 h. 326
Figure A6.29 ^{19}F NMR (282 MHz, C_6D_6, **A**) spectra of Ni(Xantphos)$_2$ + CTFE in benzene after 12 h, then changed the solvent to DCM. 327
Figure A6.30 ^{19}F NMR (282 MHz, C_6D_6) spectrum of Ni($C_4Cl_2F_6$)(dppe) (**6-5c**) and Ni(C_2ClF_3)(dppe)[($P(O^iPr)_3$] (**6-7c**) plus $ZnCl_2$. 327
Figure A6.31 ^{19}F NMR (282 MHz, C_6D_6) spectrum of Ni($C_4Cl_2F_6$)(dppp) (**6-5b**) and Ni(C_2ClF_3)(dppp)[(P(OiPr)$_3$] (**6-7b**) plus $ZnCl_2$. 328
Figure A6.32 ^{19}F NMR (282 MHz, C_6D_6) spectrum of Ni[$C_4(OCF_3)_2F_6$](dppe) (**6-2c**) and Ni[$C_2(OCF_3)F_3$](dppe)[$P(O^iPr)_3$] (**6-3**) with TMSOTf. 328
Figure A6.33 ^{19}F NMR (282 MHz, C_6D_6) spectrum of Ni[$C_4Cl_2F_6$][dppe][($P(O^iPr)_3$] (**6-5c**) and Ni[C_2ClF_3][dppe][($P(O^iPr)_3$] (**6-7c**) plus TMSOTf. 329
Figure A6.34 ^{19}F NMR (282 MHz, C_6D_6, **A**) spectra of Ni(Xantphos)$_2$ + CTFE in benzene, then changed the solvent to DCM and added TMSOTf. 329
Figure A6.35 ^{19}F NMR (282 MHz, C_6D_6) spectrum of Ni[$C_4Cl_2F_6$](dppp) and Ni[C_2ClF_3](dppp)-[($P(O^iPr)_3$] (green line) plus trifluoroacetic acid after 7 h (black line) and 16 h (red line). 330

List of Tables

Table 3.1 Fluoroalkylation of benzoyl chloride in different solvents. 73
Table 3.2 Aroyl chloride fluoroalkylation substrate scope 74
Table 3.3 Optimization of the preparation of "ligandless" Cu[$CF(OCF_3)CF_2H$]..... 76
Table 4.1 Addition and elimination energy barriers (kcal/mol) for transfer of three different fluoroalkyl groups to iodobenzene……..... 103
Table 4.2 Addition and elimination energy barriers (kcal/mol) associated with -CF_2CF_2H transfer to iodobenzene from three different $LCuR^F$ complexes..... 104
Table 4.3 Addition and elimination energy barriers (kcal/mol) associated with -CF_2CF_2H transfer to five different organic electrophiles. 104
Table 4.4 Largest barriers associated with a given R^F, electrophile, and ancillary ligand. **Bold** = oxidative addition rate limiting, Italics = reductive elimination rate-limiting. 105
Table 4.5 Largest barriers associated with a given R^F, electrophile, and ancillary ligand taking account of ligand association pre-equilibria. **Bold** = oxidative addition rate limiting, *Italics* = reductive elimination rate-limiting..... 106
Table 4.6 Optimization of 4-iodobenzonitrile tetrafluoroethylation using "ligandless" Cu(C_2F_4H). 107
Table 4.7 Optimization of R^F transfer from **4-1** to 4-iodouracil. 110
Table 4.8 Information of homology model of *F. graminearum* SDH. 120
Table 5.1 Ligand Angle Effects in Metallacycle Formation (DFT/B3LYP-D3/LACV3P**/gas)…… .134
Table A3.1 Details of X-ray diffraction data collection and refinement……..216
Table A3.2 Time course reaction of complex **3-1** with CuBr/DMSO and 4-iodo-benzonitrile monitored by ^{19}F NMR using the internal standard ($PhCF_3$) to calculate the concentration of product and starting material. 268
Table A5.1 Details of X-ray diffraction data collection and refinement …….……301
Table A6.1 Details of X-ray diffraction data collection and refinement…….....312

List of New Compounds

Metal complexes

Label	Complex	Label	Complex	Label	Complex
2-1	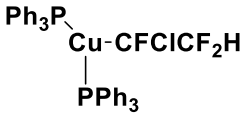	2-2	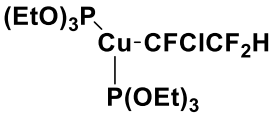	2-3	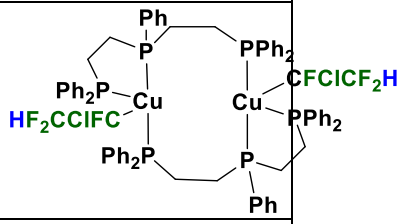
3-1	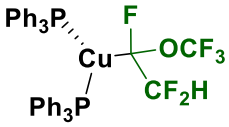	3-2	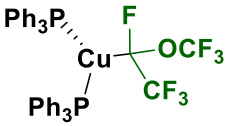	3-4a	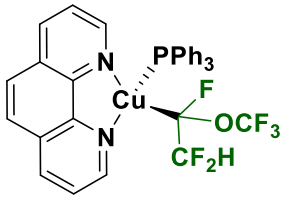
3-4b	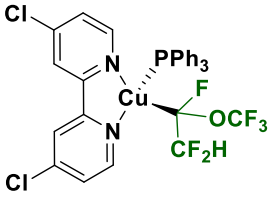	3-5	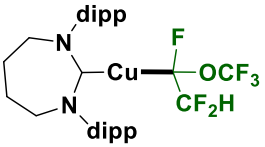	4-2	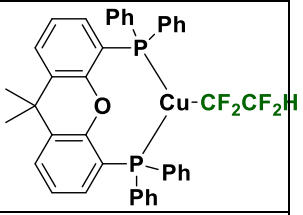
5-1a	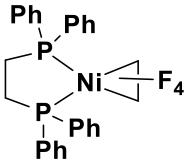	5-1b	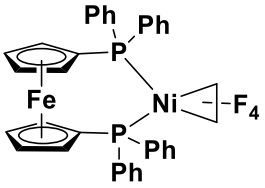	5-2b	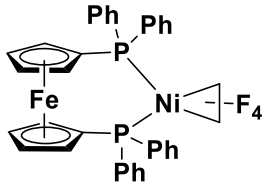
5-2a	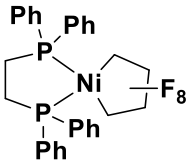	5-1c	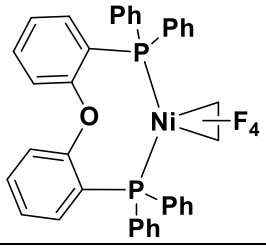	5-2c	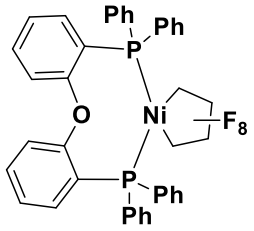
5-3	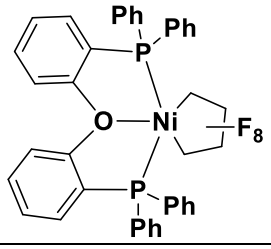	5-4a	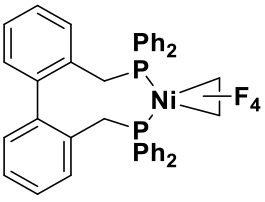	5-4b	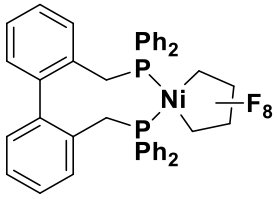
5-4c	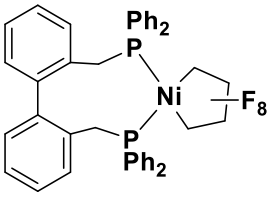	5-2d	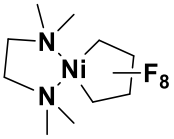	5-2e	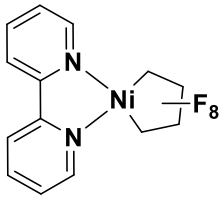

5-2f	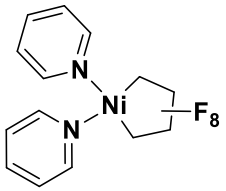	6-1a	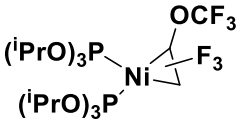	6-2a	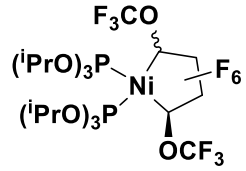
6-2c	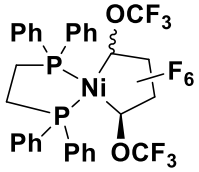	6-3	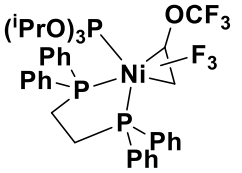	6-1b	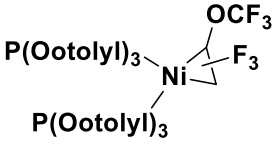
6-1c	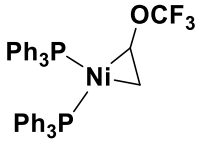	6-1d	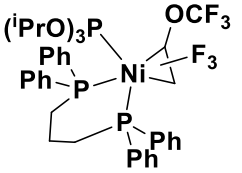	6-4a	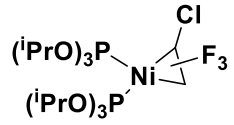
6-5	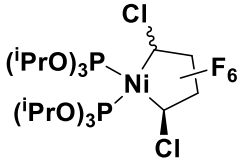	6-6a	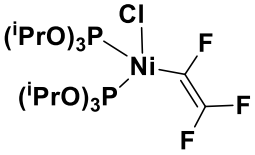	6-5a	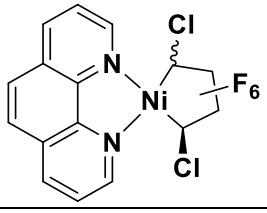
6-5b	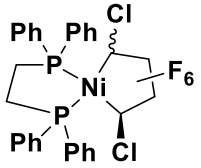	6-5c	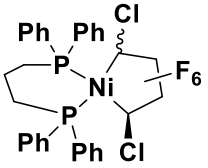	6-7a	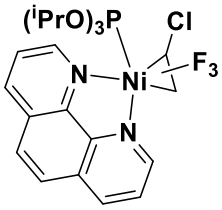
6-7b	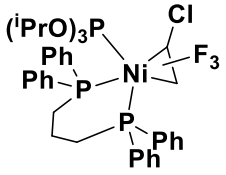	6-7c	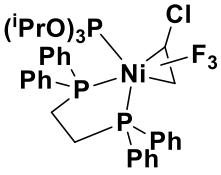	6-4e	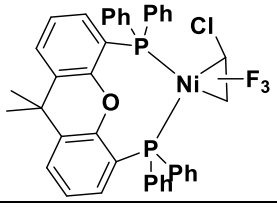
6-6e	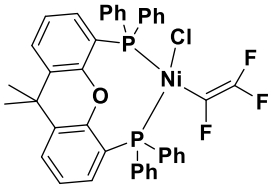	6-5d	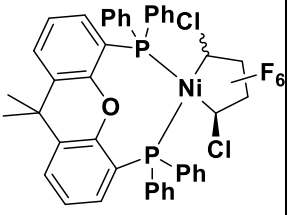	6-8a,b	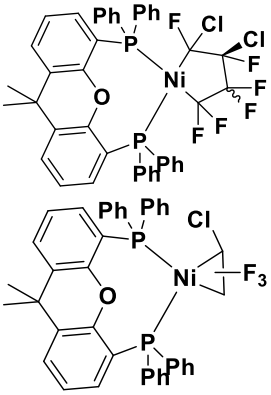

6-10	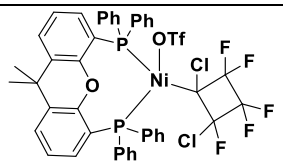	6-10a,b	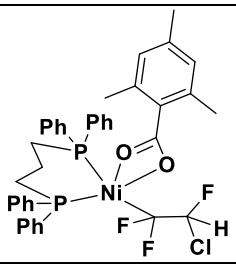	6-4b	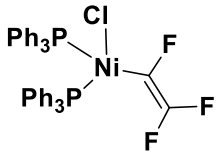
6-	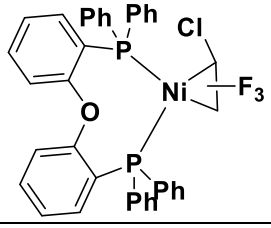				

Organic compounds

Label	Compound	Label	Compound	Label	Compound
2-4a	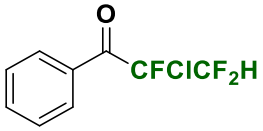	2-4b	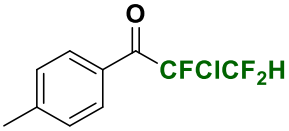	2-4c	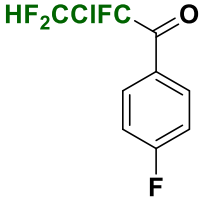
2-4d	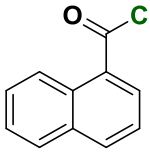	2-4e	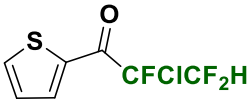	2-4f	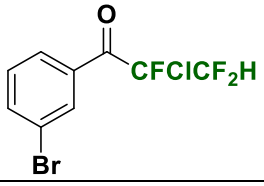
2-4g	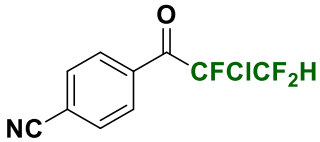	2-4h	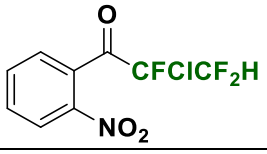	2-4i	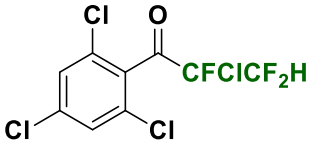
3-3a	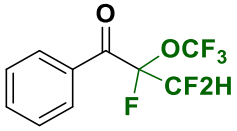	3-3b	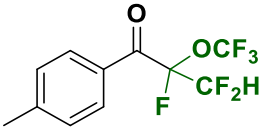	3-3c	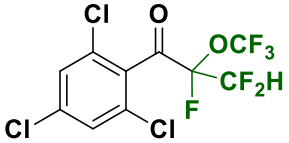
3-3d	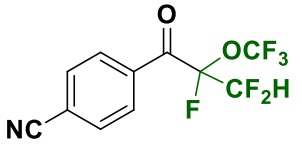	3-3e	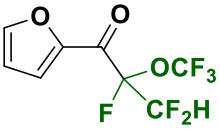	3-3f	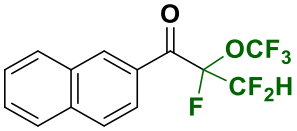
3-3g	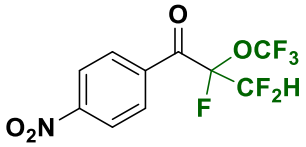	3-3h	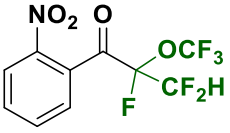	3-3i	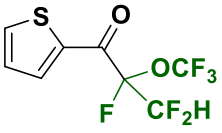

3-6a	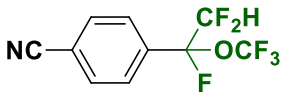	3-7a	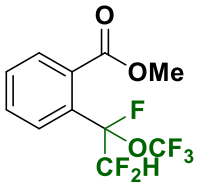	3-7c	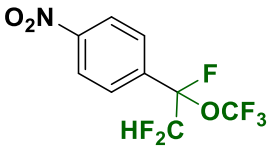
3-7d	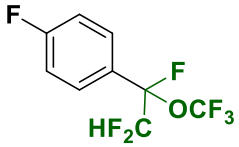	3-7e	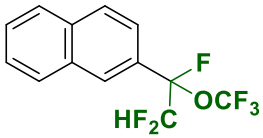	3-7f	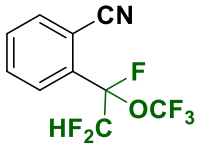
3-7g	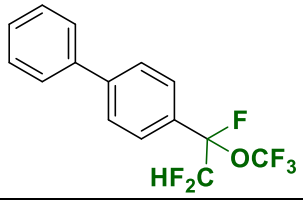	3-3h	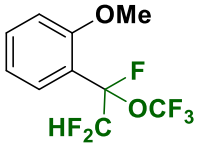	3-7i	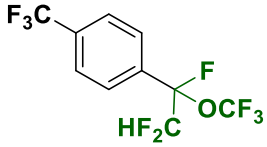
3-7j	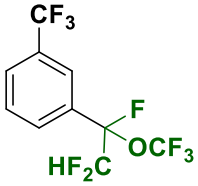	3-7k	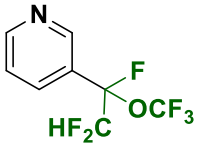	3-7l	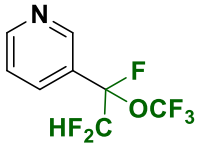
3-7m	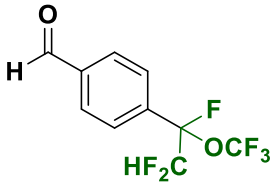	3-7n	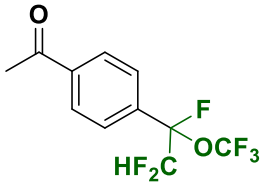	3-7o	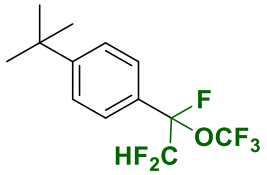
4-3a	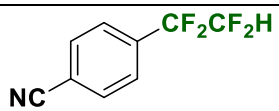	4-4a	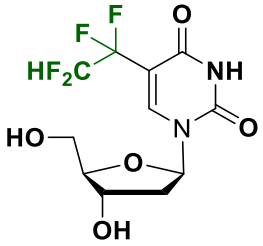	4-4b	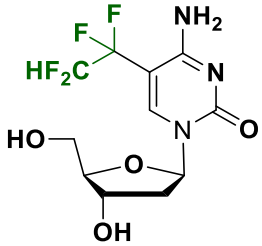
4-4c	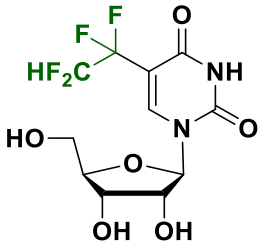	4-4d	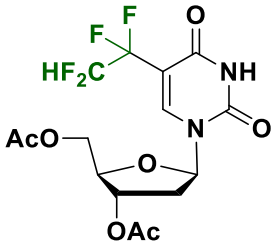	4-4e	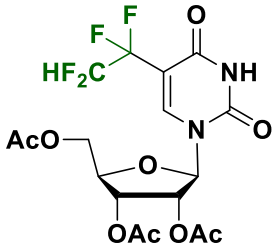
4-4f	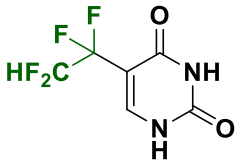	4-4g	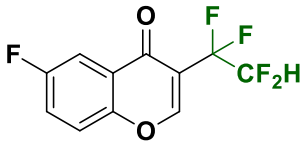	4-4h	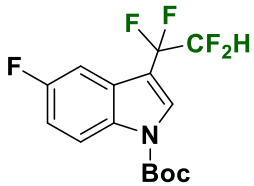

4-4i	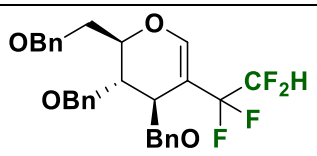	**4-4j**	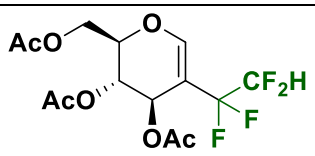	**4-4k**	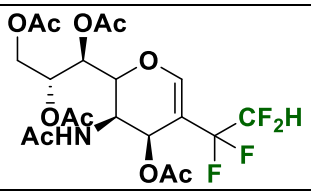
4-4l	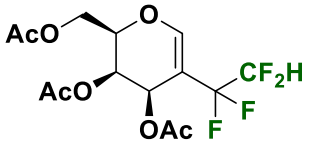	**4-4m**	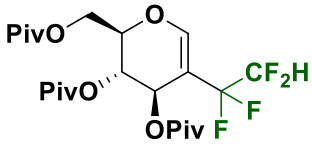	**4-4n**	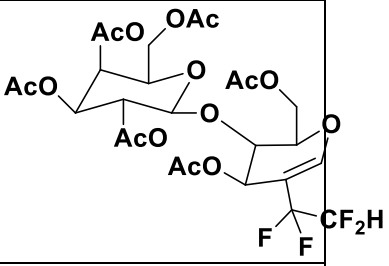
4-5a	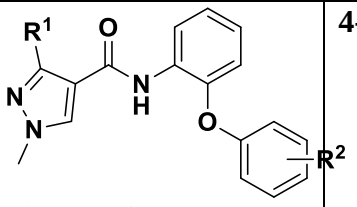 R^1 = H, R^2 = H	**4-5b**	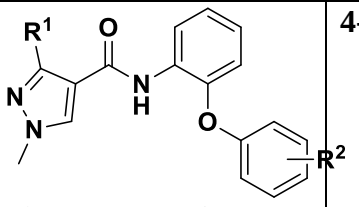 R^1 = CF_2CF_3, R^2 = 2-Cl	**4-5c**	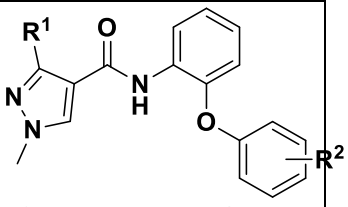 R^1 = CF_2CF_2H, R^2 = 2-Cl
4-5d	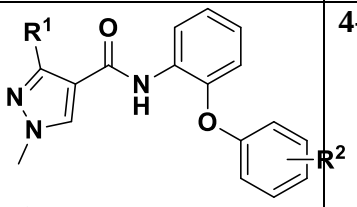 R^1 = (R)-$CF(OCF_3)CF_2H$, R^2 = 2-Cl	**4-5e**	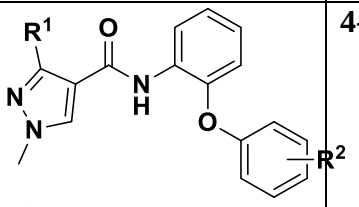 R^1 = (S)-$CF(OCF_3)CF_2H$, R^2 = 2-Cl	**4-5f**	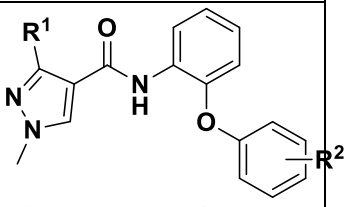 R^1 = CF_2CF_3, R^2 = 4-F
4-5g	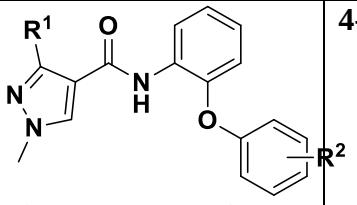 R^1 = CF_2CF_2H, R^2 = 4-F	**4-5h**	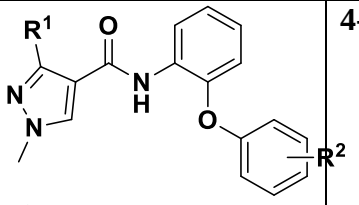 R^1 = (R)-$CF(OCF_3)CF_2H$, R^2 = 4-F	**4-5i**	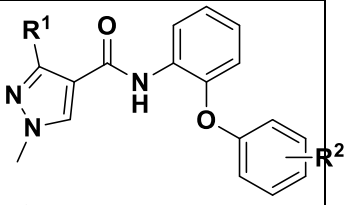 R^1 = (S)-$CF(OCF_3)CF_2H$, R^2 = 4-F
4-6a	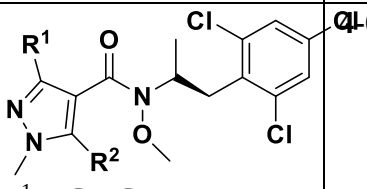 R^1 = CF_2CF_3, R_2 = H	**4-6b**	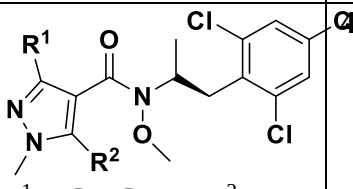 R^1 = CF_2CF_2H, R^2 = H	**4-6c**	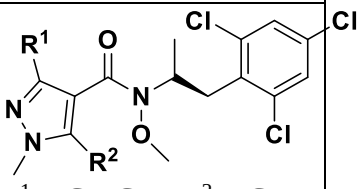 R^1 = CF_2CF_3, R^2 = CH_3

4-6d	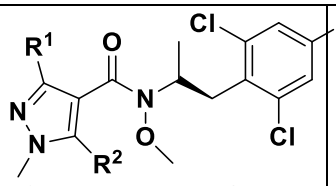 $R^1 = CF_2CF_2H$, $R^2 = CH_3$	**4-6e**	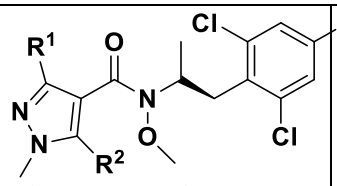 $R^1 = CF_2H$, $R^2 = CF_2CF_3$	**4-6f**	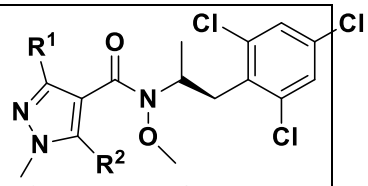 $R^1 = CF_2H$, $R^2 = CF_2CF_2H$
4-6g	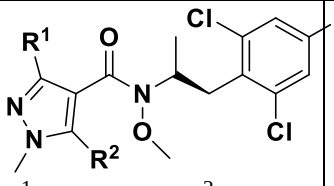 $R^1 = CF_2CF_3$, $R^2 = CF_2CF_3$	**4-6h**	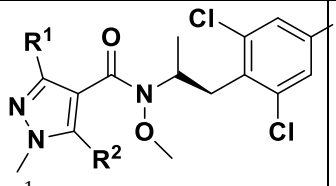 R^1 = (R)-$CF(OCF_3)CF_2H$, $R^2 = H$	**4-6i**	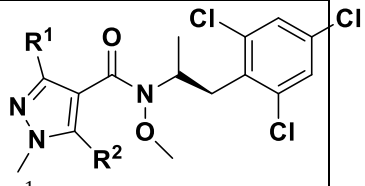 R^1 = (S)-$CF(OCF_3)CF_2H$, $R^2 = H$

CHAPTER 1. INTRODUCTION

1. The Power of Fluorine

1.1 Properties of fluorine

Fluorine (F) is the most abundant halogen in the Earth's crust,[258]although it is much less abundant in sea water (1.1% as NaF).[259] It was isolated as elemental F_2 gas for the first time by Henri Moissan in 1886 by electrolysis of potassium hydrogen difluoride (KHF_2) in anhydrous hydrogen fluoride (HF).[1] Incorporation of fluorine into organic molecules was initiated by Swarts at the end of the 19th century through the conversion of chlorocarbons to fluorocarbons in the presence of SbF_3.[2] Later, the first and most recognized fluoropolymer [poly(tetrafluoroethylene) – PTFE or Teflon™] was discovered by Roy Plunkett at DuPont in 1938, essentially initiating the commercial application of organofluorine compounds (**Scheme 1**).[3]

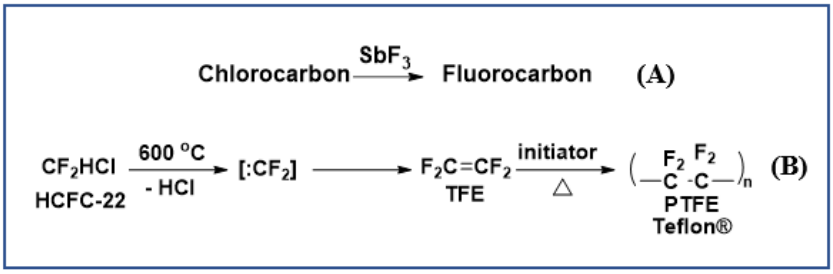

Scheme 1.1 (**A**) Incorporation of fluorine in organic molecules; (**B**) PTFE synthesis.

The widespread use of fluorine is due to specific features (also called fluorine magic)[4] such as high electronegativity (Pauling scale = 4), small size (van der Waals radius = 1.47 Å), low polarizability (less van der Waals attraction) and high C-F bond energy (480 kJ/mol) accounted for by electrostatic interactions between $F^{\delta-}$ and $C^{\delta+}$ which increase upon accumulation of additional fluorine atoms. A significant dipole moment (μ) influences the anti-planar conformational preference of the C-F bond to amide carbonyl, reducing conforming to the weaker dipole functional group. Additionally, the hyperconjugation effect from anomeric stabilization of low lying $\sigma^*_{C\text{-}F}$ antibonding orbital contributes to axial stabilization/gauche conformational preference (known as the fluorine gauche effect).[5–9]

Fluorinated compounds have both HOMO (highest occupied molecular orbital) and LUMO (lowest unoccupied molecular orbital) at lower energies than hydrogen compounds, which explains their higher reactivity toward reductants (electron donation to LUMO) and lower reactivity toward oxidants (accepting an electron from HOMO).[8] Consequently, the substitution of H with F can drastically change a molecule's properties. For example, changing one H in acetic acid (present in vinegar, CH_3COOH) to F forms fluoroacetic acid (CH_2FCOOH), which is highly poisonous. Nonetheless, desirable properties can also be achieved by adding F into a molecule, so there is a rapidly growing number of fluorine-substituted compounds applied across multiple industry sectors.[10] Therefore, the future of fluorine chemistry is bright, as reflected in all sections of this thesis.

1.2 Application of fluorine in industry: Fluorocarbon refrigerants

Refrigeration systems have a significant impact on food preservation; extending the shelf life of fresh foods to increase food safety and decrease food waste.[11–13] Refrigerants are essential components of Heating, Ventilation, and Air-conditioning (HVAC) systems responsible for transferring heat from indoors to outdoor. The first fluorinated gases produced on a large scale were chlorofluorocarbons (CFCs), constituting the first-generation of fluorocarbon refrigerants. Within this group, CFC-12 (CF_2Cl_2) showed the most suitable properties (high stability, low flammability and toxicity) and production in commercial quantities began in 1935 with the addition of HF to CCl_4 in the presence of an antimony catalyst (**Scheme 1.2A**).[9,10] After many decades of useful service, however, 1995 Nobel prize winners Molina, Rowland and Crutzen discovered that the stability of CFCs allowed them to enter the Earth's stratosphere, where UV radiation generated chlorine atoms that depleted the ozone layer that serves to protect us from the sun's radiation.[14] This led to a 1978 ban on CFCs by the US Environmental Protection Agency (EPA) and the subsequent 1987 Montreal Protocol to phase out their production.

The second generation hydrochlorofluorocarbons (HCFCs) were prepared by similar routes (**Scheme 1.2B**), providing a number of useful refrigerants and foam-blowing agents with a lower ozone depletion potential (ODP). Working with a DuPont team, Baker demonstrated an alternate route to HCFCs using metal-catalyzed hydrodefluorination to afford

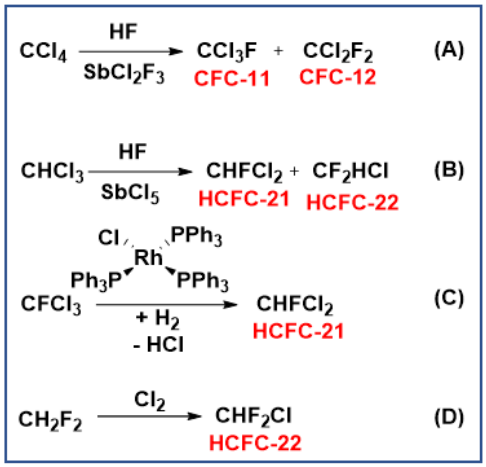

Scheme 1.2 Synthesis of CFC-12 (**A**), HCFC-21 and HCFC-22 (**B**, **C** and **D**).

HCFC-21 in 95% yield (**Scheme 1.2C**)[15] and Iikubo *et al.* used oxidative chlorination of CH_2F_2 at 200 ºC to obtain HCFC-22 (**Scheme 1.2D**).[16]

In 1998 HCFCs were also phased out with the advent of third generation hydrofluorocarbons (HFCs) that have no adverse effects on the ozone layer. The CFC-12 substitute, HFC-134a (1,1,1,2-tetrafluoroethane)[17] was initially prepared from trifluoroethylene (TrFE, $CHF=CF_2$) using SnF_4 in HF[18] (**Scheme 1.3A**) or PbO_2/SF_4[19] (**Scheme 1.3B**). In 1999, Hughes and Smith reported the formation of 134a from stoichiometric hydrodefluorination of an Ir-C_2F_5 complex via $C_\alpha F_2$ hydrogenolysis (**Scheme 1.3C, C_α coordinated to Ir**).[20] Vinylidene chloride (1,1-dichloroethylene) can also be utilized in the presence of F_2 followed by catalyzed HF addition (**Scheme 1.3D**)[21] or using the PbO_2/SF_4 system[19] (**Scheme 1.3E**). In spite of their zero ODP, the atmospheric lifetime of HFCs species is still too long, and they contribute greatly to the greenhouse effect; HFC-134a, for example, has a 14 year lifetime and a Global Warming Potential (GWP) of 1430 (vs. CO_2 as 1).[10,22,23]

Finally, the fourth-generation refrigerants known as hydrofluoroolefins (HFOs) are composed of species containing at least one carbon-carbon double bond (C=C) and exhibit low GWP. For example, HFO-1234yf (2,3,3,3-tetrafluoroprop-1-ene) possesses low flammability, zero ODP, and GWP of 4 with 11 days atmospheric lifetime (gets converted to CF_3CO_2H), and is already being used to replace HFC-134a in automobile air-conditioners.[24–26] There are many

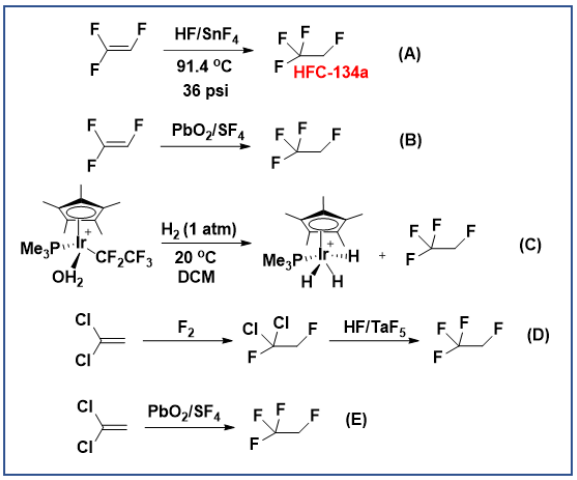

Scheme 1.3 Synthesis of HFC-134a.

routes to HFO-1234yf discussed in the literature,[10,27,28] including hydrodehalogenation of chlorotrifluoroethylene (CTFE) in the presence of SbF_5 catalyst and methyl fluoride (CH_3F) (**Scheme 1.4A**).[29] It can also be obtained from hydrodefluorination of hexafluoropropylene (HFP) catalyzed by palladium in the presence of hydrogen (**Scheme 1.4B**)[30] or copper with 10 mol% of co-ligands and 10 eq. of siloxane (**Scheme 1.4C**).[31]

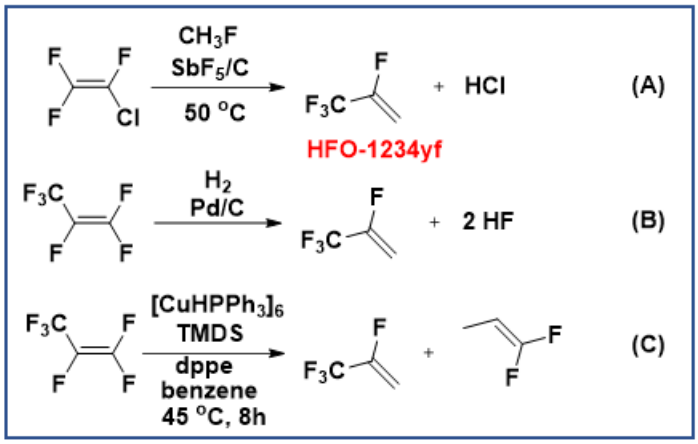

Scheme 1.4 Synthesis of HFO-1234yf. Picture changed: ClH_2 to HCl (A) and 2 HF (B)

1.3 Metal organofluorine chemistry

1.3.1 Perfluoroalkyl metal complexes

The expansion of organofluorine chemistry in the 1950s was soon followed by its organometallic counterpart.[32] In the early 1960s, Stone *et al.* and McClellan reported the first

examples of perfluoroalkyl transition metal derivatives with general formula $M(R^F)(CO)_5$ from decarbonylation of perfluoroacyl compounds using $NaM(CO)_5$ in which M = manganese (Mn) or rhenium (Re) (**Scheme 1.5A**). They also reported a stable Mn prop-1-enyl complex from

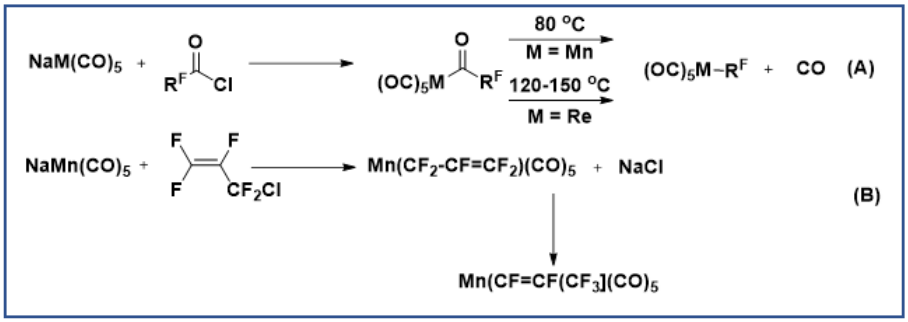

Scheme 1.5 Synthesis of transition metal perfluoro-alkyl and -alkenyl complexes.

perfluoroallyl chloride and $NaMn(CO)_5$ via rearrangement of the initially formed Mn prop-2-enyl complex (**Scheme 1.5B**).[33,34]

Stone and co-workers expanded the range of metals to prepare perfluoroalkyl derivatives. In 1961, for example, they demonstrated the oxidative addition of perfluoroalkyl iodides to iron carbonyl (**Scheme 1.6A**) and showed that their thermolysis at 120 °C afforded fluoro-alkenes and -alkanes (**Scheme 1.6B**).[35] An analogous Co complex was also prepared (**Scheme 1.6C**).[35]

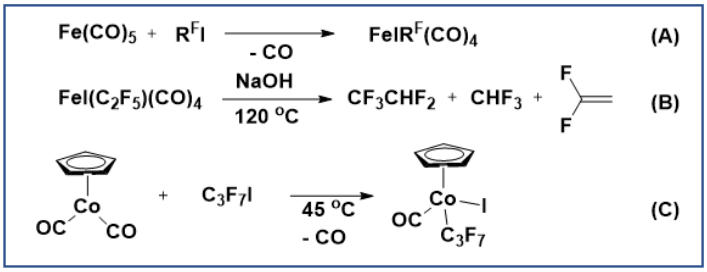

Scheme 1.6 Oxidative addition of R^FI to form perfluoroalkyl metal iodides.

1.3.2 Perfluorometallacycles: 3- vs. 5-membered ring

In the 1960s, Stone showed that the reaction product obtained from photolysis of iron carbonyl and tetrafluoroethylene (TFE), previously assigned as an Fe bis(TFE) complex by Wilkinson,[36] was actually the first example of a perfluorometallacyclopentane.[37] The remarkable stability of this Fe dialkyl complex is evidenced by its reactivity: heating at 160 ^{o}C for 12 days gave tetrafluorocyclobutene, or in the presence of bromine (Br_2) at 70 ^{o}C for 120 h yielded perfluorocyclobutane in 70% yield.[37]

Later, Stone expanded this chemistry to low-valent nickel (Ni), showing that ligand sterics dictate the size of the metallacycle formed (3- vs. 5-membered ring).[38] He also noted that Ni(II) metallacycles could easily undergo ligand-exchange reactions from the stable precursor $Ni(C_4F_8)[(P(n\text{-}Bu)_3]_2$.[36,39] Building on these studies, Ogoshi et al. confirmed the need for a smaller ligand to form metallacyclopentanes, regardless of basicity. He then investigated bidentate ligands, showing exclusive formation of three-membered metallacyclopropane in the presence of 1,2-bis(dicyclohexylphosphino)ethane (DCPE) or 1,4-bis(dicyclohexylphosphino)butane (DCPB).[40]

Vicic and co-workers prepared a nickel perfluorocyclopentane without the use of TFE using a dizinc reagent $[(MeCN)_2Zn((CF_2)_4)_2Zn(NCMe)_2]$ and $[(DME)NiBr_2]$ in acetonitrile, which is a safer methodology compared to using TFE. Vicic also prepared a cobalt complex. $[Co(C_4F_8)(NCMe)_4]$, using the same method, and both Co and Ni products undergo ligand substitution using two equivalents of the desired ligand in THF. [38,41,42]

The reaction of two molecules of TFE with d^{10} platinum bis(η-cyclo-octa-1,5-diene, cod), unlike $Ni(cod)_2$, gives a bis(μ-C_2F_4)-bridged dimer via electron transfer from Pt to TFE (**Scheme 1.7**).[43] Treatment of tetrakis(triphenylphosphine) platinum with different fluoro-olefins yields a σ-bonded metallacyclopropane three-membered ring exclusively (**Figure 1.1).**[44] A robust Pt-C^F bond is observed for **1-1a** (X= CF_3) with a geminal ^{19}F-^{19}F coupling constant of 200 Hz, suggesting a σ-bonded fluorocarbon to the metal. Heating **1-1b** (X = Cl) at 208 ^{o}C causes a molecular rearrangement, affording vinyl complex **1-1c** for which the ^{19}F-^{31}P coupling constant suggests a *trans*-phosphine complex.[44,45]

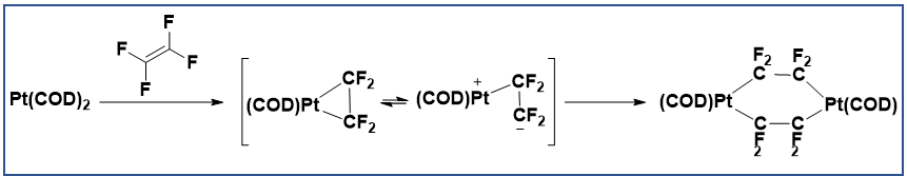

Scheme 1.7 $Pt(cod)_2$ reaction with tetrafluoroethylene.

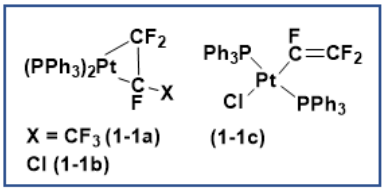

Figure 1.1 Perhalo-organoplatinum products from PtL_4 and fluoro-olefins.

Another study that shows different types of TFE reactivity with metal variation observed strong binding of TFE with tris(triphenylphosphine) rhodium (I) chloride (Wilkinson's catalyst), which was not displaced by an excess of triphenylphosphine, ethylene, amines, nitriles, cyanide ion, or heating to 37 °C in benzene. However, treatment with 1,5-cyclooctadiene or CO displaces the TFE at 70 °C as its hydrogenated product ($C_2F_4H_2$). Meanwhile, TFE displaces one molecule of ethylene from [Rh(acac)(C_2H_4)$_2$], supporting the increased stability of fluoroalkene vs. hydrocarbon alkenes to electron-rich metal centers (acac = acetylacetonate).[46–48] Rhodacyclopentane complexes can be generated from addition of fluoro-olefins to [Rh(acac)(PPh_2Me)$_2$] (**Figure 1.2**). The insertion of CTFE yields a head-to-tail metallacyclopentane with *trans*-phosphine ligands (**1-2a**) and TFE affords a similar perfluororhodacyclopentane (**1-2b**). However, switching the halogen to bromide (bromotrifluoroethylene, $BrFC=CF_2$) generates only the rhodacyclopropane (**1-2c**).[49]

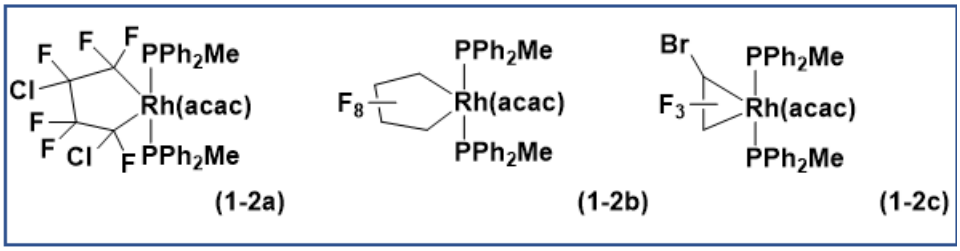

Figure 1.2 Structures of rhodium fluorometallacycles derived from fluoroolefins and Rh(acac)(PPh_2Me)$_2$.

Palladium tetrakis(methyldiphenylphosphine), [Pd(PPh_2Me)$_4$], reacts with an excess of hexafluoroacetone at 25 ^oC yielding the three-membered ring complex (**1-3a**), which, after three days at 60 ^oC, expands to the five-membered ring product (**1-3b**). As for Ni chemistry, there is a dependence on the ligand, such that the triphenylphosphite analog does not generate the fluorometallacyclopentane.[50] In contrast, a similar reaction of nickel tetrakis(*t*-butylisocyanide), followed by hexafluoroisopropylidene amine, gave a 5-membered ring complex (**1-3d**).[51]

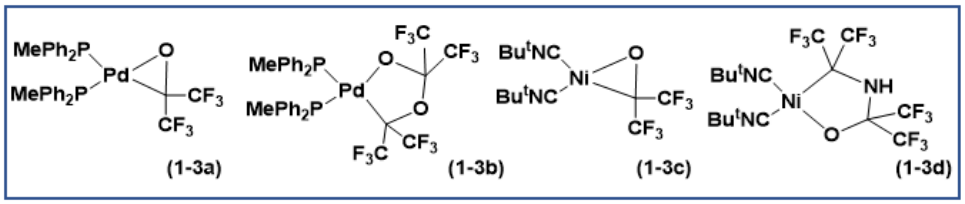

Figure 1.3 Structures of Group 10 metallacycles derived from fluorinated ketone and imine.

1.3.3 Reactivity of nickel fluorometallacyclopentanes

Nickel fluorometallacyclopentanes are most widely studied, representing the bulk of our knowledge of their reactivity. In 1996 Baker *et al.*, working at DuPont, developed a TFE hydrodimerization process showing unique reactivity of nickelacycles bearing π-acid ligands that enhance the acidity of presumed dihydrogen complex, allowing for hydrogenolysis of the Ni-C^F bond (**Scheme 1.8**).[52] Also at Dupont, Burch and co-workers demonstrated the reactivity of Cα-F bonds towards BF_3 Lewis acid, followed by phosphine migration to C_α. A dicationic product is created after a second equivalent of BF_3, and a stable product is isolated after bis(phosphine) ligand addition (**Scheme 1.9**).[53]

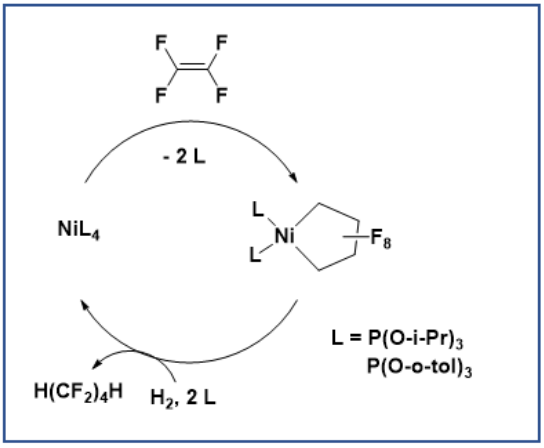

Scheme 1.8 Nickel-complex catalyzed TFE hydrodimerization to generate octafluorobutane.

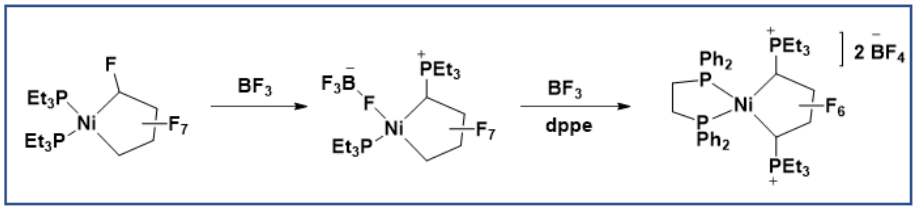

Scheme 1.9 Reactivity of perfluoronickelacycle with Lewis acid.

In 2015, Andrella, Baker *et al.* reported a stable 3-coordinate NHC nickel perfluorocyclopentane (**1-4a**) prepared by displacement of two phosphite ligands by one bulky NHC ligand (**Scheme 1.10**).[54] This complex reacts with Lewis acid Me_3SiOTf to undergo C_α-F abstraction, followed by C-C bond-forming ring contraction, affording perfluorocyclobutyl complex **1-4b**. Heating (**1-4b**) at 80 ^oC for 24 h then afforded perfluorocyclobutene via C_β-F elimination.

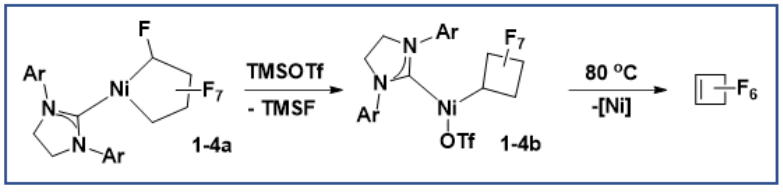

Scheme 1.10 Reactivity of 3-coordinate perfluoronickelacycle with Lewis acid.

Building on the Burch work, Giffin, Baker *et al.* found selective ligand migration of the P donor using bidentate [P-S] (**1-4c**) and [P-N] ligands on treatment with a strong Lewis acid

(**Scheme 1.11**).[55] Complex **1-4d**, upon hydrolysis, afforded a single isomer of hexafluorobut-1-ene, whereas treatment with three equiv of 2,6-dimethylphenylisocyanide (CNAr) induces ring-opening to yield the cationic product (**1-4e**), in which the phosphine traps eliminated Cβ-F. Finally, addition of a second equiv of TMSOTf enables fluoride abstraction from P to generate complex (**1-4f**).[55]

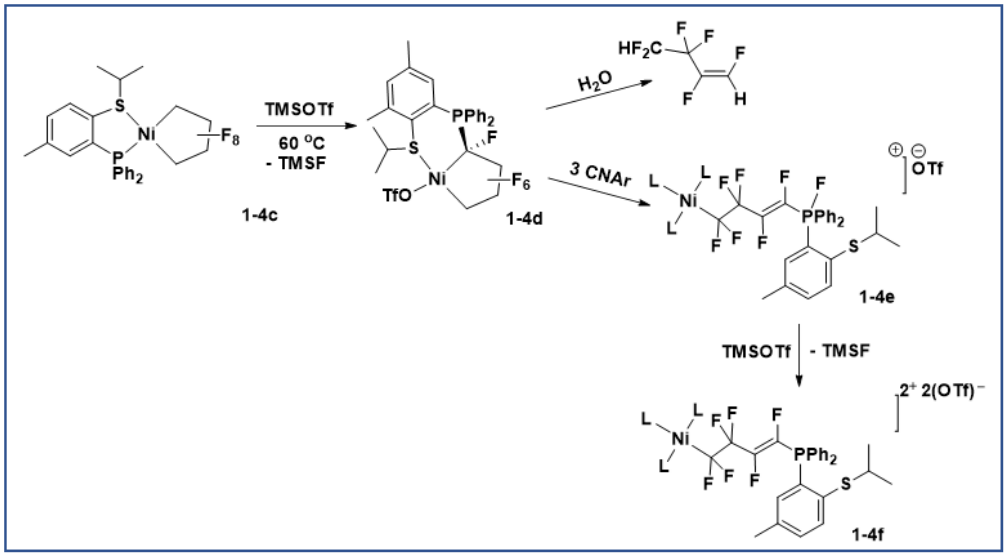

Scheme 1.11 Cα-F abstraction and phosphine migration to Cα.

Additional understanding of fluorometallacycle reactivity has resulted from the use of additional fluoroalkenes. Giffin, Baker *et al.* showed that the regioselectivity of metallacyclopentane formation using trifluoroethylene (TrFE) depends on the steric bulk of the phosphorus ligand. While DFT studies indicated that the head-to-head isomers with all four Fs on the α carbons are the most stable, 50% of the observed products consisted of the *cis*- and *trans*-head-to-tail regioisomers even with the smallest PMe_3 ligand (**Figure 1.4**).[56] In contrast, small amounts of the tail-to-tail isomer were only observed for the largest ligands, PPh_3 and $P(O\text{-}o\text{-}tol)_3$. While the reaction of the head-to-head isomer with 2 equiv of TMSOTf resulted in double phosphine migration followed by double Cβ-F elimination, the head-to-tail isomers yielded tetrafluorocyclobutene or tetrafluorobutadiene, depending on whether BF_3 or TMSOTf was used as the Lewis acid for the double fluoride abstraction (**Scheme 1.12**).

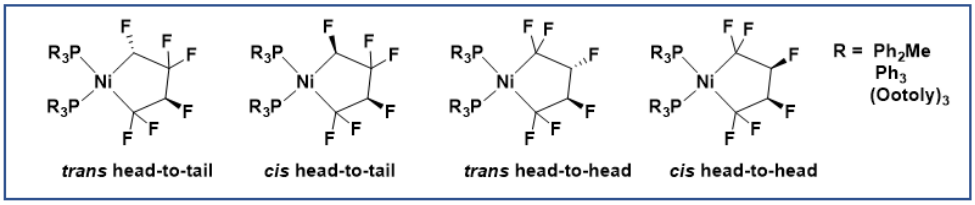

Figure 1.4 Reactivity of Ni^0 with TrFE.

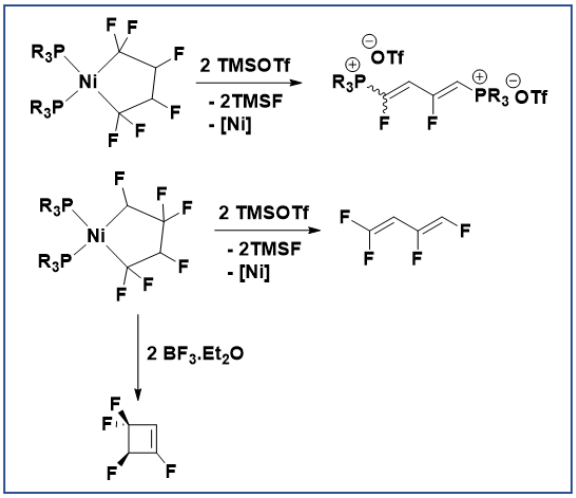

Scheme 1.12 C-F bond activation of metallacyclopentanes derived from Ni^0 and TrFe.

Sicard, Baker *et al.* then showed the first example of fluoroalkene homologation using vinylidene difluoride (CH_2=CF_2, VDF). They observed the three-membered ring metallacycle using small phosphines (**Scheme 1.13a**) whereas large phosphines or NHC ligands gave μ-F dimer derived from the metallacyclopentane by selective C_β-F elimination (**Scheme 1.13b**). Furthermore, by addition of silanes they demonstrated the Ni-catalyzed hydrodefluorodimerization (HDFD) of VDF to 2,4,4-trifluorobut-1-ene (HFO-1363pyf) (**Scheme 1.13c**). This new reaction has great potential for the creation of a variety of fluoroalkenes via the creation of mixed metallacycles from two different fluoroalkenes.

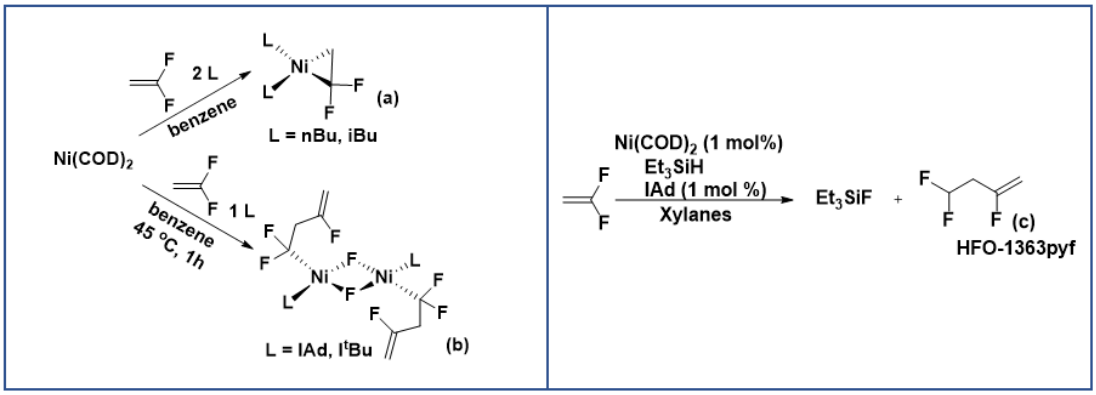

Scheme 1.13 Reactivity of Ni^0 with VDF.

1.4 Fluorine in medicinal chemistry

1.4.1 Fluorine in pharmaceutical compounds

The incorporation of fluorine into medicinal compounds often improves the biochemical and therapeutic aspects by impacting pharmacokinetics (PK) and pharmacodynamic (PD) properties. In 1953 fludrocortisone was shown to exhibit a 10-fold increase in anti-inflammatory activity compared to its non-fluorinated analogue.[57] Four years later, Heidelberger and co-workers reported antimetabolic 5-fluorouracil (5-FU) for cancer treatment (**Figure 1.5**).[58] Since then, many examples of fluorinated-containing pharmaceuticals for diverse diseases have been reported, comprising 20% of total commercial pharmaceuticals and 45% of the 38 small molecules approved by the U.S Food and Drug Administration (FDA) in 2018.[59] These classes include anticancer[60,61], antifungals[62], antivirals[63], antidepressants[64], antipsychotics[65], anticonvulsants[66], antidiabetics[67], treatment for heart failure[68] and antilipemic[69]. We will not discuss all these classes in this chapter, but just the most relevant for the work done in this thesis.

The significant impact of fluorine incorporation on drug development is reflected in the improved drug potency. For example, fluorastrol is 5-times more potent than monastrol (inhibitor of ATPase activity of Eg5 for cancer treatment) given the three additional interactions involving the 4-fluoro-aryl group and Arg221, Glu217, and Ala218 (**Figure 1.5A)**.[70] Interestingly, the fluorine effect enhanced the metabolic stability of thalidomide, so the fluorinated derivative (*S*)-fluorothalidomide is more potent and stable than (*R*)-fluorothalidomide avoiding the racemization *in vivo*. This was a great discovery after the "thalidomide tragedy"[71] since this drug is still approved

for multiple myeloma (MM) and erythema nodosum leprosum (ENL).[72] Enhancing lipophilicity increases the rate of absorption, transportation to cells, and oral bioavailability.

Another essential factor to be considered is the drug permeability. Many drugs need a high permeability and CNS penetration to achieve their target; for example, C-F bond inclusion in β-site amyloid precursor protein-cleaving enzyme 1 (BACE1) inhibitors decreases the efflux ratio from the P-glycoprotein efflux pump from 19 to 2, increasing the drug concentration in the brain (**Figure 1.5B**).[73]

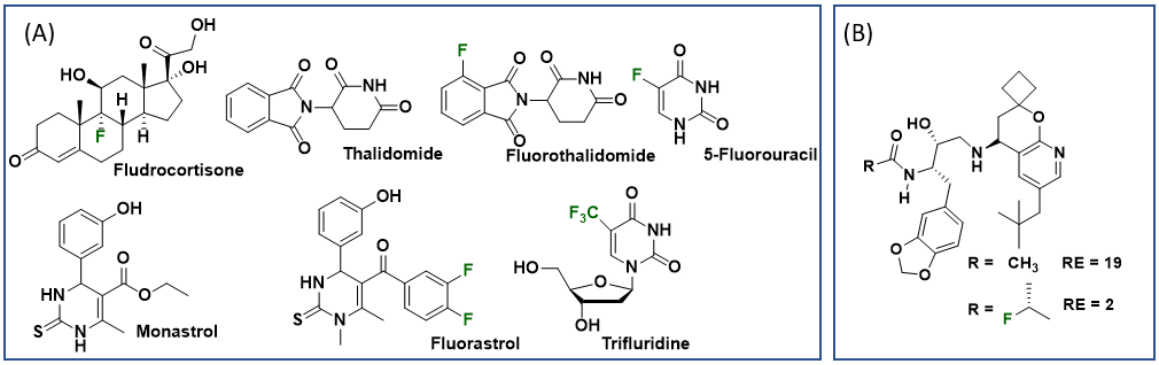

Figure 1.5 (**A**) Structures of fludrocortisone, 5-FU, trifluridine, thalidomide, fluorothalidomide, fluorastrol, monastrol, and (**B**) BACE-1 inhibitor. RE = Efflux ratios.

1.4.2 Fluorine in nucleoside analogs: Anticancer and antiviral activity

Modification of DNA structure, synthesis of nucleotides, and modification of nucleobases have attracted scientists.[74,75] Nucleoside analogs of uridine, thymidine, and cytidine can inhibit viral replication and act as antivirals,[76] or their metabolites can incorporate into the DNA strand and cause apoptosis of cancer cells.[77] Fluorine-containing-nucleoside analogs (NAs) have become a significant class among FDA-approved drugs and those in development.[78] Fluorinated-NAs have different dipole-dipole and gauche interactions, anomeric effects, and F-base interactions, besides the features typical of fluorine incorporation such as metabolic stability and increased lipophilicity, which explains their improvement in both PD and PK drug properties compared to NAs.[79]

We noted above the second fluorinated drug developed as 5-FU, an analog of nucleobase uracil that inhibits thymidylate synthase (TS). However, we did not mention this molecule's poor tumor activity and high toxicity. Many strategies have been addressed to decrease this toxicity; a pro-

drug called Capecitabine was developed that selectively delivers the fluorouracil after metabolizing by carboxylesterase (CES), cytidine deaminase (CDA), and thymidine phosphorylase (TP) (enzymes highly expressed in tumours).[80–83] Furthermore, numerous studies have been exploited extensively in the development process of pyrimidine analogs with fewer adverse effects and higher activity.

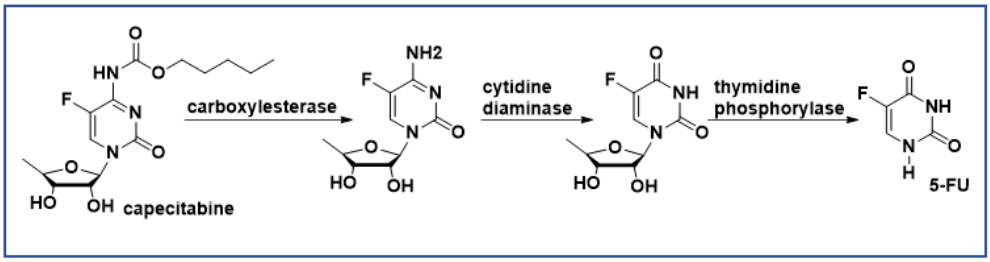

Scheme 1.14 Metabolic reactions of capecitabine to afford 5-FU.

Trifluridine (trifluorinated thymidine-based nucleoside analog, TFD) (**Figure 1.5A**) is another example of fluorinated-NA in the market, synthesized in 1964 by Heidelberger and co-workers as an antitumor reagent.[84] The cytotoxicity of TFD is due to the phosphorylation by thymidine kinase 1 (TK1) instead of thymidine (the usual substrate). Then TFD can incorporate the DNA during phase S and TS inhibition (analog to 5-FU mechanism).[85] Interactions of the trifluoromethyl group with Cys198 and Tyr146 are essential for the TS inhibition mechanism.[86] In 2015, to prevent the degradation of TFD from TP; it was combined with tipiracil (TP inhibitor) and approved for metastatic colorectal cancer.[87] Moreover, it is the first-choice treatment for herpes simplex virus type 1 and 2 (HSV-1 and HSV-2) keratitis and keratoconjuctivitis.[88–90]

1.4.3 Fluorine in drugs for COVID-19 treatment

Not surprisingly, fluorine participated actively during the latest pandemic that affected over 170 countries in less than three months (COVID-19 pandemic) as part of potential adjuvants against SARS-CoV-2 disease (COVID-19). Paxlovid™ is the first oral antiviral therapeutic approved for the treatment of COVID-19 by the FDA (December 2021), followed by Health Canada, Australia, and the European Union (January 2022).[91,92] Paxlovid™ combines nirmatrelvir plus ritonavir; nirmatrelvir is an inhibitor of the SARS-CoV-2 main protease and contains a trifluoromethyl group[93] ritonavir is a CYP3A4 inhibitor (which keeps the concentration of

nirmatrelvir high) and human immunodeficiency virus type 1 (HIV-1) protease inhibitor (**Figure 1.6**).[94] Besides the super-star drug first approved, more than ten fluorinated drugs have been reported for COVID-19 treatment, solidifying fluorine's importance in health science.[95]

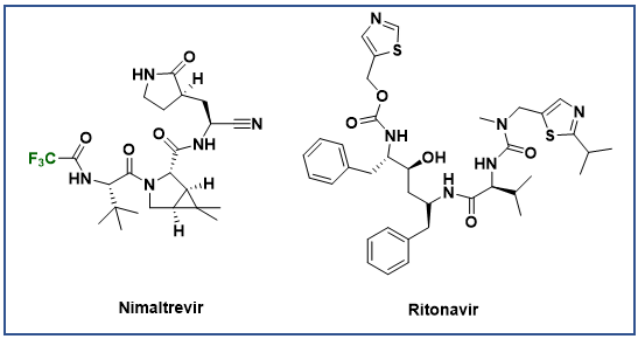

Figure 1.6 Structures of Paxlovid active ingredients.

1.4.4 Fluorine in agrochemicals

The continuing growth of the world's population pushes agriculture to improve its production by reducing plant illness/crop losses and enhancing food quality. A 4.5% annual growth rate for agrochemicals has been projected worldwide.[96] Among them, fluorinated pesticides constitute 70% of new agrochemical products in the 21st century; they are displayed in the top-selling agricultural products such as insecticides, fungicides, acaricides, and herbicides.[97,98] The most common fluoroalkyl groups incorporated into agrochemicals are trifluoromethyl ($-CF_3$), difluoromethyl ($-CF_2H$), trifluoromethoxy ($-OCF_3$), difluoromethoxy ($-OCF_2H$), difluoromethyl-sulfonyl (SO_2CF_2H), heptafluoroisopropyl [$-CF(CF_3)_2$] and methoxy-heptafluoroisopropyl [$-C(OMe)(CF_3)_2$] (**Figure 1.7**).[99]

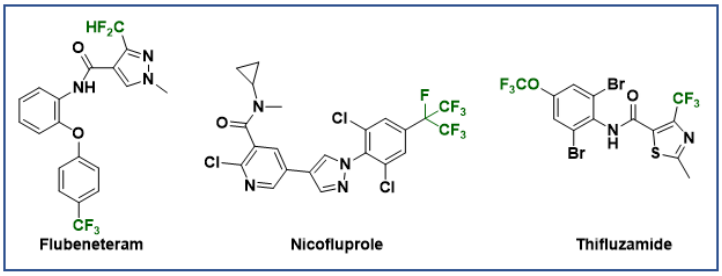

Figure 1.7 Examples of agrochemicals containing fluoroalkyl groups.

All fluorine properties discussed earlier in this chapter (**section 1.1**), such as electronic effects, steric effects, dipole effect, H-bond interaction, lipophilicity modulation, stereochemical

behaviour, and improvement in metabolic stability, explain the importance of building fluorinated blocks into agrochemical compounds. [4,7,100]

While late-stage fluorination of pharmaceuticals and agrochemicals is quite similar, the choice of process for commercialization is very different. For example, the cost of production may render the final product inaccessible to developing countries and has an environmental impact since they are not readily biodegradable. Moreover, lipophilicity may interfere with the bioaccumulation inside living organisms. Both properties are more significant due to the high volume necessary for the use of agrochemicals vs. pharmaceuticals. Although ecological implications are discussed in the current literature, discovering a novel fluorinated agrochemical that is more selective, specific, and less dangerous to human health is urgent for protecting crop production, ensuring we can feed the population in coming years.[97,101,102]

1.4.4.1 Fungicides

Fungicides control mycotoxins produced by fungi, kill fungi and can be used to treat plant diseases.[103] There are several fungicide groups with their respective target site: methyl-benzimidazole fungicides (MBCs), demethylation inhibitor fungicides (DMIs), quinone-outside inhibitor fungicides (QoIs), succinate dehydrogenase inhibitors (SDHis), carboxylic acid amides (CAAs), dicarboximide fungicides (DCFs) and keto-reductase inhibitors (KRIs).[104] However, SDHis have become the most commonly used fungicide class on the market due to their high broad-based activity and are now the center of research in modern agriculture.

The main mode of action of fungicides is inhibition of succinate dehydrogenase (SDH), also known as mitochondrial complex II or ubiquinone oxidoreductase. The SDH contains four polypeptide nuclear-encoded subunits (SdhA, SdhB, SdhC, and SdhD) inside mitochondria. Inhibition of this enzyme interferes with the functional mitochondrial respiratory chain and tricarboxylic acid cycle (TCA).[103,105] SDHis bind in the ubiquinone binding pocket (Q site) and avoid the reduction of succinate to fumarate and ubiquinone to ubiquinol (instead of panthenol), thereby inhibiting fungal respiration, leading to fungal death.[103]

Carboxin was the first-generation SDHi commercially available in the late 1960s.[106] 1990 saw the development of the second generation, represented by thifluzamide, and in the 21st century, the third generation appeared, represented by structurally variable compounds.[103] Carboximide fungicides block the Q site efficiently. Many researchers have proposed a structure-activity relationship (SAR) of SDHi developing a new succinate dehydrogenase subclass based on molecular docking and molecular dynamics simulations. They observed hydrogen bonding from the pyrazole ring closer than pyridines and π-π interaction of aromatic ring and the target protein; they also described the importance of the carbonyl linker connecting the amide attached to the amine portion and the pyrazole ring (acid part), the last component usually contains fluoroalkyl groups.[106–111] These descriptions clearly define Pydiflumetofen and Isoflucypram, which entered the market in 2016 and 2019 (**Figure 1.8**).[112] The unique properties of these compounds as SDHi have been applied against the devastating disease of wheat and barley crops known as fusarium head blight (FHB) caused by *Fusarium graminearium* (Fg).[112–114]

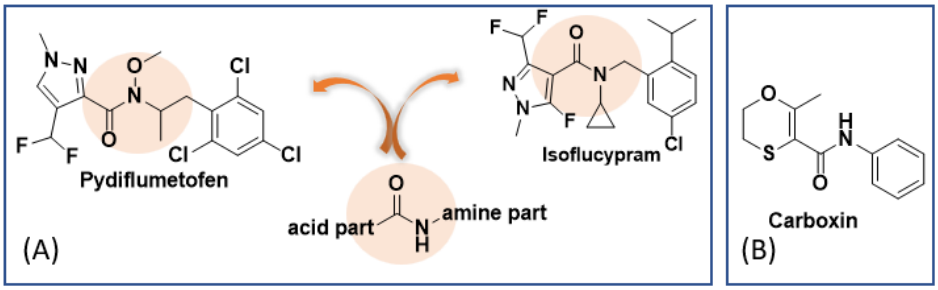

Figure 1.8 Structures of Ag chemicals pydiflumetofen, isoflucypram (**A**), and carboxin (**B**).

1.5 Late-stage fluorination

1.5.1 Incorporation of fluorine

The development of synthetic protocols to incorporate fluorine into drugs or agricultural chemicals is an expanding field, with many new options becoming available.[115] There are problems associated with the use of simple fluorine sources, such as fluorine gas (F_2) and fluoride ion, for functionalization at a late stage of the bioactive molecule's synthesis. The high reactivity of F_2 gas leads to functional group intolerance and fluoride ion's poor nucleophilicity in the presence of an H-bond donor, and its high basicity often causes side-reactions leading to poor yields.[116]

There are two types of fluorinating reagents: nucleophilic and electrophilic. Electrophilic fluorination provides a source of F^+, starting with elemental F_2 and xenon difluoride (XeF_2) (more stable than F_2 but expensive);[116,117] F_2 gas is a good choice for fluorination of nanographene to the 2D diamond in a free-radical cross-linking mechanism[118]. Also, O-F reagents (like CF_3OF[119], CH_3CO_2F[120], CF_3CO_2F[121], and $CsOSO_2OF$[122]) were used for many years; however, they possess many challenges, as we discussed before.

In the early 1990s, a new class of electrophilic fluorination reagents became popular due to their milder and safer properties. Having a general structure of R_2N-F (neutral) or R_3N^+-F (quaternary ammonium), N-fluorobis(phenyl)sulfonimide (NFSI), N-fluoropyridinium salts (NFPy), and 1-chloromethyl-4-fluoro-1,4-diazoniabicyclo[2.2.2]octane bis(tetrafluoroborate) (Selectfluor®) (**Figure 1.9**) are the most used reagents that helped to develop more tolerable fluorination methods. These organonitrogen groups promote reactivity of the N-F bond after suffering a nucleophilic attack (**Scheme 1.15a**) or a single-electron transfer (SET) reaction with nucleophiles (**Scheme 1.15b**).[123–126]

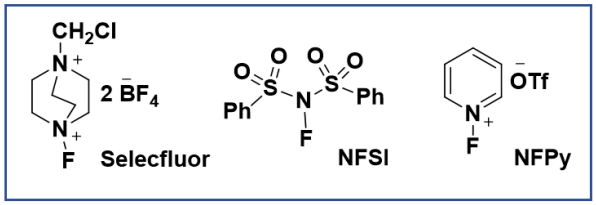

Figure 1.9 Structures of Selectfluor®, NFSI, and NFPy.

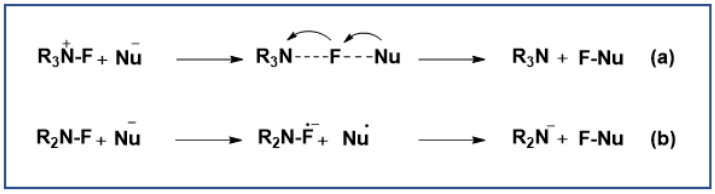

Scheme 1.15 a. Reactivity of fluorine with nucleophile using quaternary salt reagents and **b**. SET pathway.

Differding and co-workers 1991 synthesized the stable crystalline solid NFSI[127], which requires high temperatures and neat conditions to fluorinate various aromatic nucleophiles (anisole, toluene, acetanilide) and so is less used.[128] Selectfluor,® reported for the first time in 1992 by Banks and co-workers,[129], is the favorite fluorinating reagent that possesses a

"fluorine-free" functional group (transition metal oxidant, fluorine cation, or radical initiator) and can also react as an oxidant or Lewis acid.[130,131]

In 2014 You and co-workers described a silver-catalyzed tandem cyclization/ fluorination of 2-alkylanilines to offer fluorinated indole derivatives using NFSI or Selectfluor® as the fluorinating reagent. They found a cyclization/ difluorohydroxylation one-pot protocol using 3.0 equiv of H_2O, 10 mol % silver nitrate ($AgNO_3$) in acetonitrile (ACN) at 80 ^oC, that was only possible to get excellent yields by adding 2.0 equiv of Selectfluor® instead of NFSI.[132] Nonetheless, Flower and co-workers[133] observed fluorination of carboxylic acids substituting the Selectfluor® from Li`s methodology[134] (**Scheme 1.16a**) with NFSI combined with sodium persulfate (**Scheme 1.16b**). Two years later, Tang *et al.* described a silver-catalyzed hydroxyfluorination of styrenes with anti-Markovnikov-type regioselectivity treating Selectfluor® with 10 mol % of AgOTf in $PhNO_2/H_2O/CH_3NO_2$ at 30 ^oC (**Scheme 1.16c**).[135] More recently, Vincent and Brioche described a combination of $AgNO_3$ and Selectfluor® capable of deoxyfluorinating cesium oxalates from their corresponding alcohols performed by radical fluorination (**Scheme 1.16d**).[136] A boron-catalyzed α-fluorination of free carboxylic acids was recently described by Feng and co-workers using SelectFluor® in organic bases (pyridine, DMAP, TMG, and DBU), yielding α-fluorocarboxylic acid bioactive molecules in 20-96% yield (**Scheme 1.16e**).[137] Examples of nickel catalyzed fluorinations use NFSI or Selectfluor® to α-fluorinate cyano-ester[138], oxindole[139], and keto-ester[140] substrates in excellent yields.[141]

Nucleophilic fluorination was developed in the early 21st century and has expanded efforts to improve its reactivity and/or ease of use. Familiar sources are poorly soluble metal fluoride salts, such as KF, CsF, and AgF (cheaper than electrophilic reagents but weak nucleophiles) and soluble tetrabutylammonium difluorotriphenylsilicate (TBAT) tetramethylammonium fluoride (TMAF), and tetrabutylammonium fluoride (TBAF).[142] One of the most successful methods is to transfer nucleophilic fluorine to a transition metal, and the fluorination proceeds via a cross-coupling mechanism.[117,143–145]

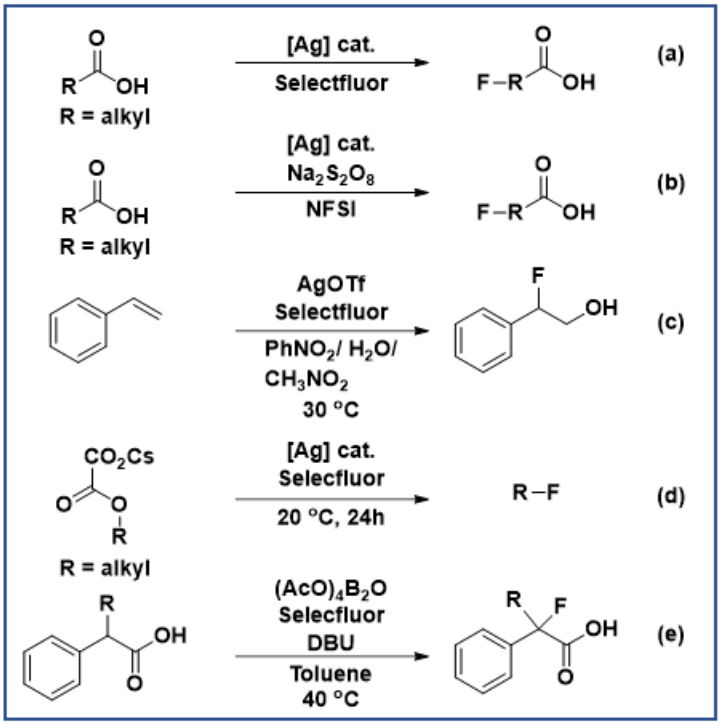

Scheme 1.16 α-Fluorination of carboxylic acids (**a**,**b,e**), styrene (**c**), and decarboxylative fluorination (**d**).

Late transition metal-catalyzed fluorination is an attractive strategy since d^{10}-metals are functional group tolerant and can be attached to different ligands to increase reactivity.[143,144] However, the difficult reductive elimination of Ar-F has been noted by Grushin.[146–148] In general, late metal-fluorine bonds are labile and reactive, and many complexes are capable of fluorinating electrophile substrates.[149–151]

The first Pd(0) system to catalyze fluorination of aryl triflates was reported by Buchwald *et al.* in 2009.[152] The same group developed a system using CsF that expanded the substrate scope to include heterocycles.[153–155] In 2014 Doyle and co-workers studied the reaction mechanism of palladium-catalyzed allylic fluorination with AgF as the fluorine source. They proposed allylpalladium(II) chloride formation after oxidative addition to Pd(0), followed by ligand exchange with AgF to produce a homobimetallic transition state from both intermediates (cationic vs. neutral allylic); which they were not able to distinguish by kinetic studies (**Scheme 1.17a**).[156] In contrast, using an electrophilic F source, Lectka and co-workers reported a radical chain mechanism based on the synthesis, kinetics and computational studies combining a copper salt and Selectfluor in acetonitrile (**Scheme 1.17b**).[157]

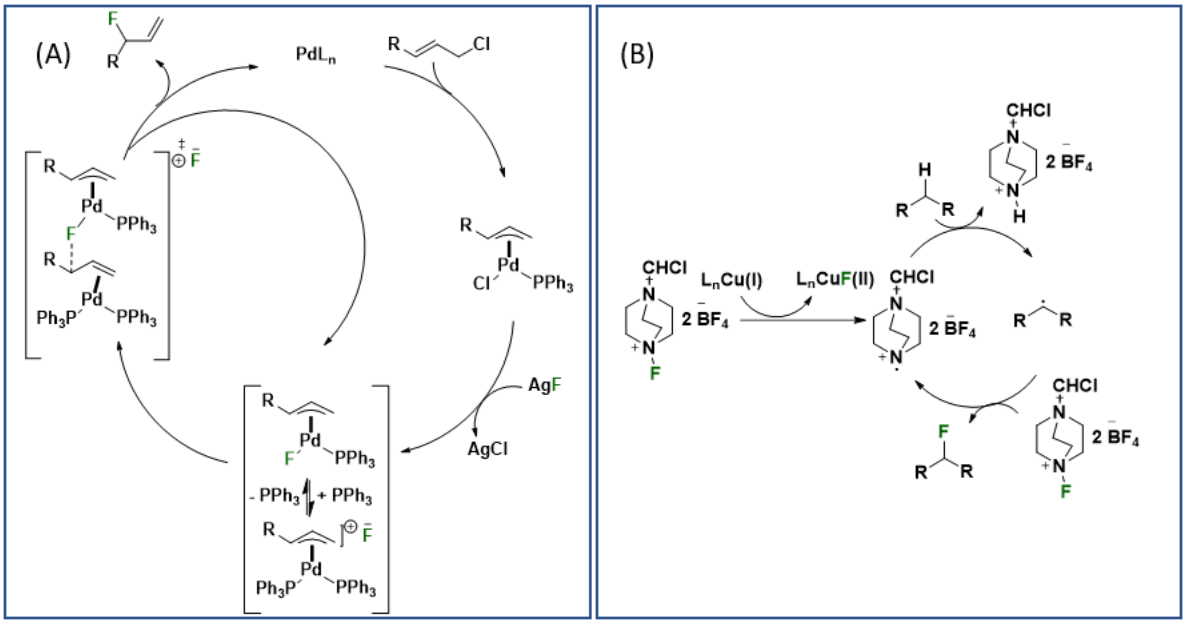

Scheme 1.17 The proposed mechanism by Doyle et al. uses a nucleophilic source (**A**), while Lectka et al. use an electrophilic source (**B**).

Motivated by Gray *et al.'s* work using a cyclometallated iridium (III) catalyst for high yield fluorination of acyl chlorides,[158] Baker *et al.* reported cobalt-catalyzed fluorination of acyl chlorides using AgF as fluoride source and CpCo (III) perfluoroalkyl halide complexes.[159] In a similar way, Licence and co-workers recently reported rhodium-catalyzed nucleophilic fluorination of acyl chlorides, including an analog of the pharmaceutical compound probenecid, in 99% yield. The reaction was performed under mild conditions, using 5 mol% of a cyclometallated rhodium complex containing a perfluorinated ligand and 1.5 equiv. of AgF in dichloromethane for 1.5 h.[160] His DFT studies also supported Baker's[1] proposed mechanism, [59] in which nucleophilic attack at the substrate is the rate-determining step with the formation of a new M-F bond (**Scheme 1.18**).[160]

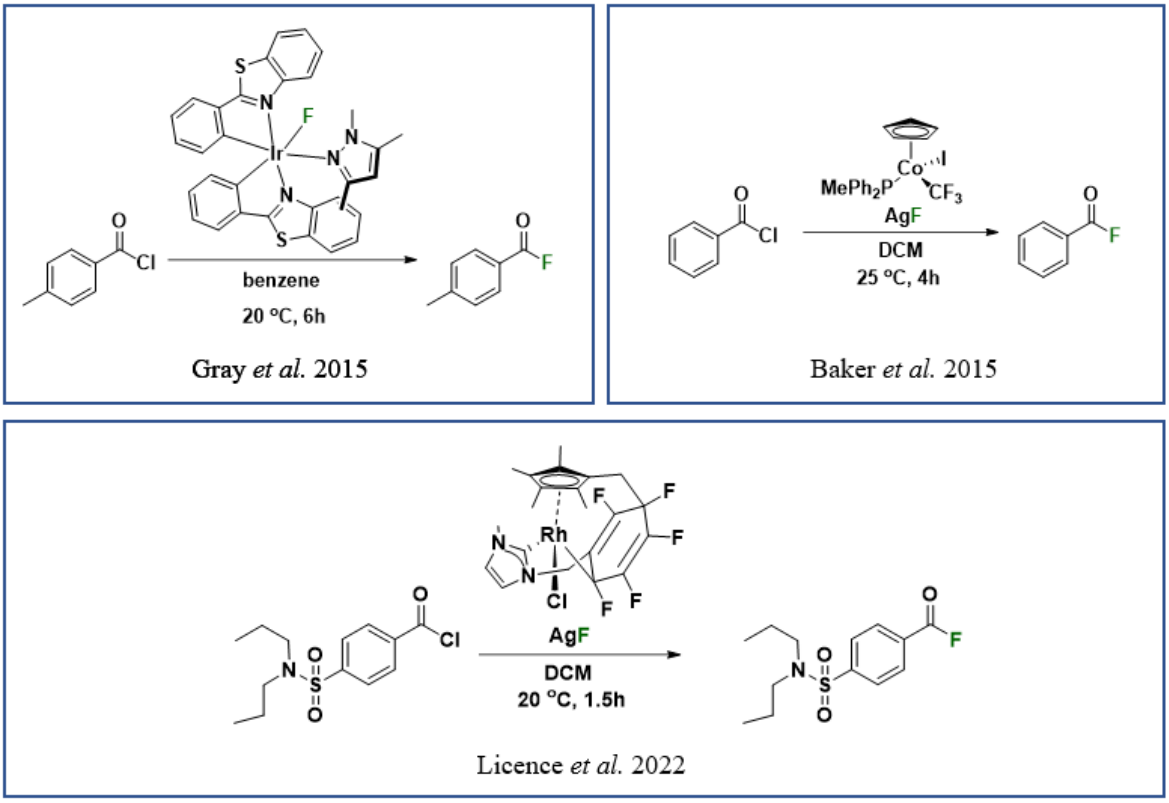

Scheme 1.18 Fluorination of acyl chloride catalyzed by perfluorinated metal (M = Rh, Ir, or Co).

1.5.2 Fluoroalkylation

An enormous number of late-stage trifluoromethylation have been described in the literature for decades.[161–164] They can be divided into four categories: nucleophilic[165,166], electrophilic[167], radical[168] and radical addition[169] (**Figure 1.10**). Ruppert *et al.* synthesized one of the most used CF_3 sources ($TMSCF_3$) of organic electrophiles, which is less toxic and more attractive, which will be detailed in the next sections.[170] It can be activated by n-Bu_4NF (TBAF), Lewis base (such as Et_3N and pyridine) or N-heterocyclic carbenes (NHC) for promoting trifluoromethylation of carbonyl groups.[171] Beier and co-workers established the trifluoromethylation of sulfonyl azides to further the generation of CF_3-containing triazoles (**Scheme 1.19a**).[171,172] In 1989, Chen and co-workers developed a nucleophilic trifluoromethylation reagent ($FSO_2CF_2CO_2Me$)[173]. A catalytic amount of copper iodide promotes the *in situ* decomposition of this reagent, generating $CuCF_3$, inducing trifluoromethylation of organohalides (**Scheme 1.19b**).[174]

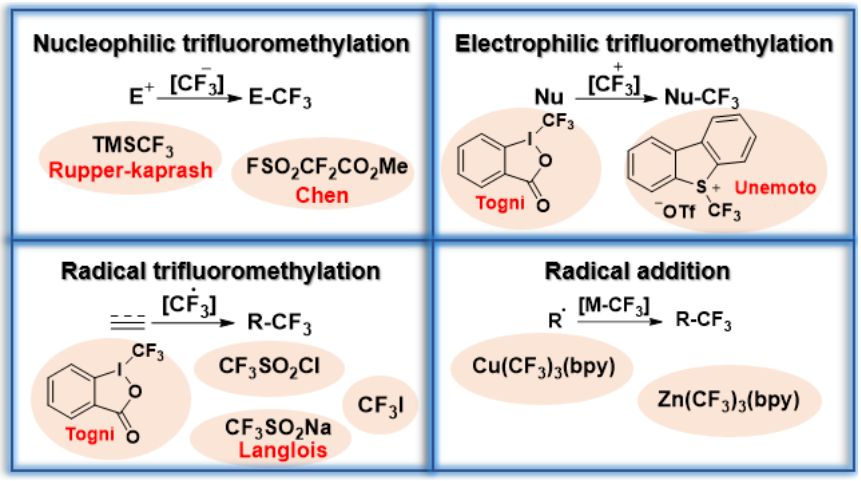

Figure 1.10 Four categories of trifluoromethylation sources.

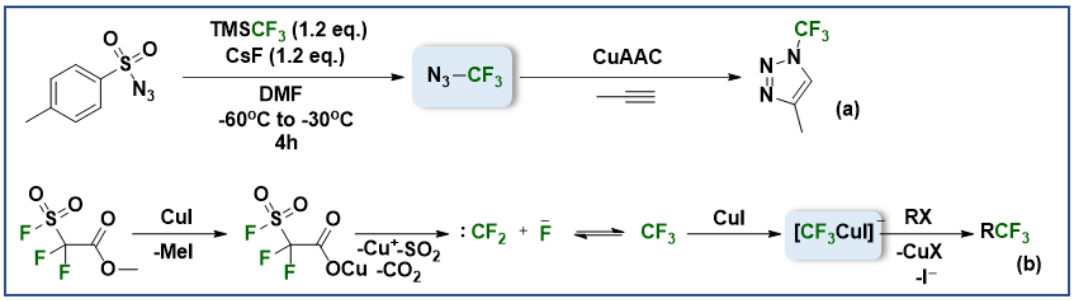

Scheme 1.19 Trifluoromethylation using nucleophilic sources.

Amii *et al*. developed a copper-catalyzed strategy of aromatic trifluoromethylation using diamine ligands to stabilize and increase the nucleophilicity of Cu-CF_3,[175]. They proposed a catalytic mechanism in which the Cu(I) iodide complex could be reused faster than trifluoromethylcopper decomposition. Years later Jover detailed by computational studies, the endergonic reaction of KCF_3 generation from $TMSCF_3$ and KF (**Scheme 1.20a**), followed by CF_3 transfer to copper through an exergonic transmetalation (**Scheme 1.20b**). They also observed the slowest step oxidative addition with +2.4 kcal/mol.[176] Very recently, Shen *et al.* for the first time isolated and characterized a five-coordinated Cu (III) complex containing two CF_3 group and a bpy ligand. They examined the reductive elimination of this complex involving a concerted pathway with a 23.0 kcal/mol energy barrier (**Scheme 1.20c**). [177]

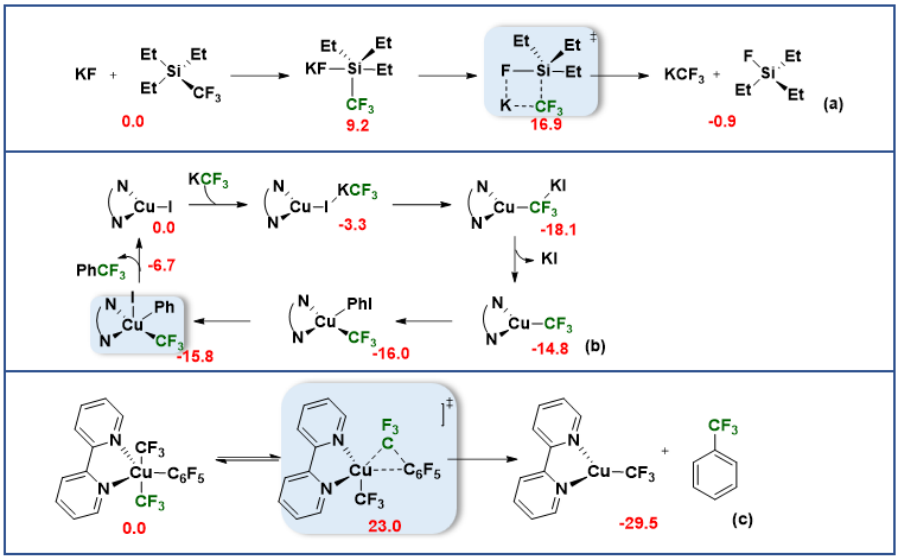

Scheme 1.20 Copper-catalyzed trifluoromethylation.

Metal-free or iron-catalyzed trifluoromethylation reactions using Togni`s hypervalent iodine reagent have been studied over the past few years.[163,178] For example, Togni`s reagent can be the electrophile source for iron-catalyzed trifluoromethylation of diallyl aryl alcohol and enamides,[179,180] as well as for trifluoromethylation of ketones and unsaturated amides under metal-free basic conditions (**Scheme 1.21**).[181,182]

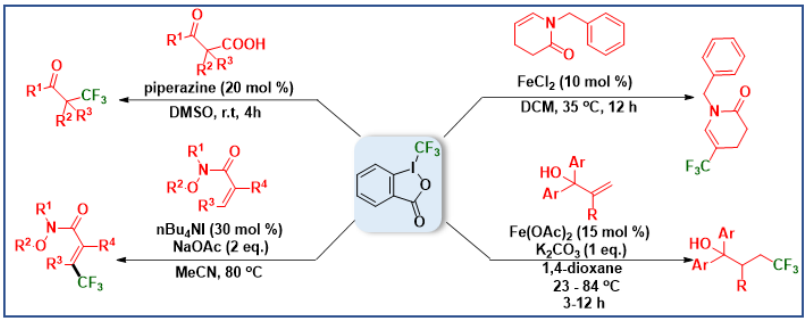

Scheme 1.21 Trifluomethylation employed by Togni`s reagent.

Synthetic approaches to afford trifluoromethylated heterocycles using radical fluorinated sources can also be metal-free.[183] Zhang *et al.* showed a direct trifluoromethylation of quinoxaline-2(1H)-ones with Langlois reagent in the presence of [bis(trifluoroacetoxy)iodo]benzene ($PhI(OTFA)_2$) (**Scheme 1.22a**).[184] Another example reported the trifluoromethylation of alkyl radicals assisted by copper.[168] Along this line, Li and co-workers disclosed that $Cu(CF_3)_2(bpy)$ complex reduced by triethylsilane gives Cu^{II}-CF_3 which becomes the electrophilic source in this reaction (**Scheme 1.22b**). [185]

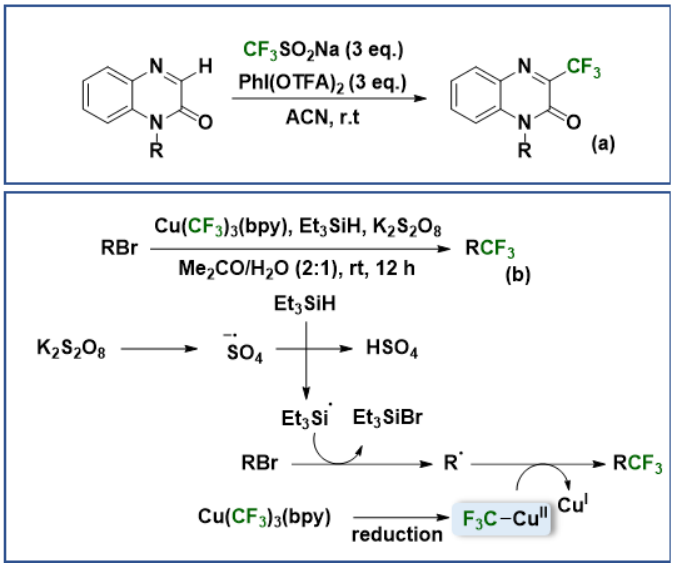

Scheme 1.22 Trifluoromethylation using radical source.

A transition metal-catalyst combined with Selectfluor® as an oxidant can mediate cross-coupling reactions and generate new fluoroorganic compounds. Although there are a few reports using transition metal catalysts and NFSI/ Selectfluor® reagents,[186] silver-catalyzed radical fluorination combined with these reagents has become more popular for hydroxyfluorination. For example, Qing *et al.* reported a silver-mediated trifluoromethylation of alcohols (**Scheme 1.23a**);[187] more than two years later; they also showed that pentafluoroalkyl ethers were incorporated into alcohols and phenol substrates mediated by silver in the presence of Selectfluor® and $TMSC_2F_5$, $TMSCF_2CO_2Et$ or $TMSCF_2CF_2CF_3$ (**Scheme 1.23b**).[188]

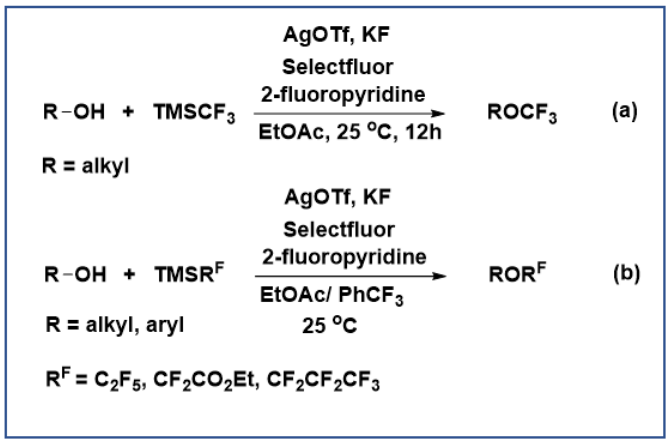

Scheme 1.23 a. Trifluoromethylation of alcohols; **b**. Pentafluoroethylation of alcohols and phenols.

1.5.3 Transition-metal catalyzed trifluoromethythiolation, trifluoromethoxylation and difluoromethylation.

Methodologies for introducing SCF_3, OCF_3, and CF_2H into organic molecules, mainly catalyzed by metal complexes, have recently gained much attention. Palladium, nickel, gold, and copper complexes have all been reported for catalyzing direct nucleophilic and electrophilic trifluoromethylthiolation. Nucleophilic sources ($CuSCF_3$, $AgSCF_3$, $Hg(SCF_3)_2$, $TMSCF_3$, Me_4NeSCF_3) and electrophilic reagents (CF_3SCl, CF_3SSCF_3, N-trifluoromethylthiophthalimide, N-Trifluoromethylthiosaccharin) have both been employed. The first Pd-catalyzed cross-coupling of aryl halides for the formation of heteroaryl-SCF_3 using a nucleophilic source was reported by Buchwald and co-workers in 2011; their optimal conditions used a combination of $[NPhEt_3]I$, $AgSCF_3$, and a sterically hindered/ electron-rich phosphine Brettphos (dicyclohexyl[3,6-dimethoxy-2',4',6'-tri(isopropyl)[1,1'-biphenyl]]-2-yl] phosphine) (**Scheme 1.24**).[189] Huang and co-workers used $Pd(OAc)_2$, 2 equiv of $AgSCF_3$, and 3.0 equiv of Selectfluor as oxidant at 60 °C to trifluoromethylthiolate phenylpyridine derivatives in high yields.[190] A catalytic amount of copper salt combined with 1.5 equiv of $AgSCF_3$ and 20 mol % of bipyridine (bpy) ligand (to increase the stability of $CuSCF_3$)[191] gave aryl trifluoromethylthioethers in good yields from oxidative trifluoromethylthiolation of boronic acids.[192] Hypervalent diaryliodonium salts are also good substrates, as shown by Anbarasan and co-workers, using 20 mol % of CuI combined with 20 mol % of SPhos (2-dicyclohexylphosphino-2',6'-dimethoxylbiphenyl) and 1.1 equiv of $AgSCF_3$

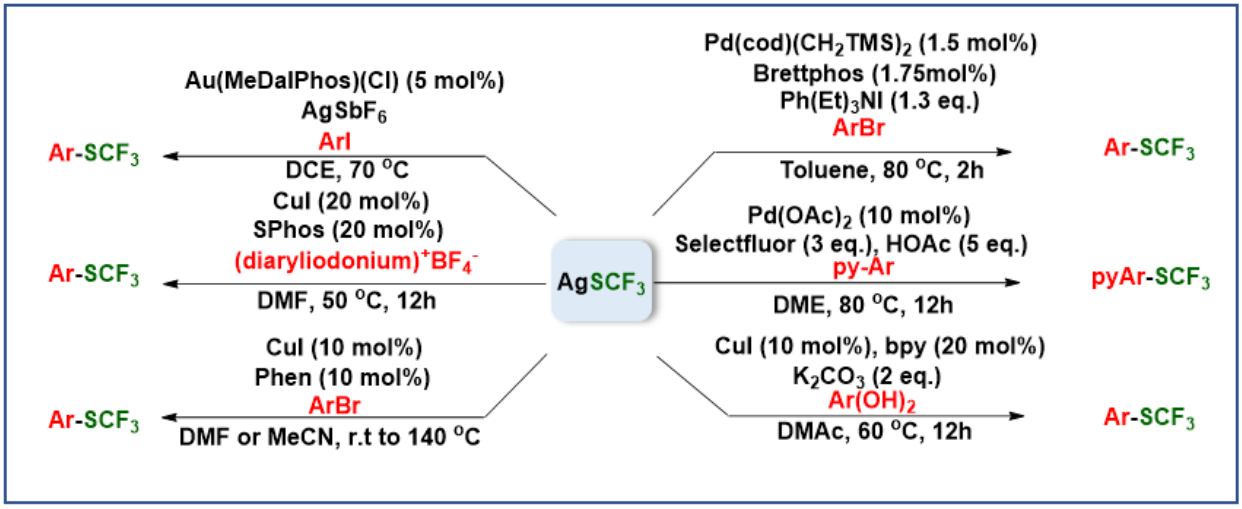

Scheme 1.24 Trifluoromethylthiolation of aryl halides using $AgSCF_3$.

at 50 °C in DMF, generating heteroaryl trifluoromethyl sulfides in up to 94% yield.[193] Phenanthroline is also a good ligand to stabilize $CuSCF_3$ (derived from $AgSCF_3$ and CuBr) and effect the trifluoromethylthiolation of aryl halides.[194] In recent work, Lu *et al.* reported a gold-catalyzed trifluoromethylthiolation of aryl halides under mild conditions, including bioactive molecules, in high yields, using $AgSCF_3$ and a silver activator ($AgSbF_6$).[195] Reactions using Me_4NSCF_3 to afford aryltrifluoromethylethers can be catalyzed by iodide-bridged palladium dimer[196] or Ni (0) using highly soluble bipyridine derivatives like 4,4'-dimethoxybipyridine (dmbpy[197]) and a wide-bite angle phosphine ligand 1,1'-bis(diphenylphosphino)ferrocene (dppf) (**Scheme 1.25**). Shoenebeck and co-workers also found this Ni-catalyzed protocol to be highly efficient in giving the respective trifluoromethyl sulfide ($ArSCF_3$) of pharmaceutical compounds.[198]

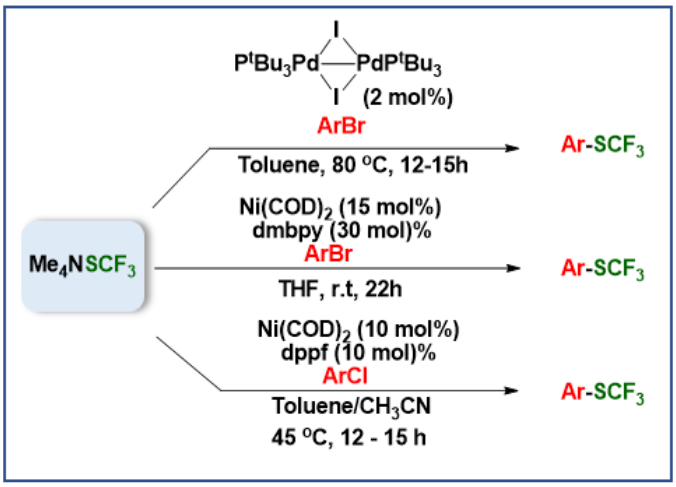

Scheme 1.25 Trifluoromethylthiolation of aryl halides using Me_4NSCF_3.

The most commonly used electrophile source, N-trifluoromethylthalimide present in the reaction mixture with a copper salt as a catalyst and boronic acids gives trifluoromethylthiolated arenes in good yields.[199,200] Alternately, Li *et al.* reported a rhodium-catalyzed C-H bond functionalization affording trifluoromethylthiolated arenes in high yields using N-trifluoromethylthiosaccharin. [201]

Many other electrophilic trifluoromethylthiolating reagents have been developed in the past decades. [202] Billard`s reagent activated by Lewis or Brønsted acids trifluoromethylthiolate

electron-rich arene and indoles (**Scheme 1.26a**),[203] while his second generation under superacid condition achieved trifluoromethylthiolation of acetanilide (**Scheme 1.26b**).[204] The recently hypervalent iodine (III) trifluoromethylthiolate designed by Zhang is able to trifluoromethylthiolate multimethoxylated arenes and naphthols without Lewis acid (**Scheme 1.26c**).[205] Expanding Friedel-Crafts substrate scopes, the trifluoromethyl sulfoxide built by Procter and co-workers was able to generate *p*-xylene trifluoromethylthiolate after activation by Tf_2O (**Scheme 1.26d**). [206]

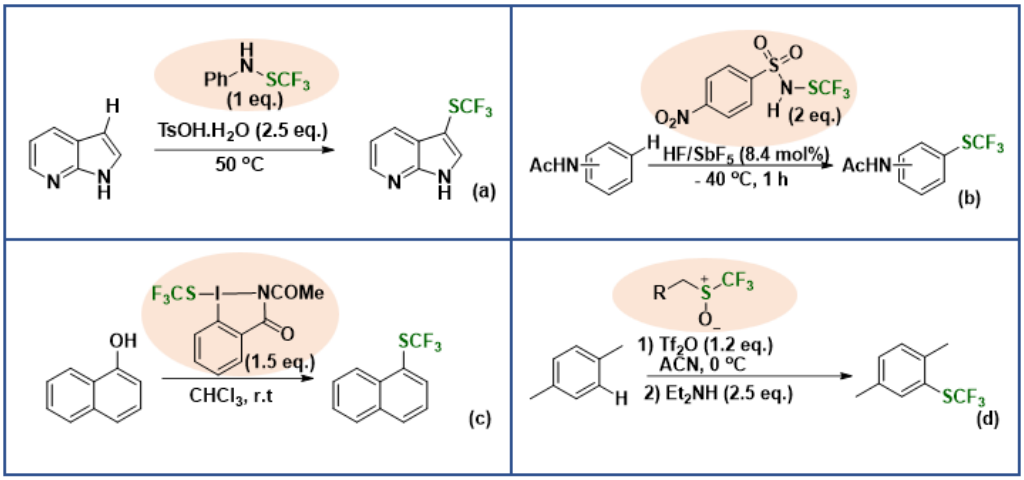

Scheme 1.26 Trifluoromethylthiolation of hetero(aryl) C-H bonds.

The trifluoromethoxy anion $(OCF_3)^-$ is highly unstable and decomposes (to fluoride and difluorophosgene) above – 20 °C,[207] highlighting the need for new trifluoromethoxylation reagents. While the first examples of arene trifluoromethoxylation generated trifluoromethoxide salts in situ[208,209], newer nucleophilic reagents include $AgOCF_3$,[210] nBu_4NOCF_3,[210] and $(Me_2N)_3SOCF_3$ ($TASOCF_3$).[211] Although the generation of trifluoromethoxy anion (OCF_3^-) from trifluoromethyl triflate (TFMT) activated by fluoride salt has enabled the development of transition-metal catalyzed protocols, few examples are found in the literature. In 2018 Hu and co-workers reported the trifluoromethoxylation-bromination of benzyne from trifluoromethylbenzoate (TFBz), trimethylsilylphenyl triflate and AgF that generates $AgOCF_3$ *in situ* (**Scheme 1.27**).[212] In the same year, Liu *et al.* described the generation of bis(trifluoromethoxylated) alkenes using $AgOCF_3$, 3.0 equiv of strong oxidant (Selectfluor-OTf), and a catalytic amount of palladium.[213] Interestingly, a catalytic amount of Pd and 2.0 equiv. of Selectfluor®/ 3.0 equiv. of $AgOCF_3$ under mild conditions provided a trifluoromethoxylation (-

OCF_3) of alkenes in 60-80% (**Scheme 1.27**). [214] In 2020, Friesen and co-workers reported a stable quaternary ammonium trifluoromethoxide (NR_4OCF_3) as a nucleophilic source of OCF_3. They formed the NR_4OCF_3 salts from the nucleophilic attack of tertiary amines on trifluoromethyl ether, followed by trifluoromethoxylation of pyranose.[215] Hopkinson *et al.* described a C-H trifluoromethoxylation of arenes from the reaction of bis(trifluoromethyl)peroxide (BTMP) and the photocatalyst $[Ru(bpy)_3][PF_6]_2$ in MeCN for 16 h at room temperature.[216] Trifluoromethoxylation of aziridines was studied by Tang *et al.* using TFMOTf as an OCF_3 source catalyzed by silver, with a nucleophilic attack of $^-OCF_3$ proceeding at the less hindered carbon of the aziridine.[217]

Difluoromethylation of organic compounds is not yet well-developed. N,N-diethylaminosulfur trifluoride (DAST), bis(2-methoxyethyl)aminosulfur trifluoride (Deoxo-fluor®), and Xtalfluor-M® have been used as difluoromethyl sources for many years, but they are limited by toxicity, functional group incompatibility, and have low scalability.[218–220] Some

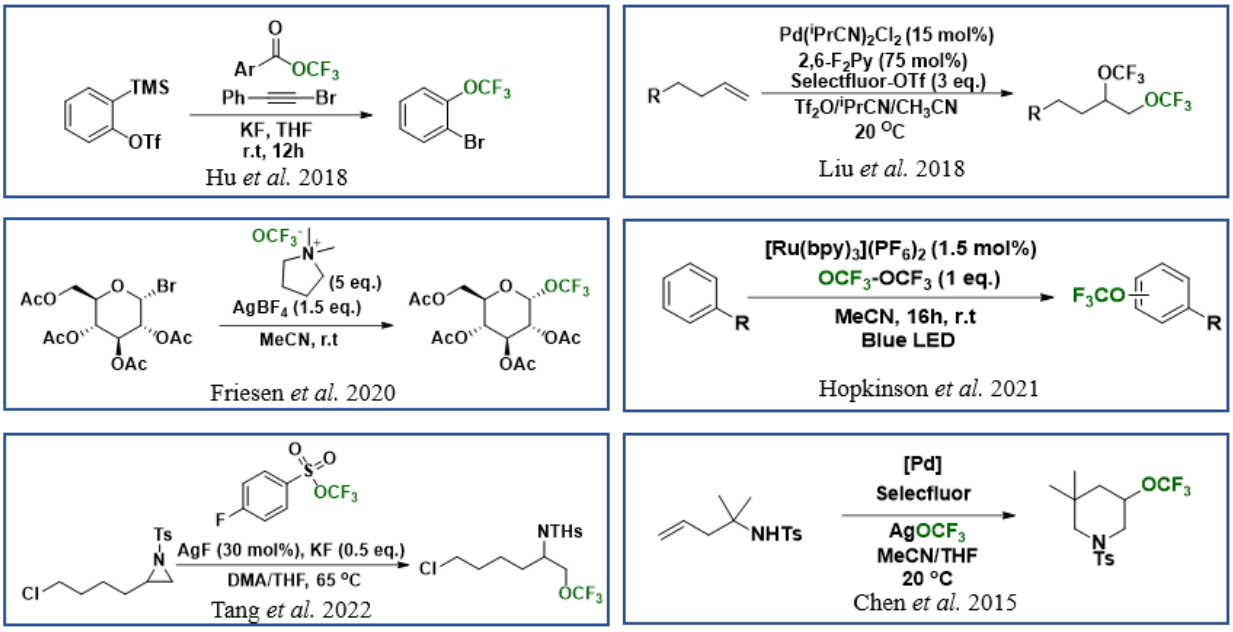

Scheme 1.27 Trifluoromethoxylation using nucleophilic sources.

successful reactions were achieved using transition metal catalysts, such as Cu,[221,222] Fe[223], Ni,[224,225] Pd,[226,227] and Pt.[228]

In 2014 Shen *et al.* reported a palladium/silver catalytic cycle for difluoromethylation of aryl halides using dppf as ligand and $TMSCF_2H$ as the fluoroalkyl source. They isolated [$Ag(CF_2H)(SIPr)$] (SIPr = 1,3-bis(2,6-diisopropyl phenyl)imidazoline-2-ylidine) in 82% by reacting [AgCl(SIPr)] with $TMSCF_2H$ in THF (**Scheme 1.28)**.[229] In 2017, the same group described a direct difluoromethylation of heteroaryl bromides and iodides using [$Ag(CF_2H)$ (SIPr)] with a catalytic amount of bis(dibenzylideneacetone) palladium(0) [$Pd(dba)_2$] and a wide bite angle phosphine bis[(2-diphenylphosphino)phenyl] ether (DPEphos) that reacted smoothly to give Ar-CF_2H, inclusive of medicinal substrate imiquimod analog (**Scheme 1.29)**.[230] Difluoromethylation of important drug/ agrochemical molecules was also achieved using a Pd catalyst discovered by Buchwald[231] with Xphos ligand.[226] A Pd-catalytic system with $TMSCF_2H$, CsF, and bulky electron-rich monodentate phosphine Brettphos conducted in moderate to good yields the difluoromethylation of aryl chlorides.[227] Mikami and co-workers developed a Cu-catalyzed difluoromethylation of aryl iodides using Vicic`s reagent, [$(DMPU)_2Zn(CF_2H)_2$] (DMPU = N, N'dimethylpropyleneurea).[232] They observed by ^{19}F NMR neutral $Cu(CF_2H)$ and

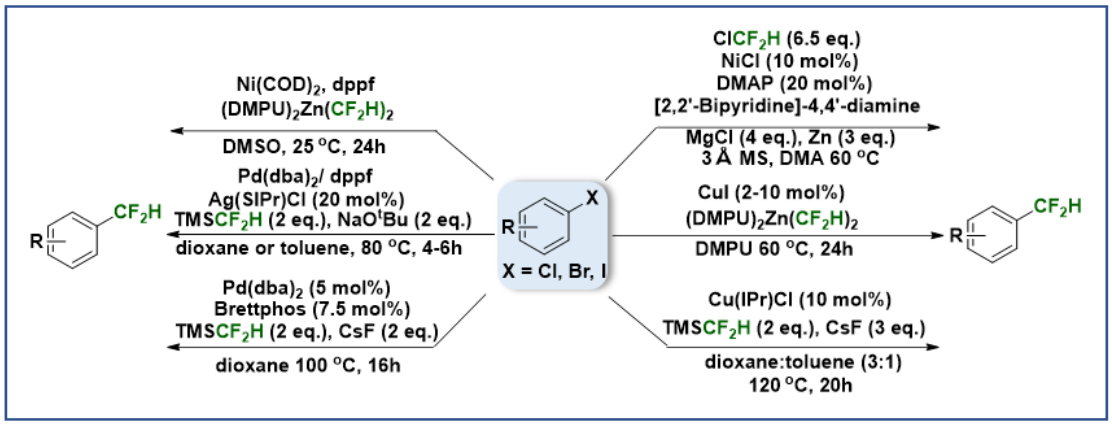

Scheme 1.28 Metal-catalyzed difluoromethylation of aryl halides.

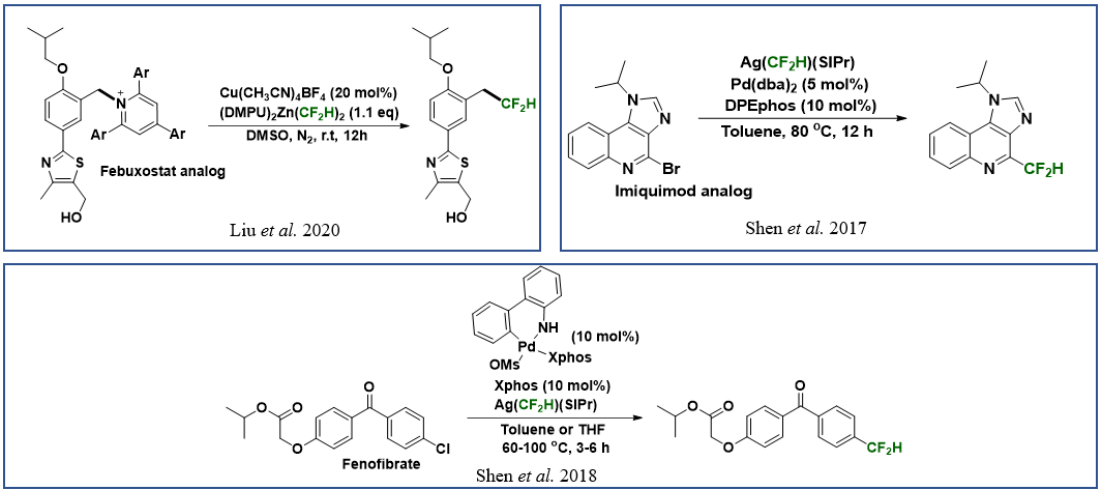

Scheme 1.29 Metal-catalyzed difluoromethylation of bioactive compounds.

cuprate $[Cu(CF_2H)_2]^-$ in equilibrium from the transmetallation of -CF_2H from the Zn complex to CuI.[222] The second example of Cu-catalyzed difluoromethylation of aryl iodides in good yields was reported by Sanford *et al.* in 2017, who explored the use of CuCl(IPr) as a catalyst with $TMSCF_2H$ and 3.0 equiv of CsF at 120 °C for 12 h.[233] Liu and co-workers reported a late-stage deaminative difluoromethylation of drug agents using Vicic`s reagent as the difluoromethyl source and $Cu(CH_3CN)_4BF_4$ as a catalyst in DMSO for 12 h at room temperature (**Scheme 1.29)**.[221] Vicic and co-workers developed a Ni-catalyzed system for difluoromethylation of a variety of electron-deficient aryl iodides using his reagent as a difluoromethyl source and dppf as a ligand.[232] $NiCl_2$ in DME can also catalyze the reaction between chlorodifluoromethane ($ClCF_2H$) and aryl chlorides at 60 °C yielding CF_2H-Ar.[224] $Fe(acac)_3$ in the presence of TMEDA catalyzed difluoromethylation of diaryl zinc reagents using 2-pyridyl sulfone ($2\text{-}PySO_2CF_2H$) as a difluoromethyl source under mild conditions yielding electron-rich and electron-poor CF_2H-Ar (**Scheme 1.30)**.[223]

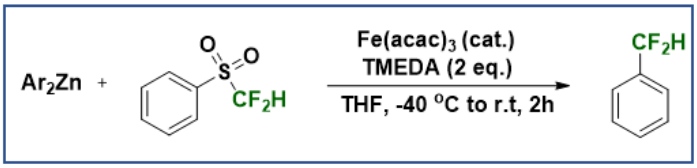

Scheme 1.30 Iron-catalyzed difluoromethylation of diaryl zinc.

1.5.4 Copper-mediated fluoroalkylation

1.5.4.1 From fluoroalkyl iodides

McLoughlin and Thrower first reported an example of a stoichiometric copper-mediated fluoroalkylation of aryl halides using fluoroalkyl iodides (R^F-I) in polar aprotic solvents (DMF or DMSO) at 100-170 ^oC (**Scheme 1.31a**).[141] Two coppers react with R^F-I to give Cu-I + Cu-R^F; The latter then reacts with aryl halide to give the product. Kondo *et al.* 1981 realized a trifluoromethylation of aryl halides using stoichiometric copper (CuI) and sodium trifluoroacetate (CF_3CO_2Na) in aprotic solvents, such as N-methylpyrrolidone (NMP) and N, N-dimethylacetamide (DMA) (**Scheme 1.31b**).[235] Likewise, trifluoromethylarenes were obtained using a more soluble precursor fluorosulphonyl difluoromethyl iodide (FSO_2CF_2I) using a stoichiometric amount of Cu (**Scheme 1.31c**). They proposed that two other reaction pathways besides trifluoromethylation interfered with the reaction yield; difluorocarbene insertion and a free-radical addition-elimination.[236]

1.5.4.2 From Zn(CF_3)Br

In 1997, Shibuya *et al.* observed a transmetallation of [(diethoxyphosphinyl)difluoromethyl] zinc with CuBr that generates organocopper species, promoting the fluoroalkylation of aryl iodides (**Scheme 1.32a)**.[237] The development of trifluoromethylation using a stable solid complex $ZnBr(CF_3)$•2 DMF (stable in a dry-box fridge for weeks)[238] showed the generation of [$Cu(CF_3)$]

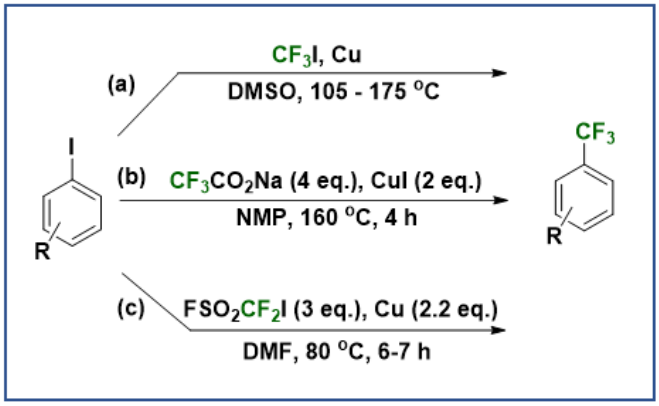

Scheme 1.31 Copper-mediated trifluoromethylation of aryl iodides using fluoroalkanes.

after transmetallation from Zn to CuBr, enabling the trifluoromethylation of electron-deficient aryl halides in moderate yields. ^{19}F NMR monitoring detected the presence of $CuCF_3$, $Cu[Cu(CF_3)_2]$, and $Cu[Cu^{III}(CF_3)_4]$; at higher temperatures (50 ^oC), using less reactive aryl halides, a small quantity of pentafluoroethyl aryl halides was observed and using a mixture of 1:2 ($ZnBr(CF_3)$•2 DMF/ CuBr) converted the trifluoromethylcopper to pentafluoroethylcopper selectively (**Scheme 1.32b**).[239]

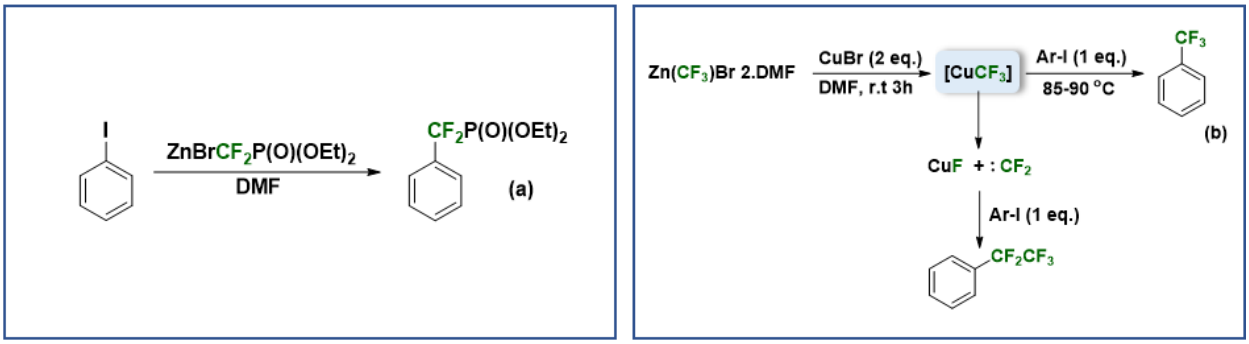

Scheme 1.32 Trifluoromethylation of aryl iodides using $Zn(R^F)Br$.

1.5.4.3 From fluoroalkylsilanes

The most efficient and successful method for trifluoromethylation is using inexpensive and readily available Ruppert-Prakash reagent ($TMSCF_3$) and its derivatives as the fluoroalkyl source.[240] The facile generation of $(CF_3)^-$ anion by addition of catalytic NaI allows for facile transmetallations, and this reagent has been used extensively to prepare different M-CF_3 complexes. For example, Vicic and co-workers in 2008 prepared a bulky $Cu(CF_3)(SIPr)$ complex by treating $[Cu(OtBu)(SIPr)]_2$ with 2.0 equiv of $TMSCF_3$. They then demonstrated stoichiometric CF_3 transfer from this complex to aryl iodides in DMF (**Scheme 1.33a**).[241] A robust and stable phen-ligated trifluoromethylcopper, $Cu(CF_3)(phen)$, known as the Trifluoromethylator,™ was obtained by Hartwig in 96% yield by treatment of [CuOtBu] with 1.0 equiv of phen and 1.1 equiv of $TMSCF_3$. The complex efficiently transferred the CF_3 group to a broad range of aryl iodides (**Scheme 1.33b**).[242] In the same year, Grushin *et al.* prepared the air-stable PPh_3 complex from CuF_2•3 H_2O, PPh_3, and $TMSCF_3$. Addition of phen generated $[Cu(CF_3)(phen)(PPh_3)]$ that was soluble in DMF and efficiently mediated the trifluoromethylation of aryl iodides in moderate yields (**Scheme 1.33c**).[243]

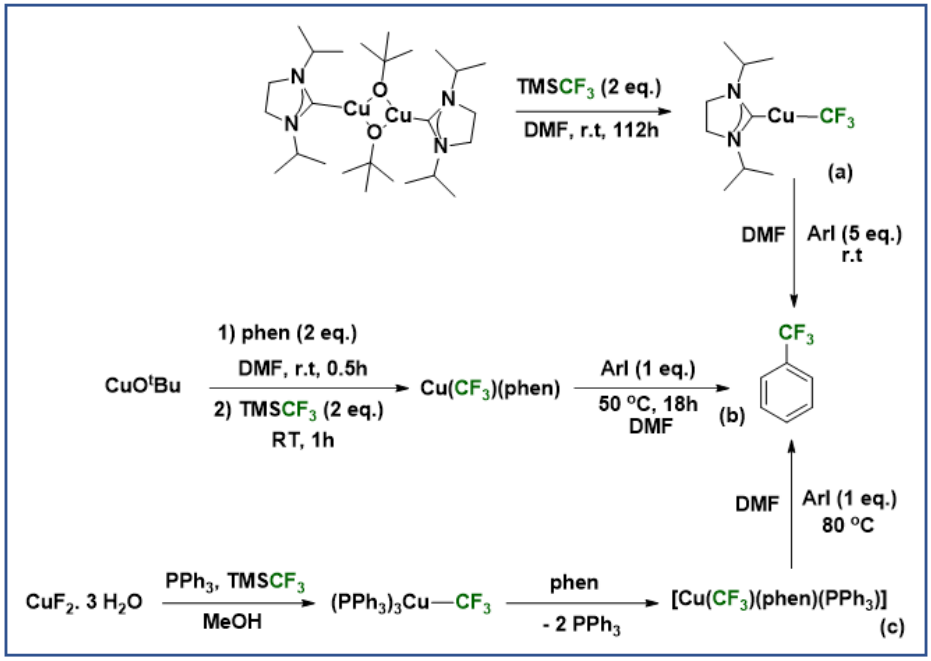

Scheme 1.33 Copper-mediated trifluoromethylation of aryl iodides using $TMSCF_3$ reagent.

Building on the work of Prakash,[244] and Lee[159] from the Baker group, Hu and co-workers used $TMSCF_3$ / NaI to generate the $CuCF_2CF_3$ group from $TMSCF_3$ and optimized conditions for the pentafluoroethylation of aryl iodides.[245] Boutureira *et al.* prepared a storable and stable "ligandless" $[Cu(C_2F_5)]$ from the treatment of excess CuBr, $TMSCF_3$, and KF in DMF at 50 °C (**Scheme 1.34a**). Using ^{19}F NMR monitoring, they adjusted reaction parameters (CuX, solvent, temperature, and reaction time) to adjust the ratio of the homologated products ($CuCF_3$ vs. CuC_2F_5 and CuC_3F_7), showing that CuCl gave a lower yield (vs CuBr) due to the formation of $[Cu(CF_3)_2]^-$. Finally, they could pentafluoroethylate electron-rich alkenyl and heterocycle iodides, including medicinal compound derivatives.[246] Recently, Hu *et al.* investigated a copper-mediated oxidative pentafluoroethylation to heteroaryl boronates and terminal alkynes using $TMSCF_3$ and phen as the ligand in DMF at 50 °C (**Scheme 1.34b**).[247]

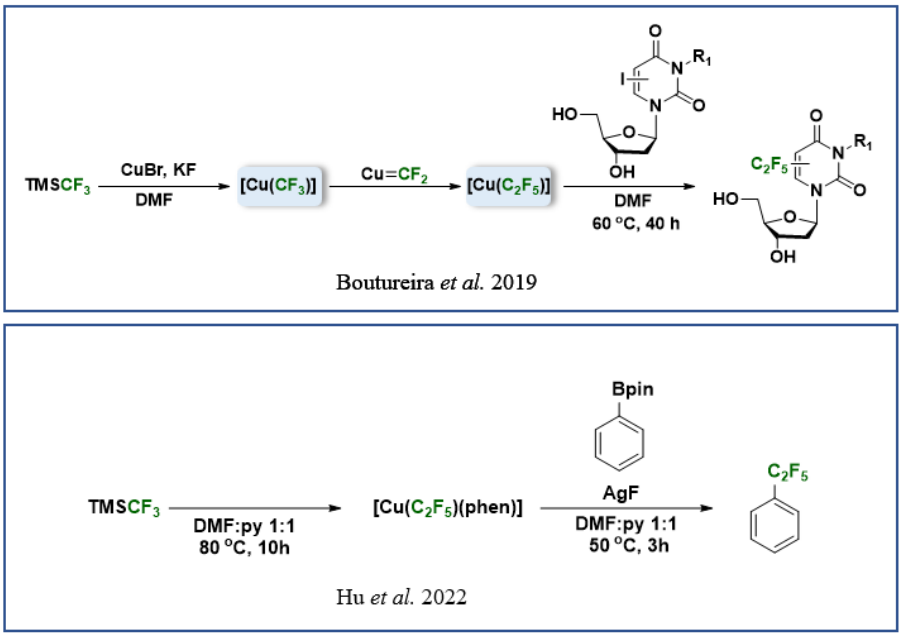

Scheme 1.34 Copper-mediated pentafluoroethylation of aryl iodide and boronate using $TMSCF_3$.

1.5.4.4 From $TMSCF_2H$

We gave many examples of metal-catalyzed difluoromethylation in the above section. However, stoichiometric difluoromethylation using copper was first reported in 2012[248], and the first isolated $[Cu(CF_2H)]$ complex, stabilized by the IPr NHC ligand was reported in 2017.[233] Unlike $[Cu(CF_3)]$, $[Cu(CF_2H)]$ is quite unstable *in situ*, and Hartwig found that using an excess of $TMSCF_2H$ could avoid this problem by conversion to more stable $[Cu(CF_2H)_2]^-$, followed by difluoromethylation of electron-rich aryl iodides in good yields[248]. Years later, Qing observed that phen as ligand combined with a soluble base tBuOK expanded the substrate scope to electron-poor aryl iodides at room temperature.[111] Shen and co-workers isolated stable $[Ag(CF_2H)(SIPr)]$ from [AgCl(SIPr)] and $TMSCF_2H$, which was able to difluoromethylate aryl iodides using CuI and diaryliodonium triflates in MeCN at room temperature.[249] Following the same thinking, two years later, Sanford and co-workers isolated a $[Cu(CF_2H)(IPr)]$ using $TMSCF_2H$ and [Cu(OtBu)(IPr)]. The reaction of electron-rich aryl iodides and 1.25 equiv of $[Cu(CF_2H)(IPr)]$ complex at 90 °C afforded aryl difluoromethylated in good yields.[233] More recently, Jinbo Hu and co-workers reported a tetrafluoroethylation of aryl iodides using $TMSCF_2H$ and $TMSCF_2Br$ as fluorinated source (**Scheme 1.35**).[250]

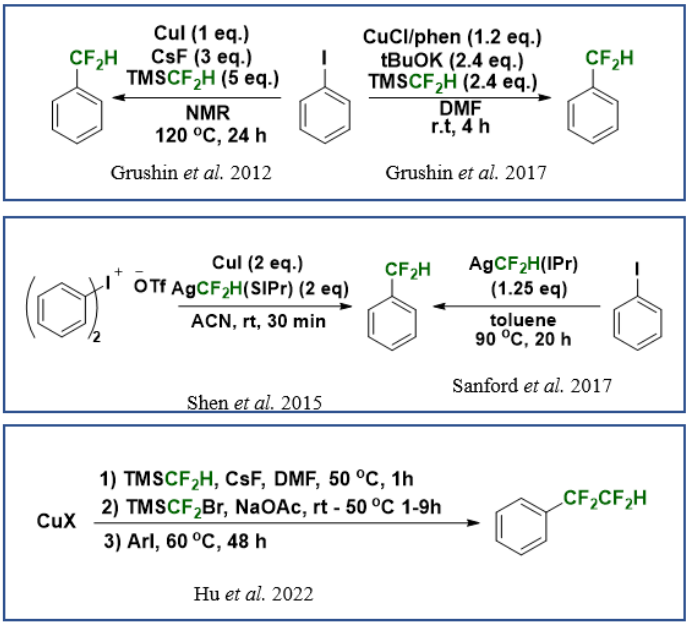

Scheme 1.35 Copper-mediated difluoromethylation using $TMSCF_2H$ as the fluorinated source.

1.5.4.5 From fluoroalkanes and -alkenes

Grushin and co-workers 2011 developed a trifluoromethyl source from a direct cupration of fluoroform (CHF_3). Treatment of CuCl with KO^tBu (1:2) in DMF quickly generates the dialkoxycuprate $K[Cu(O^tBu)_2]$ that directly metallates CHF_3 at room temperature to afford $K[Cu(CF_3)(O^tBu)]$ and Bu^tOH. Addition of $Et_3NF•3HF$ (TREAT HF) stabilizes the $CuCF_3$, preventing defluorination from K^+, and allows for good trifluoromethylation yields for a wide range of electron-deficient and -rich aryl iodides.[251] Two years later, they reported a direct cupration of C_2F_5H under the same conditions, isolating $[K(DMF)_2][Cu(C_2F_5)(O^tBu)]$. This complex gave high yields of pentafluoroethylated boronic acids, benzyl, aryl, and alkenyl bromides (**Scheme 1.36a**).[252]

Building on a previous report in which inexpensive hexafluoropropene gas [CF_2=$CF(CF_3)$, HFP] was inserted into the Ag-F bond to generate an Ag heptafluoroisopropyl (hfip) complex, [253,254] Baker and co-workers in 2018 prepared $Cu[CF(CF_3)_2](PPh_3)_2$ by direct insertion of HFP into the Cu-F bond of $CuF(PPh_3)_3$. Given the insolubility of the latter, they then developed an improved procedure using Stryker`s reagent $[CuH(PPh_3)]_6$, PPh_3 and HFP. Furthermore, inspired by Hartwig[242] and Grushin[243], they prepared the phen adduct $Cu[CF(CF_3)_2](phen)(PPh_3)]$ and observed perfluoroalkylation of aroyl chlorides (**Scheme 1.36b**).[255]

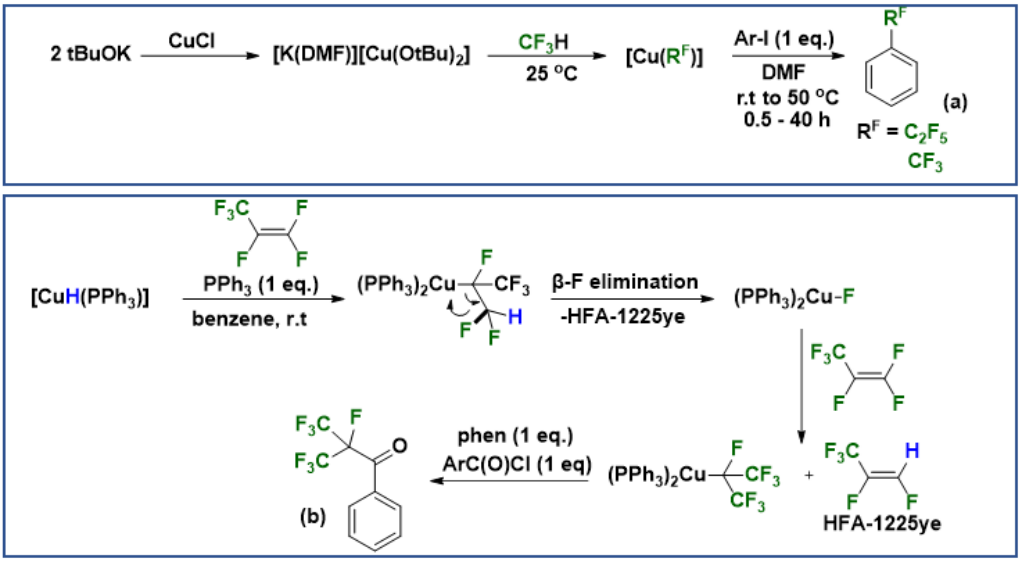

Scheme 1.36 Perfluoroalkylation of aryl iodides using CF_3H (**a**) and HFP (**b**).

1.6 Summary and thesis outline

The powerful and unique features of fluorine allow for its use in a wide range of applications. Moreover, fluorine's very important but often unpredictable behaviour enables us to divide this thesis into two parts, highlighting the special essence of fluorine discussed in this chapter for both the fluorochemical and pharmaceutical industries.

In Chapter 1, we highlight the importance of fluorine in medicinal chemistry and the creation of new fluoroalkyl groups derived from the insertion of fluoroalkenes into Cu-H. Chapter 2 details the synthesis and stabilization of $Cu(CFClCF_2H)$ using the triphos ligand after regioselective insertion of $CFCl=CF_2$ (CTFE) into Cu-H. While our initial attempts to transfer this new R^F group gave only poor to fair yields using aroyl chlorides, further work is needed given the possibility of further functionalization of the C-Cl bond. In Chapter 3, we expand on this work using perfluoro(methyl vinyl ether) (PMVE) to generate a new bifunctional fluoroalkyl containing two important groups (OCF_3 and CF_2H). An extensive study of the ancillary ligands on Cu allowed us to develop the Cu-mediated transfer of the $-CF(OCF_3)CF_2H$ group to aryl iodides; the first example using such a large fluoroalkyl. Further insight into these transfers was provided by our computational chemistry collaborator Christian Ehm (Naples). Chapter 4 builds on Andrella`s work[31,256] with the synthesis and reactivity of $Cu-CF_2CF_2H$ complexes using the stable gas mixture

TFE:CO_2 (1:1) and focuses on the inorganic/bio-organic interface using solvent-stabilized 'ligandless' Cu-CF_2CF_2H reagent for the fluoroalkylation of biologically-active compounds, including nucleosides synthesized in collaboration with the Omar Boutureira group at URV in Tarragona, Spain. In another collaboration with the Michelle Loewen lab at NRC Ottawa, we investigated bioisosteric interactions of different fluoroalkylated compounds with a specific enzyme for antifungal potential.

Environmental concerns relating to GWP mitigated by hydrofluoroalkenes and the necessity to develop new fluorocarbon refrigerants drove us to explore further the reactivity of low-valent nickel precursors with fluoroalkenes in part 2. For Chapter 5, we collaborated with computational fluorine chemist Russell P. Hughes (Dartmouth College) to better understand the electronic factors and ancillary ligand effects associated with metallacyclopentane formation. In Chapter 6, we examine the reactivity of low-valent nickel precursors with functionalized fluoroalkenes (CTFE and PMVE) containing C-Cl and C-OCF_3 bonds, revealing fundamental effects of the ancillary ligands (phosphines, phosphites, and NHCs) on the metallacycle regioselectivity and reactivity with Lewis and Brønsted acids.

Finally, in Chapter 7 we consider our new discoveries within the context of the current state of the art and propose some new directions that they will hopefully enable.

REFERENCES

(1) Wisniak, J. Henri Moissan – The Discoverer of Fluorine. *Educ. Química* **2002**, *13*, 267–274. https://doi.org/10.22201/fq.18708404e.2002.4.66285.

(2) Dolbier, W. R. Fluorine Chemistry at the Millennium. *J. Fluor. Chem.* **2005**, *126* (2), 157–163. https://doi.org/https://doi.org/10.1016/j.jfluchem.2004.09.033.

(3) Shah, P.; Westwell, A. D. The Role of Fluorine in Medicinal Chemistry. *J. Enzyme Inhib. Med. Chem.* **2007**, *22* (5), 527–540. https://doi.org/10.1080/14756360701425014.

(4) O'Hagan, D. Understanding Organofluorine Chemistry. An Introduction to the C–F Bond. *Chem. Soc. Rev.* **2008**, *37* (2), 308–319. https://doi.org/10.1039/B711844A.

(5) Reichenbächer, K.; Süss, H. I.; Hulliger, J. Fluorine in Crystal Engineering—"the Little Atom That Could." *Chem. Soc. Rev.* **2005**, *34* (1), 22–30. https://doi.org/10.1039/B406892K.

(6) Uneyama, K. *Organofluorine Chemistry*, Wiley-Blackwell, 2006, pp 1–100. https://doi.org/https://doi.org/10.1002/9780470988589.ch1.

(7) Bondi, A. Van Der Waals Volumes and Radii. *J. Phys. Chem.* **1964**, *68* (3), 441–451. https://doi.org/10.1021/j100785a001.

(8) Dinoiu, V. Fluorine Chemistry: Past, Present and Future. *Rev. Roum. Chim.* **2007**, *51*, 1141–1152. https://doi.org/10.1002/chin.200744226.

(9) Okazoe, T. Overview on the History of Organofluorine Chemistry from the Viewpoint of Material Industry. *Proc. Jpn. Acad. Ser. B. Phys. Biol. Sci.* **2009**, *85* (8), 276–289. https://doi.org/10.2183/pjab.85.276.

(10) Sicard, A. J.; Baker, R. T. Fluorocarbon Refrigerants and Their Syntheses: Past to Present. *Chem. Rev.* **2020**, *120* (17), 9164–9303. https://doi.org/10.1021/acs.chemrev.9b00719.

(11) Holsteijn, F. van; Kemna, R. Minimizing Food Waste by Improving Storage Conditions in Household Refrigeration. *Resour. Conserv. Recycl.* **2018**, *128*, 25–31. https://doi.org/https://doi.org/10.1016/j.resconrec.2017.09.012.

(12) Cardoso, B. J.; Lamas, F. B.; Gaspar, A. R.; Ribeiro, J. B. Refrigerants Used in the Portuguese Food Industry: Current Status. *Int. J. Refrig.* **2017**, *83*, 60–74. https://doi.org/https://doi.org/10.1016/j.ijrefrig.2017.07.013.

(13) Duret, S.; Hoang, H.-M.; Derens-Bertheau, E.; Delahaye, A.; Laguerre, O.; Guillier, L. Combining Quantitative Risk Assessment of Human Health, Food Waste, and Energy Consumption: The Next Step in the Development of the Food Cold Chain? *Risk Anal.* **2019**, *39* (4), 906–925. https://doi.org/https://doi.org/10.1111/risa.13199.

(14) Holt, LC.; Mattison, E. L. Production of Fluorinated Acyclic Hydrocarbons. US patent 2,0005,713, 1933.

(15) Baker, R. T. Homogeneous Catalytic Hydrodechlorination of Chlorofluorocarbons. US patents 5,300,712, and 5,326,914, 1994.

(16) Iikubo, Y.; Hedrick, V.; Brandstadter, S. C. M. Materials and Methods for the Conversion of Hydrofluorocarbons. Patent WO2004060842, 2004.

(17) Spauschus, H. O. HFC 134a as a Substitute Refrigerant for CFC 12. *Int. J. Refrig.* **1988**, *11* (6), 389–392. https://doi.org/https://doi.org/10.1016/0140-7007(88)90063-1.

(18) Pennetreau, P.; Janssens, F.; Braun, M.; Eicher J.; Rudolph W.; Hausmann, E. Process for the Preparation of 1,1,1,2-Tetrafluoroethane. US patent 5,382,721, 1995.

(19) Bissell, E. R.; Fields, D. B. The Addition of Fluorine to Halogenated Olefins. *J. Org. Chem.* **1964**, *29* (6), 1591–1593. https://doi.org/10.1021/jo01029a078.

(20) Hughes, R. P.; Smith, J. M. Hydrogenolysis of Aliphatic Carbon−Fluorine Bonds in Fluoroalkyl−Iridium Complexes to Give Hydrofluorocarbons. *J. Am. Chem. Soc.* **1999**, *121* (25), 6084–6085. https://doi.org/10.1021/ja990490z.

(21) Giddis, C. R.; Stewart, P. H. Production of Hydrofluoroalkanes, patent WO2002018304A3, 2005.

(22) Ciconkov, R. Refrigerants: There Is Still No Vision for Sustainable Solutions. *Int. J. Refrig.* **2018**, *86*, 441–448. https://doi.org/https://doi.org/10.1016/j.ijrefrig.2017.12.006.

(23) Ko, M.; Shia, R.-L.; Sze, N.-D.; Magid, H.; Bray, R. G. Atmospheric Lifetime and Global Warming Potential of HFC-245fa. *J. Geophys. Res. Atmos.* **1999**, *104* (D7), 8173–8181. https://doi.org/https://doi.org/10.1029/1998JD100097.

(24) Pabon, J. J. G.; Khosravi, A.; Belman-Flores, J. M.; Machado, L.; Revellin, R. Applications of Refrigerant R1234yf in Heating, Air Conditioning and Refrigeration Systems: A Decade of Researches. *Int. J. Refrig.* **2020**, *118*, 104–113. https://doi.org/https://doi.org/10.1016/j.ijrefrig.2020.06.014.

(25) Raabe, G. Molecular Simulation Studies on the Vapor–Liquid Phase Equilibria of Binary Mixtures of R-1234yf and R-1234ze(E) with R-32 and CO_2. *J. Chem. Eng. Data* **2013**, *58* (6), 1867–1873. https://doi.org/10.1021/je4002619.

(26) Nielsen, O. J.; Javadi, M. S.; Sulbaek Andersen, M. P.; Hurley, M. D.; Wallington, T. J.; Singh, R. Atmospheric Chemistry of CF_3CFCH_2: Kinetics and Mechanisms of Gas-Phase Reactions with Cl Atoms, OH Radicals, and O_3. *Chem. Phys. Lett.* **2007**, *439* (1), 18–22. https://doi.org/https://doi.org/10.1016/j.cplett.2007.03.053.

(27) Arora, P.; Tyagi, A.; Seshadri, G. Fourth Generation Refrigerant: HFO 1234 Yf. *Curr. Sci.* **2018**, *115*, 1497. https://doi.org/10.18520/cs/v115/i8/1497-1503.

(28) Vollmer, M. K.; Reimann, S.; Hill, M.; Brunner, D. First Observations of the Fourth Generation Synthetic Halocarbons HFC-1234yf, HFC-1234ze(E), and HCFC-1233zd(E) in the Atmosphere. *Environ. Sci. Technol.* **2015**, *49* (5), 2703–2708. https://doi.org/10.1021/es505123x.

(29) Van der Puy, M. Process for the Preparation of 2,3,3,3-Tetrafluoropropene (HFO-1234yf).US patent US8071826B2, 2011.

(30) Terazono, S.; Wang, X.; Kanda, M.; Kawaguchi, S.; Kasagawa, M. Process for Producing Hydrofluoroolefin. Patent EP3187477A4, 2005

(31) Andrella, N. O.; Xu, N.; Gabidullin, B. M.; Ehm, C.; Baker, R. T. Selective Copper Complex-Catalyzed Hydrodefluorination of Fluoroalkenes and Allyl Fluorides: A Tale of Two Mechanisms. *J. Am. Chem. Soc.* **2019**, *141* (29), 11506–11521. https://doi.org/10.1021/jacs.9b03101.

(32) Murphy, E. F.; Murugavel, R.; Roesky, H. W. Organometallic Fluorides: Compounds Containing Carbon−Metal−Fluorine Fragments of d-Block Metals. *Chem. Rev.* **1997**, *97* (8), 3425–3468. https://doi.org/10.1021/cr960365v.

(33) Kaesz, H. D.; King, R. B.; Stone, F. G. A. Chemistry of the Metal Carbonyls VIII: Perfluoroacyl and Perfluoroalkyl Derivatives of Manganese and Rhenium. *Z. Naturforsch. B* **1960**, *15* (12), 763–764. https://doi.org/doi:10.1515/znb-1960-1202.

(34) McClellan, W. R. Perfluoroalkyl and Perfluoroacyl Metal Carbonyls. *J. Am. Chem. Soc.* **1961**, *83* (7), 1598–1600. https://doi.org/10.1021/ja01468a012.

(35) King, R. B.; Stafford, S. L.; Treichel, P. M.; Stone, F. G. A. Chemistry of the Metal Carbonyls. XV. Fluorocarbon Derivatives of Iron Carbonyl. *J. Am. Chem. Soc.* **1961**, *83* (17), 3604–3608. https://doi.org/10.1021/ja01478a016.

(36) Browning, J.; Cundy, C. S.; Green, M.; Stone, F. G. A. Hexafluoroacetone and Hexafluorothioacetone Nickel Complexes. *J. Chem. Soc. A Inorganic, Phys. Theor.* **1969**, No. 0, 20–23. https://doi.org/10.1039/J19690000020.

(37) Manuel, T. A.; Stafford, S. L.; Stone, F. G. A. Chemistry of the Metal Carbonyls. VII. Perfluoroalkyl Iron Compounds. *J. Am. Chem. Soc.* **1961**, *83* (1), 249–250. https://doi.org/10.1021/ja01462a052.

(38) Kaplan, P. T.; Xu, L.; Chen, B.; McGarry, K. R.; Yu, S.; Wang, H.; Vicic, D. A. Mild, Safe, and Versatile Reagents for (CF2)n Transfer and the Construction of Fluoroalkyl-Containing Rings. *Organometallics* **2013**, *32* (24), 7552–7558. https://doi.org/10.1021/om401016k.

(39) Cundy, C. S.; Green, M.; Stone, F. G. A. Reactions of Low-Valent Metal Complexes with Fluorocarbons. Part XII. Fluoro-Olefin Reactions of Zerovalent Nickel Complexes. *J. Chem. Soc. A Inorganic, Phys. Theor.* **1970**, No. 0, 1647–1653. https://doi.org/10.1039/J19700001647.

(40) Ohashi, M.; Shibata, M.; Saijo, H.; Kambara, T.; Ogoshi, S. Carbon–Fluorine Bond Activation of Tetrafluoroethylene on Palladium(0) and Nickel(0): Heat or Lewis Acidic Additive Promoted Oxidative Addition. *Organometallics* **2013**, *32* (13), 3631–3639. https://doi.org/10.1021/om400255t.

(41) Xue, T.; Cramer, R. E.; Vicic, D. A. Access to Perfluorometallacyclopentane Complexes of Cobalt through the $[(MeCN)_4Co(C_4F_8)][PF_6]$ Precursor. *Organometallics* **2021**, *40* (21), 3585–3590. https://doi.org/10.1021/acs.organomet.1c00469.

(42) Yu, S.; Dudkina, Y.; Wang, H.; Kholin, K. V; Kadirov, M. K.; Budnikova, Y. H.; Vicic, D. A. Accessing Perfluoroalkyl Nickel(II), (III), and (IV) Complexes Bearing a Readily Attached $[C_4F_8]$ Ligand. *Dalton Trans.* **2015**, *44* (45), 19443–19446. https://doi.org/10.1039/C5DT01771H.

(43) Green, M.; Laguna, A.; Spencer, J. L.; Stone, F. G. A. Reactions of Low-Valent Metal Complexes with Fluorocarbons. Part 31. Bis(η-Cyclo-Octa-1,5-Diene)-Platinum and -Palladium, with Fluoroolefins. *J. Chem. Soc., Dalton Trans.* **1977**, No. 10, 1010–1016. https://doi.org/10.1039/DT9770001010.

(44) Green, M.; Osborn, R. B. L.; Rest, A. J.; Stone, F. G. A. Fluorocarbon Platinum Complexes. *J. Chem. Soc. A Inorganic, Phys. Theor.* **1968**, No. 0, 2525–2530. https://doi.org/10.1039/J19680002525.

(45) Green, M.; Osborn, R. B. L.; Rest, A. J.; Stone, F. G. A. Fluorocarbon Platinum Complexes. *Chem. Commun.* **1966**, No. 15, 502–503. https://doi.org/10.1039/C19660000502.

(46) Mays, M. J.; Wilkinson, G. 1220. Transition-Metal Fluorocarbon Complexes. Part VII. Some Complexes of Cobalt and Rhodium with Tetrafluoroethylene, Chlorotrifluoroethylene, and Hexafluorobut-2-Yne. *J. Chem. Soc.* **1965**, No. 0, 6629–6634. https://doi.org/10.1039/JR9650006629.

(47) Evans, J. A.; Russell, D. R. The Crystal Structures of Ethylene and Tetrafluoroethylene

Complexes of Rhodium(I). *J. Chem. Soc. D Chem. Commun.* **1971**, No. 4, 197–198. https://doi.org/10.1039/C29710000197.

(48) Cramer, R.; Parshall, G. W. Tetrafluoroethylene Complexes of Transition Metals. *J. Am. Chem. Soc.* **1965**, *87* (6), 1392–1393. https://doi.org/10.1021/ja01084a048.

(49) Mukhedkar, A. J.; Mukhedkar, V. A.; Green, M.; Stone, F. G. A. Reactions of Low-Valent Metal Complexes with Fluorocarbons. Part XV. Acetylacetonatobis(Methyldiphenyl- or Triphenyl-Phosphine)Rhodium. *J. Chem. Soc. A Inorganic, Phys. Theor.* **1970**, No. 0, 3166–3171. https://doi.org/10.1039/J19700003166.

(50) Empsall, H. D.; Green, M.; Stone, F. G. A. Reactions of Low-Valent Metal Complexes with Fluorocarbons. Part XXI. Five-Membered Ring Complexes from Phosphine, Arsine, and Phosphite Palladium (0) Compounds. *J. Chem. Soc., Dalton Trans.* **1972**, No. 1, 96–101. https://doi.org/10.1039/DT9720000096.

(51) Green, M.; Shakshooki, S. K.; Stone, F. G. A. Reactions of Low-Valent Metal Complexes with Fluorocarbons. Part XVIII t-Butyl Isocyanide–Nickel Complexes. *J. Chem. Soc. A Inorg. Phys. Theor.* **1971**, No. 0, 2828–2834. https://doi.org/10.1039/J19710002828.

(52) Baker, R. T.; Beatty R. P.; Farnham, W. B.; Wallace, R. L. Process for the Manufacturing of Selected Halogenated Hydrocarbons Containing Fluorine and Hydrogen and Compositions Provided Therein. U. S. patents 5,670,679, 1996 and 5,760,282, 1998.

(53) Burch, R. R.; Calabrese, J. C.; Ittel, S. D. Fluoroorganometallic Chemistry: Carbon-Fluorine Bond Activation in Perfluorometallacyclopentane Complexes. *Organometallics* **1988**, *7* (7), 1642–1648. https://doi.org/10.1021/om00097a030.

(54) Andrella, N. O.; Sicard, A. J.; Gorelsky, S. I.; Korobkov, I.; Baker, R. T. A T-Shaped Ni[κ^2-$(CF_2)_4$–] NHC Complex: Unusual C_{Sp3}–F and M–C^F Bond Functionalization Reactions. *Chem. Sci.* **2015**, *6* (11), 6392–6397. https://doi.org/10.1039/C5SC01886B.

(55) Giffin, K. A.; Harrison, D. J.; Korobkov, I.; Baker, R. T. Activation of C–F and Ni–C Bonds of [P,S]-Ligated Nickel Perfluorometallacycles. *Organometallics* **2013**, *32* (24), 7424–7430. https://doi.org/10.1021/om400933k.

(56) Giffin, KA; Pua, LA; Piotrkowski, S; Gabidullin, BM; Korobkov, I; Hughes, RP; Baker, R. Generation of Hydrofluoronickelacycles from Trifluoroethylene and Ni(0): Ligand Effects on Regio-/Stereoselectivity and Reactivity. *J. Am. Chem. Soc.* **2017**, *139* (11), 4075–4086. https://doi.org/10.1021/jacs.6b12607.

(57) Fried, J.; Sabo, E. F. Synthesis of 17α-Hydroxycorticosterone and Its 9α-Halo Derivatives from 11-Epi-17α-Hydroxycorticosterone. *J. Am. Chem. Soc.* **1953**, *75* (9), 2273–2274. https://doi.org/10.1021/ja01105a527.

(58) Longley, D. B.; Harkin, D. P.; Johnston, P. G. 5-Fluorouracil: Mechanisms of Action and Clinical Strategies. *Nat. Rev. Cancer* **2003**, *3* (5), 330–338. https://doi.org/10.1038/nrc1074.

(59) Inoue, M.; Sumii, Y.; Shibata, N. Contribution of Organofluorine Compounds to Pharmaceuticals. *ACS Omega* **2020**, *5* (19), 10633–10640. https://doi.org/10.1021/acsomega.0c00830.

(60) Cohen, MH; Williams, GA; Sridhara, R; Chen, G; McGuinn, WDJr; Morse, D.; Abraham, S; Rahman, A; Liang, C; Lostritto, R; Baird, A; Pazdur, R. United States Food and Drug Administration Drug Approval Summary: Gefitinib (ZD1839; Iressa) Tablets. *Clin. Cancer Res.* **2004**, *10* (4), 1212–1218. https://doi.org/10.1158/1078-0432.ccr-03-0564.

(61) Wilhelm, S. M.; Adnane, L.; Newell, P.; Villanueva, A.; Llovet, J. M.; Lynch, M. Preclinical Overview of Sorafenib, a Multikinase Inhibitor That Targets Both Raf and VEGF and PDGF Receptor Tyrosine Kinase Signaling. *Mol. Cancer Ther.* **2008**, *7* (10), 3129–3140. https://doi.org/10.1158/1535-7163.MCT-08-0013.

(62) Herbrecht, R. Voriconazole: Therapeutic Review of a New Azole Antifungal. *Expert Rev. Anti. Infect. Ther.* **2004**, *2* (4), 485–497. https://doi.org/10.1586/14787210.2.4.485.

(63) Dorr, P; Westby, M; Dobbs, S; Griffin, P; Irvine, B; Macartney, M; Mori, J; Rickett, G; Smith-Burchnell, C; Napier, C; Napier, C; Webster, R; Armour, D.; Price, D Stammen, Blanda Wood, A;Perros, M. Maraviroc (UK-427,857), a Potent, Orally Bioavailable, and Selective Small-Molecule Inhibitor of Chemokine Receptor CCR5 with Broad-Spectrum Anti-Human Immunodeficiency Virus Type 1 Activity. *Antimicrob. Agents Chemother.* **2005**, *49* (11), 4721–4732. https://doi.org/10.1128/AAC.49.11.4721-4732.2005.

(64) Sánchez, C.; Bøgesø, K. P.; Ebert, B.; Reines, E. H.; Braestrup, C. Escitalopram versus Citalopram: The Surprising Role of the R-Enantiomer. *Psychopharmacology (Berl).* **2004**, *174* (2), 163–176. https://doi.org/10.1007/s00213-004-1865-z.

(65) Caccia, S.; Pasina, L.; Nobili, A. New Atypical Antipsychotics for Schizophrenia: Iloperidone. *Drug Des. Devel. Ther.* **2010**, *4*, 33–48. https://doi.org/10.2147/dddt.s6443.

(66) Wheless, J. W.; Vazquez, B. Rufinamide: A Novel Broad-Spectrum Antiepileptic Drug. *Epilepsy Curr.* **2010**, *10* (1), 1–6. https://doi.org/10.1111/j.1535-7511.2009.01336.x.

(67) Hansen, B; Hsiao, Y; Xu, F; Rivera, N; Clausen, A; Kubryk, M; Krska, S; Rosner, T; Simmons, B; Balsells, J; Ikemoto, N; Sun, Y; Spindler, F; Malan, C; Grabowski, E; Armstrong, J. Highly Efficient Asymmetric Synthesis of Sitagliptin. *J. Am. Chem. Soc.* **2009**, *131* (25), 8798–8804. https://doi.org/10.1021/ja902462q.

(68) Veverka, A.; Salinas, J. L. Nebivolol in the Treatment of Chronic Heart Failure. *Vasc. Health Risk Manag.* **2007**, *3* (5), 647–654.

(69) Murdoch, D.; Scott, L. J. Ezetimibe/Simvastatin. *Am. J. Cardiovasc. Drugs* **2004**, *4* (6), 405–422. https://doi.org/10.2165/00129784-200404060-00009.

(70) Kaan, HYK; Ulaganathan, V.; Rath, O; Prokopcová, H; Dallinger, D; Kappe, CO Kozielski, F. Structural Basis for Inhibition of Eg5 by Dihydropyrimidines: Stereoselectivity of Antimitotic Inhibitors Enastron, Dimethylenastron and Fluorastrol. *J. Med. Chem.* **2010**, *53* (15), 5676–5683. https://doi.org/10.1021/jm100421n.

(71) Kim, J. H.; Scialli, A. R. Thalidomide: The Tragedy of Birth Defects and the Effective Treatment of Disease. *Toxicol. Sci.* **2011**, *122* (1), 1–6. https://doi.org/10.1093/toxsci/kfr088.

(72) Tokunaga, E.; Akiyama, H.; Soloshonok, V. A.; Inoue, Y.; Hara, H.; Shibata, N. Biological Evaluation of Both Enantiomers of Fluoro-Thalidomide Using Human

Myeloma Cell Line H929 and Others. *PLoS One* **2017**, *12* (8), e0182152.

(73) Gillis, E. P.; Eastman, K. J.; Hill, M. D.; Donnelly, D. J.; Meanwell, N. A. Applications of Fluorine in Medicinal Chemistry. *J. Med. Chem.* **2015**, *58* (21), 8315–8359. https://doi.org/10.1021/acs.jmedchem.5b00258.

(74) Kumar, V.; Rozners, E. Fluorobenzene Nucleobase Analogues for Triplex-Forming Peptide Nucleic Acids. *ChemBioChem* **2022**, *23* (3), e202100560. https://doi.org/https://doi.org/10.1002/cbic.202100560.

(75) Chan, K. Y.; Kinghorn, A. B.; Hollenstein, M.; Tanner, J. A. Chemical Modifications for a Next Generation of Nucleic Acid Aptamers. *ChemBioChem* **2022**, *n/a* (n/a), e202200006. https://doi.org/https://doi.org/10.1002/cbic.202200006.

(76) Kataev, V. E.; Garifullin, B. F. Antiviral Nucleoside Analogs. *Chem. Heterocycl. Compd.* **2021**, *57* (4), 326–341. https://doi.org/10.1007/s10593-021-02912-8.

(77) Matsuda, A.; Sasaki, T. Antitumor Activity of Sugar-Modified Cytosine Nucleosides. *Cancer Sci.* **2004**, *95* (2), 105–111. https://doi.org/https://doi.org/10.1111/j.1349-7006.2004.tb03189.x.

(78) Bassetto, M.; Slusarczyk, M. Therapeutic Use of Fluorinated Nucleosides – Progress in Patents. *Pharm. Pat. Anal.* **2018**, *7* (6), 277–299. https://doi.org/10.4155/ppa-2018-0028.

(79) Cavaliere, A.; Probst, K. C.; Westwell, A. D.; Slusarczyk, M. Fluorinated Nucleosides as an Important Class of Anticancer and Antiviral Agents. *Future Med. Chem.* **2017**, *9* (15), 1809–1833. https://doi.org/10.4155/fmc-2017-0095.

(80) McGavin, J. K.; Goa, K. L. Capecitabine: A Review of Its Use in the Treatment of Advanced or Metastatic Colorectal Cancer. *Drugs* **2001**, *61 15*, 2309–2326.

(81) Wagstaff, A. J.; Ibbotson, T.; Goa, K. L. Spotlight on Capecitabine in the Management of Advanced Breast Cancer. *Am. J. Cancer* **2003**, *2* (2), 137–140. https://doi.org/10.2165/00024669-200302020-00008.

(82) Walko, C. M.; Lindley, C. Capecitabine: A Review. *Clin. Ther.* **2005**, *27* (1), 23–44. https://doi.org/10.1016/j.clinthera.2005.01.005.

(83) Koukourakis, G. V; Kouloulias, V.; Koukourakis, M. J.; Zacharias, G. A.; Zabatis, H.; Kouvaris, J. Efficacy of the Oral Fluorouracil Pro-Drug Capecitabine in Cancer Treatment: A Review. *Molecules*. 2008. https://doi.org/10.3390/molecules13081897.

(84) Heidelberger, C.; Parsons, D. G.; Remy, D. C. Syntheses of 5-Trifluoromethyluracil and 5-Trifluoromethyl-2'-Deoxyuridine1,2. *J. Med. Chem.* **1964**, *7* (1), 1–5. https://doi.org/10.1021/jm00331a001.

(85) Kataoka, Y; Iimori, M; Niimi, S; Tsukihara, H; Wakasa, T.; Saeki, H; Oki, E; Maehara, Y; Kitao, H. Cytotoxicity of Trifluridine Correlates with the Thymidine Kinase 1 Expression Level. *Sci. Rep.* **2019**, *9* (1), 7964. https://doi.org/10.1038/s41598-019-44399-6.

(86) Johnson, B. M.; Shu, Y.-Z.; Zhuo, X.; Meanwell, N. A. Metabolic and Pharmaceutical Aspects of Fluorinated Compounds. *J. Med. Chem.* **2020**, *63* (12), 6315–6386.

https://doi.org/10.1021/acs.jmedchem.9b01877.

(87) Chan, B. M.; Hochster, H. S.; Lenz, H.-J. The Safety and Efficacy of Trifluridine-Tipiracil for Metastatic Colorectal Cancer: A Pharmacy Perspective. *Am. J. Heal. Pharm.* **2019**, *76* (6), 339–348. https://doi.org/10.1093/ajhp/zxy006.

(88) Spertus, C. B.; Mohammed, H. O.; Ledbetter, E. C. Effects of Topical Ocular Application of 1% Trifluridine Ophthalmic Solution in Dogs with Experimentally Induced Recurrent Ocular Canine Herpesvirus-1 Infection. *Am. J. Vet. Res.* **2016**, *77* (10), 1140–1147. https://doi.org/10.2460/ajvr.77.10.1140.

(89) Skevaki, C. L.; Galani, I. E.; Pararas, M. V; Giannopoulou, K. P.; Tsakris, A. Treatment of Viral Conjunctivitis with Antiviral Drugs. *Drugs* **2011**, *71* (3), 331–347. https://doi.org/10.2165/11585330-000000000-00000.

(90) Wu, W.; You, Y.; Weng, Z. Recent Advances in the Synthesis of Fluoroalkylated Compounds Using Fluoroalkyl Anhydrides. *Chin. Chem. Lett.* **2022**. https://doi.org/https://doi.org/10.1016/j.cclet.2022.01.038.

(91) McDonald, E. G.; Lee, T. C. Nirmatrelvir-Ritonavir for COVID-19. *Can. Med. Assoc. J.* **2022**, *194* (6), E218 LP-E218. https://doi.org/10.1503/cmaj.220081.

(92) Lamb, Y. N. Nirmatrelvir Plus Ritonavir: First Approval. *Drugs* **2022**, *82* (5), 585–591. https://doi.org/10.1007/s40265-022-01692-5.

(93) Owen, DR; Allerton, CMN; Anderson AS; Aschenbrenner, L; Avery, M; Berritt, S; Boras, B; Cardin, RD; Carlo, A; Coffman, K.; Dantonio, A; Di, L; Eng, H; Ferre, R; Gajiwala, KS; Gibson, SA; Greasley, S.; Hurs, BL; Kadar, E.; Kalgutkar, AS; Lee JC; Lee, J; Liu W; Mason, SW; Noell, S.; Novak, JJ; Obach RS; Ogilvie, K; Patel, NC; Pettersson, M.; Rai, DK; Reese, MR; Sammons, MF; Sathish, J.; Singh, RSP; Steppan, C.; Stewart, AE; Tuttle, J.; Lawrence, U; Verhoest, P.; Liuqing, W; Qingyi, Y; Yuao, Z. An Oral SARS-CoV-2 Mpro Inhibitor Clinical Candidate for the Treatment of COVID-19. *Science* **2021**, *374* (6575), 1586–1593. https://doi.org/10.1126/science.abl4784.

(94) Saravolatz, L. D.; Depcinski, S.; Sharma, M. Molnupiravir and Nirmatrelvir-Ritonavir: Oral COVID Antiviral Drugs. *Clin. Infect. Dis.* **2022**, ciac180. https://doi.org/10.1093/cid/ciac180.

(95) Zhang C. Fluorine in Medicinal Chemistry: In Perspective to COVID-19. *ChemRxiv. Cambridge Open Engag.* **2022**.

(96) Grillo, R.; Fraceto, L. F.; Amorim, M. J. B.; Scott-Fordsmand, J. J.; Schoonjans, R.; Chaudhry, Q. Ecotoxicological and Regulatory Aspects of Environmental Sustainability of Nanopesticides. *J. Hazard. Mater.* **2021**, *404*, 124148. https://doi.org/https://doi.org/10.1016/j.jhazmat.2020.124148.

(97) Ogawa, Y.; Tokunaga, E.; Kobayashi, O.; Hirai, K.; Shibata, N. Current Contributions of Organofluorine Compounds to the Agrochemical Industry. *iScience* **2020**, *23* (9), 101467. https://doi.org/https://doi.org/10.1016/j.isci.2020.101467.

(98) Jeschke, P. Current Trends in the Design of Fluorine-Containing Agrochemicals. in *Organofluorine Chemistry*, Szabo, K; Selander, N., Eds. Wiley, 2021, pp 363–395.

https://doi.org/https://doi.org/10.1002/9783527825158.ch11.

(99) Jeschke, P. Latest Generation of Halogen-Containing Pesticides. *Pest Manag. Sci.* **2017**, *73* (6), 1053–1066. https://doi.org/https://doi.org/10.1002/ps.4540.

(100) Kiel, M.; Engesser, K.-H. The Biodegradation vs. Biotransformation of Fluorosubstituted Aromatics. *Appl. Microbiol. Biotechnol.* **2015**, *99* (18), 7433–7464. https://doi.org/10.1007/s00253-015-6817-5.

(101) Alexandrino, D. A. M.; Almeida, C. M. R.; Mucha, A. P.; Carvalho, M. F. Revisiting Pesticide Pollution: The Case of Fluorinated Pesticides. *Environ. Pollut.* **2022**, *292*, 118315. https://doi.org/https://doi.org/10.1016/j.envpol.2021.118315.

(102) Wang, Q.; Song, H.; Wang, Q. Fluorine-Containing Agrochemicals in the Last Decade and Approaches for Fluorine Incorporation. *Chin. Chem. Lett.* **2022**, *33* (2), 626–642. https://doi.org/https://doi.org/10.1016/j.cclet.2021.07.064.

(103) Li, S.; Li, X.; Zhang, H.; Wang, Z.; Xu, H. The Research Progress in and Perspective of Potential Fungicides: Succinate Dehydrogenase Inhibitors. *Bioorg. Med. Chem.* **2021**, *50*, 116476. https://doi.org/https://doi.org/10.1016/j.bmc.2021.116476.

(104) Hawkins, N. J.; Fraaije, B. A. Contrasting Levels of Genetic Predictability in the Evolution of Resistance to Major Classes of Fungicides. *Mol. Ecol.* **2021**, *30* (21), 5318–5327. https://doi.org/https://doi.org/10.1111/mec.15877.

(105) Luo, B.; Ning, Y. Comprehensive Overview of Carboxamide Derivatives as Succinate Dehydrogenase Inhibitors. *J. Agric. Food Chem.* **2022**, *70* (4), 957–975. https://doi.org/10.1021/acs.jafc.1c06654.

(106) Xiong, L; Li, H; Jiang, L.; Ge, J; Yang, W; Zhu, XLY; Guang, F. Structure-Based Discovery of Potential Fungicides as Succinate Ubiquinone Oxidoreductase Inhibitors. *J. Agric. Food Chem.* **2017**, *65* (5), 1021–1029. https://doi.org/10.1021/acs.jafc.6b05134.

(107) Zhu, X.-L.; Xiong, L.; Li, H.; Song, X.-Y.; Liu, J.-J.; Yang, G.-F. Computational and Experimental Insight into the Molecular Mechanism of Carboxamide Inhibitors of Succinate-Ubquinone Oxidoreductase. *ChemMedChem* **2014**, *9* (7), 1512–1521. https://doi.org/https://doi.org/10.1002/cmdc.201300456.

(108) Xu, L.; Du, S.; Li, Z.; Tian, Z. Synthesis, Antifungal Activity and QSAR of Novel Pyrazole Amides as Succinate Dehydrogenase Inhibitors. *Heterocycles* **2018**, *96*, 74.

(109) Li, S.; Li, D.; Xiao, T.; Zhang, S.; Song, Z.; Ma, H. Design, Synthesis, Fungicidal Activity, and Unexpected Docking Model of the First Chiral Boscalid Analogues Containing Oxazolines. *J. Agric. Food Chem.* **2016**, *64* (46), 8927–8934. https://doi.org/10.1021/acs.jafc.6b03464.

(110) Zhang, L.; Li, W.; Xiao, T.; Song, Z.; Csuk, R.; Li, S. Design and Discovery of Novel Chiral Antifungal Amides with 2-(2-Oxazolinyl)Aniline as a Promising Pharmacophore. *J. Agric. Food Chem.* **2018**, *66* (34), 8957–8965. https://doi.org/10.1021/acs.jafc.8b02778.

(111) Yang, Z.; Sun, Y.; Liu, Q.; Li, A.; Wang, W.; Gu, W. Design, Synthesis, and Antifungal Activity of Novel Thiophene/Furan-1,3,4-Oxadiazole Carboxamides as Potent Succinate

Dehydrogenase Inhibitors. *J. Agric. Food Chem.* **2021**, *69* (45), 13373–13385. https://doi.org/10.1021/acs.jafc.1c03857.

(112) Desbordes, P.; Essigmann, B.; Gary, S.; Gutbrod, O.; Maue, M.; Schwarz, H.-G. Isoflucypram, the First Representative of a New Succinate Dehydrogenase Inhibitor Fungicide Subclass: Its Chemical Discovery and Unusual Binding Mode. *Pest Manag. Sci.* **2020**, *76* (10), 3340–3347. https://doi.org/10.1002/ps.5951.

(113) Shao, W; Wang, J.; Wang, H; Wen, Z; Liu, C; Zhang, Y; Zhao, Y; Ma, Z. Fusarium Graminearum FgSdhC1 Point Mutation A78V Confers Resistance to the Succinate Dehydrogenase Inhibitor Pydiflumetofen. *Pest Manag. Sci.* **2022**, *78* (5), 1780–1788. https://doi.org/https://doi.org/10.1002/ps.6795.

(114) Maienfisch, P.; Mangelinckx, S. Chapter 1 - Recent Innovation in Crop Protection Research, in *Recent Highlights in the Discovery and Optimization of Crop Protection Products*, Maienfisch, P., Mangelinckx, S., Eds. Academic Press, 2021; pp 1–23. https://doi.org/https://doi.org/10.1016/B978-0-12-821035-2.00001-2.

(115) Britton, R; Gouverneur, V; Lin, J; Meanwell, M; Ni, C; Pupo, G; Xiao, J; Hu, J. Contemporary Synthetic Strategies in Organofluorine Chemistry. *Nat. Rev. Methods Prim.* **2021**, *1* (1), 47. https://doi.org/10.1038/s43586-021-00042-1.

(116) Campbell, M. G.; Ritter, T. Modern Carbon–Fluorine Bond Forming Reactions for Aryl Fluoride Synthesis. *Chem. Rev.* **2015**, *115* (2), 612–633. https://doi.org/10.1021/cr500366b.

(117) Liang, T.; Neumann, C. N.; Ritter, T. Introduction of Fluorine and Fluorine-Containing Functional Groups. *Angew. Chem. Int. Ed.* **2013**, *52* (32), 8214–8264. https://doi.org/https://doi.org/10.1002/anie.201206566.

(118) Liu, J.; Li, X.; Zhang, L.; Liu, X.; Wang, X. Direct Fluorination of Nanographene Molecules with Fluorine Gas. *Carbon N. Y.* **2022**, *188*, 453–460. https://doi.org/https://doi.org/10.1016/j.carbon.2021.12.043.

(119) Barton, D. H. R. The Invention of Reactions Useful for the Synthesis of Specifically Fluorinated Natural Products. *Pure Appl. Chem.* **1977**, *49* (9), 1241–1249. https://doi.org/doi:10.1351/pac197749091241.

(120) Rozen, S.; Lerman, O.; Kol, M.; Hebel, D. Electrophilic Fluorination of Unsaturated Systems with the Recently Developed Acetyl Hypofluorite. *J. Org. Chem.* **1985**, *50* (24), 4753–4758. https://doi.org/10.1021/jo00224a019.

(121) Rozen, S.; Lerman, O. A New Approach toward the Synthesis and Chemistry of Fluoroxy Compounds. *J. Am. Chem. Soc.* **1979**, *101* (10), 2782–2784. https://doi.org/10.1021/ja00504a073.

(122) Appelman, E. H.; Basile, L. J.; Thompson, R. C. Fluoroxysulfate: A Powerful New Oxidant and Fluorinating Agent. *J. Am. Chem. Soc.* **1979**, *101* (12), 3384–3385. https://doi.org/10.1021/ja00506a046.

(123) Tressaud, A. Fluorine, a Key Element for the 21St Century. In *Progress in Fluorine Science*; Tressaud, A. B. T.-F., Ed.; Elsevier, 2019; Vol. 5, pp 77–150.

https://doi.org/https://doi.org/10.1016/B978-0-12-812990-6.00002-7.

(124) Nyffeler, P. T.; Durón, S. G.; Burkart, M. D.; Vincent, S. P.; Wong, C.-H. Selectfluor: Mechanistic Insight and Applications. *Angew. Chem. Int. Ed.* **2005**, *44* (2), 192–212. https://doi.org/https://doi.org/10.1002/anie.200400648.

(125) Lal, G. S.; Pez, G. P.; Syvret, R. G. Electrophilic NF Fluorinating Agents. *Chem. Rev.* **1996**, *96* (5), 1737–1756. https://doi.org/10.1021/cr941145p.

(126) Setiawan, D.; Sethio, D.; Cremer, D.; Kraka, E. From Strong to Weak NF Bonds: On the Design of a New Class of Fluorinating Agents. *Phys. Chem. Chem. Phys.* **2018**, *20* (37), 23913–23927. https://doi.org/10.1039/C8CP03843K.

(127) Differding, E.; Ofner, H. N-Fluorobenzenesulfonimide: A Practical Reagent For Electrophilic Fluorinations. *Synlett* **1991**, *1991*, 187–189.

(128) Umemoto, T.; Yang, Y.; Hammond, G. B. Development of N-F Fluorinating Agents and Their Fluorinations: Historical Perspective. *Beilstein J. Org. Chem.* **2021**, *17*, 1752–1813. https://doi.org/10.3762/bjoc.17.123.

(129) Banks, R. E.; Mohialdin-Khaffaf, S. N.; Lal, G. S.; Sharif, I.; Syvret, R. G. 1-Alkyl-4-Fluoro-1,4-Diazoniabicyclo[2.2.2]Octane Salts: A Novel Family of Electrophilic Fluorinating Agents. *J. Chem. Soc., Chem. Commun.* **1992**, No. 8, 595–596. https://doi.org/10.1039/C39920000595.

(130) Stavber, S.; Zupan, M. Selectfluor (TM)-TEDA-BF_4 as a Versatile Mediator or Catalyst in Organic Chemistry. *ACTA Chim. Slov.* **2005**, *52* (1), 13-26 WE-Science Citation Index Expanded (SCI-E.

(131) Stavber, S. Recent Advances in the Application of Selectfluor TMF-TEDA-BF_4 as a Versatile Mediator or Catalyst in Organic Synthesis. *Molecules* 2011. https://doi.org/10.3390/molecules16086432.

(132) Yang, L.; Ma, Y.; Song, F.; You, J. Silver-Catalyzed One-Pot Cyclization/Fluorination of 2-Alkynylanilines: Highly Efficient Synthesis of Structurally Diverse Fluorinated Indole Derivatives. *Chem. Commun.* **2014**, *50* (23), 3024–3026. https://doi.org/10.1039/C3CC49851D.

(133) Patel, N. R.; Flowers, R. A. Mechanistic Study of Silver-Catalyzed Decarboxylative Fluorination. *J. Org. Chem.* **2015**, *80* (11), 5834–5841. https://doi.org/10.1021/acs.joc.5b00826.

(134) Yin, F.; Wang, Z.; Li, Z.; Li, C. Silver-Catalyzed Decarboxylative Fluorination of Aliphatic Carboxylic Acids in Aqueous Solution. *J. Am. Chem. Soc.* **2012**, *134* (25), 10401–10404. https://doi.org/10.1021/ja3048255.

(135) Li, Y.; Jiang, X.; Zhao, C.; Fu, X.; Xu, X.; Tang, P. Silver-Catalyzed Anti-Markovnikov Hydroxyfluorination of Styrenes. *ACS Catal.* **2017**, *7* (3), 1606–1609. https://doi.org/10.1021/acscatal.6b03529.

(136) Vincent, É.; Brioche, J. Synthesis of Alkyl Fluorides by Silver-Catalyzed Radical Decarboxylative Fluorination of Cesium Oxalates. *Eur. J. Org. Chem.* **2021**, *2021* (17),

2421–2430. https://doi.org/https://doi.org/10.1002/ejoc.202100344.

(137) Hu, H; Wang, C; Wu, X; Liu, Y; Yue, G; Su, G; Feng, J. Boron-Catalyzed α-C–H Fluorination of Aryl Acetic Acids. *Org. Chem. Front.* **2022**, *9* (5), 1315–1320. https://doi.org/10.1039/D1QO01814K.

(138) Jacquet, O.; Clément, N. D.; Blanco, C.; Belmonte, M. M.; Benet-Buchholz, J.; van Leeuwen, P. W. N. M. SPANphos Ligands in Palladium-Catalyzed Asymmetric Fluorination. *Eur. J. Org. Chem.* **2012**, *2012* (25), 4844–4852. https://doi.org/https://doi.org/10.1002/ejoc.201200223.

(139) Deng, Q.-H.; Wadepohl, H.; Gade, L. H. The Synthesis of a New Class of Chiral Pincer Ligands and Their Applications in Enantioselective Catalytic Fluorinations and the Nozaki–Hiyama–Kishi Reaction. *Chem. – Eur. J.* **2011**, *17* (52), 14922–14928. https://doi.org/https://doi.org/10.1002/chem.201102375.

(140) Kang, S. H.; Kim, D. Y. Catalytic Enantioselective Fluorination of α-Chloro-β-Keto Esters in the Presence of Chiral Nickel Complexes. *Adv. Synth. Catal.* **2010**, *352* (16), 2783–2786. https://doi.org/https://doi.org/10.1002/adsc.201000515.

(141) Marchese, A. D.; Adrianov, T.; Lautens, M. Recent Strategies for Carbon−Halogen Bond Formation Using Nickel. *Angew. Chem. Int. Ed.* **2021**, *60* (31), 16750–16762. https://doi.org/https://doi.org/10.1002/anie.202101324.

(142) Iashin, V.; Wirtanen, T.; Perea-Buceta, J. E. Tetramethylammonium Fluoride: Fundamental Properties and Applications in C-F Bond-Forming Reactions and as a Base. *Catalysts* **2022**. https://doi.org/10.3390/catal12020233.

(143) Ajenjo, J.; Destro, G.; Cornelissen, B.; Gouverneur, V. Closing the Gap between ^{19}F and ^{18}F Chemistry. *EJNMMI Radiopharm. Chem.* **2021**, *6* (1), 33. https://doi.org/10.1186/s41181-021-00143-y.

(144) Sather, A. C.; Buchwald, S. L. The Evolution of Pd^{0}/Pd^{II}-Catalyzed Aromatic Fluorination. *Acc. Chem. Res.* **2016**, *49* (10), 2146–2157. https://doi.org/10.1021/acs.accounts.6b00247.

(145) Grushin, V. V. The Organometallic Fluorine Chemistry of Palladium and Rhodium: Studies toward Aromatic Fluorination. *Acc. Chem. Res.* **2010**, *43* (1), 160–171. https://doi.org/10.1021/ar9001763.

(146) Marshall, W. J.; Grushin, V. V. Palladium(II) and Palladium(0) Complexes of BINAP(O) (2-(Diphenylphosphino)-2‘-(Diphenylphosphinyl)-1,1‘-Binaphthyl). *Organometallics* **2003**, *22* (3), 555–562. https://doi.org/10.1021/om020838q.

(147) Grushin, V. V. Palladium Fluoride Complexes: One More Step toward Metal-Mediated C−F Bond Formation. *Chem. – Eur. J.* **2002**, *8* (5), 1006–1014. https://doi.org/https://doi.org/10.1002/1521-3765(20020301)8:5<1006::AID-CHEM1006>3.0.CO;2-M.

(148) Fraser, S. L.; Antipin, M. Y.; Khroustalyov, V. N.; Grushin, V. V. Molecular Fluoro Palladium Complexes. *J. Am. Chem. Soc.* **1997**, *119* (20), 4769–4770. https://doi.org/10.1021/ja963984u.

(149) Laitar, D. S.; Müller, P.; Gray, T. G.; Sadighi, J. P. A Carbene-Stabilized Gold(I) Fluoride: Synthesis and Theory. *Organometallics* **2005**, *24* (19), 4503–4505. https://doi.org/10.1021/om050619f.

(150) Hollingworth, C.; Gouverneur, V. Transition Metal Catalysis and Nucleophilic Fluorination. *Chem. Commun.* **2012**, *48* (24), 2929–2942. https://doi.org/10.1039/C2CC16158C.

(151) Campbell, M. G.; Hoover, A. J.; Ritter, T. Transition Metal-Mediated and Metal-Catalyzed Carbon–Fluorine Bond Formation, in *Organometallic Fluorine Chemistry*, Braun, T., Hughes, R. P., Eds.; Springer International: 2015; pp 1–53. https://doi.org/10.1007/3418_2014_88.

(152) A., W. D.; Mingjuan, S.; Georgiy, T.; Yong, Z.; Jorge, G.-F.; Tom, K.; L., B. S. Formation of ArF from LPdAr(F): Catalytic Conversion of Aryl Triflates to Aryl Fluorides. *Science.* **2009**, *325* (5948), 1661–1664. https://doi.org/10.1126/science.1178239.

(153) Noël, T.; Maimone, T. J.; Buchwald, S. L. Accelerating Palladium-Catalyzed C-F Bond Formation: Use of a Microflow Packed-Bed Reactor. *Angew. Chem. Int. Ed.* **2011**, *50* (38), 8900–8903. https://doi.org/https://doi.org/10.1002/anie.201104652.

(154) Milner, P. J.; Kinzel, T.; Zhang, Y.; Buchwald, S. L. Studying Regioisomer Formation in the Pd-Catalyzed Fluorination of Aryl Triflates by Deuterium Labeling. *J. Am. Chem. Soc.* **2014**, *136* (44), 15757–15766. https://doi.org/10.1021/ja509144r.

(155) Su, M.; Buchwald, S. L. A Bulky Biaryl Phosphine Ligand Allows for Palladium-Catalyzed Amidation of Five-Membered Heterocycles as Electrophiles. *Angew. Chem. Int. Ed.* **2012**, *51* (19), 4710–4713. https://doi.org/https://doi.org/10.1002/anie.201201244.

(156) Katcher, M. H.; Norrby, P.-O.; Doyle, A. G. Mechanistic Investigations of Palladium-Catalyzed Allylic Fluorination. *Organometallics* **2014**, *33* (9), 2121–2133. https://doi.org/10.1021/om401240p.

(157) Pitts, C. R.; Bloom, S.; Woltornist, R.; Auvenshine, D. J.; Ryzhkov, L. R.; Siegler, M. A.; Lectka, T. Direct, Catalytic Monofluorination of Sp_3 C–H Bonds: A Radical-Based Mechanism with Ionic Selectivity. *J. Am. Chem. Soc.* **2014**, *136* (27), 9780–9791. https://doi.org/10.1021/ja505136j.

(158) Maity, A.; Stanek, R. J.; Anderson, B. L.; Zeller, M.; Hunter, A. D.; Moore, C. E.; Rheingold, A. L.; Gray, T. G. Fluoride Complexes of Cyclometalated Iridium(III). *Organometallics* **2015**, *34* (1), 109–120. https://doi.org/10.1021/om5009555.

(159) Leclerc, M. C.; Bayne, J. M.; Lee, G. M.; Gorelsky, S. I.; Vasiliu, M.; Korobkov, I.; Harrison, D. J.; Dixon, D. A.; Baker, R. T. Perfluoroalkyl Cobalt(III) Fluoride and Bis(Perfluoroalkyl) Complexes: Catalytic Fluorination and Selective Difluorocarbene Formation. *J. Am. Chem. Soc.* **2015**, *137* (51), 16064–16073. https://doi.org/10.1021/jacs.5b12003.

(160) Morgan, P. J.; Saunders, G. C.; Macgregor, S. A.; Marr, A. C.; Licence, P. Nucleophilic Fluorination Catalyzed by a Cyclometallated Rhodium Complex. *Organometallics* **2022**,

41 (7), 883–891. https://doi.org/10.1021/acs.organomet.2c00052.

(161) Tomashenko, O. A.; Grushin, V. V. Aromatic Trifluoromethylation with Metal Complexes. *Chem. Rev.* **2011**, *111* (8), 4475–4521. https://doi.org/10.1021/cr1004293.

(162) Langlois, B. R.; Billard, T.; Roussel, S. Nucleophilic Trifluoromethylation: Some Recent Reagents and Their Stereoselective Aspects. *J. Fluor. Chem.* **2005**, *126* (2), 173–179. https://doi.org/https://doi.org/10.1016/j.jfluchem.2004.11.007.

(163) Vaishak, T. B.; Soumya, P. K.; Saranya, P. V.; Anilkumar, G. Recent Advances and Prospects in the Iron-Catalyzed Trifluoromethylation Reactions. *Catal. Sci. Technol.* **2021**, *11* (14), 4690–4701. https://doi.org/10.1039/D1CY00499A.

(164) Amal Joseph, P. J.; Priyadarshini, S. Copper-Mediated C–X Functionalization of Aryl Halides. *Org. Proc. Res. Dev.* **2017**, *21* (12), 1889–1924. https://doi.org/10.1021/acs.oprd.7b00285.

(165) Prakash, G. K. S.; Yudin, A. K. Perfluoroalkylation with Organosilicon Reagents. *Chem. Rev.* **1997**, *97* (3), 757–786. https://doi.org/10.1021/cr9408991.

(166) Alonso, C.; Martínez de Marigorta, E.; Rubiales, G.; Palacios, F. Carbon Trifluoromethylation Reactions of Hydrocarbon Derivatives and Heteroarenes. *Chem. Rev.* **2015**, *115* (4), 1847–1935. https://doi.org/10.1021/cr500368h.

(167) Shibata, N.; Matsnev, A.; Cahard, D. Shelf-Stable Electrophilic Trifluoromethylating Reagents: A Brief Historical Perspective. *Beilstein J. Org. Chem.* **2010**, *6*, 65. https://doi.org/10.3762/bjoc.6.65.

(168) Zhu, L.; Fang, Y.; Li, C. Trifluoromethylation of Alkyl Radicals: Breakthrough and Challenges. *Chin. J. Chem.* **2020**, *38* (7), 787–789. https://doi.org/https://doi.org/10.1002/cjoc.202000095.

(169) Studer, A. A "Renaissance" in Radical Trifluoromethylation. *Angew. Chem. Int. Ed.* **2012**, *51* (36), 8950–8958. https://doi.org/10.1002/anie.201202624.

(170) Ruppert, I.; Schlich, K.; Volbach, W. Die Ersten CF_3-Substituierten Organyl(Chlor)Silane. *Tetrahedron Lett.* **1984**, *25* (21), 2195–2198. https://doi.org/https://doi.org/10.1016/S0040-4039(01)80208-2.

(171) Ojima I. *Frontiers of Organofluorine Chemistry*, World Scientific, 2019, Chapter 2, pp 93–176. https://doi.org/doi:10.1142/q0217.

(172) Blastik, Z. E.; Voltrová, S.; Matoušek, V.; Jurásek, B.; Manley, D. W.; Klepetářová, B.; Beier, P. Azidoperfluoroalkanes: Synthesis and Application in Copper(I)-Catalyzed Azide–Alkyne Cycloaddition. *Angew. Chem. Int. Ed.* **2017**, *56* (1), 346–349. https://doi.org/https://doi.org/10.1002/anie.201609715.

(173) Chen, Q.-Y.; Wu, S.-W. Methyl Fluorosulphonyldifluoroacetate; a New Trifluoromethylating Agent. *J. Chem. Soc., Chem. Commun.* **1989**, No. 11, 705–706. https://doi.org/10.1039/C39890000705.

(174) Xie, Q.; Hu, J. Chen's Reagent: A Versatile Reagent for Trifluoromethylation,

Difluoromethylenation, and Difluoroalkylation in Organic Synthesis. *Chin. J. Chem.* **2020**, *38* (2), 202–212. https://doi.org/https://doi.org/10.1002/cjoc.201900424.

(175) Oishi, M.; Kondo, H.; Amii, H. Aromatic Trifluoromethylation Catalytic in Copper. *Chem. Commun.* **2009**, No. 14, 1909–1911. https://doi.org/10.1039/B823249K.

(176) Jover, J. Computational Insights into Nucleophilic Copper-Catalyzed Trifluoromethylation of Aryl Halides. *ACS Catal.* **2014**, *4* (12), 4389–4397. https://doi.org/10.1021/cs500872m.

(177) Wang, G.; Li, M.; Leng, X.; Xue, X.; Shen, Q. Neutral Five-Coordinate Arylated Copper(III) Complex: Key Intermediate in Copper-Mediated Arene Trifluoromethylation. *Chin. J. Chem.* **2022**, *n/a* (n/a). https://doi.org/https://doi.org/10.1002/cjoc.202200230.

(178) Chen, J.-Y.; Huang, J.; Sun, K.; He, W.-M. Recent Advances in Transition-Metal-Free Trifluoromethylation with Togni's Reagents. *Org. Chem. Front.* **2022**, *9* (4), 1152–1164. https://doi.org/10.1039/D1QO01504D.

(179) Egami, H.; Shimizu, R.; Usui, Y.; Sodeoka, M. Iron-Catalyzed Trifluoromethylation with Concomitant C–C Bond Formation via 1,2-Migration of an Aryl Group. *Chem. Commun.* **2013**, *49* (66), 7346–7348. https://doi.org/10.1039/C3CC43936D.

(180) Rey-Rodriguez, R.; Retailleau, P.; Bonnet, P.; Gillaizeau, I. Iron-Catalyzed Trifluoromethylation of Enamide. *Chem. – Eur. J.* **2015**, *21* (9), 3572–3575. https://doi.org/https://doi.org/10.1002/chem.201406333.

(181) Kong, W.; Casimiro, M.; Fuentes, N.; Merino, E.; Nevado, C. Metal-Free Aryltrifluoromethylation of Activated Alkenes. *Angew. Chem. Int. Ed.* **2013**, *52* (49), 13086–13090. https://doi.org/https://doi.org/10.1002/anie.201307377.

(182) Zhang, R.; Ni, C.; He, Z.; Hu, J. Organocatalyzed Decarboxylative Trifluoromethylation of β-Ketoacids. *Top. Catal.* **2018**, *61* (7), 664–673. https://doi.org/10.1007/s11244-018-0973-7.

(183) Baishya, G.; Dutta, N. B. Recent Advances in Direct C−H Trifluoromethylation of N-Heterocycles. *ChemistrySelect* **2021**, *6* (47), 13384–13408. https://doi.org/https://doi.org/10.1002/slct.202103407.

(184) Wang, L.; Zhang, Y.; Li, F.; Hao, X.; Zhang, H.-Y.; Zhao, J. Direct C−H Trifluoromethylation of Quinoxalin-2(1H)-Ones under Transition-Metal-Free Conditions. *Adv. Synth. Catal.* **2018**, *360* (20), 3969–3977. https://doi.org/https://doi.org/10.1002/adsc.201800863.

(185) Shen, H.; Liu, Z.; Zhang, P.; Tan, X.; Zhang, Z.; Li, C. Trifluoromethylation of Alkyl Radicals in Aqueous Solution. *J. Am. Chem. Soc.* **2017**, *139* (29), 9843–9846. https://doi.org/10.1021/jacs.7b06044.

(186) Britton, R; Gouverneur, V.; Lin, J; Meanwell, M; Ni, C.; Pupo, G; Xiao, J; Hu, J. Contemporary Synthetic Strategies in Organofluorine Chemistry. *Nat. Rev. Methods Prim.* **2021**, *1* (1), 47. https://doi.org/10.1038/s43586-021-00042-1.

(187) Liu, J.-B.; Xu, X.-H.; Qing, F.-L. Silver-Mediated Oxidative Trifluoromethylation of

Alcohols to Alkyl Trifluoromethyl Ethers. *Org. Lett.* **2015**, *17* (20), 5048–5051. https://doi.org/10.1021/acs.orglett.5b02522.

(188) Fu, M.-L.; Liu, J.-B.; Xu, X.-H.; Qing, F.-L. Synthesis of Pentafluoroethyl Ethers by Silver-Mediated Oxidative Pentafluoroethylation of Alcohols and Phenols. *J. Org. Chem.* **2017**, *82* (7), 3702–3709. https://doi.org/10.1021/acs.joc.7b00190.

(189) Teverovskiy, G.; Surry, D. S.; Buchwald, S. L. Pd-Catalyzed Synthesis of Ar-SCF_3 Compounds under Mild Conditions. *Angew. Chem. Int. Ed.* **2011**, *50* (32), 7312–7314. https://doi.org/10.1002/anie.201102543.

(190) Yin, W.; Wang, Z.; Huang, Y. Highly Ortho-Selective Trifluoromethylthiolation Reactions Using a Ligand Exchange Strategy. *Adv. Synth. Catal.* **2014**, *356* (14–15), 2998–3006. https://doi.org/https://doi.org/10.1002/adsc.201400362.

(191) Weng, Z.; He, W.; Chen, C.; Lee, R.; Tan, D.; Lai, Z.; Kong, D.; Yuan, Y.; Huang, K.-W. An Air-Stable Copper Reagent for Nucleophilic Trifluoromethylthiolation of Aryl Halides. *Angew. Chem. Int. Ed.* **2013**, *52* (5), 1548–1552. https://doi.org/https://doi.org/10.1002/anie.201208432.

(192) Wu, W.; Wang, B.; Ji, X.; Cao, S. Direct Copper-Catalyzed Oxidative Trifluoromethylthiolation of Aryl Boronic Acids with $AgSCF_3$. *Org. Chem. Front.* **2017**, *4* (7), 1299–1303. https://doi.org/10.1039/C7QO00198C.

(193) Saravanan, P.; Anbarasan, P. Copper-Catalyzed Trifluoromethylthiolation of Di(Hetero)Aryl-Λ3-Iodanes: Mechanistic Insight and Application to Synthesis of (Hetero)Aryl Trifluoromethyl Sulfides. *Adv. Synth. Catal.* **2015**, *357* (16–17), 3521–3528. https://doi.org/https://doi.org/10.1002/adsc.201500606.

(194) Xu, J.; Mu, X.; Chen, P.; Ye, J.; Liu, G. Copper-Catalyzed Trifluoromethylthiolation of Aryl Halides with Diverse Directing Groups. *Org. Lett.* **2014**, *16* (15), 3942–3945. https://doi.org/10.1021/ol501742a.

(195) Mudshinge, S. R.; Yang, Y.; Xu, B.; Hammond, G. B.; Lu, Z. Gold (I/III)-Catalyzed Trifluoromethylthiolation and Trifluoromethylselenolation of Organohalides. *Angew. Chem. Int. Ed.* **2022**, *61* (12), e202115687. https://doi.org/https://doi.org/10.1002/anie.202115687.

(196) Yin, G.; Kalvet, I.; Schoenebeck, F. Trifluoromethylthiolation of Aryl Iodides and Bromides Enabled by a Bench-Stable and Easy-To-Recover Dinuclear Palladium(I) Catalyst. *Angew. Chem. Int. Ed.* **2015**, *54* (23), 6809–6813. https://doi.org/https://doi.org/10.1002/anie.201501617.

(197) Zhang, C.-P.; Vicic, D. A. Nickel-Catalyzed Synthesis of Aryl Trifluoromethyl Sulfides at Room Temperature. *J. Am. Chem. Soc.* **2012**, *134* (1), 183–185. https://doi.org/10.1021/ja210364r.

(198) Yin, G.; Kalvet, I.; Englert, U.; Schoenebeck, F. Fundamental Studies and Development of Nickel-Catalyzed Trifluoromethylthiolation of Aryl Chlorides: Active Catalytic Species and Key Roles of Ligand and Traceless MeCN Additive Revealed. *J. Am. Chem. Soc.* **2015**, *137* (12), 4164–4172. https://doi.org/10.1021/jacs.5b00538.

(199) Pluta, R.; Nikolaienko, P.; Rueping, M. Direct Catalytic Trifluoromethylthiolation of Boronic Acids and Alkynes Employing Electrophilic Shelf-Stable N-(Trifluoromethylthio)Phthalimide. *Angew. Chem. Int. Ed.* **2014**, *53* (6), 1650–1653. https://doi.org/https://doi.org/10.1002/anie.201307484.

(200) Kang, K.; Xu, C.; Shen, Q. Copper-Catalyzed Trifluoromethylthiolation of Aryl and Vinyl Boronic Acids with a Shelf-Stable Electrophilic Trifluoromethylthiolating Reagent. *Org. Chem. Front.* **2014**, *1* (3), 294–297. https://doi.org/10.1039/C3QO00068K.

(201) Hamzehloo, M.; Hosseinian, A.; Ebrahimiasl, S.; Monfared, A.; Vessally, E. Direct C-H Trifluoromethylthiolation of (Hetero)Arenes: A Review. *J. Fluor. Chem.* **2019**, *224*, 52–60. https://doi.org/https://doi.org/10.1016/j.jfluchem.2019.05.004.

(202) Xu, C.; Wang, S.; Shen, Q. Recent Progress on Trifluoromethylthiolation of (Hetero)Aryl C–H Bonds with Electrophilic Trifluoromethylthiolating Reagents. *ACS Sustain. Chem. Eng.* **2022**. https://doi.org/10.1021/acssuschemeng.2c01006.

(203) Ferry, A.; Billard, T.; Bacqué, E.; Langlois, B. R. Electrophilic Trifluoromethanesulfanylation of Indole Derivatives. *J. Fluor. Chem.* **2012**, *134*, 160–163. https://doi.org/https://doi.org/10.1016/j.jfluchem.2011.02.005.

(204) Milandou, L.J.C.; Carreyre, H.; Alazet, S.; Greco, G.; Martin-Mingot, C.; Nkounkou, L.; Ouamba, J.M.; Bouazza, F.; Billard, T.; Thibaudeau, S. Superacid-Catalyzed Trifluoromethylthiolation of Aromatic Amines. *Angew. Chem. Int. Ed.* **2017**, *56* (1), 169–172. https://doi.org/https://doi.org/10.1002/anie.201609574.

(205) Yang, X.-G.; Zheng, K.; Zhang, C. Electrophilic Hypervalent Trifluoromethylthio-Iodine(III) Reagent. *Org. Lett.* **2020**, *22* (5), 2026–2031. https://doi.org/10.1021/acs.orglett.0c00405.

(206) Wang, D.; Carlton, C. G.; Tayu, M.; McDouall, J. J. W.; Perry, G. J. P.; Procter, D. J. Trifluoromethyl Sulfoxides: Reagents for Metal-Free C−H Trifluoromethylthiolation. *Angew. Chem. Int. Ed.* **2020**, *59* (37), 15918–15922. https://doi.org/https://doi.org/10.1002/anie.202005531.

(207) Seppelt, K. Trifluoromethanol, CF_3OH. *Angew. Chem. Int. Ed. Engl.* **1977**, *16* (5), 322–323. https://doi.org/https://doi.org/10.1002/anie.197703221.

(208) Trainor, G. L. The Preparation of O-Trifluoromethyl Carbohydrates. *J. Carbohydr. Chem.* **1985**, *4* (4), 545–563. https://doi.org/10.1080/07328308508082676.

(209) Redwood, M. E.; Willis, C. J. Fully Fluorinated Alkoxides: Part I. Trifluoromethoxides of Alkali Metals. *Can. J. Chem.* **1965**, *43* (7), 1893–1898. https://doi.org/10.1139/v65-251.

(210) Kolomeitsev, A. A.; Vorobyev, M.; Gillandt, H. Versatile Application of Trifluoromethyl Triflate. *Tetrahedron Lett.* **2008**, *49* (3), 449–454. https://doi.org/https://doi.org/10.1016/j.tetlet.2007.11.105.

(211) Farnham, W. B.; Smart, B. E.; Middleton, W. J.; Calabrese, J. C.; Dixon, D. A. Crystal and Molecular Structure of Tris(Dimethylamino)Sulfonium Trifluoromethoxide. Evidence for Negative Fluorine Hyperconjugation. *J. Am. Chem. Soc.* **1985**, *107* (15), 4565–4567. https://doi.org/10.1021/ja00301a043.

(212) Zhou, M.; Ni, C.; Zeng, Y.; Hu, J. Trifluoromethyl Benzoate: A Versatile Trifluoromethoxylation Reagent. *J. Am. Chem. Soc.* **2018**, *140* (22), 6801–6805. https://doi.org/10.1021/jacs.8b04000.

(213) Chen, C.; Luo, Y.; Fu, L.; Chen, P.; Lan, Y.; Liu, G. Palladium-Catalyzed Intermolecular Ditrifluoromethoxylation of Unactivated Alkenes: CF_3O-Palladation Initiated by Pd(IV). *J. Am. Chem. Soc.* **2018**, *140* (4), 1207–1210. https://doi.org/10.1021/jacs.7b11470.

(214) Chen, C.; Chen, P.; Liu, G. Palladium-Catalyzed Intramolecular Aminotrifluoromethoxylation of Alkenes. *J. Am. Chem. Soc.* **2015**, *137* (50), 15648–15651. https://doi.org/10.1021/jacs.5b10971.

(215) Newton, J. J.; Jelier, B. J.; Meanwell, M.; Martin, R. E.; Britton, R.; Friesen, C. M. Quaternary Ammonium Trifluoromethoxide Salts as Stable Sources of Nucleophilic OCF_3. *Org. Lett.* **2020**, *22* (5), 1785–1790. https://doi.org/10.1021/acs.orglett.0c00099.

(216) Dix, S.; Golz, P.; Schmid, J. R.; Riedel, S.; Hopkinson, M. N. Radical C−H Trifluoromethoxylation of (Hetero)Arenes with Bis(Trifluoromethyl)Peroxide. *Chem. – Eur. J.* **2021**, *27* (45), 11554–11558. https://doi.org/https://doi.org/10.1002/chem.202101621.

(217) Xin, J.; Deng, X.; Tang, P. Silver-Catalyzed Trifluoromethoxylation of Aziridines. *Org. Lett.* **2022**, *24* (3), 881–885. https://doi.org/10.1021/acs.orglett.1c04226.

(218) Szpera, R.; Kovalenko, N.; Natarajan, K.; Paillard, N.; Linclau, B. The Synthesis of the 2,3-Difluorobutan-1,4-Diol Diastereomers. *Beilstein J. Org. Chem.* **2017**, *13*, 2883–2887. https://doi.org/10.3762/bjoc.13.280.

(219) Rewcastle, G.W.; Gamage, S.A.; Flanagan J.U.; Frederick, R.; Denny, W.A.; Baguley, B.B.; Kestell, P.; Singh, R.; Kendall, J.D.; Marshall, E.S.; Lill, C.L.; Lee, W.-J.; Kolekar, S.; Buchanan, C.M.; Jamieson, S.M.F.; Shepard, P.R. Synthesis and Biological Evaluation of Novel Analogues of the Pan Class I Phosphatidylinositol 3-Kinase (PI3K) Inhibitor 2-(Difluoromethyl)-1-[4,6-Di(4-Morpholinyl)-1,3,5-Triazin-2-Yl]-1H-Benzimidazole (ZSTK474). *J. Med. Chem.* **2011**, *54* (20), 7105–7126. https://doi.org/10.1021/jm200688y.

(220) Beaulieu, F.; Beauregard, L.-P.; Courchesne, G.; Couturier, M.; LaFlamme, F.; L'Heureux, A. Aminodifluorosulfinium Tetrafluoroborate Salts as Stable and Crystalline Deoxofluorinating Reagents. *Org. Lett.* **2009**, *11* (21), 5050–5053. https://doi.org/10.1021/ol902039q.

(221) Zeng, X.; Yan, W.; Zacate, S.B.; Cai, A.; Wang, Y.; Yang, D; Yang, K; Liu, W. Copper-Catalyzed Deaminative Difluoromethylation. *Angew. Chem. Int. Ed.* **2020**, *59* (38), 16398–16403. https://doi.org/10.1002/anie.202006048.

(222) Serizawa, H.; Ishii, K.; Aikawa, K.; Mikami, K. Copper-Catalyzed Difluoromethylation of Aryl Iodides with (Difluoromethyl)Zinc Reagent. *Org. Lett.* **2016**, *18* (15), 3686–3689. https://doi.org/10.1021/acs.orglett.6b01733.

(223) Miao, W.; Zhao, Y.; Ni, C.; Gao, B.; Zhang, W.; Hu, J. Iron-Catalyzed Difluoromethylation of Arylzincs with Difluoromethyl 2-Pyridyl Sulfone. *J. Am. Chem.*

Soc. **2018**, *140* (3), 880–883. https://doi.org/10.1021/jacs.7b11976.

(224) Xu, C.; Guo, W.-H.; He, X.; Guo, Y.-L.; Zhang, X.-Y.; Zhang, X. Difluoromethylation of (Hetero)Aryl Chlorides with Chlorodifluoromethane Catalyzed by Nickel. *Nat. Commun.* **2018**, *9* (1), 1170. https://doi.org/10.1038/s41467-018-03532-1.

(225) Sheng, J.; Ni, H.-Q.; Bian, K.-J.; Li, Y.; Wang, Y.-N.; Wang, X.-S. Nickel-Catalyzed Direct Difluoromethylation of Aryl Boronic Acids with $BrCF_2H$. *Org. Chem. Front.* **2018**, *5* (4), 606–610. https://doi.org/10.1039/C7QO00934H.

(226) Lu, C.; Lu, H.; Wu, J.; Shen, H.; Hu, T.; Gu, Y.; Shen, Q. Palladium-Catalyzed Difluoromethylation of Aryl Chlorides and Triflates and Its Applications in the Preparation of Difluoromethylated Derivatives of Drug/Agrochemical Molecules. *J. Org. Chem.* **2018**, *83* (2), 1077–1083. https://doi.org/10.1021/acs.joc.7b02989.

(227) Ferguson, D. M.; Malapit, C. A.; Bour, J. R.; Sanford, M. S. Palladium-Catalyzed Difluoromethylation of Aryl Chlorides and Bromides with $TMSCF_2H$. *J. Org. Chem.* **2019**, *84* (6), 3735–3740. https://doi.org/10.1021/acs.joc.9b00324.

(228) Zhong, J.-J.; Yang, C.; Chang, X.-Y.; Zou, C.; Lu, W.; Che, C.-M. Platinum(II) Photo-Catalysis for Highly Selective Difluoroalkylation Reactions. *Chem. Commun.* **2017**, *53* (64), 8948–8951. https://doi.org/10.1039/C7CC03823B.

(229) Gu, Y.; Leng, X.; Shen, Q. Cooperative Dual Palladium/Silver Catalyst for Direct Difluoromethylation of Aryl Bromides and Iodides. *Nat. Commun.* **2014**, *5* (1), 5405. https://doi.org/10.1038/ncomms6405.

(230) Lu, C.; Gu, Y.; Wu, J.; Gu, Y.; Shen, Q. Palladium-Catalyzed Difluoromethylation of Heteroaryl Chlorides, Bromides and Iodides. *Chem. Sci.* **2017**, *8* (7), 4848–4852. https://doi.org/10.1039/C7SC00691H.

(231) Bruno, N. C.; Tudge, M. T.; Buchwald, S. L. Design and Preparation of New Palladium Precatalysts for C–C and C–N Cross-Coupling Reactions. *Chem. Sci.* **2013**, *4* (3), 916–920. https://doi.org/10.1039/C2SC20903A.

(232) Xu, L.; Vicic, D. A. Direct Difluoromethylation of Aryl Halides via Base Metal Catalysis at Room Temperature. *J. Am. Chem. Soc.* **2016**, *138* (8), 2536–2539. https://doi.org/10.1021/jacs.6b00053.

(233) Bour, J. R.; Kariofillis, S. K.; Sanford, M. S. Synthesis, Reactivity, and Catalytic Applications of Isolable (NHC)Cu(CHF_2) Complexes. *Organometallics* **2017**, *36* (7), 1220–1223. https://doi.org/10.1021/acs.organomet.7b00025.

(234) Mcloughlin, V. C. R.; Thrower, J. A Route to Fluoroalkyl-Substituted Aromatic Compounds Involving Fluoroalkylcopper Intermediates. *Tetrahedron* **1969**, *25* (24), 5921–5940. https://doi.org/https://doi.org/10.1016/S0040-4020(01)83100-8.

(235) Matsui, K.; Tobita, E.; Ando, M.; Kondo, K. A Convenient Trifluoromethylation of Aromatic Halides with Sodium Trifluoroacetate. *Chem. Lett.* **1981**, *10* (12), 1719–1720. https://doi.org/10.1246/cl.1981.1719.

(236) Chen, Q.-Y.; Wu, S.-W. Studies on Fluoroalkylation and Fluoroalkoxylation. Part 33.

Direct Trifluoromethylation of Aryl Halides with Fluorosulphonyldifluoromethyl Iodide in the Presence of Copper: An Electron Transfer Induced Process. *J. Chem. Soc. Perkin Trans. 1* **1989**, No. 12, 2385–2387. https://doi.org/10.1039/P19890002385.

(237) Yokomatsu, T.; Murano, T.; Suemune, K.; Shibuya, S. Facile Synthesis of Aryl(Difluoromethyl)Phosphonates through CuBr-Mediated Cross Coupling Reactions of [(Diethoxyphosphinyl)Difluoromethyl]Zinc Bromide with Aryl Iodides. *Tetrahedron* **1997**, *53* (3), 815–822. https://doi.org/https://doi.org/10.1016/S0040-4020(96)01063-0.

(238) Naumann, D.; Tyrra, W.; Kock, B.; Rudolph, W.; Wilkes, B. Preparation and Properties of $ZnBr(CF_3)\cdot 2L$ — a Convenient Route for the Preparation of CF_3I. *J. Fluor. Chem.* **1994**, *67* (1), 91–93. https://doi.org/https://doi.org/10.1016/0022-1139(93)02937-A.

(239) Kremlev, M. M.; Tyrra, W.; Mushta, A. I.; Naumann, D.; Yagupolskii, Y. L. The Solid Complex $Zn(CF_3)Br\cdot 2DMF$ as an Alternative Reagent for the Preparation of Both, Trifluoromethyl and Pentafluoroethyl Copper, $CuCF_3$ and CuC_2F_5. *J. Fluor. Chem.* **2010**, *131* (2), 212–216. https://doi.org/https://doi.org/10.1016/j.jfluchem.2009.10.011.

(240) Prakash, G. K. S.; Krishnamurti, R.; Olah, G. A. Synthetic Methods and Reactions. 141. Fluoride-Induced Trifluoromethylation of Carbonyl Compounds with Trifluoromethyltrimethylsilane (TMS-CF_3). A Trifluoromethide Equivalent. *J. Am. Chem. Soc.* **1989**, *111* (1), 393–395. https://doi.org/10.1021/ja00183a073.

(241) Dubinina, G. G.; Furutachi, H.; Vicic, D. A. Active Trifluoromethylating Agents from Well-Defined Copper(I)−CF_3 Complexes. *J. Am. Chem. Soc.* **2008**, *130* (27), 8600–8601. https://doi.org/10.1021/ja802946s.

(242) Morimoto, H.; Tsubogo, T.; Litvinas, N. D.; Hartwig, J. F. A Broadly Applicable Copper Reagent for Trifluoromethylations and Perfluoroalkylations of Aryl Iodides and Bromides. *Angew. Chem. Int. Ed.* **2011**, *50* (16), 3793–3798. https://doi.org/10.1002/anie.201100633.

(243) Tomashenko, O. A.; Escudero-Adán, E. C.; Martínez Belmonte, M.; Grushin, V. V. Simple, Stable, and Easily Accessible Well-Defined $CuCF_3$ Aromatic Trifluoromethylating Agents. *Angew. Chem. Int. Ed.* **2011**, *50* (33), 7655–7659. https://doi.org/https://doi.org/10.1002/anie.201101577.

(244) Luo, G.; Luo, Y.; Qu, J. Direct Nucleophilic Trifluoromethylation Using Fluoroform: A Theoretical Mechanistic Investigation and Insight into the Effect of Alkali Metal Cations. *New J. Chem.* **2013**, *37* (10), 3274–3280. https://doi.org/10.1039/C3NJ00686G.

(245) Xie, Q.; Li, L.; Zhu, Z.; Zhang, R.; Ni, C.; Hu, J. From C_1 to C_2: $TMSCF_3$ as a Precursor for Pentafluoroethylation. *Angew. Chem. Int. Ed.* **2018**, *57* (40), 13211–13215. https://doi.org/https://doi.org/10.1002/anie.201807873.

(246) Mestre, J.; Castillón, S.; Boutureira, O. "Ligandless" Pentafluoroethylation of Unactivated (Hetero)Aryl and Alkenyl Halides Enabled by the Controlled Self-Condensation of $TMSCF_3$-Derived $CuCF_3$. *J. Org. Chem.* **2019**, *84* (23), 15087–15097. https://doi.org/10.1021/acs.joc.9b02001.

(247) Pan, S.; Xie, Q.; Wang, X.; Wang, Q.; Ni, C.; Hu, J. Copper-Mediated

Pentafluoroethylation of Organoboronates and Terminal Alkynes with $TMSCF_3$. *Chem. Commun.* **2022**, *58* (33), 5156–5159. https://doi.org/10.1039/D2CC00975G.

(248) Fier, P. S.; Hartwig, J. F. Copper-Mediated Difluoromethylation of Aryl and Vinyl Iodides. *J. Am. Chem. Soc.* **2012**, *134* (12), 5524–5527. https://doi.org/10.1021/ja301013h.

(249) Gu, Y.; Chang, D.; Leng, X.; Gu, Y.; Shen, Q. Well-Defined, Shelf-Stable (NHC)Ag(CF_2H) Complexes for Difluoromethylation. *Organometallics* **2015**, *34* (12), 3065–3071. https://doi.org/10.1021/acs.organomet.5b00350.

(250) Wang, X.; Pan, S.; Luo, Q.; Wang, Q.; Ni, C.; Hu, J. Controllable Single and Double Difluoromethylene Insertions into C–Cu Bonds: Copper-Mediated Tetrafluoroethylation and Hexafluoropropylation of Aryl Iodides with $TMSCF_2H$ and $TMSCF_2Br$. *J. Am. Chem. Soc.* **2022**, *144* (27), 12202–12211. https://doi.org/10.1021/jacs.2c03104.

(251) Zanardi, A.; Novikov, M. A.; Martin, E.; Benet-Buchholz, J.; Grushin, V. V. Direct Cupration of Fluoroform. *J. Am. Chem. Soc.* **2011**, *133* (51), 20901–20913. https://doi.org/10.1021/ja2081026.

(252) Lishchynskyi, A.; Grushin, V. V. Cupration of C_2F_5H: Isolation, Structure, and Synthetic Applications of $[K(DMF)_2][(t\text{-}BuO)Cu(C_2F_5)]$. Highly Efficient Pentafluoroethylation of Unactivated Aryl Bromides. *J. Am. Chem. Soc.* **2013**, *135* (34), 12584–12587. https://doi.org/10.1021/ja407017j.

(253) Dyatkin, B. L.; Martynov, B. I.; Martynova, L. G.; Kizim, N. G.; Sterlin, S. R.; Stumbrevichute, Z. A.; Fedorov, L. A. On the Enteraction of Perfluoroalkyl Carbanions with Silver Salts. *J. Organomet. Chem.* **1973**, *57* (2), 423–433. https://doi.org/https://doi.org/10.1016/S0022-328X(00)86623-1.

(254) Miller, W. T.; Burnard, R. J. Perfluoroalkylsilver Compounds. *J. Am. Chem. Soc.* **1968**, *90* (26), 7367–7368. https://doi.org/10.1021/ja01028a047.

(255) Andrella, N. O.; Liu, K.; Gabidullin, B.; Vasiliu, M.; Dixon, D. A.; Baker, R. T. Metal Heptafluoroisopropyl (M-Hfip) Complexes for Use as Hfip Transfer Agents. *Organometallics* **2018**, *37* (3), 422–432. https://doi.org/10.1021/acs.organomet.7b00837.

(256) Andrella, N. O. Synthesis of Organo-Fluorine Compounds by Metal Complex-Mediated and -Catalyzed Transformations of Fluoro-Alkenes and Fluoro-Arenes, University of Ottawa PhD thesis, 2019.

(258) Koga, K. T.; Rose-Koga, E. F. Fluorine in the Earth and solar system, where does it come from and can it be found?. *C. R. Chimie* **2018**, 21, 749-756.

(259) Miller, G.R and Kester, D.R. Sodium fluoride ion-pairs in seawater. *Mar. Chem.* **1975**, 4, 67-82.

Chapter 2. Generation of Copper Fluoroalkyl Complexes (CuR^FLn) from Chlorotrifluoroethylene and -R^F Transfer to Benzoyl Chloride

Contributions to knowledge:

Generation of Copper Fluoroalkyl Complexes (CuR^FL_n) from Chlorotrifluoroethylene and -R^F transfer to Benzoyl Chloride

Luana L. T. N. Porto, Moutasem Seifi, Nicole Johnson, and R. Tom Baker

Submitted to *Can. J. Chem.,* Sept. 2022 (invited article in honour of Prof. Cathleen Crudden)

Chapter contributions: Luana Porto performed the experiments and wrote the first draft. Moutasem Seifi performed substrate scope of aroyl chlorides and Nicole Johnson performed the reactions with aryl iodides. Prof. Baker helped plan the experiments and refine the manuscript text.

Abstract: Given the importance of fluorinated drugs and agrochemicals, fluoroalkylation of organic electrophiles that can be performed at a late stage of chemical synthesis has attracted a flurry of contributions. New fluoroalkyl groups can be obtained by insertion of fluoroalkenes into Cu-H bonds. Chlorotrifluoroethylene undergoes regioselective insertion in its reaction with Stryker's reagent, $[CuH(PPh_3)]_6$, and triphos to give $[Cu(CFClCF_2H)(\mu\text{–}\kappa^1,\kappa^2\text{-triphos})]_2$ which mediates the fluoroalkylation of several aroyl chlorides [triphos = bis(2-diphenylphosphinoethyl)- phenylphosphine]. In contrast, attempted -R^F transfer to aryl iodides instead affords aryl-aryl coupling products.

2.1 INTRODUCTION

The development of new methodologies for perfluoroalkylation of organic electrophiles has been extensively explored by scientists over the last decade due to the widespread application of fluorine in pharmaceutical, agrochemicals and material science.[1–4] Since McLoughlin and Thrower developed the first copper-mediated perfluoroalkylation of aryl halides in 1969,[5] diverse methodologies to afford fluoroalkylated arenes have been found in the literature.[6] In 2011 Hartwig and co-workers demonstrated the stabilization of $CuCF_3$ generated in situ from the Ruppert-Prakash reagent (Me_3SiCF_3) using 1,10-phenanthroline (phen) as a ligand; the Trifluoromethylator® effects the trifluoromethylation of aryl iodides in good yields.[7] However, there are still few examples of perfluoroalkylation methodologies that transfer -CF_2CF_2H, -CF_2CF_3, -OCF_3, -SCF_3, and -CF_2H to organic electrophiles.[8-11] In 2019, Boutureira and co-workers reported the pentafluoroethylation of aryl iodides using CuBr and Me_3SiCF_3 in DMF.[12] Jinbo Hu *et al.* showed that adding the phen ligand and AgF in the reaction of Me_3SiCF_3 and CuCl could perform the pentafluoroethylation of heteroaryl boronates.[13] Sanford *et al.* demonstrated difluoromethylation of aryl iodides using $Cu(CF_2H)(IPr)$ generated from Me_3SiCF_2H.[14] Building on the

work of Miller and Burnard who first prepared Ag(hfip) by reaction of hexafluoropropene (HFP) with AgF,[15] the Baker group prepared Cu-hfip complexes from insertion of HFP first into Cu-H and then Cu-F (hfip = heptafluoroisopropyl; **Scheme 2.1**).[16] They then showed that Cu(hfip)(phen)(PPh_3) transfers the hfip group to aroyl chlorides in moderate to good yields. Moreover, insertion of tetrafluoroethylene into Cu-H gave Cu(CF_2CF_2H)($PMePh_2$)$_3$ that enabled the tetrafluoroethylation of aryl halides.[17] Chlorotrifluoroethylene (CTFE, $CFCl=CF_2$) is a readily available fluoroalkene that we thought could give access to a functionalizable fluoroalkyl group (cf., post-synthetic replacement of C-Cl bond). Herein, we report a new fluoroalkyl R^F group (-$CFClCF_2H$) derived from regioselective insertion of CTFE into Cu-H. After testing several different N-, P-, and C-donor ligands, we found that the tridentate triphos ligand [bis-(2-diphenylphosphinoethyl)phenylphosphine)] stabilizes the Cu-R^F linkage sufficiently to allow for its Cu-mediated transfer to aroyl chlorides.

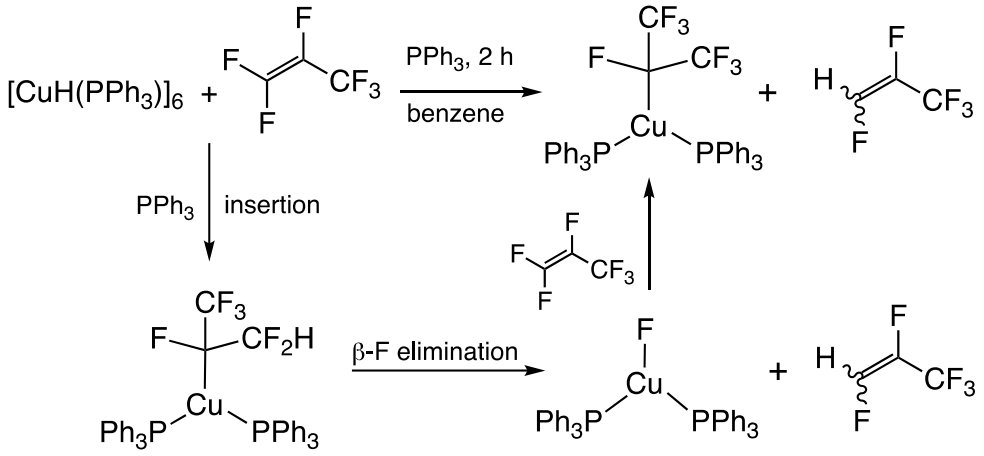

Scheme 2.1 Synthesis of Cu(hfip)(PPh_3)$_2$ from HFP + Cu-F generated from Cu-H + HFP

2.2 RESULTS AND DISCUSSION

2.2.1 Synthesis of Cu($CFClCF_2H$)Ln complexes: Reactions of Stryker's reagent, [CuH(PPh_3)]$_6$, with CTFE after addition of a variety of ligands including triisopropylphosphite [P(O^iPr)$_3$], tri-*o*-tolylphosphite (P(O-*o*-tol)$_3$], methyldiphenylphosphine (PPh_2Me), 1,1,1-tris(diphenylphosphino-methyl)ethane (tripod), 1,10-phenanthroline (phen), 2,2';6',2"-terpyridine (terpy) and N,N,N′,N″,N″-pentamethyldiethylenetriamine (PMDTA) gave mostly hydrodehalogenation (CHF=CHF) and/or hydrogenolysis products ($CHFClCF_2H$) (see Appendix). In contrast, both triethylphosphite and triphenylphosphine afforded the regioselective insertion products, Cu($CFClCF_2H$)L_n (**2-1,2**) as evidenced by ^{19}F NMR spectroscopy (**Scheme 2.2**). For

$Cu(CFClCF_2H)[P(OEt)_3]_3$ (**2-1**) the phosphite ligand presumably undergoes facile dissociation (rapid on NMR time scale) as evidenced by the broad ^{31}P resonance and lack of P-F coupling to Ca-F in the ^{19}F NMR. The diastereotopic CF_2 groups of **2-1,2** show characteristically large F-F (264 and 280 Hz) and F-H two-bond couplings (ca. 59 Hz). Unfortunately, upon solvent removal, the signals for **2-1** disappeared (Fig. A2.5) and those for $Cu(CFClCF_2H)(PPh_3)_2$ (**2-2)** were accompanied by a number of additional side-products (Fig. A2.8) as confirmed by an unsuccessful scale-up attempt.

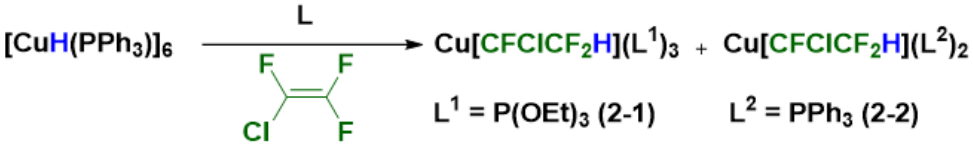

Scheme 2.2 Generation of Cu-$CFClCF_2H$ complexes **2-1,2**.

Finally, a stable analogue was obtained using the potentially tridentate bis(2-diphenylphosphinoethyl)phenyl phosphine (triphos) ligand that generates the dinuclear complex $[Cu(CFClCF_2H)(\mu–\kappa^1,\kappa^2\text{-triphos})]_2$ (**2-3**) as determined by ^{19}F NMR and mass spectrometry (**Scheme 2.3**). Triphos reacts with expulsion of PPh_3 from Stryker`s reagent to give a hydride intermediate that we could not characterize (both ^{31}P and ^{1}H NMR show broad resonances as shown in Appendix). Although we could not obtain a suitable crystal of **2-3** for X-ray crystallographic analysis, we assign the dimeric structure based on the molecular structure of the iodide analog determined by White and co-workers in 1991.[18]

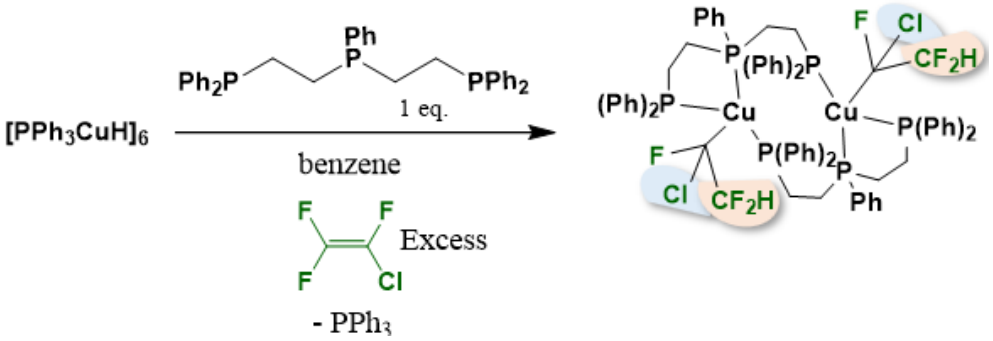

Scheme 2.3 Synthesis of $[Cu(CFClCF_2H)(\mu–\kappa^1,\kappa^2\text{-triphos})]_2$ (**2-3**).

The two-resonance ^{19}F NMR spectrum of **2-3** in benzene is overly simplistic due to the similarity of the diastereotopic CF_2 chemical shifts. Adding 8 equiv of dimethylsulfoxide (DMSO) sharpens the resonances and distinguishes the diastereotopic CF_2 group resonances (**Figure 2.1**). Another S ligand, tetrahydrothiophene (THT), also sharpens the resonances, and the CF_2 chemical shifts are further distinguished using THT as the solvent. The ^{31}P NMR spectra of **2-3** provides evidence for a fluxional process that equilibrates the two PPh_2 arms of the triphos ligand. At -40 °C in THT solvent, the three broad resonances appear at 9, -4 and -8.5 ppm while at 22 °C two broad resonances at -8 and -12 ppm in a 2:1 ratio are observed (Fig. A2.28,29). Unfortunately, heating a solution of **2-3** to obtain the high-temperature limiting spectrum led to decomposition.

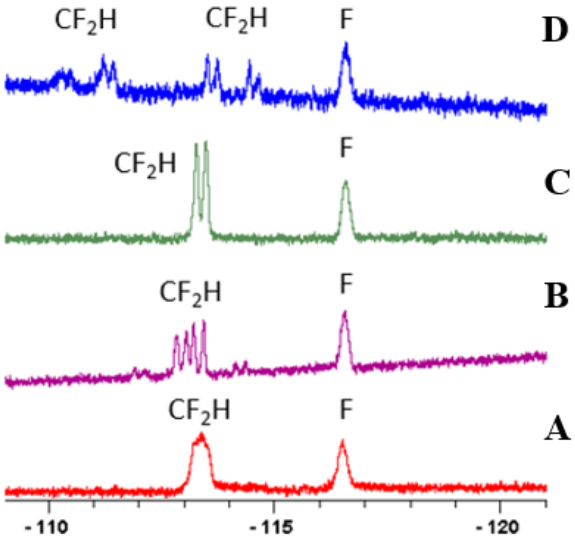

Figure 2.1 ^{19}F NMR spectra of complex **2-3** in benzene (**A**), with 8 eq. of DMSO (**B**), 8 eq. of THT (**C**), and THT as solvent (**D**).

*2.2.2 Reactivity of **2-3** with aroyl chlorides:* To investigate the reactivity of **2-3** towards organic electrophiles, we started our studies by screening aroyl chlorides and *p*-fluoro-benzyl bromide in benzene. Although we still observed the presence of **2-3** after 24 h, none of the desired product was obtained. Next, we tried DMSO, in which the solution changed from yellow to green (**Figure 2.2**). Indeed, conducting the reaction in DMSO as a solvent at room temperature (25 °C), the R^F group (-$CFClCF_2H$) could be

transferred to electron-poor or -rich benzoyl chlorides (**2-4a-i**), albeit in low yield (**Scheme 2.4**). Unfortunately, neither addition of other ligands such as phen, additives such as CuBr, or increasing the

Figure 2.2 Variation of reaction color in DMSO after addition of substrate.

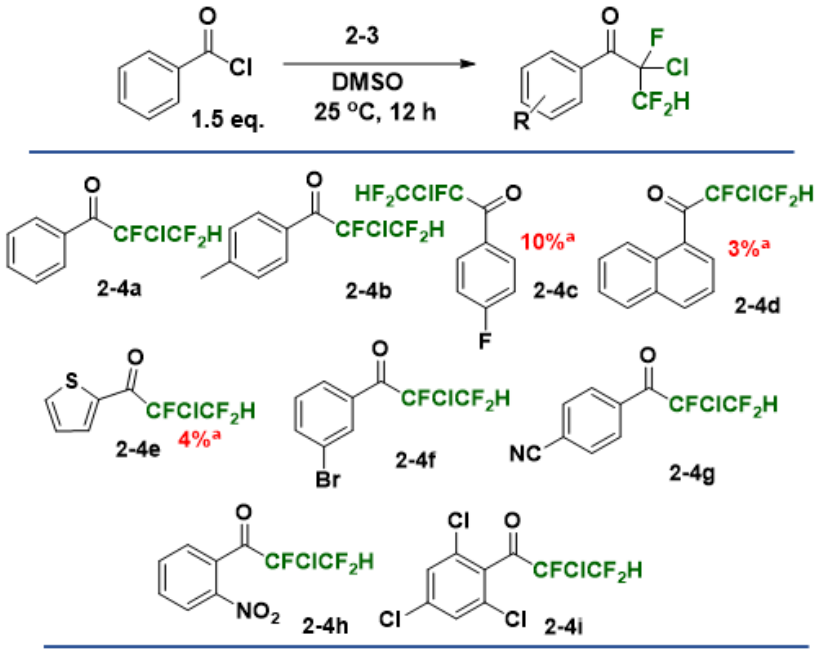

[a]Yields determined by ^{19}F NMR with trifluorotoluene as the internal standard.

Scheme 2.4 Perfluoroalkylation of aroyl chlorides. All reactions gave poor yields; those shown included the internal standard.

temperature had a positive effect on the yield. Nonetheless, the -$CFClCF_2H$ group is transferred to 4-fluorobenzoyl chloride using DMSO as solvent (10%) or ligand in benzene (16%). We also observed by-products, including LCu-CF_2H, a common side product in the following chapters' reactions. The ^{19}F NMR spectrum shows a significant shift of the C*F*Cl fluorine resonance after being transferred to the organic

electrophile (**Figure 2.3**). Although most products were characterized only by ^{19}F NMR spectroscopy, the composition of the *p*-tolyl derivative **2-4b** was confirmed by GC-MS observation of M^+.

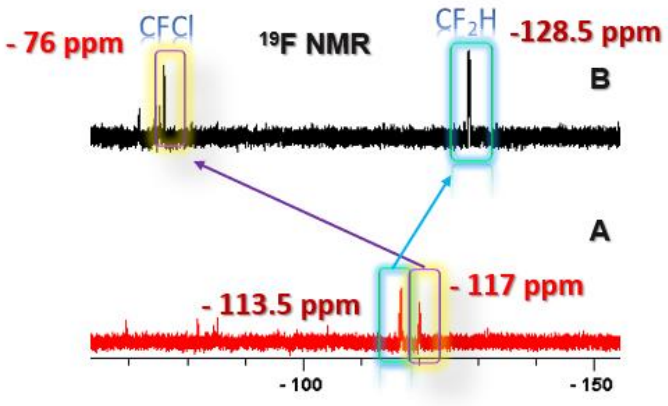

Figure 2.3 ^{19}F NMR (282 MHz) spectra of **2-3** (**A**) and benzoyl-R^F (**B**) in DMSO at 25 °C.

*2.2.3. Reactivity of **2-3** with aryl iodides:* A further investigation of the electrophile scope showed that in the presence of aryl iodide, oxidative aryl-aryl homocoupling products are dominant, besides the *cis*-CHF=CFH hydrodehalogenation product. Aryl-aryl homocoupling products suggest a transmetallation from CuR^FArI to another Cu center, perhaps favoured by the bimetallic structure proposed in this work. Although aryl-aryl coupling between complex **2-3** and electron-poor electrophile 4-fluoro-iodobenzene was observed in different solvents (benzene, DMF, DMPU and DMSO), decomposition of the complex is also occurring simultaneously. Unfortunately, raising the temperature only accelerated the decomposition of **2-3**.

2.3 CONCLUSION

This work expands our knowledge of Cu-R^F synthesis using Cu-H and fluoroalkenes with a variety of ligands. CTFE certainly turned out to be the most challenging fluoroalkene with $P(OEt)_3$ generating an observable CuR^F product and $P(O^iPr)_3$ not. With PPh_3 we see the product but not with $PMePh_2$. Moreover, only with triphos could we obtain a product that is stable upon removal of the CTFE and solvent. Based on our observation of high m/e cations in the mass spectrum and a previous molecular structure determination for the iodide analog, we propose a dimeric structure for the CuR^F(triphos) complex **2-3.** In addition, transfer to aroyl chlorides gave low yields even after addition of nitrogen ligands (PMDTA, DMAP, TMEDA) or CuBr. These reactions were also accompanied by HF formation, suggesting

formation of Cu-CCl=CF_2 (cf. formation of Cu-CF=CF_2 from trifluoroethylene insertion into Cu-F reported previously by Andrella[16]) but we were unable to identify this species by NMR spectroscopy.

2.4 EXPERIMENTAL SECTION

2.4.1. General Procedures: Experiments were conducted under nitrogen, using Schlenk techniques or a 164 MBraun glove box. All solvents were deoxygenated by purging with nitrogen. Tetrahydrofuran (THF), acetonitrile (MeCN) and toluene were dried on columns of activated alumina using a J. C. Meyer (formerly Glass Contour®) solvent purification system. Cyclopentyl methyl ether (CPME) and benzene-d_6 (C_6D_6) were dried by stirring over activated alumina (ca. 10 wt. %) overnight, followed by filtration. All solvents were stored over activated (heated at ca. 250 °C for >10 h under vacuum) 4 Å molecular sieves. Glassware was oven-dried at 120 °C for >2 h. The following chemicals were obtained commercially, as indicated: dimethylformamide (DMF, Alfa Aesar anhydrous, 99.8%), dimethylsulfoxide (DMSO, Alfa Aesar anhydrous, 99.8%), N,N′- dimethylpropyleneurea (DMPU, Alfa Aesar anhydrous, 98%), cyclopentyl methyl ether (CPME, Sigma-Aldrich, >99.9%), iodobenzene (Alfa Aesar, 98 %), all aroyl chlorides and aryl iodides (SiGMA), triphenylphosphine (PPh3, Oakwood chemicals, 99%), triisopropylphosphite [$P(OiPr)_3$, Sigma-Aldrich, 98%], triethylphosphite [$P(OEt)_3$, Sigma-Aldrich, 98%], methyldiphenylphosphine ($PMePh_2$, Acros Organics, 99%). bis(2-diphenylphosphinoethyl)phenyl phosphine (triphos, Sigma-Aldrich), 1,1,1-tris(diphenylphosphinomethyl) (tripod, Sigma Aldrich), 1,10-phenanthroline (phen, Sigma-Aldrich), pyridine (pyr, Sigma-Aldrich, 99.8%), 2,2';6',2"-terpyridine (terpy, Sigma-Aldrich,) N,N,N',N",N"-pentamethyldiethylenetriamine (PMDTA, Sigma-Aldrich, 99%). The [CuH(PPh3)]6 was synthesized as previously reported.[23] Electrospray ionization mass spectral data were collected using an Applied Biosystem API2000 triple quadrupole mass spectrometer. GC-MS analyses were performed on an Agilent Technologies 6890N GC system equipped with an Agilent Technologies 5973 Network mass selective detector. NMR spectra were recorded on a 300 MHz Bruker Avance instrument at room temperature (21-23 °C) unless stated otherwise. $^{31}P\{^1H\}$ NMR data were referenced to external H_3PO_4 (85 % aqueous solution) set to 0.0 pm. Unless stated otherwise, ^{19}F NMR spectra were referenced to internal standard α,α,α-trifluorotoluene ($PhCF_3$; Sigma-Aldrich, 99%), deoxygenated by purging with nitrogen, stored over activated 4 Å molecular sieves), set to –63.5 ppm.

2.4.2. Synthesis of copper complexes:

*Generation of $Cu(CFClCF_2H)[P(OEt)_3]_3$ (**2-1**):* The red complex $[(PPh_3)_3CuH]_6$ (10 mg, 0.03 mmol) was loaded into an NMR tube and dissolved in 0.5 mL of benzene. $P(OEt)_3$ (10 mg, 0.06 mmol) was added to the solution and the NMR tube was sealed with a cap. Using a gas-tight syringe, 5 equiv of CTFE were then added to the same NMR tube. The reaction was left to sit at room temperature for 12 h. ^{19}F NMR –115.9 (ddd, $^2J_{FF}$ = 264, 2 J_{FH} = 60, $^3J_{FF}$ = 9 Hz, CF_2H), –116.2 (dd, $^2J_{FF}$ = 264, $^2J_{FH}$ = 59, $^3J_{FF}$ = 12 Hz CF_2H), –118.7 ppm (ddd, $^3J_{FF}$ = 12, 9, 3 JFH = 8 Hz, CF). $^{31}P\{^1H\}$ NMR 131.9 ppm. (Figs. A2-A4). Upon removal of the CTFE and solvent in vacuo, no ^{19}F NMR resonances were observed (Fig. A5) and the ^{31}P NMR spectrum showed a singlet resonance at 140 ppm due to $CuR^F[P(OEt)_3]_2$.

*Generation of $Cu(CFClCF_2H)(PPh_3)_2$ (**2-2**): The* red complex $[(PPh_3)_3CuH]_6$ (10 mg, 0.03 mmol) was loaded into an NMR tube and dissolved in 0.5 mL of benzene. PPh_3 (15 mg, 0.06 mmol) was added to the solution and the NMR tube swas ealed with a cap. Using a gas-tight syringe, 5 equivalent of CTFE were then added to the same NMR tube. The reaction was left to sit at room temperature for 12 h. ^{19}F NMR –121.1 (mult, CF), –121.8 (dd, $^2J_{FF}$ = 280, $^2J_{FH}$ = 59 Hz, CF_2H), –124.2 ppm (dd, $^2J_{FF}$ = 280, $_2$JFH = 59 Hz, CF2H) (Fig. S7). On removal of the CTFE and solvent in vacuo, a number of new resonances were observed (Fig. A8).

*Synthesis of $[Cu(CFClCF_2H)(\mu–\kappa^1,\kappa^2\text{-triphos})]_2$ (**2-3**):* The red complex $[(PPh_3)_3CuH]_6$ (150 mg, 0.46 mmol) was loaded into a vial glass and dissolved in 5 mL of benzene. Triphos (248 mg, 0.46 mmol) was added to the solution and the vial was sealed with a cap. Using a gas-tight syringe, 5 equiv of CTFE were added to the vial and the reaction was left to sit at room temperature for 24 h. The reaction mixture changed from deep red to light brown. The solvent was removed under vacuum, and the residue was washed with Et_2O. The resulting oil was triturated with hexane, and the ensuing precipitate was collected as a light brown solid: 503 mg = 75% yield. ^{19}F NMR (C_6D_6) –116.7 (dmult, $^2J_{FH}$ = 60 Hz, CF_2H), –116.8 (dmult, $^2J_{FH}$ = 60 Hz, CF_2H), –119.9 ppm (mult, CFCl). $^{31}P\{^1H\}$ NMR (C_6D_6) (br, ^1P), -12 ppm (br, ^2P). ^1H NMR (C_6D_6) δ 8.5-6.5 (ov mult, aryl CH), 6.17 ppm (trd, $^2J_{HF}$ = 60, $^3J_{HF}$ = 10 Hz, CF_2H), 2-1.5 (br, CH_2) (Figs. 214 A215-A218). High-resolution electrospray ionization MS: mass calculated for [(H_3O-M]+ 215 $C_{72}H_{63}Cl_2Cu_2F_6NaOP_6$ 1449.1597 m/z, 1447.1797 found (Fig. A2.20).

2.4.3. General experimental procedure for fluoroalkylation of aroyl chlorides, NMR scale: Complex **2-3** (10 mg, 0.007 mmol) was loaded into an NMR tube and mixed with 0.5 mL of DMSO. Benzoyl chloride (0.01 mmol) and $PhCF_3$ (20 μL, 0.01 mmol/mL) were added to the solution and the reaction was analyzed by ^{19}F NMR after 12 h.

PhC(O)CFCl(CF_2H) (**2-4a**): ^{19}F NMR –72.4 (t, $^3J_{FF}$ = 12 Hz, C*F*Cl), -124.8 ppm (dd, $^2J_{FH}$ = 60, $^3J_{FF}$ = 12 Hz, C*F*$_2$H).

p-CH_3-PhC(O)CFCl(CF_2H) (**2-4b**): ^{19}F NMR –72.5 (t, $^3J_{FF}$ = 12 Hz, C*F*Cl), -124.9 ppm (dd, $^2J_{FH}$ = 56, $^3J_{FF}$ = 12 Hz, C*F*$_2$H). GC-MS expected 236 m/z, found 234 m/z (1%) and 119 m/z (90%).

p-F-PhC(O)CFCl(CF_2H) (**2-4c**): ^{19}F NMR –73.9 (t, $^3J_{FF}$ = 14 Hz, C*F*Cl), -101.6 (s, C*F*), -125 ppm (dd, $^2J_{FH}$ = 54, $^3J_{FF}$ = 14 Hz, C*F*$_2$H).

naphthyl-C(O)CFCl(CF_2H) (**2-4d**): ^{19}F NMR –72 (t, $^3J_{FF}$ = 14 Hz, C*F*Cl), -124.8 ppm (dd, $^2J_{FH}$ = 55, $^3J_{FF}$ = 14 Hz, C*F*$_2$H).

2-thiophenyl-C(O)CFCl(CF_2H) (**2-4e**): ^{19}F NMR –71.8 (t, $^3J_{FF}$ = 13 Hz, C*F*Cl), -124.2 ppm (dd, $^2J_{FH}$ = 54, $^3J_{FF}$ = 13 Hz, C*F*$_2$H).

m-Br-PhC(O)CFCl(CF_2H) (**2-4f**): ^{19}F NMR –71.9 (t, $^3J_{FF}$ = 14 Hz, C*F*Cl), -124.3 ppm (dd, $^2J_{FH}$ = 53, $^3J_{FF}$ = 14 Hz, C*F*$_2$H).

p-NC-PhC(O)-CFCl(CF_2H) (**2-4g**): ^{19}F NMR –71.8 (t, $^3J_{FF}$ 12 Hz, C*F*Cl), -124.3 ppm (dd, $^2J^{FH}$ = 53, $^3J_{FF}$ = 12 Hz, C*F*$_2$H).

2-NO_2-PhC(O)CFCl(CF_2H) (**2-4h**): ^{19}F NMR –71.6 (t, $^3J_{FF}$ 14 Hz, C*F*Cl), -124.1 ppm (dd, $^2J_{FH}$ = 53, $^3J_{FF}$ = 14 Hz, C*F*$_2$H).

2,4,6-Cl_3-PhC(O)CFClCF_2H (**2-4i**): ^{19}F NMR – 71.8 (t, $^3J_{FF}$ = 14 Hz, C*F*Cl), -124.3 ppm (dd, $^2J_{FH}$ = 55, $^3J_{FF}$ = 14 Hz, C*F*$_2$H).

General experimental procedure for attempted fluoroalkylation of aryl iodides, NMR scale: Complex **2-3** (10 mg, 0.007 mmol) was loaded into an NMR tube and mixed with 0.5 mL of solvent (DMSO, benzene or CPME). 1.5 equiv. of substrate 4-fluoro-iodobenzene (1.2 μL, 0.0105 mmol), methyl 2- iodobenzoate (1.5 μL, 0.0105 mmol), or 4-iodo-benzonitrile (2.4 mg, 0.0105 mmol) were then added to the solution and the reaction was analyzed by ^{19}F NMR after 7 h at the reported

temperature. In another NMR tube, complex **2-3** (10 mg, 0.007 mmol) in benzene, 1.5 equiv. of substrate and 8 equiv. of ligands pyridine (4.5 μL , 0.056 mmol), DMSO (4 μL, 0.056 mmol) or DMF (4,3 μL, 0.056 mmol) were added to the solution. The reactions were left for 7 h at the reported temperature and analyzed by ^{19}F NMR. Finally, a mixture of **2-3** (10 mg, 0.007 mmol) in benzene, 1.5 equiv of methyl 2-iodobenzoate (1.5 255 μL, 0.0105 mmol), 28 equiv of DMSO and 2 equiv of CuBr (2 mg, 0.014 mmol) were stirred for 12 h and monitored by ^{19}F NMR (Fig. A2.70).

2.5 REFERENCES

(1) Richardson, P. Applications of fluorine to the construction of bioisosteric elements for the purposes of novel drug discovery. *Expert Opin. Drug Discov.* **2021**, *16* (11), 1261–1286. https://doi.org/10.1080/17460441.2021.1933427.

(2) Yu, Y.; Liu, A.; Dhawan, G.; Mei, H.; Zhang, W.; Izawa, K.; Soloshonok, V. A.; Han, J. Fluorine-containing pharmaceuticals approved by the FDA in 2020: Synthesis and biological activity. *Chin. Chem. Lett.* **2021**, *32* (11), 3342–3354. https://doi.org/https://doi.org/10.1016/j.cclet.2021.05.042.

(3) Jeschke, P. Manufacturing approaches of new halogenated agrochemicals. *Eur. J. Org. Chem.* **2022**, *2022* (12), e202101513. https://doi.org/https://doi.org/10.1002/ejoc.202101513.

(4) Nerella, S. G.; Bhattacharya, A.; Thacker, P. S.; Tulja, S. Synthetic methodologies and PET imaging applications of fluorine-18 radiotracers: A patent review. *Expert Opin. Ther. Pat.* **2022**, *32* (4), 455–473. https://doi.org/10.1080/13543776.2022.2032649.

(5) McLoughlin, V. C. R.; Thrower, J. A route to fluoroalkyl-substituted aromatic compounds involving fluoroalkylcopper intermediates. *Tetrahedron* **1969**, *25* (24), 5921–5940. https://doi.org/https://doi.org/10.1016/S0040-4020(01)83100-8.

(6) Castillo-Pazos, D.J.; Lasso, J.D.; Li, C.-J. Modern methods for the synthesis of perfluoroalkylated aromatics. *Org. Biomol. Chem.* **2021**, *19,* 7116-7128.

(7) Morimoto, H.; Tsubogo, T.; Litvinas, N. D.; Hartwig, J. F. A broadly applicable copper reagent for trifluoromethylations and perfluoroalkylations of aryl iodides and bromides. *Angew. Chem. Int. Ed.* **2011**, *50* (16), 3793–3798. https://doi.org/10.1002/anie.201100633.

(8) Saranya, P. V.; Aneeja, T.; Anilkumar, G. Palladium-catalyzed difluoromethylation and difluoroalkylation reactions: An overview. *Appl. Organomet. Chem.* **2022**, *36* (2), e6503. https://doi.org/https://doi.org/10.1002/aoc.6503.

(9) Ispizua-Rodriguez, X.; Barrett, C.; Krishamurti, V.; Surya Prakash, G. K. Silicon-based difluoromethylations, difluoromethylenations, pentafluoroethylations, and related fluoroalkylations. *Prog. Fluorine Sci.* **2021**, *6*, 117-218. https://doi.org/https://doi.org/10.1016/B978-0-12-819874-2.00012-6.

(10) Xie, Q.; Hu, J. The development of new reagents and reactions for synthetic organofluorine chemistry by understanding the unique fluorine effects. in *Organofluorine Chemistry: Synthesis, Modeling and Applications*, Szabo, K.; Selander, N., Eds. Wiley, 2021, pp 1–22. https://doi.org/https://doi.org/10.1002/9783527825158.ch1

(11) Yin, W.; Wang, Z.; Huang, Y. Highly ortho-selective trifluoromethylthiolation reactions using a ligand exchange strategy. *Adv. Synth. Catal.* **2014**, *356* (14–15), 2998–3006. https://doi.org/https://doi.org/10.1002/adsc.201400362.

(12) Mestre, J.; Castillón, S.; Boutureira, O. "Ligandless" pentafluoroethylation of unactivated (hetero)aryl and alkenyl halides enabled by the controlled self-condensation of $TMSCF_3$-derived $CuCF_3$. *J. Org. Chem.* **2019**, *84* (23), 15087–15097. https://doi.org/10.1021/acs.joc.9b02001.

(13) Pan, S.; Xie, Q.; Wang, X.; Wang, Q.; Ni, C.; Hu, J. Copper-mediated pentafluoroethylation of organoboronates and terminal alkynes with $TMSCF_3$. *Chem. Commun.* **2022**, *58* (33), 5156–5159. https://doi.org/10.1039/D2CC00975G.

(14) Bour, J. R.; Kariofillis, S. K.; Sanford, M. S. Synthesis, reactivity, and catalytic applications of isolable (NHC)Cu(CHF_2) complexes. *Organometallics* **2017**, *36* (7), 1220–1223. https://doi.org/10.1021/acs.organomet.7b00025.

(15) Miller, W.T.; Burnard, R.J. Perfluoroalkylsilver compounds. *J. Am. Chem. Soc.*, **1968**, ***90*** , 7367.

(16) Andrella, N. O.; Liu, K.; Gabidullin, B.; Vasiliu, M.; Dixon, D. A.; Baker, R. T. Metal heptafluoroisopropyl (M-hfip) complexes for use as hfip transfer agents. *Organometallics* **2018**, *37* (3), 422–432. https://doi.org/10.1021/acs.organomet.7b00837.

(17) Andrella, N. O.; Xu, N.; Gabidullin, B. M.; Ehm, C.; Baker, R. T. Selective copper complex-catalyzed hydrodefluorination of fluoroalkenes and allyl fluorides: A tale of two mechanisms. *J. Am. Chem. Soc.* **2019**, *141* (29), 11506–11521. https://doi.org/10.1021/jacs.9b03101.

(18) Hart, R. D.; Skelton, B. W.; White, A. H. Lewis-base adducts of group 11 metal(I) compounds. LXI. The 1 : 1adducts of the copper(I) halides (Cl, Br, I) with bis(2-diphenylphosphinoethyl)phenylphosphine, "Triphos." *Aust. J. Chem.* **1991**, *44* (7), 919–925.

(19) Lee, D.-W.; Yun, J. Direct synthesis of Stryker's reagent from a Cu(II) salt. *Tet. Lett.* **2005**, *12*, 2037-2039.

Chapter 3. Copper-Mediated -$CF(OCF_3)CF_2H$ Transfer to Organic Electrophiles

Contributions to Knowledge:

Copper-Mediated -$CF(OCF_3)(CF_2H)$ Transfer to Organic Electrophiles
Luana L. T. N. Porto, Nicole Johnson, Jeffrey A. Ovens, Christian Ehm and R. Tom Baker**
To be submitted, Sept. 2022.

Chapter Contributions: Our collaborator Dr. Christian Ehm (University of Naples, Italy) performed DFT calculations, Inorganic Chemistry Exchange (ICE) undergraduate student Nicole Johnson helped to expand the substrate scope, and Dr. Jeffrey Ovens collected and refined the X-ray diffraction data for molecular structure determination. Prof. Baker helped plan the experiments and refine the manuscript text. The first draft of the paper and all other experiments were performed by Luana Porto.

Abstract: Fluoroalkyl groups containing the -CF_2H functional group have drawn interest for their ability to simultaneously increase lipohilicity and provide a hydrogen-bonding function in bioactive compounds. Regioselective insertion of commercially available perfluoro(methyl vinyl ether), CF_2=$CF(OCF_3)$, into Cu-H, derived from $[CuH(PPh_3)]_6$ (Stryker`s reagent) and ancillary ligands L, affords a series of stable $Cu[CF(OCF_3)CF_2H]L_n$ complexes, some of which mediate the fluoroalkylation of aroyl chlorides. Reaction optimization and computational analysis identified a unique role for dimethylsulfoxide as a privileged co-ligand, enabling fluoroalkylation of a broad scope of aryl iodides.

3.1 INTRODUCTION

As noted in previous chapters, the success of organofluorine compounds in the pharmaceutical (more than 20% contain at least one fluorine)[1] and agrochemical (more than 40% contain at least one fluorine)[2] markets have been inspiring many scientists and researchers to develop more efficient late-stage fluorination[3] and fluoroalkylation protocols.[4] While there are many methodologies to incorporate the trifluoromethyl group into organic substrates[5], fewer examples have been reported for other fluoroalkyl groups such as -C_2F_5,[6] -OCF_3[7], and -CF_2H.[8] Nonetheless, such functional groups have already appeared in useful drugs: *cf.* -OCF_3 in Riluzole® (glutamate antagonist used as an anticonvulsant)[9] and Triflumuron (pesticide)[10] and -CF_2H in PQR620 (mTOR inhibitor, anti-cancer)[11] and Pantoprazole (proton pump inhibitor; **Figure 3.1**).[12] Increased interest in these two substituents results from their bioisosteric properties (cf., CF_2H for OH and SH). In contrast to the OCH_3 group, the OCF_3 group is not co-planar with its attached aryl ring, and adjacent σ bonds can interact with the low-energy σ* orbital of the O-C_{CF3} bond.[13] The -CF_2H group has been intensively studied over the past few years due to its unique properties, such as Brønsted acidity and ability to act as a hydrogen-bond donor while still modulating lipophilicity.[14]

Moreover, its small steric signature allows it to adopt an optimal conformation based on specific drug targets.[15,16]

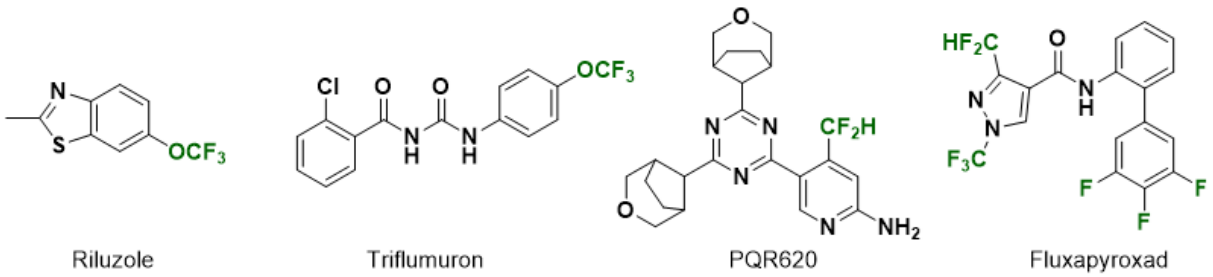

Figure 3.1 Bioactive compounds containing -OCF_3 and -CF_2H groups.

As detailed in Chapter 1, the Baker group recently reported the perfluoroisopropylation of aroyl chlorides with a phenanthroline copper heptafluoroisopropyl complex, [Cu(hfip)(PPh_3)(phen)].[17] Although phenanthroline was necessary for successful fluoroalkylation, stabilization of the hfip group was initially achieved by inserting hexafluoropropene (HFP) into the Cu-F bond of $CuF(PPh_3)_3$. However, the hfip group transfer was limited to aroyl chlorides, other important electrophiles like aryl iodides or allyl halides remained inaccessible.

In this work, we employ commercially available perfluoro(methyl vinyl ether), PMVE, CF_2=CF(OCF_3), in the synthesis of new copper fluoroalkyls Cu[CF(OCF_3)CF_2H]L_n that contain geminal -OCF_3 and -CF_2H groups. We also demonstrate, both experimentally and computationally, the privileged role of the dimethylsulfoxide co-ligand in enabling trifluoroalkylation of a range of aryl iodides. Finally, our computational studies show that the elimination step resembles S_N2 $(R^F)^-$ anion attack at the carbonyl carbon.

3.2 RESULTS AND DISCUSSION

3.2.1 Synthesis and characterization of Cu[CF(OCF_3)CF_2H]Ln: Reaction of 5 equiv of PMVE with a mixture of $[CuH(PPh_3)]_6$, PPh_3 (3 equiv per Cu) and tetramethyldisiloxane (TMDSO) (1.5 equiv) gave a light red solution of Cu[CF(OCF_3)CF_2H](PPh_3)$_2$ (**3-1**) from which pink crystals could be isolated in 90% yield. Addition of the siloxane converted any Cu-F (by-product of β-F elimination) back to Cu-H to avoid the formation of Cu[CF(OCF_3)CF_3](PPh_3)$_2$ (**3-2; Scheme 3.1**). No evidence for the other regioisomer [Cu-

$CF_2CHF(OCF_3)(PPh_3)_2$] was obtained. Similar reactions using the more basic $PMePh_2$ ligand did not selectively afford the desired product, generating P-F bonds and additional uncharacterized side products.

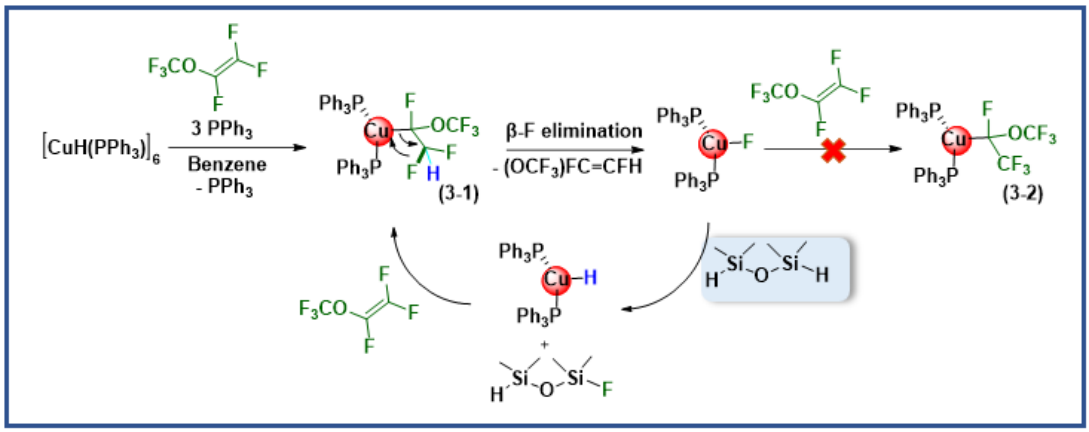

Scheme 3.1 Synthesis of $Cu[CF(OCF_3)CF_2H](PPh_3)_2$ (**3-1**)

The ^{19}F NMR spectrum of **3-1** in C_6D_6 displayed a doublet for the OCF_3 ($^4J_{FF}$ = 4 Hz), a multiplet for Ca-*F* and typical diastereotopic CF_2 resonances at -120.8 (ddd, $^2J_{FF}$ = 280, $^3J_{FH}$ = 58, $^3J_{FF}$ = 5 Hz), and -127.0 ppm (ddd, $^2J_{FF}$ = 280, $^2J_{FH}$ = 60, $^3J_{FF}$ = 5 Hz) (Figs. S1,2). The molecular structure of **3-1** shows a distorted trigonal-planar copper with a P-Cu-P angle of 114.5º and P-Cu-C angles of 126.6 and 118.5º (**Figure 3.2**). The Cu-C bond distance (2.062 Å) is slightly longer than that observed in Cu-hfip (2.003 Å)[17] and Cu-CF_2CF_3 complexes (1.99 Å),[18] presumably reflecting the influence of the bulky OCF_3 group. Moreover, the C_α-F bond distance (1.55 Å) is also longer *vs* Cu-hfip (1.44 Å) and Cu-CF_2CF_3 (1.40 Å).

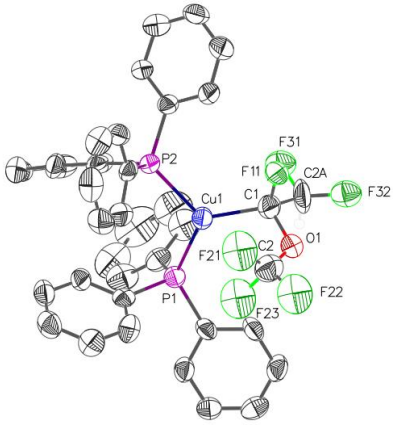

Figure 3.2 Molecular diagram representation of the molecular structure of **3-1**. Thermal ellipsoid probabilities are set at 50%, and hydrogens atoms and alternate conformations of disordered ttfet group are omitted. Selected bond distances (Å) and angles (deg): Cu-C 2.012(18)-2.062(16) Cu-P1 2.271(2) Cu-P2 2.286(2) P1-Cu-C1 118.50(4)-120.5(5), P1-Cu-P2 114.50(9), P2-Cu-C1 121.2(4)-126.7(4).

*3.2.2 Reactivity of **3-1** with aroyl chlorides:* Beginning with benzoyl chloride, we added 1 equiv of **3-1** in a range of solvents (**Table 3.1**, entries 1-9) and monitored the reaction using ^{19}F NMR spectroscopy. In contrast to our previous results with transfer of the hfip group that required dimethylformamide (DMF) solvent,[17] successful transfer of the 1-trifluoromethyl-1,2,2-trifluoromethoxy-ethyl (ttfet) group to give **3-3a** was only realized in dimethylsulfoxide (DMSO); using **3-1** with other coordinating polar solvents led to decomposition of the Cu complex after 2 h. Moderate heating (40 °C) of the reactions in dry tetrahydrofuran (THF), toluene, diethyl ether (Et_2O) or hexane gave fluoroalkane [$CHF(OCF_3)CF_2H$] from the decomposition of **3-1**. Formation of the fluorinated ketone was indicated by the shift of the C_α-F ^{19}F NMR resonance from -119.9 ppm in **3-1** to -81 ppm in **3-3a.**

Table 3.1 Fluoroalkylation of benzoyl chloride in different solvents.

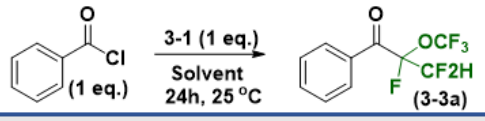

Entry	Solvent	Yield[a] (%)
1	THF	0
2	Et_2O	0
3	DMF	0
4	DMA	0
5	MeCN	0
6	CPME	0
7	DMSO	70
8	Toluene	0
9	Hexane	0

[a]yields determined by ^{19}F NMR with trifluorotoluene as internal standard

After identifying the optimal solvent, we next examined a limited aroyl chloride substrate scope (**Table 3.2**). Substituted aroyl chlorides were treated with complex **3-1** in DMSO to give the corresponding fluoroalkyl ketones (**3-3b-i)** in low to good yields. The ^{19}F NMR spectra of **3-3b-i** are all very similar to that of **3-3a** (see Appendix). The fluoroalkyl transfer was most successful with electron-poor substrates, although poor or no yield was obtained from the 4-cyano and 4-nitro analogs. No attempts were made to separate the products from the high-boiling dmso solvent.

3.2.3 Influence of ancillary ligands on fluoroalkylation efficiency: Chelating nitrogen ligands have been shown previously to promote Cu-mediated fluoroalkyl transfer to organic electrophiles.[17-19] Although the

reaction product of **3-1** with 1,10-phenanthroline (**3-4a)** could be characterized by ^{19}F NMR spectroscopy, the formation of several by-products hampered its full characterization, whereas reaction of **3-1** with

Table 3.2 Aroyl chloride fluoroalkylation substrate scope

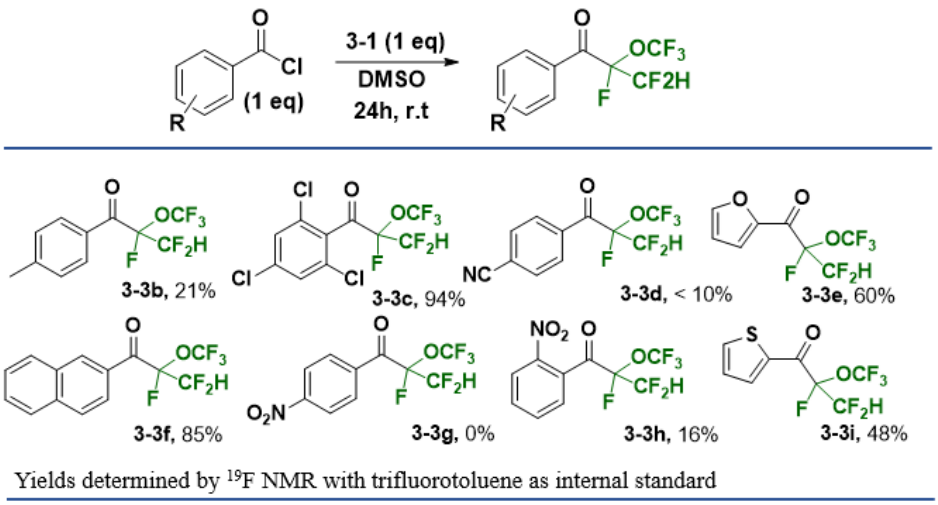

4,4'-dichloro-2,2'-bipyridine proceeded smoothly to afford 4-coordinate Cu[CF(OCF$_3$)CF$_2$H](PPh$_3$)(bpy-Cl$_2$) (**3-4b).** Finally, reaction of **1** with the 7-Dipp NHC ligand gave 2-coordinated analogue **3-5** (**Scheme 3.2**). The molecular structure of **3-4b** exhibits a distorted tetrahedral geometry around Cu **(**C1-Cu-P1 = 133^o) analogous to the previously reported Cu(hfip)(phen)(PPh$_3$) complex.[17] The molecular structure of **3-5** features the R^F group and the seven-membered ring NHC in a linear geometry, with shorter Cu-C$_\alpha$ and C$_\alpha$-F bond distances than those in **3-1** or **3-4b** (**Figure 3.3**). Complexes **3-4a,b** could not effect fluoroalkylation of benzoyl chloride in DMSO**.** Although the **^{19}**F NMR spectra of reactions of **3-5** with several aroyl chlorides reveal new products, chemical shifts are not consistent with transfer of the *ttfet* group (i.e., no Cα-F resonance at -81 ppm; see Appendix).

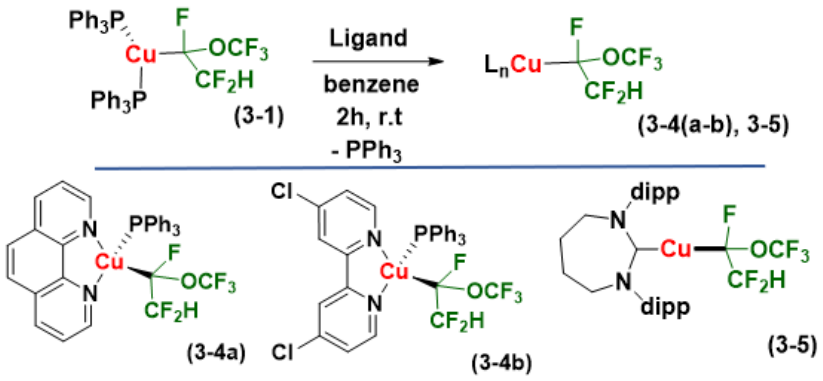

Scheme 3.2 Synthesis of additional Cu-ttfet complexes.

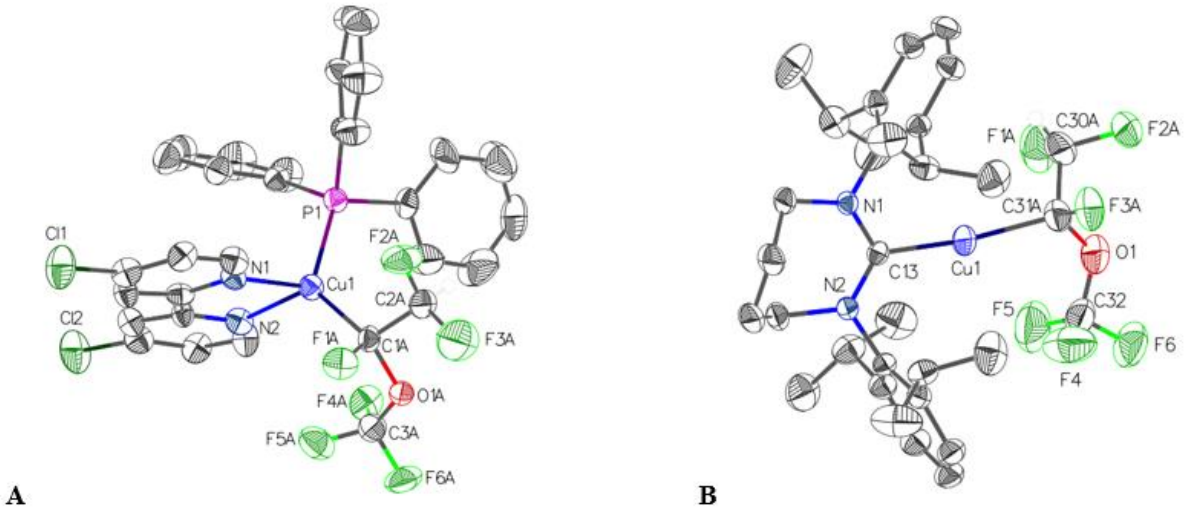

Figure 3.3 Molecular diagram representation of the molecular structures of **3-4b** (**A**) and **3-5** (**B**). Thermal ellipsoid probabilities are set to 50%, with hydrogen atoms and alternate conformations for disordered ttfet group omitted for clarity. Selected bond distances (Å) and angles (deg) for **3-4b**: Cu-C1 1.99(2)-2.02(2), C1-F1 1.42(2)-1.44(2), C1-Cu-P1 123(1)-133(1) and for **3-5**: Cu-C31 1.976(5)-2.033(7), Cu-C13 1.920(2), C31-F3 1.414(9)-1.436(7), C31-Cu-C13 165.1(2).

3.2.4 Fluoroalkylation of aryl iodides: In previous work, we were unable to transfer the hfip group from Cu(hfip)(phen)(PPh_3) to aryl iodides.[17] Similarly, using **3-1** in DMSO led only to decomposition before any transfer could occur. Curiously, when conducting the reaction in benzene solvent at 50 ˚C with just 8 equiv of DMSO, we observed some ttfet transfer to several electron-poor aryl iodides (methyl-2-iodobenzoate, 4-fluoro-iodobenzene, 4-nitro-iodobenzene, 3-iodobenzonitrile and 2-iodopyridine). ^{19}F NMR spectra shows that the C_α-F resonance shifts from -119.9 ppm in **3-1** to -131 ppm in the fluoroalkylated arenes (see Appendix). Increasing the concentration beyond 8 equiv led to more decomposition of complex **3-1** (see A3). In his work on pentafluoroethylation, Hartwig reported that less

electron-donating bpy ligands increased the rate of R^F transfer from Cu to aryl chlorides.[20] Indeed, heating **3-4b** with electron-poor aryl iodides at 85 °C in toluene provided our second example of successful transfer of the ttfet group. However, yields were limited due to poor selectivity (see A3).

Given these first results with DMSO and bpy-Cl_2, we sought to optimize the fluoroalkylation of aryl halides. Inspired by previous work by Grushin et al.[21] and Boutureira and co-workers[22], we aimed to access a polar solvent-stabilized, "ligandless" Cu[$CF(OCF_3)CF_2H$] complex generated from complex **3-1** and Cu halide salts, Cu-X, to trap the PPh_3 ligands. To avoid decomposition of **3-1**, we created a new protocol using a minor amount of coordinating solvent to stabilize the copper salt in benzene, followed by precipitation of $(PPh_3)_2CuX$. The ArR^F (**3-6a**) yield decreased to less than 5% when DMF was used as co-solvent (**Table 3.3**, entries 4, 8 and 12). Further screening of different CuX identified CuBr as the most efficient copper salt, producing **3-6a** in 82% when used with a 2:1:1 ratio of CuBr/substrate/**3-1** (entry 11). Next, to optimize the DMSO concentration we conducted experiments under our best conditions (Table 3, entry 11) with less reactive substrate, 4-iodoanisole (**Figure 3.4**), which showed 25 equiv of DMSO gave the highest yield. The reaction time course for **3-1** and 3-iodobenzonitrile demonstrated fast transfer over the first 10 min, with progressive slowing thereafter, as expected for a bimolecular reaction (Fig. A3.106). To our satisfaction, this methodology could also be employed for the larger hfip group that we were unable to transfer previously. Unoptimized perfluoroalkylation of methyl 2-iodobenzoate using $Cu(hfip)(PPh_3)_2$ and 2 equiv of CuBr gave 20% of the desired product (Fig. A3.104).

Table 3.3 Optimization of the preparation of "ligandless" Cu[$CF(OCF_3)CF_2H$].

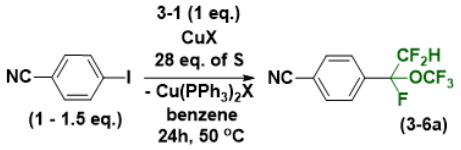

Entry	CuX (equiv.)	Substrate (equiv.)	Solv. (S)	Yield[a] (%)
1	CuCl (1.5)	1.5	DMSO	< 10
2	CuCl (2)	1.5	DMSO	66
3	CuCl (2)	1	DMSO	59
4	CuCl (2)	1	DMF	< 5
5	CuI (1.5)	1.5	DMSO	18
6	CuI (2)	1.5	DMSO	37
7	CuI (2)	1	DMSO	29
8	CuI (2)	1	DMF	< 5
9	CuBr (1.5)	1.5	DMSO	53
10	CuBr (2)	1.5	DMSO	55
11	CuBr (2)	1	DMSO	82
12	CuBr (2)	1	DMF	< 5

yields determined by ^{19}F NMR with trifluorotoluene as the internal standard.

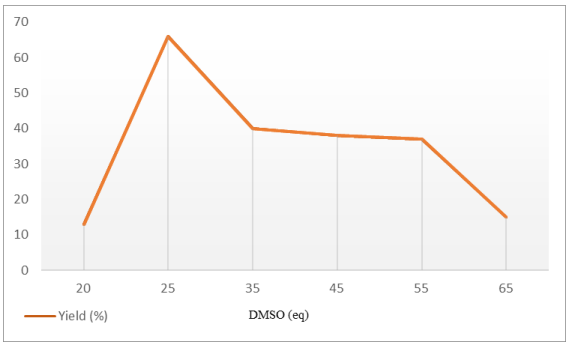

Figure 3.4 Yield of 4-iodoanisole fluoroalkylation product as a function of added DMSO in benzene after 24 h at 50 °C with a substrate/**3-1** ratio of 1.5/1.

3.2.5 Aryl iodide substrate scope: With the optimal conditions in hand, we examined the substrate scope for *ttfet* transfer to a series of substituted aryl iodides. As shown in **Scheme 3.3**, all reactions furnished the desired product in moderate to very good yields. High yields were obtained with *ortho*-substituted substrates (**3-7a,f,h)**, as observed by Grushin *et al.* for trifluoromethylations,[20] but electron-donating *para* substituents generally led to decreased product yields (**3-7g,i,m,n,o**) compared to electron-withdrawing ones (**3-7b-d**). Again, the ^{19}F NMR spectra of **3-7b-o** are all very similar to that of **3-7a** (see Appendix).

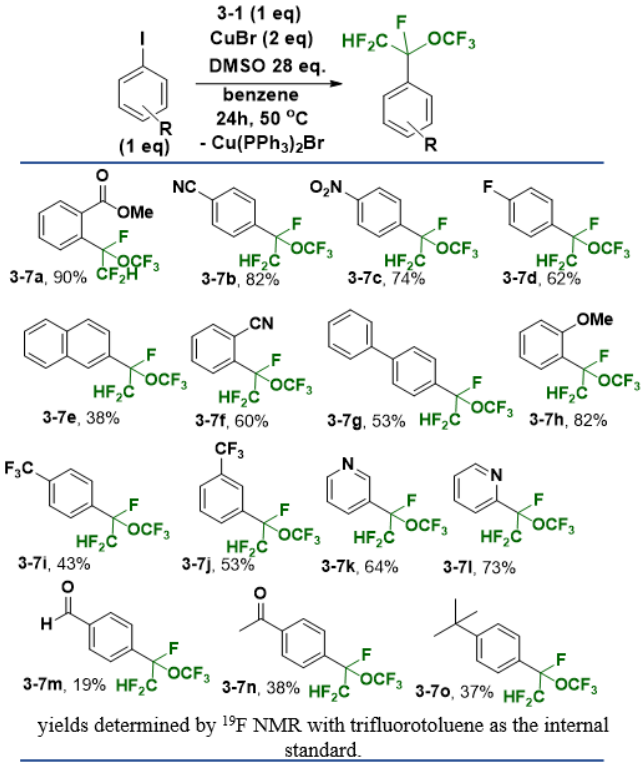

Scheme 3.3 Substrate scope for –[CF(OCF$_3$)CF$_2$H] transfer to aryl iodides.

3.2.6 Computational insights into the role of DMSO: The reaction of complex **3-1** with benzoyl chloride was computationally interrogated at the DFT level (TPSSh-D0/TZ//TPSSTPSS/DZ) utilizing an approach previously employed in studying selective copper complex-catalyzed hydrodefluorination of fluoroalkenes.[23]

Potential Energy Surface. Modeling the effect of solvent employing solvent corrections indicated only minimal (polarizable continuum model, PCM: 1.5 kcal/mol)[24] or absent (solvation model based on density, SMD)[25] effects of increased solvent polarity with respect to gas phase calculations, which does not reflect experimental observations. Therefore, we decided to model solvent coordination explicitly; **Scheme 3.4** depicts the Gibbs free energy surface for the reaction of **3-1** with benzoyl chloride. Dissociation of one PPh_3 ligand (L) from **3-1** precedes oxidative addition of benzoyl chloride and is strongly endergonic (**LCu-R^F**: 18.5 kcal/mol). The barrier for oxidative addition from **3-1** is sizable (**OxAd TS**: 25.7 kcal/mol) and predominantly due to formation of the monoligated **LCu-R^F** complex. Formation of the square-planar, formally Cu(III), intermediate is endergonic (+12.2 kcal/mol). Rate limiting is the reductive elimination (**RedEl TS**: 25.7 kcal/mol) which is strongly exergonic (L_2Cu-Cl + product: -23 kcal/mol). β-F elimination from the LCu-R^F complex is not competitive because it is endergonic (+2.6 kcal/mol); there is no obvious escape route, and the resulting olefin would only reinsert into Cu-F under the experimental conditions. Coordination of two solvent molecules stabilizes the mono-phosphine complex, however, DMSO (LCu(2DMSO)-R^F: 2.2 kcal/mol) is much more effective than either acetone (12.7 kcal/mol) or acetonitrile (11.9 kcal/mol). The oxidative addition TS is stabilized by coordination of a single solvent molecule, with all three solvents showing similar stabilization (≈ 4 kcal/mol). Then again, of the three tested solvents, only DMSO stabilizes the square-pyramidal formal Cu(III)-intermediate and the **RedEl TS** strongly enough to overcome the entropic penalty for solvent coordination (**RedEl TS**: 21.1 kcal/mol). This barrier height is in line with the slow reaction observed experimentally. Five-coordinate Cu(III)-complexes have recently been isolated by Xue and Shen.[26] In order to understand the effect that solvent coordination has on the barrier heights and stability of the intermediate it is instructive to analyze those species in more detail.

Cu(III) or Cu(I)? Snyder was the first to propose that the formal Cu(III) square-planar $[Cu(CF_3)_4]^-$ anion is best thought of as Cu(I).[27] He postulated an inverted ligand field, with the LUMO being primarily ligand-centered and the d_{x2-y2} orbital heavily occupied. The ligand field inversion has been proven spectroscopically by Lancaster and co-workers.[28,29] They ascertained that "copper's limited

capacity to be oxidized necessitates localization of electron hole character on the supporting ligands; consequently the physical d^8 description for these formally Cu(III) species is inaccurate." Overgaard has also confirmed the Cu(I) oxidation state by high-resolution X-ray single-crystal diffraction.[30]

In the present case, several observations align with Snyder's findings. Although the intermediate is nearly perfectly square planar (depending on the level of theory) pointing to Cu(III), the frontier molecular orbitals are ligand-centered (**Figure 3.5**). Natural resonance theory (NRT)[31] and intrinsic bond orbital theory (IBO)[32-34] were used to further elucidate the nature of the intermediate. NRT allows us to determine the weights of contributing resonance structures to an idealized Lewis structure. In Knizia's IBO method, a set of local orbitals (IBOs) is determined, exactly representing the computed Kohn-Sham

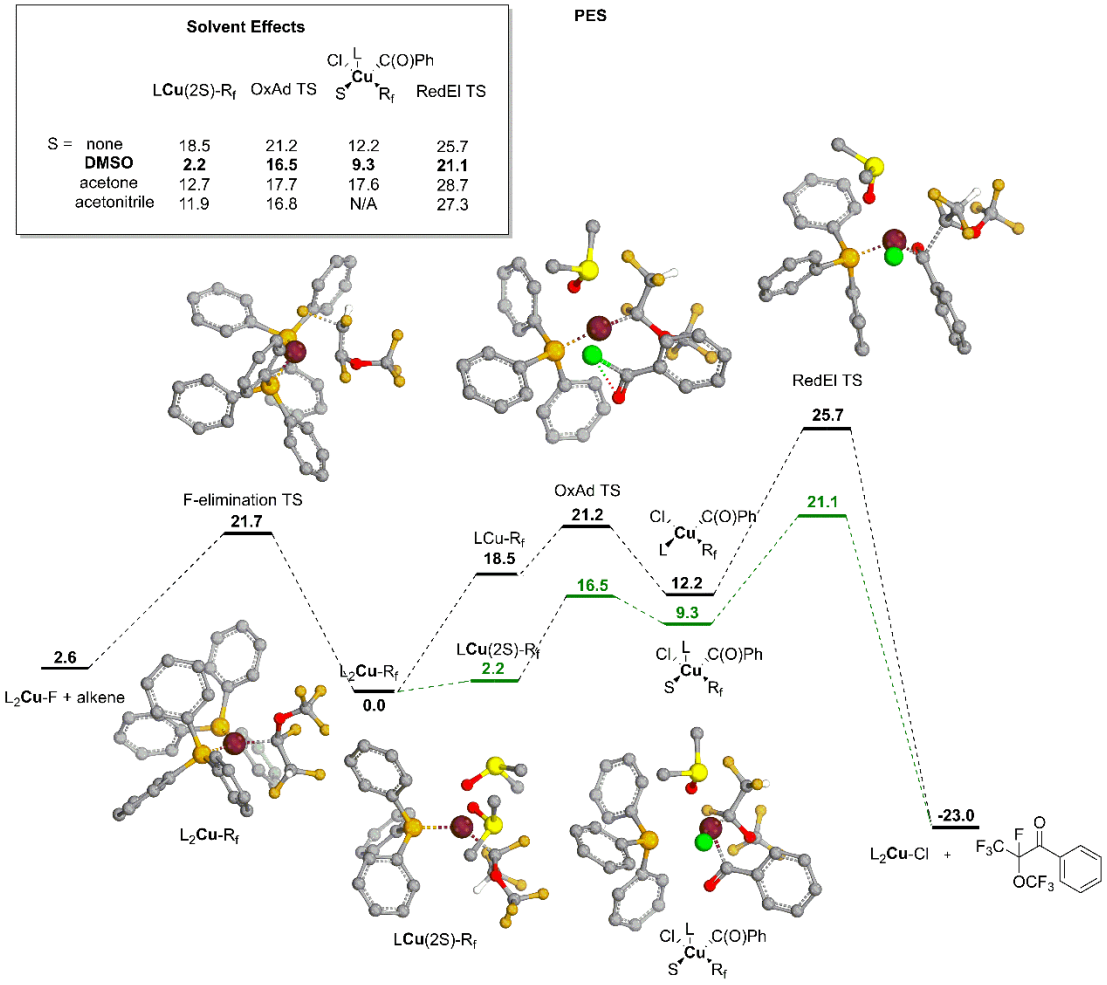

Scheme 3.4 Potential energy surface for the reaction of **3-1** with benzoyl chloride. Black trace without coordinated solvent, green trace with coordinated DMSO. Insert shows relative energies of key species for different solvents with respect to **3-1** ($L_2Cu\text{-}R^F$). T = 298 K.

significantly. The apical Cu-P bond is very long (3.076 Å). NRT now conforms with more Cu(III) character, albeit with substantial Cu(I) (22.4%). The effective oxidation state of copper computed with IBOview according to the formalisms by Ramos-Cordoba, Postils and Salvador[35,36] is in both cases +1.

The rate-limiting reductive elimination is concerted but decidedly asynchronous. In fact, in the solventless system, the Cu-C_{aroyl} bond length is even shorter in the TS than it is in the intermediate (by 0.005 Å, **Figure 3.6**) and only minimally elongated in the DMSO case. Contrarily, the Cu-R_f bond is elongated by 0.33 Å (no DMSO) and 0.41 Å (DMSO). Wiberg bond indices reflect these changes, with the Cu-C_{aroyl} bond order changing only minimally while the one for the Cu-R^F bond decreases from around 0.4 to around 0.15. Minimal changes occur in the bond Cu-C_{aroyl} bond composition while the electron density of the forming C-C bond stems mostly from the R^F fragment (approx. 2:1). **Figure 3.7** shows wave function. Because IBOs intuitively depict occupied orbitals, they allow for a direct interpretation of chemical bonding. Charges are assigned to individual atoms without free parameters and electrons in doubly occupied IBOs are assigned proportionately to individual atoms allowing further quantitative interpretation of bonding. NRT conforms to a Cu(I) species with an oxidized benzoyl ligand.

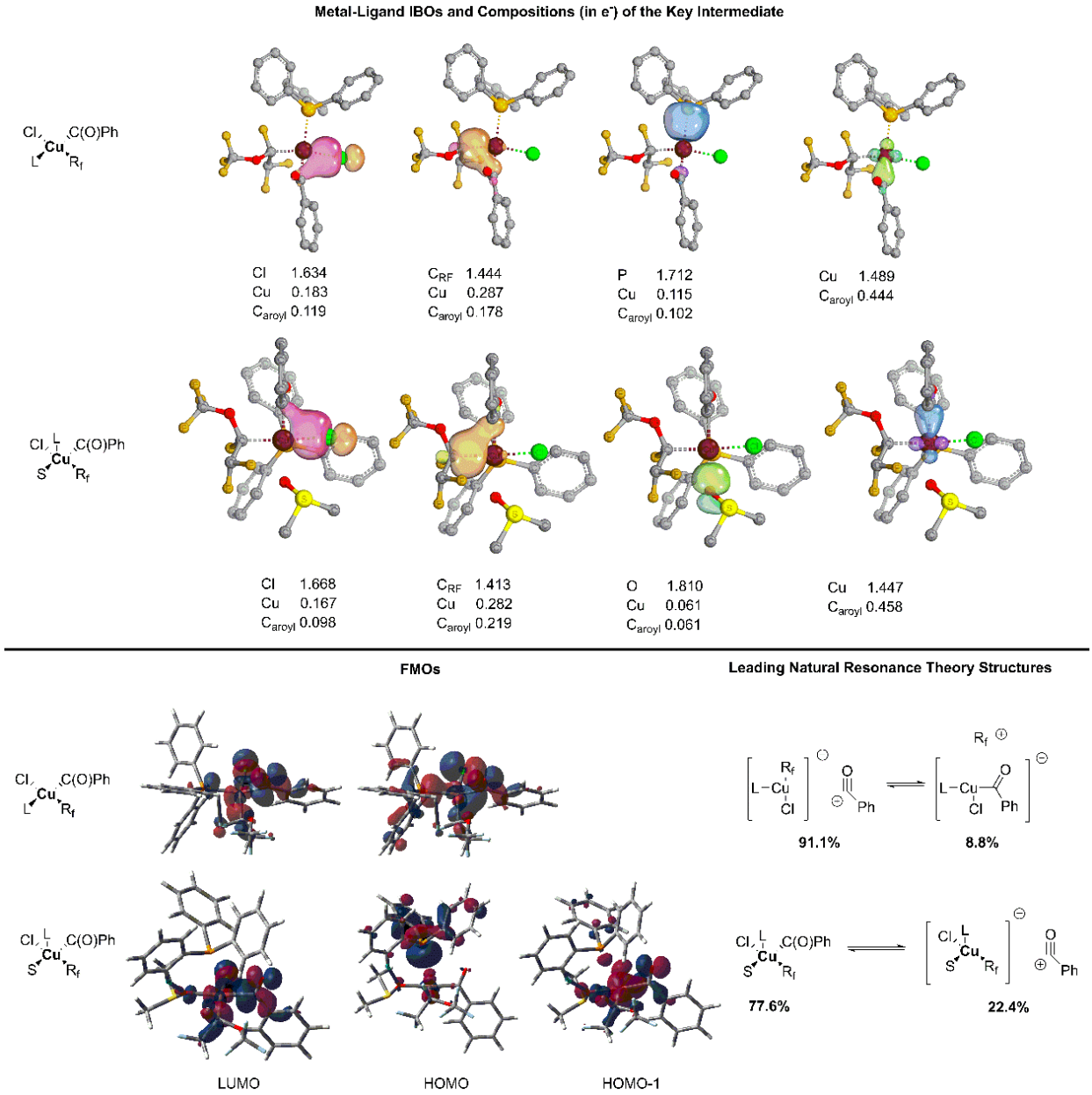

Figure 3.5 Metal-ligand IBOs, frontier molecular orbitals and NRT structures for the key intermediate.

IBO as well as natural bond orbital theory describe the Cu-P, Cu-Cl and Cu-R^F bonds as heavily polarized and ligand centered (>72% ligand contribution) while the Cu-C_{aroyl} bond is heavily copper-centered (75% Cu). Wiberg bond indices are < 0.4, indicating substantial ionic contribution to the bond. Moreover, the Cu-P, Cu-Cl and Cu-R^F IBOs are partially localized on the aroyl fragment (5-9%), with the Cu-R^F bond showing the largest contribution from C_{aroyl}. FMOs change only minimally when DMSO is coordinated.

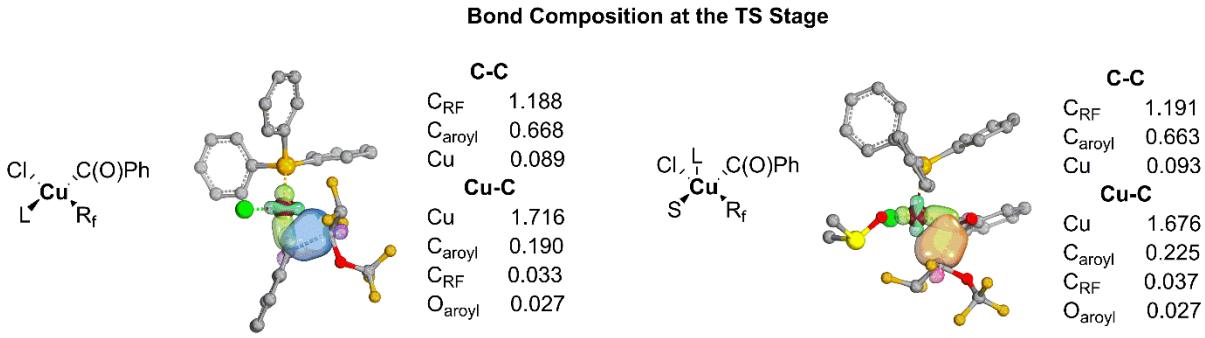

Key Metric Parameters, Charges, WBI

	Bond Lengths				IBO Charges)				WBI		
	Cu-C_{RF}	Cu-C_{aroyl}	C_{RF}-C_{aroyl}	Cu-P	Cu	C_{aroyl}	C_{RF}	O_{aroyl}	C_{RF}-C_{aroyl}	Cu-C_{RF}	Cu-C_{aroyl}
	intermediate										
none	1.990	1.970	2.818	2.401	0.888	0.150	0.062	-0.289	-	0.375	0.397
DMSO	1.988	1.947	2.803	3.076	0.947	0.163	0.085	-0.284	-	0.382	0.463
	TS										
none	2.327	1.965	2.094	2.326	0.788	0.191	0.213	-0.336	0.463	0.145	0.316
DMSO	2.401	1.997	2.093	2.348	0.838	0.167	0.215	-0.346	0.448	0.149	0.347

Figure 3.6 IBO bond composition at the TS stage, key metric parameters, charges and WBIs.

the bond composition of the Cu-Cl and Cu-R^F bonds and the Cu-C_{aroyl} bond also do not change depicts the electron flow along the reaction coordinate, emphasizing the asynchronicity of the elimination.

Consequences of the Inverted Ligand Field and Solvent Stabilization. Regardless of whether one regards the intermediates as Cu(III) or Cu(I), a picture emerges of a species in which the Cu-R^F bond is heavily concentrated on the ligand, while the Cu-C_{aroyl} bond is more concentrated on the metal. This biases the complex for an easy reductive elimination more reminiscent of nucleophilic attack of the R^F group on the electrophilic aroyl fragment than traditional concerted reductive elimination mechanisms. In essence, this resembles acid-base chemistry. These findings align with Lancaster's analysis of reductive elimination in $[Cu(benzyl)(CF_3)_3]^{-}$[28] and Klein's[37] findings for Sanford's Ni-system.[38]

Square-pyramidal Cu-species like the DMSO-stabilized one here are severely crowded, as emphasized by the long Cu-P in the intermediate (3.076 Å vs 2.401 Å in the square-planar species). DMSO, with its javelin shaped O=S unit, develops steric bulk further away from the central metal than, for example, acetone. Furthermore, the strong negative point-charge stabilizes the charge transfer during

the elimination. N-donors like acetonitrile, on the other hand, seem incapable of stabilizing such species sufficiently.

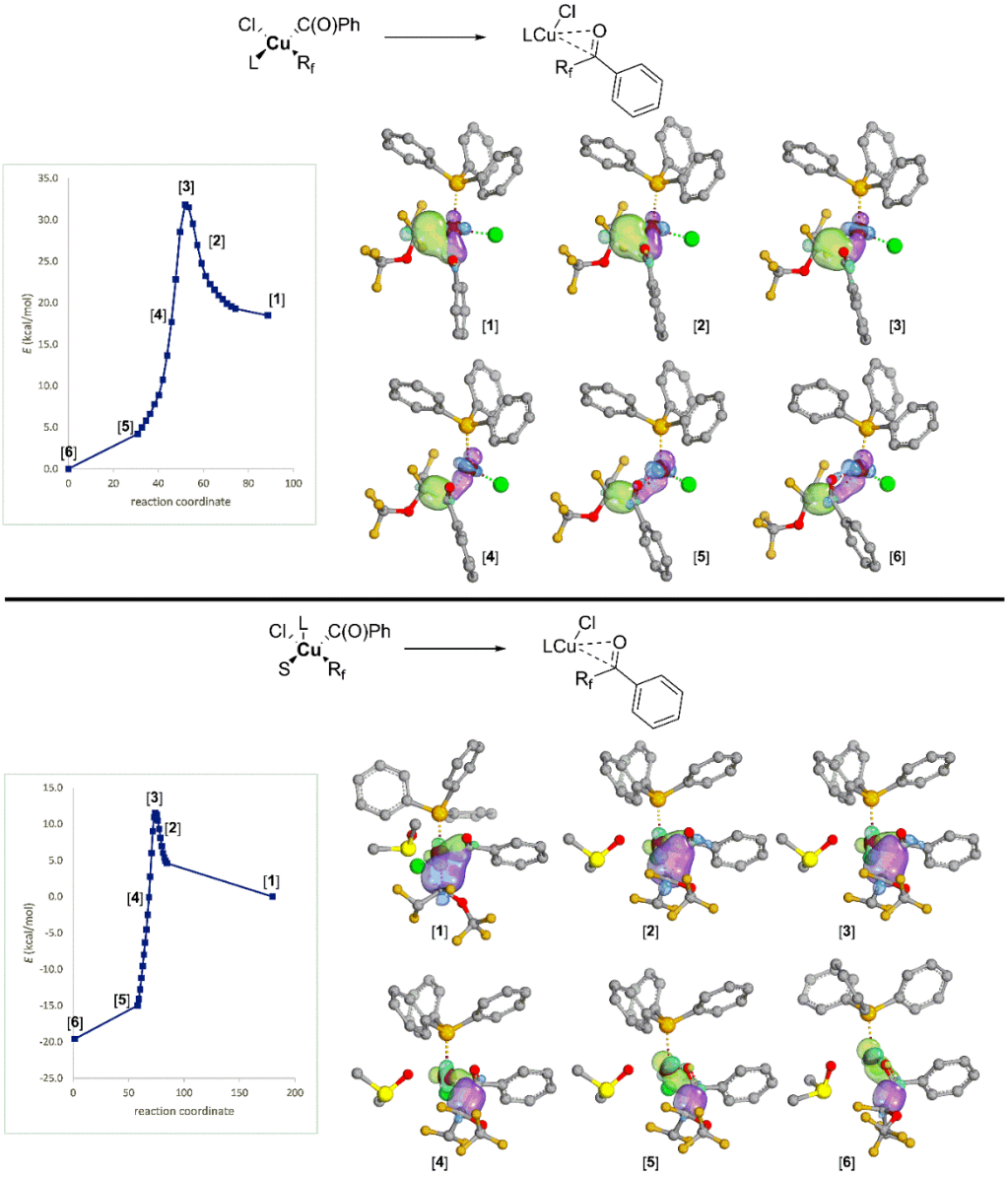

Figure 3.7 Electron flow along the intrinsic reaction coordinate (IRC) during reductive elimination. Hydrogen atoms omitted for clarity. The two IBOs with the largest changes along the reaction pathway are depicted.

3.3 CONCLUSIONS

The results described herein build significantly on the Baker group's previous work with Cu-hfip transfer to aroyl chlorides. In that case the optimal reaction conditions involved use of the phenanthroline ancillary ligand in DMF solvent with the PPh_3 ligand presumably dissociating with addition of the substrate. For the present work with Cu-ttfet, DMSO outperformed other solvents in spite of its propensity to eventually decompose **3-1**. As a result, optimal reaction conditions were obtained using just 28 equiv of DMSO in arene solvents. Accompanying DFT calculations showed that the unique properties of DMSO (polar S=O bond and steric bulk further from Cu *vs* other polar coordinating

solvents) contribute to a lower energy transition state for rate-determining reductive elimination. Moreover, the unusual characteristics of the formal Cu(III) addition product (Cu-C_{aroyl} bond concentrated on the metal and Cu-C^F bond on the carbon) give rise to an asynchronous C-C bond formation more reminiscent of an acid/base reaction than a typical concerted reductive elimination. Finally, employing the "ligandless" strategy previously developed by others for transfer of the -CF_3[21] and -C_2F_5 groups,[22] we were able to transfer the *ttfet* group to a range of aryl iodides, thus providing a new R^F group capable of increasing lipophilicity and serving as an H-bond donor in new bioactive target molecules. Extension of this concept to include other commercially available fluoroalkenes will provide additional R^F groups for late-stage fluoroalkylation approaches.

3.4 EXPERIMENTAL SECTION

3.4.1 General Procedures: Experiments were conducted under nitrogen, using Schlenk techniques or an MBraun glove box. All solvents were deoxygenated by purging with nitrogen. Tetrahydrofuran (THF), acetonitrile (MeCN), diethyl ether (Et_2O), hexanes and toluene were dried on columns of activated alumina using a J. C. Meyer (formerly Glass Contour®) solvent purification system. Benzene-d_6 (C_6D_6) was dried by stirring over activated alumina (ca. 10 wt. %) overnight, followed by filtration. All solvents were stored over activated (heated at ca. 250 °C for >10 h under vacuum) 4 Å molecular sieves. Glassware was oven-dried at 120 °C for >2 h. The following chemicals were obtained commercially, as indicated: perfluoro(methyl vinyl ether) (PMVE, Synquest), pentane (Sigma-Aldrich, anhydrous, >99%), benzene (Sigma-Aldrich, anhydrous, 99.8%), dimethylformamide (DMF, Alfa Aesar, anhydrous, 99.8%), dimethylsulfoxide (DMSO, Alfa Aesar Anhydrous, 99.8%), cyclopentyl methyl ether (Sigma-Aldrich, anhydrous, >99%), N,N-dimethylformamide (Sigma-Aldrich, anhydrous, 99.8%),

N,N-dimethylacetamide (Sigma-Aldrich, anhydrous, >99%), dimethylsulfoxide (Sigma-Aldrich, anhydrous, >99%), trifluorotoluene (Sigma-Aldrich, anhydrous, >99%), iodobenzene (Alfa Aesar, 98 %), all other aryl iodides (SIGMA), all acid chlorides (SIGMA), 1,10-phenanthroline (Sigma-Aldrich, phen), 4,4'-dichloro-2,2'-bipyridine (SIGMA, bipy), triphenylphosphine (PPh_3, Oakwood chemicals, 99%), methyldiphenylphosphine ($PMePh_2$, Acros Organics, 99%), tetramethyldisiloxane (Sigma-Aldrich, 97%), copper bromide ((Sigma-Aldrich, 98%). The following chemicals were synthesized as previously reported: hexahydro-1,3-bis(2,4,6-trimethylphenyl)-1,3-diazepin-2-ylidene (7-dipp),[39] 1,3-bis(2,3,6-trimethylphenyl)imidazolidene (IMes),[40] and $[CuH(PPh_3)]_6$.[41] Electrospray ionization mass spectral data were collected using an Applied Biosystem API2000 triple quadrupole mass spectrometer. For electron impact (EI), solid samples were prepared by drying products under vacuum, and spectra obtained using a Kratos Concept S1 instrument (Hres 7000−10000). X-ray diffraction data were collected on a Bruker Smart or Kappa diffractometer equipped with an ApexII CCD detector and a sealed-tube Mo K source (λ = 0.71073 Å) (see Table A3.1 for details). NMR spectra were recorded on a 300 MHz Bruker Avance instrument at room temperature (21-23 °C) unless stated otherwise. ^{1}H NMR spectra were referenced to residual proton peaks associated with the deuterated solvents (C_6D_6: 7.16) and $^{31}P\{^1H\}$ NMR data were referenced to external H_3PO_4 (85 % aqueous solution), set to 0.0 pm. ^{19}F NMR spectra were referenced to internal standard α,α,α-trifluorotoluene (CF_3Ph) (unless stated otherwise) set to – 63.5 ppm. NMR spectra for the title compounds are displayed in the Appendix.

3.4.2 Synthesis of Copper Complexes

*Synthesis of $Cu[CF(OCF_3)CF_2H](PPh_3)_2$ (**3-1**):* The red complex $[(PPh_3)_3CuH]_6$ (150 mg, 0.46 mmol) was dissolved in 5 mL of benzene in a glass vial. Triphenylphosphine (365 mg, 1.39 mmol) and tetramethyldisiloxane (122 µL, 0.69 mmol) were added to the solution and the vial was sealed with a septum. Five equiv of PMVE were then added to the vial using a gas-tight syringe. The reaction changed from deep red to light red and was left to sit at room temperature for 24 h. The solvent was then removed under vacuum, and the residue washed with Et_2O. The resulting oil was triturated with hexane, and the ensuing precipitate was collected as a light red solid and dried to give 320 mg (95% yield). ^{19}F NMR (C_6D_6) -53.8 (d, $^3J_{FF}$ = 4 Hz, OC*F*$_3$), -119.9 (mult, C*F*), -120.8 (ddd, $^2J_{FF}$ = 280, $^2J_{FH}$ = 58, $^3J_{FF}$ = 5 Hz, C*F*$_2$H) and -126.8 ppm (ddd, $^2J_{FF}$ = 280, $^2J_{FH}$ = 60, $^3J_{FF}$ = 5 Hz, C*F*$_2$H). $^{31}P\{^1H\}$ NMR -2.4 ppm (br s). ^{1}H NMR d 7.24 (overlapping, PPh_3) and 5.58 ppm (tmult $^2J_{FH}$ = 58 Hz, CF_2*H*). MS results: (Figs A3.1-S7).

*Addition of co-ligands to **3-1:*** To a solution of 10 mg (0.013 mmol) **3-1** in C_6D_6 was added 5 µL (0.026 mmol) of $PMePh_2$ in one experiment and 4 mg (0.013 mmol) of IMes in another. ^{19}F NMR spectra

indicated decomposition (Figs. S8, S9). In another experiment, 10 mg (0.013 mmol) of **3-1** was dissolved in 0.8 mL of DMSO-d_6, resulting in decomposition of the R^F group. (Figs. S16-S18).

*Synthesis of Cu[CF(OCF₃)CF₂H](phen) (**3-4a**):* Complex **1** (150 mg, 0.20 mmol) and 1,10-phenanthroline (36 mg, 0.20 mmol) were loaded into a 20 mL vial glass along with 5 mL of benzene. After 2 h, the resulting brown-black solid was washed with hexane to remove PPh_3, filtered using a glass frit and dried, yielding 106 mg of **3-4a** (80% yield). ^{19}F NMR -50.2 ppm (s, OC*F*$_3$), –111.1 ppm (m, C*F*), -118.8 ppm (dd, $^2J_{FF}$ = 278, $^2J_{FH}$ = 60 Hz, C*F*$_2$H) and -120.7 ppm (dd, $^2J_{FF}$ = 278,$^2J_{FH}$ = 60 Hz, C*F*$_2$H) (Fig. S30).

*Synthesis of Cu[CF(OCF₃)CF₂H](bpyCl₂)(PPh₃) (**3-4b**):* Complex **1** (200 mg, 0.26 mmol) and 4,4'-dichloro-2,2'-bipyridine (60 mg, 0.26 mmol) were loaded into a 20 mL vial glass along with 5 mL of benzene. The reaction was left stirring for 2 h and then dried under vacuum. The residue was dissolved in Et_2O, and pentane was used to precipitate a yellow solid that was filtered off and dried, yielding 96 mg of **3-4b** (80% yield). ^{19}F NMR (C_6D_6) -50.1 ppm (s, OC*F*$_3$), – 113.9 ppm (m, C*F*), -119.27 ppm (ddd, $^2J_{FF}$ = 280, $^2J_{FH}$ = 53 Hz, C*F*$_2$H) and -121.4 ppm (ddd, $^2J_{FF}$ = 290, $^2J_{FH}$ = 54 Hz, C*F*$_2$H). ^{31}P{^{1}H} NMR – 2.9 ppm (m, PPh_3). ^{1}H NMR d 7.6 – 7.25 (overlapping, PPh_3 and H aromatics from pyridine), 5.38 (trd, $^2J_{FH}$ = 58, $^2J_{FH}$ = 9 Hz). High-resolution electrospray ionization: mass calculated for $C_{13}H_9F_6N_2OCu$ 385.99 m/z, Found m/z 389 (99%); $C_{28}H_{23}CuN_2P$ expected 481 m/z, Found 481.13 (20%). (Fig. S31-33).

*Synthesis of Cu[CF(OCF₃)CF₂H](7-dipp) (**3-5**):* Complex **3-1** (100 mg, 0.13 mmol) and hexahydro-1,3-bis(2,4,6-trimethylphenyl)-1,3-diazepin-2-ylidene (7-dipp) (44 mg, 0.13 mmol) were loaded into a 20 mL vial glass and dissolved in 5 mL of benzene. The reaction was left stirring for 2 h and then dried under vacuum. The resulting residue was washed with Et_2O and pentane was used to precipitate a colorless solid that was filtered and dried to give 70 mg of **3-5** (90% yield). ^{19}F NMR -53.6 ppm (s, OC*F*$_3$), -119.8 (mult, C*F*), -120.6 (ddd, $^2J_{FF}$ = 282, $^2J_{FH}$ = 56, $^3J_{FF}$ = 7 Hz, C*F*$_2$H) and -126.9 ppm (ddd, $^2J_{FF}$ = 284, $^2J_{FH}$ = 58, $^3J_{FF}$ = 5 Hz, C*F*$_2$H). ^{1}H NMR d 5.74 (trd, $^2J_{FH}$ = 59 Hz, $^3J_{HF}$ = 12 Hz, CF_2H). High-resolution electrospray ionization: mass calculated for $[C_{26}H_{32}F_6N_2OCuNa]_2(H_2O)]^{2+}$ expected 597 m/z, found 597 (Figs. S34-S36).

3.4.3 R^F Transfer Reactions:

General experimental procedure for perfluoroalkylation of aroyl chlorides in DMSO. Complex **3-1** (13 mg, 0.01 mmol) was loaded into an NMR tube and mixed with 0.5 mL of DMSO. Benzoyl chloride (0.01

mmol) and $PhCF_3$ (20 μL, 0.01 mmol/mL) were added to the solution and the reaction was analyzed by ^{19}F NMR spectroscopy after 24 h.

PhC(O)CF(OCF_3)CF_2H (**3-3a**): ^{19}F NMR -54.0 (d, $^4J_{FF}$ = 10 Hz, OC*F*$_3$), -81.2 (mult, C*F*), -133.2 (ddq, $^2J_{FF}$ = 288, $^2J_{FH}$ = 54, $^3J_{FF}$ = 10 Hz, C*F*$_2$H), -134.6 ppm (ddq, $^2J_{FF}$ = 288, $^2J_{FH}$ = 54, $^3J_{FF}$ = 10 Hz, C*F*$_2$H.

MePhC(O)CF(OCF_3)CF_2H (**3-3b**): ^{19}F NMR -53.9 (d, $^4J_{FF}$ = 10 Hz, OC*F*$_3$), -81.2 (mult, C*F*), -132.7 (ddq, $^2J_{FF}$ = 288, $^2J_{FH}$ = 54, $^3J_{FF}$ = 8 Hz, C*F*$_2$H), -135.1 ppm (ddq, $^2J_{FF}$ = 288, $^2J_{FH}$ = 51, $^3J_{FF}$ = 8 Hz, C*F*$_2$H).

2,4,6-Cl_3PhC(O)CF(OCF_3)CF_2H (**3-3c**): ^{19}F NMR -53.9 (d, $^4J_{FF}$ = 10 Hz, OC*F*$_3$), -81.2 (mult, C*F*), -132.7 (ddq, $^2J_{FF}$ = 288, $^2J_{FH}$ = 53, $^3J_{FF}$ = 10 Hz, C*F*$_2$H), -135.1 ppm (ddq, $^2J_{FF}$ = 288, $^2J_{FH}$ = 53, $^3J_{FF}$ = 9 Hz, C*F*$_2$H).

4-CNPhC(O)CF(OCF_3)CF_2H (**3-3d**): ^{19}F NMR –53.9 (d, $^4J_{FF}$ = 10 Hz, OC*F*$_3$), -81.2 (mult, C*F*), -132.7 (ddq, $^2J_{FF}$ = 288, $^2J_{FH}$ = 52, $^3J_{FF}$ = 8 Hz, C*F*$_2$H), -135.1 ppm (ddq, , $^2J_{FF}$ = 288, $^2J_{FH}$ = 51, $^3J_{FF}$ = 9 Hz, C*F*$_2$H).

2-(-CHCHCHCHO-)C(O)CF(OCF_3)CF_2H (**3-3e**): ^{19}F NMR -53.9 (d, $^4J_{FF}$ 10 Hz, OC*F*$_3$), -81.2 (mult, C*F*), -132.7 (ddq, $^2J_{FF}$ = 288, $^2J_{FH}$ = 53, $^3J_{FF}$ = 9 Hz, C*F*$_2$H), -135.1 ppm (ddq, , $^2J_{FF}$ = 288, $^2J_{FH}$ = 52, $^3J_{FF}$ = 8 Hz, C*F*$_2$H).

Ph-PhC(O)CF(OCF_3)CF_2H (**3-3f**): ^{19}F NMR -54 (d, $^4J_{FF}$ = 10 Hz, OC*F*$_3$), -81.3 (mult, C*F*), -133.2 (ddq, , $^2J_{FF}$ = 287, $^2J_{FH}$ = 51, $^3J_{FF}$ = 8 Hz, C*F*$_2$H), -134.6 ppm (ddq, $^2J_{FF}$ = 287, $^2J_{FH}$ = 52, $^3J_{FF}$ = 9 Hz, C*F*$_2$H).

2-NO_2PhC(O)CF(OCF_3)CF_2H (**3-3h**): ^{19}F NMR -53.9 (d, $^4J_{FF}$ = 10 Hz, OCF_3), - 81.2 (mult, C*F*), -133.1 (ddq, $^2J_{FF}$ = 288, $^2J_{FH}$ = 53, $^3J_{FF}$ = 7 Hz, C*F*$_2$H) and -134.5 ppm (ddq, $^2J_{FF}$ = 288, $^2J_{FH}$ = 53, $^3J_{FF}$ = 7 Hz, C*F*$_2$H).

2-(-C_4H_4S)C(O)CF(OCF_3)CF_2H (**3-3i**): ^{19}F NMR -53.9 (d, $^4J_{FF}$ =10 Hz, OC*F*$_3$), - 81.2 (mult, C*F*), -133.2 (ddq, $^2J_{FF}$ = 287, $^2J_{FH}$ = 53, $^3J_{FF}$ = 8 Hz, C*F*$_2$H), -134.6 ppm (ddq, $^2J_{FF}$ = 287, $^2J_{FH}$ = 52, $^3J_{FF}$ = 9 Hz, C*F*$_2$H).

General experimental procedure for perfluoroalkylation of aryl iodides. CuBr (3.8 mg, 0.026 mmol) was dissolved in 28 equiv of DMSO (0.36 mmol) and then added to complex **3-1** (10 mg, 0.01 mmol) in an NMR tube with 0.5 mL of benzene. The aryl iodide (0.013 mmol) and $PhCF_3$ (20 μL, 0.01 mmol/mL) were added to the solution, and the reaction was analyzed by ^{19}F NMR after 24 h at 50 ^oC.

2-Methylbenzoate-CF(OCF_3)CF_2H (**3-7a**): ^{19}F NMR -52.9 (d, $^4J_{FF}$ = 10 Hz, OC*F*$_3$), -132.1 (s, C*F*), –134.5 (ddd, $^2J_{FF}$ = 288, $^2J_{FH}$ = 55, $^3J_{FF}$ = 13 Hz, C*F*$_2$H), –136.1 ppm (ddd, $^2J_{FF}$ = 288, $^2J_{FH}$ = 55, $^3J_{FF}$ = 10 Hz, C*F*$_2$H). ^1H NMR d 7.62 (dd, $^3J_{FF}$ = 8, $^4J_{FF}$ = 1 Hz), 7.48 (dd, $^3J_{FF}$ = 8, $^4J_{FF}$ = 1 Hz), 7.4 (dd, $^3J_{FF}$ = 8, $^4J_{FF}$ =

1.5 Hz), 7.24 (dmult), 6.80 (overlapped, CF_2H), 3.34 (s, OCH_3). GC-MS: (retention time: 12.483 min) expected 302.17 m/z (100%), found 302.1 m/z (20%) and 251 m/z (99%).

4-cyanophenyl-CF(OCF_3)CF_2H (**3-7b**): ^{19}F NMR -52.9 (d, $^4J_{FF}$ = 9 Hz, OCF_3), -132.9 (s, C*F*), -133.1 (ddd, $^2J_{FF}$ = 287, $^2J_{FH}$ = 54, $^3J_{FF}$ = 4 Hz, CF_2H), –133.6 ppm (ddd, $^2J_{FF}$ = 287, $^2J_{FH}$ = 54, $^3J_{FF}$ = 7 Hz, CF_2H). ^{1}H NMR d 7-5.5 (ov aromatic C-H), 5.53 (trd, $^2J_{FH}$ = 54, $^3J_{FH}$ = 5 Hz, CF_2H). GC-MS: (retention time: 6.791 min) expected 269.15 m/z (100%), found 269 m/z (30%), 218 m/z (80%) and 130.1 (99%).

4-nitrophenyl-CF(OCF_3)CF_2H (**3-7c**): ^{19}F NMR -51.5 (d, $^4J_{FF}$ = 9 Hz, OCF_3), -131.7 (s, C*F*), –133.2 (ddd, $^2J_{FF}$ = 293, $^2J_{FH}$ = 53, $^3J_{FF}$ = 8 Hz, CF_2H), –133.3 ppm (ddd, $^2J_{FF}$ = 293, $^2J_{FH}$ = 53, $^3J_{FF}$ 8 Hz, CF_2H). GC-MS (retention time: 14.357 min) expected 289.13 m/z (100%), found 289 m/z (20%) and 238 m/z (99%).

4-fluorophenyl-CF(OCF_3)CF_2H (**3-7d**): ^{19}F NMR –52.0 (d, $^4J_{FF}$ = 8 Hz, OCF_3), -108.9 (s, C*F*), -131.5 (s, C*F*), –133.4 (ddd, $^2J_{FF}$ = 289, $^2J_{FH}$ = 52, J_{FF} = 6 Hz, CF_2H) –134.8 ppm (ddd, $^2J_{FF}$ = 289, $^2J_{FH}$ = 52, J_{FF} = 6 Hz, CF_2H).

1-naphthyl-CF(OCF_3)CF_2H (**3-7e**): ^{19}F NMR –52.7 (d, $^4J_{FF}$ = 9 Hz OCF_3), -131.5 (s, C*F*), –131.9 (ddd, $^2J_{FF}$ = 286, $^2J_{FH}$ = 53, $^3J_{FF}$ = 10 Hz, CF_2H), –134.5 ppm (ddd, $^2J_{FF}$ = 286, $^2J_{FH}$ = 53, $^3J_{FF}$ = 10 Hz, CF_2H).

2-cyanophenyl-CF(OCF_3)CF_2H (**3-7f**): ^{19}F NMR –52.7 (d, $^4J_{FF}$ = 9 Hz OCF_3), -129.9 (s, C*F*), –131.8 (ddd, $^2J_{FF}$ = 295, $^2J_{FH}$ = 54, $^3J_{FF}$ = 5 Hz, CF_2H) –134.5 ppm (ddd, $^2J_{FF}$ = 295, $^2J_{FH}$ = 54, $^3J_{FF}$ = 8 Hz, CF_2H).

4-biphenyl-CF(OCF_3)CF_2H (**3-7g**): ^{19}F NMR -51.8 (d, $^4J_{FF}$ = 10 Hz, OCF_3), -132.3 (m, C*F*), –133.3 (ddd, $^2J_{FF}$ = 291, $^2J_{FH}$ = 53, $^3J_{FF}$ = 5 Hz, CF_2H) –134.7 ppm (ddd, $^2J_{FF}$ = 291, $^2J_{FH}$ = 53, $^3J_{FF}$ = 8 Hz, CF_2H).

2-methoxyphenyl-CF(OCF_3)CF_2H (**3-7h**): ^{19}F NMR –52.7 (d, $^4J_{FF}$ = 9 Hz OCF_3), -129.9 (s, C*F*), –132.7 (dd, $^2J_{FF}$ = 284, $^2J_{FH}$ = 53, $^3J_{FF}$ = 14 Hz, CF_2H), –139.1 ppm (dd, $^2J_{FF}$ = 284, $^2J_{FH}$ = 54, $^3J_{FF}$ = 9 Hz, CF_2H). ^{1}H NMR d 7.62 (dt, J_{HH} = 8, J_{HH} = 1.5 Hz), 6.8 (dt, $^3J_{HH}$ = 8, J_{HH} = 1 Hz), 6.33 (dt, $^2J_{HH}$ = 8, $^3J_{HH}$ = 1.5 Hz), 6.18 (dt, $^2J_{HH}$ = 8, $^3J_{HH}$ = 1.5 Hz), 6.28 (ddd, $^2J_{FH}$ = 55, $^2J_{HF}$ = 12 Hz, CF_2H), 3.0 (s, OCH_3).

4-trifluoromethylphenyl-CF(OCF_3)CF_2H (**3-7i**): ^{19}F NMR –52.7 (d, $^4J_{FF}$ = 9 Hz OCF_3), -129.9 (s, C*F*), –132.7 (dd, $^2J_{FF}$ = 284, $^2J_{FH}$ = 53, $^3J_{FF}$ = 14 Hz, CF_2H), –139.1 ppm (dd, $^2J_{FF}$ = 284, $^2J_{FH}$ = 54, $^3J_{FF}$ = 9 Hz, CF_2H). ^{1}H NMR d 7.62 (dt, J_{HH} = 8, J_{HH} = 1.5 Hz), 6.8 (dt, $^3J_{HH}$ = 8, J_{HH} = 1 Hz), 6.33

(dt, $^{2}J_{HH}$ = 8, $^{3}J_{HH}$ = 1.5 Hz), 6.18 (dt, $^{2}J_{HH}$ = 8, $^{3}J_{HH}$ = 1.5 Hz), 6.28 (ddd, $^{2}J_{FH}$ = 55, $^{2}J_{HF}$ = 12 Hz, CF_2H), 3.0 (s, OCH_3).

3- trifluoromethylphenyl -$CF(OCF_3)CF_2H$ (**3-7j**): ^{19}F NMR – 52.8 (d, $^{4}J_{FF}$ = 9 Hz OCF_3), - 62.6 (s, CF_3), -132.1 (mult, C*F*), –133.6 (ddd, J_{FF} = 288, J_{FH} = 55, J_{FF} = 5 Hz, CF_2H), –133.6 ppm (ddd, J_{FF} = 288, J_{FH} = 55, J_{FF} = 7 Hz, CF_2H).

3-pyridyl-$CF(OCF_3)CF_2H$ (**3-7k**): ^{19}F NMR – 52.2 (d, $^{4}J_{FF}$ = 9 Hz, OCF_3), -132.8 (m, C*F*), – 133.1 (dt, $^{2}J_{FF}$ = 278, $^{2}J_{FH}$ = 55 Hz, CF_2H), –134.6 ppm (dt, $^{2}J_{FF}$ = 278, $^{2}J_{FH}$ = 51 Hz, CF_2H). ^{1}H NMR 7.6 ppm (ddt, J_{FF} 8 Hz, J_{FF} 12 Hz), 7.36 ppm (d, J_{FF} 8 Hz), 7.31 ppm (d, J_{FF} 8 Hz), 7 ppm (overlapped), 5.55 ppm (dt, $^{2}J_{FH}$ = 54, $^{3}J_{FH}$ = 4 Hz, CF_2H).

2-pyridyl-$CF(OCF_3)CF_2H$ (**3-7l**): ^{19}F NMR – 52.9 (d, $^{4}J_{FF}$ = 8 Hz, OCF_3), -142.5 (m, C*F*), – 135.15 (dd, $^{2}J_{FF}$ = 289, $^{2}J_{FH}$ = 55, $^{3}J_{FF}$ = 11 Hz, CF_2H) – 139.8 ppm (dd, $^{2}J_{FF}$ = 289, $^{2}J_{FH}$ = 53, $^{3}J_{FF}$ = 9 Hz, CF_2H). ^{1}H NMR d 8.16 (dm, J_{HH} = 5 Hz), 7.25 (dm, J_{HH} = 8 Hz), 6.5 (dd, J_{HH} = 8 Hz, J_{HH} = 1 Hz), 6.2 (dd, J_{HF} = 54, $^{3}J_{HF}$ = 12 Hz, CF_2H).

4-formylphenyl-$CF(OCF_3)CF_2H$ (**3-7m**): ^{19}F NMR –52.2 (d, $^{4}J_{FF}$ = 8 Hz, OCF_3), -133 (m, C*F*), – 134 (ddt, $^{2}J_{FF}$ = 240, $^{2}J_{FH}$ = 53, $^{3}J_{FF}$ = 5 Hz, CF_2H) and –134.8 ppm (ddt, $^{2}J_{FF}$ = 240, $^{2}J_{FH}$ = 53, $^{3}J_{FF}$ = 7 Hz, CF_2H).

4-acetylphenyl-$CF(OCF_3)CF_2H$ (**3-7n**): ^{19}F NMR –52.3 (d, $^{4}J_{FF}$ = 8 Hz, OCF_3), -132.3 (m, C*F*), – 133.0 (ddd, $^{2}J_{FF}$ = 293, $^{2}J_{FH}$ = 54, $^{3}J_{FF}$ = 4 Hz, CF_2H), –134.4 ppm (ddd, $^{2}J_{FF}$ = 293, $^{2}J_{FH}$ = 54, $^{3}J_{FF}$ = 6 Hz, CF_2H). ^{1}H NMR d 7.37 (dt, $^{3}J_{FF}$ = 9, J_{FF} = 1.5 Hz), 7.21 (dt, $^{3}J_{FF}$ = 9, J_{FF} = 1.5 Hz), 5.56 (dt, $^{2}J_{FH}$ = 54, $^{3}J_{HF}$ = 5 Hz, CF_2H) and 1.98 (s, CH_3).

4-t-butylphenyl-$CF(OCF_3)CF_2H$ (**3-7o**): ^{19}F NMR –51.9 (d, $^{4}J_{FF}$ = 9 Hz, OCF_3), -131.6 (mult, C*F*), –133.0 (dt, $^{2}J_{FF}$ = 290, $^{2}J_{FH}$ = 54 Hz, CF_2H), –134.3 ppm (dt, $^{2}J_{FF}$ = 290, $^{2}J_{FH}$ = 55 Hz, CF_2H).

Time course reaction: Complex **3-1** (10 mg, 0.013 mmol) was loaded into an NMR tube and mixed with 25 μL of DMSO. 4-Iodobenzonitrile (0.013 mmol) and $PhCF_3$ (20 μL, 0.01 mmol/mL) were then added to the solution and the reaction was analyzed by ^{19}F NMR every 5 min for 4 h.

Computational Details: All geometries were fully optimized using the Gaussian 16 software package[42] in combination with the BOpt software package.[43] Following a previously proposed protocol,[44] all relevant minima and transition states were fully optimized at the TPSSTPSS level[45]

of theory employing correlation-consistent polarized valence double-ζ Dunning (DZ) basis sets with cc-pVDZ quality[46,47] from the EMSL basis set exchange library, using a small core pseudopotential on Cu.[48] The density fitting approximation (Resolution of Identity, RI)[49-52] was used at the optimization stage and for single-point energy corrections. Solvent effects (benzene, ε = 2.2706) were included with the polarizable continuum model approach (PCM) at both stages.[53] All calculations were performed at the standard Gaussian 16 SCF convergence using an ultrafine grid [Scf = tight and Int(grid = ultrafine)]. The nature of each stationary point was checked with an analytical second-derivative calculation (no imaginary frequency for minima, exactly one imaginary frequency for transition states, corresponding to the reaction coordinate). The accuracy of TS was confirmed with an intrinsic reaction coordinate (IRC) scan. Transition states were located using a suitable guess and the Berny algorithm (Opt = TS)[54] or a relaxed potential energy scan to arrive at a suitable transition-state guess, followed by a quasi-Newton or eigenvector-following algorithm to complete the optimization. Final single-point energies were calculated at the TPSSh level of theory[45] employing triple-ζ Dunning (TZ) basis sets (cc-pVTZ quality).[46] Grimme dispersion corrections without damping (keyword -zero) were added at this stage using the standalone dftd3 program.[55,56] Enthalpies and Gibbs free energies were then obtained from TZ single-point energies and thermal corrections from the TPSSTPSS/cc-pVDZ-(PP) vibrational analyses; entropy corrections were scaled by a factor of 0.67 to account for decreased entropy in the condensed phase.[57-59] IBOview was used for intrinsic bond orbital theory (IBO)calculations.[32,33]

3.5 REFERENCES

1. Zhou, Y.; Wang, J.; Gu, Z.; Wang, S.; Zhu, W.; Acena, J.L.; Soloshonok, V.A.; Izawa, K.; Liu, H. Next generation of fluorine-containing pharmaceuticals, compounds currently in phase II–III clinical trials of major pharmaceutical companies: New structural trends and therapeutic areas. *Chem. Rev.* **2016**, *116*, 422–518.

2. Ogawa, Y.; Tokunaga, E.; Kobayashi, O.; Hirai, K.; Shibata, N. Current contributions of organofluorine compounds to the agrochemical industry, *iScience* **2020**, *23*, 101467.

3. a) Neumann, C.N.; Ritter, T. Late-stage fluorination: Fancy novelty or useful tool? Angew. Chem. Int. Ed. 2015, 54, 3216-3221. b) Szpera, R.; Moseley, D.F.J.; Smith, L.B.; Sterling, A.J.; Gouverneur, V. The fluorination of C−H bonds: Developments and perspectives. Angew. Chem. Int. Ed. 2019, 58, 14824-14848.

4. a) Han, Z.-Z.; Zhang, C.-P. Fluorination and fluoroalkylation reactions mediated by hypervalent iodine reagents. *Adv. Synth. Catal.* **2020**, *362*, 4256-4292. b) Britton, R.; Gouverneur, V.; Lin, J.-H.; Meanwell, M.; Ni, C.; Pupo, G.; Xiao, J.-C.; Hu, J. Contemporary synthetic strategies in organofluorine chemistry. *Nature Rev.* **2021**, *1*, 47.

5. a) Barata-Vallejo, S.; Lantano, B.; Postigo, A. Recent advances in trifluoromethylation reactions with electrophilic trifluoromethylating reagents. *Chem. Eur. J.* 2014, *20*, 16806-16829. b) Li, G.-B.; Zhang, C.; Song, C.; Ma, Y.-D. Progress in copper-catalyzed trifluoromethylation. *Beilstein J. Org. Chem.* **2018**, *14*, 155–181. c) Xiao, H.; Zhang, Z.; Fang, Y.; Zhu, L.; Li, C. Radical trifluoromethylation. *Chem. Soc. Rev.* 2021, *50*, 6308-6319.

6. a) Ohashi, M.; Ishida, N.; Ando, K.; Hashimoto, Y.; Shigaki, A.; Kikushima, K. Ogoshi, S. Cu^{I}-catalyzed pentafluoroethylation of aryl iodides in the presence of tetrafluoroethylene and cesium fluoride: Determining the route to the key pentafluoroethyl Cu^{I} intermediate. *Chem. Eur. J.* **2018**, 24, 9794-9798. b) Xie, Q.; Li, L.; Zhu, Z.; Zhang, R.; Ni, C.; Hu, J. From C_1 to C_2: $TMSCF_3$ as a precursor for pentafluoroethylation. *Angew. Chem. Int. Ed.* **2018**, *57*, 13211-13215. c) Xie, Q.; Zhu, Z.; Li, L.; Ni, C.; Hu, J. Controllable double CF_2 insertion into sp^2 C-Cu bond using $TMSCF_3$: A facile access to tetrafluoroethylene-bridged structures. *Chem. Sci*. **2019**, *1*1, 276-280.

7. a) Landelle, G.; Panossian, A.; Leroux, F.R. Trifluoromethyl ethers and -thioethers as tools for medicinal chemistry and drug discovery. *Curr. Top. Med. Chem*. **2014**, *14*, 941-951. b) Lee, K.N.; Lee, J.W.; Nga, M.-Y. Recent development of catalytic trifluoromethoxylation reactions. *Tetrahedron* **2018**, *74*, 7127–7135. c) Deng, Z.; Zhao, M.; Wang, F.; Tang, P. Selective C-H trifluoromethoxylation of (hetero)arenes as limiting reagent, *Nature Commun.* **2020**, *11*, 2569.

8. a) Fier, P.S.; Hartwig, J.F. Copper-mediated difluoromethylation of aryl and vinyl iodides. *J. Am. Chem. Soc*. **2012**, *134*, 5524-5527. b) Sap, J.B.I.; Meyer, C.F.; Straathof, N.J.W.; Iwumene, N.; am Ende, C.W.; Trabanco, A.A.; Gouverneur, V. Late-stage difluoromethylation: Concepts, developments and perspective. *Chem. Soc. Rev.* **2021**, *50*, 8214-8247. c) Zhang, W.; Xiang, X.-X.; Chen, J.; Yang, C.; Pan, Y.-L.; Cheng, J.-P.; Meng, Q.; Li, X. Direct C–H difluoromethylation of heterocycles via organic photoredox catalysis. *Nature Commun.* **2020**, *11*, 638.

9. Doble, A. The pharmacology and mechanism of action of riluzole. *Neurol.* **1996**, *47*, 233S LP-241S.

10. Belinato, T.A.; Martins, A.J.; Lima, J.B.P.; de Lima-Camara, T.N.; Peixoto, A.A.; Valle, D. Effect of the chitin synthesis inhibitor triflumuron on the development, viability and reproduction of *Aedes aegypti*. *Mem. Inst. Oswaldo Cruz*. **2009**, *104*, 43-47.

11. Rageot, D.; Bohnacker, T.; Melone, A.; Langlois, J.-B.; Borsari, C.; Hillmann, P.; Sele, A.M.; Beaufils, F.; Zvelebil, M.; Hebeisen, P.; Löscher, W.; Burke, J.; Fabbro, D.; Wymann, M.P. Discovery and preclinical characterization of 5-[4,6-Bis({3-oxa-8-azabicyclo[3.2.1]octan-8-yl})-1,3,5-triazin-2-yl]-4-(difluoromethyl)pyridin-2-amine (PQR620), a highly potent and selective mTORC1/2 inhibitor for cancer and neurological disorders. *J. Med. Chem*. **2018**, *61*, 10084–10105.

12. Liu, K.; Wen, Z.; Ma, Z., Shao, W. Biological and molecular characterizations of fluxapyroxad-resistant isolates of *Botrytis cinerea*. *Phytopathol. Res*. **2022**, *4*, 2.

13. Xing, L.; Blakemore, D.C.; Narayanan, A.; Unwalla, R.; Lovering, F.; Denny, R.A.; Zhou, H.; Bunnage, M.E. Fluorine in drug design: A case study with fluoroanisoles. *ChemMedChem*. **2015**, *10*, 715-726.

14. Abraham, M.H.; Abraham, R.J. A simple and facile NMR method for the determination of hydrogen bonding by amide N–H protons in protein models and other compounds. *New J. Chem*. **2017**, *41*, 6064-6066.

15. Miele, M.; D'Orsi, R.; Sridharan, V.; Holzer, W.; Pace, V. Highly chemoselective difluoromethylative homologation of iso(thio)cyanates: Expeditious access to unprecedented α,α-difluoro(thio)amides. *Chem. Commun*. **2019**, *55*, 12960-12963.

16. Berger, M.; Herszman, J. D.; Kurimoto, Y.; de Kruiff, G.H.M.; Schüll, A.; Ruf, S.; Waldvogel, S. R. Metal-free electrochemical fluorodecarboxylation of aryloxyacetic acids to fluoromethyl aryl ethers. *Chem. Sci*. **2020**, *11*, 6053-6057.

17. Andrella, N.O.; Liu, K.; Gabidullin, B.M.; Vasiliu, M.; Dixon, D.A.; Baker, R.T. Metal heptafluoroisopropyl (M-hfip) complexes for use as hfip transfer agents. *Organometallics* **2018**, *37*, 422-432.

18. a) Tomashenko, O.A.; Escudero-Adàn, E.C.; Belmonte, M.M.; Benet-Bucholz, J.; Grushin, V.V. Simple, stable and easily accessible well-defined $CuCF_3$ aromatic trifluoromethylating agents. *Angew. Chem. Int. Ed.* **2011**, *50*, 7655-7659. b) Panferova, L. I.; Miloserdov, F.M.; Lishchynskyi, A.; Belmonte, M.M.; Benet-Bucholz, J.; Grushin, V.V. Well-defined CuC_2F_5 complexes and pentafluoroethylation of acid chlorides. *Angew. Chem. Int. Ed.* **2015**, *54*, 5218-5222.

19. Morimoto, H.; Tsubogo, T.; Litvinas, N.D.; Hartwig, J.F. A broadly applicable copper reagent for trifluoromethylations and perfluoroalkylations of ary iodides and bromides. *Angew. Chem. Int. Ed.* **2011**, *50*, 3793-3798.

20. Kalkman, E.D.; Mormino, M.G.; Hartwig, J.F. Unusual electronic effects of ancillary ligands on the perfluoroalkylation of aryl iodides and bromides mediated by copper(I)

pentafluoroethyl complexes of substituted bipyridines. *J. Am. Chem. Soc*. **2019**, *141*, 19458-19465.

21. Lishchynskyi, A.; Novikov, M.A.; Martin, E.; Escudero-Adàn, E.C.; Novàk, P.; Grushin, V. V. Trifluoromethylation of aryl and heteroaryl halides with fluoroform-derived $CuCF_3$: Scope, limitations and mechanistic features. *J. Org. Chem*. **2013**, *78*, 11126-11146.

22. Mestre, J.; Castillón, S.; Boutureira O. "Ligandless" pentafluoroethylation of unactivated (hetero)aryl and alkenyl halides enabled by the controlled self-condensation of $TMSCF_3$-derived $CuCF_3$. *J. Org. Chem*. **2019**, *84*, 15087-15097.

23. Andrella, N.O.; Xu, N.; Gabidullin, B.M.; Ehm, C.; Baker, R.T. Selective copper complex-catalyzed hydrodefluorination of fluoroalkenes and allyl fluorides: A tale of two mechanisms. *J. Am. Chem. Soc.* **2019**, *141*, 11506–11521.

24. Tomasi, J. Thirty years of continuum solvation chemistry: a review, and prospects for the near future. *Theor Chem Acc*. **2004**, 112, 184–203.

25. A. V Marenich, C.J. Cramer, D.G. Truhlar, Universal solvation model based on solute electron density and on a continuum model of the solvent defined by the bulk dielectric constant and atomic surface tensions, *J. Phys. Chem. B.* **2009**, 113, 63786396.

26. Wang, G,; Li, M.; Leng, X.; Xue, X.; Shen, Q. Neutral five-coordinate arylated copper(III) complex: Key intermediate in copper-mediated arene trifluoromethylation. *Chin. J. Chem.* **2022**, *40*, 1924-1930.

27. Snyder, J.P. Elusiveness of Cu^{III} complexation: Preference for trifluoromethyl oxidation in the formation of $[Cu(CF_3)_4]^-$ salts. *Angew. Chem. Int. Ed.* **1995**, *34*, 80-81.

28. DiMucci, I.M.; Lukens, J.T.; Chatterjee, S.; Carsch, K.M.; Titus, C.J.; Lee, S.J.; Nordlund, D.; Betley, T.A.; MacMillan, S.N.; Lancaster, K.M. The myth of d^8 Cu(III). *J. Am. Chem. Soc.* **2019**, *141*, 18508-18520.

29. Hoffmann, R.; Alvarez, S.; Mealli, C.; Falceto, A.; Cahill, T. J. III,; Zeng, T.; Manca, G. From widely accepted concepts in coordination chemistry to inverted ligand fields. *Chem. Rev.* **2016**, *116*, 8173-8192.

30. Gao, C.; Macetti, G.; Overgaard, J. Experimental X-ray electron density study of atomic charges, oxidations states and inverted ligand field in $[Cu(CF_3)_4]$- . *Inorg. Chem*. **2019**, *58*, 2133-2139.

31. Glendening, E. D.; Weinhold, F. Natural resonance theory: I. General formalism. *J. Comput. Chem.* **1998**, *19*, 593-609.

32. Knizia, G. Intrinsic atomic orbitals: An unbiased bridge between quantum theory and chemical concepts. *J. Chem. Theor. Comput.* **2013**, 9, 4834-4843.

33. Knizia, G.; Klein, J.E.M.N. Electron flow in reaction mechanisms – Revealed from first principles. *Angew. Chem. Int. Ed.* **2015**, *54*, 5518-5522.

34. dos Santos Comprido, L.N.; Klein, J.E.M.N.; Knizia, G.; Kästner, J.; Hashmi, A.S.K. The stabilizing effects in gold carbene complexes. *Angew. Chem. Int. Ed.* **2015,** *54*, 10336-10340.

35. Ramos-Cordoba, E.; Postils, V.; Luis, J.M.; Salvador, P. Oxidation states from wave function analysis. *J. Chem. Theory, Comput.* 2015, 11, 1501-1508.

36. Postils, V.; Delgado-Alonso, C.; Luis, J.M.; Salvador, P. An objective alternative to IUPAC's approach to assign oxidation states. *Angew. Chem. Int. Ed.* **2018,** *57*, 10525-10529.

37. Steen, J. S.; Knizia, G.; Klein, J.E.M.N. s-noninnocence: Masked phenyl cation transfer at formal Ni^{IV}. *Angew. Chem. Int. Ed.* **2019,** *58*, 13133-13139.

38. Bour, J.R.; Camasso, N.M.; Sanford, M.S. Oxidation of Ni(II) to Ni(IV) with aryl electrophiles enables Ni-mediated aryl-CF_3 coupling. *J. Am. Chem. Soc.* **2015**, *137*, 8034-8037.

39. Rzhevsky, S.A.; Topchiy, M.A.; Lyssenko, K.A.; Philippova, A.N.; Belaya, M.A.; Ageshina, A.A.; Bermeshev, M.V.; Nechaev, M.S.; Asachenko, A.F. New expanded-ring NHC platinum(0) complexes: Synthesis, structure and highly efficient diboration of terminal alkenes. *J. Organomet. Chem.* **2020**, *912*, 121140.

40. Arduengo, A.J., III.; Krafczyk, R.; Schmutzler, R.; Craig, H. A.; Goerlich, J.R.; Marshall, W. J. Unversagt, M. Imidazolylidenes, imidazolinylidenes and imidazolines. *Tetrahedron* **1999**, *55*, 14523-14534.

41. Lee, D.-W.; Yun, J. Direct synthesis of Stryker's reagent from a Cu(II) salt. *Tet. Lett.* **2005**, *12*, 2037-2039.

42. Gaussian 16, Revision C.01, Frisch, M. J.; Trucks, G. W.; Schlegel, H. B.; Scuseria, G. E.; Robb, M. A.; Cheeseman, J. R.; Scalmani, G.; Barone, V.; Petersson, G. A.; Nakatsuji, H.; Li, X.; Caricato, M.; Marenich, A. V.; Bloino, J.; Janesko, B. G.; Gomperts, R.; Mennucci, B.; Hratchian, H. P.; Ortiz, J. V.; Izmaylov, A. F.; Sonnenberg, J. L.; Williams-Young, D.; Ding, F.; Lipparini, F.; Egidi, F.; Goings, J.; Peng, B.; Petrone, A.; Henderson, T.; Ranasinghe, D.; Zakrzewski, V. G.; Gao, J.; Rega, N.; Zheng, G.; Liang, W.; Hada, M.; Ehara, M.; Toyota, K.; Fukuda, R.; Hasegawa, J.; Ishida, M.; Nakajima, T.; Honda,

Y.; Kitao, O.; Nakai, H.; Vreven, T.; Throssell, K.; Montgomery, J. A., Jr.; Peralta, J. E.; Ogliaro, F.; Bearpark, M. J.; Heyd, J. J.; Brothers, E. N.; Kudin, K. N.; Staroverov, V. N.; Keith, T. A.; Kobayashi, R.; Normand, J.; Raghavachari, K.; Rendell, A. P.; Burant, J. C.; Iyengar, S. S.; Tomasi, J.; Cossi, M.; Millam, J. M.; Klene, M.; Adamo, C.; Cammi, R.; Ochterski, J. W.; Martin, R. L.; Morokuma, K.; Farkas, O.; Foresman, J. B.; Fox, D. J. Gaussian, Inc., Wallingford CT, 2016.

43. Budzelaar, P. H. M. Geometry optimization using generalized, chemically meaningful constraints. *J. Comput. Chem.* **2007**, *28*, 2226− 2236.

44. Ehm, C.; Budzelaar, P. H. M.; Busico, V. Calculating accurate barriers for olefin insertion and related reactions. *J. Organomet. Chem.* **2015**, *775*, 39−49.

45. Tao, J.; Perdew, J. P.; Staroverov, V. N.; Scuseria, G. E. Climbing the Density Functional Ladder: Nonempirical Meta-Generalized Gradient Approximation Designed for Molecules and Solids. *Phys. Rev. Lett.* **2003**, *91*, 146401.

46. Balabanov, N. B.; Peterson, K. A. Systematically convergent basis sets for transition metals. I. All-electron correlation consistent basis sets for the 3d elements Sc−Zn. *J. Chem. Phys.* **2005**, *123*, 064107.

47. Balabanov, N. B.; Peterson, K. A. Basis set limit electronic excitation energies, ionization potentials, and electron affinities for the 3d transition metal atoms: Coupled cluster and multireference methods. *J. Chem. Phys.* **2006**, *125*, 074110.

48. Schuchardt, K. L.; Didier, B. T.; Elsethagen, T.; Sun, L. S.; Gurumoorthi, V.; Chase, J.; Li, J.; Windus, T. L. Basis set exchange: A community database for computational sciences. *J. Chem. Inf. Model.* **2007**, *47*, 1045−1052.

49. Whitten, J. L. Coulombic potential energy integrals and approximations. *J. Chem. Phys.* **1973**, *58*, 4496.

50. Baerends, E. J.; Ellis, D. E.; Ros, P. Self-consistent molecular Hartree-Fock-Slater calculations I. The computational procedure. *Chem. Phys.* **1973**, *2*, 41−51.

51. Feyereisen, M.; Fitzgerald, G.; Komornicki, A. Use of approximate integrals in *ab initio* theory. An application in MP2 energy calculations. *Chem. Phys. Lett.* **1993**, *208*, 359−363.

52. Vahtras, O.; Almlöf, J.; Feyereisen, M.W. Integral approximations for LCAO-SCF calculations. *Chem. Phys. Lett.* **1993**, *213*, 514−518.

53. Tomasi, J. Thirty years of continuum solvation chemistry: A review and prospects for the near future. *Theor. Chem. Acc.* **2004**, *112*, 184−203.

54. The Berny algorithm was never fully published; see the Gaussian documentation for details.

55. Grimme, S. Density functional theory with London dispersion corrections. *Wiley Interdiscip. Rev. Comput. Mol. Sci.* **2011**, *1*, 211−228.

56. Grimme, S.; Ehrlich, S.; Goerigk, L. Effect of the damping function in dispersion corrected density functional theory. *J. Comput. Chem.* **2011**, *32*, 1456−1465.

57. Tobisch, S.; Ziegler, T. Catalytic oligomerization of ethylene to higher linear α-olefins promoted by the cationic group 4 $[(\eta^5\text{-Cp-}(CMe_2\text{-bridge})\text{-Ph})M^{II}(\text{ethylene})_2]^+$ (M = Ti, Zr, Hf) active catalysts: A density functional investigation of the influence of the metal on the catalytic activity and selectivity. *J. Am. Chem. Soc.* **2004**, *126*, 9059− 9071.

58. Dunlop-Briere, A. F.; Budzelaar, P. H. M.; Baird, M. C. α- and β-Agostic alkyl-titanocene complexes. *Organometallics* **2012**, *31*, 1591−1594.

59. Raucoules, R.; de Bruin, T.; Raybaud, P.; Adamo, C. Theoretical unraveling of selective 1-butene oligomerization catalyzed by iron−bis(arylimino)pyridine. *Organometallics* **2009**, *28*, 5358−536

Chapter 4. Copper-mediated Tetrafluoroethylation of Bioactive Compounds

Contributions to Knowledge:

Copper-Mediated Tetrafluoroethylation of Aroyl Chlorides and Aryl Halides

Nicholas O. Andrella, Luana L. T. N. Porto, Nancy Xu, Christian Ehm and R. Tom Baker,** to be submitted, 2022.

Copper-mediated Tetrafluoroethylation of Bioactive Alkenyl Iodides

Luana L. T. N. Porto, Isabel Bascuas, Nicole Johnson, Omar Boutureira and R. Tom Baker,** manuscript in preparation.

Fluoroalkylated Carboxamides as Potential Succinate Dehydrogenase Inhibitors

Luana L. T. N. Porto, Antony St.-Jacques, R. Tom Baker and Michele C. Loewen,** manuscript in preparation.

Chapter Contributions: Our collaborator Dr. Christian Ehm (University of Naples, Italy), performed the DFT calculations. The Xantphos-Cu mediated tetrafluoroethylation of aroyl chlorides and aryl halides performed by Luana Porto built on previous work in the Baker group by Nicholas O. Andrella using the $PMePh_2$ ancillary ligand. Development of the ligandless -CF_2CF_2H transfer to alkenyl iodides was performed by Luana Porto and ICE undergraduate Nicole Johnson with substrates provided by our collaborator Prof. Omar Boutureira and his PhD student Isabel Bascuas (Universitat Rovira i Virgili, Tarragona, Spain). The molecular docking studies were performed by Dr. Antony St.-Jacques working with our collaborator Dr. Michele Loewen (National Research Council, Ottawa).

Abstract: The tetrafluoroethyl group (-CF_2CF_2H) has attracted attention in pharmaceutical and agrochemical research due to its lipohilicity and H-bonding capability. In this chapter we show that the readily available Xantphos ligand allows for the Cu-mediated tetrafluoroethylation of aroyl chlorides and aryl iodides in toluene at 90°C, albeit in poor to fair yields (Xantphos = 4,5-bis(diphenylphosphino)-9,9-dimethylxanthene). We then describe an efficient 'ligandless' Cu system that mediates the tetrafluoroethylation of alkenyl iodides, affording products with potential biological activity. Finally, we propose fluoroalkylated-carboxamide analogues as potential fungicides based on molecular *docking* studies.

4.1 INTRODUCTION

Fluoroalkyl groups containing the -CF_2H functionality have attracted attention as lipophilic H-bond donors.[1] However, the -CF_2CF_2H group offers both increased lipophilicity and a more acidic C-H bond (*vs.* -CF_2H).[2] Although there are a number of strategies to access difluoromethylarenes ($ArCF_2H$),[3] direct incorporation of -CF_2CF_2H has been limited in terms of both step economy and cost efficiency. An early example of cobalt carbonyl-catalyzed direct addition of

tetrafluoroethylene (TFE) to arenes at 135°C (**Scheme 4.1A**)[4] would be unsuitable for late-stage fluoroalkylation, and deoxyfluorination, by treating Ar-C(O)C(O)H compounds with deoxofluor

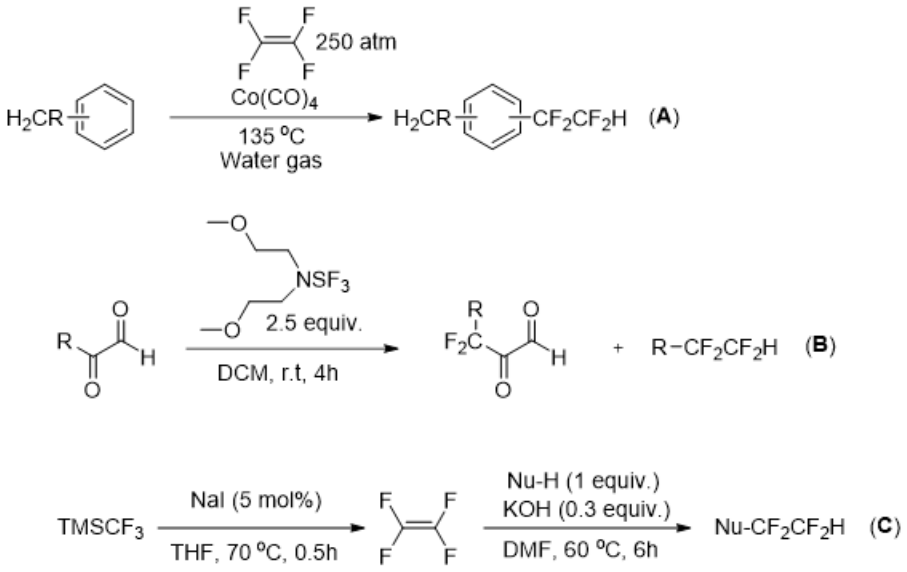

Scheme 4.1 Several arene tetrafluoroethylation strategies.

[bis(2-methoxyethyl)aminosulfur trifluoride][5] requires specialized starting materials (**Scheme 4.1B**). Hu and co-workers prepared heteroatom-containing -CF_2CF_2H compounds by addition of E-H nucleophiles to TFE generated from $TMSCF_3$ using a custom two-chamber reactor (**Scheme 4.1C**).6 In 2018 Andrella, working in the Baker group, reported the synthesis of $Cu(CF_2CF_2H)(PMePh_2)_3$ (**4-1**)[7] from reaction of Stryker's reagent, $CuH(PPh_3]_6$, with $PMePh_2$ and so-called Safe-Supply™ mixture of 1:1 TFE:CO_2, easily generated by thermolysis of potassium perfluoropropionate.[8] Moreover, they demonstrated for the first time the direct tetrafluoroethylation of aroyl chlorides and, in the presence of catalytic CuCl(IPr), the tetrafluoroethylation of aryl iodides (**Scheme 4.2**).[9]

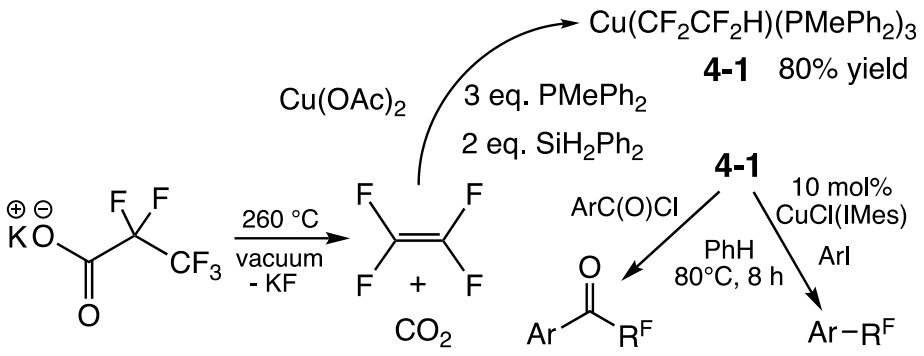

Scheme 4.2 Synthesis of **4-1** and tetrafluoroethylation of aroyl chlorides and aryl iodides.

In a later report, citing safety concerns associated with the use of TFE gas, Hu et al. optimized the generation of TFE from $TMSCF_3$ to effect the pentafluoroethylation of aryl iodides and double insertion of CF_2 of heteroatom-$CF_2CF_2C_6F_5$ compounds (**Scheme 4.3A**).[10] Finally, Hu et al. recently employed Me_3SiCF_2Br with $CuCF_2H$ to effect the direct tetrafluoroethylation of aryl iodides and bromides (**Scheme 4.3B**).[11] In an effort to expand the synthesis of M-R^F complexes pioneered by Miller and Burnard with silver fluoride and hexafluoropropene (as described in Chapter 1),[12] we have accessed Cu-R^F complexes by insertion of fluoroalkenes into Cu-F or Cu-H bonds.[13] In an effort to expand the scope of tetrafluoroethylations, we build on Boutureira's work on alkenyl iodide pentafluoroethylation[14] to develop solvent-stabilized 'ligandless' Cu-CF_2CF_2H transfer to analogous bioactive compounds under mild conditions. Moreover, working with DFT collaborator Christian Ehm, we show the contribution of pre-equilibria to the activation energies for transfer of a variety of R^F groups to several organic electrophiles as a function of the ancillary ligands on copper. Finally, we propose fluoroalkylated-carboxamide analogues as potential fungicides based on molecular *docking* studies.

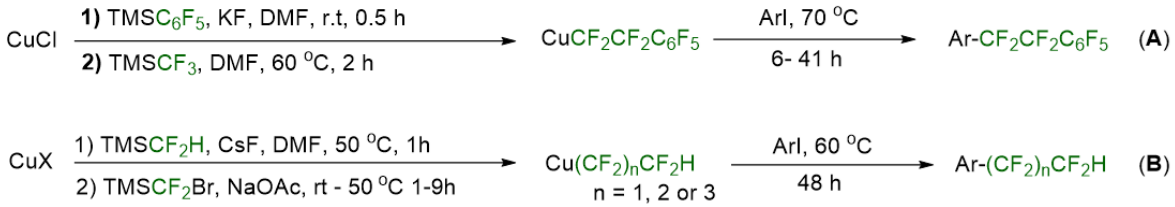

Scheme 4.3 Hu's fluoroalkyl-trimethylsilane routes to arene tetrafluoroethylation.

4.2 RESULTS AND DISCUSSION

4.2.1 Ligand effects in -CH_2CH_2F transfer to aryl iodides: In previous work it was reported that $Cu(CF_2CF_2H)(PMePh_2)_3$ (**4-1**) could be obtained in high yield from the reaction of Stryker's reagent, $[CuH(PPh_3)]_6$, with $PMePh_2$ and so-called Safe-Supply™ mixture of 1:1 TFE:CO_2, whereas synthesis of the Xantphos analog, $Cu(CF_2CF_2H)$(Xantphos) (**4-2**) could only be prepared using pure TFE (Xantphos = 4,5-bis(diphenylphosphino)-9,9-dimethylxanthene).[7] In contrast, we found that changing the reaction solvent from benzene to N,N-dimethylformamide (DMF) afforded complex **4-2** from the TFE:CO_2 mixture. Moreover, **4-2** slowly transferred the -CF_2CF_2H group to 4-nitro-iodobenzene at 50 °C (**Figure 4.1**); addition of 10% CuCl(SIMes) gave 22% yield after 12 h at 90 °C (**Figure 4.2**).

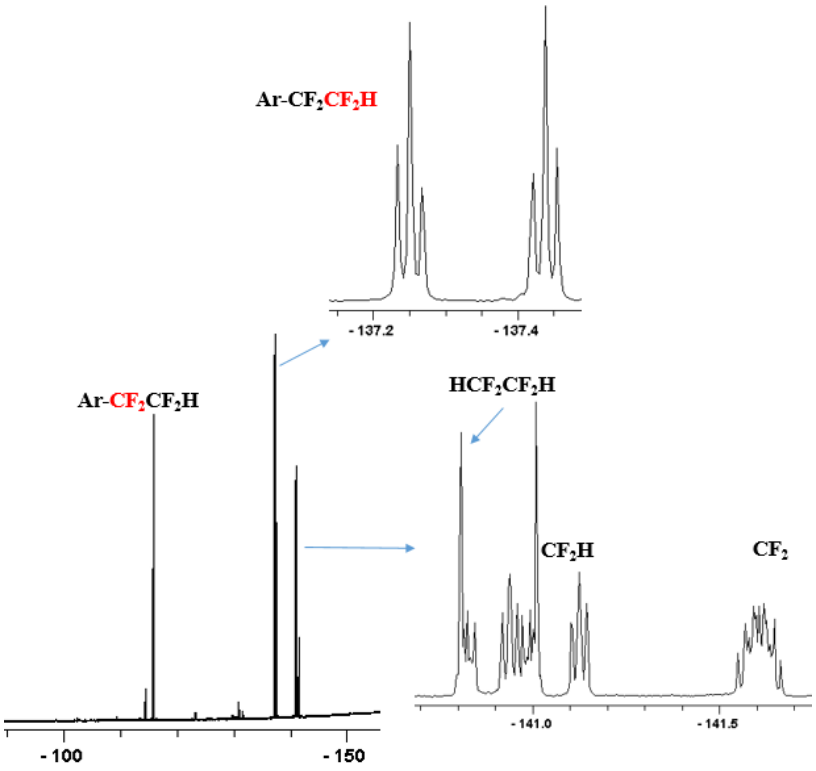

Figure 4.1 ^{19}F NMR spectrum of $[CuH(PPh_3)]_6$ + Xantphos + tetramethyldisiloxane + TFE:CO_2 + methyl-4-iodobenzoate in DMF after 7 h at 50 °C.

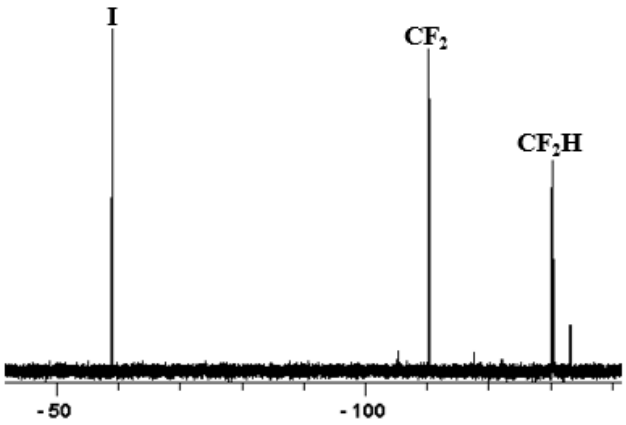

Figure 4.2 ^{19}F NMR spectrum of Cu(CF_2CF_2H)(Xantphos) (**4-2)** + 4-nitro-iodobenzene + 10 mol% CuCl(SIMes) in toluene at 90 ˚C after 12 h. I = internal standard $PhCF_3$.

Vicic previously identified N-heterocyclic carbenes as one of the best ligand classes that he evaluated for Cu-mediated trifluoromethylation, suggesting that they reduce the rate-determining energy barrier for oxidative addition.[15] As a detailed computational analysis of ligand effects for several different R^F groups and organic electrophiles had not been undertaken, we engaged Dr. Christian Ehm from Naples, Italy as a collaborator.

4.2.2 DFT studies of Cu-mediated R^F transfer to organic electrophiles: DFT calculations were performed using the TPSSh-D0 /TZ//TPSSTPSS/DZ level of theory. Solvent effects were included at the single point energy correction stage employing the polarizable continuum model; this approach was employed previously in studying selective copper complex-catalyzed hydrodefluorination of fluoroalkenes.[7]

A simplified mechanistic scheme is depicted in **Figure 4.3** using a single PPh_3 ligand on the Cu(CF_2CF_2H) fragment and iodobenzene as the substrate, i.e., ignoring any pre-equilibria that can affect the stability of LCu-R^F complexes. The reaction has a strong driving force due to the weak Cu-C^F bond (vs. Cu-X) and strong product C-C bond between the aryl carbon and fluorinated benzylic carbon. Using this linear model, the activation energies for both the 'oxidative' addition and 'reductive' elimination steps are similar for the -CF_3, -CF_2CF_2H and -$CF(CF_3)_2$ R^F groups showing little dependence on sterics (**Table 4.1**); this is hardly surprising, considering that PPh_3 is not a large phosphine and, in linear d^{10} copper systems, the steric bulk of the phosphine ligand is in the opposing hemisphere from the R^F group. In contrast, replacing the PPh_3 ancillary ligand

with either bulky SIMes or bidentate phenanthroline ligand increased the energy barriers for both addition and elimination steps (**Table 4.2**), especially for the SIMes system. Finally, five different electrophiles were screened, and the oxidative addition barriers follow the expected C-X bond strengths with PhC(O)Cl < Ph-I < Ph-Br < $PhCH_2Br$ < PhCl (**Table 4.3**); reductive elimination becomes rate-determining only when oxidative addition has very low barriers, *i.e.*, only for benzoyl chloride as shown in Chapter 3.

Having explored the effects of L-type ligand, R^F group and electrophile, we decided to interrogate the trends for R^F and electrophile variation for two copper ligands: SIMes and phen. The largest barriers associated with a given R^F, electrophile, and ancillary ligand are listed in **Table 4.4**. Cells marked in red in the table indicate that the predicted rate-limiting barrier in a given system is above 25 kcal/mol, *i.e.*, no reactivity (or very slow conversion) would be expected under experimental conditions. Inspection of the results indicates that most barriers are predicted to be below 25 kcal/mol, regardless of the ligand; this is not in line with experimental observation. However, in a general sense, barriers increase with increasing size of L, R^F and C-X bond strength. On the face of it, there is no apparent indication as to why the phen complex gives the best transfer of the hfip group to aroyl chlorides or why SIMes is a privileged ligand for transfer of the $-CF_2H$ and $-CF_2CF_2H$ groups to aryl iodides. However, once one considers the potential role of ligand association pre-equilibria as significant contributors to the oxidative addition step, everything falls rapidly into place.

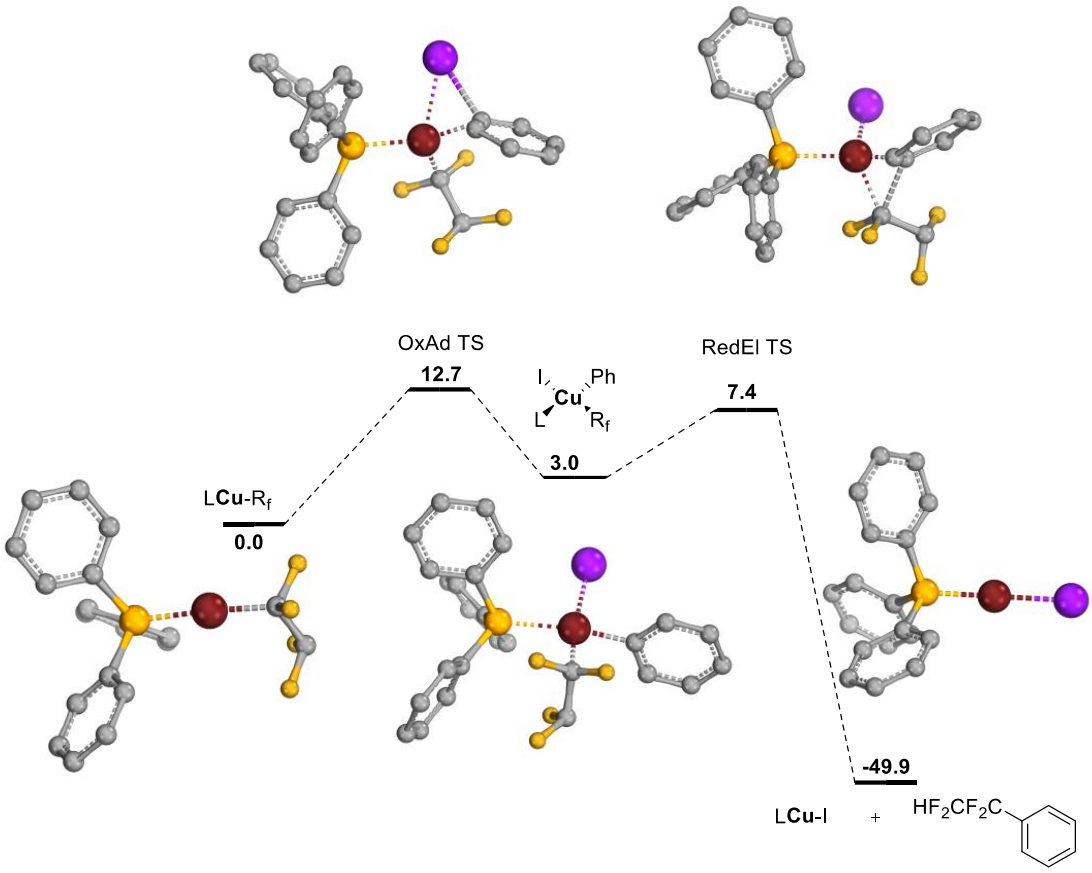

Figure 4.3 Calculated reaction coordinate for R^F transfer from $Cu(CF_2CF_2H)(PPh_3)$ to iodobenzene in toluene (energies are in kcal/mol).

R_f Variation		
	OxAd TS	**RedEl TS**
R_f = CF_3	**11.8**	8.7
CF_2CF_2H	**12.7**	7.4
i-C_3F_7	**11.8**	8.7

Table 4.1 Addition and elimination energy barriers (kcal/mol) for transfer of three different fluoroalkyl groups to iodobenzene.

Table 4.2 Addition and elimination energy barriers (kcal/mol) associated with -CF_2CF_2H transfer to iodobenzene from three different $LCuR^F$ complexes.

	Ligand Variation	
	OxAd TS	**RedEl TS**
L = SIMes	**19.4**	13.7
Phen	**13.9**	9.4
PPh_3	**12.7**	7.4

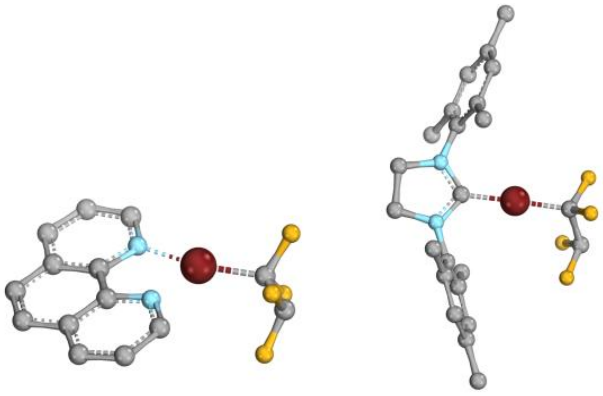

Phen **SIMes**

Table 4.3 Addition and elimination energy barriers (kcal/mol) associated with -CF_2CF_2H transfer to five different organic electrophiles.

	Electrophiles	
	OxAd TS	**RedEl TS**
Ph-I	**12.7**	7.4
Ph-Br	**17.4**	10.0
Ph-Cl	**22.6**	10.6
Bn-Br	**20.3**	8.2
Ph-C(O)Cl	9.6	**13.4**

Table 4.4 Largest barriers associated with a given R^F, electrophile, and ancillary ligand. **Bold** = oxidative addition rate limiting, Italics = reductive elimination rate-limiting.

	PhCl	PhBr	PhI	BnBr	PhC(O)Cl
R = CF_3					
SIMes	**23.9**	**18.9**	**14.5**	**21.6**	*13.3*
Phen	**20.8**	**16.3**	**11.3**	*19.4*	*15.0*
PPh_3	**22.1**	**16.8**	**11.8**	**19.8**	*12.4*
R = CF_2CF_2H					
SIMes	**29.2**	**23.4**	**19.4**	*20.5*	**15.2**
Phen	**22.6**	**19.0**	**13.9**	*20.5*	*13.9*
PPh_3	**22.6**	**17.4**	**12.7**	**20.3**	*13.4*
R = i-C_3F_7					
SIMes	*28.3*	*26.6*	*25.3*	*32.2*	*26.1*
Phen	*25.3*	*22.3*	*20.2*	**26.7**	*22.6*
PPh_3	**22.1**	**16.8**	**11.8**	**19.8**	*12.4*
R = $CF{=}CF_2$					
Phen	**24.2**	**20.3**	**15.3**	**19.6**	**11.7**
R = $CFCF_3OCF_3$					
Phen	*24.4*	*21.9*	*18.1*	*23.1*	*19.3*

We identified several different possible equilibria. Most notably, depending on the size of the R^F group, $L_3Cu\text{-}R^F$ or $L_2Cu\text{-}R^F$ (L = triphenylphosphine) is predicted to be the lowest energy structure, *i.e.*, phosphine dissociation to provide space for the subsequent oxidative addition is a non-negligible contribution, in fact raising the barrier in all cases above the useful threshold (25 kcal/mol). The phen ligand does not displace all coordinated phosphines and $(phen)(PPh_3)Cu\text{-}R^F$ is lowest in energy for CF_2CF_2H and hfip. Nonetheless, addition of phen is predicted to improve R^F transfer, as the phosphine is much more weakly-bound to copper than in the homoleptic copper phosphine complexes, likely due to steric reasons.

Additionally complicating the pre-equilibria are dimeric copper complexes, depending on the R^F ligand (in the case of R^F = perfluorovinyl) and the halide ligand (X-ligand). The latter is only relevant for catalytic performance, when dimerization of the reaction products (X stemming from the electrophile after the first reductive elimination) can increase the barrier for regeneration

Table 4.5 Largest barriers associated with a given R^F, electrophile, and ancillary ligand taking account of ligand association pre-equilibria. **Bold** = oxidative addition rate limiting, Italics = reductive elimination rate-limiting.

	PhCl	PhBr	PhI	BnBr	PhC(O)Cl
R = CF_3					
SIMes	**24.2**	**19.5**	**16.7**	**22.2**	*13.3*
Phen	**20.9**	**17.3**	**15.5**	**19.5**	*15*
PPh_3	**50.6**	**45.3**	**40.3**	**48.3**	**39**
R = CF_2CF_2H					
SIMes	**29.2**	**23.4**	**19.4**	*20.5*	**15.2**
Phen	**25.2**	**21.6**	**16.5**	*20.5*	*13.9*
PPh_3	**45.1**	**39.9**	**35.2**	**42.8**	**32.1**
R = i-C_3F_7					
SIMes	**33.4**	**28.7**	*25.3*	*32.2*	*26.1*
Phen	**39.2**	**34.3**	**29.3**	**26.7**	*22.6*
PPh_3	**37.4**	**32.1**	**27.1**	**35.1**	**25.8**
R = $CF=CF_2$					
Phen	**34.2**	**30.3**	**25.6**	**29.9**	**22.0**

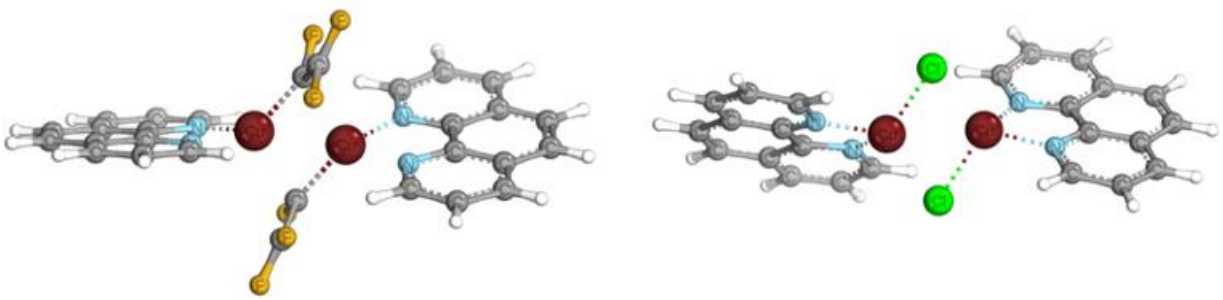

Figure 4.4 R^F- and halo-bridged copper dimers.

of the catalyst. Note that bimolecular decomposition pathways have been implicated in the decomposition of Cu-R^F complexes, for example. SIMes is only a privileged ligand, and only for small R^F groups, because it affects the pre-equilibria.[15] Reductive elimination becomes rate-limiting for bulkier R^F groups and even for smaller R^F groups, barriers from the active LCu-R^F species are larger than for the corresponding phosphine system and only the suppression of pre-equilibria tips the scales. The smaller phen ligand seems to offer the best compromise here between influencing pre-equilibria and activation barriers of the active species. In fact, the existence of

these pre-equilibria leads to non-trivial tuning effects for this type of catalysis, partially explaining why Hartwig observed "unusual electronic effects of ancillary ligands on the perfluoroalkylation of aryl iodides and bromides" in his copper bipy systems.[16] Correctly identifying the role that these pre-equilibria play is challenging due to the complexity of the hyperspace and the results presented above represent a necessary first step in this direction.

4.2.2 Tetrafluoroethylation of bioactive compounds using 'ligandless' CuR^F strategy: Ever since Burton and co-workers used Zn and Cd reagents to prepare '$Cu(CF_3)$' stabilized solely by coordinating solvents, and demonstrated the stoichiometric trifluoromethylation of aryl iodides,[17] this strategy has been employed by Grushin and co-workers using fluoroform (CHF_3)[18] and by Boutureira et al. using Me_3SiCF_3 to effect the pentafluoroethylation of glycals, nucleosides and nucleobases.[19] Building on our work in Chapter 3, our initial investigation adding Cu(I) halide salts to complex **4-1** in DMF afforded two different Cu-CF_2CF_2H species that eventually converted to a single Cu complex that was stable for at least four months. To better understand the reactivity of this solvated complex, we treated **4-1** with 2 equiv. of CuX and 1 equiv. of 4-iodobenzonitrile using two solvent systems: DMSO/benzene (0.05:1) and pure DMF. Using the DMSO/benzene mixture with CuCl, CuBr and CuI afforded 4-(C_2F_4H)-benzonitrile (**4-3a**) in 16, 11 and 9%, yield, respectively (**Table 4.6**, entries 1-3). Fortunately, pure DMF gave the same product with CuBr in 80% yield vs. 26 for CuI and 12 for CuCl.

Table 4.6 Optimization of 4-iodobenzonitrile tetrafluoroethylation using "ligandless" $Cu(C_2F_4H)$.

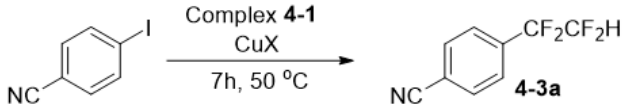

Entry	Solvent	CuX	Yield[a] (%)
1	DMSO/benzene	CuCl	16
2	DMSO/benzene	CuBr	11
3	DMSO/benzene	CuI	9
4	DMF	CuCl	12
5	DMF	CuBr	80
6	DMF	CuI	26

[a]yields determined by ^{19}F NMR with trifluorotoluene as the internal standard.

With these conditions in hand, we moved to alkenyl iodides, investigating the scope with protected and unprotected nucleobases, indoles (**Scheme 4.4**) and protected (benzyl, pivalate and acetate) iodoglycols, including disaccharides with acid-labile linkages (D-lactose and D-glucose) and Neu5Ac2en (**Scheme 4.5**). All afforded moderate to high yields, except the deprotected cytidine (**4-4b**) obtained in 20% yield. Traces of HCF_2CF_2H by-product (^{19}F NMR resonance at *ca.* -141 ppm) were detected for all reactions. Of note, unprotected NH_2 and N-H groups gave lower yields (cf. **4-4b** and **4-4f)** with formation of HCF_2CF_2H predominating. In contrast, the same behaviour was not observed for free OH as evidenced by **4-4a** and **4-4c**. Furthermore, the electron-rich iodinated analog of the antiviral trifluridine (Viroptic®)[19] gave product **4-4d** in only 10% higher yield than **4-4a** from the deprotected substrate. Both fluorinated indole iodides afforded C_2F_4H-derivatives **4-4g** and **4-4h** in high yield, including the analog of vitamin P core (**4-4g**). In **Scheme 4.5**, we show the fluoroalkylation of the iodinated analog of antiviral zanamivir (Relenza®)[20] that generates **4-4k** in 80% yield. Among D-glucose analogs, those with the pivalate protecting group (**4-4m**) showed the most efficient reaction compared to similar results obtained with benzyl (**4-4i**) or acetate (**4-4j**).

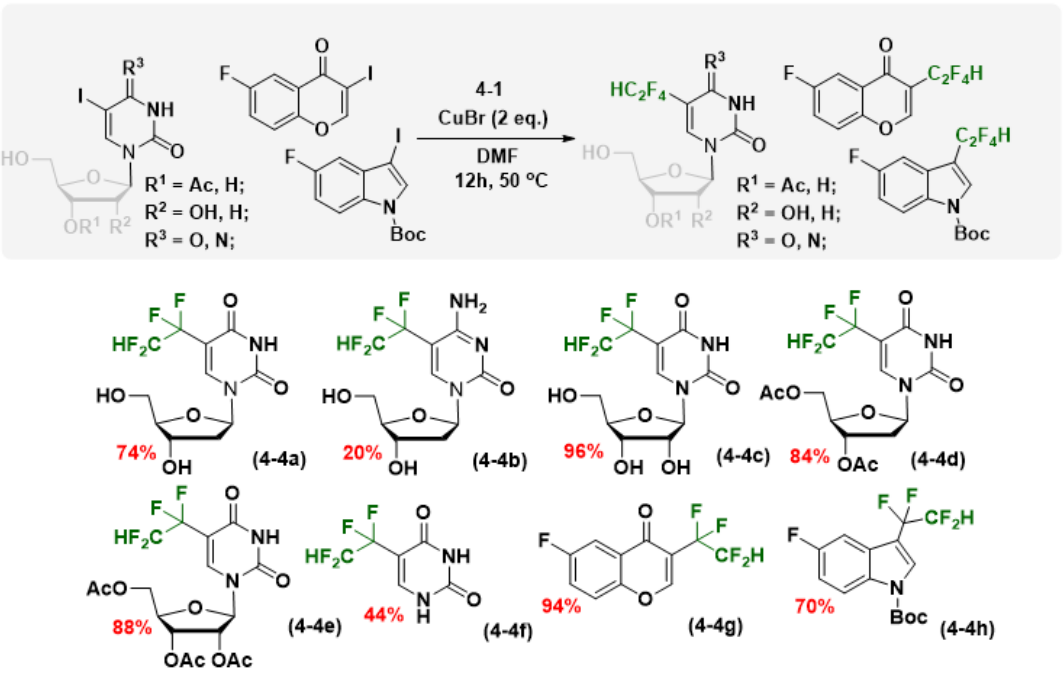

Scheme 4.4 Tetrafluoroethylation of electron-rich heterocyclic alkenyl iodides. Yields determined by ^{19}F NMR with trifluorotoluene as internal standard.

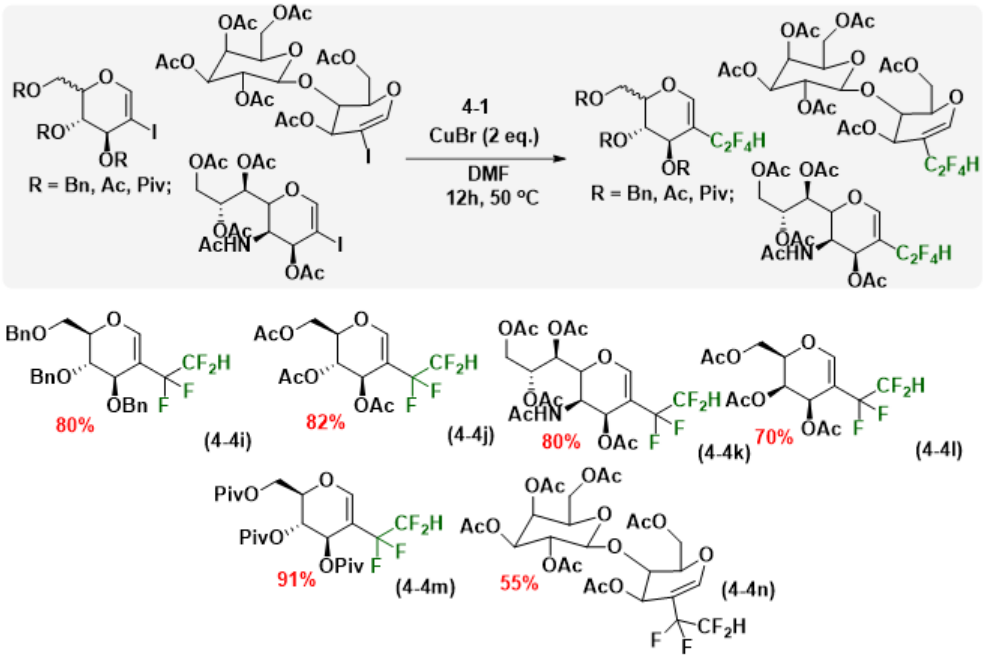

Scheme 4.5 Tetrafluoroethylation of electron-rich iodoglycols. Yields determined by ^{19}F NMR with trifluorotoluene as internal standard.

Motivated by the above success and attempting to get a higher yield, considering the side product reactions are coming from interaction with the substrate, we increased the substrate to 1.5 equiv. We observed a slightly higher yield for some products (including unprotected **4-4a**). 4-Iodouracil analog of the antiviral fluorouracil (Adrucil®) improved almost twice the effectiveness of fluoroalkylation, but no significant changes were observed for protected **4-4d**, **4-4e**, **4-4i**, and **4-4j** (**Scheme 4.6**). Further experiments confirmed by ^{1}H NMR an interaction between 4-iodouracil and CuBr, resulting in a higher yield with an excess of the substrate (See Appendix). Additional optimization of this reaction (**Table 4.7**) showed that the **4-1**/CuBr/substrate (1:2:1) system in DMSO/toluene (0.05:1) gave 77% of product **4-4n** with evident precipitation of $CuBr(PPh_2Me)_3$. Even though scale-up reactions were not successful due to generation of a large quantity of hydrogenolysis product, in collaboration with Dr. Boutureira we decided to scale up the fluorouracil (Adrucil®) (**4-4f**) and trifluridine (Viroptic®) (**4-4e**) analogues containing (-CF_2CF_2H and -CF_2CF_3). These compounds tested as antivirals by another collaborator lab, Dr. John Pezacki at uOttawa. Purification of the crude material started during my visit in prof. Boutureira's laboratory and will be continued by them to characterize all the compounds.

4.2.3 Synthesis and molecular docking studies of potential succinate dehydrogenase inhibitors (SDHi): As discussed in Chapter 1, novel fluorine-containing agrochemicals have critical relevance for agrochemical research. One of the most common modes of action for fungicides is

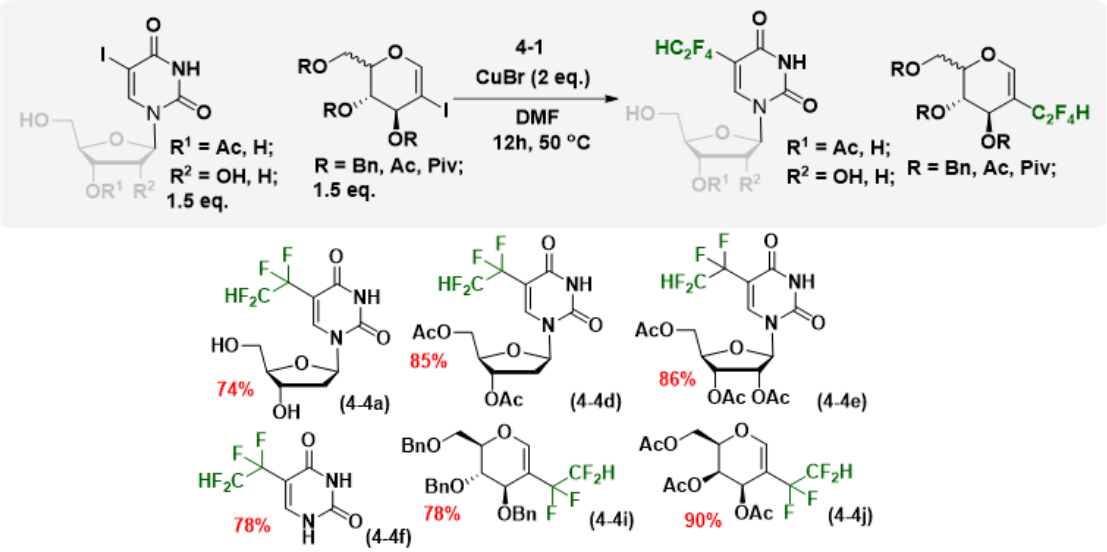

Scheme 4.6 Tetrafluoroethylation of electron-rich heterocyclic alkenyl iodides using 1.5 equiv. of substrate.

Table 4.7 Optimization of R^F transfer from **4-1** to 4-iodouracil.

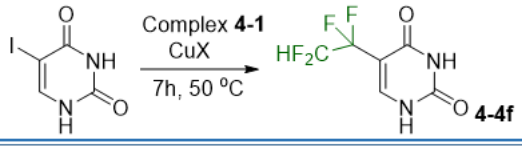

Entry	Solvent	Complex 1 (eq.)	CuBr (eq.)	Iodouracil (eq.)	Yield[a]
1	DMF	1.5	0.5	1	0
2	DMF	1.5	1	1	0
3	DMF	1	1	1.5	0
4	DMF	1	2.5	1.5	0
5	Et_2O/DMF	1	2	1.5	0
6	Et_2O/DMF	1	2	1	0
7	THF/DMF	1	2	1.5	0
8	Toluene/DMF	1	2	1	42
9	Toluene/DMF	1	3	1	43
10	Toluene/DMSO	1	2	1	77

[a]yields determined by ^{19}F NMR with trifluorotoluene as the internal standard.

the inhibition of the succinate dehydrogenase (SDH) enzyme involved in the tricarboxylic acid cycle, as its inhibition leads to the arrest of fungal growth.[20] Motivated by our successful ligandless fluoroalkylation system for aryl iodides, nucleobases and glycals, we decided to go further and pursue novel fluoroalkylated carboxamides as potential succinate dehydrogenase inhibitors. In a collaboration with Dr. Michele Loewen of the National Research Council lab in Ottawa, *in silico* molecular docking analysis on potential fluorinated-carboxamides containing the three R^F group (-$CF(OCF_3)CF_2H$, -CF_2CF_3 and CF_2CF_2H) with *Fusarium graminearum* succinate dehydrogenase (fgSDH) structure were performed by Dr. Antony St.-Jacques.

4.2.3.1 In silico molecular docking results: We initiated our studies using *in silico* docking molecular strategy to find the most successful fluorinated-carboxamide analogue (**4-5a-i**, **4-6a-i**) for synthesis and *in vitro* studies (**Figure 4.5**). To the best of our knowledge, no crystal structure has been solved for fgSDH. Thus, we built two homology models using SWISS_MODEL.[21] The major difference between the two models is the positions of W72C and F73C (**Figure 4.6**). In order to gauge the predictability of the docking simulations, we compared the docking results to how N-[(4-*t*-butylphenyl)methyl]-2-(trifluoromethyl)benzamide (NAQ) binds the crystal structure of Sus scrofa (feral pig) SDH (PDB ID: 4YTP, **Figure 4.6**). NAQ binds ssSDH in an orientation consistent with how Sierotzki *et al*.[22] described how SDHIs bind SDHs: Trp173B and Tyr128D hydrogen bond to the carbonyl oxygen of the amide group; the trifluoromethylbenzene group is in the cavity, 5.9 Å from the Cα of His216B, the residue at the end of the pocket, and p-stacking with Arg46C. The isopropyl benzene group is at the mouth of the pocket and interacts with Ile30C, Trp35C, and Ile43C. This orientation of the carboxy side ring and the amide side ring in the binding site is consistent with the pharmacophore reported for carboxamide SDHIs.[23]

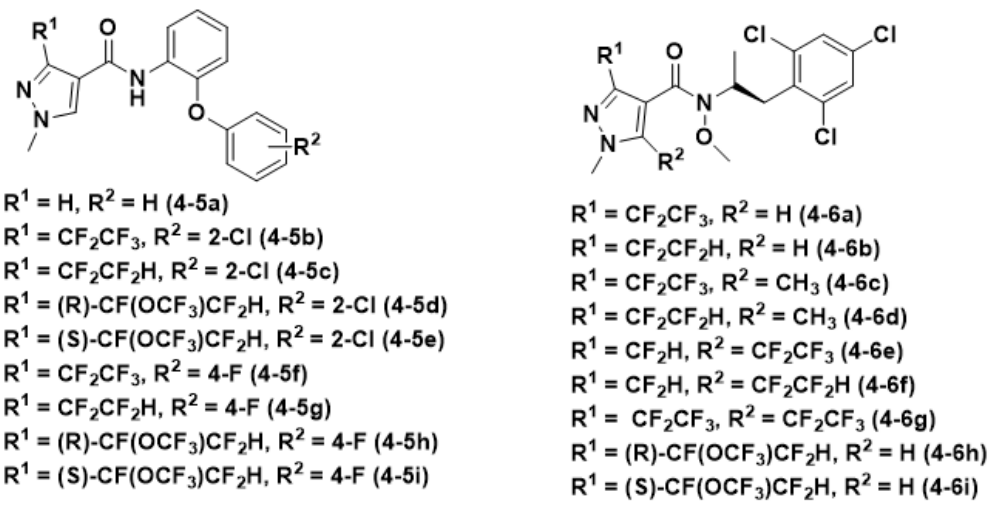

Figure 4.5 Fluoroalkylated carboxamide analogues proposed for molecular docking studies.

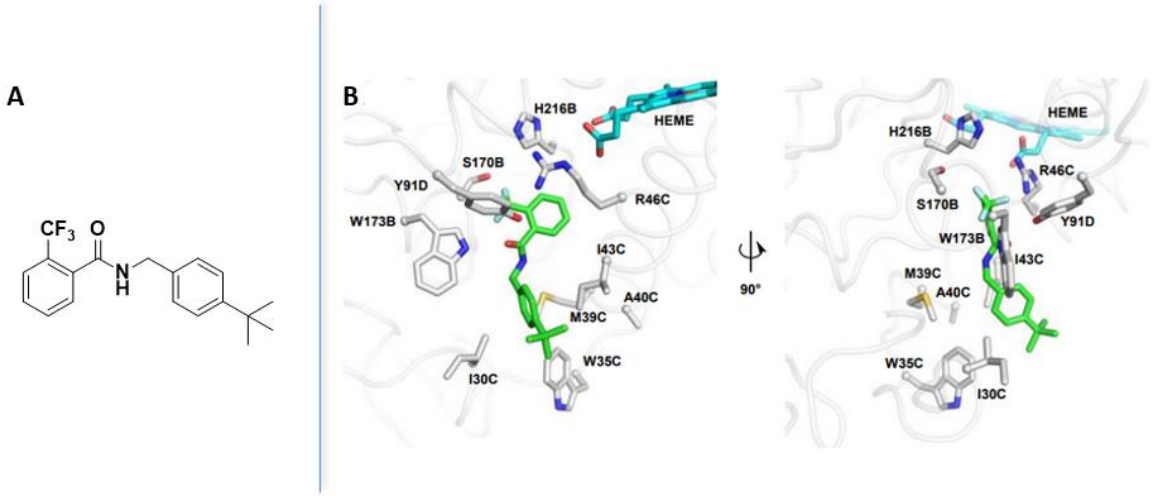

Figure 4.6 (a) Structure of N-[(4-tert-butylphenyl)methyl]-2-(trifluoromethyl)benzamide (NAQ). (b) NAQ (green) binding mode with Sus scrofa SDH (PDB ID: 4YTP). The heme group is shown in cyan. The binding site residues are labelled with a 1-letter amino acid code, and the chain letter near the Cα shown as spheres.

4.2.3.2 Docking simulations of known SDHi: The SDHIs isoflucypram, thifluzamide, (S)-pydiflumetofen, pyflubimide, and flubendiamide (**Figure 4.7**) were docked onto the fgSDH models (**Figures 4.8** and **4.9**). The azole rings of isoflucypram (model 2), thifluzamide (model 1), (S)-pydiflumetofen (models 1 and 2) are predicted to interact with the binding pocket. In these cases, π-stacking with Arg80C is predicted.

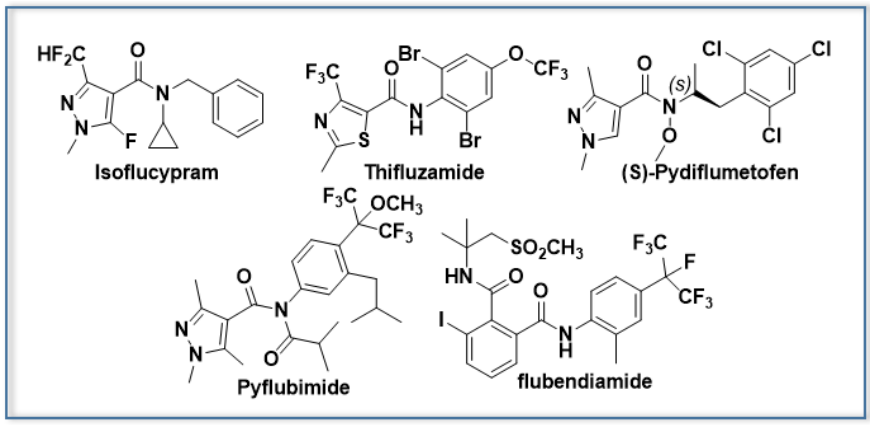

Figure 4.7 Chemical structures of known SDH inhibitors.

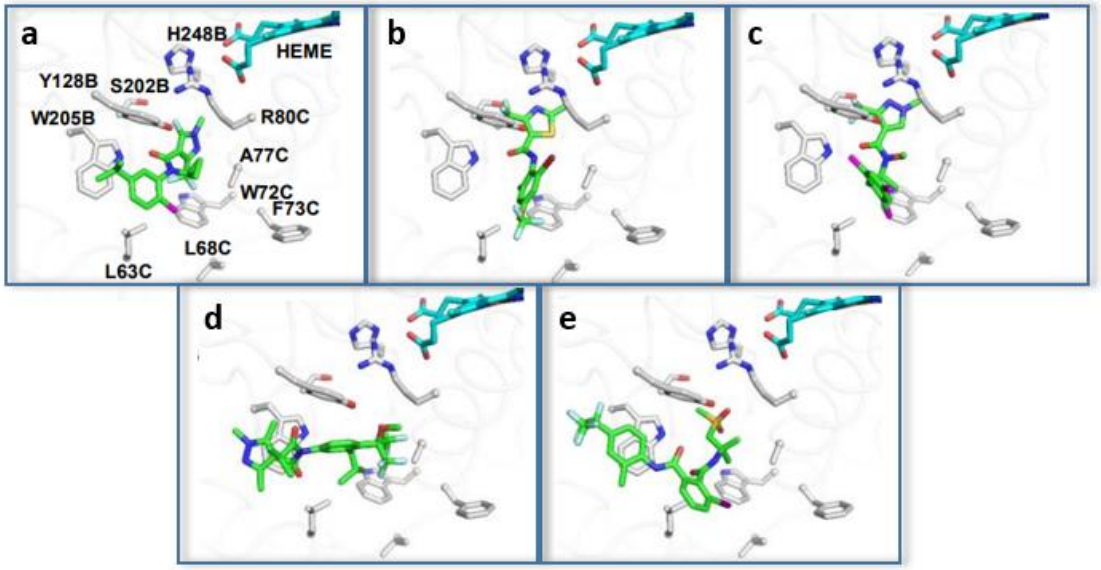

Figure 4.8 Simulation results of known SDHIs docked into the binding site of fgSDH homology model 1. (**a**) isoflucypram, (**b**) thifluzamide, (**c**) (S)-pydiflumetofen, (**d**) pyflubimide and (**e**) flubendiamide. The SDHIs and heme groups are shown as green and cyan sticks, respectively. Chlorine and fluorine atoms are shown in pink and light green, respectively.

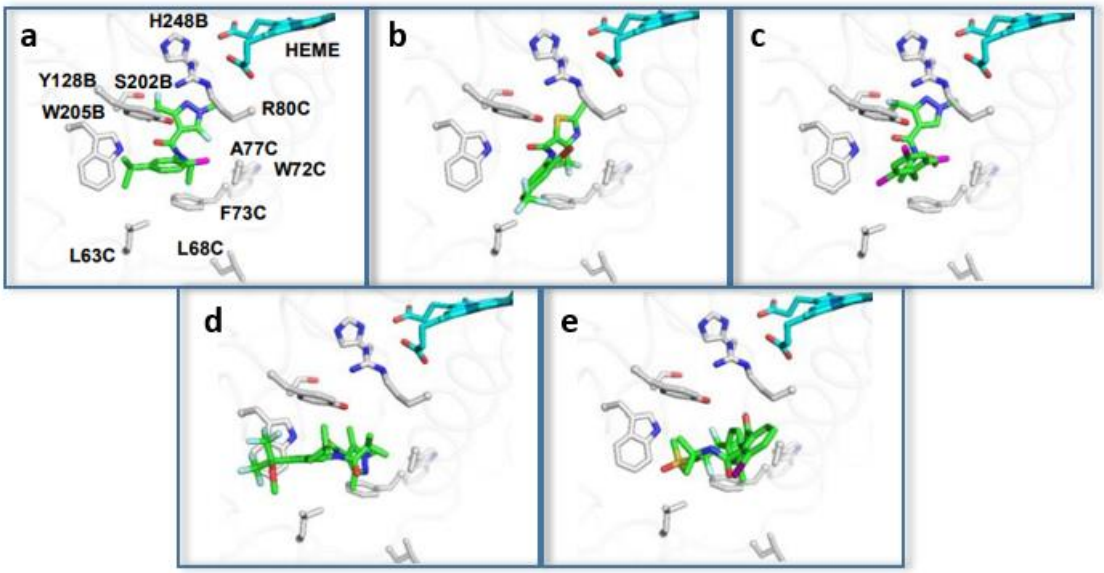

Figure 4.9 Simulation results of known SDHis docked into the binding site of fgSDH homology model 2. (**a**) isoflucypram, (**b**) thifluzamide, (**c**) (S)-pydiflumetofen, (**d**) pyflubimide and (**e**) flubendiamide. The SDHIs and heme groups are shown as green and cyan sticks, respectively. Chlorine and fluorine atoms are shown in pink and light green, respectively.

4.2.3.2 Docking of fluoroalkylated SDHi analogues: The next step was to try fluorinated-carboxamide analogues (**4-5a-i**, **4-6a-i**). Since the azole rings of (S)-pydiflumetofen were predicted to bind the fgSDH site in the orientation hypothesized to inhibit the enzyme in both models and (S)-pydiflumetofen has been reported to act as a fungicide of *F. graminearum*, 4 fluoroalkyl-substituted analogues of (S)-pydiflumetofen (**Figure 4.10**) were also docked onto the fgSDH binding site to predict the effect of the proposed R^F groups (-$CF(OCF_3)CF_2H$, -CF_2CF_3, CF_2CF_2H). In short, only analogues that contained the -CF_2CF_2H and -CF_2CF_3 at the R^1 position of both compounds were docked in an orientation with the carboxy side azole ring inside the pocket, interacting with W72C, W205B and R80C. Hydrogen bonding is predicted between the Trp and the amide-oxygen of compounds **4-5f**, **4-5g**, **4-6**a and **4-6**c. Alternatively, Trp is predicted to form a hydrogen bond with the N-methoxy-oxygen of compound **4-6b**.

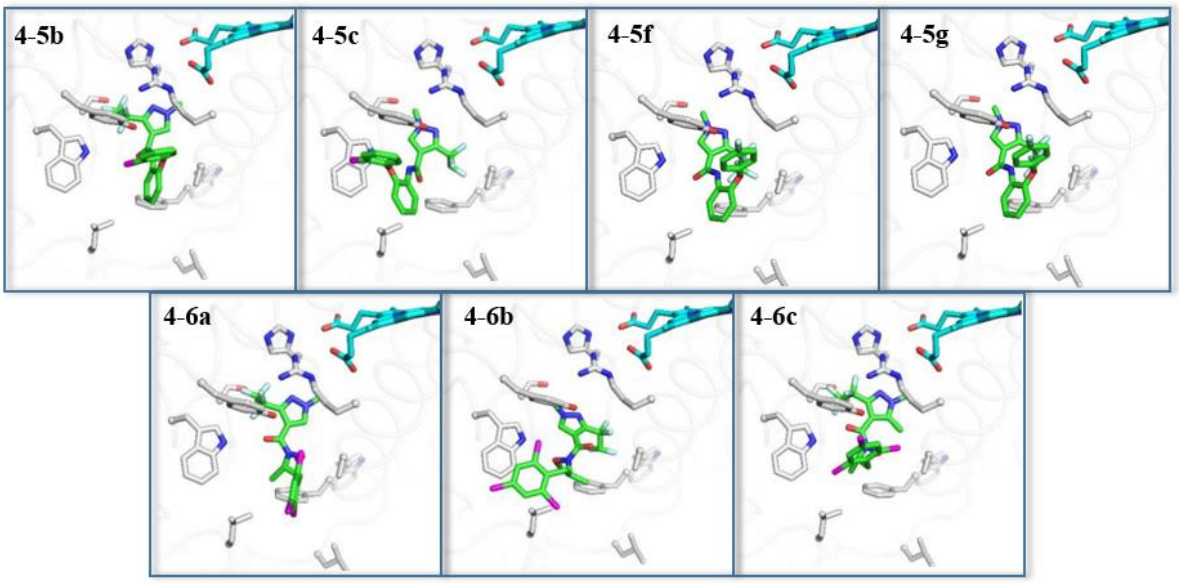

Figure 4.10 Simulation results of fluoroalkylated-carboxamides (**4-5b**,**c**,**f**,**g** and **4-6a**,**b**,**c**) docked into the binding site of fgSDH homology model 2.

4.3 CONCLUSIONS

Building on previous work in the Baker group by Andrella, we showed that the readily available Xantphos ligand can be used (instead of NHC ligands) in concert with the easily prepared 1:1 mixture of CO_2 and TFE to facilitate the fluoroethylation of aryl iodides. Our computational studies confirmed that, in contrast to the aroyl chlorides studied in Chapter 3, the oxidative addition step is rate-limiting for aryl iodides as determined previously by others.[24] Moreover, contributions of ligand exchange pre-equilibria at copper to the oxidative addition barrier helped to explain the efficiency of the 'ligandless' approach in which stronger binding ligands can be scavenged by added CuBr. Our evaluation of different R^F groups revealed that transfer of the perfluorovinyl group should be energetically feasible unless prevented by its dimerization.

Building on Boutureira's work with pentafluoroethylation,[14] we demonstrated the efficient tetrafluoroethylaiton of nucleosides, nucleobases and glycols in fair to high yields. Work is in progress to scale up the fluorouracil (**4-4f**) and trifluridine (**4-4e**) analogues containing $-CF_2CF_2H$ and $-CF_2CF_3$ groups for antiviral testing in the John Pezacki labs at uOttawa. Finally, in efforts aimed at developing antifungal fluoroalkylated carboxamides, a molecular docking investigation

identified these same two R^F groups as potentially active SDH inhibitors. Two analogues have been scaled up in the Boutureira lab for testing by the Loewen lab in Ottawa.

4.4 EXPERIMENTAL SECTION

4.4.1 General Procedures: Experiments were conducted under nitrogen, using Schlenk techniques or an MBraun glove box. All solvents were deoxygenated by purging with nitrogen. Tetrahydrofuran (THF), acetonitrile (MeCN) and toluene were dried on columns of activated alumina using a J. C. Meyer (formerly Glass Contour®) solvent purification system. 1,2-Dimethoxyethane (DME), cyclopentyl methyl ether (CPME) and benzene-d_6 (C_6D_6) were dried by stirring over activated alumina (ca. 10 wt. %) overnight, followed by filtration. All solvents were stored over activated (heated at ca. 250 °C for >10 h under vacuum) 4 Å molecular sieves. Glassware was oven-dried at 120 °C for >2 h. The following chemicals were obtained commercially, as indicated: dimethylformamide (DMF, Alfa Aesar anhydrous, 99.8%), dimethylsulfoxide (DMSO, Alfa Aesar anhydrous, 99.8%), 4-iodo-benzonitrile (Alfa Sigma, 98 %), triphenylphosphine (PPh_3, Oakwood chemicals, 99%), 4,5-bis(diphenylphosphino)-9,9-dimethylxanthene (Xantphos, Accela ChemBio Inc., 99%), methyldiphenylphosphine ($PMePh_2$, Acros Organics, 99%). The following chemicals were synthesized as previously reported: 1,3-bis(2,3,6-trimethylphenyl)imidazolidin-2-ylidene (SIMes),[25] $[(PPh_3)CuH]_6$,[26] (SIMes)CuCl[27] and $Cu(CF_2CF_2H)(PMePh_2)_3$ (**4-1**).[9] All bioactive substrates were provided by our collaborator Omar Boutureira. Electrospray ionization mass spectral data were collected using an Applied Biosystem API2000 triple quadrupole mass spectrometer. NMR spectra were recorded on a 300 MHz Bruker Avance instrument at room temperature (21-23 °C) unless stated otherwise. ^1H NMR spectra were referenced to residual proton peaks associated with the deuterated solvents (C_6D_6: δ 7.16) and $^{31}P\{^1H\}$ NMR data were referenced to external H_3PO_4 (85 % aqueous solution), set to 0.0 pm. ^{19}F NMR spectra were referenced to internal standard α,α,α-trifluorotoluene (CF_3Ph, Sigma-Aldrich, 99%, deoxygenated by purging with nitrogen, stored over activated 4 Å molecular sieves) set to –63.5 ppm. NMR spectra for the title compounds are displayed in the Appendix.

*4.4.2 Synthesis of $Cu(CF_2CF_2H)$(Xantphos (**4-2**):* The red complex $[(PPh_3)_3CuH]_6$ (150 mg, 0.46 mmol) was placed in a 40 mL vial glass and mixed with 4 mL of DMF. Xantphos (266 mg, 0.46 mmol) and tetramethyldisililoxane (TMDSO) (107 µL, 0.69 mmol) were then added to the solution and sealed with cap. In the same vial glass, 5 equivalents of TFE:CO_2 was inserted using a syringe.

The reaction was left to sit at room temperature for 24 h at room temperature. The deep red color changed to a light orange-red colour. The solvent was removed using vacuum and the residue heated at 50 ºC for 2 h, washed with Et_2O and then triturated with pentane. The resulting light orange solid was collected and dried to give 239 mg of **4-2** (70%). ^{19}F NMR (282 MHz, acetone-d_6): −107.7 (m, CF_2), −129 ppm (d, $^2J_{FH}$ = 58 Hz, CF_2H). $^{31}P\{^1H\}$ NMR (121 MHz, acetone-d_6): -19.2 ppm (br) ^1H NMR (300 MHz, acetone-d^6): d x.yy (ov mult, Ar-H), 5.65 (trtr, $^2J_{HF}$ = 58, $^3J_{HF}$ = 9 Hz, CF_2H).

*4.4.3 Procedures for R^F transfer using **4-2**:* Complex **4-2** (10 mg, 0.013 mmol) was loaded into an NMR tube and mixed with 4-nitro-iodobenzene (0.013 mmol) and internal standard $PhCF_3$ (20 μL, 0.01 mmol/mL) in 0.5 mL of DMF and the reaction was analyzed by ^{19}F NMR spectroscopy after 7 h at 50 ºC.

In a second procedure, complex **4-2** (10 mg, 0.013 mmol) was loaded into an NMR tube and mixed with 4-nitro-iodobenzoate (0.013 mmol), Cu(SIMes)Cl (0.052 mg, 0.0013 mmol) and $PhCF_3$ (20 μL, 0.01 mmol/mL) in 0.5 mL of toluene and the reaction was analyzed by ^{19}F NMR after 12 h at 90 ºC. ^{19}F NMR -109.6 (brs, CF_2) and –133.1 ppm (dt, $^2J_{FH}$ = 55 and $^3J_{FF}$ = 10 Hz, CF_2H).

*4.4.4 General procedure for 'ligandless' R^F transfer using **4-1** / CuBr:* The colorless complex $Cu(CF_2CF_2H)(PPh_2Me)_3$ (**4-1**) (10 mg, 0.013 mmol) and CuBr (3.75 mg, 0.026 mmol) were loaded into an NMR tube and dissolved in 0.5 mL of DMF. The (hetero)aryl iodide (0.013 mmol) and internal standard $PhCF_3$ (20 μL, 0.01 mmol/mL) were then added to the tube and the reaction was analyzed by ^{19}F NMR spectroscopy after heating at 50 ºC for 12 h.

2'-deoxy-5-tetrafluoroethyl-uridine (**4-4a**): ^{19}F NMR –116.5 and –118.2 (d, $^2J_{FF}$ = 268 Hz, CF_2), –138.6 and –139.9 ppm (ddd, $^2J_{FF}$ = 297, $^2J_{FH}$ = 51 Hz, CF_2H).

2'-deoxy-5-tetrafluoroethyl-cytidine (**4-4b**): ^{19}F NMR –113.2 (m, CF_2), –136.8 ppm (dm, $^2J_{FH}$ = 53 Hz, CF_2H).

5-tetrafluoroethyl uridine (**4-4c**): ^{19}F NMR –116.6 and -118.2 (d, $^2J_{FF}$ = 267 Hz, CF_2), –138.6 and –139.9 ppm (dd, J_{FF} = 293, $^2J_{FH}$ = 51 Hz, CF_2H).

2'-5-o-acetyl-5-tetrafluoroethyl-uridine (**4-4d**): ^{19}F NMR –117.5 and –118.2 (br d, $^2J_{FF}$ = 268 Hz, CF_2), –131.1 ppm (br d, J_{FH} = 55 Hz, CF_2H)

5-tetrafluoroethyl-2',3',5'-triacetate uridine (**4-4e**): ^{19}F NMR –117.8 (br s, C*F*$_2$), –139.1 ppm (br d, $^2J_{FH}$ = 54 Hz, C*F*$_2$H).

4-tetrafluoroethyl-uracil (**4-4f**): ^{19}F NMR –118.6 (br s, C*F*$_2$), –140.1 ppm (d, $^2J_{FH}$ = 55 Hz, C*F*$_2$H).

6-fluoro-3-tetrafluoroethylchromone (**4-4g**): ^{19}F NMR –119.9 (mult, C*F*$_2$), –139.2 ppm (dt, $^2J_{FH}$ = 52, $^3J_{FF}$ = 7 Hz, C*F*$_2$H).

t-butyl-5-fluoro-3-tetrafluoroethyl-1H-indole-1-carboxylate (**4-4h**): ^{19}F NMR –110.8 (br s, C*F*$_2$), –136.4 ppm (d, $^2J_{FH}$ = 53 Hz, C*F*$_2$H).

1,5-anhydro-3,4,6-tri-O-benzyl-2-deoxy-2-tetrafluoroethyl-D-lyxo-hex-1-enitol (**4-4i**): ^{19}F NMR –111.7 and –122.1 (dm, $^2J_{FF}$ = 265, $^3J_{FF}$ = 12 Hz, C*F*$_2$), –137.1 and –139.2 ppm (ddd, $^2J_{FF}$ = 287, $^2J_{FH}$ = 55, $^3J_{FF}$ = 12 Hz, C*F*$_2$H).

1,5-anhydro-3,4,6-tri-O-acetyl-2-deoxy-2-tetrafluoroethyl-D-lyxo-hex-1-enitol (**4-4j**): ^{19}F NMR –112.5 and -117.1 (dd, $^2J_{FF}$ = 270, $^3J_{FF}$ = 10 Hz, C*F*$_2$), –136.6 (ddd, $^2J_{FF}$ = 292, $^2J_{FH}$ = 52, $^3J_{FF}$ = 10 Hz, C*F*$_2$H), -138.6 ppm (ddtr, $^2J_{FF}$ = 292, $^2J_{FH}$ = 54, $^3J_{FF}$ = 8 Hz, C*F*$_2$H).

methyl 5-acetamido-4,7,8,9-tetra-O-acetyl-2,6-anhydro-3,5-dideoxy-3-tetrafluoroethyl-D-glycero-D-galacto-non-2-enonate (**4-4k**): ^{19}F NMR –109.2 and –115.0 (d, J_{FF} = 275 Hz, C*F*$_2$), –136.2 ppm (d, $^2J_{FH}$ = 53 Hz, C*F*$_2$H).

methyl 5-acetamido-4,7,8,9-tetra-O-acetyl-2,6-anhydro-3,5-dideoxy-3-tetrafluoroethyl-D-glycero-D-galacto-non-2-enonate (**4-4l**): ^{19}F NMR –112.5 (dd, J_{FF} = 271, $^3J_{FF}$ = 10 Hz, C*F*$_2$), –117.2 (dq, $^2J_{FF}$ = 271, $^3J_{FF}$ = $^3J_{FH}$ = 9 Hz, C*F*$_2$), –136.6 (dddd, $^2J_{FF}$ = 290, $^2J_{FH}$ = 52, $^3J_{FF}$ = 10, 2 Hz, C*F*$_2$H), –138.5 ppm (ddtr, $^2J_{FF}$ = 290, $^2J_{FH}$ = 52, $^3J_{FF}$ = 12 Hz, C*F*$_2$H).

1,5-anhydro-3,4,6-tri-O-pivaloyl-2-deoxy-2-tetrafluoroethyl-D-arabino-hex-1-enitol (**4-4m**): ^{19}F NMR –112.1 and –113.4 (d, $^2J_{FF}$ = 275 Hz, C*F*$_2$), –136.6 and –137.7 ppm (dd, $^2J_{FF}$= 296 Hz, $^2J_{FH}$ = 50 Hz, C*F*$_2$H).

1,5-anhydro-3,6-di-O-acetyl-2-deoxy-4-O-(2,3,4,6-tetra-O-acetyl-β-D-galactopyranosyl)-2 tetrafluoroethyl-D-arabino-hex-1-enitol (**4-4n**): ^{19}F NMR – 113.7 and - 117.0 (d, $^2J_{FF}$ = 271 Hz, C*F*$_2$), –137.5 ppm (dmult, $^2J_{FH}$ = 53 Hz, C*F*$_2$H).

4.4.5 Computational details: All geometries were fully optimized using the Gaussian 16 software package[28] in combination with the BOpt software package.[29] Following a previously proposed protocol,[30] all relevant minima and transition states were fully optimized at the TPSSTPSS level[31] of theory employing correlation-consistent polarized valence double-ζ Dunning (DZ) basis sets with cc-pVDZ quality[32,33] from the EMSL basis set exchange library, using a small core pseudopotential on Cu.[34] The density fitting approximation (Resolution of Identity, RI)[35-37] was used at the optimization stage and for single-point energy corrections. Solvent effects (benzene, ε = 2.2706) were included with the polarizable continuum model approach (PCM) at both stages.[38] All calculations were performed at the standard Gaussian 16 SCF convergence using an ultrafine grid [Scf = tight and Int(grid = ultrafine)]. The nature of each stationary point was checked with an analytical second-derivative calculation (no imaginary frequency for minima, exactly one imaginary frequency for transition states, corresponding to the reaction coordinate). The accuracy of TS was confirmed with an intrinsic reaction coordinate (IRC) scan. Transition states were located using a suitable guess and the Berny algorithm (Opt = TS)[39] or a relaxed potential energy scan to arrive at a suitable transition-state guess, followed by a quasi-Newton or eigenvector-following algorithm to complete the optimization. Final single-point energies were calculated at the TPSSh level of theory[40] employing triple-ζ Dunning (TZ) basis sets (cc-pVTZ quality).[32] Grimme dispersion corrections without damping (keyword -zero) were added at this stage using the standalone dftd3 program.[41,42] Enthalpies and Gibbs free energies were then obtained from TZ singlepoint energies and thermal corrections from the TPSSTPSS/cc-pVDZ-(PP) vibrational analyses; entropy corrections were scaled by a factor of 0.67 to account for decreased entropy in the condensed phase.[43-45]

4.4.6 Molecular docking studies: The amino acid sequence of Sus scrofa succinate dehydrogenase was retrieved from a crystal structure (PDB ID: 4YXD);[46] the subunit consists of 4 unique chains. The *F. graminearum* SDH amino acid sequence was retrieved via a TBLASTN search using the Sus scrofa SDH sequences as the query and the organism as "Fusarium graminearum species complex (taxid:569360)". The accession numbers for each chain are: XM_011328820 (NCBI), JX869230.1 (Genebank), JX869216.1 (Genebank), JX869209 (Genebank) for chains A, B, C, and D, respectively. The 4 chains were then used as a "Multiple Target" input for homology modeling using the SWISS-MODEL server,[21] which yielded 26 different templates. Models were then built for the top scored (by GMQE and QSQE) 2 unique templates (Table 3). Each model was

superimposed with the crystal structure of their respective template. Coordinates of ligands from the template structure that were missing (flavin-adenine dinucleotide and heme group) were added to the model. Then, each model was superimposed to the template from model 2. The coordinates of the NAQ were then copied into each model to guide selection of the SDHI binding site residues.

Table 4. 8 Information of homology model of F. graminearum SDH.

Model	PDB ID	Sequence Identity (%)	GMQE[1] score (%)	QSQE[6] score	Ramachandran favoured (%)	Enzyme
1	3SFD[7]	63.05	0.74	0.78	94.08	*S. srofa* SDH
2	4YTP[5]	60.82	0.74	0.77	94.20	*S. srofa* SDH

The coordinates of the model were opened in the Molecular Operating Environment (MOE) software,[47] and hydrogens were added with the Protonate3D utility. Using the AMBER99 force field[48] with a combined explicit solvent and implicit reaction field solvent model set up using the MOE software package, the model was minimized to a RMSG of < 0.1 kcal mol-1 Å -1 with the backbones tethered to prevent deviation from the starting structure. The coordinates of NAQ from the crystal structure of Sus scrofa SDH used as a template in model 2 (PDB ID: 4YTP) was placed into the binding sites of each model. Active site residues within 5 Å were selected as the binding pocket residues. Then, a library of conformers for each ligand was generated in MOE using a systematic search with the MMFF94x force field[49] as implemented by MOE. Docking was performed with the 'Induced Fit' docking protocol. One thousand ligand conformations were generated, and the docking was performed using the 'Triangle Matcher' placement method. All 1000 conformations per ligand were scored using the 'London dG' scoring function, submitted to a refinement step based on molecular mechanics and rescored with the 'GBVI/WSA dG' scoring function.11-12 GBVI/WSA dG, a forcefield-based scoring function, determines the binding free energy (kcal mol-1) of the ligand from a given pose.[50,51]

4.5 REFERENCES

1. (a) Fier, P.S.; Hartwig, J.F. Copper-mediated difluoromethylation of aryl and vinyl iodides. *J. Am. Chem. Soc.* **2012**, *134*, 5524–5527. https://doi.org/10.1021/ja301013h (b) Bour, J.R.; Kariofillis, S.K.; Sanford, M.S. Synthesis, reactivity, and catalytic applications of isolable

(NHC)Cu(CHF_2) complexes. *Organometallics* **2017**, *36*, 1220–1223. (c) Zhang, W.; Xiang, X.-X.; Chen, J.; Yang, C.; Pan, Y.-L.; Cheng, J.-P.; Meng, Q.; Li, X. Direct C–H Difluoromethylation of heterocycles via organic photoredox catalysis. *Nature Commun.* **2020**, *11*, 638.

2. (a) Linclau, B.; Wang, Z.; Compain, G.; Paumelle, V.; Fontenelle, C.Q.; Wells, N.; Weymouth-Wilson, A. Investigating the influence of (deoxy)fluorination on the lipophilicity of non-UV-active fluorinated alkanols and carbohydrates by a new log *p* determination method. *Angew. Chem. Int. Ed.*, **2016**, *55*, 674–678. (b) Václavík, J.; Klimánková, I.; Budinská, A.; Beier, P. Advances in the synthesis and application of tetrafluoroethylene- and 1,1,2,2-tetrafluoroethyl-containing compounds. *Eur. J. Org. Chem.* **2018**, 3554-3593.
3. Sap, J. B. I.; Meyer, C. F.; Straathof, N. J. W.; Iwumene, N.; am Ende, C. W.; Trabanco, A. A.; Gouverneur, V. Late-stage difluoromethylation: concepts, developments and perspective. *Chem. Soc. Rev.* **2021**, *50*, 8214-8247.
4. Sieglitz, A.; Bestian, H.; Rehn, K. New aromatic compounds containing tetrafluoroethyl tetrafluoroethyl side chains and a process for preparing them. US patent 2,862,974, 1958.
5. (a) Singh, R.P.; Shreeve, J.M. Concentration-dependent reactions of deoxofluor with arylglyoxal hydrates: A new route to polyfluoro ethers. *Org. Lett.* **2001**, *3*, 2713–2715. b) Singh, R.P.; Twamley, B.; Shreeve, J.M. Polyfluoroether derivatives via nucleophilic fluorination of glyoxal hydrates with deoxofluor. *J. Org. Chem.* **2002**, *67*(6), 1918-1924.
6. Li, L.; Ni, C.; Xie, Q.; Hu, M.; Wang, F.; Hu, J. $TMSCF_3$ as a convenient source of CF_2=CF_2 for pentafluoroethylation, (aryloxy)tetrafluoroethylation, and tetrafluoroethylation. *Angew. Chem. Int. Ed.* **2017**, *56*, 9971–9975.
7. Andrella, N.O.; Xu, N.; Gabidullin, B.M.; Ehm, C.; Baker, R.T. Selective copper complex-catalyzed hydrodefluorination of fluoroalkenes and allyl fluorides: a tale of two mechanisms. *J. Am. Chem. Soc.* **2019**, *141*, 11506–11521.
8. Hercules, D.A.; Parrish, C.A.; Sayler, T.S.; Tice, K.T.; Williams, S.M.; Lowery, L.E.; Brady, M.E.; Coward, R.B.; Murphy, J.A.; Hey, T.A.; Scavuzzo, A.R.; Rummler, L.M.; Burns, E.G.; Matsnev, A.V.; Fernandez, R.E.; McMillen, C.D.; Thrasher, J.S. Preparation of tetrafluoroethylene from the pyrolysis of pentafluoropropionate salts. *J. Fluor. Chem.* **2017**, *196*, 107–116.

9. Andrella, N. O. Synthesis of organo-fluorine compounds by metal complex-mediated and -catalyzed transformations of fluoro-alkenes and fluoro-arenes. University of Ottawa PhD thesis, **2019**.
10. Xie, Q.; Zhu, Z.; Li, L.; Ni, C.; Hu, J. Controllable Double CF_2 Insertion into sp^2 C-Cu Bond using $TMSCF_3$: A Facile access to tetrafluoroethylene-bridged structures. *Chem. Sci*. **2019**, *11*, 276-280.
11. Wang, X.; Pan, S.; Luo, Q.; Wang, Q.; Ni, C.; Hu, J. Controllable single and double difluoromethylene insertions into C−Cu bonds: Copper-mediated tetrafluoroethylation and hexafluoropropylation of aryl iodides with $TMSCF_2H$ and $TMSCF_2Br$. *J. Am. Chem. Soc.* **2022**, *144*, ASAP https://doi.org/10.1021/jacs.2c03104
12. Miller, W.T.; Burnard, R.J. Perfluoroalkyl silver compounds. *J. Am. Chem. Soc.* **1968**, *90*, 7367−7368.
13. Andrella, N.O.; Liu, K.; Gabidullin, B.M.; Vasiliu, M.; Dixon, D. A.; Baker, R.T. Metal heptafluoroisopropyl (M-hfip) complexes for use as hfip transfer agents. *Organometallics* **2018**, *37*, 422-432.
14. Mestre, J.; Castillón, S.; Boutureira, O. "Ligandless" pentafluoroethylation of unactivated (hetero)aryl and alkenyl halides enabled by the controlled self-condensation of $TMSCF_3$-derived $CuCF_3$. *J. Org. Chem*. **2019**, *84*, 15087-15097.
15. Dubunina, G.G.; Furutachi, H.; Vicic, D.A. Active trifluoromethylating agents from well-defined copper(I)−CF_3 complexes. *J. Am. Chem. Soc.* **2008**, *130*, 8600–8601.
16. Kalkman, E.D.; Mormino, M.G.; Hartwig, J.F. Unusual electronic effects of ancillary ligands on the perfluoroalkylation of aryl iodides and bromides mediated by copper(I) pentafluoroethyl complexes of substituted bipyridines. *J. Am. Chem. Soc*. **2019**, *141*, 19458-19465.
17. Wiemers, D. M.; Burton, D. J. Pregeneration, spectroscopic detection, and chemical reactivity of (trifluoromethyl) copper, an elusive and complex species. *J. Am. Chem. Soc.* **1986**, *108*, 832-835.
18. Lishchynskyi, A.; Novikov, M.A.; Martin, E.; Escudero-Adán, E.C.; Novák, P.; Grushin,V.V. Trifluoromethylation of aryl and heteroaryl halides with fluoroform-derived $CuCF_3$: Scope, limitations, and mechanistic features. *J. Org. Chem.* **2013**, *78*, 11126–11146.
19. Spertus, C.B.; Mohammed, H.O.; Ledbetter, E.C. Effects of topical ocular application of 1%

trifluridine ophthalmic solution in dogs with experimentally induced recurrent ocular canine herpes virus-1 infection. *Am. J. Vet. Res*. **2016**, *7*, 1140-1147.

20. Luo, B.; Ning, Y. Comprehensive overview of carboxamide derivatives as succinate dehydrogenase inhibitors. *J. Agric. Food Chem*. **2022**, *70*, 957-975.
21. Waterhouse, A.; Bertoni, M.; Bienert, S.; et al. SWISS-MODEL: homology modelling of protein structures and complexes. *Nucleic Acids Res*. **2018**, *46*, W296-W303.
22. Sierotzki, H.; Scalliet, G. A review of current knowledge of resistance aspects for the next-generation succinate dehydrogenase inhibitor fungicides. *Phytopathol.* **2013,** *103*, 880-887.
23. Yao T.-T.; Fang, S.-W.; Li, Z.-S.; Xiao, D.-Z.; Cheng, J.-L.; Ying, H.-J.; Du, Y.-J.; Zhao, J.-H.; Dong, X.-W.Discovery of novel succinate dehydrogenase inhibitors by the integration of *in silico* library design and pharmacophore mapping. *J. Agric. Food Chem*. **2017**, *65*, 3204-3211.
24. Jover, J. Computational insights into nucleophilic copper-catalyzed trifluoromethylation of aryl halides. *ACS Catal.* **2014**, *4*, 4389-4397.
25. (a) Arduengo, A.J., III.; Krafczyk, R.; Schmutzler, R.; Craig, H.A.; Goerlich, J.R.; Marshall, W.J. Unversagt, M. Imidazolylidenes, imidazolinylidenes and imidazolines. *Tetrahedron* **1999**, *55*, 14523-14534. (b) Gautier, A.; Cisnetti, F.; Diez-Gonzalez, S.; Gibard, C. Synthesis of 1,3–bis(2,4,6–trimethylphenyl)–imidazolinium salts: SIMes•HCl, SIMes•HBr, SIMes•HBF_4 and SIMes•HPF_6. *Nat. Protoc. Exchange.* Published online October 10, 2012. doi:10.1038/protex.2012.04
26. Lee, D.-W.; Yun, J. Direct synthesis of Stryker's reagent from a Cu(II) salt. *Tet. Lett.* **2005**, *12*, 2037-2039.
27. Citadelle, C.A.; Le Nouy, E.; Bisaro, F.; Slawin, A.M.Z.; Cazin, S.C.J. Simple and versatile synthesis of copper and silver N-heterocyclic carbene complexes in water or organic solvents. *Dalton Trans*. **2010**, *39*, 4489-4491.
28. Gaussian 16, Revision C.01, Frisch, M.J.; Trucks, G.W.; Schlegel, H. B.; Scuseria, G. E.; Robb, M. A.; Cheeseman, J. R.; Scalmani, G.; Barone, V.; Petersson, G. A.; Nakatsuji, H.; Li, X.; Caricato, M.; Marenich, A. V.; Bloino, J.; Janesko, B. G.; Gomperts, R.; Mennucci, B.; Hratchian, H. P.; Ortiz, J. V.; Izmaylov, A. F.; Sonnenberg, J. L.; Williams-Young, D.; Ding, F.; Lipparini, F.; Egidi, F.; Goings, J.; Peng, B.; Petrone, A.; Henderson, T.; Ranasinghe, D.; Zakrzewski, V. G.; Gao, J.; Rega, N.; Zheng, G.; Liang, W.; Hada, M.;

Ehara, M.; Toyota, K.; Fukuda, R.; Hasegawa, J.; Ishida, M.; Nakajima, T.; Honda, Y.; Kitao, O.; Nakai, H.; Vreven, T.; Throssell, K.; Montgomery, J. A., Jr.; Peralta, J. E.; Ogliaro, F.; Bearpark, M. J.; Heyd, J. J.; Brothers, E. N.; Kudin, K. N.; Staroverov, V. N.; Keith, T. A.; Kobayashi, R.; Normand, J.; Raghavachari, K.; Rendell, A. P.; Burant, J. C.; Iyengar, S. S.; Tomasi, J.; Cossi, M.; Millam, J. M.; Klene, M.; Adamo, C.; Cammi, R.; Ochterski, J. W.; Martin, R. L.; Morokuma, K.; Farkas, O.; Foresman, J. B.; Fox, D. J. Gaussian, Inc., Wallingford CT, 2016.

29. Budzelaar, P. H. M. Geometry Optimization Using Generalized, Chemically Meaningful Constraints. *J. Comput. Chem.* **2007**, *28*, 2226− 2236.
30. Ehm, C.; Budzelaar, P. H. M.; Busico, V. Calculating Accurate Barriers for Olefin Insertion and Related Reactions. *J. Organomet. Chem.* **2015**, *775*, 39−49.
31. Tao, J.; Perdew, J. P.; Staroverov, V. N.; Scuseria, G. E. Climbing the Density Functional Ladder: Nonempirical Meta-Generalized Gradient Approximation Designed for Molecules and Solids. *Phys. Rev. Lett.* **2003**, *91*, 146401.
32. Balabanov, N. B.; Peterson, K. A. Systematically Convergent Basis Sets for Transition Metals. I. All-electron Correlation Consistent Basis Sets for the 3d Elements Sc−Zn. *J. Chem. Phys.* **2005**, *123*, 064107.
33. Balabanov, N. B.; Peterson, K. A. Basis Set Limit Electronic Excitation Energies, Ionization Potentials, and Electron Affinities for the 3d Transition Metal Atoms: Coupled Cluster and Multireference Methods. *J. Chem. Phys.* **2006**, *125*, 074110.
34. Schuchardt, K. L.; Didier, B. T.; Elsethagen, T.; Sun, L. S.; Gurumoorthi, V.; Chase, J.; Li, J.; Windus, T. L. Basis Set Exchange: A Community Database for Computational Sciences. *J. Chem. Inf. Model.* **2007**, *47*, 1045−1052.
35. Whitten, J. L. Coulombic Potential Energy Integrals and Approximations. *J. Chem. Phys.* **1973**, *58*, 4496.
36. Baerends, E. J.; Ellis, D. E.; Ros, P. Self-Consistent Molecular Hartree-Fock-Slater Calculations I. The Computational Procedure. *Chem. Phys.* **1973**, *2*, 41−51.
37. Feyereisen, M.; Fitzgerald, G.; Komornicki, A. Use of Approximate Integrals in Ab Initio Theory. An Application in MP2 Energy Calculations. *Chem. Phys. Lett.* **1993**, *208*, 359−363.

38. Vahtras, O.; Almlöf, J.; Feyereisen, M. W. Integral Approximations for LCAO-SCF Calculations. *Chem. Phys. Lett.* **1993**, *213*, 514−518.
39. Tomasi, J. Thirty Years of Continuum Solvation Chemistry: A Review and Prospects for the Near Future. *Theor. Chem. Acc.* **2004**, *112*, 184−203.
40. The Berny algorithm was never fully published; see the Gaussian documentation for details.
41. Grimme, S. Density Functional Theory with London Dispersion Corrections. *Wiley Interdiscip. Rev. Comput. Mol. Sci.* **2011**, *1*, 211−228.
42. Grimme, S.; Ehrlich, S.; Goerigk, L. Effect of the Damping Function in Dispersion Corrected Density Functional Theory. *J. Comput. Chem.* **2011**, *32*, 1456−1465.
43. Tobisch, S.; Ziegler, T. Catalytic Oligomerization of Ethylene to Higher Linear α-Olefins Promoted by the Cationic Group 4 $[(\eta^5\text{-Cp-}(CMe_2\text{-bridge})\text{-Ph})M^{II}(\text{ethylene})_2]^+$ (M = Ti, Zr, Hf) Active Catalysts: A Density Functional Investigation of the Influence of the Metal on the Catalytic Activity and Selectivity. *J. Am. Chem. Soc.* **2004**, *126*, 9059− 9071.
44. Dunlop-Briere, A. F.; Budzelaar, P. H. M.; Baird, M. C.` α- and β-Agostic Alkyl-Titanocene Complexes. *Organometallics* **2012**, *31*, 1591−1594.
45. Raucoules, R.; de Bruin, T.; Raybaud, P.; Adamo, C. Theoretical Unraveling of Selective 1-Butene Oligomerization Catalyzed by Iron−Bis(arylimino)pyridine. *Organometallics* **2009**, *28*, 5358−5367.
46. Inaoka, D.K.; Shiba, T.; Sato, D.; Balogun, E.O.; Sasaji, T.; Nagahama, M.; Oda, M.; Matsuoka, S.; Ohmori, J.; Honma, T.; inoue, M.; Kita, K.; Harada, S. Structural insights into the molecular design of flutolanil derivatives targeted for fumarate respiration of parasite mitochondria. *Int. J. Mol. Sci*. **2015**, *16*, 15287-15308.
47. Inc CCG. Molecular Operating Environment (MOE): Montreal, QC, Canada, H3A 2R7, 2014.09.
48. Wang, J.; Cieplak, P.; Kollman, P.A. How well does a restrained electrostatic potential (RESP) model perform in calculating conformational energies of organic and biological molecules? *J. Comput. Chem*. **2000**, *21*, 1049-1074.
49. Halgren, T.A. Merck molecular force field. I. Basis, form, scope, parameterization, and performance of MMFF94. *J. Comput. Chem*. **1996**, *17*, 490-519.

50. Wojciechowski, M.; Lesyng, B. Generalized Born Model: Analysis, Refinement, and Applications to Proteins. *J. Phys. Chem. B.* **2004**, *108*, 18368-18376.
51. Labute, P. The generalized Born/volume integral implicit solvent model: Estimation of the free energy of hydration using London dispersion instead of atomic surface area. *J. Comput. Chem*. **2008**, *29*, 1693-1698.

Chapter 5: Mechanism of Perfluoronickelacyclopentane Formation from Tetrafluoroethylene

Contributions to Knowledge:

Mechanism of Perfluoronickelacyclopentane Formation from Tetrafluoroethylene: Ancillary Ligand Steric and Bite Angle Effects on Cyclization Pathways.

Luana L. T. N. Porto, Jeffrey A. Ovens, Russell P. Hughes and R. Tom Baker,** to be submitted, Oct. 2022.

Chapter Contributions: Our collaborator Dr. Russell P. Hughes (Dartmouth College, USA) performed DFT calculations, Luana Porto performed all the experiments and wrote the first draft. Dr. Jeffrey Ovens collected and refined the X-ray diffraction data for molecular structure determination, and Prof. Baker conceived the project, helped plan the experiments and refined the manuscript text.

Abstract: Metallacyclopentanes are important reaction intermediates for catalytic processes such as selective ethylene oligomerization and diene cyclooligomerization. Reactions of fluoroalkenes with low-valent first row transition metal complexes tend to form stable fluorometallacyclopentane products (unless precluded by bulky ancillary ligands). DFT studies conducted herein indicate that conversion of L_2Ni bis(fluoroalkene) complexes to fluorometallacycle products is accompanied by a dramatic increase in the L-Ni-L angle. An experimental investigation of wide bite-angle bis(phosphine) ligands such as DPEphos confirms formation of isomeric metallacyclobutane products.

5.1 INTRODUCTION

Formation of metallacyclopentanes from alkenes has been pursued intensively with early metals for selective ethylene oligomerization to 1-hexene[1-5] and with late metals for diene cyclooligomerization[6-11] and ethylene dehydrodimerization to butadiene.[12] The history of nickelacyclopentanes is particularly fascinating. In 1974 Binger and co-workers showed that reactions of $Ni(cod)_2$ with strained cyclopropenes gave cyclobutane products, proposed to result from reductive elimination of the substituted metallacyclopentane intermediate (**Scheme 5.1**).[13] Subsequent synthesis of $Ni(\kappa^2\text{-}C_4H_6)(bpy)$ demonstrated its considerable thermal stability (now to b-H elimination), although the complex could not be obtained from ethylene.[14,15] Several years later Grubbs and Miyashita prepared triphenylphosphine nickelacyclopentanes at low temperature and showed that their decomposition pathways depended on the P:Ni ratio (**Scheme 5.2**).[16,17] Labeling studies indicated reversible formation of the nickelacyclopentane from the bis(alkene)

complex[18] and proposed the former as catalysts for alkene cycylodimerization.[19] These results prompted an early EHMO computational study on concerted cyclization of $Fe(\eta^2\text{-}C_2H_3R)_2(CO)_3$

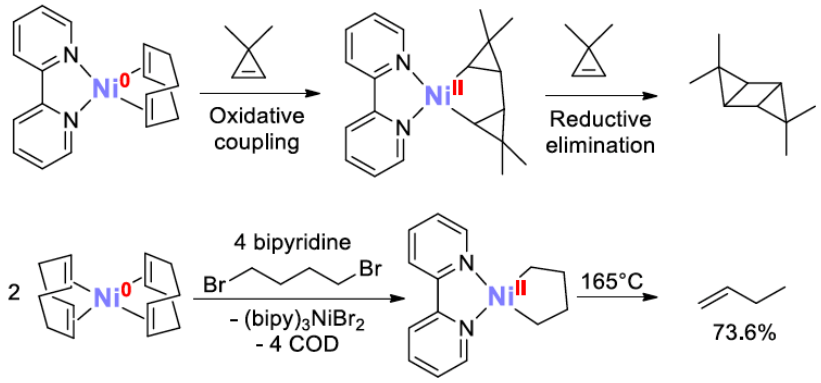

Scheme 5.1 First synthesis and reactivity demonstration of nickelacyclopentanes.

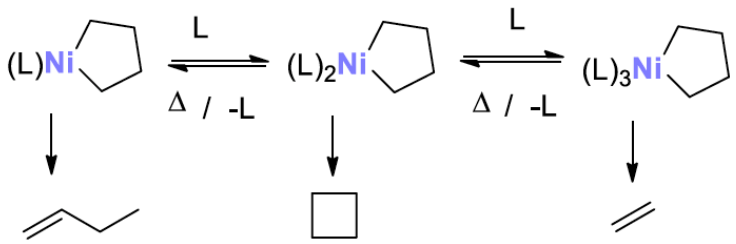

Scheme 5.2 Nature of decomposition products derived from PPh_3 nickelacycles depends on P:Ni ratio.

that correctly predicted the kinetic regioselectivity of metallacycle formation based on relative lobe size of the unsymmetrical alkene's π* orbital.[20] In contrast, both Ogoshi and coworkers,[21] and Olivier-Bourbigou, Breuil and coworkers[22] did not observe formation of cyclobutane or 1-butene while using $Ni(C_2H_4)_2(PCy_3)$ and $Ni(C_2H_4)(PPh_3)_2$, respectively, with ethylene. In 1998 a DFT study showed that in the lowest energy pathway the incoming ethylene molecule reacts not at the metal center, but at the carbon of a coordinated ethylene, generating a 1,5-diradical that then collapses to the metallacycle.[23]

The discovery of perfluorometallacyclopentane complexes by Stone and Wilkinson in 1960 (prepared by photolysis of $Fe(CO)_5$ and tetrafluoroethylene, TFE) demonstrated their high thermal stability.[24,25] Subsequent studies with low-valent nickel precursors showed that steric effects dictated formation of the alkene complex vs. metallacycle.[26–30] Electronic effects were also identified by the same group with π-accepting ancillary ligands favoring metallacycle formation[31].

Later work by Pörschke and co-workers confirmed this effect in their demonstration that Ni(η^2-C_2F_4)(tmeda) does not form the nickelacyclopentane on exposure to excess TFE under elevated pressure and temperature,[32,33] even though the latter is stable and easily obtained by ligand substitution from Ni[κ^2-$(CF_2)_4$)-][$P(O^iPr)_3$]$_2$.[34]

Although the metal-mediated cyclization of alkenes and alkynes has been investigated computationally,[1,18,19] given the unique roles played by organofluorine compounds in physical organic chemistry[35] we sought to investigate the Ni-mediated cyclization of TFE in detail. Herein we report a combined experimental-computational study of the effects of ancillary ligands. For bidentate chelating ligands, and for all but the most sterically demanding monodentate ligands, an 18-electron four-coordinate pathway is energetically favored, proceeding via an unusual pseudotetrahedral metallacyclopentane intermediate. In the cases of bidentate ligands, large bite angles accelerate the overall reaction.

5.2 RESULTS AND DISCUSSION

The standard reaction we employed for the synthesis of perfluoronickelacyclopentanes is reaction of $Ni(cod)_2$ with 2 equiv of a monodentate ligand, L or 1 equiv of a bidentate ligand, L-L followed by addition of 3-5 equiv of TFE. In some cases, the first reaction was conducted at low temperature to minimize formation of NiL_4 or $Ni(L\text{-}L)_2$, although some of these react smoothly with TFE. Monitoring the reaction by ^{19}F NMR spectroscopy typically shows initial formation of the olefin complex, followed by the metallacycle with no evidence of the bis(olefin) complex prior to cyclization. As a result computational studies started with L_2Ni- or (L-L)Ni TFE olefin complex + 1 equiv TFE.

5.2.1 Computational studies: Experimentally, the only relevant species observed in solution has been the mono(alkene) complex (or metallacyclopropane), Ni(η^2-C_2F_4)(L_2) (**5-1)** and the metallacyclopentane Ni($CF_2CF_2CF_2CF_2$)L_2 (**5-2**), several examples of which have been characterized crystallographically.[31-34,36,37] Potential pathways for conversion of **5-1** to **5-2** were studied computationally using Density Functional Theory (DFT/B3LYP-D3/LACV3P**). As the reactions typically proceed in non-polar solvents, no solvent corrections were employed.

5.2.1.1 Pathways for metallacycle formation: We began by evaluating potential species present in solution from which metallacycle formation might originate. Assumptions were that **5-1** is the

starting material, spectroscopically observed *in situ*, and that coupling to form the new C-C bond occurs within the coordination sphere, requiring two molecules of coordinated C_2F_4. Alternative pathways, in which exogenous C_2F_4 attacks ligated C_2F_4 to give a diradical intermediate[38] prior to closure to give the metallacycle were considered but excluded (*vide infra*). Two coordinated C_2F_4 ligands are accommodated by coordination of an additional C_2F_4 to $L_2Ni(C_2F_4)$ (**A**) to give the pseudo-tetrahedral 18-electron intermediate $L_2Ni(C_2F_4)_2$ (**B**), or by subsequent loss of L from **B** to afford the trigonal planar 16-electron mono(phosphine) species $LNi(C_2F_4)_2$ (**C**). DFT optimization of **A**, **B**, and **C** using several monodentate ligands afforded their closed-shell singlet ground state structures and free energies, and further exploration of the singlet energy landscape afforded the transition structures and intermediates connecting them. The resultant relative free energy landscapes are shown in **Figure 5.1**. In all systems described herein, calculated free energies are given relative to $G[L_2Ni(C_2F_4) + \text{free } C_2F_4] = 0.0$ kcal/mol. Since singlet/triplet energy gaps for starting materials and product **A**, **B**, and **C** are calculated to be large (e.g., L= PMe_3; **A** 23.7; **B** 27.0; **C** 34.9 kcal/mol) only closed-shell singlet reaction pathways have been examined in detail. Calculated structures (**A-I**) for L = PMe_3 are presented in **Figure 5.2**. Full structural information on all calculated species is provided in the Appendix.

As shown in Figure 5.1, formation of the final metallacyclic product **F** is strongly downhill in all cases. Binding of a second C_2F_4 ligand to $L_2Ni(C_2F_4)$ (**A**) to give **B** is an uphill process except for the PMe_3 complex, which is essentially thermoneutral. A transition state for C_2F_4 binding to **A** to give **B** (L=PMe_3) was located at 6.4 kcal/mol above the starting materials; coordination is clearly a low activation energy process and details have not been examined for other systems. Unsurprisingly, both steric and electronic effects play significant roles in these reactions to form the key bis(alkene) intermediates **B** and **C** and are discussed in detail later.

In all cases, the transition structure ($\mathbf{D}^{\ddagger}$) for C-C coupling via four-coordinate intermediate **B** is more favorable than that ($\mathbf{G}^{\ddagger}$) from three-coordinate **C**. For the three-coordinate pathway, examination of the relevant structures in **Figure 5.2** reveals that the two alkenes in the ground state of **C** are already in the conformationally required coplanar arrangement for metallacycle formation. The C-C coupling occurs concertedly via $\mathbf{D}^{\ddagger}$, which then descends to a second transition structure $\mathbf{G}^{\ddagger}$ leading to a bifurcated pathway to the two identical T-shaped intermediates (**I**); a similar pathway

has been computed for cyclization of CF_2=CH_2 using Ni(NHC) as a template.[39] Coordination of L affords the final metallacycle **F**.

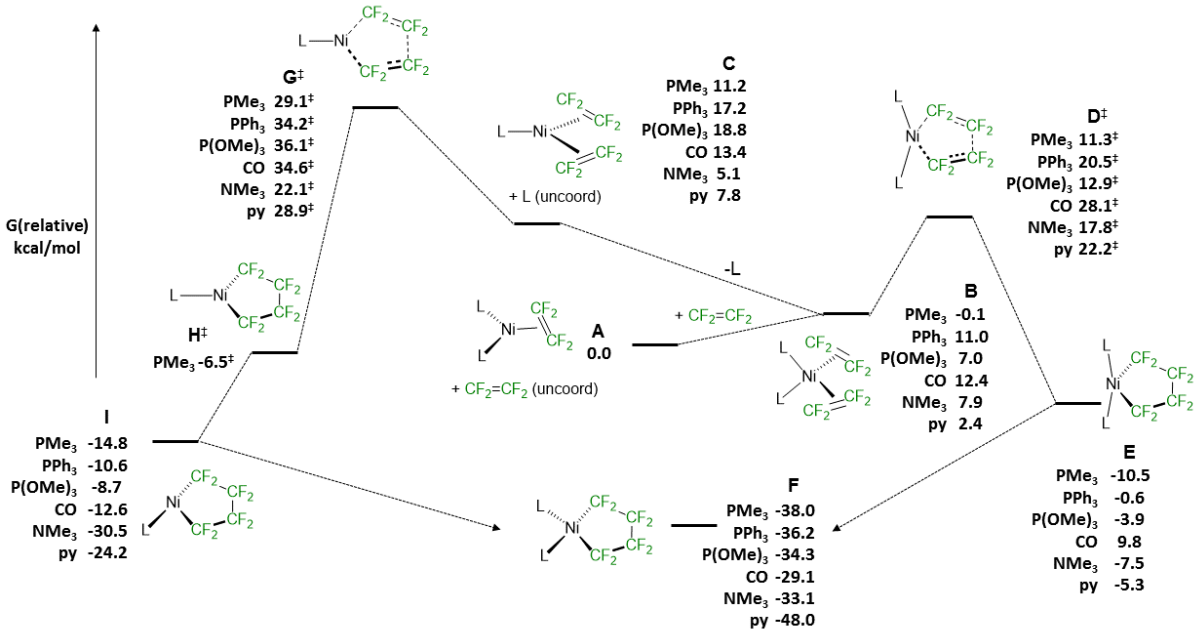

Figure 5.1 Calculated relative free energy landscape (not to scale) for Ni-metallacycle formation from two molecules of C_2F_4 using monodentate ancillary ligands. G values are relative to G[$L_2Ni(C_2F_4)$ + free C_2F_4] = 0.0 kcal/mol.

In contrast, binding of a second C_2F_4 to **A** results in a substantial contraction of the L-Ni-L angle from 119.3° to 108.9° (L = PMe_3) that must have a steric price (*vide infra*). In the ground state of the resultant four-coordinate **B** the two alkenes are mutually skewed, with each of their C-C axes eclipsing a Ni-P bond and are not conformationally oriented for coplanar C-C bond formation. Fortunately, as expected, the barrier to propeller rotation about the Ni-alkene axis is small (calculated ~6 kcal/mol) in pseudotetrahedral **B**, allowing low energy access to the coplanar conformation required to generate transition structure **D**‡. Other than this rotational component, four-coordinate transition structure **D**‡ for formation of the new C-C bond requires significantly less distortion of the two alkenes and occurs earlier along the reaction coordinate (C-C = 2.311Å) compared to **G**‡ (C-C = 1.970Å) (L = PMe_3), contributing to its lower energy. The concerted C-C

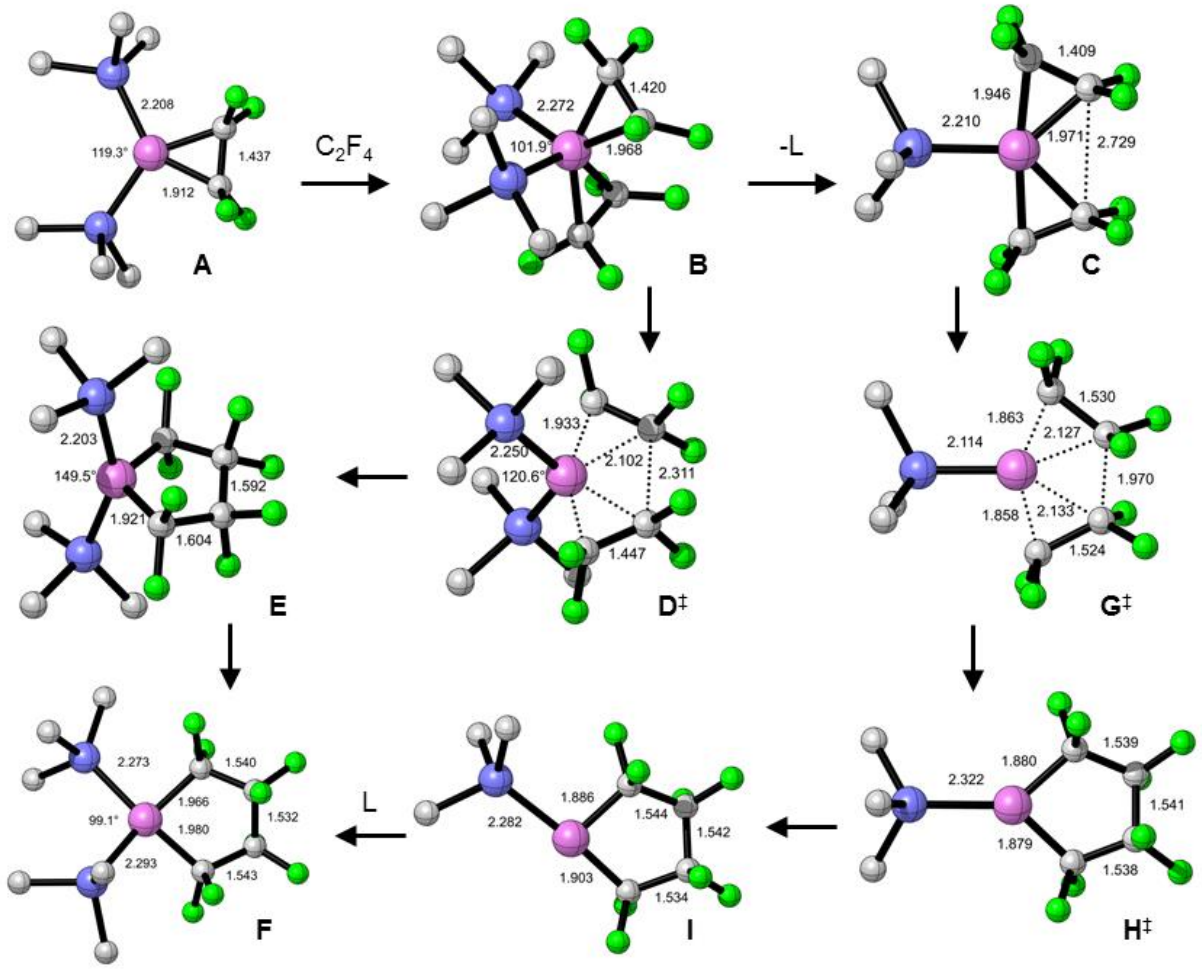

Figure 5.2 Calculated structures for Ni-C_2F_4 complexes **A-I** (Figure 5.1) using PMe_3 as the ancillary ligand. Hydrogen atoms are omitted for clarity.

coupling reaction via **D**‡ leads to an unusual kinetic metallacycle **E**. The L-Ni-L angle is dramatically increased in both the transition structure **D**‡ (120.6°) and kinetic metallacycle product **E** (149.5°) (L = PMe_3). Subsequently **E** rearranges to the thermodynamically observed square planar metallacycle **F**. We have been unable to observe a direct transition structure for this **E-F** isomerization computationally. Intermediate **E** is remarkable for a four coordinate, formally Ni(II), species, which has an exceptionally obtuse L-Ni-L angle. Rather than a pseudotetrahedral geometry, it resembles a trigonal bipyramid with a missing equatorial ligand. We speculate that one of the additional donors present *in situ* (L or COD) can bind to the vacant coordination site in **E** to afford a trigonal bipyramidal intermediate, which can then pseudorotate to a square pyramid, with ultimate loss of the exogenous donor to afford the final product metallacycle (**F**). We have not examined this

isomerization in any detail, but significant computational evidence for an intramolecular version of this isomerization is presented later.

In contrast, when the ancillary ligand becomes sufficiently bulky (e.g., P^iPr_3), the energy landscape is flipped, as shown in **Figure 5.3**. Formation of four-coordinate **B** is now strongly disfavored compared to three-coordinate **C** and coupling proceeds via the three-coordinate pathway**.** Here the steric demands of the phosphine make even the four-coordinate metallacycle **F** unstable with respect to phosphine dissociation to give **I**. Similar T-shaped metallacycles **I** with very bulky NHC ligands have been previously observed experimentally and studied computationally.[39,40] Further discussion here is therefore limited to the four-coordinate pathway.

5.2.1.2 Energy components in the four-coordinate pathway: The overall activation free energy of metallacycle formation from four-coordinate **B**, reflected by the free energy of transition structure **D**‡, involves two important components; initial binding of the second alkene to **A** to give **B**, followed by the actual intramolecular cyclization step in which **B** transitions to **E** via **D**‡. The former represents a reversible, and in most cases thermodynamically unfavorable, pre-equilibrium in which $\ln K_{eq}$ is inversely proportional to DG(**B-A**), with the second barrier DG(**D-B**) corresponding to the barrier for C-C bond formation via irreversible generation of the kinetic metallacycle **E** directly from **B**. Ancillary ligand effects on both steps define their impact on the overall facility of the reaction and are considered separately.

Relative G values, Ni-L distances, and L-Ni-L angles in the important species along the four-coordinate path are compiled in **Table 5-1** for those monodentate ligands already discussed (entries 1-6), and for several bidentate analogues to be discussed later.

5.2.1.3 Monodentate ligands (Table 5-1; entries 1-6): Relative to the PMe_3 example, in which the electron-rich and relatively sterically unencumbered Ni readily binds an additional C_2F_4 to give **B**, this reaction is disfavored for the larger cone angle PPh_3 (as it is even more strongly for P^iPr_3; *vide supra*) but is also disfavored for the better p-acceptor $P(OMe)_3$ and notably for the sterically undemanding but strongly p-accepting CO ligand. Electronic effects clearly play an important effect on this pre-cyclization process. Replacement of PMe_3 by NMe_3 also results in less favorable

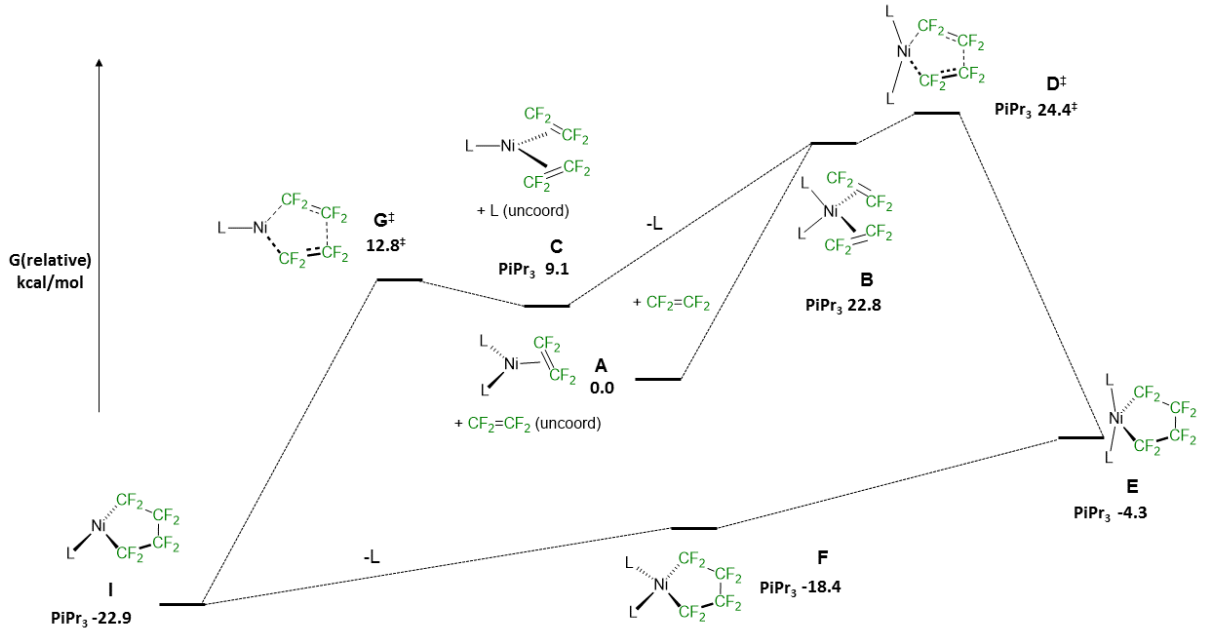

Figure 5.3 Calculated relative free energy landscapes (not to scale) for Ni-metallacycle formation from two molecules of C_2F_4 using the P^iPr_3 ligand.

Table 5.1 Ligand Angle Effects in Metallacycle Formation (DFT/B3LYP-D3/LACV3P**/gas)

Entry	Ligand (**L_2**)	Relative **G**[a] (L-Ni-Langle °) {Ni-L distances Å}				
		$L_2Ni(C_2F_4)$ $_2$ **B**	Transition structure **D‡**	Kinetic Metallacycle **E**	Final Metallacycle **F**	***ΔG (D‡-B)***[b]
1	2 x PMe_3	**-0.1** (101.9) {2.271}	**11.3** (120.6) {2.252}	**-10.5** (149.5) {2.202}	**-38.0** (99.1) {2.273, 2.293}	***11.4***
2	2 x PPh_3	**11.0** (105.0) {2.348, 2.354}	**20.5** (114.9) {2.275, 2.342}	**-0.6** (142.6) {2.210, 2.220}	**-36.2** (99.8) {2.288, 2.348}	***9.5***
3	2 x $P(OMe)_3$	**7.0** (96.2) {2.227}	**12.9** (119.6) {2.210}	**-3.9** (143.9) {2.177}	**-34.3** (95.4) {2.222, 2.250}	***5.9***
4	2 x CO	**12.4** (103.9) {1.859}	**28.1** (127.5) {1.833}	**9.8** (158.2) {1.813}	**-29.1** (99.3) {1.873}	***15.7***

5	2 x NMe_3	**7.9** (101.8) {2.248}	**17.8** (109.3) {2.168, 2.171}	**-7.5** (146.7) {1.989}	**-33.1** (99.3) {2.102, 2.320}	***9.9***
6	2 x py	**2.4** (93.8) {2.057}	**22.2** (113.6) {1.958. 2.114}	**-5.3** (157.5) {1.913}	**-48.0** (90.5) {2.025}	***19.8***
7	bipy	**2.1** (80.5) {2.028}	**26.0** (82.3) {1.946, 2.069}	**18.8** (85.5) {1.971}	**-50.1** (81.3) {2.009}	***23.9***
8	$Me_2N(CH_2)_2NMe_2$ tmeda	**8.3** (84.2) {2.214, 2.223}	**24.8** (88.0) {1.984, 2.343}	**12.9** (95.9) {2.048}	**-48.6** (86.0) {2.078}	***16.5***
9	*cis*-$Me_2N(CH=CH)NMe_2$	**8.6** (81.6) {2.190, 2.198}	**26.4** (83.4) {2.010, 2.336)	**14.8** (91.2) {2.062}	**-47.9** (84.8) {2.078}	***17.8***
10	$Me_2N(CH_2)_3NMe_2$	**15.5** (90.6) {2.278}	**29.4** (98.8) {2.146, 2.168}	**10.2** (120.3) {1.996}	**-35.4** (94.6) {2.132}	***13.9***
11	$Me_2N(CH_2)_4NMe_2$	**15.5** (98.4) {2.172, 2.277}	**29.4** (110.2) 2.018, 2.444}	**6.5** (136.5) {1.975, 1.990}	**-21.6** (97.1) {2.163, 2.228}	***13.9***
12	$Me_2P(CH_2)_2PMe_2$ dmpe	**-3.8** (88.5) {2.286}	**14.4** (95.0) {2.207, 2.266}	**-0.5** (104.5) {2.165}	**-49.5** (88.4) {2.211}	***18.2***
13	$Me_2P(CH_2)_3PMe_2$ dmpp	**4.4** (93.9) {2.301}	**18.9** (103.5) {2.230, 2.236}	**0.9** (118.2) {2.157}	**-41.8** (93.6) {2.243}	***14.5***
14	$Me_2P(CH_2)_4PMe_2$ dmpb	**1.0** (98.5) {2.247, 2.269}	**14.1** (115.5) {2.238, 2.250}	**-7.3** (138.9) {2.189}	**-39.6** (98.2) {2.270}	***13.1***

15	DPEphos	**8.0** (102.0) {2.305, 2.377} {Ni-O 3.251}	**17.8** (111.4) {2.280, 2.297} {Ni-O 3.126}	Isomer 1[c] **-3.5** (132.1) {2.202, 2.212} {Ni-O 2.892} Isomer 2[c] **-24.5** (117.9) {2.248, 2.461} {Ni-O 2.120}	**-33.2** (100.6) {2.324, 2.371} {Ni-O 3.088}	***9.8***
16	XantPhos	**5.3** (104.3) {2.336, 2.351} {Ni-O 3.382}	**12.1** (116.9) {2.274, 2.301} {Ni-O 3.181}	Isomer 1 **-8.4** (137.2) {2.202, 2.212} {Ni-O 2.797} Isomer 2 **-25.7** (125.4) {2.276, 2.345} {Ni-O 2.059}	**-26.6** (99.5) {2.315, 2.321} {Ni-O 2.546}	***6.8***

[a] For each L_2, all G values (**bold**) are relative to $L_2Ni(C_2F_4)$ + C_2F_4(free) = 0.0 kcal/mol
[b] This value represents the free energy change for the actual cyclization step.
[c] Different intermediate structures are due to different conformations of the DPE ring systems; the Ni, P, and metallacycle components are essentially superimposable.

binding of alkene, perhaps due to increased intra-ligand steric effects which are enhanced due to the short Ni-N bonds, as the L-Ni-L angle must contract from **A** to **B**. Indeed, loss of NMe_3 from **B** to give **C** is slightly downhill. In contrast the planar pyridine (py) ligand provides for more favorable alkene binding, and unfavorable py dissociation from **B**. Loss of L from **B** to give the trigonally coordinated species (**C**) is also a significantly uphill process for all phosphorus ligands (excepting P^iPr_3; *vide supra*), while NMe_3 is slightly downhill (*vide supra*) and CO is only slightly uphill. Clearly, the facility of initial binding of a second alkene to afford the crucial intermediate **B** is strongly dependent both on the ancillary ligand donor/acceptor properties and intraligand steric effects, with no clear predictable pattern emerging. However, despite unfavorable binding constants in almost all cases, it is clear that the preferred pathway for metallacycle formation originates from **B** via transition structure $\mathbf{D}^{\ddagger}$; the corresponding transition state $\mathbf{G}^{\ddagger}$ for cyclization in a three coordinate species is always a significantly higher energy reaction.

Not unexpectedly, as with the initial binding step, examination of the activation free energies of the cyclization step (reflected in DG(**D**‡**-B**); entries 1-6, **Table 5-1**) reveals no clear correlation between steric effects and electron donor/acceptor properties of the monodentate ligands studied. However, some more useful correlations can be made between individual monodentate ligands and their bidentate analogues.

*5.2.1.4 Bidentate ligands (**Table 5-1**; entries 7-16):* Since the favored pathway for metallacycle formation for monodentate ligand complexes requires a four-coordinate intermediate we were initially mystified as to why the previously reported compounds $L_2Ni(C_2F_4)$ [L_2 = bipy, tmeda] were resistant to reaction with more C_2F_4 to give a metallacycle, even though the metallacycle can be prepared independently by alternative means (see below). This clearly implicates a kinetic barrier to cyclization, and we posited that the obtuse L-Ni-L angle in the corresponding intermediate **E** and in the transition structure **D**‡ leading to it, might not be readily achievable by chelates with small bite angles. Accordingly, we examined the energy landscapes of these bidentate chelates, as shown in **Figure 5.4**.

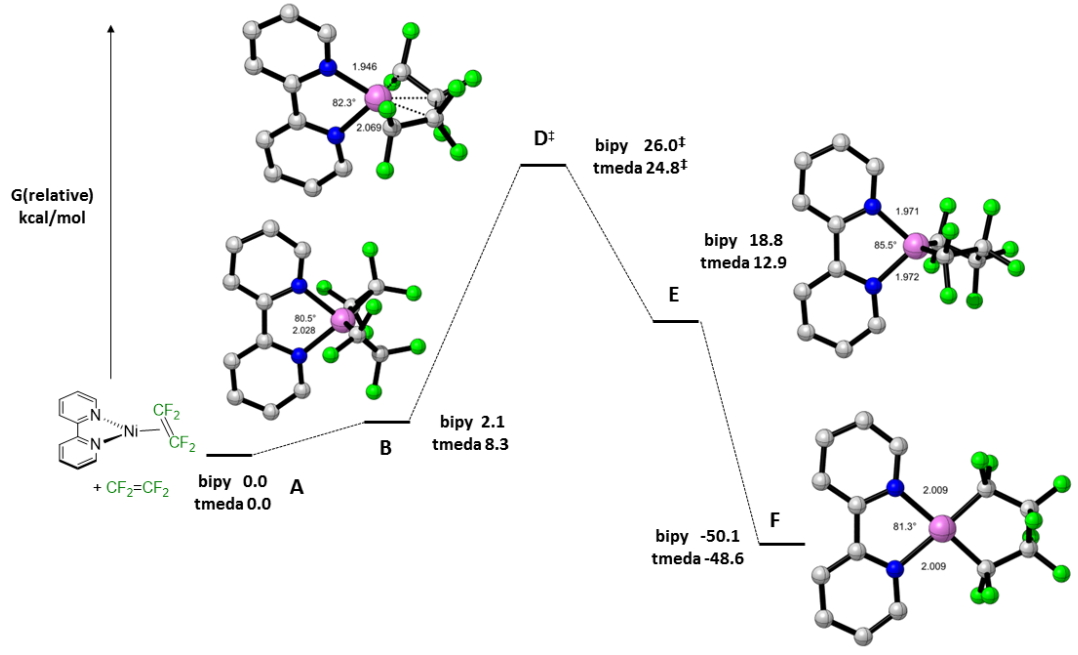

Figure 5.4 Calculated relative free energy landscapes (not to scale) for Ni-metallacycle formation from two molecules of C_2F_4 using bipy and tmeda chelate ligands. Structures for the bipy complexes are shown, with hydrogen atoms omitted for clarity.

The pathway to metallacycle formation via transition structure **D**‡ is indeed higher than for the monodentate ligands in both cases (**Figure 5.1**). Due to the constrained bite angles of these chelating ligands, the kinetic metallacycle **E** has a much more pseudotetrahedral structure than in the monodentate ligand cases in which the L-Ni-L angle can expand. Comparison of the tmeda data with those of the analogous untethered bis(NMe_3) system (Table 5.1; entries 8 and 5) reveals significantly different overall activation free energies. These arise not from binding energies differences for the second alkene, which are almost identical, but from significant differences in the values of DG(**D**‡**-B**); transition structure **D**‡ is significantly higher in energy for the bidentate ligand, as is the energy of the kinetic metallacycle **E**. The structure of **D**‡ shows an N-Ni-N angle of 88.0° for the bidentate tmeda ligand, with significantly different Ni-N distances (1.984, 2.343Å). Formation of intermediate **E** expands this angle slightly to 95.9°, with equal Ni-N distances (2.048Å). In contrast, the untethered bis(NMe_3) analogue allows a much larger N-Ni-N angle of 109.3° in the transition structure **D**‡, with essentially equal Ni-N distances, and also allows an even more expanded angle of 146.7° in the kinetic metallacycle **E**. Introduction of additional conformational constraint in the bidentate ligand using *cis*-$Me_2NCH{=}CHNMe_2$ (entry 9) affords essentially identical conclusions. Thus constraint of the bite angle is a significant factor in the tmeda system, which accommodates the additional strain by elongating one Ni-N distance in the transition structure **D**‡. Likewise, comparison of the data for chelating bipy and its untethered bis(py) analogue (**Table 5-1**; entries 6 and 7) yields similar conclusions concerning bite angle constraints, with the exception that the transition structure **D**‡ for the bis(py) derivative also shows two different Ni-N distances.

The results of increasing the bite angle of the chelating nitrogen ligands using added methylene groups (entries 8, 10, and 11) are initially suprising, as the overall activation free energy actually increases, despite the more flexible ligands. However this difference arises from increased steric cost of alkene binding to form intermediate **B**; the actual cyclization step has a slightly lower activation energy DG**(D**‡**-B)**, in agreement with a more flexible bite angle.

Comparison of the bis(PMe_3) system with the chelating dmpe analogue (entries 1 and 12) is also enlightening. Even though the dmpe derivative binds the second alkene more strongly than the monodentate analogue, the overall activation free energy is larger due to the constrained bite, as reflected in the DG**(D**‡**-B)** values. Two significantly different Ni-P distances are found in the

dmpe transition structure **D**‡. Comparison of dmpe with its ring-expanded analogues dppp and dppb (entries 12-14) illustrates differential C_2F_4 binding as the chelate ring bite expands, but examination of the DG**(D**‡**-B)** values illustrates that the more flexible bite angle leads to progressive lowering of the activation barrier to the actual cyclization step.

Bidentate ligands having larger bite angles were also examined computationally (Table 5-1: entries 15-16). In addition, these ligands have an O-atom in the chelate backbone with added ligating potential. The energy landscape for the DPEphos system (entry 15) is shown in **Figure 5.5**, along with computed structures. The energetics are remarkably similar to those for the untethered bis(PPh_3) system (entry 2) indicating that the bite angle constraint is attenuated for this large bite angle ligand. In particular, the activation barrier for the actual cyclization step DG(**D**‡**-B**) is almost identical to that for the untethered PPh_3 analogue. The backbone O-atom appears to play no significant role until after the cyclization transition state, with the Ni-O distance essentially unchanged from **B** (3.251Å) to **D**‡ (3.126Å) Transition structure **D**‡ intially evolves into intermediate **E**(isomer 1) in which the Ni-O distance (2.797Å) shortens slightly but is not significantly stabilized relative to the PPh_3 analogue. However, a subsequent conformational flip of the DPEphos ligand generates a truly five-coordinate isomer **E**(isomer2) in which the Ni-O distance is 2.120Å and which is strongly stabilized relative to its isomer. Alternative views of these two isomeric intermediates **E** for the DPEphos system are provided in **Figure 5.6**, illustrating that **E**(isomer2) is a truly five-coordinate trigonal bipyramidal structure. A trigonal twist serves to isomerize this to the final square planar metallacyclic product **F** in which the Ni-O interaction is substantially lengthened to 3.088Å. This serves as a model for exogenous donors to help stabilize intermediates **E** in other systems (*vide supra*), and to facilitate isomerization to the final product **F**.

The energy profile of the corresponding XantPhos system (entry 16) is similar, though with a significantly lower activation barrier fro the cyclization step, consistent with its larger bite angle. Notably for XantPhos the final square planar product **F** (entry 16) is very close in energy to **E** (intermediate2).

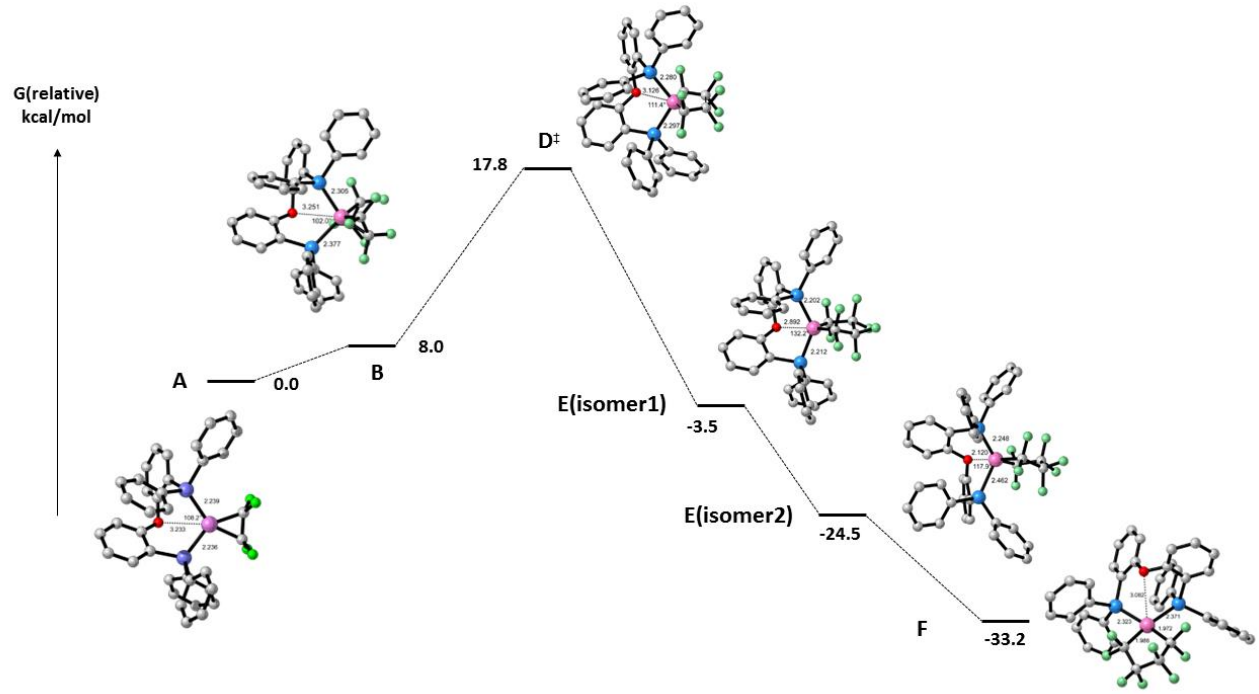

Figure 5.5 Calculated free energy landscape for metallacycle formation using DPEphos. H-atoms omitted for clarity.

5.2.2 Experimental Studies: In light of the remarkable P-Ni-P angle increase observed computationally for C-C bond formation using TFE, we investigated reactions with several bis(phosphines) having a wide natural bite angle (β_n).[41-43] Reactions of 5 equiv of TFE with Ni(cod)(dppe) (β_n = 78 °) and Ni(cod)(dppf) (β_n = 99 °) proceeded as expected with initial formation of the olefin complexes, **5-1a,b** and subsequent conversion to nickelacyclopentanes, **5-2a,b** characterized by ^{19}F and ^{31}P NMR spectroscopy [**Figure 5.7** and Appendix; dppe = 1,2-bis(diphenylphosphino)ethane; dppf = 1,1'-bis(diphenylphosphino)ferrocene]. The structure of **5-1b** was confirmed by X-ray crystallography (**Figure 5.8**). In contrast, using DPEphos (b_n = 102 °), olefin complex **5-1c** as well as two different metallacycles **5-2c** and **5-3** were observed {**Scheme 5.3**; DPEphos = bis[(2-diphenylphosphino)-phenyl] ether}. While complex **5-2c** gave rise to sharp ^{19}F NMR resonances (**Figure 5.9**), those due to **5-3** were indicative of a fluxional process with the low-temperature spectrum indicating no apparent mirror plane containing the metallacycle ring (**Figure 5.10**). This process could involve a flexing of the ligand backbone or reversible Ni-O bond cleavage; the activation barrier could be estimated as $\Delta G^{\neq}$ = -13.5 kcal/mol) assuming coalescence at 238K. Crystallization of **5-2c** from the reaction mixture allowed us to demonstrate its distorted square planar structure (**Figure 5.11**) that matched well the calculated structure (**E** isomer 1). The

other metallacyclopentane isomer (**5-3**) is presumably that with Ni coordinated to the oxygen of the DPEphos diaryl ether backbone (**E** isomer 2).

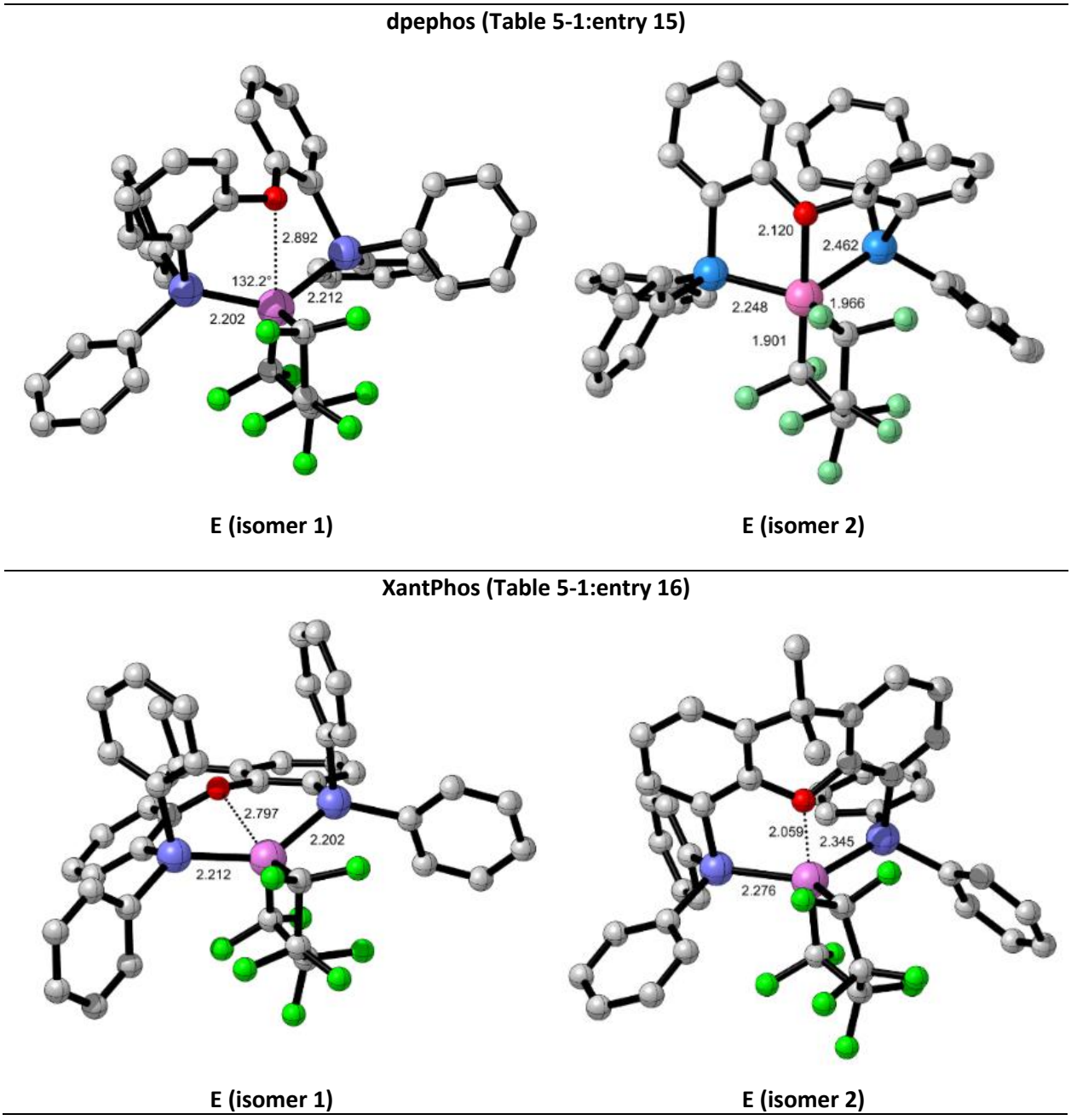

Figure 5.6 Alternative views of the computed structures of the **E** isomers in the DPEphos and Xantphos cyclization reactions, with H-atoms omitted for clarity.

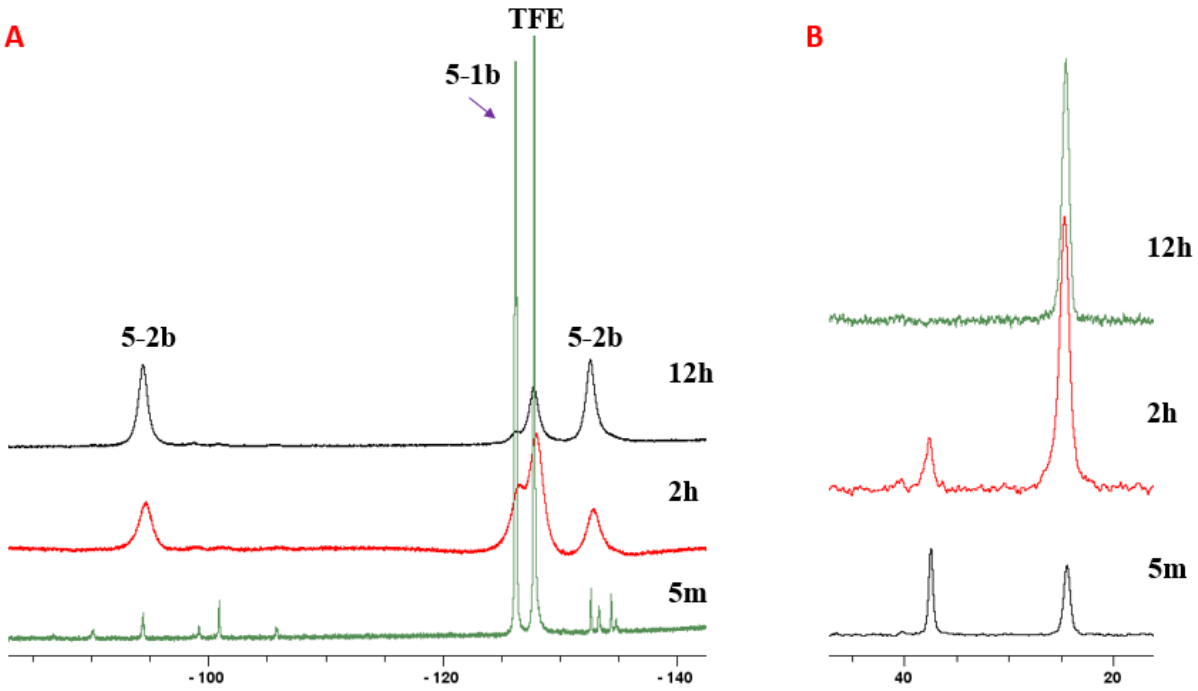

Figure 5.7 ^{19}F (**A**) and $^{31}P\{^{1}H\}$ (**B**) NMR spectra of $Ni(cod)_2$ + dppf + 3 equiv TFE in C_6D_6.

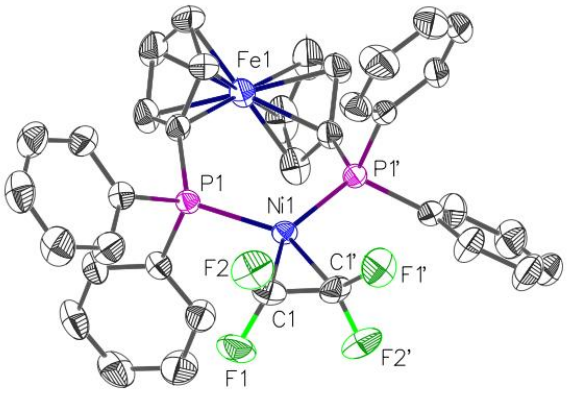

Figure 5.8 *Molecular diagram representation of the molecular structure of Ni(η^2-C_2F_4)(dppf) (**5-1b**). Thermal ellipsoid probabilities are set to 30% with hydrogen atoms and co-crystallized solvent omitted for clarity. Selected bond distances (Å) and angles (deg): Ni-P1 2.2003(4); Ni-C1 1.8839(14); C1-C1' 1.409(3); Ni-Centroid(C1,C1') 1.7471(10); Ni-Fe 4.1955(4); P1-Ni-P1' 106.6(1); C1-Ni-P1 104.95(5); C1-Ni-P1' 148.2(1); P1-Ni-Centroid(C1,C1') 126.7(1).*

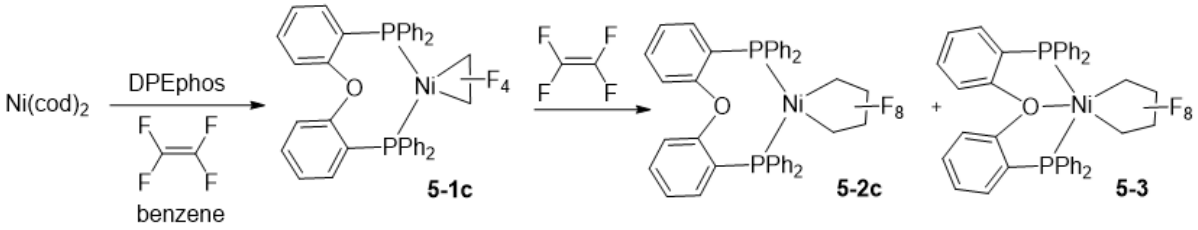

Scheme 5.3 Reaction of Ni(cod)(DPEphos) with TFE in THF.

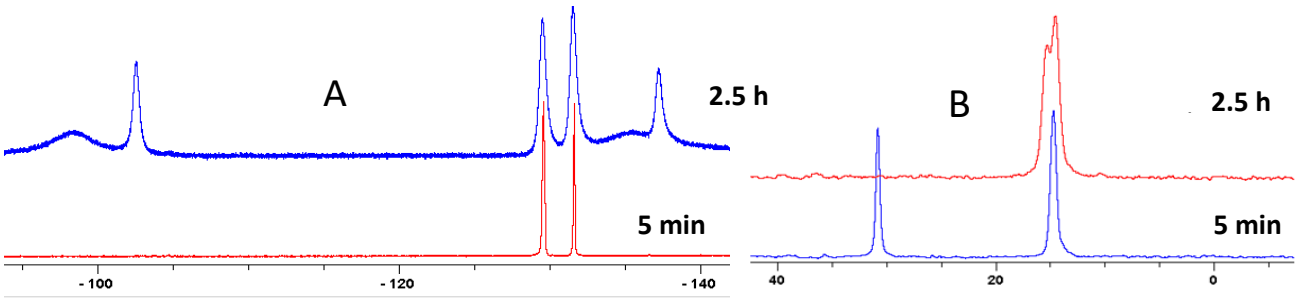

Figure 5.9 ^{19}F (**A**) and $^{31}P\{^{1}H\}$ (**B**) NMR spectra of $Ni(cod)_2$ + DPEphos + 3 equiv TFE in C_6D_6.

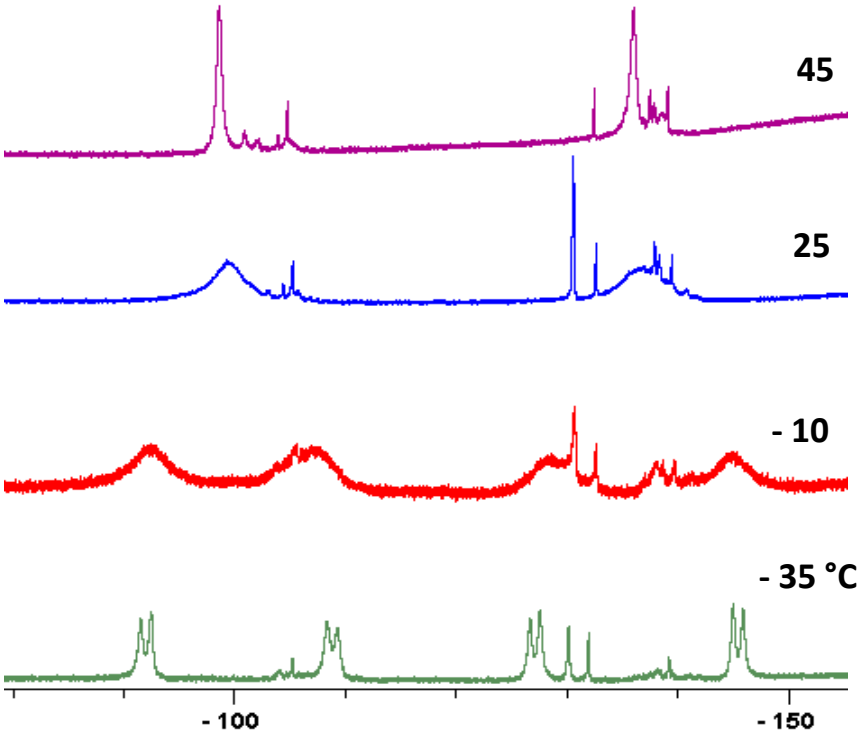

Figure 5.10 Variable temperature ^{19}F NMR spectra of metallacycle **5-3.**

Finally, using Bisbi (β_n = 113 °), which does not contain an oxygen donor, we again observed a mixture of metallacycles (**Figure 5.12**). Although several of the resonances shifted on

addition of acetonitrile (see Appendix), crystals obtained from this solvent revealed formation of .a bis(phosphine)-bridged complex with one acetonitrile ligand coordinated to each Ni (**Figure 5.13**). It is thus possible that with this largest bite-angle bis(phosphine), chelating a single Ni center is disfavored with respect to bridging two nickels.

Returning then to the chelating N-N ligands investigated originally by Pörschke, after confirming their observation of no reaction between the TFE complex and additional TFE in THF solvent even at 60 °C, we found that simply switching the solvent to acetone with gentle heating (40 °C) afforded previously reported Ni(C_4F_8)(bipy) (**5-2e**) in high yield (see Appendix). Indeed, even in 2,5-dimethyl-dihydrofuran solvent metallacycle formation was observed after heating at 60 °C overnight. As a result, rather than smaller solvent molecules promoting metallacycle formation via an associative pathway, it is more likely, based on the calculations above, that tight binding of THF to Ni(η^2-C_2F_4)(bipy) accounts for Pörschke's original observation.

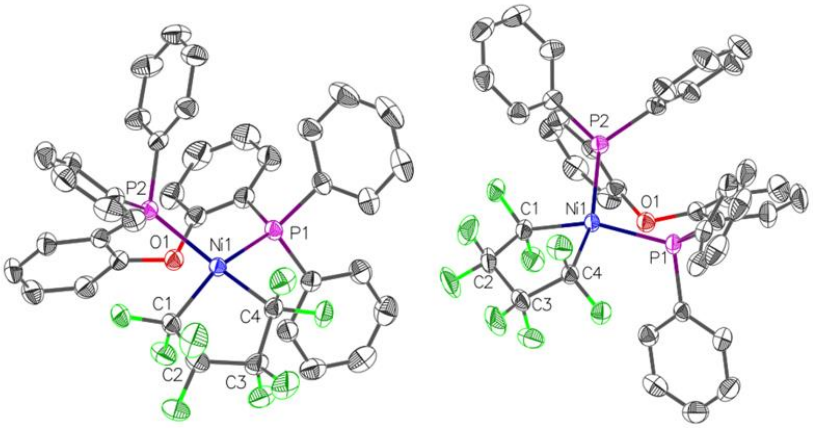

Figure 5.11 Molecular diagram representation of molecular structure of **5-2c**. Thermal ellipsoid probabilities are set to 30% with hydrogen atoms, co-crystallized solvent and alternate conformations of the disordered nickelacyclopentane ring are omitted for clarity. Selected bond distances (Å) and angles (deg): Ni-C1 1.956(3); Ni-C4 1.948(3); Ni-P1 2.2403(8); Ni-P2 2.2512(9); Ni----O 2.947(2); C1-Ni-P1 153.01(10); C4-Ni-P2 157.29(10); C1-Ni-C4 84.32(13); P1-Ni-P2 100.43(3); C1-Ni-P2 91.44(10); C4-Ni-P4 93.13(9).

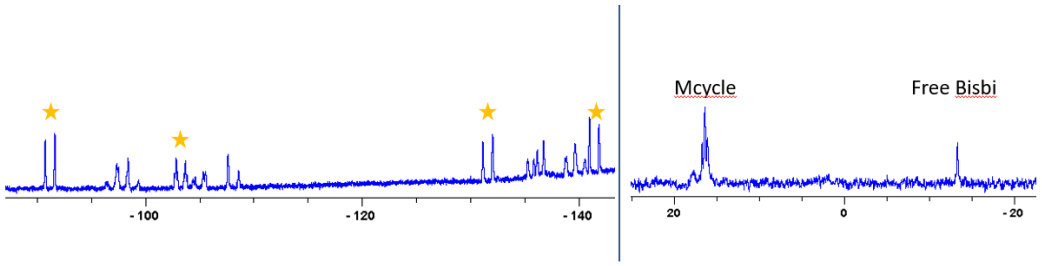

Figure 5.12 ^{19}F (**A**) and $^{31}P\{^{1}H\}$ (**B**) NMR spectra of Ni(cod)(Bisbi) + 3 equiv TFE in benzene.

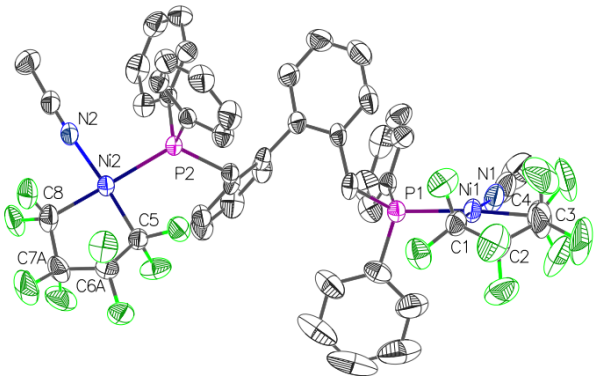

Figure 5.13 Molecular diagram representation of molecular structure of **5-5**. Thermal ellipsoid probabilities are set to 30% with hydrogen atoms, co-crystallized solvent and alternate conformations of disordered nickelacyclopentane ring are omitted for clarity. Selected bond distances (Å) and angles (deg): Ni-C1 1.898(3)-1.899(3); Ni-C2 1.940(3)-1.943(4); Ni-P1 2.2589(9)-2.2734(8); Ni-N1 1.885(3)-1.897(3); C1-Ni-N1 175.12(13)-175.27(11); C2-Ni-P1 174.29(11)-175.01(14); C1-Ni-C4 85.68(13)-85.92(16); C1-Ni-P1 92.91(10)-93.23(9); C4-Ni-N1 89.20(15)-89.95(12); P1-Ni-N1 90.95(7)-91.98(9)

5.3 CONCLUSIONS

In this work, DFT calculations, together with experiments, elucidated several unique features in reactions of TFE with zerovalent Ni complexes. The effects of ancillary ligands are derived first from both the kinetic energy barrier to binding the second TFE molecule, as well as the thermodynamic stability of this intermediate. Second, in the transit from bis(alkene) complex to metallacycle, C-C bond formation occurs in a plane that is perpendicular to the L-Ni-L plane and is accompanied by a dramatic opening of the L-Ni-L angle to afford a kinetic metallacycle product in which the geometry about Ni resembles a trigonal bipyramid with one vertex missing. We then proposed that reversible coordination of a third ligand could facilitate conversion of this kinetic metallacycle to the most stable distorted square planar analogue. We showed that using wide bite-angle ligands such as DPEphos permits the 'trapping' of the kinetic metallacycle by Ni coordination to the oxygen of the ligand's diaryl ether backbone. These observations represent a rare example of mechanistic studies of perfluorometallacycles and could help to develop new and more efficient catalytic systems.

5.4 EXPERIMENTAL SECTION

5.4.1 General procedures: Experiments were conducted under nitrogen, using Schlenk techniques or an MBraun glove box. All solvents were deoxygenated by purging with nitrogen. Toluene, hexanes, diethyl ether (DEE) and tetrahydrofuran (THF) were dried on columns of activated alumina using a J. C. Meyer (formerly Glass Contour®) solvent purification system. Benzene-d_6 (C_6D_6) was dried by stirring over activated alumina (ca. 10 wt.%) overnight, followed by filtration. Acetonitrile (CH_3CN) and dichloromethane (DCM) were dried by refluxing over calcium hydride under nitrogen. After distillation, they were dried further by stirring over activated alumina (ca. 5 wt.%) overnight, followed by filtration. All solvents were stored over activated (heated at ca. 250 ^oC for >10 h under vacuum) 4 Å molecular sieves. Glassware was oven-dried at 150 ^oC for >2 h. The following chemicals were obtained commercially without further purification, as indicated: 1,2-bis(diphenylphosphino)ethane, (dppe, AlfaAesar, 97%), 1,1′-Ferrocenediyl-bis(diphenylphosphine), (dppf, Sigma-Aldrich, 97%), Bis[(2-diphenylphosphino)phenyl] ether (DPEphos, Sigma-Aldrich, 97%), Bis[(2-diphenylphosphino)phenyl] ether (DPEphos, Sigma-Aldrich, 98%), 2,2'-Bis(diphenylphosphinomethyl)-1,1'-biphenyl, 99% (Bisbi, Strem, 99%), acetone (Sigma-Aldrich, ≥99.8%, HPLC grade), 1,4-Dioxane (Sigma-Aldrich, ≥99.8%, anhydrous), nickel(II) acetylacetonate (EMD Millipore, >98%), 1,5-cyclooctadiene (TCI America, >98%), di-n-butylmagnesium (Sigma-Aldrich, 1.0 M solution in heptane) and n-butyl-s-butylmagnesium (Sigma-Aldrich, 0.7 M solution in hexane). Tetrafluoroethylene (TFE) was made by pyrolysis of polytetrafluoroethylene (Scientific Polymer Products, powdered) under vacuum, using a slightly modified literature procedure [10-20 mTorr, 650 °C, 30 g scale, product stabilized with R(+)-limonene (Aldrich, 97%), giving TFE of ca. 97% purity].[44] Bis(1,5-cyclooctadiene)nickel (0) [$Ni(cod)_2$] was prepared using a new literature procedure.[45] ^{19}F and $^{31}P\{^1H\}$ NMR spectra were recorded on a 300 MHz Bruker Avance instrument at room temperature (21-23 °C) unless stated otherwise. Electrospray ionization mass spectral data were collected using an Applied Biosystem API2000 triple-quadrupole mass spectrometer.

5.4.2 X-ray crystallography: Single crystals were mounted on MiTeGen MicroMounts using parabar oil and X-ray diffraction data were collected on a Bruker Kappa or Smart ApexII single crystal diffractometer equipped with a sealed tube Mo Kα source (λ= 0.71073 Å), a graphite monochromator, and an Apex II CCD detector. Samples were held at a low temperature using a

dry compressed-air cooling system. Raw data collection and processing were performed with the Apex3 software package from Bruker.[46] Initial unit cell parameters were determined from 36 data frames from select $\boldsymbol{\omega}$ scans. Semi-empirical absorption corrections based on equivalent reflections were applied.[47] Systematic absences in the diffraction data-set and unit-cell parameters were consistent with the assigned space group. The initial structural solutions were determined using ShelxT direct methods,[48], and refined with full-matrix least-squares procedures based on $\boldsymbol{F2}$ using ShelXL and ShelXle.[49] Hydrogen atoms were placed geometrically and refined using a riding model.

5.4.3 Computational Methods: All calculations were carried out using the Jaguar quantum mechanical program from Schrodinger.[50] Structures were optimized with the M06 functional[51] combined with the LACVP** basis set.[52] Single point energies for the optimized structures were calculated using M06 and the def2-TZVP[53] basis set. Stationary point structures were confirmed to be minima or first-order saddle points by calculating the vibrational frequencies using analytical second derivatives. Images were produced using CYLView.[54]

Reported free energies are:

(U)M06/def2-TZVP(THF)//(U)M06/LACVP**(gas) at 298 K and 1 atm

$\Delta G = \Delta E_{(def2\text{-}TZVP)} + \Delta G_{solv(def2\text{-}TZVP)} + \Delta E_{ZPE(LACVP**)} + \Delta U_{(LACVP**)} + nRT - T\Delta S_{(gas\ phase)}$. $\Delta G_{solv(def2\text{-}TZVP)}$.

5.4.4 Synthesis:

Generation of Ni(η^2-C_2F_4)(dppe) (5-1a) and Ni(C_4F_8)(dppe) (5-2a)

Solid $Ni(cod)_2$ (10 mg, 0.036 mmol) and dppe (14 mg, 0.036 mmol) were dissolved in 0.5 mL of C_6D_6 in an NMR tube sealed with rubber cap. Using a 3 mL syringe, 1 mL of TFE was inserted directly into the NMR tube. The reaction mixture was light orange and left at RT. ^{19}F NMR spectra were recorded after 5 min, 1 and 2 h. **5-1a**: -125.6 ppm (t, $^3J_{FP}$ = 31 Hz, 4F). **5-2a**: -97.7 (s, $2F_\alpha$), -134.7 ppm (s, $2F_\beta$). $^{31}P\{^1H\}$ NMR: **5-1a**: -2.98 ppm **5-2a**: -0.7 ppm.

Generation of Ni(η^2-C_2F_4)(dppf) (5-1b) and Ni(C_4F_8)(dppf) (5-2b)

Solid $Ni(cod)_2$ (10 mg, 0.036 mmol) and dppf (20 mg, 0.036 mmol) were dissolved in 0.5 mL of C_6D_6 in a NMR tube sealed with rubber cap. Using a 3 mL syringe, 1 mL of TFE was inserted directly into the NMR tube. The reaction mixture was light orange and left at RT. ^{19}F NMR spectra were recorded after 5 min, 2 and 8 h. ^{19}F NMR (benzene) **5-1b**: δ -130.1 ppm (t, $^3J_{FP}$ = 24 Hz, 4F) and **5-2b**: δ -98.4 ppm (t, $^3J_{FP}$ = 29 Hz, $2F_\alpha$), -136.6 ppm (s, $2F_\beta$). $^{31}P\{^1H\}$ NMR: **5-1b**:18.5 ppm **5-2b**: 18.5 ppm. ^{19}F NMR (THF) **5-1b**: δ -127.8 ppm (t, $^3J_{FP}$ = 24 Hz, 4F) and **5-2b**: δ -96.1 (t, $^3J_{FP}$ = 28 Hz, $2F_\alpha$), -134.2 (s, $2F_\beta$). $^{31}P\{^1H\}$ NMR: **5-1b**:22 ppm **5-2b**: 22 ppm. ^{19}F NMR (acetone) **5-1b**: δ -131.6 ppm (t, $^3J_{FP}$ = 23 Hz, 4F) and **5-2b**: δ -100.4 ppm (t, $^3J_{FP}$ = 28 Hz, $2F_\alpha$), -137.6 ppm (s, $2F_\beta$). $^{31}P\{^1H\}$ NMR: **5-1b**:18.1 ppm **5-2b**: 18.1 ppm.

Generation of Ni(η^2-C_2F_4)(DPEphos) (5-1c), Ni(C_4F_8)(κ^2-DPEphos) (5-2c) and Ni(C_4F_8)(κ^3-DPEphos) (5-3)

Solid $Ni(cod)_2$ (10 mg, 0.036 mmol) and DPEphos (20 mg, 0.036 mmol) were dissolved in 0.5 mL of benzene in a NMR tube sealed with rubber cap. Using a 3 mL syringe, 1 mL of TFE was inserted directly into the NMR tube. The reaction mixture was light orange and left at RT. ^{19}F NMR spectra were recorded after 5 min, 1 and 2 h. **5-1c**: -130.6 (s, 4F), **5-2c**: δ -101.6 (s, $2F_\alpha$), -136.3 (s, $2F_\beta$) and **5-3** δ -97.5 (br s, $2F_\alpha$), -134.3 ppm (br s, $2F_\beta$). **5-3** at -35 °C: -92, -109.02 ppm (d, $^2J_{FF}$ = 262 Hz, F_α), -127.2, -145.5 ppm (d, $^2J_{FF}$ = 255 Hz, F_b) $^{31}P\{^1H\}$ NMR: **5-1c**: 16.3 ppm **5-2c**: 16.3 ppm **5-3** 15.38 ppm.

In another identical experiment, after 12 h complex **5-2c** crystallized quantitatively from the reaction mixture and, after filtration, ^{19}F NMR spectra were obtained at different temperatures to investigate the fluxional process occurring for **5-3.** MS of **5-2c** [EI], m/z calculated for $C_{40}H_{28}F_8NiOP_2$. 797.7, found 796.7 $(M-H)^+$.

Synthesis of Ni(Bisbi)(COD)

Solid $Ni(cod)_2$ (100 mg, 0.36 mmol) was placed in a 15 mL vial glass and dissolved in 5 mL of benzene. Solid Bisbi (200 mg, 0.36 mmol) was added to the solution and the color changed from light yellow to orange. After stirring for 2 h at RT, the reaction mixture was concentrated in vacuo and precipitated with pentane. The product was filtered and dried affording an orange powder (252 mg, 98%). $^{31}P\{^1H\}$ NMR: 36.7 ppm.

Synthesis of Ni(C_4F_8)(Bisbi) (5-4)

Solid Ni(COD)(Bisbi) was dissolved in 0.5 mL of benzene in a NMR tube sealed with rubber cap. Using a 3 mL syringe, 1 mL of TFE was inserted directly into the NMR tube. The reaction mixture did not change color and was left at RT. ^{19}F NMR spectra were recorded after 5 min, 1 and 2 h. ^{19}F NMR (282 MHz, toluene) **5-4a**: -124.5 (dm, $^{2}J_{FF}$ = 182 Hz, 2*F*), -129.6 ppm (dm, $^{2}J_{FF}$ = 182 Hz, 2*F*); **5-4b**: -99.1 (s, 1F), -133.8 ppm (s, F); **5-4c** -87.7 (dd, $^{2}J_{FF}$ = 253 Hz, CF_2), - 99.8 (dt, $^{2}J_{FF}$ = 253, $^{3}J_{FP}$ = 30 Hz, CF_2), -128 (dd, $^{2}J_{FF}$ = 247 Hz, CF_2), -137.8 ppm (dd, $^{2}J_{FF}$ = 247 Hz, CF_2).

Synthesis of Ni(C_4F_8)(TMEDA) (5-2d)

Solid Ni(cod)$_2$ (10 mg, 0.036 mmol) and TMEDA (4.2 mg, 0.036 mmol) were dissolved in 0.5 mL of acetone in an NMR tube sealed with rubber cap. Using a 3 mL syringe, 1 mL of TFE was inserted directly into the NMR tube. The reaction mixture was light orange and left at 50 ^{o}C. ^{19}F NMR **5-2d**: -111.6 (s, 2F), -140.6 ppm (s, 2F).

Synthesis of Ni(C_4F_8)(bipyridine) (5-2e)

Solid Ni(cod)$_2$ (10 mg, 0.036 mmol) and bipyridine (6 mg, 0.036 mmol) were dissolved in 0.5 mL of THF in a NMR tube sealed with rubber cap. Using a 3 mL syringe, 1 mL of TFE was inserted directly into the NMR tube. The reaction mixture was light orange and left at 50 ^{o}C. ^{19}F NMR **5-2e**: -105.9 (s, 2F), -136.5 ppm (s, 2F).

Synthesis of Ni(C_4F_8)(pyridine)$_2$ (5-2f)

Solid Ni(cod)$_2$ (10 mg, 0.036 mmol) and pyridine (6 mg, 0.072 mmol) were dissolved in 0.5 mL of acetone in a NMR tube sealed with rubber cap. Using a 3 mL syringe, 1 mL of TFE was inserted directly into the NMR tube. The reaction mixture was light orange and left at 50 ^{o}C. ^{19}F NMR **5-2f**: -112.18 (s, 2F), -139.51 ppm (s, 2F).

5.5 REFERENCES

1. Petit, J.; Magna, L.; Mézailles, N. Alkene oligomerization via metallacycles: Recent advances and mechanistic insights. *Coord. Chem. Rev*. **2022**, *450*, 214-227.
2. a) Sydora, O. L. Selective ethylene oligomerization. *Organometallics* **2019**, *38*, 997–1010. b) Kwon, D.-H.; Maley, S. M.; Stanley, J.; Sydora, O. L.; Bischof, S. M.; Ess, D. H. Why

less coordination provides higher reactivity chromium phosphinoamidine ethylene trimerization catalysts. *ACS Catal*. **2020**, *10*, 9674-9683.

3. Ishii, S.; Nakano, T.; Kawamura, K.; Kinoshita, S.; Ichikawa, S.; Fujita, T. Development of new selective ethylene trimerization catalysts based on highly active ethylene polymerization catalysts. *Catal. Today* **2018**, *303*, 263–270.
4. Venderbosch, B.; Oudsen, J.-P. H.; Martin, D. J.; de Bruin, B.; Korstanje, T. J.; Tromp, M. Investigating the active species in a [(R-SN(H)S-R)$CrCl_3$] ethene trimerization system: Mononuclear or dinuclear? *ChemCatChem* **2020**, *12*, 881-892.
5. Steelman, D. K.; Aluthge, D. C.; Lehman, M.C.; Labinger, J.A.; Bercaw, J. E. Mechanistic studies on selective trimerization of linear a-olefins over a supported titanium catalyst. *ACS Catal.* **2017**, *7*, 4922–4926.
6. Bouwkamp, M. W.; Bowman, A. C.; Lobkovsky, E.; Chirik, P. J. Iron-catalyzed [2p+2p] cycloaddition of a,w-dienes: The importance of redox-active supporting ligands. *J. Am. Chem. Soc.***2006**, *128*, 13340–13341.
7. Hoyt, J. M.; Sylvester, K. T.; Semproni, S. P.; Chirik, P. J. Synthesis and electronic structure of bis(imino)pyridine iron metallacyclic intermediates in iron-catalyzed cyclization reactions. *J. Am. Chem. Soc.* **2013**, *135*, 4862–4877.
8. Hoyt, J. M.; Schmidt, V.A.; Tondreau, A.M.; Chirik, P. J. Iron-catalyzed intermolecular [2+2] cycloadditions of unactivated alkenes. *Science* **2015**, *349*, 960–963.
9. Hu, L.; Chen, H. Substrate-dependent two-state reactivity in iron-catalyzed alkene [2+2] cycloaddition reactions. *J. Am. Chem. Soc.* **2017**, *139*, 15564–15567.
10. Joannou M.V.; Hoyt, J.M.; Chirik, P. J. Investigations into the mechanism of inter- and intramolecular iron-catalyzed [2+2] cycloaddition of alkenes. *J. Am. Chem. Soc.* **2020**, *142*, 5314–5330.
11. Schmidt, V. A.; Hoyt, J. M.; Margulieux, G. W.; Chirik, P.J. Cobalt-catalyzed [2p+2p] cycloadditions of alkenes: Scope, mechanism, and elucidation of electronic structure of catalytic intermediates. *J. Am. Chem. Soc.* **2015**, *137*, 7903–7914.
12 Gao, Y.; Emge, T. J.; Krogh-Jespersen, K.; Goldman, A. S. Selective dehydrogenative coupling of ethylene to butadiene via an iridacyclopentane complex. *J. Am. Chem. Soc.* **2018**, *140*, 2260–2264.

13. Doyle, M. J. Binger, P. Nickelacyclopentane derivatives as intermediates in the nickel(0) catalysed cyclodimerization of strained ring olefins. *J. Chem. Soc., Chem. Commun*. **1976**, 376–377.
14. Binger, P. Metallacycloalkanes: I. Preparation and characterisation of α,α′-bipyridyl-5-nickela-3,3,7,7-tetramethyl-*trans*-tricyclo[4.1.0.$0^{2,4}$]heptane. *J. Organomet. Chem.* **1977**, *135*, 405–414.
15. Binger, P.; Doyle, M. J.; Krüger, C.; Tsay, Y. Metallacycloalkane. III. Darstellung und charakterisierung von a,a′-dipyridyl-nickelacyclopentan /Preparation and characterisation of a,a′-bipyridyl-nickelacyclopentane. *Z. Naturforsch.* **1979**, *34b*, 1289–1292.
16. Grubbs, R.H.; Miyashita, A.; Liu, M.; Burk, P. The preparation and reactions of nickelocyclopentanes. *J. Am. Chem. Soc.* **1977**, *99*, 3863–3864.
17. Grubbs, R.H.; Miyashita, A.; Liu, M.; Burk, P. Preparation and reactions of phosphine nickelocyclopentanes. *J. Am. Chem. Soc.* **1978**, *100*, 2418–2425.
18. Grubbs, R.H.; Miyashita, A. The relationship beween metallacyclopentanes and bis(olefin) metal complexes. *J. Am. Chem. Soc.* **1978**, *100*, 1300–1302.
19. Grubbs, R.H.; Miyashita, A. Metallacyclopentanes as catalysts for the linear and cyclodimerization of olefins. *J. Am. Chem. Soc.* **1978**, *100*, 7416–7418.
20. Ohashi, M.; Kawashima, T.; Taniguchi, T.; Kikushima, K.; Ogoshi, S. 2,2,3,3-Tetrafluoronickelacyclopentanes generated via the oxidative cyclization of tetrafluoroethylene and simple alkenes: A key intermediate in nickel-catalyzed C–C bond-forming reactions *Organometallics* **2015**, *34*, 1604–1607.
21. Moser, E.; Jeanneau, E.; Mézailles, N.; Olivier-Bourbigou, H.; Breuil, P.-A. R. Simplified and versatile access to low valent Ni complexes by metal-free reduction of Ni(II) precursors. *Dalton Trans.* **2019**, *28*, 4101–4104.
22. Stockis, A.; Hoffmann, R. Metallacyclopentanes and bisolefin complexes. *J. Am. Chem. Soc*. **1980**, *102*, 2952-2962.
23. Bernardi, F.; Bottoni, A.; Rossi, I. A DFT investigation of ethylene dimerization catalyzed by Ni(O) complexes. *J. Am. Chem. Soc.* **1998**, *120*, 7770–7775.
24. a) Manuel, T. A.; Stafford, S.L.; Stone, F. G. A. Chemistry of the metal carbonyls. Part VII. Perfluoroalkyl iron compounds. *J. Am Chem. Soc*. **1961**, *83*, 249-250. b) Hoehn, H. H.; Pratt,

L.; Watterson, K. F.; Wilkinson, G. Transition-metal fluorocarbon complexes. Part I. Derivatives of perfluoro-olefins. *J. Chem. Soc.* **1961**, 2738–2745.

25. Clarke, B.; Green, M.; Stone, F. G. A. Reactions of low-valent metal complexes with fluorocarbons. Part XI. Chlorocarbonylbis(methyldiphenylphosphine)iridium and chlorodinitrogenbis(triphenylphosphine)iridium. *J. Chem. Soc. A, Inorg., Phys. Theor*. **1970**, 951-955.
26. Greco, A.; Green, M.; Shakshooki, S. K.; Stone, F. G. A. Ring expansion reactions in organonickel chemistry. *J. Chem. Soc. D, Chem. Commun*. **1970**, 1374-1375.
27. Green, M.; Shakshooki, S. K.; Stone, F. G. A. Reactions of low-valent metal complexes with fluorocarbons. Part XVIII *t*-Butyl isocyanide–nickel complexes. *J. Chem. Soc. A, Inorg. Phys. Theor*. **1971**, 2828-2834.
28. Browning, J.; Green, M.; Stone, F. G. A. Reactions of low-valent metal complexes with fluorocarbons. Part XVII. Tertiary arsine–nickel complexes. *J. Chem. Soc. A, Inorg. Phys. Theor* . **1971**, 453-457.
29. Maples, P. K.; Green, M.; Stone, F. G. A. Reactions of low-valent metal complexes with fluorocarbons. Part XXVI. 1,1,1-Tris(diphenylphosphinomethyl)- and 1,1,1-tris(diphenylarsinomethyl)-ethane. *J. Chem. Soc., Dalton Trans*. **1973**, 388-392.
30. Stone, F. G. A. The role of fluorocarbons in oxidative-addition and reductive-elimination reactions. *Pure Appl. Chem*. **1972**, *30*, 551-574.
31. Ohashi, M.; Shibata, M.; Saijo, H.; Kambara, T.; Ogoshi, S. Carbon–fluorine bond activation of tetrafluoroethylene on palladium(0) and nickel(0): Heat or Lewis acidic additive promoted oxidative addition. *Organometallics* **2013**, *32*, 3631-3639.
32. Kaschube, W.; Schröder, W.; Pörschke, K. R.; Angermund, K.; Krüger, C. Amin-nickel-komplexe VI. Synthese, struktur und reaktivität von (tmeda)Ni(C_2F_4). *J. Organomet. Chem*. **1990**, *389*, 399-408.
33. Schröder, W.; Bonrath, W.R.; Pörschke, K. Synthese und reactivität von (2,6-iPr_2Ph-dad)Ni(C_2F_4). *J. Organomet. Chem*. **1991**, *408*, C25-C29.
34. Hunter, N.M. High-valent perfluoronickelacycles: Intermediates for “green” routes to fluorocarbons and their derivatives. University of Ottawa MSc thesis, 2011.
35. Uneyama, K. *Organofluorine Chemistry*, Wiley-Blackwell, 2006.

36. Ni-TFE complexes: (a) Browning, J.; Penfold, P.R. Crystal and molecular structure of tetrafluoroethylene-1,1,1-tris-(diphenylphosphinomethyl)ethane nickel. *J. Chem. Soc., Chem. Commun.* **1973**, 198-199. (b) Ohashi, M.; Saijo, H.; Shibata, M.; Ogoshi, S. Palladium-catalyzed base-free Suzuki–Miyaura coupling reactions of fluorinated alkenes and arenes via a palladium fluoride key intermediate. *Eur. J. Org. Chem.* **2013**, 443-447.

37. Ni(C_4F_8) metallacycles: (a) Burch, R.R.; Calabrese, J.C.; Ittel, S.D. Fluoroorganometallic chemistry: Carbon-fluorine bond activation in perfluorometallacyclopentane complexes. *Organometallics* **1988**, *7*, 1642-1648. b) Gasafi-Martin, W.; Oberendfellner G.; von Werner, K. A facile synthesis of metalla-octafluorocyclopentane complexes of ruthenium and nickel. *Can. J. Chem.* **1996**, *74*, 1922-1924. (c) Kaplan, P.T.; Xu, L.; McGarry, K.R.; Yu, S.; Wang, H.; Vicic, D.A. Mild, safe, and versatile reagents for $(CF_2)_n$ transfer and the construction of fluoroalkyl-containing rings. *Organometallics* **2013**, *32*, 7552-7558. (d) Yu, S.; Dudkina, Y.; Wang, H.; Kholin, K.V.; Kadirov, M.K.; Budnikova, Y.H.; Vicic, D.A. Accessing perfluoroalkyl nickel(II), (III), and (IV) complexes bearing a readily attached [C_4F_8] ligand. *Dalton Trans.* **2015**, *44*, 19443-19446. (e) Kosobokov, M.D.; Sandleben, A.; Vogt, N.; Klein, A.; Vicic, D.A. Nitrogen–nitrogen bond formation via a substrate-bound anion at a mononuclear nickel platform. *Organometallics* **2018**, *37*, 521-525. (f) Bour, J.R.; Ferguson, D.M.; McLain, E.J.; Kampf, J.W.; Sanford, M.S. Connecting organometallic Ni(III) and Ni(IV): Reactions of carbon-centered radicals with high -valent organonickel complexes *J. Am. Chem. Soc.* **2019**, *141*, 8914-8920. (g) Shirataki, H.; Ono, T.; Ohashi, M.; Ogoshi, S. Ni(0)-catalyzed three-component coupling reaction of tetrafluoroethylene and *N*-sulfonyl-substituted imines with silanes via aza-nickelacycles. *Org. Lett.* **2019**, *21*, 851-856.

38. Fuller, J. T.; Harrison, D. J.; Leclerc, M. C.; Baker, R. T.; Ess, D. H.; Hughes, R. P. A new stepwise mechanism for formation of a metallacyclobutane via a singlet diradical intermediate. *Organometallics* **2015**, *34*, 5210-5213.

39. Sicard, A.J.; Ghaffari, B.; Gabidullin, B.M.; Ovens, J.S.; Hughes, R.P.; Baker, R.T. Nickel-catalyzed homologation of vinylidene difluoride (CH_2=CF_2): Selective β-F vs β-H elimination. *J. Am. Chem. Soc.* **2022**, *144*, in press.

40. Andrella, N.O.; Sicard, A.J.; Gorelsky, S.I.; Korobkov, I.; Baker, R.T. A T-shaped Ni[κ^2-$(CF_2)_4$–] NHC complex: Unusual C_{sp3}–F and M–C^F bond functionalization reactions. *Chem. Sci*. **2015**, *6*, 6392-6397.
41. Casey, C. P.; Whiteker, G. T. The Natural Bite Angle of Chelating Diphosphines. *Isr. J. Chem*. **1990**, *30*, 299-304.
42. van Leeuwen, P. W. N. M.; Kamer, P. C. J.; Reek, J. N. H.; Dierkes, P. Ligand Bite Angle Effects in Metal-catalyzed C−C Bond Formation. *Chem Rev*. **2000**, *100*, 2741-2770.
43. Adams, G. M.; Weller, A. S. POP-type ligands: Variable coordination and hemilabile behaviour. *Coord. Chem. Rev*. **2018**, *355*, 150-172.
44. Hunadi, R. J.; Baum, K. Tetrafluoroethylene: A convenient laboratory preparation. *Synthesis* **1982**, *39*, 454.
45. Sicard, A. J.; Baker; R. T. Safe and Expeditious Preparation of $Ni(cod)_2$ for Same Day High-Throughput Screening," *Org. Proc. Res. Devel.* **2020**, *24***,** 2950-2952.
46. APEX Software Suite v 2010 Bruker AXS Inc. Madison Wisconsin USA, 2010.
47. Blessing, R. H. An Empirical Correction for Absorption Anisotropy. *Acta Crystallogr.* **1995**, *A51*, 33–38.
48. Sheldrick, G. M. A Short History of SHELX *Acta Crystallogr.* **2008**, *A64*, 112–122.
49. Hübschle, C. B.; Sheldrick, G. M.; Dittrich, B. *ShelXle*: A Qt Graphical User Interface for *SHELXL*. *J. Appl. Crystallogr.* **2011**, *44*, 1281–1284.
50. (a) Bochevarov, A. D.; Harder, E.; Hughes, T. F.; Greenwood, J. R.; Braden, D. A.; Philipp, D. M.; Rinaldo, D.; Halls, M. D.; Zhang, J.; Friesner, R. A. Jaguar: A high performance quantum chemistry software program with strengths in the life and materials sciences. *Int. J. Quantum Chem.* **2013**, *113*, 2110-2142; (b) Jaguar, versions 7.0-9.3, Schrödinger, LLC, New York, NY: 2007-2016.
51. (a) Zhao, Y.; Truhlar, D. G. The M06 suite of density functionals for main group thermochemistry, thermochemical kinetics, noncovalent interactions, excited states, and transition elements: two ne functionals and systematic testing of four M06 class functionals and 12 other functionals. *Theor. Chem. Acc.* **2008**, *120*, 215-241; (b) Zhao, Y.; Truhlar, D. G. Density functionals with broad applicability in chemistry. *Acc. Chem. Res.* **2008**, *41*, 157-167.

52. (a) Dunning, T. H.; Hay, P. J., In *Modern Theoretical Chemistry, Vol. 4: Applications of Electronic Structure Theory.* Schaefer, H. F., III (Editor); Plenum, NY: 1977 ; (b) Wadt, W. R.; Hay, P. J. *Ab initio* effective core potentials for molecular calculations. Potentials for main group elements Na to Bi. *J. Chem. Phys.* **1985**, *82*, 284-298; (c) Hay, P. J.; Wadt, W. R. *Ab initio* effective core potentials for molecular calculations. Potentials for K to Au including the outermost core orbitals. *J. Chem. Phys.* **1985**, *82*, 299-310; (d) Hay, P. J.; Wadt, W. R. *Ab initio* effective core potentials for molecular calculations. Potentials for the transition metal atoms Sc to Hg. *J. Chem. Phys.* **1985**, *82*, 270-283.

53. (a) Schaefer, A.; Huber, C.; Ahlrichs, R. Fully optimized contracted Gaussian basis sets of triple zeta valence quality for atoms Li to Kr. *J. Chem. Phys.* **1994**, *100*, 5829-5835; (b) Schaefer, A.; Horn, H.; Ahlrichs, R. Fully optimized contracted Gaussian basis sets of triple zeta valence quality for atoms Li to Kr. *J. Chem. Phys.* **1992**, *97*, 2571-2577

54. Legault, C. Y. CYLview, 1.0b, Université de Sherbrooke: Université de Sherbrooke, 2009.

Chapter 6: Synthesis and Reactivity of Functionalized Fluoro-Nickelacyclopentanes

Contributions to Knowledge:

Synthesis and Reactivity of Functionalized Fluoro-Nickelacyclopentanes

*Luana L. T. N. Porto, Loic P. F. Mangin, Jeffrey A. Ovens and R. Tom Baker,** to be submitted, 2022.

Chapter Contributions: Luana Porto performed all the experiments and wrote the first draft. Dr. Jeffrey Ovens and Dr. Loic P. F. Mangin collected and refined the X-ray diffraction data for molecular structure determination and Prof. Baker helped plan the experiments, analyze NMR data, and refine the manuscript text.

Abstract: Fluoronickelacyclopentanes, typically formed by reactions of low-valent nickel complexes with fluoroalkenes, are key intermediates in the synthesis of hydrofluorocarbons (by hydrogenolysis or b-F elimination / organosilane reduction) and fluorinated ketones (by cycloaddition / β-H elimination). In an effort to better understand substituent effects on their reactivity, we have prepared a series of nickel complexes from perfluoro(methyl vinyl ether) (PMVE) and chlorotrifluoroethylene (CTFE). In addition to L_2Ni olefin complexes, both fluoroalkenes react with $Ni(cod)_2$ + 2 equiv of $P(O^iPr)_3$ to give regioselective formation of the nickelacyclopentanes, $Ni[-CFX(CF_2)_2CFX-][P(O^iPr)_3]_2$ (X = OCF_3, Cl) as *trans*-diastereomers. While the complex with X = OCF_3 is stable, removal of solvent with X = Cl affords CTFE and $Ni(cod)[P(O^iPr)_3]_2$. Reaction of both metallacycles with dppp [1,3-bis(diphenylphosphino)-propane] displaces the phosphite ligands, affording a single diastereomer of electron-rich congeners Ni[-CFX$(CF_2)_2$CFX-](dppp) that are both stable to solvent removal. In contrast, reaction of CTFE with $Ni(cod)_2$ and 2 equiv of PPh_3 yields the perfluorovinyl complex, $NiCl(CF{=}CF_2)(PPh_3)_2$ from oxidative addition of the C-Cl bond. Using the wide bite-angle Xantphos ligand, however, affords the alkene complex and metallacyclopentanes that include two diastereomers of the head-to-tail regioisomer, Ni[-$CFClCF_2CFClCF_2$-](Xantphos). While the CTFE-derived dppp metallacycle does not react with Lewis acids such as $ZnCl_2$ and Me_3SiOTf, the Xantphos analog undergoes selective Cα-F bond cleavage with the latter reagent to form a new complex proposed to be the dichloropentafluorocyclobutyl complex, Ni(OTf)(σ-$CFCF_2CF_2CFCl$-](Xantphos). In contrast, reaction of a mixture of the dppp CTFE alkene complex and metallacycle with trifluoroacetic acid protonated the Ni-C^F bond of the alkene complex exclusively, providing insight into substituent effects on reactivity of fluoronickelacycles.

6.1 INTRODUCTION

Advantages of fluorocarbons (vs. hydrocarbons), such as the strength of C-F bonds due to high polarity, small size, and low polarizability, as well as reduced flammability, reflect their increased demand as refrigerants, foam-blowing agents, and monomers for high-value fluoropolymers.[1] Development of the 4th generation of F-gases, hydrofluoroolefins (HFOs), in air-conditioning and

refrigeration came with the necessity of decreasing their global warming potential.[2] One effective way to synthesize HFOs is by transition metal catalysis and environmental concerns with traditional methods employing HF and heavy metals have stimulated development of this area.[3] Organometallic nickel chemistry has played an important role in this field, allowing for the functionalization of easily accessed fluorometallacycles as described in Chapters 1 and 5.[4,5]

In 1996, Baker *et al.*, working at DuPont CR&D, demonstrated hydrogenolysis of the Ni-C^F bond in phosphite-ligated Ni perfluoronickelacyclopentanes at elevated temperature, giving rise to the catalytic hydrodimerization of TFE to $H(CF_2)_4$.[6] This process was also successful with trifluoroethylene (CF_2=CFH, TrFe) giving predominantly $HCF_2(CHF)CF_2CH_2F$) and $HCF_2(CHF)_2CF_2H$)], and with a 10:1 mixture of ethylene and TFE to give 1,1,2,2-tetrafluoro-n-butane. In later work, Andrella of the Baker group prepared the three-coordinate NHC perfluoronickelacyclopentane which undergoes hydrogenolysis at room temperature and 1 atm (**Scheme 6.1**). Building on earlier work by Burch (also at Dupont CR&D), C_α-F abstraction from

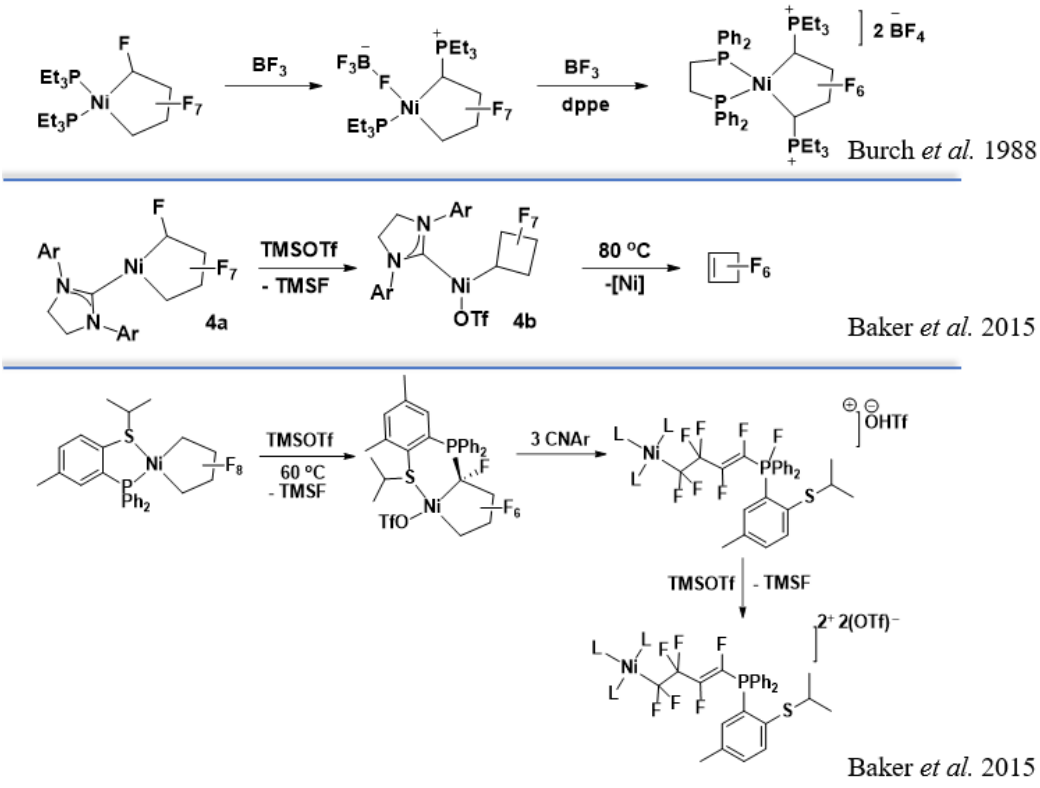

Scheme 6.1 Reactivity of perfluoronickelacyclopentanes with Lewis acids.

Andrella's complex using trimethylsilyl trifluoromethanesulfonate (TMSOTf) was accompanied by Ni-C^F bond cleavage, C^F-C^F bond formation, and subsequent β-F elimination to give perfluorocyclobutene.[7] Baker *et al.* also showed that xylylisocyanide ligand substitution promoted cleavage of both Ni-C^F and C_β-F bonds.[8]

Following up on Stone's cyclization of Ni(0) with TrFe and PPh_2Me,[9,10] Baker *et al.* showed that regioselectivity could be influenced significantly by ancillary ligands (**Scheme 6.2)**. Treatment of the head-to-tail isomers of the $Ni(PMePh_2)_2$ metallacycles with boron trifluoride etherate ($BF_3.OEt_2$) or TMSOTf resulted in multiple C-F bond activations (**Scheme 6.3**).[11] In contrast, reaction of Andrella's 3-coordinate, TFE derived Ni(NHC) metallacycle with Brønsted acids gave HF or C^Fα-H bond formation depending on the acid strength (**Scheme 6.4**).[7] Finally, employing the monoligand nickel strategy with vinylidene fluoride (CF_2=CH_2, VDF) afforded dimeric $[Ni(\mu\text{-}F)(CF_2CH_2CF{=}CH_2)L]_2$ via β-F elimination from the head-to-tail metallacycle. Inclusion of a hydrosiloxane then gave 2,4,4-trifluorobut-1-ene exclusively via Ni-catalyzed hydrodefluorodimerization (**Scheme 6.5**).[12]

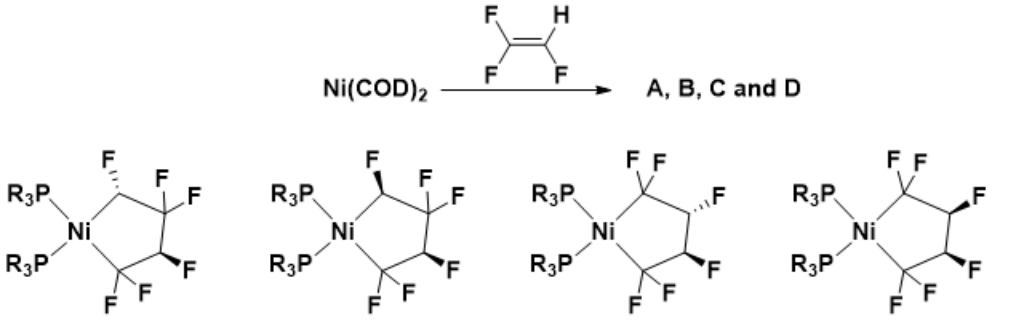

P	A (%)	B (%)	C (%)	D (%)
PPh_2Me	25	53	20	2
PPh_3	25	53	17	4
$P(O\text{-}o\text{-}tolyl)_3$	20	53	21	6

Scheme 6.2 Controlling fluoronickelacycle regioselectivity with ancillary ligands

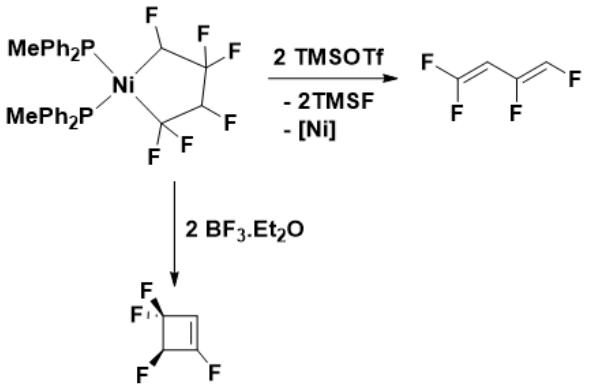

Scheme 6.3 Reactions of Ni TrFE metallacycle with Lewis acids.

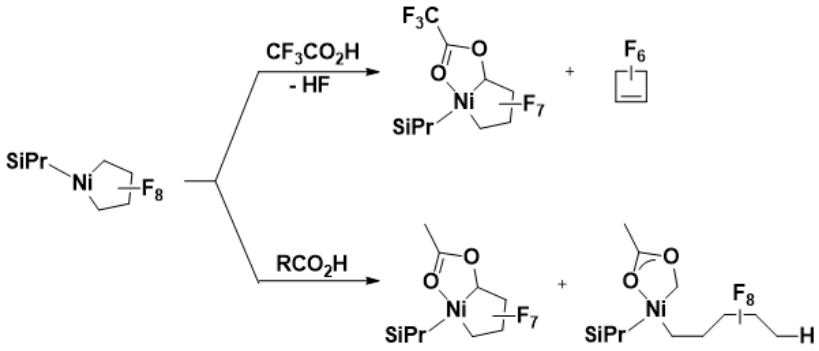

Scheme 6.4 Reactions of $Ni(C_4F_8)(SIPr)$ with carboxylic acids

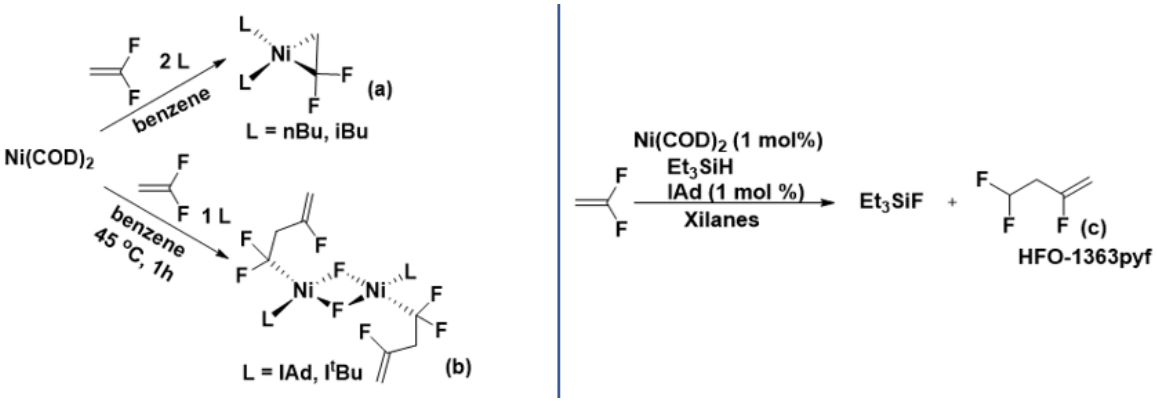

Scheme 6.5 Ni-catalyzed hydrodefluorodimerization of VDF

Inspired by this work, we expanded the scope to include the functionalized fluoroalkenes, chlorotrifluoroethylene (CF_2=CFCl, CTFE) and trifluoromethyl vinyl ether ($CF(OCF_3)$=CF_2,

PMVE) with several different ancillary ligands on nickel. We also explored the reactivity of the resulting fluoronickelacyclopentanes with several Lewis and Brønsted acids.

6.2 RESULTS AND DISCUSSION

6.2.1 Synthesis of functionalized nickelacyclopentanes and nickel alkene complexes from perfluoro(methyl vinyl ether) (PMVE)

Treatment of $Ni(cod)_2$ (cod = 1,5-cyclooctadiene) with 2 equiv of triisopropylphosphite, $P(O^iPr)_3$, and excess (5 equiv) perfluoro(methyl vinyl ether) [PMVE, $CF_2=CF(OCF_3)$] at room temperature in benzene after 4 h gave a 1:1 mixture of the nickel alkene complex, $Ni[\eta^2\text{-}CF_2=CF(OCF_3)][P(OiPr)_3]_2$ (**6-1a**) and regio- and stereospecific formation of nickelacyclopentane, $Ni[\text{-}CF(OCF_3)\text{-}CF_2CF_2CF(OCF_3)\text{-}][P(O^iPr)_3]_2$ (**6-2a; Scheme 6.6)**. Interestingly, the **6-1a:6-2a** ratio remains unchanged in the presence of PMVE after several days, suggesting that metallacyclopentane formation is reversible. The ^{19}F NMR spectrum of the reaction mixture displayed two new broad OCF_3 resonances at -51.6 and -51.9 ppm in a 2:1 ratio due to **6-2a** and **6-1a**, respectively (**Figure 6.1A**). For **6-2a** the two broad doublets for the diastereotopic CF_2 groups show a typical sp^3 $^2J_{FF}$ coupling of 249 Hz but the C_α-F resonance does not show coupling to P which is 46 Hz from the triplet ^{31}P NMR resonance (**Figure 6.1B**). In contrast, **6-1a** shows a single triplet CF_2 resonance and a singlet CF resonance in keeping with the $^3J_{FP}$ coupling of 42 Hz observed in the $^{31}P\{^1H\}$ NMR spectrum (see Appendix). The molecular structure of **6.2a**, confirmed by single-crystal X-ray diffraction analysis, consists of a distorted square planar nickel center with C_2-Ni-C_5 and P_1-Ni-P_2 angles of 87.5 and 95.4°, respectively (**Figure 6.2**).

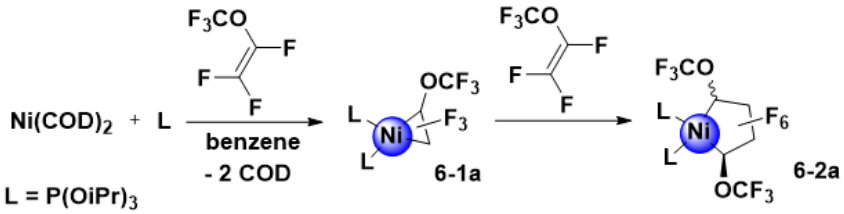

Scheme 6.6 Synthesis of complexes **6-1a** and **6-2a** from Ni(0), $P(O^iPr)_3$ and PMVE.

As seen previously with TFE,[13] use of bulkier ancillary ligands often afford the alkene complex (or metallacyclopropane) exclusively. Indeed, treatment of $Ni(cod)_2$ with 2 equiv of tri-*o*-tolylphosphite, $P(O\text{-}o\text{-}tol)_3$, and excess (5 equiv) PMVE at room temperature in benzene after 4 h gave exclusively the alkene complex, $Ni[\eta^2\text{-}CF_2{=}CF(OCF_3)][P(O\text{-}o\text{-}tol)_3]_2$ (**6-1b; Scheme 6.7**).

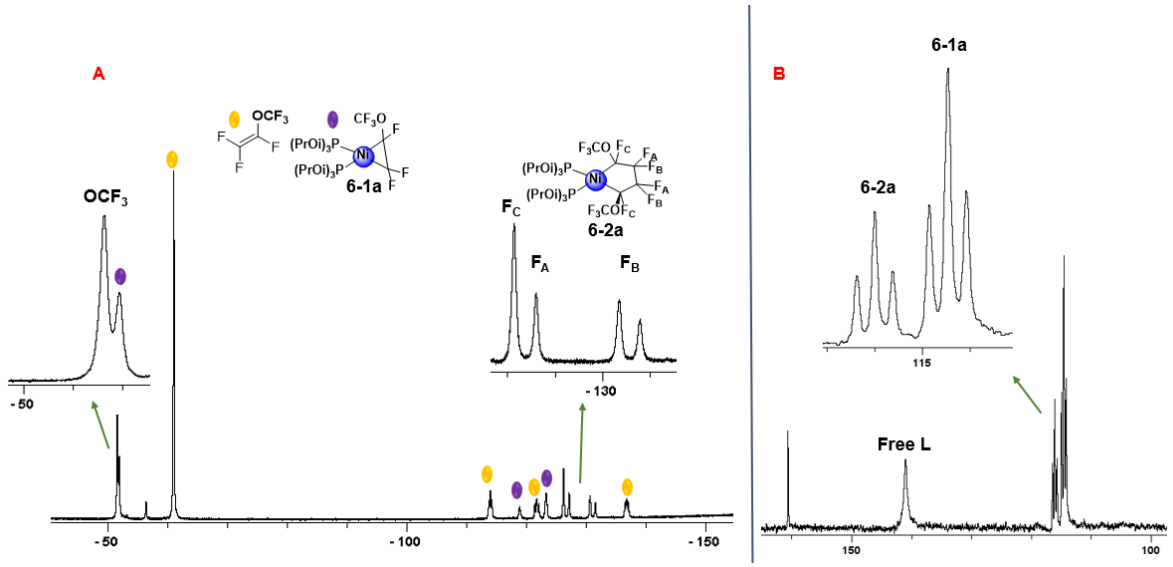

Figure 6.1 ^{19}F (**A**) and $^{31}P\{^1H\}$ NMR spectra (**B**) of **6-1a** and **6-2a**

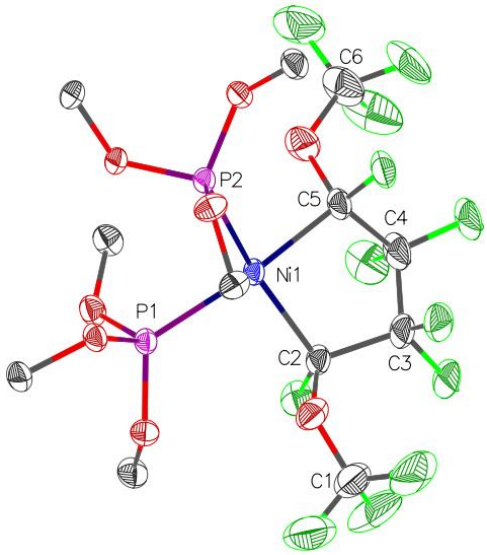

Figure 6.2 Molecular diagram representation of molecular structure of **6-1a**. Thermal ellipsoid probabilities are set to 30% with hydrogen atoms, disordered OCF_3 and terminal Me of i-Pr are omitted. Selected bond distances (Å) and angles (deg): Ni-P1: 2.2085(5) Ni-P2 2.2108(4) Ni-C2: 1.9416(17) NiC5: 1.9448(18) P1-Ni-P2: 95.41(2) P1-Ni-C2: 92.36(6) P1-Ni-C5: 159.35(7) P2-Ni-C5: 91.90(6) P2-Ni-C2: 159.00(6), C1-Ni-C5: 87.54(8).

The ^{19}F NMR spectrum of **6-1b** features two broad doublet resonances for the CF_2 ($^2J_{FF}$ = 176 Hz) one of which is also coupled significantly to the other F ($^3J_{FF}$ = 76 Hz). The $^{31}P\{^1H\}$ NMR spectrum showed a single resonance at 127.6 ppm, indicative of fast rotation of the alkene with respect to the Ni-centroid axis. Similar results were obtained with PPh_3 (**6-1c**) (cone angle = 145° vs. 140° for P(O-*o*-tol)$_3$) and chelating bis(phosphine) 1,3-bis-(diphenylphosphino)propane

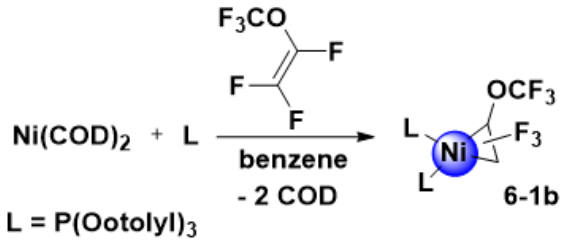

Scheme 6.7 Synthesis of complex **6-1b** from Ni(0), P(O-*o*-tol)$_3$ and PMVE.

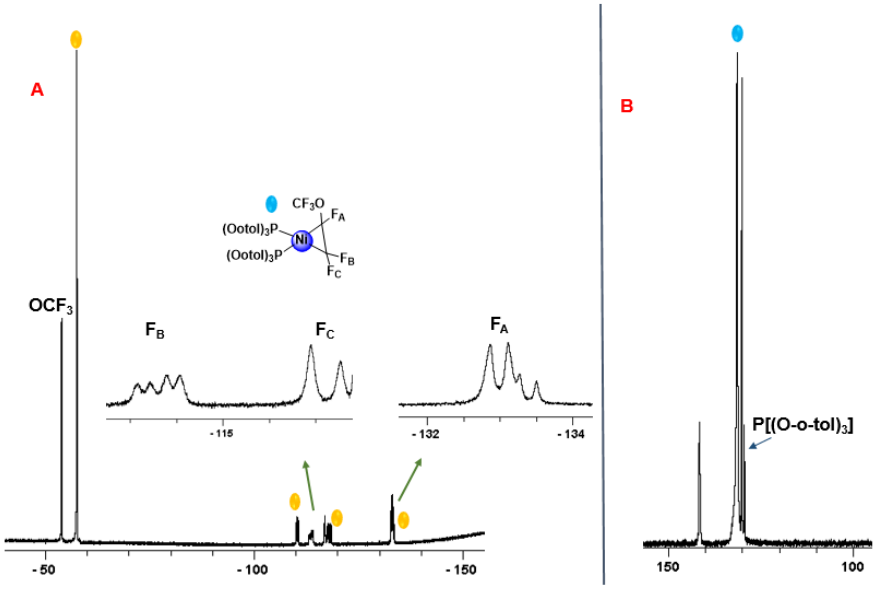

Figure 6.3 ^{19}F (**A**) and $^{31}P\{^1H\}$ NMR spectra (**B**) of **6-2**

(dppp, **6-1d**; see Appendix). In contrast, the reaction of NiL_2 with PMVE, in which L is the wide bite angle bis(phosphine) Xantphos, afforded both alkene complex (**6-1e**) and nickelacyclopentane (**6-2b**). Attempts with more electron-rich phosphines such as tricyclohexyl or tricyclopentyl phosphines, however, led to significant by-product formation including formation of P-F bonds. As a result, we pursued ligand substitution of the **6-1a/6-2a** reaction mixture. Although we were

unable to obtain clean reactions with NHC ligands or electron-rich P^iPr_3, reaction of **6-1** with 1,2-bis(diphenylphosphino)ethane (dppe) gave metallacycle Ni[-CF(OCF_3)-CF_2CF_2CF(OCF_3)-](dppe) (**6-2c**) and a five-coordinate alkene complex, Ni[η^2-CF_2=CF(OCF_3)][dppe][$P(O^iPr)_3$] (**6-3; Scheme 6.8)** as confirmed by ^{31}P NMR. The similarity of the ^{19}F NMR spectrum of **6-2c** and **6-3** to that of **6-2a** and **6-1a** is apparent (**Figure 6.4**). The alkene complex **6-3** was characterized further by single crystal X-ray

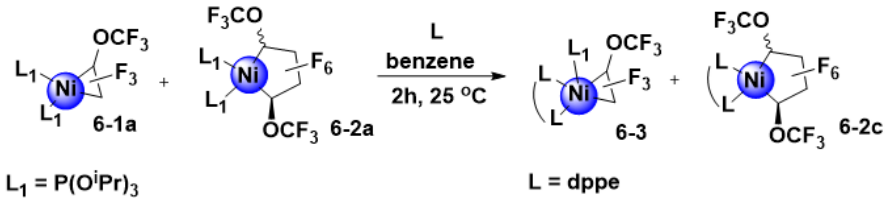

Scheme 6.8 Synthesis of complexes **6-2c** and **6-3** from reaction of **6-1a/6-2a** with dppe.

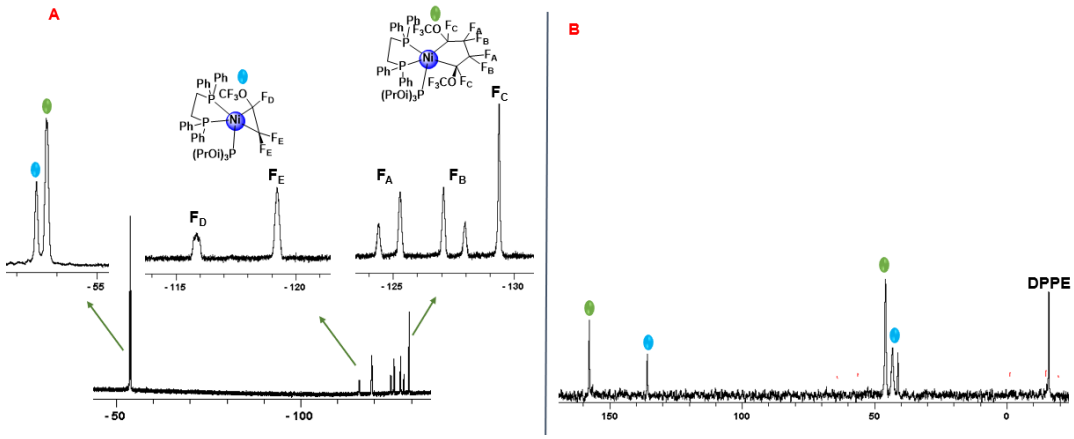

Figure 6.4 ^{19}F (**A**) and ^{31}P{^{1}H} NMR spectra (**B**) of **6-2c** and **6-3**.

diffraction (**Figure 6.5**). The structure consists of a distorted tetrahedral geometry about Ni with C1-C2 centroid angles to P of 120.5(1)-121.8(1)º, 124,4(1)-125.7(1)° and 114.7(1)º. The disparate Ni-C bond distances to the PMVE ligand with alternate conformations (Ni-C1 = 1.868(6)-1.892(2) Å, Ni-C2 = 1.926(2)-1.948(5) Å) reflect the bulky (OCF_3) group on C2.

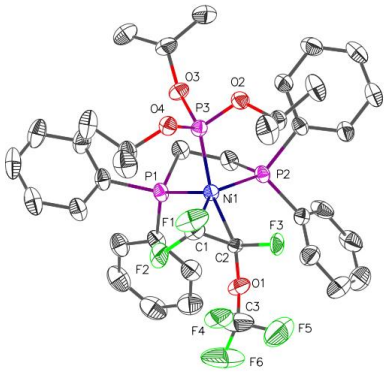

Figure 6.5 Molecular diagram representation of the molecular structure of **6-3**. Thermal ellipsoid probabilities are set to 50% with hydrogen atoms omitted. Selected bond distances (Å) and angles (deg): Ni-P1 2.2185(4) Ni-P2 2.2895(4) Ni-P3 2.1827(4) Ni-C1 1.868(6)-1.892(2) Ni-C2 1.926(2)-1.948(5) P1-Ni-P2 86.453(14) P1-Ni-P3 102.166(15) Ni-$C_{1,2centroid}$ 1.775(1) P1-Ni-$C_{1,2centroid}$ 120.5(1)-121.8(1) P2-Ni-P3 101.995(15) P2-Ni-$C_{1,2centroid}$ 124.4(1)-125.7(1) P3-Ni- $C_{1,2centroid}$ 114.7(1).

6.2.2 Synthesis of functionalized nickelacyclopentanes, nickel alkene, and -vinyl complexes from chlorotrifluoroethylene (CTFE)

In assessing the reactions of Ni(0) complexes with chlorotrifluoroethylene (CTFE, CF_2=CFCl) it became apparent that phosphite ligands were most suitable as the majority of others led rapidly to the perfluorovinyl complexes via C-Cl oxidative addition (see below). The reaction of $Ni(cod)_2$ and 3 equiv of $P(O^iPr)_3$ with 5 equiv of CTFE in benzene after 2 h at room temperature yielded a mixture of alkene complex, $Ni(\kappa^2\text{-}CF_2{=}CFCl)[P(O^iPr)_3]_2$ (**6-4a**) and selective formation of metallacyclopentane (**6-5**); after 24 h the main product was vinyl complex, $NiCl(\kappa^1\text{-}CF{=}CF_2)[P(O^iPr)_3]_2$ (**6-6a**). (**Scheme 6.9**). In contrast to the PMVE reactions, removal of solvent left only the vinyl complex, demonstrating the reversibility of both alkene and metallacyclopentane complexes. As observed for PMVE the reaction with bulkier phosphite P(O-*o*-tol)$_3$ gave initially the alkene complex (**6-4b**) and then the vinyl complex **(6-6b**) (see Chapter 6 Appendix). Similar behavior was observed for the wide bite-angle bis(phosphine), DPEphos, (forming alkene complex **6-4c** and then vinyl complex **6-6c**), whereas PPh_3 led directly to the vinyl complex (**6-6d**). Interestingly, chiral ligand BINAP gave two diastereomeric alkene complexes **6-4d/6-4d'**without formation of the vinyl complex (Fig. A6.23). In order to obtain a more stable electron-rich metallacycle, we assessed reactions of the above mixture at short reaction times with alternate ancillary ligands.

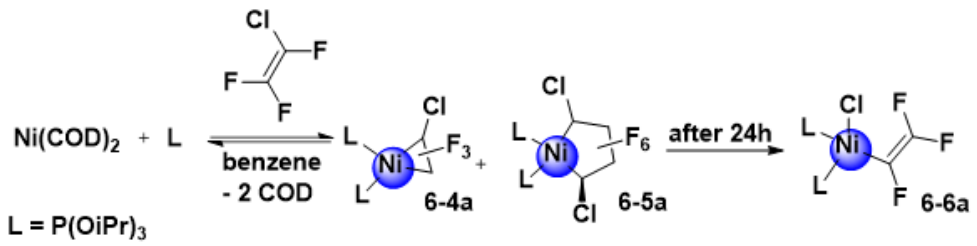

Scheme 6.9 Synthesis of **6-4a, 6-5** and **6-6a** from $Ni(cod)_2$, $P(O^iPr)_3$ and CTFE.

Monitoring by ^{19}F NMR spectroscopy, 1 equiv of L (L = phenanthroline, dppp and dppe) reacted with **6-4a** and **6-5** with phosphite ligand displacement yielding **6-7a-c** and **6-5a-c**. To investigate their stability, the solution from the NMR tube was transferred to a glass vial and dried in vacuum. Upon redissolution, ^{19}F NMR confirmed the presence of both **6-5a-c** and **6-7a-c**. Due to solubility issues, we only scaled up the reaction to isolate **6-7b** and **6-5a-c** complexes. Although the solid-state molecular structure for **6-7b** obtained by single crystal X-ray diffraction was of poor quality, the crystal for olefin complex **6-7c** confirmed the five-coordinate structure (**Figure 6.6**).

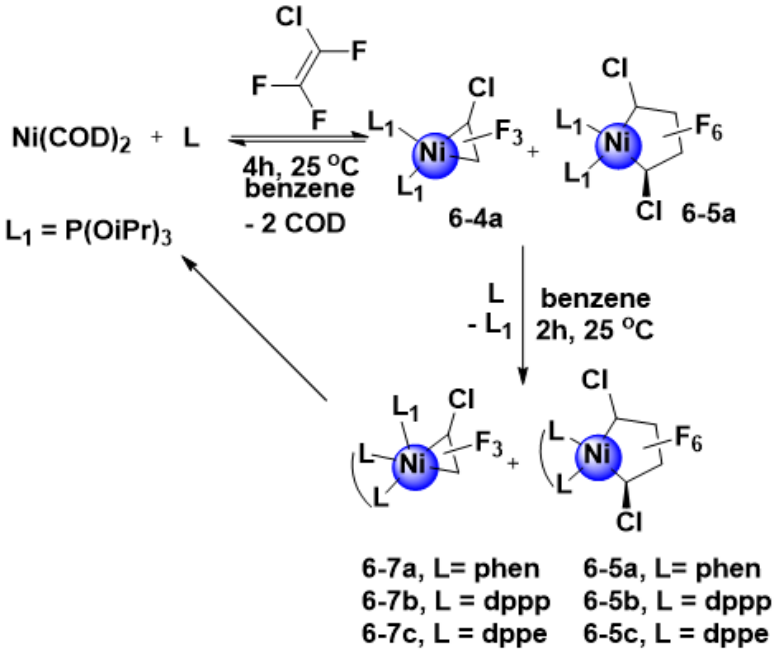

Scheme 6.10 Synthesis of stable CTFE-derived nickelacycles.

Finally, reaction of CTFE with $Ni(Xantphos)_2$ again gave both alkene complex (**6-4e)** and metallacycle products (and at longer reaction times vinyl complex **6-6e**). However, in addition to the tail-to-tail regioisomer (**6-5d**) observed with PMVE, we now see two stereoisomers of the

head-to-tail regioisomer (**6-8a,b**; **Scheme 6.11**). The structure of the latter is confirmed in the ^{19}F NMR spectrum by observation of P-F coupling in both Cα*F* and diastereotopic CαF_2 groups. The ^{19}F-^{19}F-COSY NMR also helped us to identify the peaks related to each product.

6.2.3 Reactions of nickelacycles with Lewis and Brønsted acids

Treatment of the 2:1 mixture of the PMVE-derived DPPE nickelacycles **6-3** and **6-2c** with Lewis acids such as $ZnCl_2$ or TMSOTf gave no reaction even after heating at 60 °C for 12 h. In contrast, treatment of the CTFE-derived Xantphos nickelacycles depicted in **Scheme 6-11** with TMSOTf afforded the dichloropentafluorocyclobutyl complex, Ni(OTf)(σ-$CFCF_2CF_2CFCl$-](Xantphos) from selective C_α-F bond cleavage of the major nickelacyclopentane isomer **(Scheme 6-12).**

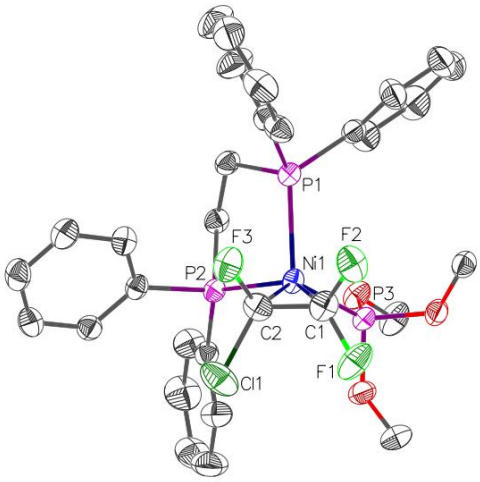

Figure 6.6 Molecular diagram representation of the molecular structure of **6-7c**. Thermal ellipsoid probabilities are set to 50% with hydrogen atoms omitted. Selected bond distances (Å) and angles (deg): Ni-P1 2.3219(4) Ni-P2 2.2074(4) Ni-P3 2.1582(4) Ni-C1 1.8970(15) Ni-C2 1.9197(16) P1-Ni-P2 88.132(14) P1-Ni-P3 107.754(15) Ni-$C_{1,2centroid}$ 1.771(2) P1-Ni-$C_{1,2centroid}$ 116.6(1) P2-Ni-P3 97.493(15) P2-Ni-$C_{1,2centroid}$ 123.5(1) P3-Ni- $C_{1,2centroid}$ 118.3(1).

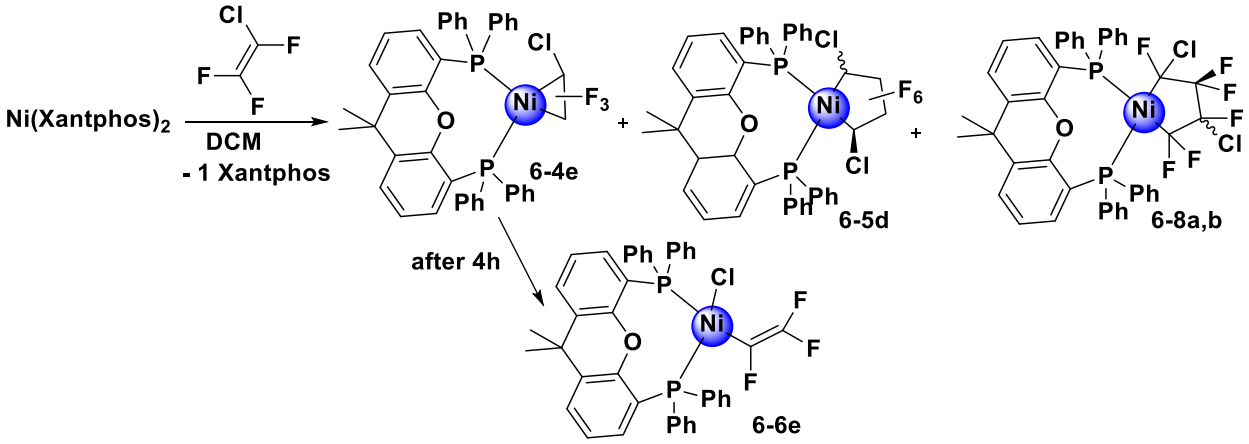

Scheme 6.11 Synthesis of Xantphos alkene complex **6-4e**, metallacycles **6-5d** and **6-8a,b** and vinyl complex **6-6e.**

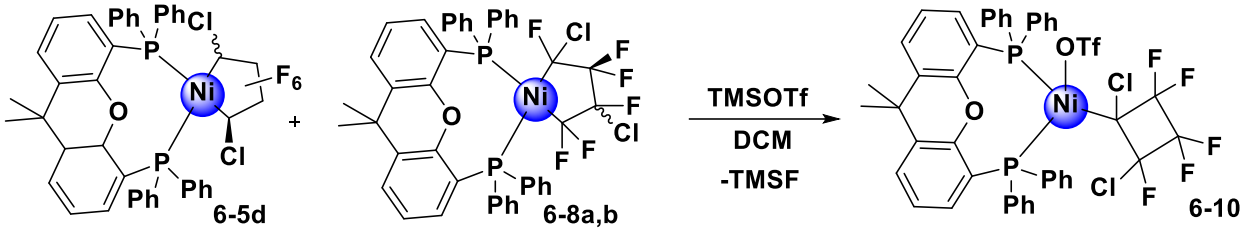

Scheme 6.12 Reaction of nickelacycle **6-5d** with TMSOTf.

On comparing the Brønsted acid reactivity of the CTFE-derived dppp mixture of nickelacycles **6-5b** and **6-7b** with that reported previously by Andrella in **Scheme 6-4** we were surprised to find exclusive and selective cleavage of the Ni-C^F bond of the alkene complex, affording two complexes bearing the Ni-CF_2CHFCl group (**Scheme 6-13**) as evidenced by ^{19}F NMR spectroscopy (**Figure 6.11**). Although we were unable to separate the reaction products from unreacted metallacyclopentane, we propose that the two products reflect the similar energies of isomers that differ in the coordination of the trifluoroacetate anion to Ni, *i.e.*, either κ^1- vs κ^2-monomeric product or bis(κ^1-bridged) dimer *vs* κ^2-monomer.

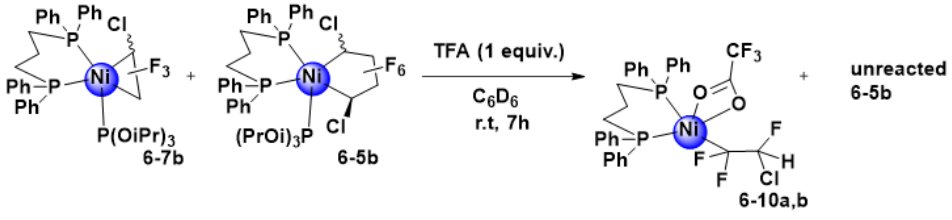

Scheme 6.13 Reaction of nickelacycle mixture **6-5b** / **6-7b** with trifluoroacetic acid.

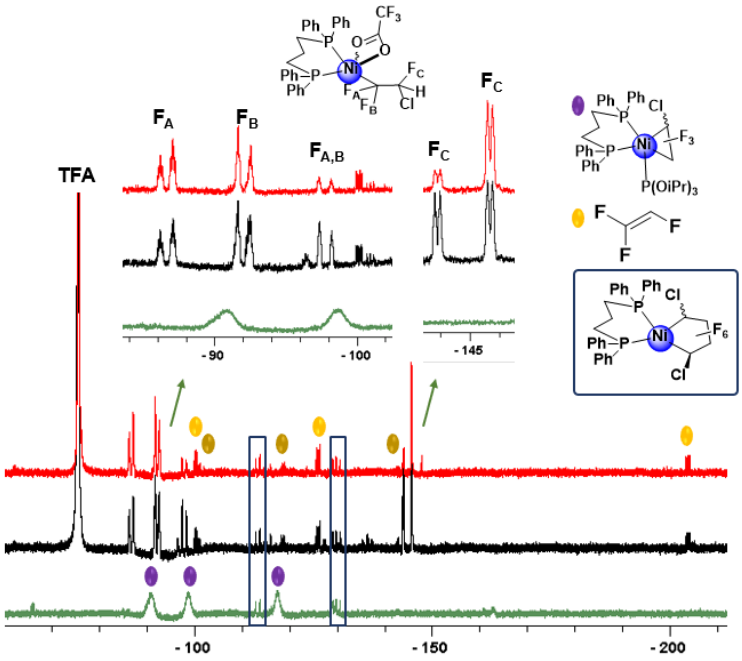

Scheme 6.14 ^{19}F NMR (282 MHz, C_6D_6) spectrum of Ni[$C_4Cl_2F_6$](dppp) (**6-5b**) and Ni[C_2ClF_3](dppp)-[(P(O^{i}Pr)$_3$] (**6-7c**) (green line) plus trifluoroacetic acid after 7 h (black line) and 16 h (red line).

6.3 CONCLUSION

The work reported in this chapter reveals how sensitive the synthesis and reactivity of fluoronickelacycles are to the substituents on carbon. While previous work had indicated a steric effect in formation of 3- vs 5-membered rings, the electronic effects in forming nickelacyclopentanes from VDF become more subtle for the fluoroalkenes studied here. While we obtained some evidence for reversibility of metallacyclopentane formation from the alkene complex using PMVE and triisopropylphosphite, with CTFE the reversibility extended to formation of the alkene complex. Moreover, only with the BINAP ligand did we not see eventual conversion of the alkene complex to the vinyl complex via C-Cl oxidative addition. On the other hand, electron-rich phosphines readily reacted with PMVE, limiting our ability to access more electron-rich metallacycles. We were successful, however, in preparing several stable electron-rich metallacycles from both PMVE and CTFE by ligand substitution of the triisopropylphosphite derivatives, although short reaction times were required for CTFE.

Regioselective formation of the tail-to-tail isomer also results presumably from electronic effects although steric effects likely dictate the stereospecificity for the *trans* disposition of the Cl

or OCF_3 groups. These results can be compared with those for VDF in which the large dipole dictates head-to-tail regioselectivity and to TrFE which typically yields at least 4 of the possible regio- and stereoisomers. This brings us to the unique reactivity of Xantphos, the only bis(phosphine) that reacts cleanly with PMVE and the only one that affords metallacycles form CTFE although now with eroded regiochemistry presumably resulting from the steric pressure of having both Cl substituents on the alpha carbons.

Finally, in comparing the metallacycle reactivity with Lewis and Brønsted acids, the stability and or structure of the PMVE-derived metallacycles seems to prevent access to the activated C_α-F bond. Such steric effects may also explain the reactivity of trifluoroacetic acid exclusively at the $C_\alpha F_2$ group of the CTFE complex which does not exist in the corresponding metallacyclopentanes. We should be able to test this hypothesis using the Xantphos metallacycles two of which appear to contain such a $C\alpha F_2$ group. In fact, scaling up the selective reaction of TMSOTf with these Xantphos metallacycles would allow us to perhaps characterize alternate cyclobutyl complexes, heating of which should yield the free dichlorocyclobutenes.

In summary, our study of these functionalized metallacycles opens the door to further studies of mixed fluoroalkene metallacycles and eventual reactivity control to develop further Ni-catalyzed homologations to new fluoroalkenes.

6.4 EXPERIMENTAL SECTION

6.3.1 General procedures: Experiments were conducted under nitrogen, using Schlenk techniques or an MBraun glove box. All solvents were deoxygenated by purging with nitrogen. Toluene, hexanes, diethyl ether (DEE) and tetrahydrofuran (THF) were dried on columns of activated alumina using a J. C. Meyer (formerly Glass Contour®) solvent purification system. Benzene-d_6 (C_6D_6) was dried by stirring over activated alumina (ca. 10 wt.%) overnight, followed by filtration. Acetonitrile (CH_3CN) and dichloromethane (DCM) were dried by refluxing over calcium hydride under nitrogen. After distillation, they were dried further by stirring over activated alumina (ca. 5 wt.%) overnight, followed by filtration. All solvents were stored over activated (heated at ca. 250 ^oC for >10 h under vacuum) 4 Å molecular sieves. Glassware was oven-dried at 150 ^oC for >2 h. The following chemicals were obtained commercially without further purification, as indicated: 1,3-Bis(diphenylphosphino)propane (Dppp, Sigma-Aldrich, 97%), trimethylsilyl

trifluoromethanesulfonate (Me_3SiOTf, Aldrich, 99%), triphenylphosphine (PPh_3. SigmaAldrich, 99%) , triisopropyl phosphite ($P(OiPr)_3$, Aldrich, 95%), tri-ortho-tolyl phosphite ($P(O\text{-}o\text{-}tolyl)_3$), Alfa Aesar, 97%), 1,2-bis(diphenylphosphino)ethane, (Dppe, AlfaAesar, 97%), 1,1′-ferrocenediyl-bis(diphenylphosphine), (Dppf, Sigma-Aldrich, 97%), bis[(2-diphenylphosphino)phenyl] ether (DPEphos, Sigma-Aldrich, 972,2'-bis(diphenylphosphinomethyl)-1,1'-biphenyl, 99% (Bisbi, Strem, 99%), acetone (Sigma-Aldrich, ≥99.8%, HPLC grade), 1,4-dioxane (Sigma-Aldrich, ≥99.8%, anhydrous), nickel(II) acetylacetonate (EMD Millipore, >98%), Trifluoroacetic acid (*ReagentPlus*®, 99%), Zinc Chloride (TCI America), 1,5-cyclooctadiene (TCI America, >98%), di-n-butylmagnesium (Sigma-Aldrich, 1.0 M solution in heptane) and n-butyl-s-butylmagnesium (Sigma-Aldrich, 0.7 M solution in hexane), Bis(1,5-cyclooctadiene)nickel [$Ni(cod)_2$] was prepared by a literature procedure.[14] ^{19}F and $^{31}P\{^1H\}$ NMR spectra were recorded on a 300 MHz Bruker Avance instrument at room temperature (21-23 °C) unless stated otherwise.. ^{19}F and ^{31}P NMR chemical shifts are reported relative to trifluorotoluene at -62 ppm. Electrospray ionization mass spectral data were collected using an Applied Biosystem API2000 triple-quadrupole mass spectrometer and EI mass spectra were collected.

6.3.2 Generation of nickelacycles from PMVE- NMR Scale: Solid $Ni(cod)_2$ (10 mg, 0.036 mmol) was suspended in ca. 0.5 mL of benzene in a NMR tube, followed by addition of the ligand for each reaction: 2 equiv of triisopropylphosphite (18 µL, 0.072 mmol), tri-*o*-tolylphosphite $P[O\text{-}o\text{-}tol)_3$ (25 µL, 0.072 mmol), triphenylphosphine, PPh_3 (19 mg, 0.072 mmol), methyldiphenylphosphine, PPh_2Me (13 µL, 0.072 mmol) or tricyclohexylphosphine, PCy_3 (20 mg, 0.072 mmol), 1 equiv of 1,3-bis(diphenylphosphino)propane, dppp (20 mg, 0.036 mmol) or Xantphos (20.8 mg,, 0.036 mmol). After adding the ligand, the NMR tube was sealed with cap and parafilm and 2.5 mL of PMVE was added by syringe. The reaction was left at 25 °C and monitored by ^{19}F NMR.

$P(OiPr)_3$: ^{19}F NMR **6.1a** -52.0 (s, OCF_3), -118.9 ppm (t, $^3J_{FP}$ = 45 Hz, CF), –123.4 (t, $^3J_{FP}$ = 44 Hz CF_2). **6.2a** -51.6 (s, OCF_3), -126.8 (s, CF), -126.3 and -131.2 ppm (d, $^2J_{FF}$ = 251 Hz, CF_2). $^{31}P\{^1H\}$ NMR **6.1a** 114.0 ppm (t, 45 Hz) **6.2a** 115.9 ppm (t, 45 Hz).

$P(O\text{-}o\text{-}tol)_3$: ^{19}F NMR **6.1b** -53.8 (s, OCF_3), -113.6 (dd, $^2J_{FF}$ = 179, $^3J_{FF}$ = 75 Hz, CF_2), -117.2 (d, $^2J_{FF}$ = 179 Hz, CF_2), -133.9 ppm (d, $^3J_{FF}$ = 75 Hz CF). $^{31}P\{^1H\}$ NMR 131.5 ppm (br s).

PPh_3: ^{19}F NMR **6.1c** -50.8 (dd, $^4J_{FF}$ = 8, $^5J_{FF}$ = 5 Hz, OCF_3), -114.4 ppm (dq, $^2J_{FF}$ 186, $^3J_{FF}$ = 79 Hz J^{FF}7 Hz CF_2), – 118.5 (d, J^{FF}186 Hz, CF_2), -134.7 (d, $^3J_{FF}$ 79 Hz, CF). $^{31}P\{^1H\}$ NMR 30.5 ppm (br s).

dppp: ^{19}F NMR **6.1d** -52.9 (s, OCF_3), -117.1 (dd, $^2J_{FF}$ = 190 Hz, $^3J_{FF}$ = 75 Hz CF_2), -119.5 (dt, $^2J_{FF}$ = 190 Hz, $^3J_{FP}$ = 30 Hz, CF_2), -137 ppm (d, $^3J_{FF}$ = 75 Hz CF).

Xantphos: ^{19}F NMR **6.1e** -52.8 (d tr, OCF_3), -123.3 (mult, CF), -123.5 ppm (mult, CF_2). **6.2b** -51.3 (d tr, OCF_3), -129.0 (s, CF), -129.4 and -132.7 ppm (d mult, $^2J_{FF}$ = 179 Hz, CF_2). $^{31}P\{^1H\}$ NMR **6.1e** 39.3 ppm (ov mult). **6.2b** 37.5 ppm (d, 22 Hz).

6.3.3 Generation of electron-rich PMVE-derived nickelacycles:

To the mixture of **6.1a** and **6.2a** from the P(OiPr)3 reaction was added 1 equiv of dppe that gave metallacycle **6.2c** and five-coordinate alkene complex **6.3**. ^{19}F NMR 6.3 -53.5 (s, OCF3), -115.8 (mult, CF), -119.2 ppm (mult, CF_2). 6.2c -53.6 (br s, OCF_3), -124.7 and 127.4 (d mult, $2J_{FF}$ = 248 Hz, CF_2), -129.2 ppm (s, CF). $^{31}P\{^1H\}$ NMR **6.3** 161.2 (br s, $P(OiPr)_3$), 46.9 ppm (br s, dppe). **6.2c** 49.4 ppm (br s).To **6.1b** from the $P(O\text{-}o\text{-}tol)_3$ reaction was added 1 equiv of IMes or 2 equiv of $PiPr_3$ but neither gave clean reactions.

6.3.4 Synthesis of nickelacycles from PMVE:

Synthesis of 6.1a

Solid $Ni(cod)_2$ (100 mg, 0.36 mmol) was dissolved/suspended in ca. 5 mL of benzene in a 20 mL glass-vial and 2 equiv of triisopropylphosphite (167 µL, 0.72 mmol) were added. The colour changed from yellow to orange. The vial was then degassed, charged with 30 mL of PMVE and stirred at 25 ^oC for 24 h. No major colour change occurred. The solvent was evaporated and the residue washed with hexane. Approximately 2 mL of toluene was then added, followed by 0.5 mL of hexane and the mixture left to sit at -35 ^oC for 24 h. Large yellow crystals of **2a** suitable for X-ray analysis formed.

Synthesis of 6-2c/6-3 mixture

Solid $Ni(cod)_2$ (100 mg, 0.36 mmol) and triisopropylphosphite (167 µL, 0.72 mmol) were charged with 30 mL of PMVE as above and stirred at 25 ^oC for 24 h. The solvent was then evaporated and the residue washed with hexane. The resulting oil was dissolved in 5 mL of benzene and 1 equiv. of DPPE (144 mg, 0.36 mmol) was added to the solution. The reaction was left stirring for 2 h at 25 ^oC. The solvent was then evaporated, washed with Et_2O and hexanes and dried in vacuo to yield 223 mg of a yellow solid 2:1 mixture of **6-2c** and **6-3** [95% based on $Ni(cod)_2$].

Synthesis of Ni[(Xantphos)$_2$]

$Ni(cod)_2$ (150 mg, 0.54 mmol) was dissolved/suspended in ca. 5 mL of benzene in a 20 mL glass-vial. 2 equivalents of (9,9-Dimethyl-9H-xanthene-4,5-diyl)bis(diphenylphosphane) (Xantphos) (631 mg, 1.09 mmol). The reaction stirred at 25 ^oC for 2 hours and precipitated a strong wine-red colour. The solvent was evaporated and washed with hexane and filtered of 30 mL medium pore fritted funnel and dried in vacuo to yield a wine-red solid 636 mg (0.52 mmol, 97% based on $Ni(cod)_2$. $^{31}P\{^1H\}$ NMR 6.8, 5.6 ppm (ov mult).

Synthesis of 6-1e/6-2b mixture

$Ni(Xantphos)_2$ (100 mg, 0.082 mmol) was dissolved/suspended in ca. 5 mL of benzene in a 20 mL glass-vial and 30 mL of PMVE was added. The reaction was stirred at 25 °C for 24 h and the colour changed to pink red. The solvent was then evaporated and the residue washed with Et_2O and hexanes, filtered and dried in vacuo to yield 64 mg of a yellow solid 1:1 mixture of **6-1e** and **6-2b** (80% based on $Ni(Xantphos)_2$).

6.3.5 Generation of nickelacycles from CTFE- NMR scale: Solid $Ni(cod)_2$ (10 mg (0.036 mmol) was dissolved/ suspended in ca. 0.5 mL of benzene in an NMR tube, followed by addition of the ligand for each reaction: 2 equiv. of triisopropylphosphite (18 µL, 0.072 mmol), tri-o-tolylphosphite $P(O\text{-}o\text{-}tol)_3$ (25 µL, 0.072 mmol), triphenylphosphine PPh_3 (19 mg, 0.072 mmol), 1 equiv of bis [(2-diphenylphosphino)phenyl] ether, DPEphos (19 mg, 0.036 mmol) or 2,2′-bis(diphenylphosphino)-1,1′-binaphthyl, BINAP (22.3 mg, 0.036 mmol). After adding the ligand, the NMR tube was sealed with cap and parafilm and 2.5 mL of CTFE was added. The reaction was then left at 25 °C and monitored by ^{19}F NMR.

$P(OiPr)_3$: ^{19}F NMR **6-4a** –109.1 (d, $^2J_{FF}$ = 172 Hz, C*F*), -112.3 (dd, $^2J_{FF}$ = 172, $^3J_{FF}$ = 174 Hz, C*F*), -140.8 ppm (d, $^3J_{FF}$ = 174 Hz, C*F*). **6-5** –112.4 (dm, $^2J_{FF}$ = 235 Hz, CF_2), -126.6 (td, J_{FP} = 57 Hz, J_{FF} = 21 Hz, C*F*α), -130.1 ppm (dm, J_{FF} = 235 Hz, CF_2). **6-6a** –89.8 (dd, $^3J_{FF}$ = 112, 39 Hz, C*F*), -132.5 (dt, $^3J_{FF}$ = 112, $^2J_{FF}$ = 107 Hz, C*F*) -161.2 ppm (dd, $^2J_{FF}$ = 107, 39 Hz, C*F*). $^{31}P\{^1H\}$ NMR **6-4a** 114.0 ppm (t, 45 Hz) **6-5** 115.9 ppm (t, 45 Hz) **6-6a.** 96.9 ppm (s).

$P(O\text{-}o\text{-}tol)_3$: ^{19}F NMR **6-4b** -108.4 ($^2J_{FF}$ = 174 Hz, C*F*), -115.3 ($^2J_{FF}$ = 174 Hz, C*F*) and –144.3 ppm ($^3J_{FP}$ = 51 Hz, C*F*). **6-6b** –84.1 (dd, $^3J_{FF}$ = 107, $^2J_{FF}$ = 40 Hz, C*F*), -128.2 (dt $^2J_{FF}$ = 109, $^3J_{FF}$ = 107 Hz, C*F*), -159.3 ppm (dd, $^2J_{FF}$ = 109, J_{FP} = 40 Hz, C*F*). $^{31}P\{^1H\}$ NMR **6-4b** 132.2 ppm (br s). **6-6b** 85.7 ppm (br mult).

PPh_3: ^{19}F NMR **6-6c** –89.1 (dd, $^2J_{FF}$ = 107, $^3J_{FF}$ = 25 Hz, C*F*), - 131.2 (t, C*F*, $^2J_{FF}$ = $^3J_{FF}$ = 107 Hz), - 157.6 ppm (dd, C*F*, $^3J_{FF}$ = 108, $^3J_{FF}$ = 25 Hz). **6-6c** $^{31}P\{^1H\}$ NMR **6-6c** 29.1 ppm (br s).

DPEphos: **6-4c** –104.7 (d, $^2J^{FF}$ = 172 Hz, CF), - 109.2 (dt, J_{FF} = 172 Hz, J_{FF} = 81 Hz,) and - 141.4 ppm (d J_{FF} = 81 Hz, CF). **6-6d** –81.7 (br, C*F*), -127.2 (br, C*F*), –154.9 ppm (br, C*F*). $^{31}P\{^1H\}$ NMR **6-4c** 20.4 ppm (br s)**.**

BINAP: ^{19}F NMR **6-4d/6-4d'** -106.1 (dmult, $^2J_{FF}$ = 171 Hz, C*F*), -107.8 (dmult, $^2J_{FF}$ = 171 Hz C*F*), -110.8 (dmult, $^2J_{FF}$ = 171 Hz, C*F*), -113.8 ppm (dmult, J_{FF} = 171 Hz, C*F*), -143.3 (mult, C*F*), -143.6 (mult, C*F*).

6.3.6 Generation of electron-rich CTFE-derived nickelacycles: To the **6-4a/6-5a** mixture from the $P(O^iPr)_3$ reaction was added 1 equiv of L in benzene at room temperature and ^{19}F NMR was analyzed after 2 hours.

phen: ^{19}F NMR **6-5a** -109.4 and -127.3 (d, $^2J_{FF}$ = 238 Hz CF_2), -125.7 ppm (t, $^3J_{FP}$ = 45 Hz, CF). **6-7a** -92 (t, $^2J_{FF}$ = 188 Hz), -93 (dt, $^2J_{FF}$ = 188 Hz, $^3J_{FF}$ = 86 Hz) -110.9 ppm (86 26 Hz, Hz).

dppe: ^{19}F NMR **6-7b** – 104.7 ppm (d, $^{2}J^{FF}$ 172 Hz, C*F*), - 109.2 ppm (dt, $^{3}J_{FF}$ 81 Hz, $^{2}J_{FF}$ 172 Hz, C*F*) and - 141.4 ppm (d $^{2}J_{FF}$ 81 Hz, C*F*). **6-5c** – 109.7 (dmult $^{2}J_{FF}$ = 236 Hz, CF_2), - 126.6 (dmult $^{2}J_{FF}$ = 236 Hz, CF_2) and – 125.6 ppm (br s, C*F*).

dppp: ^{19}F NMR **6-7c** – 95.2 ppm (dmult, $^{2}J_{FF}$ = 182 Hz, C*F*), - 95.6 ppm (dmult, $^{2}J_{FF}$ =182 Hz, C*F*) and - 114.1 ppm (dmult $^{2}J_{FF}$ = 81 Hz, C*F*). **6-5d** – 112.7 ppm (dmult $^{2}J_{FF}$ = 236 Hz, CF_2), - 130.6 ppm (dmult $^{2}J_{FF}$ = 236 Hz, CF_2) and – 128.9 ppm (qt, $^{2}J_{FF}$ = 41 Hz $^{3}J_{FF}$ = 16 Hz, C*F*).

6.3.7 Synthesis of nickel complexes from CTFE:

Synthesis of 6-6c

Solid Ni(cod)$_2$ (100 mg, 0.36 mmol) was dissolved/suspended in ca. 5 mL of benzene in a 20 mL glass-vial and 2 equiv of triphenylphosphine (188.64 mg, 0.72 mmol) were added, giving an orange solution. The vial was capped, degassed, charged with 30 mL of CTFE and stirred at 25 ºC for 24 h. The solvent was then evaporated and the residue washed with Et_2O, and hexanes, filtered and dried in vacuo to yield 224 mg of **6-6c** as a yellow solid (0.32 mmol, 90% based on Ni(cod)$_2$.

Synthesis of 6-7a/6.5a mixture

Solid Ni(cod)$_2$ (100 mg, 0.36 mmol) was dissolved/suspended in ca. 5 mL of benzene in a 20 mL glass-vial and 2 equiv of triisopropylphosphite (167 µL, 0.72 mmol) were added. The vial was capped, degassed, charged with 30 mL of CTFE and stirred at 25 ºC for 24 h. The solvent was then evaporated and the residue was washed with hexane. The resulting oil was dissolved in 5 mL of benzene and 1 equiv of 1,10-phenanthroline (64.8 mg, 0.36 mmol) was added. After 2 h at 25 ºC the solvent was evaporated and the residue washed with Et_2O and hexanes, filtered and dried in vacuo to yield 119 mg of a yellow solid (70% based on Ni(cod)$_2$. Metallacycle: -109.4 ppm (d CF_2, J^{FF} 240 Hz), -125.7 ppm (t CF, J^{FF} 45 Hz), – 127.3 ppm (d CF_2, J^{FF} 237 Hz). Olefin complex-92 ppm (t 188 Hz), -93 ppm (dt, 188 Hz, 86 Hz) -110.90 ppm (26 Hz, 86 Hz) and vinyl complex: -79.24 ppm (dd, broadened), -115.1 ppm (broadened), -139.3 ppm (m, broadened).

Synthesis of 6-7b/6-5b mixture

This reaction was conducted as for **6-7a/6.5a** using 1 equiv of dppp (148.5 mg, 0.36 mmol) to yield 230 mg of a yellow solid mixture of **6-7b** and **6.5b** (90% based on Ni(cod)$_2$.

Synthesis of 6-7c/6-5c mixture

This reaction was conducted as for **6-7b** using 1 equiv of dppe (143.4 mg, 0.36 mmol) to yield 226 mg of a yellow solid mixture of **6-7c** and **6.5c** (88 % based on Ni(cod)$_2$). Olefin complex: ^{19}F NMR – 104.7 ppm (d CF, J^{FF} 172 Hz), - 109.2 ppm (dt CF, J^{FF} 81 Hz, J^{FF} 172 Hz) and - 141.4 ppm (d CF, J^{FF} 81 Hz). ^{31}P{^{1}H} NMR 20.4. Vinyl complex: ^{19}F NMR – 81.7 ppm, -127.18 ppm and – 154.9 ppm.

Synthesis of 6-8

$Ni(Xantphos)_2$ (10 mg, 0.008 mmol) was dissolved/suspended in ca. 0.5 mL of benzene in an NMR tube and 2.5 mL of CTFE was added. After stirring at 25 °C for 2 h the colour changed to pink red. ^{19}F NMR (benzene): -109.1 (dmult, $^2J_{FF}$ = 168 Hz C*F*), -111.5 ppm (dt, $^2J_{FF}$ = 174 Hz, C*F*) and -111.79 (dt, $^2J_{FF}$ = 174 Hz, C*F*). $^{31}P\{^1H\}$ NMR 10.9 ppm.

6.3.8 Reactions of CTFE-derived nickelacycles with Lewis and Brønsted acids

Reaction of 6-7b/6-5b mixture with $ZnCl_2$

The solution mixture of the solid **6-7b** and **6-5b** was treated with 1 equiv of $ZnCl_2$ in benzene, no color changed, or precipitate was formed.

Reaction of 6-7c/6-5c mixture with TMSOTf

The solution mixture of the solid **6-7b** and **6-5b** was treated with 1 equiv of TMSOTf in benzene, the color changed to red/ orange.

Reaction of 6-5d/6-8a,b mixture with TMSOTf

The solution mixture of the solid **6-5d** and **6-8a,b** was treated with 1 equiv of TMSOTf in DCM, the light yellow color turned strong yellow after 30 minutes.

Reaction of 6-7b/6-5b mixture with trifluoroacetic acid

The solid mixture of **6-7b** and **6-5b** was treated with 1 equiv of trifluoroacetic acid and colour changed to strong yellow. ^{19}F NMR: **6-10a** -86.6 (dmult, $^2J_{FF}$ = 252 Hz, CF_2), -92.1 (dt, $^2J_{FF}$ = 252, J_{FF} = 30 Hz, CF_2), – 145.7 ppm (dt, $^2J_{FH}$ = 48, $^3J_{FF}$ = 8 Hz, C*F*HCl). **6-10b** -97.8 (dmult, $^2J_{FF}$ = 243 Hz, CF_2),– 143.7 ppm (d, $^2J_{FH}$ = 48 Hz, C*F*HCl)

6.5. REFERENCES

1. Dolbier, W. R. Fluorine Chemistry at the Millennium. *J. Fluorine Chem*. 2005, *126* (2), 157-163. doi:https://doi.org/10.1016/j.jfluchem.2004.09.033
2. Yancey, A.D.; Terian, S. J.; Shaw, B. J.; Bish, T. M.; Corbin, D. R.; Shiflett, M. B. A Review of Fluorocarbon Sorption on Porous Materials. *Microporous Mesoporous Mater*. **2022**, *331*, 111654. doi:https://doi.org/10.1016/j.micromeso.2021.111654
3. Sicard A. J.; Baker, R. T. Fluorocarbon Refrigerants and their Syntheses: Past to Present. *Chem Rev*. **2020**, *120* (17), 9164-9303. doi:10.1021/acs.chemrev.9b00719
4. Kotha, S.; Brahmachary, E.; Lahiri, K. Transition Metal Catalyzed [2+2+2] Cycloaddition and Application in Organic Synthesis. *Eur. J. Org. Chem*. **2005**, *2005* (22), 4741-4767. doi:https://doi.org/10.1002/ejoc.200500411

5. Saito, S.;, Yamamoto, Y. Recent Advances in the Transition-Metal-Catalyzed Regioselective Approaches to Polysubstituted Benzene Derivatives. *Chem. Rev*. **2000**, *100* (8), 2901-2916. doi:10.1021/cr990281x
6. Baker, R. T.; Beatty R. P.; Farnham, W. B.; Wallace R. L. Process for the Manufacturing of Selected Halogenated Hydrocarbons Containing Fluorine and Hydrogen and Compositions Provided Therein. US patents 5,670,679 (1997) and 5,760,282 (1998.
7. Andrella, N. O.; Sicard, A. J.; Gorelsky, S. I.; Korobkov, I.; Baker, R. T. A T-shaped Ni[κ^2-$(CF_2)_4$–] NHC Complex: Unusual C_{sp3}–F and M–C^F Bond Functionalization Reactions. *Chem Sci*. **2015**, *6* (11), 6392-6397. doi:10.1039/C5SC01886B
8. Giffin, K. A.; Harrison, D. J.; Korobkov, I.; Baker, R. T. Activation of C–F and Ni–C Bonds of [P,S]-Ligated Nickel Perfluorometallacycles. *Organometallics* **2013**, *32* (24), 7424-7430. doi:10.1021/om400933k
9. Browning, J.; Cundy, C. S.; Green, M.; Stone, F. G. A. Hexafluoroacetone and Hexafluorothioacetone Nickel Complexes. *J Chem Soc A Inorg, Phys, Theor* . **1969**, 20-23. doi:10.1039/J19690000020
10. Cundy, C. S.; Green, M.; Stone, F. G. A.. Reactions of Low-valent Metal Complexes with Fluorocarbons. Part XII. Fluoro-olefin Reactions of Zerovalent Nickel Complexes. *J Chem Soc A Inorg, Phys, Theor* **1970**, 1647-1653. doi:10.1039/J19700001647
11. Giffin, K. A.; Pua, L. A.; Piotrkowski, S.; Gabidullin, B. M.; Korobkov, I.; Hughes, R. P.; Baker, R. T. Generation of Hydrofluoronickelacycles from Trifluoroethylene and Ni(0): Ligand Effects on Regio-/Stereoselectivity and Reactivity. *J Am Chem Soc*. 2017, *139* (11), 4075-4086. doi:10.1021/jacs.6b12607
12. Sicard, A. J. Organometallic Manipulations of Fluoroolefins Mediated or Catalyzed by Low-coordinate Nickel. University of Ottawa MSc. thesis, 2016.
13. Ohashi, M.; Kawashima, T.; Taniguchi, T.; Kikushima, K,.;Ogoshi S. 2,2,3,3-Tetrafluoronickelacyclopentanes Generated via the Oxidative Cyclization of Tetrafluoroethylene and Simple Alkenes: A Key Intermediate in Nickel-Catalyzed C–C Bond-Forming Reactions. *Organometallics* **2015**, *34* (9), 1604-1607. doi:10.1021/acs.organomet.5b00218

14. Sicard, A. J.; Baker, R. T. Safe and Expeditious Preparation of $Ni(cod)_2$ for Same-Day High-Throughput Screening. *Org. Process Res. Dev*. **2020**, *24* (12), 2950-2952. doi: https://doi.org/10.1021/acs.oprd.0c00435

Chapter 7. Conclusions and Future Work

As discussed above, the addition of fluorine or a fluoroalkyl group can significantly alter the ADME properties and improve the bioactivity of a molecule. The large number of fluorine-containing pharmaceutical compounds approved by the FDA is reflected in the fast growth of this class over the last decades. Although enormous improvements have been made in synthesizing fluorinated organic compounds, the development of selective methods using fluorinating reagents, such as those based on nucleophilic, electrophilic, and radical strategies, have shown limitations. Some reagents are unstable, expensive, readily decompose, and are not selective. Fluoroalkylation has been limited primarily to addition of a CF_3 group with much fewer strategies reported for small fluoroalkyl groups like CF_2H, OCF_3, and SCF_2H. Therefore, further development of fluorinating reagents with economical and convenient methods is still needed.

Building on earlier work by the Baker group in which R^F groups were generated by insertion of tetrafluoroethylene[1] or hexafluoropropene[2] gas into Cu-H bonds, and subsequently transferred to organic electrophiles, we investigated similar protocols using CTFE and PMVE. In Chapter 2 we used the tridentate tris(phosphine) ligand triphos to stabilize the R^F group derived from regioselective insertion of CTFE into Cu-H. In addition, we transferred the resulting -$CFCl(CF_2H)$ group to benzoyl chlorides in DMSO at 25 ^oC, albeit in low yield. In contrast, attempted transfer to aryl iodides afforded aryl-aryl cross coupling, presumably due to facile transmetallation in the proposed dimeric $[CuR^F(triphos)]_2$ complex. One potential advantage of this particular R^F group is its potential for further functionalization by reaction with the C-Cl bond. By exchanging the C-Cl for pseudohalides such as cyanide or isocyanate or even for H or methyl, new R^F groups could be accessed that may give higher yields for transfer to a broader slate of organic electrophiles. Additional halofluoroalkenes such as bromotrifluoroethylene or perfluoroallyl chloride [$ClFC=C(CF_3)F$] may also prove useful in this Cu-H insertion protocol followed by additional C-X bond functionalization. Finally, in this chapter, we also started noticing the DMSO solvent's importance and unique effect on fluoroalkylation reactions, which expanded our strategies and methodologies for Chapters 3 and 4.

In Chapter 3 we observed another regioselective insertion using PMVE and by controlling the DMSO concentration in benzene and using CuBr to sequester strong binding ligands, were now able to transfer the resulting -$CF(OCF_3)CF_2H$ group to a variety of aryl halides in good yields.

This new R^F group is also special not just for its stability (isolated 2-, 3- and 4-coordinate CuR^F complexes) but in containing both CF_2H and OCF_3 groups which have proven useful in previous drug development. These reactions gave us a better understanding of ligand effects in our systems and how they can affect stability vs. fluoroalkylation. We first observed some fluoroalkylation of electron-poor benzoyl chlorides using the electron-rich 7-dipp NHC ligand and of electron-poor aryl iodides in low yield using the 4,4-diCl-bpy co-ligand in benzene at 25 °C. In DMSO solvent at 25 °C, however, the Cu $R^F(PPh_3)_2$ complex (**3-1**) transfers the R^F group to a variety of benzoyl chlorides in good to moderate yields. Herein, with our DFT collaborator Christian Ehm we also showed an unusual rate-determining elimination mechanism for aroyl chlorides. With the inverted ligand field often seen for formal Cu(III), only DMSO solvent stabilizes the square-pyramidal formal Cu (III) intermediate with the strong negative point charge stabilizing the charge transfer during the elimination. The synthesis of these complexes can be easily scaled up and used to develop new bioactive compounds. Many substrate scopes can be explored, which opens the opportunity to improve the bioactivity and bioavailability of agrochemicals and drugs already existent in the market.

Chapter 4 builds on Baker and Andrella's first report of aryl iodide tetrafluoroalkylation using $Cu(CF_2CF_2H)(PMePh_2)_3$ and a catalytic amount of Cu(SIMes)Cl.[1] We showed that the "Safe Supply" TFE:CO_2 can be used to generate the Xantphos complex which can also perform the tetrafluoroethylation of aryl iodides. Computational studies by Christian Ehm showed the importance of pre-equilibria in raising the barrier for rate-determining "oxidative addition" of aryl iodides. In the same chapter, we initiated two other crucial collaborations: with Omar Boutureira, we developed the tetrafluoroethylation of nucleobases, nucleosides and glycals in moderate to fair yields using a ligandless system. The complex $[CuCF_2CF_2H]$ is stabilized in DMF solvent after CuBr salt addition before the oxidative addition and reductive elimination steps.

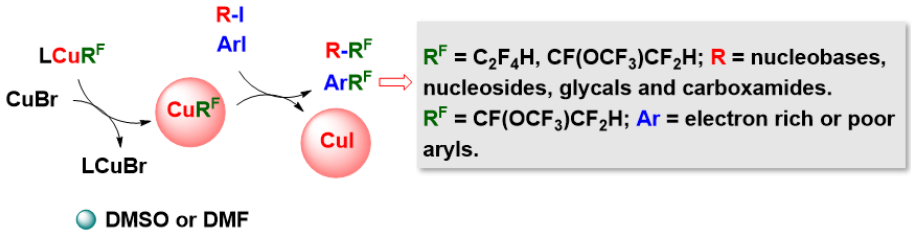

Figure 7.1. Summary description of "ligandless" system used in this work.

With Michele Loewen, we further explored by molecular docking analysis the interactions of -$CF(OCF_3)CF_2H$-, CF_2CF_2H- and CF_2CF_3-substituted carboxamides with the active site of succinate dehydrogenase enzyme (SDH), and we found that both tetrafluoroethyl- and pentafluoroethyl-substituted analogs are strong candidates as SDH inhibitors since they interact deeply in the active site of the enzyme.

The first part of this thesis contributes significantly to copper-mediated fluoroalkylation chemistry. Further work can be done to construct new fluoroalkyl groups using different fluoroalkene gases, such as perfluorocyclobutene. There is also future interest in photochemical reactions of these R^F groups to eliminate HCl or $HOCF_3$ and create a Cu-fluorovinyl complex as another potential bioisostere of amides. Furthermore, the "ligandless" approach inspired by our collaborator Omar Boutureira opens the door for fluoroalkylation of a wide range of substrates, including electron-poor hetero (aryl) iodides.

For pharmaceutical applications, the next step of this work is the biological testing of these fluorinated nucleobases/ nucleosides and glycals that can be easily scaled-up. We are in the process of scaling up the most promising candidates for antivirus activity. Biological tests will be performed in the lab of our collaborator Prof. John Pezacki at uOttawa.

Another exciting future project for the development of agrochemical compounds in collaboration with Michele Loewen and Omar Boutureira involves the synthesis of a new fluorinated-carboxamide containing the best two candidates based on our *in-silico* studies with R^F (-C_2F_4H and -C_2F_5) followed by biological testing in plants for potential antifungal activity that will be performed at NRC Ottawa. Encouraging results from synthesizing these compounds using the "ligandless" system were achieved, and reactions were performed at the SINTCARB lab in Tarragona, Spain, during my visit in July.

Another potential growth field in organofluorine chemistry is synthetic methodologies to produce new fluoroalkenes as many existing protocols still generate intermediate ozone-depleting chlorofluorocarbons. This topic constituted the second part of this thesis. Nickel-catalyzed hydrodefluorodimerization from mixed alkene metallacycles is being explored in Baker`s group in collaboration with Arkema, Inc. However, in spite of several studies on the synthesis and reactivity of fluoronickelacyclopentanes, there was a lack of knowledge in the mechanism for its formation.

In chapter 5, we discovered via a combination of computational results by Russell Hughes and our experimental work with wide bite-angle bis(phosphines) that C-C bond formation perpendicular to the P-Ni-P plane gives rise to a large P-Ni-P angle expansion and a kinetic metallacycle whose geometry resembles a trigonal bipyramid with one vertex missing. After decades since the first example of perfluoronickelacyclopentane was observed by Stone, this is the first work to probe the mechanism of perfluoronickelacyle formation. Indeed, using the DPEphos ligand allowed us to observe the kinetic metallacycle product, stabilized by Ni-O bonding.

Finally, In Chapter 6 we learned additional facts about the effects of C-substituents on fluoronickelacycle stability and reactivity. Inspired by Dr. Giffin's work with trifluoroethylene (CF_2=CFH, TrFE), we investigated the reactivity of two inexpensive and functionalized fluoroalkenes (CTFE and PMVE) with zerovalent Ni precursors. The oxidative cyclization of PMVE at $Ni(cod)_2$ with triisopropylphosphite was found to be -regio and stereoselective towards the formation of tail-to-tail fluoronickelacyclopentane with both OCF_3 groups at Cα, **6-2a**. However, interconversion of the alkene complex + PMVE with the metallacycle was reversible. Ligand exchange with dppe afforded a stable metallacycle but no reactivity was seen with Lewis or Brønsted acids or even high temperatures. Similar results were obtained with CTFE and triisopropylphosphite at $Ni(cod)_2$, affording stereo- and regioselective **6-5a** with both Cl atoms at Cα. However, now both reactions were reversible so that removal of the CTFE led to the disappearance of both complexes. Moreover, extended reaction times led to formation of the perfluorovinyl NiCl complex. Surprisingly, the oxidative cyclization of CTFE at $Ni(Xantphos)_2$ afforded stable nickelacyclopentanes but with erosion of regioselecivity as head-to-tail regioisomers were also formed. The latter reacted readily with Lewis acid TMSOTf to give selective Cα-F (vs. Cα-Cl) activation, forming the Ni dichloropentafluorobutyl complex.

In summary, chapter 6 investigates the reactivity of functionalized fluoroalkenes at Ni(0). Future studies in this area would benefit from preparing mixed metallacycles to afford new fluoroalkenes. For example, the oxidative cyclization of PMVE + CTFE, or PMVE + VDF at Ni(0) followed by β-F elimination and hydrosilylation could generate novel fluoroalkenes (**Scheme 7.1**). Furthermore, the chemistry with $Ni(Xantphos)_2$ can be applied with other fluoroalkenes (VDF, HFP and HTFE) to improve the efficiency of oxidative cyclization.

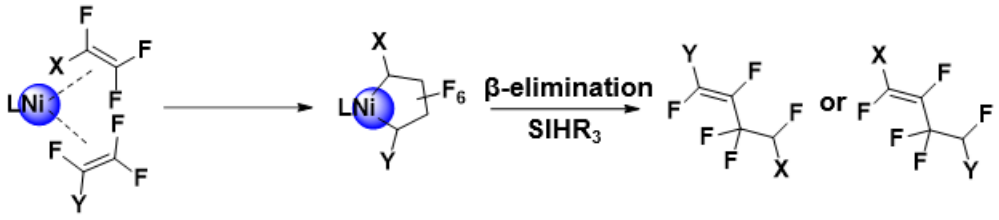

Scheme 7.1. Schematic synthesis of new fluoroolefins from a mixed metallacycle.

Overall, this thesis fleshes out a conceptual strategy to create new fluoroalkyl groups and improve the efficiency of late-stage fluorination. The last two chapters also amplified our design knowledge to obtain new fluoroolefins from metallacycle intermediates, understanding the mechanism of their formation and the reactivity of functionalized metallacycles.

7.1 REFERENCES

1. Andrella, N.O.; Xu, N.; Gabidullin, B.M.; Ehm, C.; Baker, R.T.Selective copper-complex catalyzed hydrodefluorination of fluoroalkenes and allyl Fluorides: A tale of two mechanisms," *J. Am. Chem. Soc.* **2019**, *141*, 11506-11521.

2. Andrella, N.O.; Liu, K.; Gabidullin, B.M.; Vasiliu, M.; Dixon, D.A.; Baker, R.T. Metal heptafluoroisopropyl (M-hfip) complexes for use as hfip transfer agents. *Organometallics* **2018**, *37*, 422-432. doi:10.1021/acs.organomet.7b00837

Appendix for
Reactions of Functionalized Fluoroalkenes: Ni Fluorometallacycles and Cu Fluoroalkyls for R^F Transfer to Organic Electrophiles
Luana L. T. N. Porto PhD thesis

Chapter 2: Generation of Copper Fluoroalkyl Complexes (CuR^FL_n) from Chlorotrifluoroethylene and -R^F Transfer to Aroyl Chlorides

Luana L. T. N. Porto, Moutasem Seifi, Nicole Johnson, and R. Tom Baker

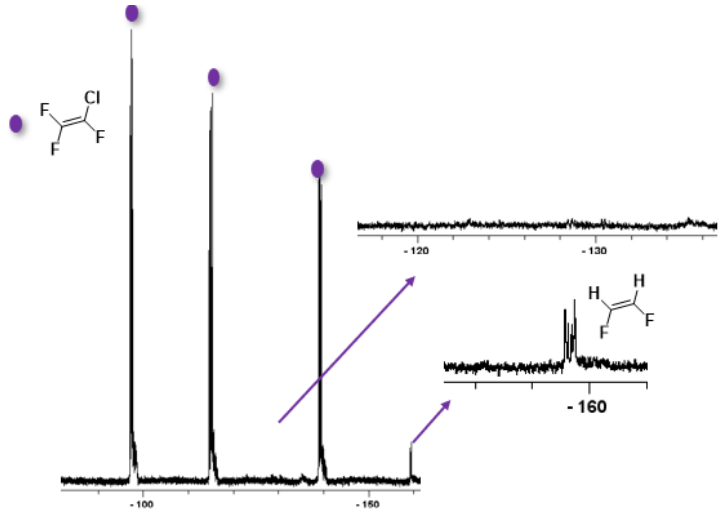

Figure A2.1 ^{19}F NMR spectrum (282 MHz) of $[CuH(PPh_3)]_6$ + 3 equiv/Cu of $P(O^iPr)_3$ + CTFE in benzene.

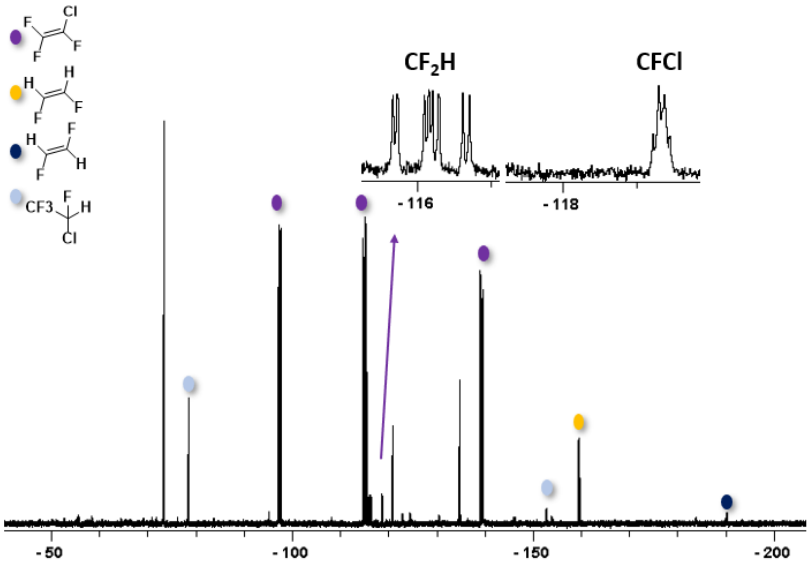

Figure A2.2 ^{19}F NMR spectrum (282 MHz) of $[CuH(PPh_3)]_6$ + 3 equiv/Cu of $P(OEt)_3$ + CTFE in benzene.

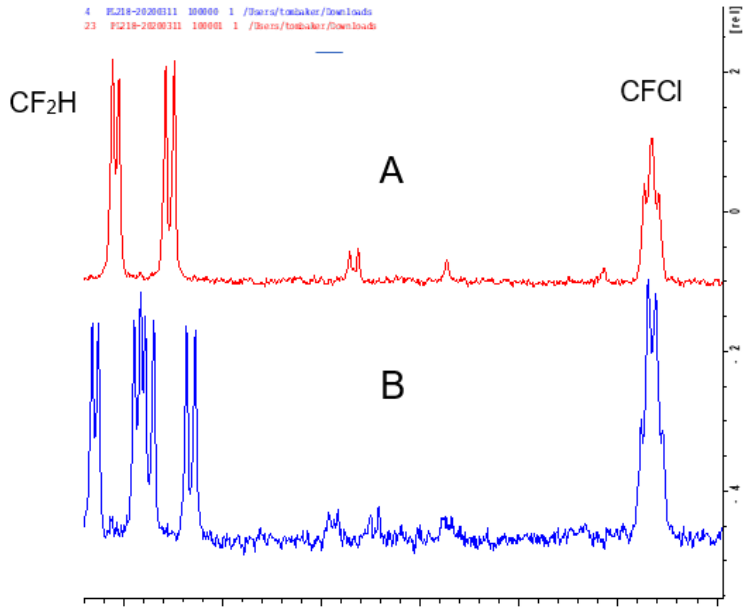

Figure A2.3 ^{19}F (**A**) and $^{19}F\{^{1}H\}$ (**B**) NMR spectra (282 MHz) of $Cu(CFClCF_2H)[(POEt)_3]_n$ (**2-1a**) in benzene.

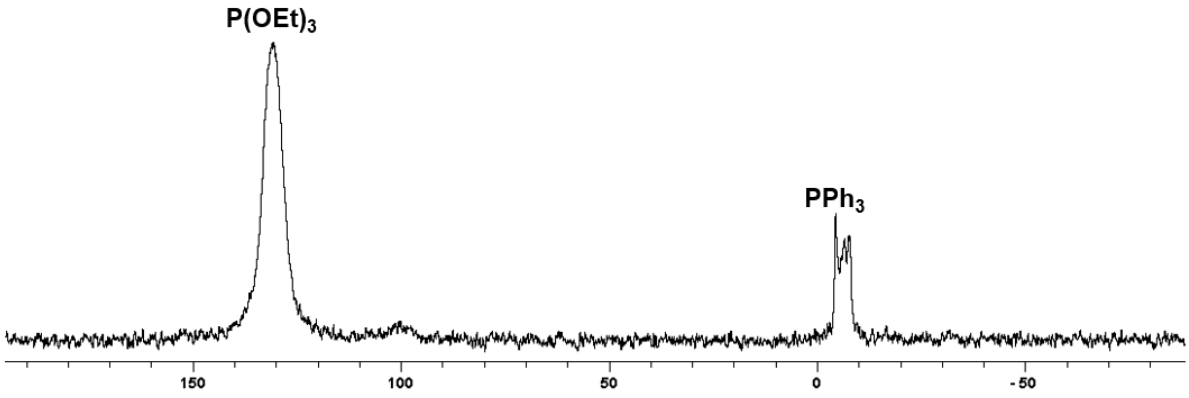

Figure A2.4 $^{31}P\{^{1}H\}$ NMR spectrum (121 MHz) of $[CuH(PPh_3)]_6$ + 3 equiv/Cu of $(POEt)_3$ + CTFE in benzene.

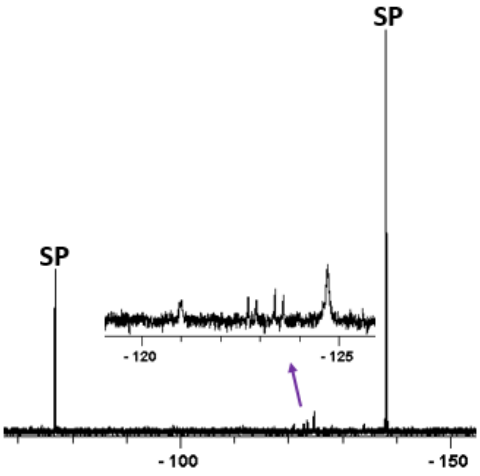

Figure A2.5 ^{19}F NMR spectrum (282 MHz) of $[CuH(PPh_3)]_6$ + 3 equiv/Cu of triethylphosphite + CTFE in benzene after removal of solvent. SP = uncharacterized side-product(s).

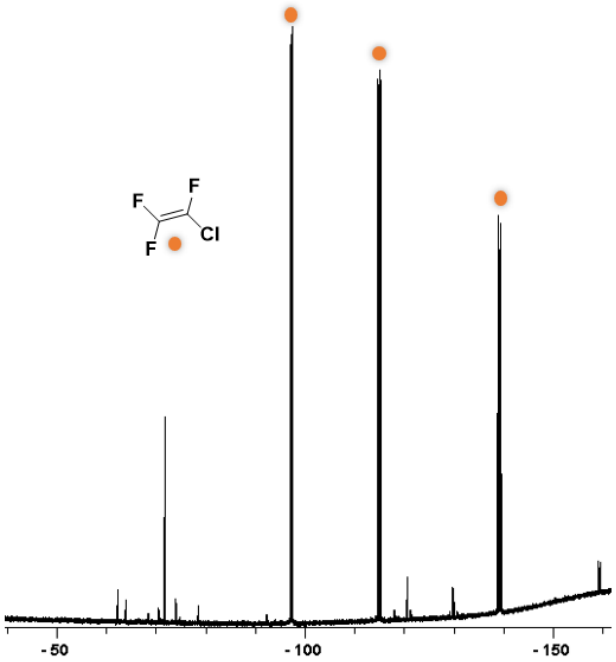

Figure A2.6 ^{19}F NMR spectrum (282 MHz) of $[CuH(PPh_3)]_6$ + 2 equiv/Cu of PPh_2Me + CTFE in benzene.

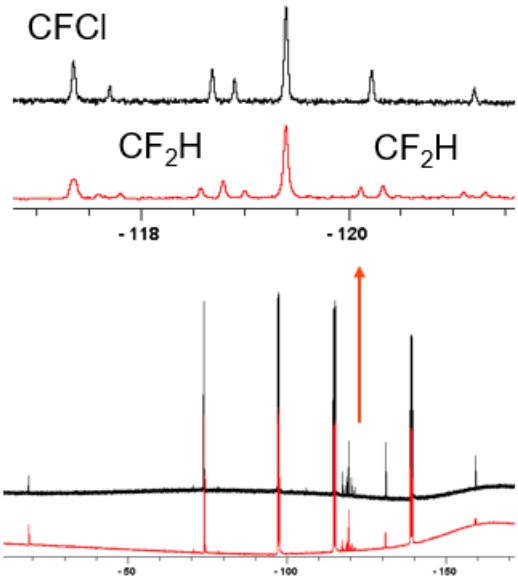

Figure A2.7 ^{19}F NMR spectrum (282 MHz) of $[CuH(PPh_3)]_6$ + 2 equiv/Cu of PPh_3 + CTFE in benzene.

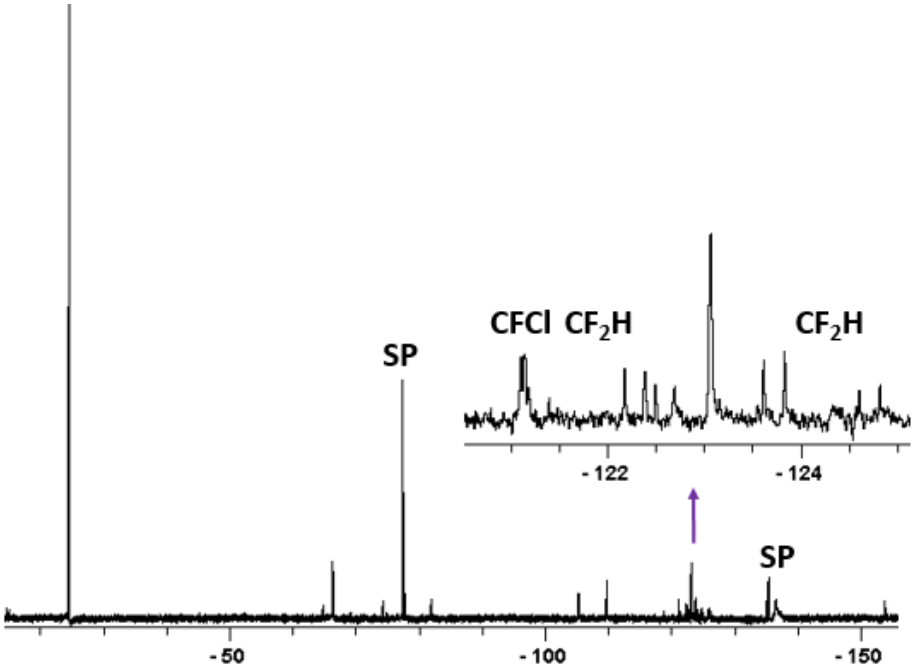

Figure A2.8 ^{19}F NMR spectrum (282 MHz) of $[CuH(PPh_3)]_6$ + 2 equiv/Cu of PPh_3 + CTFE in benzene after removal of solvent. SP = uncharacterized side-products

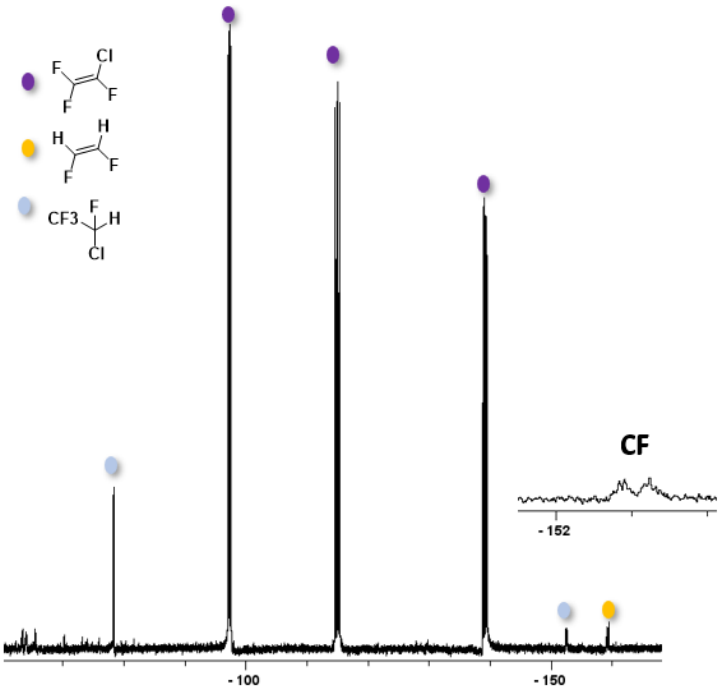

Figure A2.9 ^{19}F NMR (282 MHz) of $[CuH(PPh_3)]_6$ + 1 equiv/Cu of phen + CTFE in benzene.

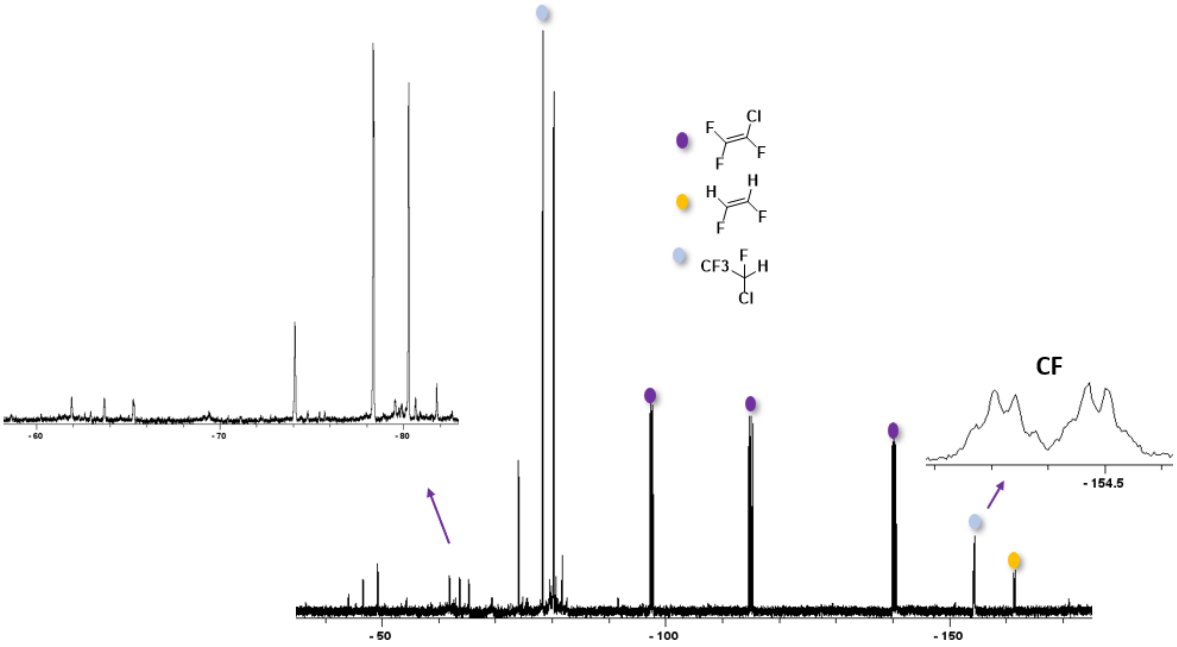

Figure A2.10 ^{19}F NMR spectrum (282 MHz) of $[CuH(PPh_3)]_6$ + 1 equiv/Cu of terpyridine + CTFE in benzene.

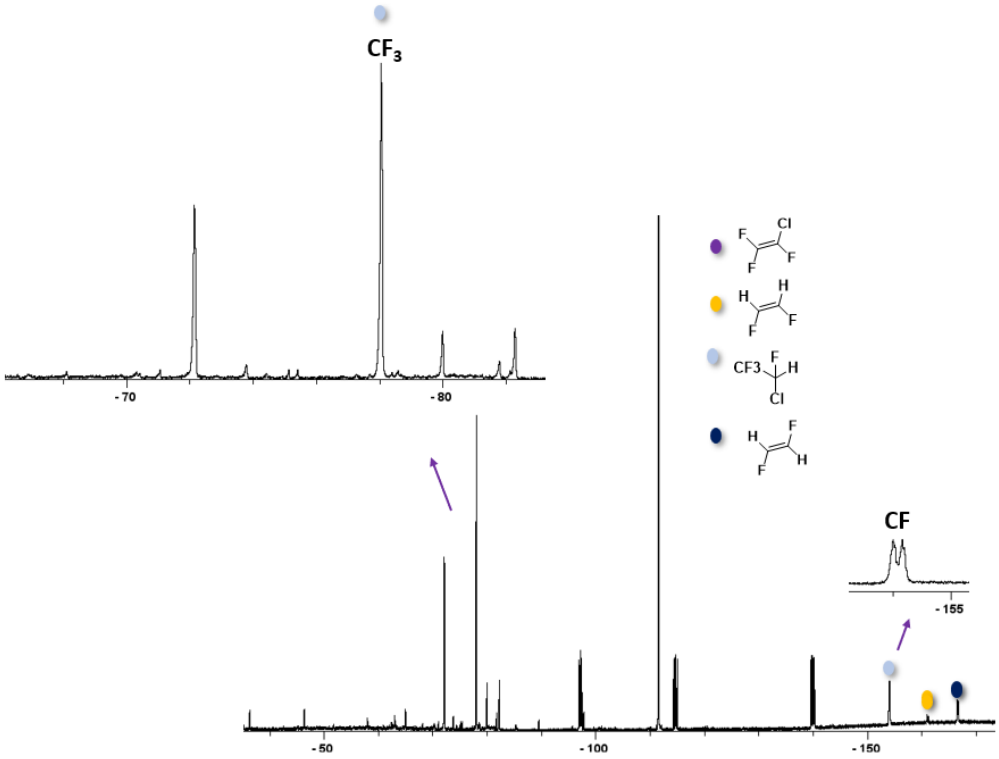

Figure A2.11 ^{19}F NMR spectrum (282 MHz) of $[CuH(PPh_3)]_6$ + 1 equiv/Cu of PMDTA+ CTFE in benzene.

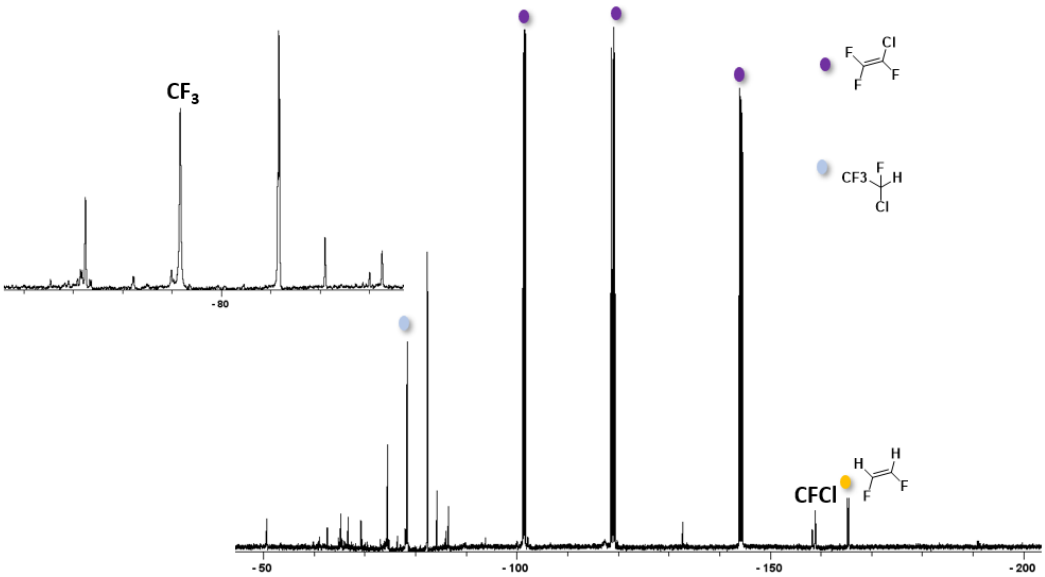

Figure A2.12 ^{19}F NMR spectrum (282 MHz) of $[CuH(PPh_3)]_6$ + 1 equiv/Cu of PMDTA + CTFE in DMF.

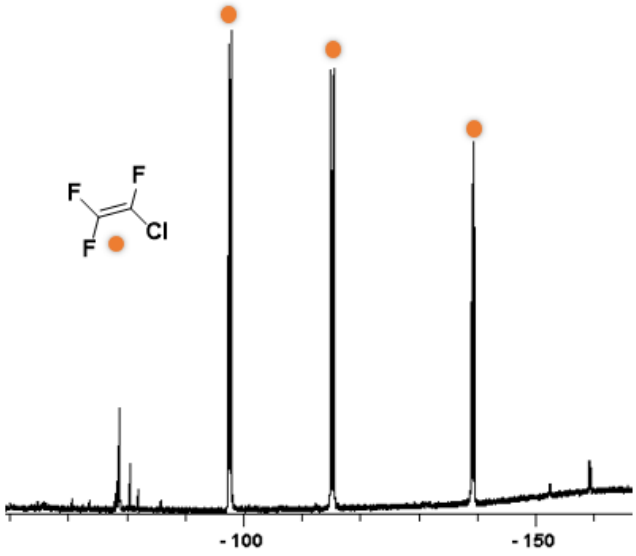

Figure A2.13 ^{19}F NMR spectrum (282 MHz) of $[CuH(PPh_3)]_6$ + 1 equiv/Cu of tripod + CTFE in benzene.

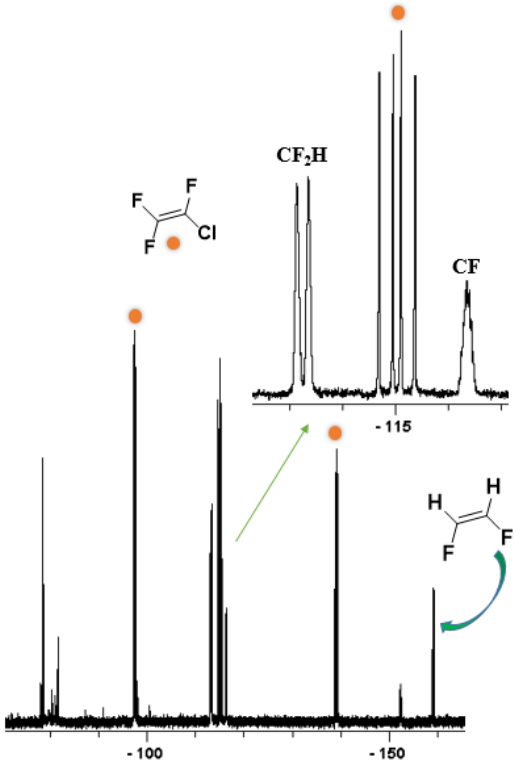

Figure A2.14 ^{19}F NMR spectrum (282 MHz) of $[CuH(PPh_3)]_6$ + 1 equiv/Cu of triphos + CTFE in benzene.

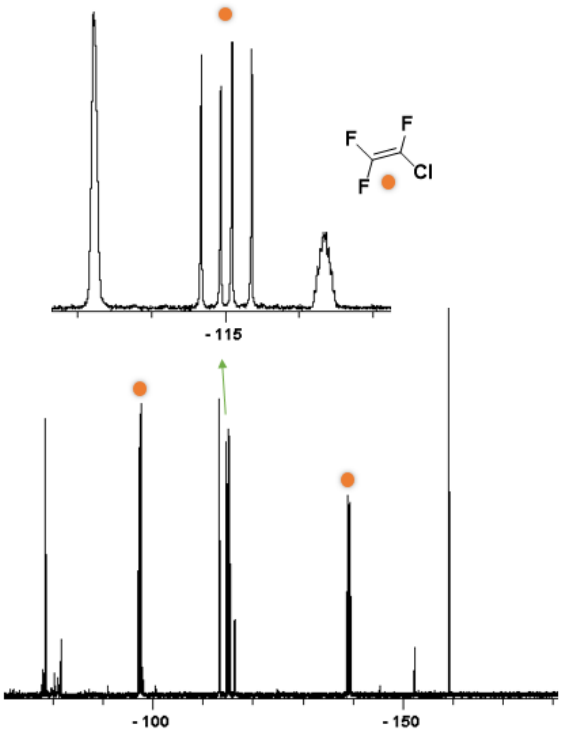

Figure A2.15 $^{19}F\{^{1}H\}$ NMR spectrum (282 MHz) of $[CuH(PPh_3)]_6$ + 1 equiv/Cu of triphos + CTFE in benzene.

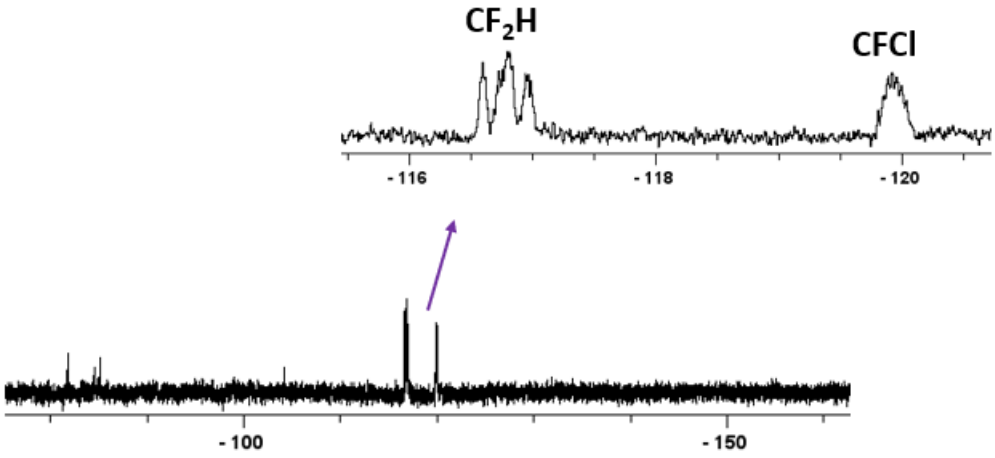

Figure A2.16 ^{19}F NMR spectrum (282 MHz, C_6D_6) of complex **2-3**.

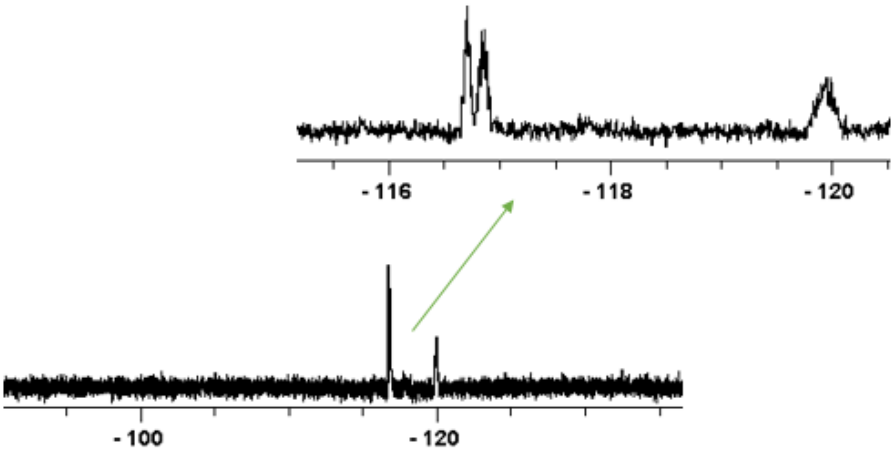

Figure A2. 17 $^{19}F\{^{1}H\}$ NMR spectrum (282 MHz, C_6D_6) of complex **2-3**.

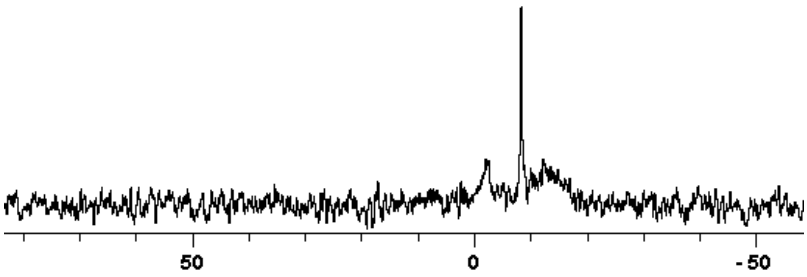

Figure A2.18 $^{31}P\{^{1}H\}$ NMR (121 MHz, C_6D_6) of complex **2-3**.

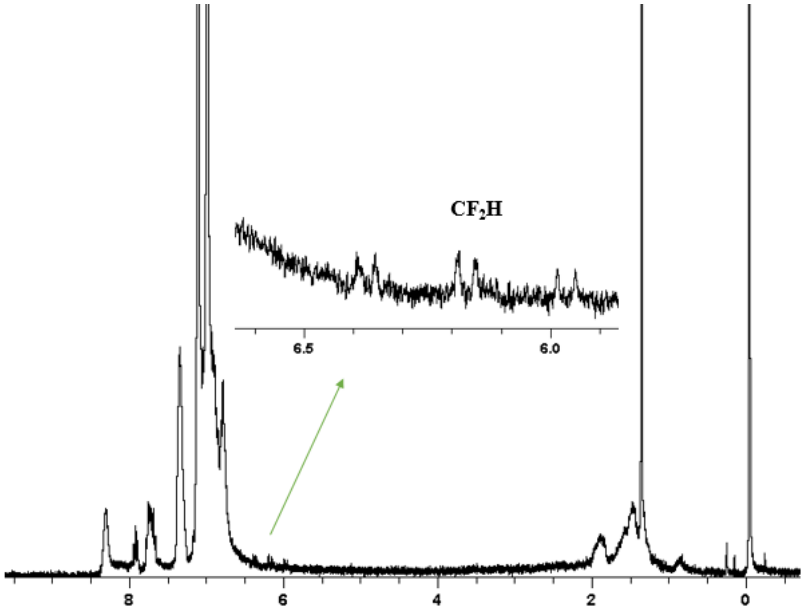

Figure A2.19 ^{1}H NMR spectrum (300 MHz, C_6D_6) of complex **2-3**.

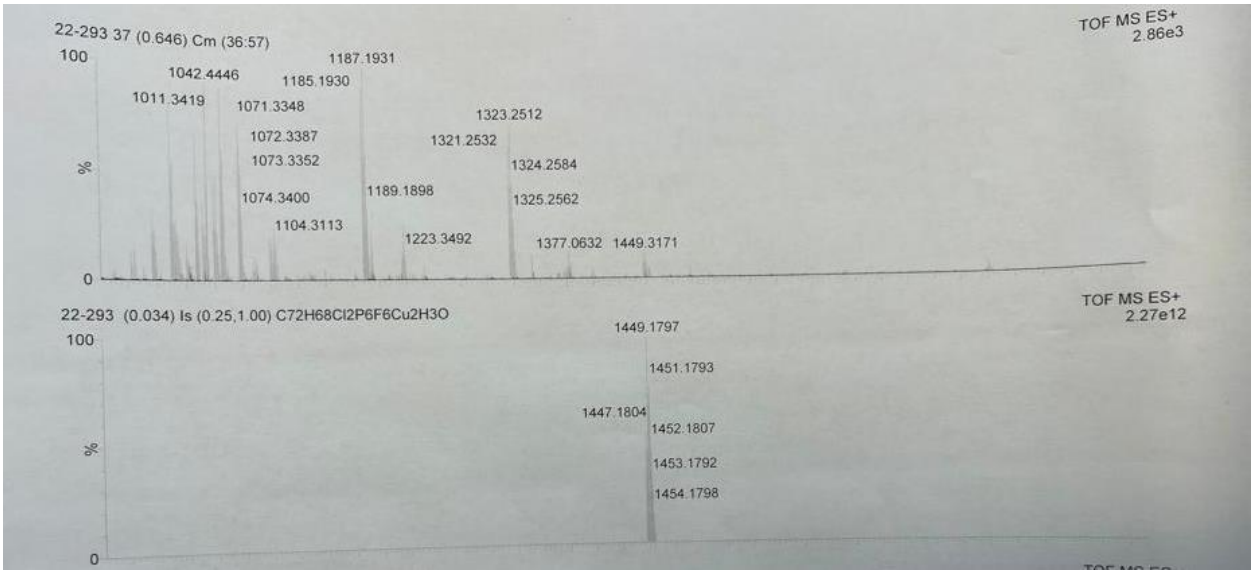

Figure A2.20 ESI-MS (positive mode) spectrum of complex **2-3**.

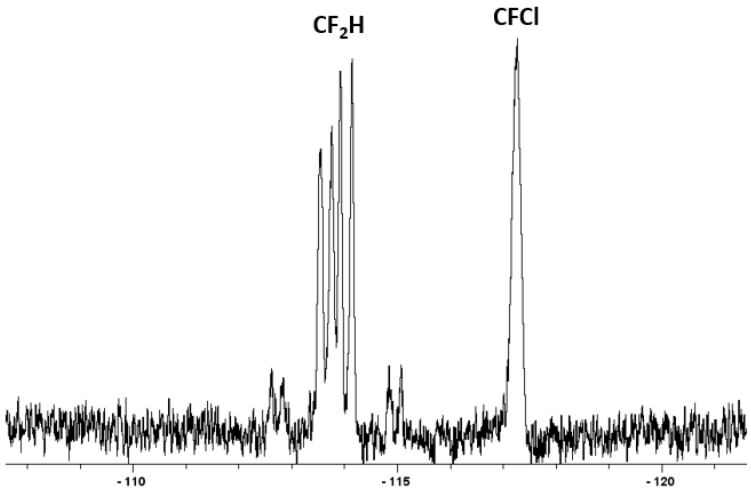

Figure A2.21 ^{19}F NMR spectrum (282 MHz) of complex **2-3** + 8 eq. of DMSO in benzene.

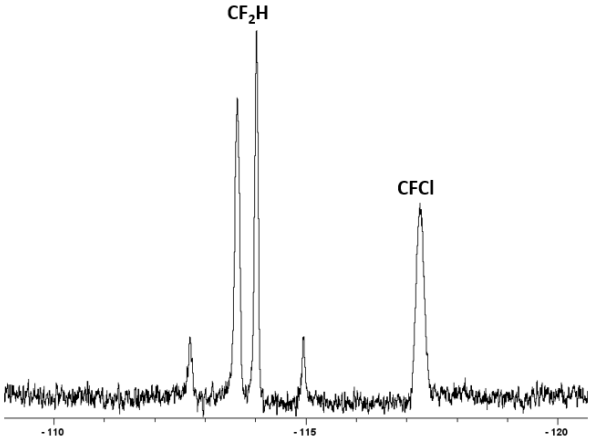

Figure A2.22 $^{19}F\{H\}$ NMR spectrum (282 MHz) of Complex **2-3** + 8 eq. of DMSO in benzene.

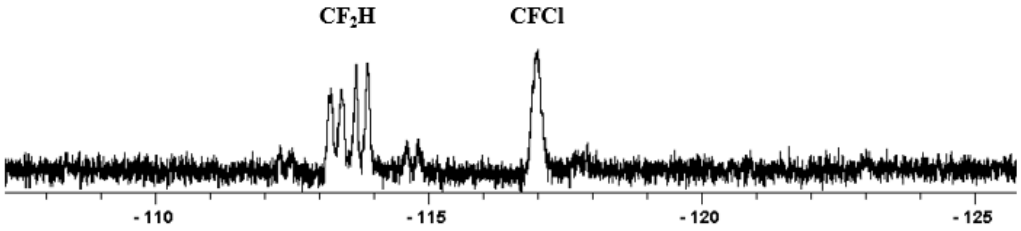

Figure A2.23 ^{19}F NMR spectrum (282 MHz) of complex **2-3** with 8 eq. of tetrahydrothiophene (THT) in benzene.

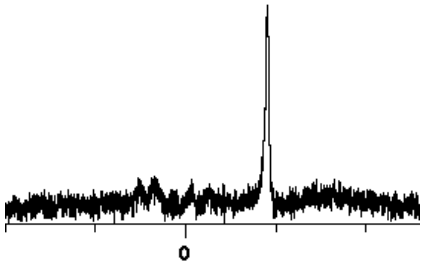

Figure A2.24 $^{31}P\{H\}$ NMR spectrum (282 MHz) of Complex **2-3** with 8 eq. of THT in benzene.

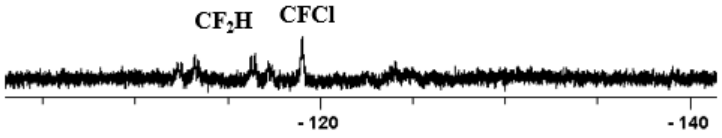

Figure A2.25 ^{19}F NMR spectrum (282 MHz) of complex **2-3** in THT.

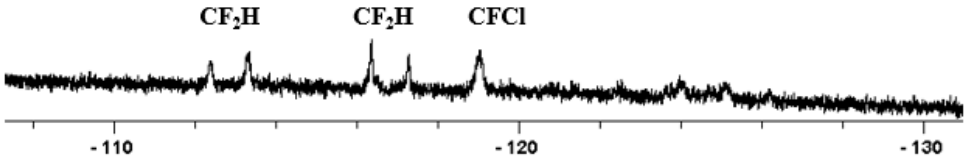

Figure A2.26 $^{19}F\{H\}$ NMR spectrum (282 MHz) of complex **2-3** in THT.

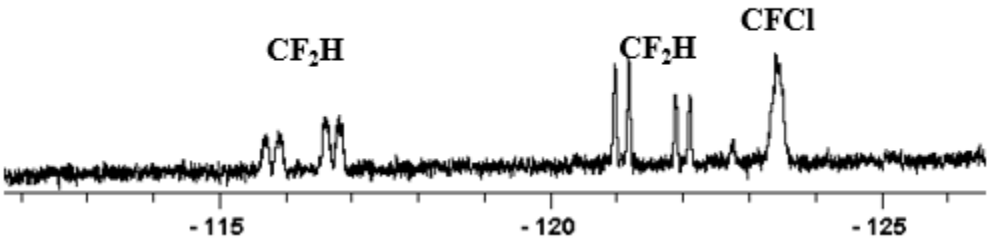

Figure A2.27 ^{19}F NMR spectrum (282 MHz) of complex **2-3** in THT at -40 °C.

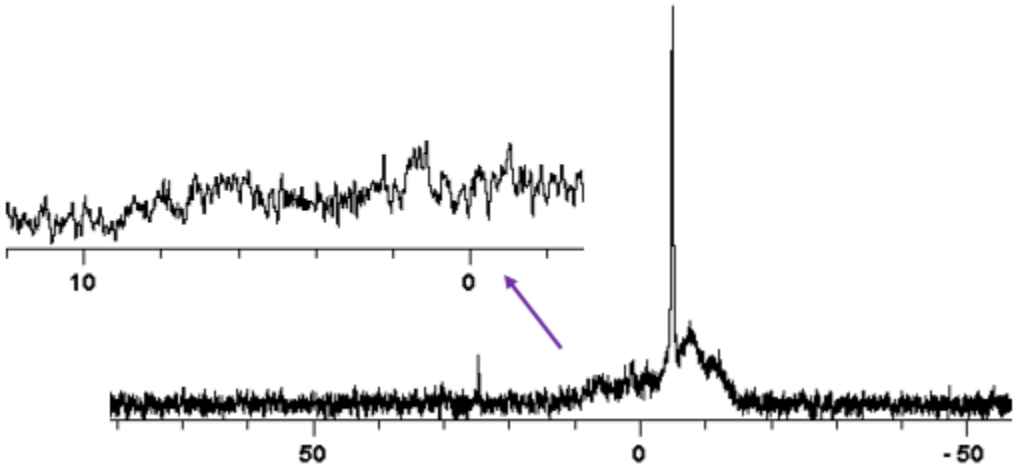

Figure A2.28 $^{31}P\{^{1}H\}$ NMR spectrum (121 MHz) of complex **2-3** in THT.

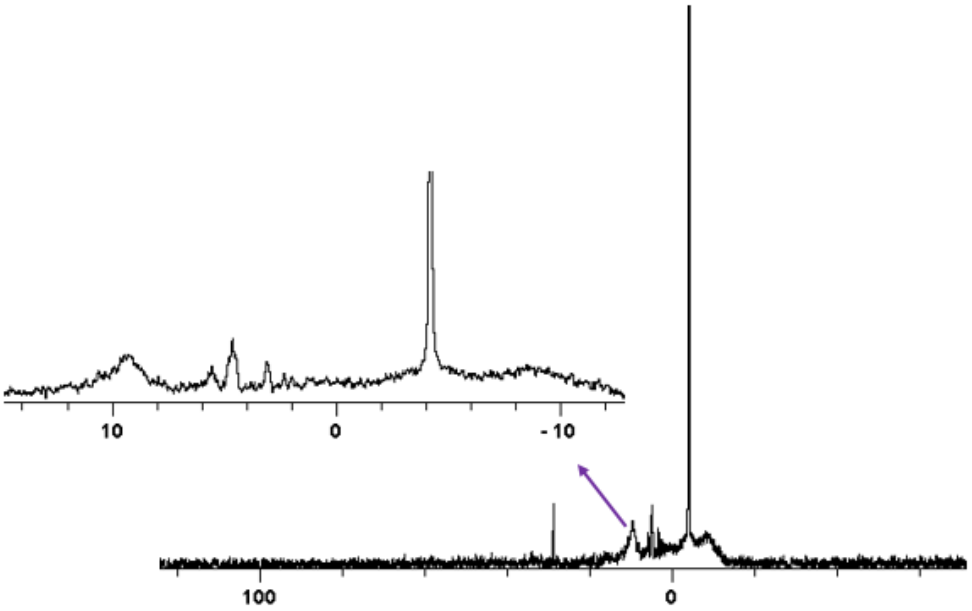

Figure A2.29 $^{31}P\{^{1}H\}$ NMR spectrum (121 MHz) of complex **2-3** in THT at -40 °C.

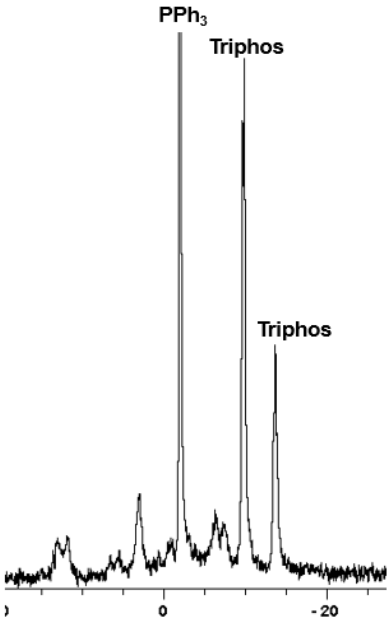

Figure A2.30 $^{31}P\{^{1}H\}$ NMR spectrum (121 MHz) of $[CuH(PPh_3)]_6$ + 2 equiv/Cu of PPh_3 + 1 equiv/Cu of triphos in benzene.

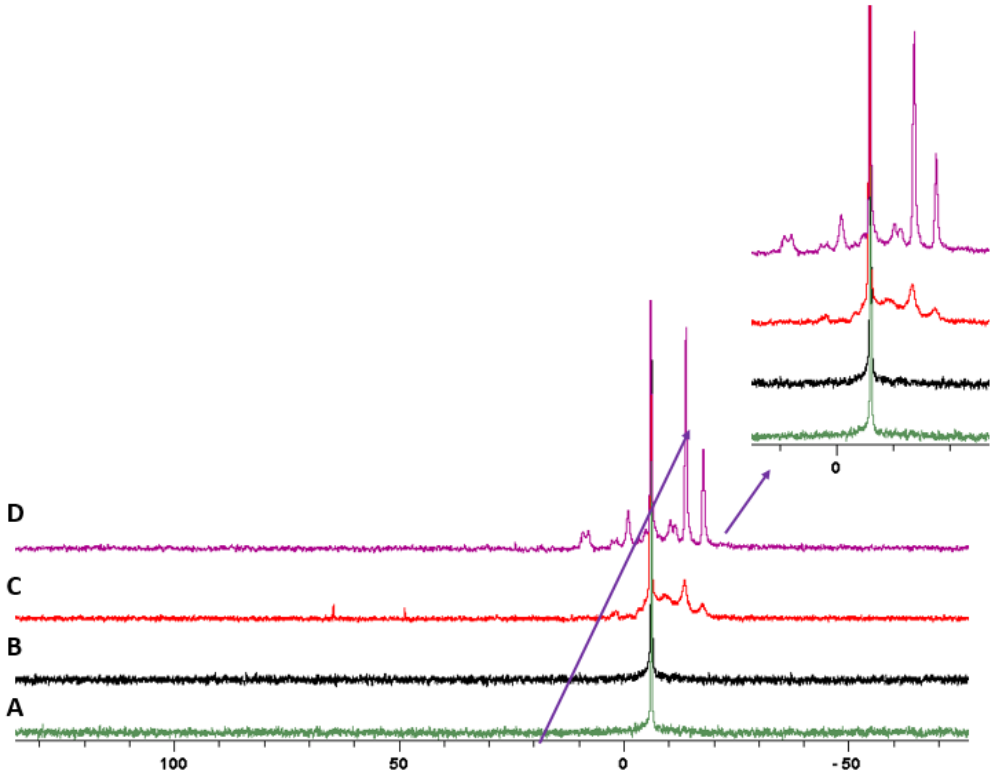

Figure A2.31 $^{31}P\{^{1}H\}$ NMR spectra (121 MHz) of reaction of $[CuH(PPh_3)]_6$ + 1 equiv/Cu of PPh_3 + 0.5 equiv/Cu of triphos (**A**) and 1 eq. of triphos (**C**) in benzene.

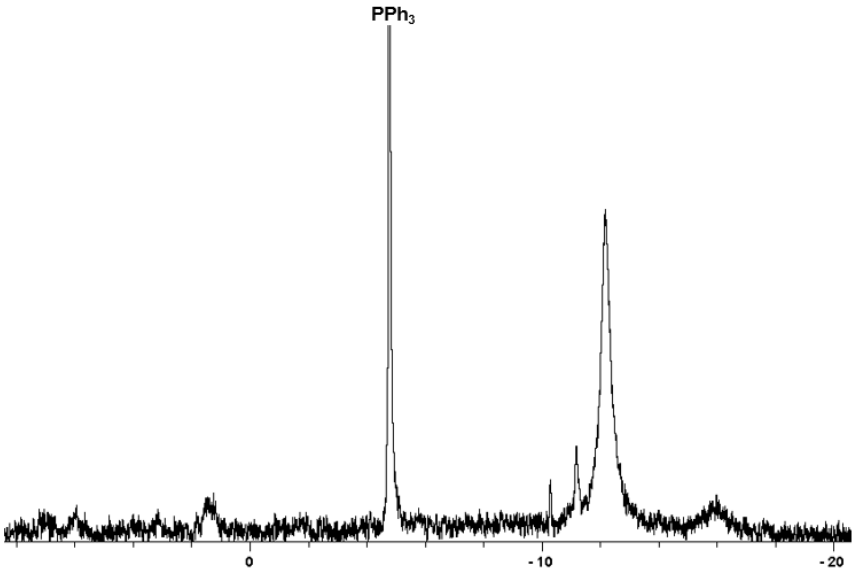

Figure A2.32 $^{31}P\{^{1}H\}$ NMR (121 MHz) of $[CuH(PPh_3)]_6$ + 1 equiv/Cu of triphos in benzene after 22 h at 50 °C.

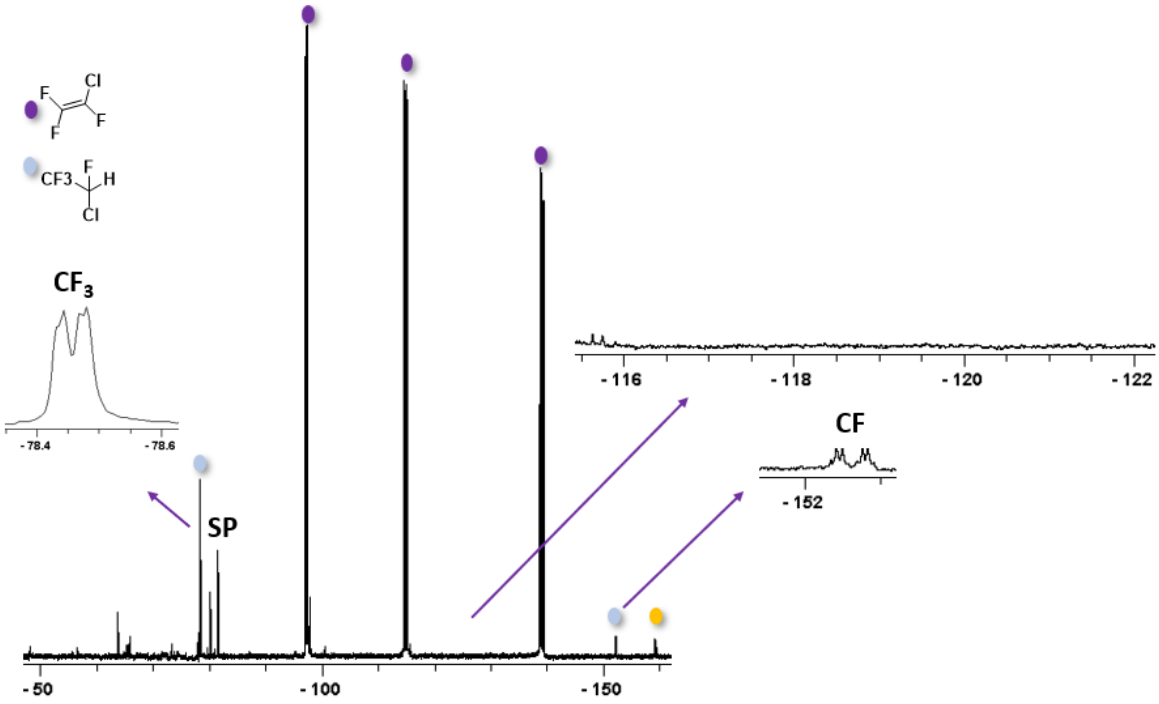

Figure A2.33 ^{19}F NMR spectrum (282 MHz) of $[CuH(PPh_3)]_6$ + 0.5 equiv/Cu of triphos + CTFE in benzene.

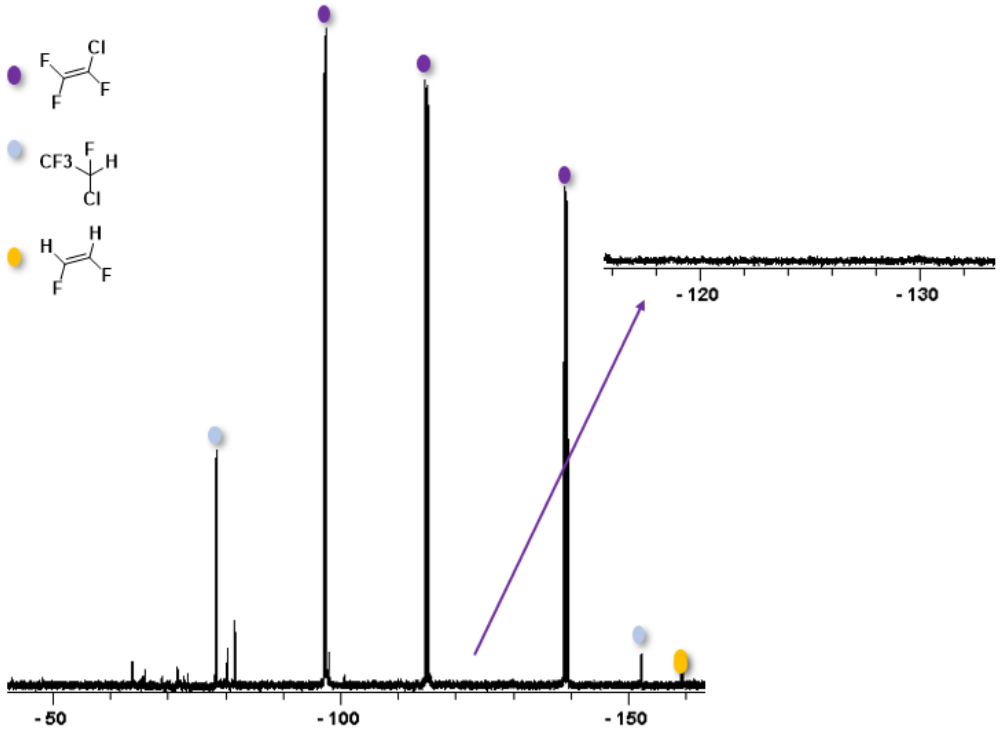

Figure A2.34 ^{19}F NMR spectrum (282 MHz) of $[CuH(PPh_3)]_6$ + 2 equiv/Cu of PPh_3 + 0.5 equiv/Cu of triphos + CTFE in benzene.

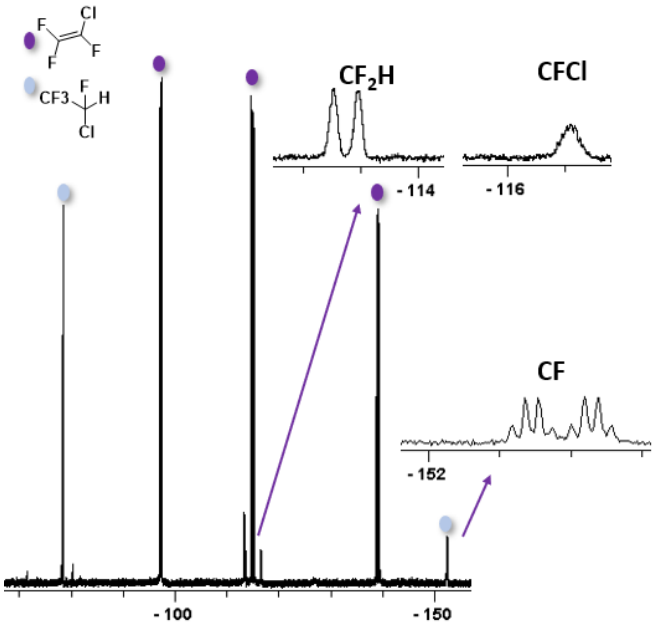

Figure A2.35 ^{19}F NMR spectrum (282 MHz) of $[CuH(PPh_3)]_6$ + 1 equiv/Cu of PPh_3 + 1 equiv/Cu of triphos + CTFE.

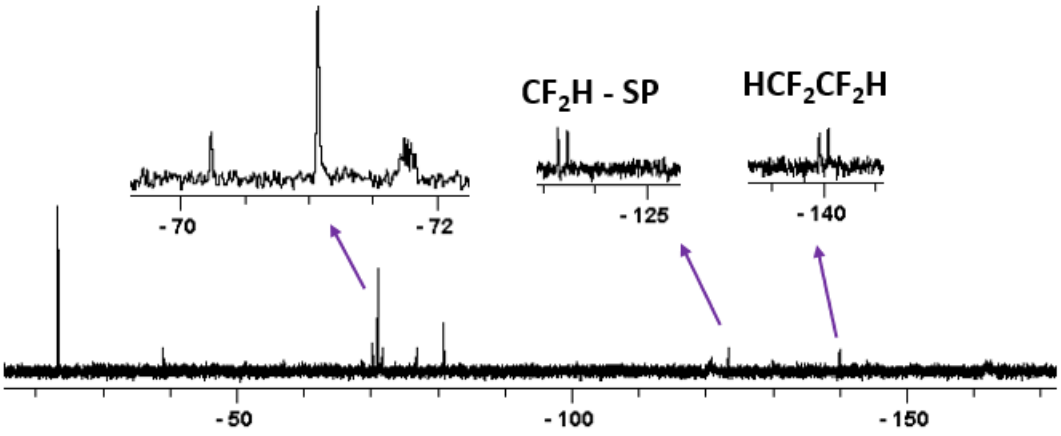

Figure A2.36 ^{19}F NMR spectrum (282 MHz) of complex **2-2** in DMSO with benzoyl chloride.

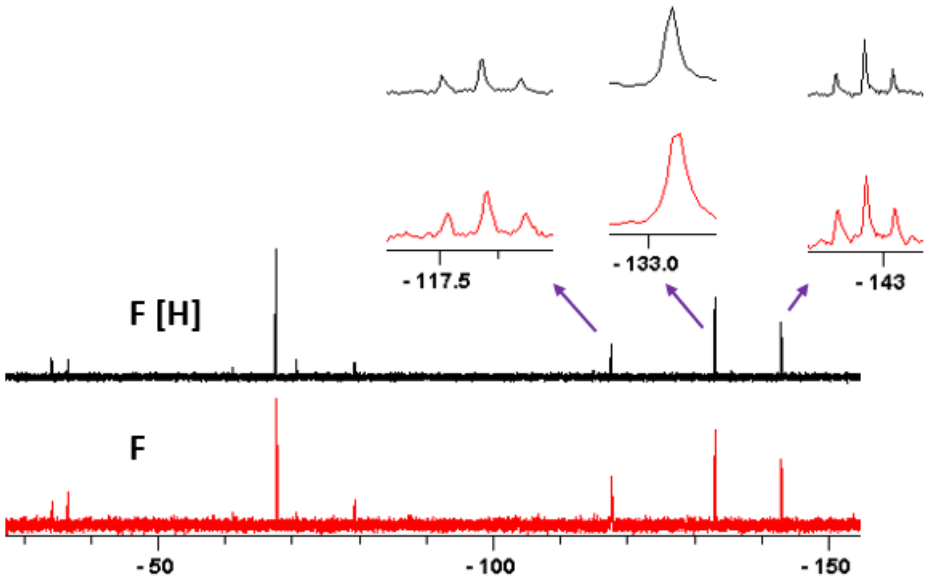

Figure A2.37 ^{19}F NMR spectrum (282 MHz) of complex **2-2** in DMF with 1 equiv of benzoyl chloride and 1 equiv of phen.

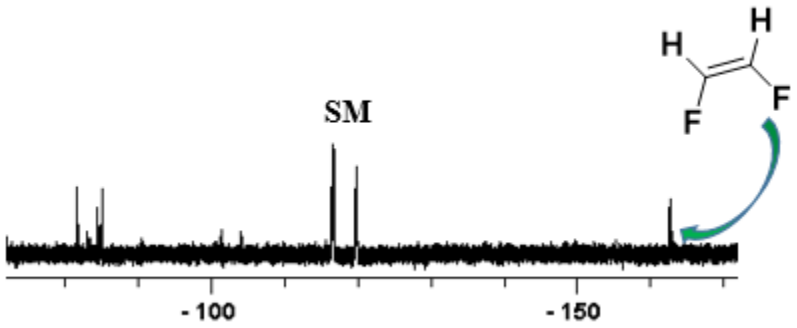

Figure A2.38 ^{19}F NMR (282 MHz) of Complex **2-3** with benzoyl chloride in benzene. SM = Starting material **2-3**.

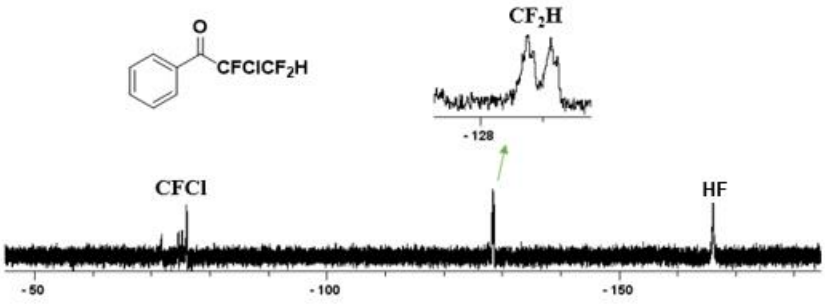

Figure A2.39 ^{19}F NMR spectrum (282 MHz) of **2-4a** from complex **2-3** with 1.5 eq. of benzoyl chloride in DMSO at 25 ^{o}C after 12 h.

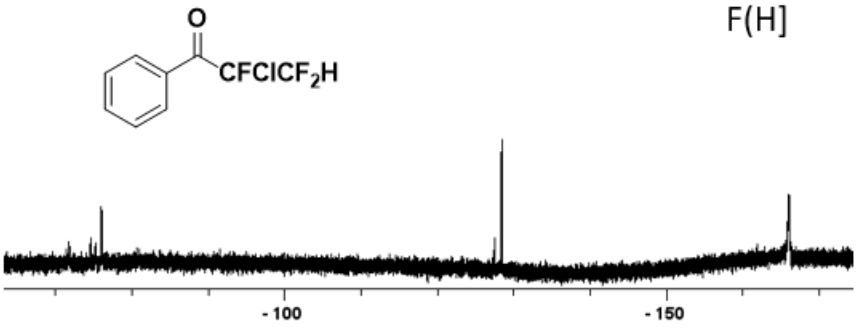

Figure A2.40 $^{19}F\{^{1}H\}$ NMR spectrum (282 MHz) of **2-4a** from complex **2-3** with 1.5 eq. of benzoyl chloride in DMSO at 25 ºC after 12 h.

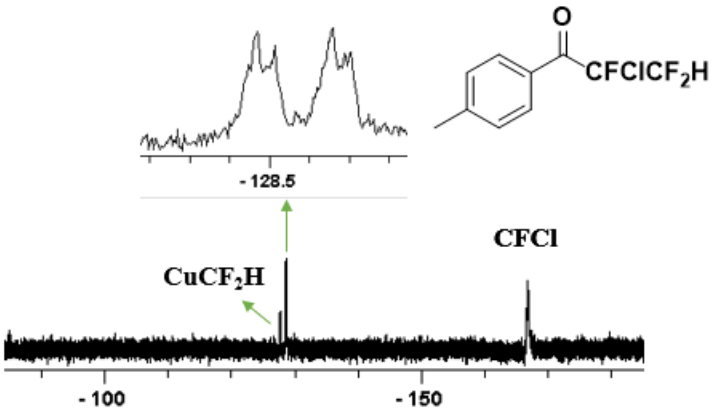

Figure A2.41 ^{19}F NMR spectrum (282 MHz) of **2-4b** from complex **2-3** with 1.5 eq. of toluoyl chloride in DMSO at 25 ºC after 12 h.

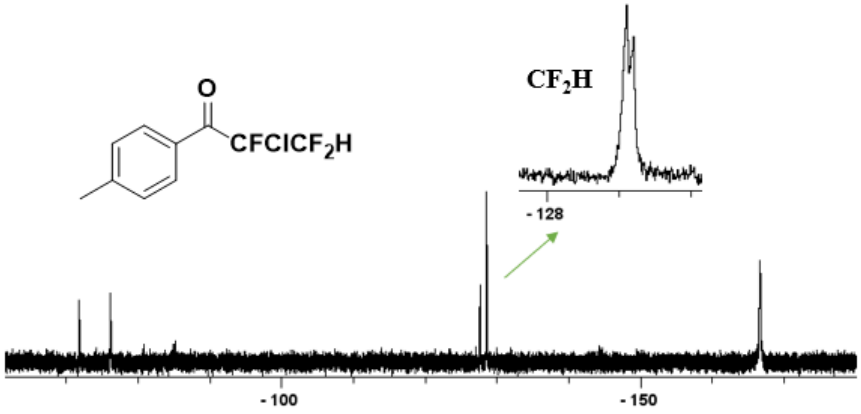

Figure A2.42 $^{19}F\{^{1}H\}$ NMR spectrum (282 MHz) of **2-4b** from complex **2-3** with 1.5 eq. of p-toluoyl chloride in DMSO at 25 ºC after 12 h.

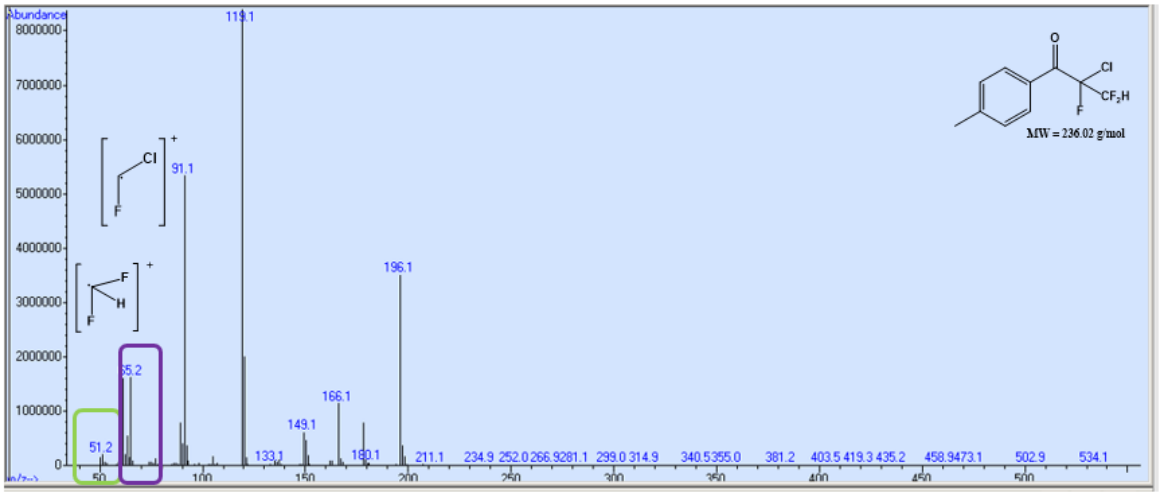

Figure A2.43 Selected GC-MS peak from reaction mixture of **2-4b** from complex **2-3** with 1.5 eq. of toluoyl chloride in DMSO at 25 ºC after 12 h (after filtration through alumina).

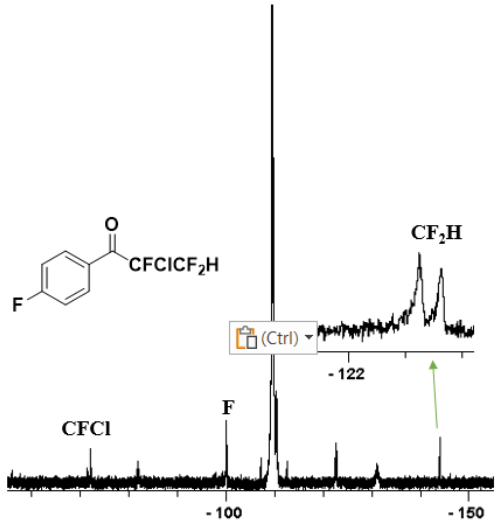

Figure A2. 44 ^{19}F NMR spectrum (282 MHz) of **2-4c** from complex **2-3** with 1.5 eq. of 4-fluoro-benzoyl chloride in DMSO at 25 ºC after 12 h.

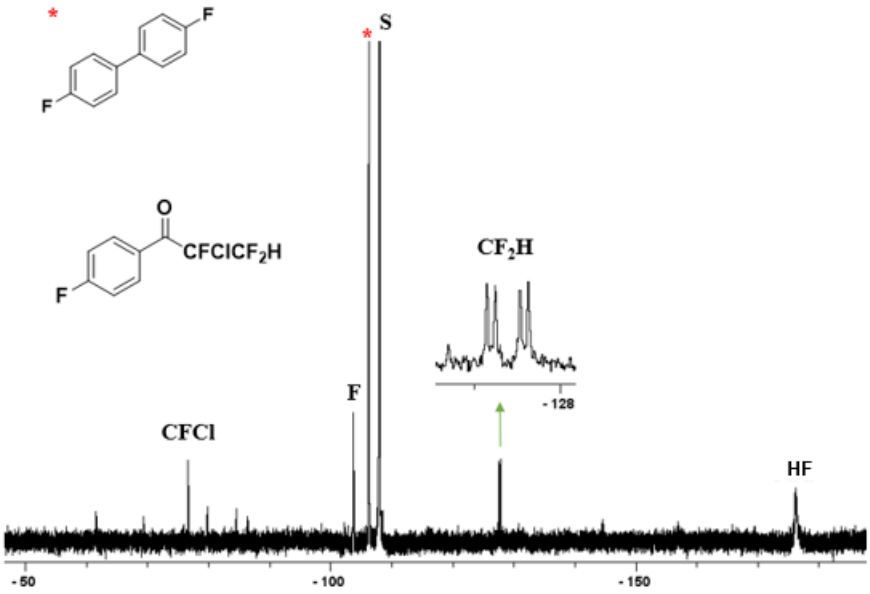

Figure A2.45 ^{19}F NMR spectrum (282 MHz) of **2-4c** from complex **2-3** with 1.5 eq. of 4-fluoro-benzoyl chloride and 8 eq. of DMSO in benzene at 50 °C after 12 h. S = substrate

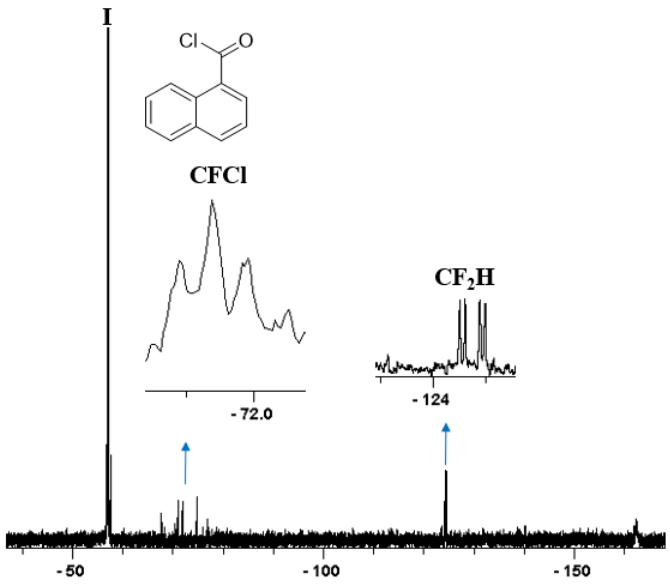

Figure A2.46 ^{19}F NMR spectrum (282 MHz) of **2-4d** from complex **2-3** with 1.5 eq. of 1-naphthoyl chloride in DMSO at 25 °C after 12 h.

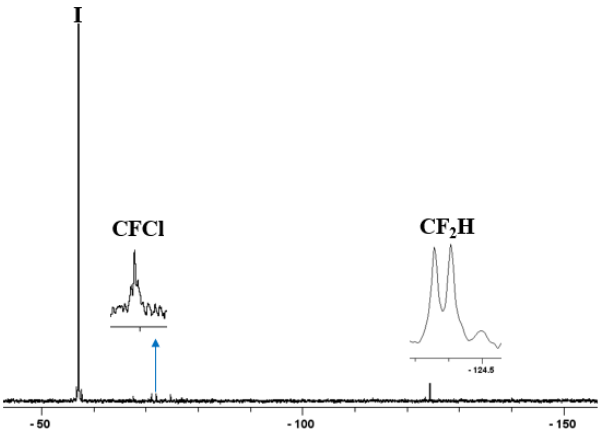

Figure A2.47 $^{19}F\{^{1}H\}$ NMR spectrum (282 MHz) of ***2-4d*** *from* complex **2-3** with 1.5 eq. of 1-naphthoyl chloride in DMSO at 25 ºC after 12 h.

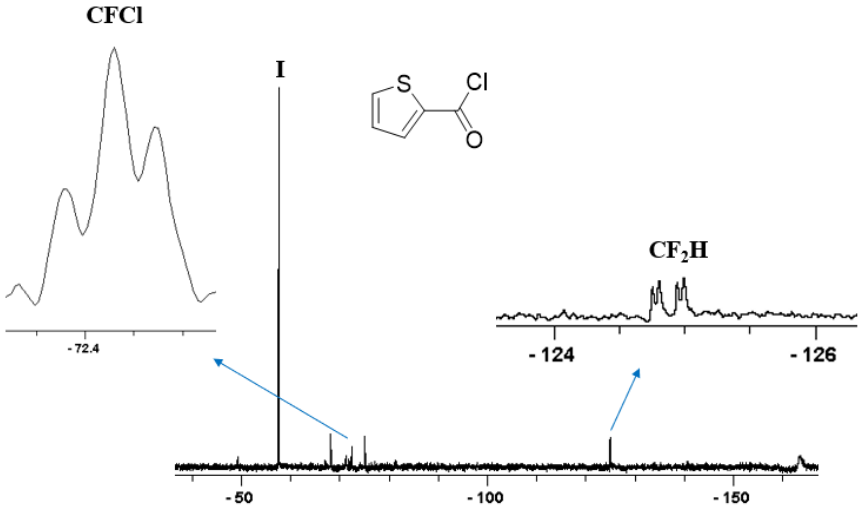

Figure A2.48 ^{19}F NMR spectrum (282 MHz) of **2-4e** from complex **2-3** with 1.5 eq. of 2-thiophenecarbonyl chloride in DMSO at 25 ºC after 12 h.

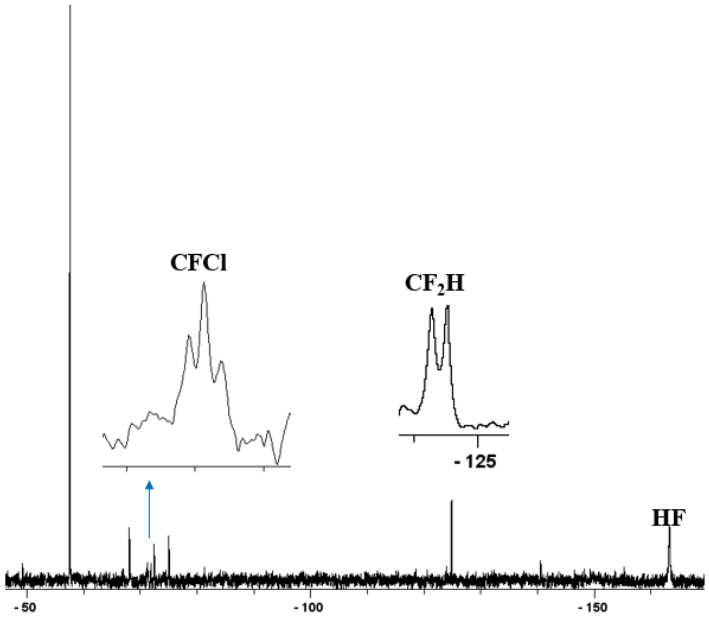

Figure A2.49 $^{19}F\{^{1}H\}$ NMR spectrum (282 MHz) of **2-4e** from complex **2-3** with 1.5 eq. of 2-thiophenecarbonyl chloride in DMSO at 25 ºC after 12 h.

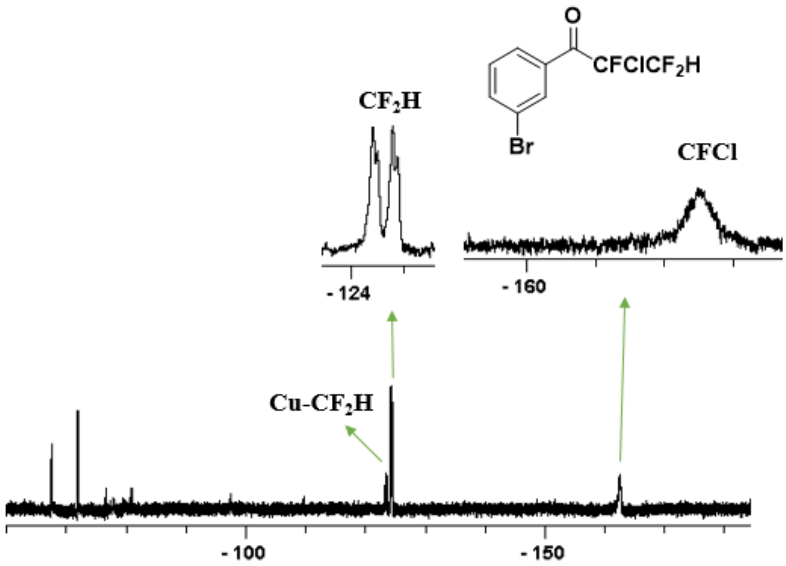

Figure A2.50 ^{19}F NMR spectrum (282 MHz) of **2-4f** from complex **2-3** with 1.5 eq. of m-Br-benzoyl chloride in DMSO at 25 ºC after 12 h

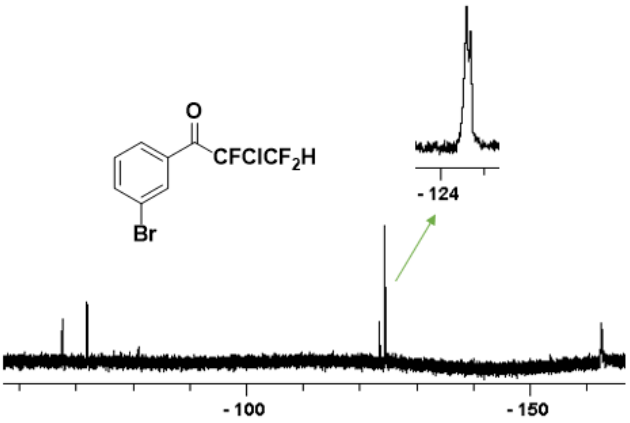

Figure A2.51 $^{19}F\{^{1}H\}$ NMR spectrum (282 MHz) of ***2-4f*** *from c*omplex **2-3** with 1.5 eq. of m-Br-benzoyl chloride in DMSO at 25 ºC after 12 h.

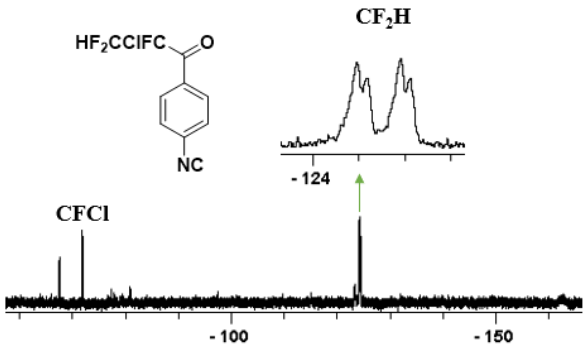

Figure A2.52 ^{19}F NMR spectrum (282 MHz) of **2-4g** from complex **2-3** with 1.5 eq. of 4-cyano-benzoyl chloride in DMSO at 25 ºC after 12 h.

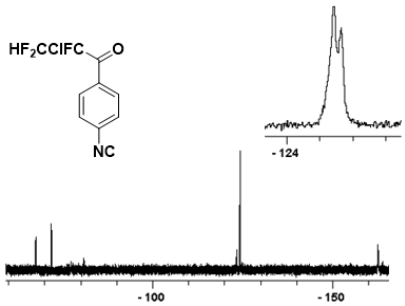

Figure A2.53 $^{19}F\{^{1}H\}$ NMR spectrum (282 MHz) of **2-4g** from complex **2-3** with 1.5 eq. of 4-cyano-benzoyl chloride in DMSO at 25 ºC after 12h.

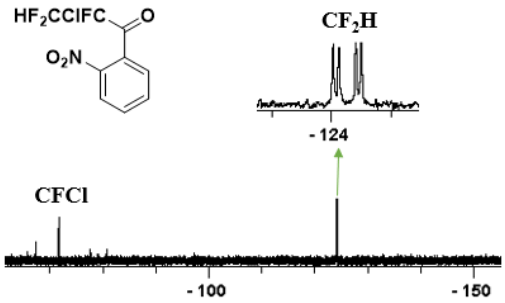

Figure A2.54 ^{19}F NMR spectrum (282 MHz) of **2-4h** from complex **2-3** with 1.5 eq. of 2-nitro-benzoyl chloride in DMSO at 25 °C after 12 h.

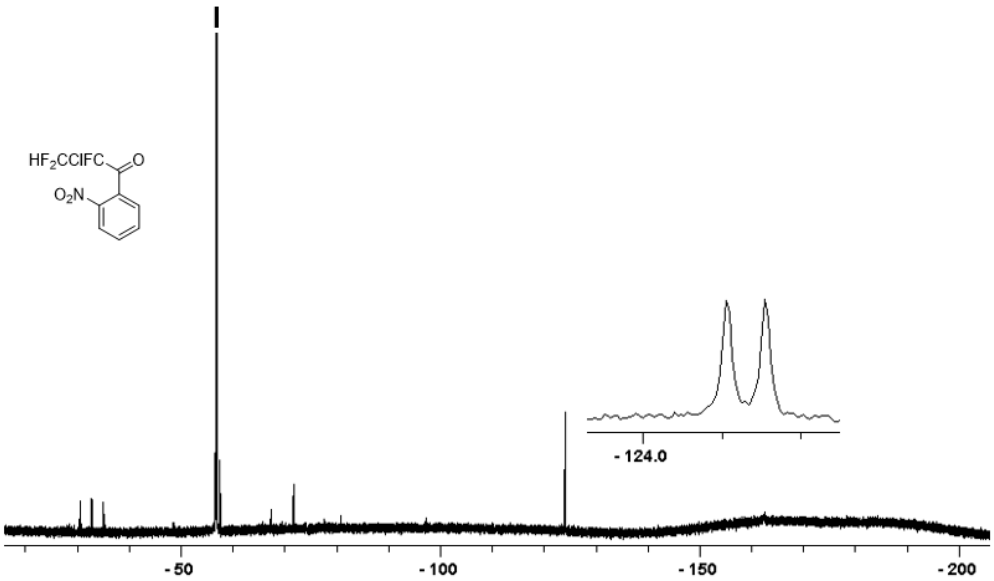

Figure A2.55 $^{19}F\{^{1}H\}$ NMR spectrum (282 MHz) of **2-4h** from complex **2-3** with 1.5 eq. of 2-nitro-benzoyl chloride in DMSO at 25 °C after 12 h.

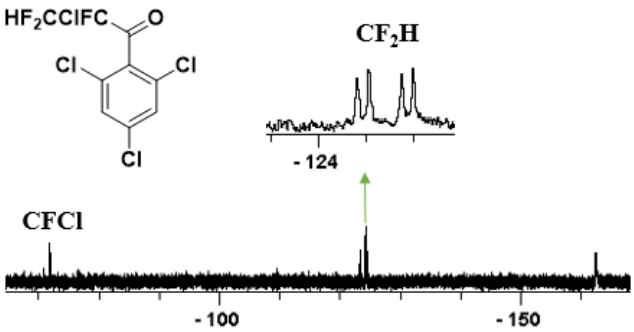

Figure A2.56 ^{19}F NMR spectrum (282 MHz) of **2-4i** from complex **2-3** with 1.5 eq. of 2,4,6-trichloro-benzoyl chloride in DMSO at 25 °C after12 h.

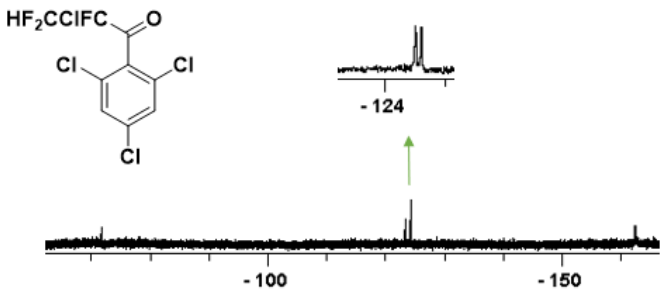

Figure A2.57 $^{19}F\{^{1}H\}$ NMR spectrum (282 MHz) of **2-4i** from complex **2-3** with 1.5 eq. of 2,4,6-trichloro-benzoyl chloride in DMSO at 25 °C after 12 h.

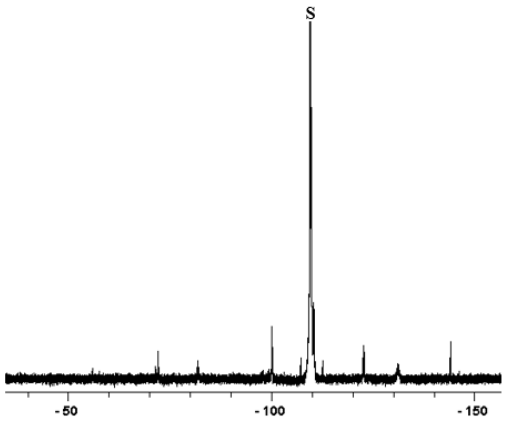

Figure A2.58 ^{19}F NMR spectrum (282 MHz) of complex **2-3** with p-F-benzyl bromide (**6**) in benzene. S = substrate.

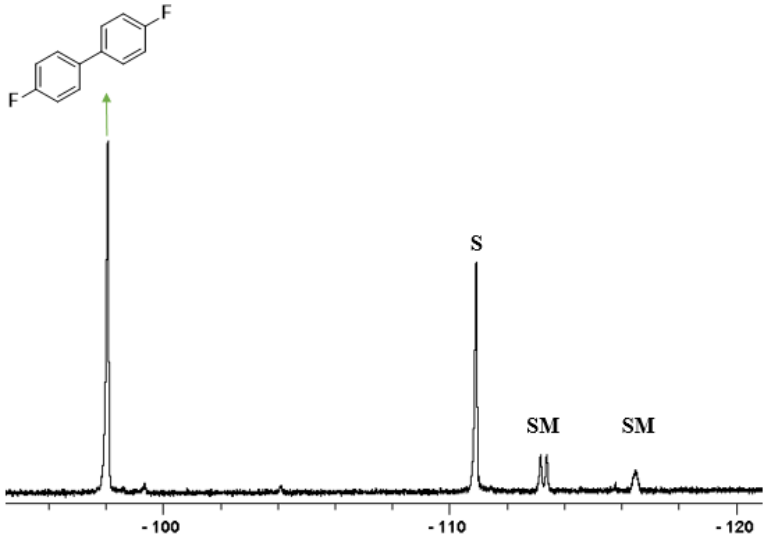

Figure A2.59 ^{19}F NMR spectrum (282 MHz) of complex **2-3** with 4-fluoro-iodobenzene in benzene. SM = starting material **2-3**, S = substrate.

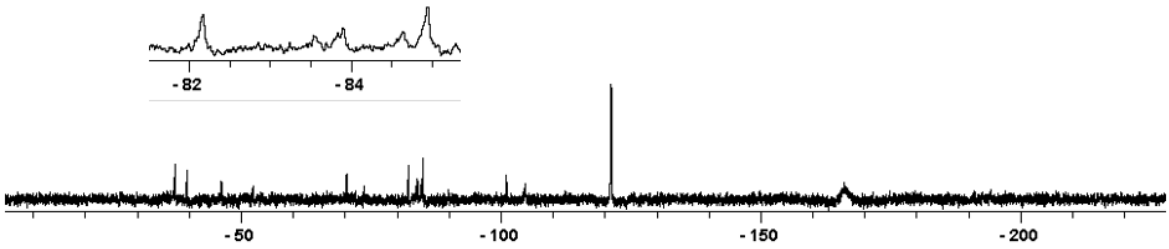

Figure A2.60 ^{19}F NMR spectrum (282 MHz) of complex **2-3** with methyl-2-iodobenzoate in DMSO at room temperature.

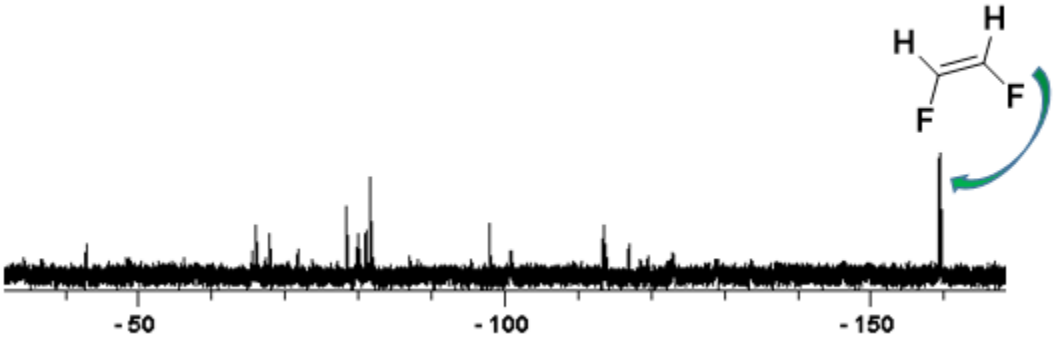

Figure A2.61 ^{19}F NMR spectrum (282 MHz) of complex **2-3** with 4-iodo-benzonitrile and 8 equiv. of DMF in benzene at 50 °C

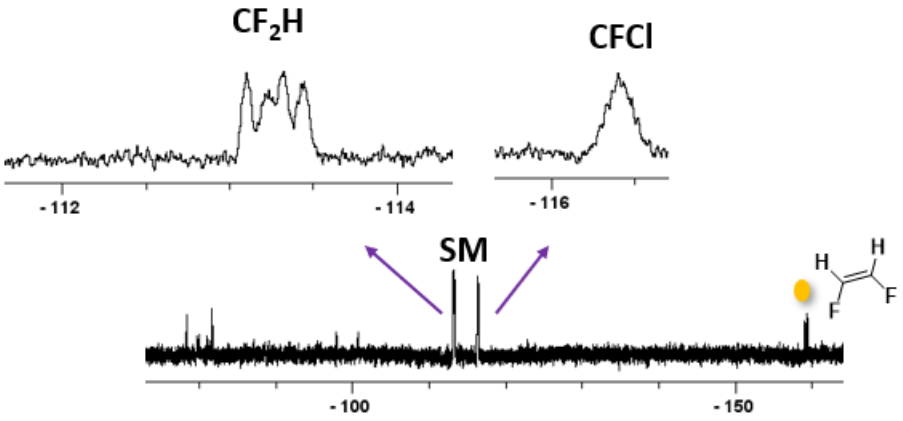

Figure A2.62 ^{19}F NMR spectrum (282 MHz) of complex 2-3 with methyl-2-iodobenzoate and 8 eq. of DMSO in benzene at 50 °C.

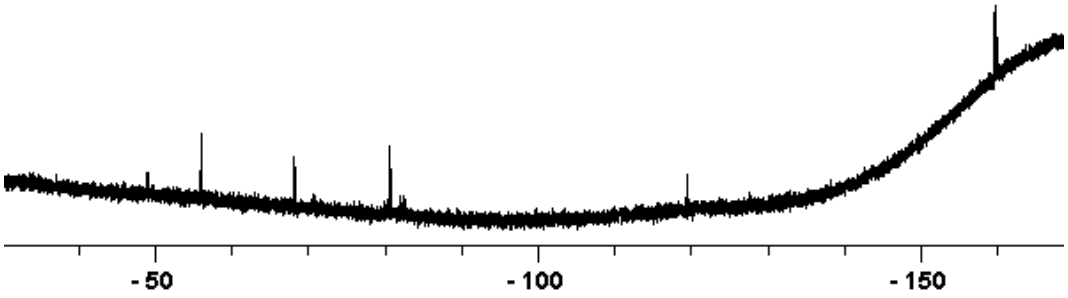

Figure A2.63 ^{19}F NMR spectrum (282 MHz) of complex **2-3** with 4-iodo-benzonitrile in benzene at 35 ^{o}C overnight.

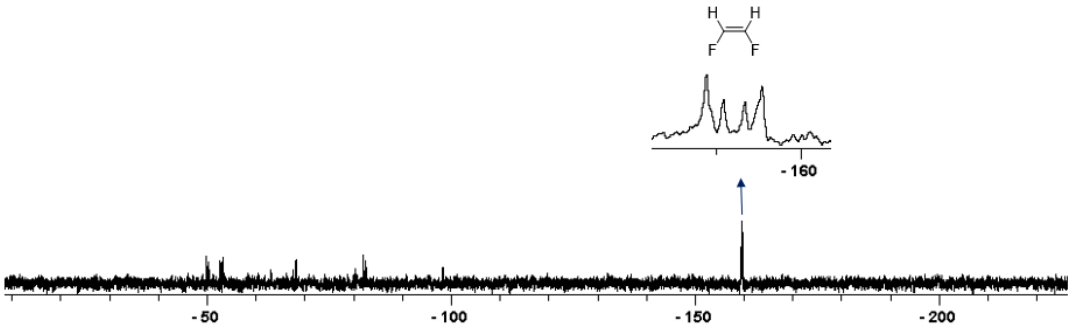

Figure A2.64 ^{19}F NMR spectrum (282 MHz) of complex **2-3** with methyl 2-iodo-benzoate in benzene at 35 ^{o}C overnight.

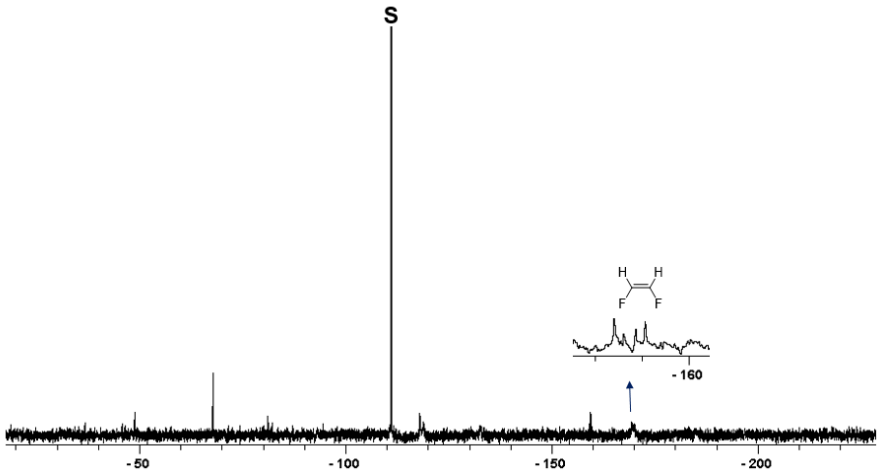

Figure A2.65 ^{19}F NMR spectrum (282 MHz) of complex **2-3** with 4-fluoro-iodobenzene and 8 eq. of DMSO in benzene at 35 ^{o}C overnight.

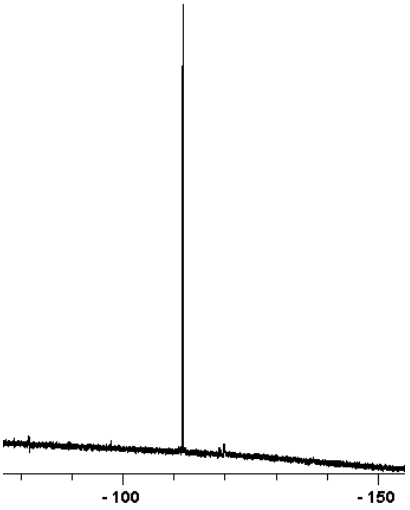

Figure A2.66 ^{19}F NMR spectrum (282 MHz) of complex **2-3** with 4-fluoro-iodobenzene in DMF diluted 2x.

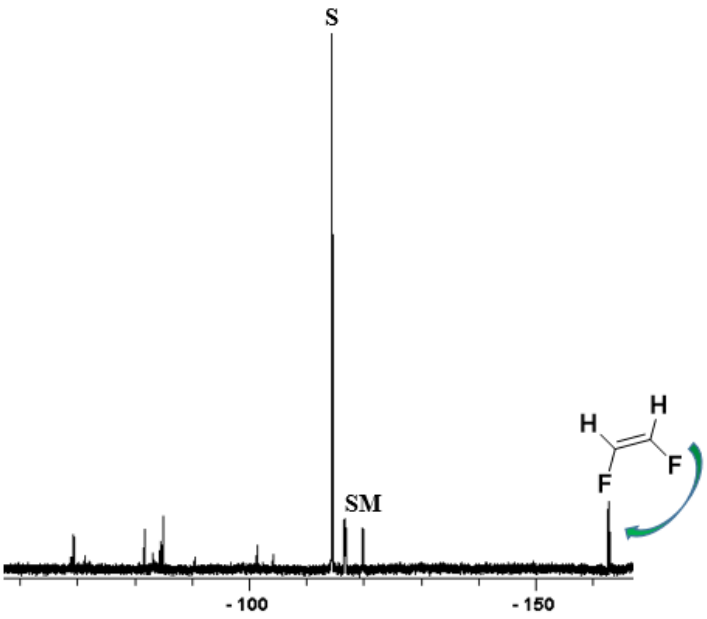

Figure A2.67 ^{19}F NMR spectrum (282 MHz) of complex **2-3** with 4-fluoro-iodobenzene in benzene diluted 2x.

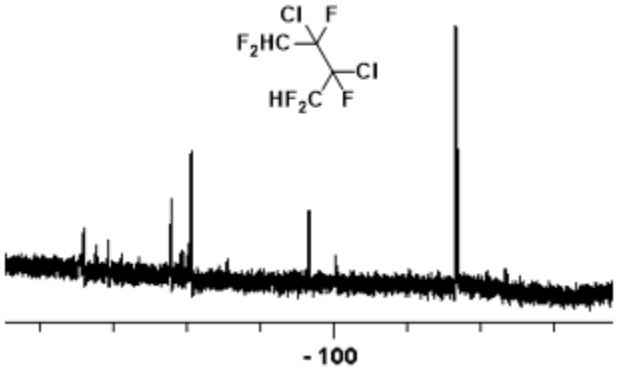

Figure A2.68 ^{19}F NMR spectrum (282 MHz) of complex **2-3** in DMSO.

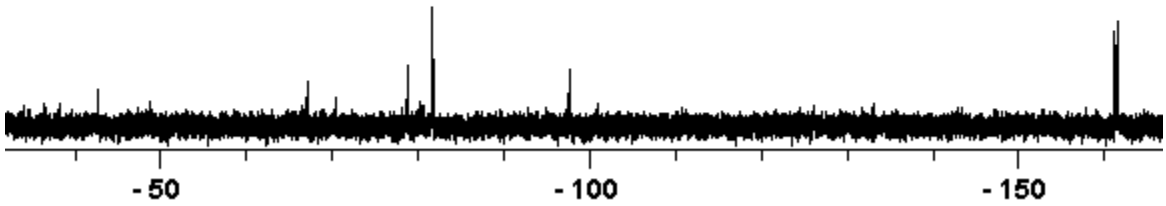

Figure A2.69 ^{19}F NMR spectrum (282 MHz) of complex **2-3** in DMF.

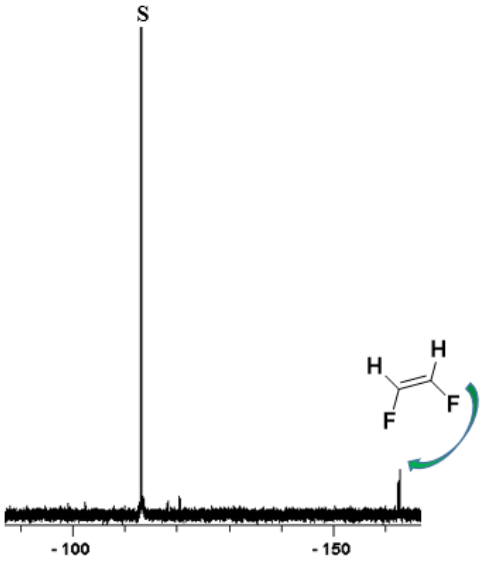

Figure A2.70 ^{19}F NMR spectrum (282 MHz) of complex **2-3** in DMPU.

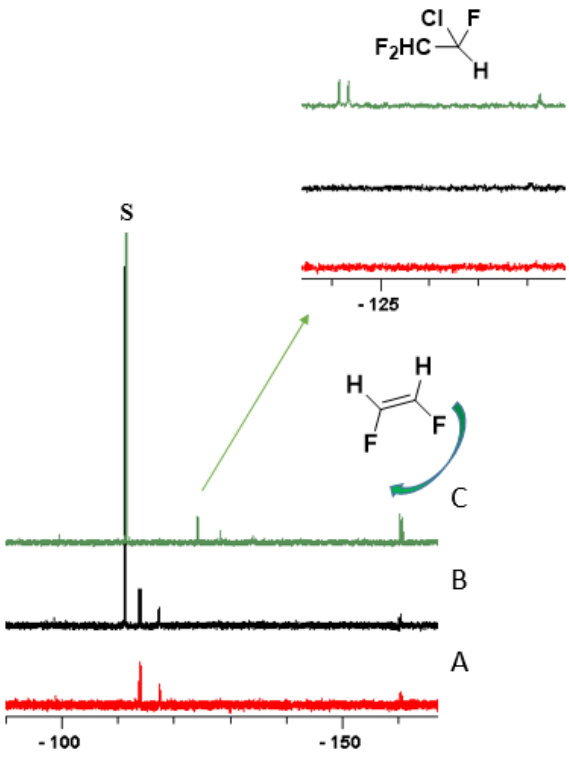

Figure A2.71 ^{19}F NMR spectrum (282 MHz) of complex **2-3** in CPME after 30 min (**A**), addition of 8 eq. of DMSO and 1.5 eq. of 4-fluoro-iodobenzene (**B**), after heating at 50 ºC overnight (**C**).

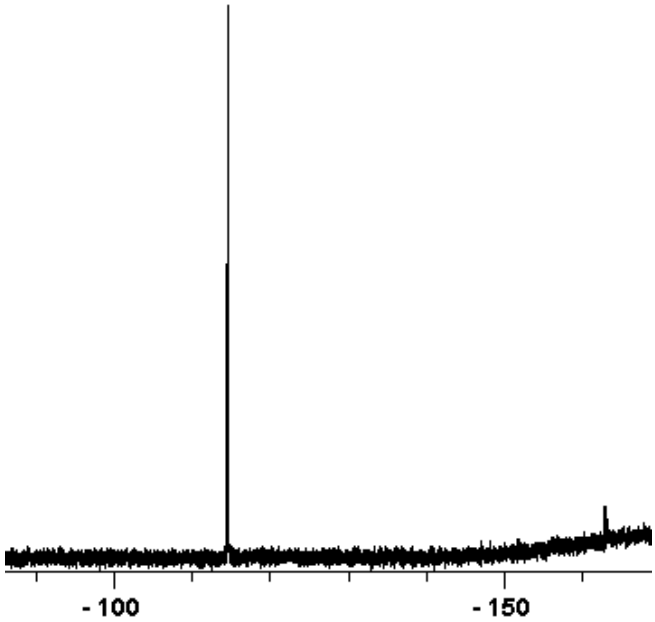

Figure A2.72 ^{19}F NMR spectrum (282 MHz) of complex **2-3** with 4- fluoro-iodobenzene + 8 eq. of DMPU in benzene diluted.

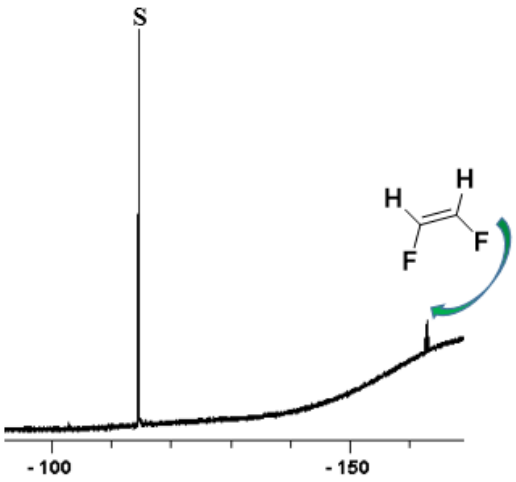

Figure A2.73 ^{19}F NMR spectrum (282 MHz) of complex **2-3** with 4-fluoro-iodobenzene in benzene diluted at 40 ^{o}C.

Figure A2.74 ^{19}F NMR spectrum (282 MHz) of complex **2-3** in 1,4-dioxane after 24 h.

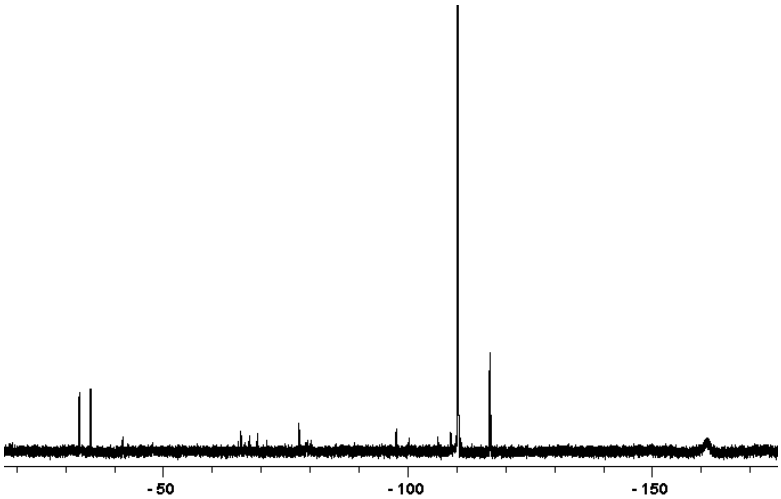

Figure A2.75 ^{19}F NMR spectrum (282 MHz) of complex **2-3** with 4-fluoro-iodobenzene in DMSO at 50 ^{o}C.

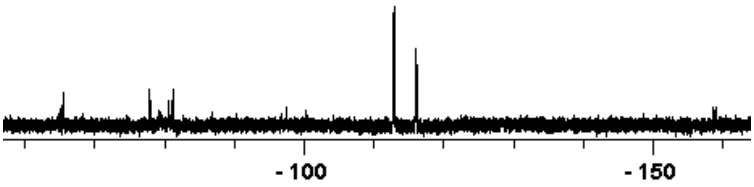

Figure A2.76 ^{19}F NMR spectrum (282 MHz) of complex **2-3** with 4-iodo-benzonitrile in benzene at 50 ^{o}C.

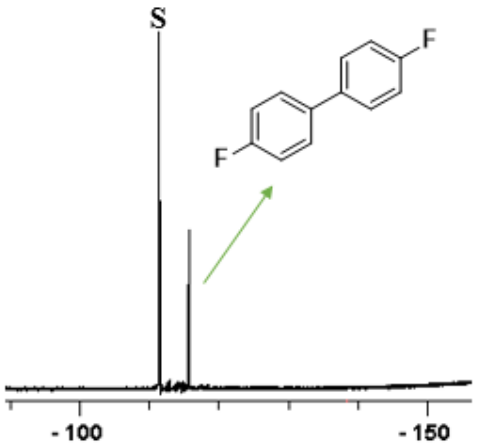

Figure A2.77 ^{19}F NMR spectrum (282 MHz) of complex **2-3** with 4-fluoro-iodobenzene in CPME at 50 ^{o}C. S = substrate.

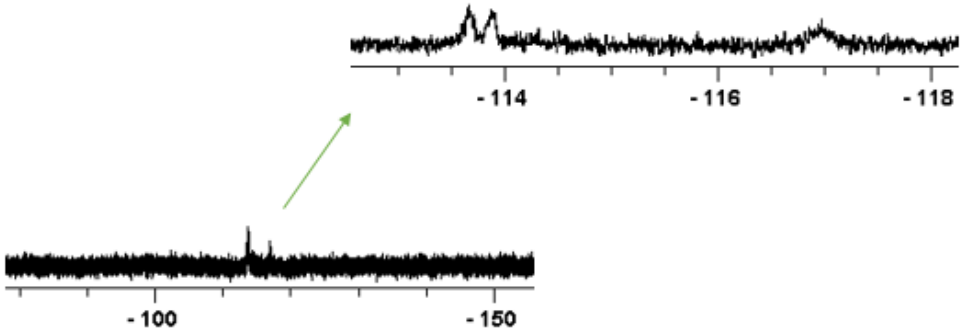

Figure A2.78 ^{19}F NMR spectrum (282 MHz) of complex **2-3** with 4-iodobenzonitrile in CPME at 100 ^{o}C.

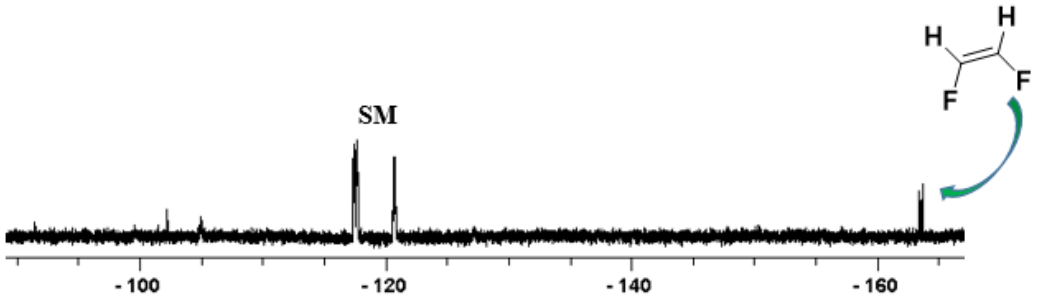

Figure A2.79 ^{19}F NMR spectrum (282 MHz) of complex **2-3** with methyl-2-iodobenzoate in benzene at 50 ºC.

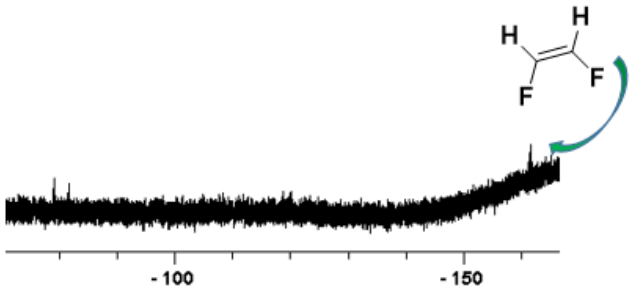

Figure A2.80 ^{19}F NMR spectrum (282 MHz) of complex **2-3** with iodo-benzonitrile in ACN at room temperature.

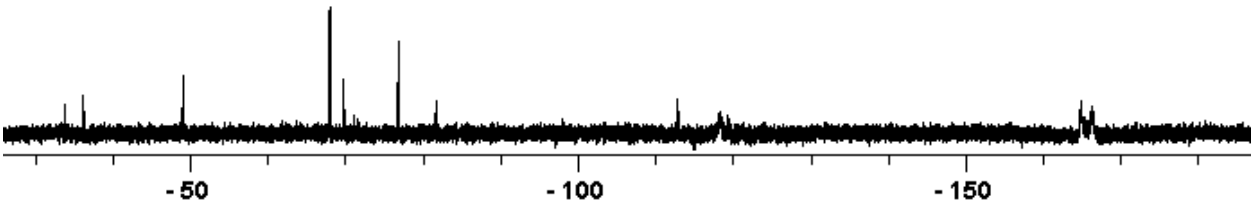

Figure A2.81 ^{19}F NMR spectrum (282 MHz) of complex **2-3** with iodo-nitrobenzene in DMSO/ benzene 1:1 at 50 ºC.

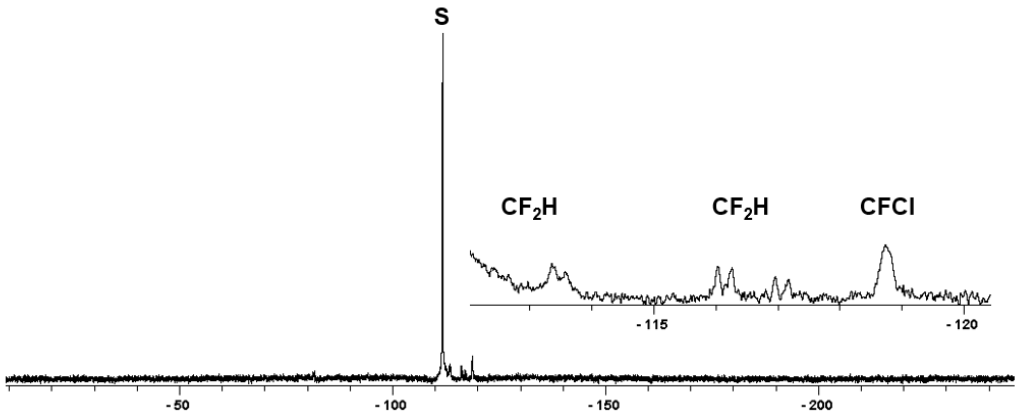

Figure A2.82 ^{19}F NMR spectrum (282 MHz) of complex **2-3** + 4-fluoro-iodobenzene + 8 equiv. of pyridine in benzene. S = substrate.

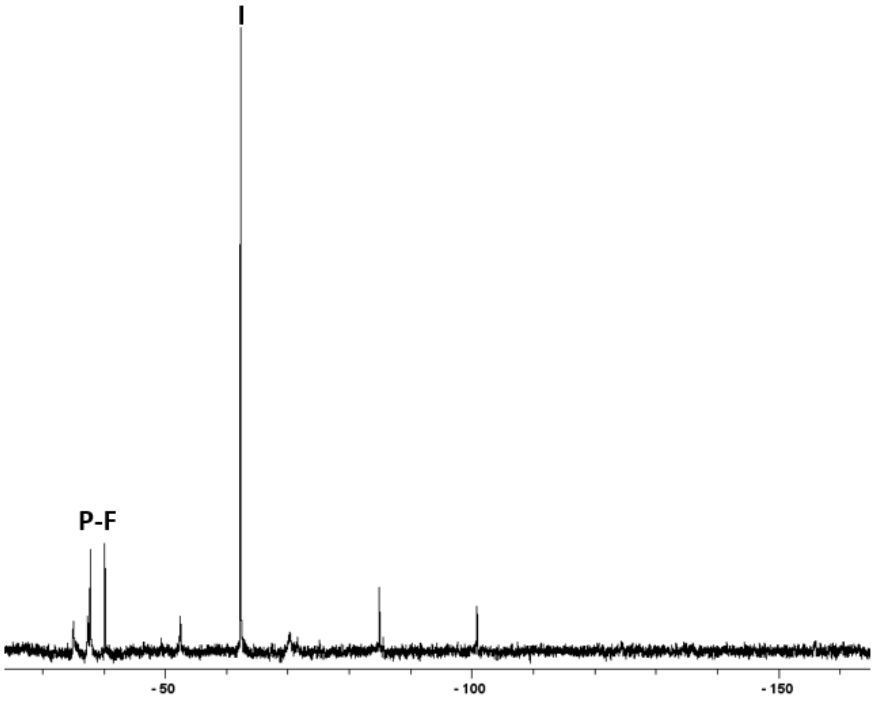

Figure A2.83 ^{19}F NMR spectrum (282 MHz) of complex **2-3** +2-methyliodo benzoate + 2 equiv. of CuBr + 28 equiv. of DMSO in benzene. I = internal standard, $PhCF_3$.

Chapter 3: Copper-Mediated -$CF(OCF_3)CF_2H$ Transfer to Organic Electrophiles

Table A3.1 Details of X-ray diffraction data collection and refinement

Identification code	K1082	K0212_F	S0379_F
Empirical formula	$C_{37}H_{34}Cl_2CuF_6N_2OP$	$C_{39}H_{31}CuF_6OP_2$	C50H58CuF6N2OP
Formula weight	802.07	755.12	110.48
Temperature/K	200.05	204(2)	200(2)
Crystal system	Triclinic	monoclinic	monoclinic
Space group	P-1	$P2_1/c$	$P2_1/n$
a/Å	10.9841(11)	19.093(3)	9.7127(4)
b/Å	18.5694(19)	10.6109(18)	16.3030(7)
c/Å	19.517(2)	18.412(3)	29.3819(13)
α/°	69.627(2)	90	90
β/°	81.123(3)	109.613(11)	95.8390(10)
γ/°	80.657(3)	90	90
Volume/$Å^3$	3661.7(6)	3513.9(10)	4628.4(3)
Z	4	4	4
$\rho_{calc}/g\cdot cm^{-3}$	1.455	1.427	1.308
μ/mm^{-1}	0.849	0.775	0.569
F(000)	1640.0	1544.0	1912.0
Crystal size/mm^3	0.16 × 0.08 × 0.07	0.286 × 0.23 × 0.098	0.415 × 0.302 × 0.292
Radiation	MoKα (λ = 0.71073)	MoKα (λ = 0.71073)	MoKα (λ = 0.71073)
2Θ range collection/°	2.238 to 52.806	4.456 to 46.536	2.786 to 61.226
Index ranges	-13 ≤ h ≤ 13 -21 ≤ k ≤ 23 0 ≤ l ≤ 24	-21 ≤ h ≤ 20 -10 ≤ k ≤ 11 -20 ≤ l ≤ 18	-13 ≤ h ≤ 13 -23 ≤ k ≤ 23 -39 ≤ l ≤ 42
Reflections collected	46359	14525	101956
Independent reflections	14544 [R_{int} = 0.0558, R_{sigma} = 0.0901]	5047 [R_{int} = 0.1019, R_{sigma} = 0.1386]	14211 [R_{int} = 0.0576, R_{sigma} = 0.0412]
Data/restraints/parameters	14544/1818/1072	5047/204/479	14211/95/604
Goodness-of-fit on F^2	1.080	1.016	1.042
Final R indexes [I>=2σ (I)]	R_1 = 0.0697 wR_2 = 0.1189	R_1 = 0.0760, wR_2 = 0.1521	R_1 = 0.0677 wR_2 = 0.1860
Final R indexes [all data]	R_1 = 0.1427 wR_2 = 0.1432	R_1 = 0.1611, wR_2 = 0.1860	R_1 = 0.1145 wR_2 = 0.2142
Largest diff. peak/hole / $e\cdot Å^{-3}$	0.58/-0.65	0.75/-0.66	0.84/-1.02

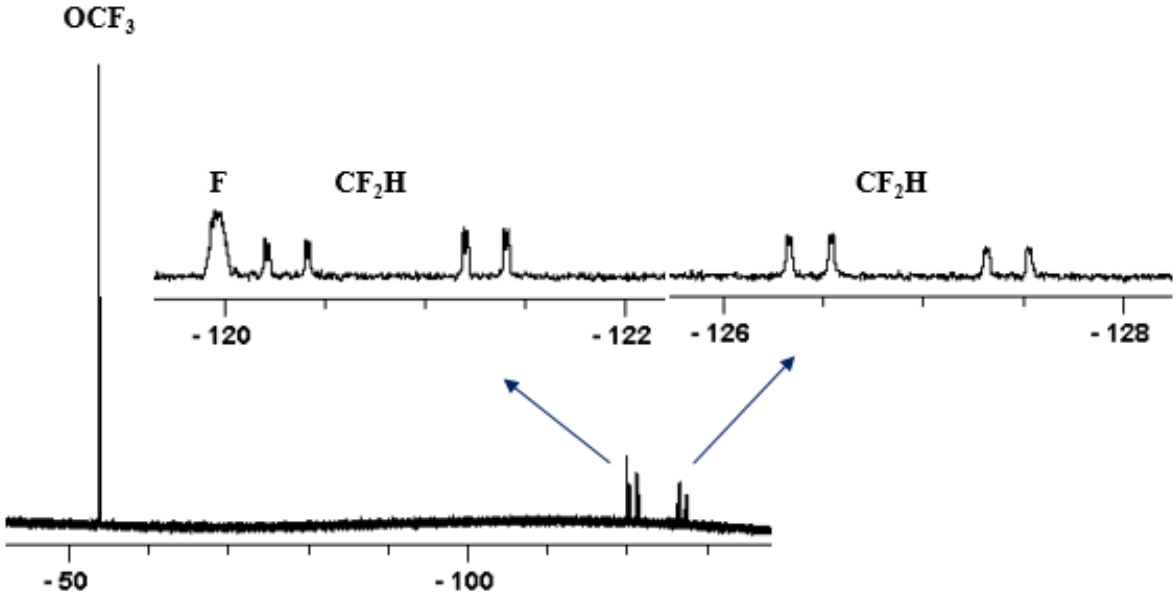

Figure A3.1 ^{19}F NMR spectrum (282 MHz, C_6D_6) of complex **3-1**.

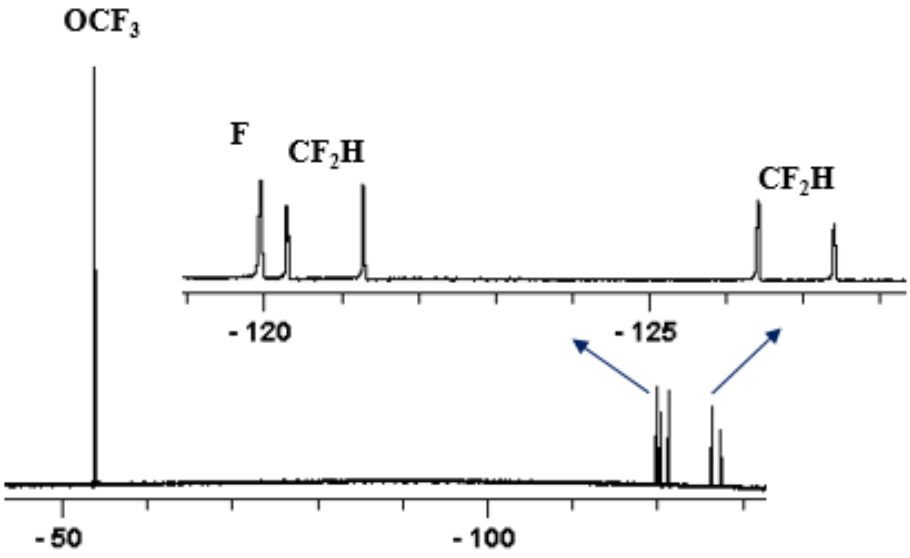

Figure A3.2 $^{19}F\{^1H\}$ NMR spectrum (282 MHz, C_6D_6) of complex **3-1**.

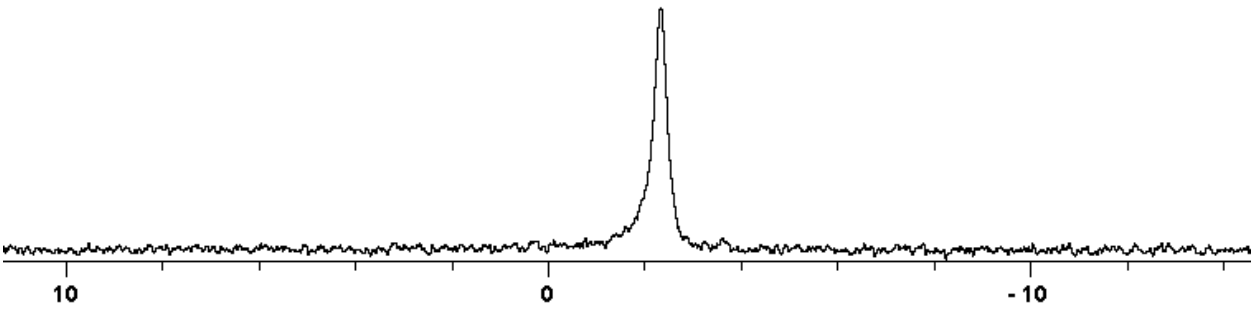

Figure A3.3 ^{31}P NMR spectrum (121 MHz, C_6D_6) of complex **3-1**.

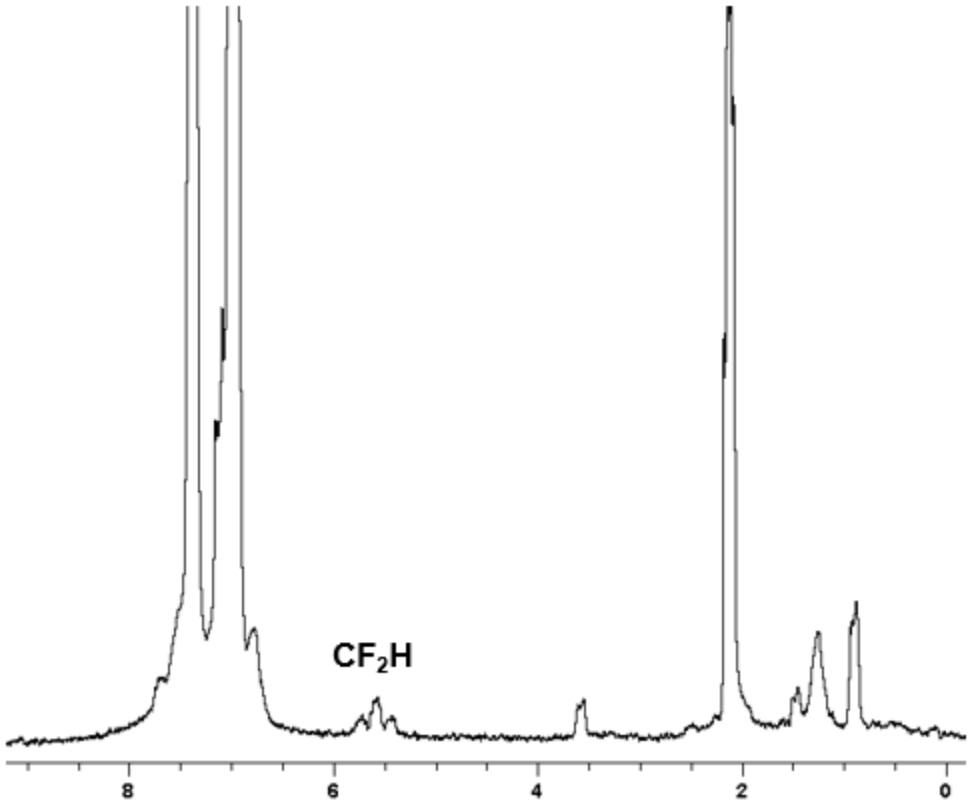

Figure A3.4 ^{1}H NMR spectrum (300 MHz, C_6D_6) of complex **3-1**.

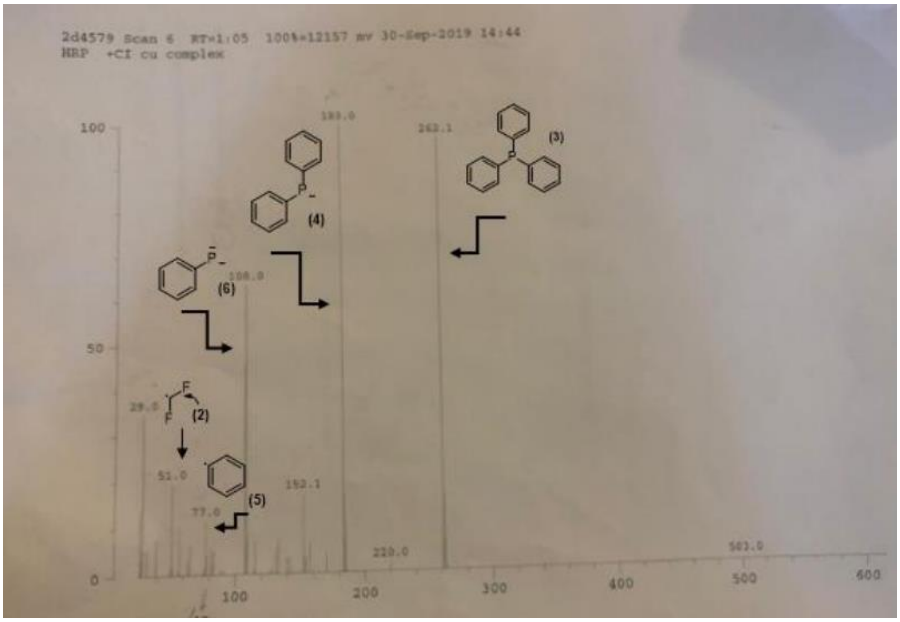

Figure A3.5 EI-MS spectrum of complex **3-1**.

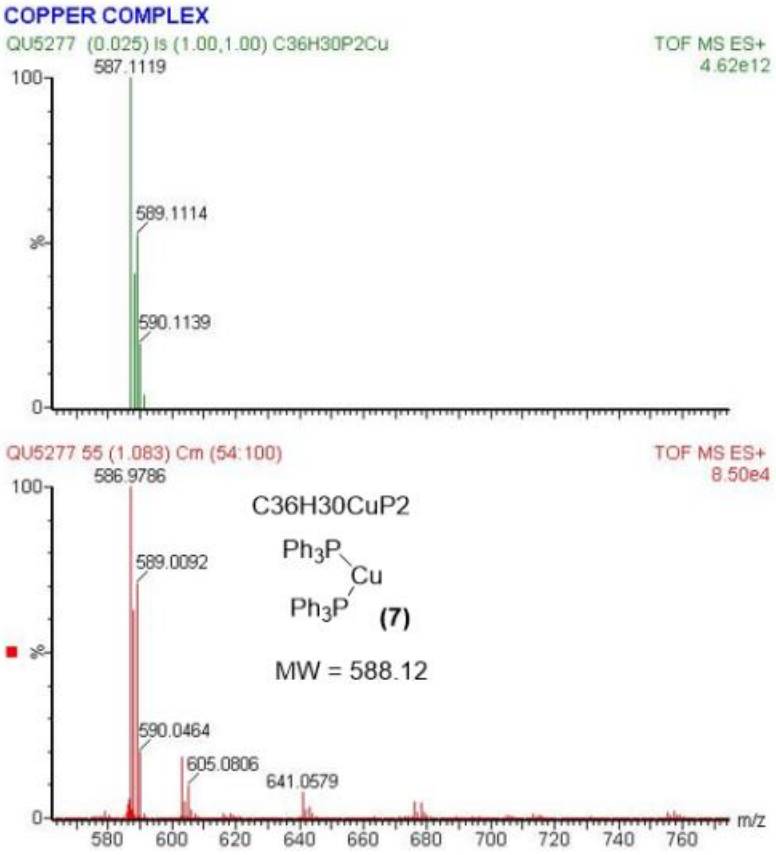

Figure A3.6 ESI-MS (positive mode) spectrum of complex **3-1**.

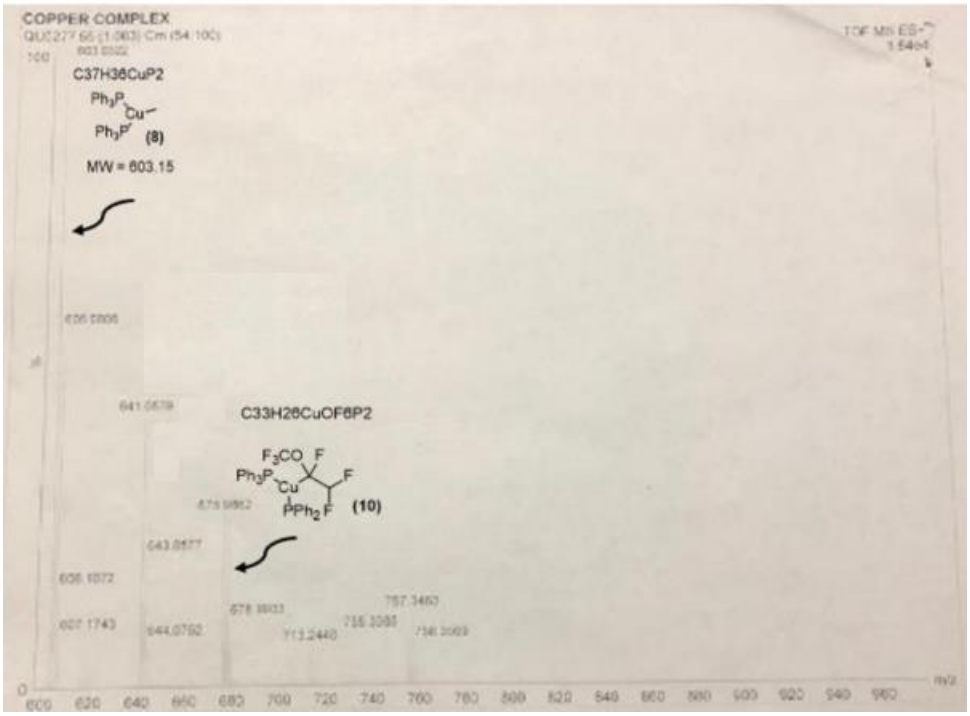

Figure A3.7 Mass spectrum of complex **3-1**.

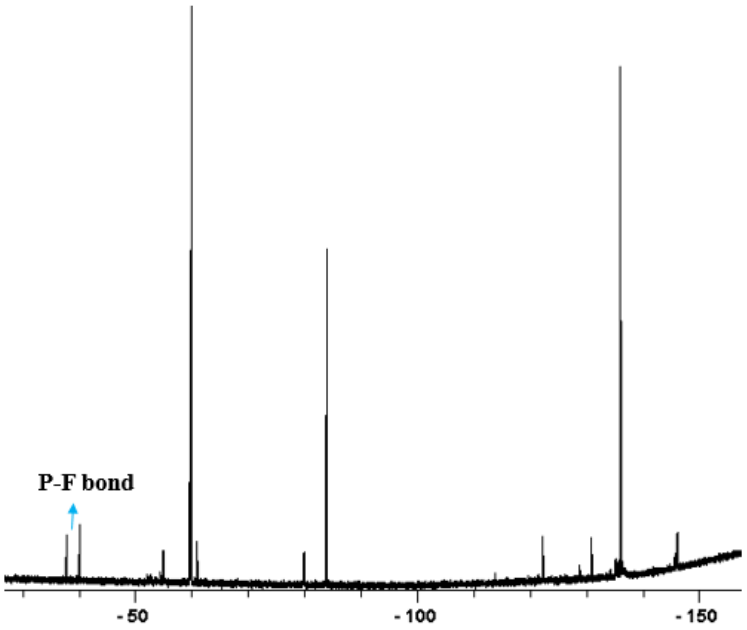

Figure A3.8 ^{19}F NMR spectrum (282 MHz, C_6D_6) of complex **3-1** and $PMePh_2$ in benzene.

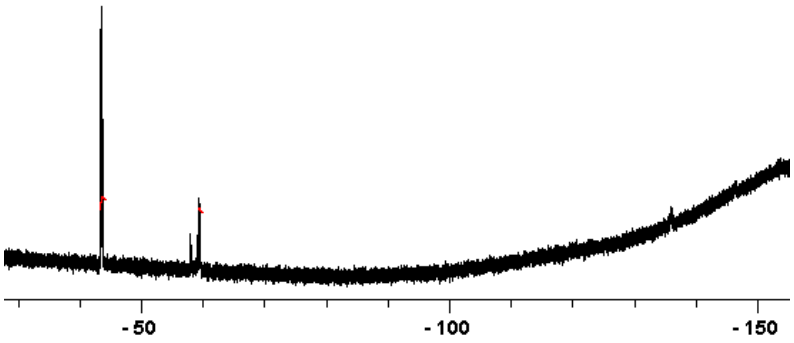

Figure A3.9 ^{19}F NMR spectrum (282 MHz, C_6D_6) of complex **3-1** and IMes in benzene.

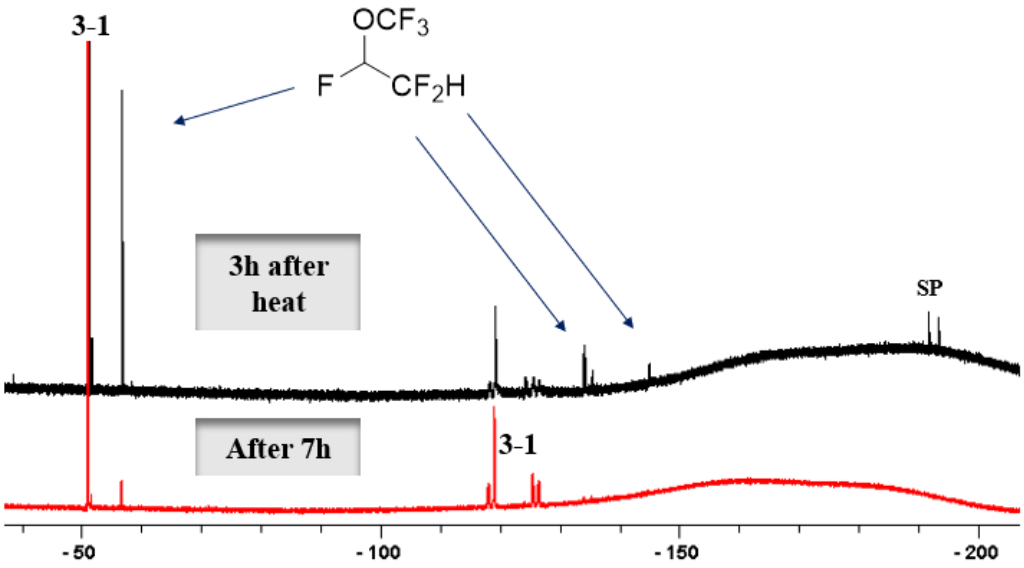

Figure A3.10 ^{19}F NMR spectra (282 MHz, C_6D_6) of complex **3-1** with 1 equiv of benzoyl chloride in THF and after heating at 40 °C. $CF_2HCHF(OCF_3)$: -56.6 (s, OCF_3), -134 (dmult, $^2J_{FH}$ = 55 Hz, CF_2H) and -144.9 ppm (dmult, $^2J_{FH}$ = 54 Hz, CF). SP = uncharacterized side product

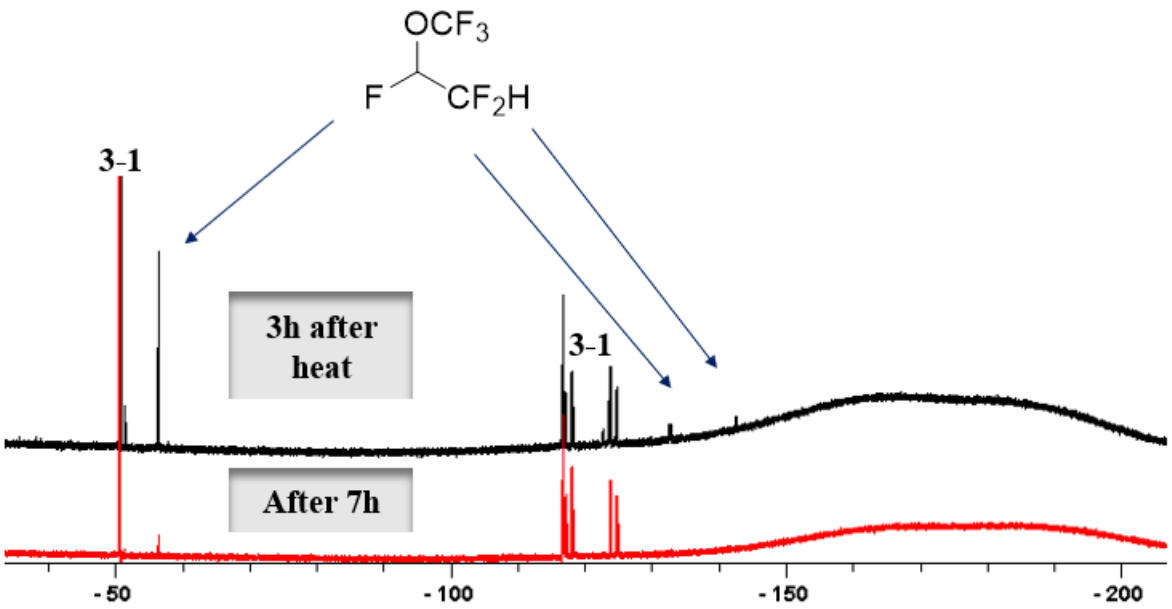

Figure A3.11 ^{19}F NMR spectrum (282 MHz, C_6D_6) of complex **3-1** with 1 equiv of benzoyl chloride in Et_2O and after heating at 40 °C.

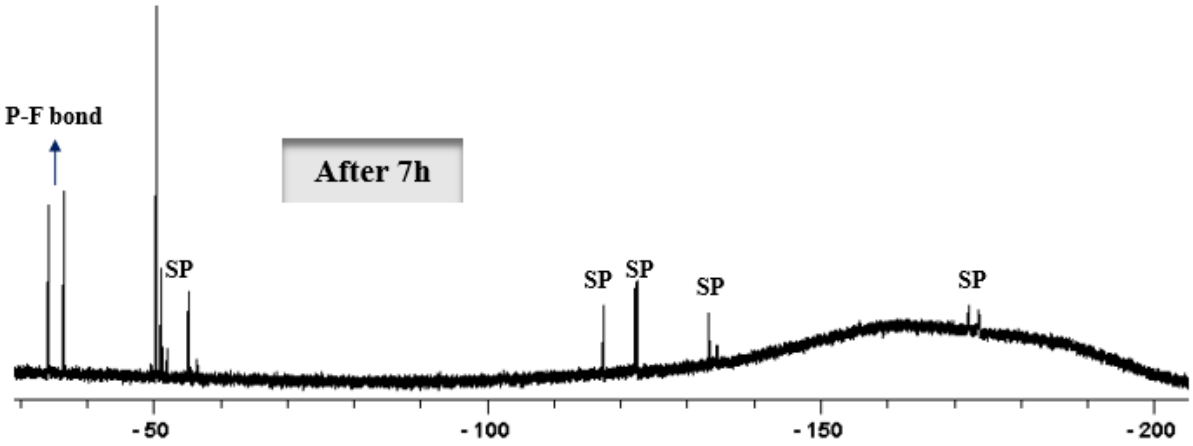

Figure A3.12 ^{19}F NMR spectrum (282 MHz, C_6D_6) of complex **3-1** with 1 equiv of benzoyl chloride in N,N-dimethylacetamide after 7 h. SP = uncharacterized side products.

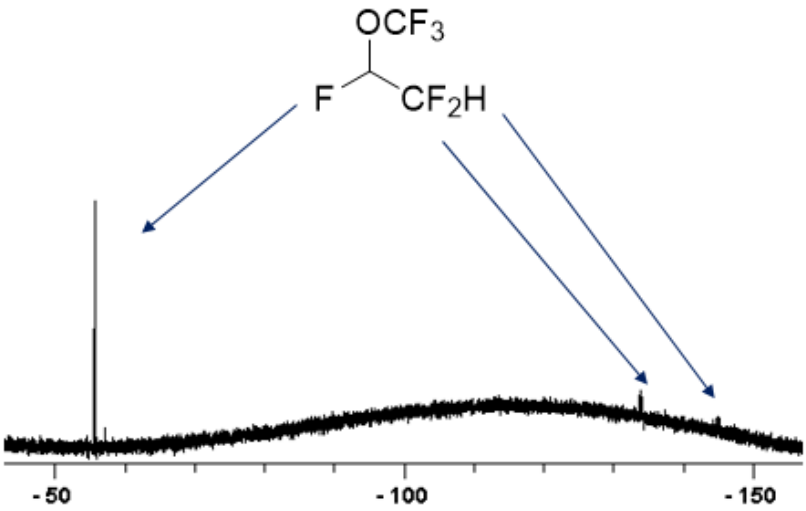

Figure A3.13 ^{19}F NMR spectrum (282 MHz, C_6D_6) of complex **3-1** with 1 equiv of benzoyl chloride in acetonitrile.

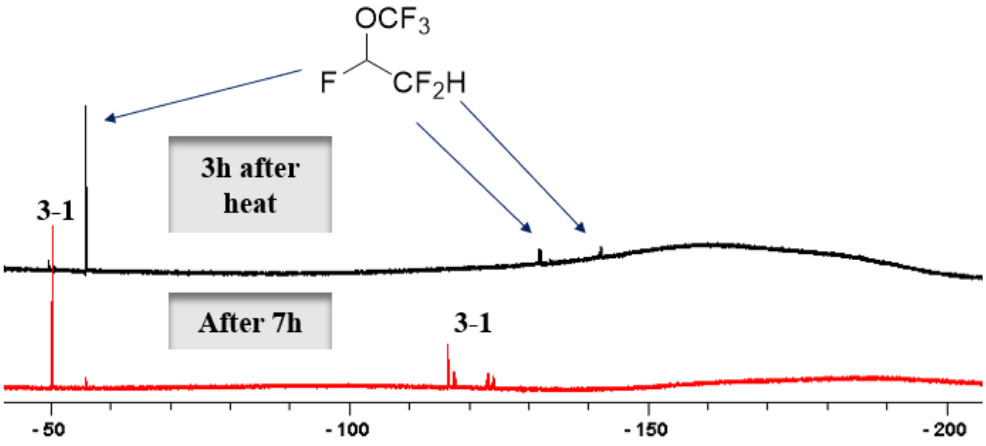

Figure A3.14 ^{19}F NMR spectrum (282 MHz, C_6D_6) of complex **3-1** with 1 equiv of benzoyl chloride in cyclopentyl methyl ether.

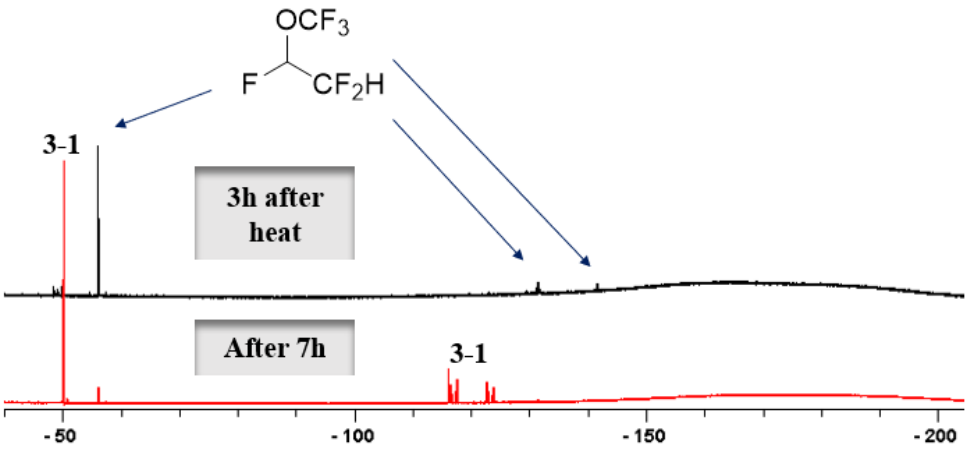

Figure A3.15 ^{19}F NMR spectrum (282 MHz, C_6D_6) of complex **3-1** with 1 equiv of benzoyl chloride in toluene.

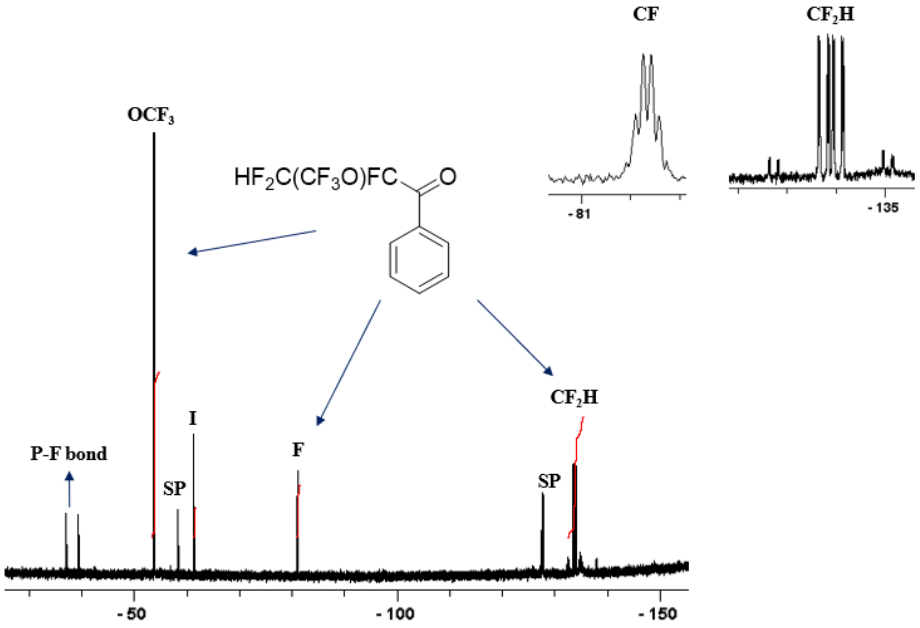

Figure A3.16 ^{19}F NMR spectrum (282 MHz, C_6D_6) of product fluorinated ketone **3-3a**, after complex **3-1** reacted with 1 equiv of benzoyl chloride in DMSO. SP = side product and I = Internal Standard ($PhCF_3$).

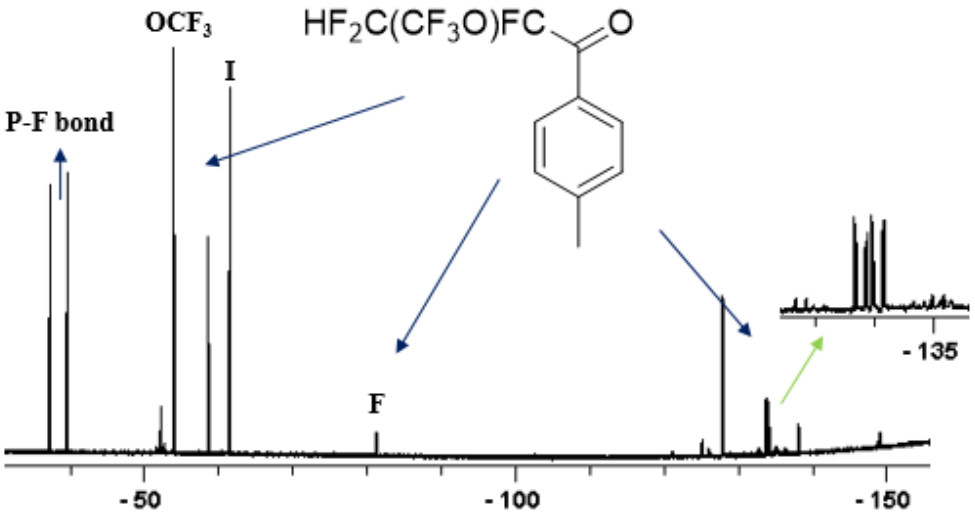

Figure A3.17 ^{19}F NMR spectrum (282 MHz, C_6D_6) of **3-3b**, after complex **3-1** reacted with 1 equiv of 4-toluoyl chloride in DMSO. I = Internal Standard ($PhCF_3$).

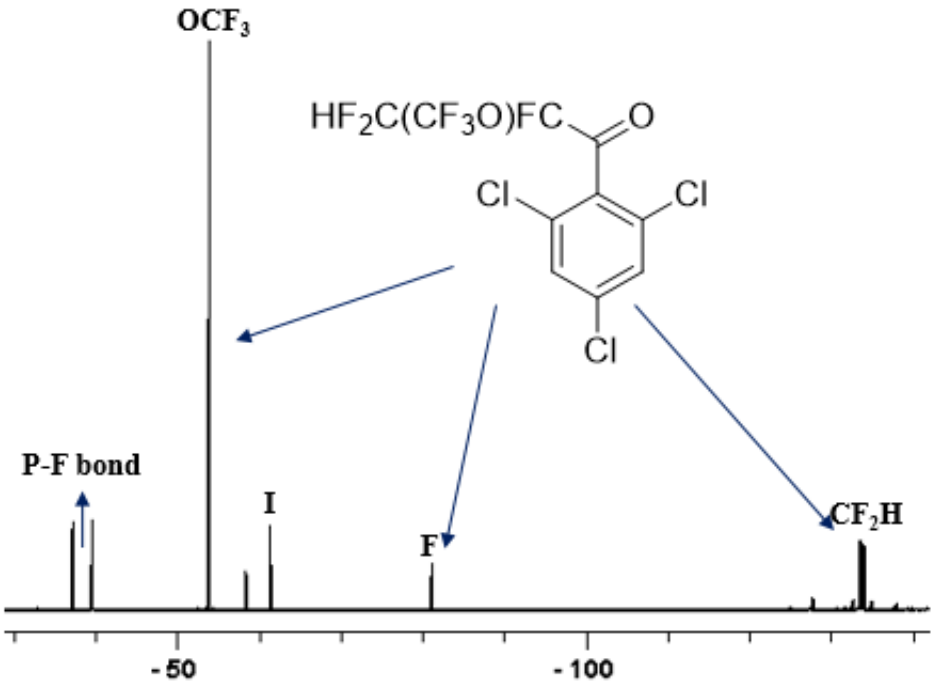

Figure A3.18 ^{19}F NMR spectrum (282 MHz, C_6D_6) of **3-3c**, after complex **3-1** reacted with 1 equiv of 2,4,6-trichlorobenzoyl chloride in DMSO. I = Internal Standard ($PhCF_3$).

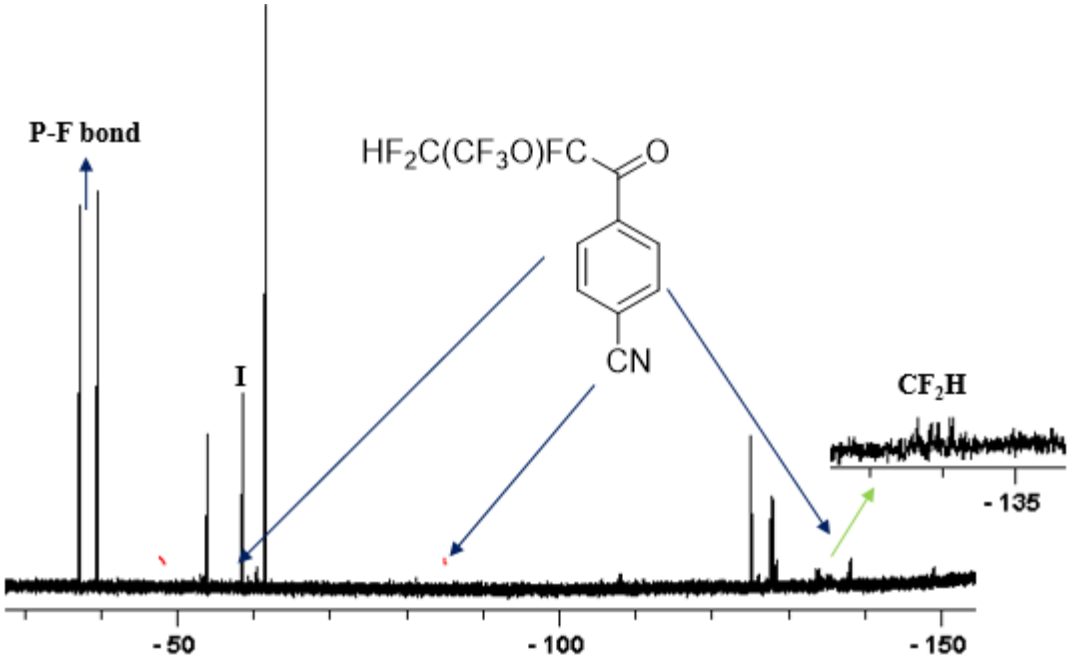

Figure A3.19 ^{19}F NMR spectrum (282 MHz, C_6D_6) of **3-3d**, after complex **3-1** reacted with 1 equiv of 4-cyanobenzoyl chloride in DMSO. I = Internal Standard ($PhCF_3$).

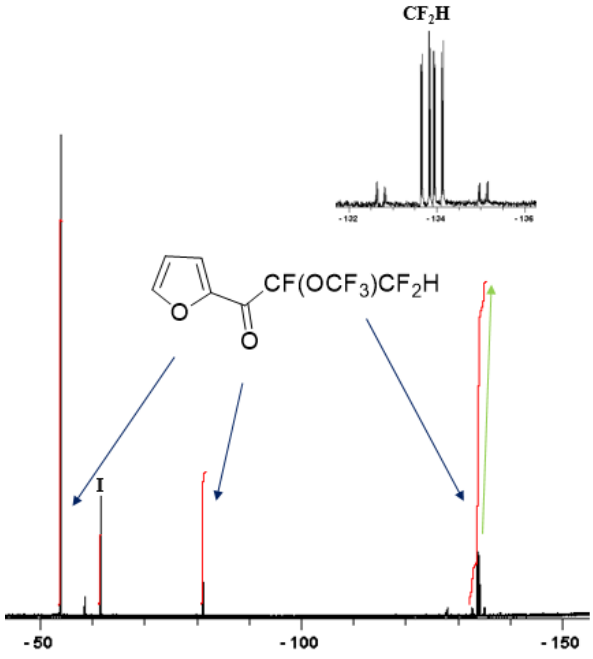

Figure A3.20 ^{19}F NMR spectrum (282 MHz, C_6D_6) of **3-3e**, after complex **3-1** reacted with 1 equiv of 2-furoyl chloride in DMSO. I = Internal Standard ($PhCF_3$).

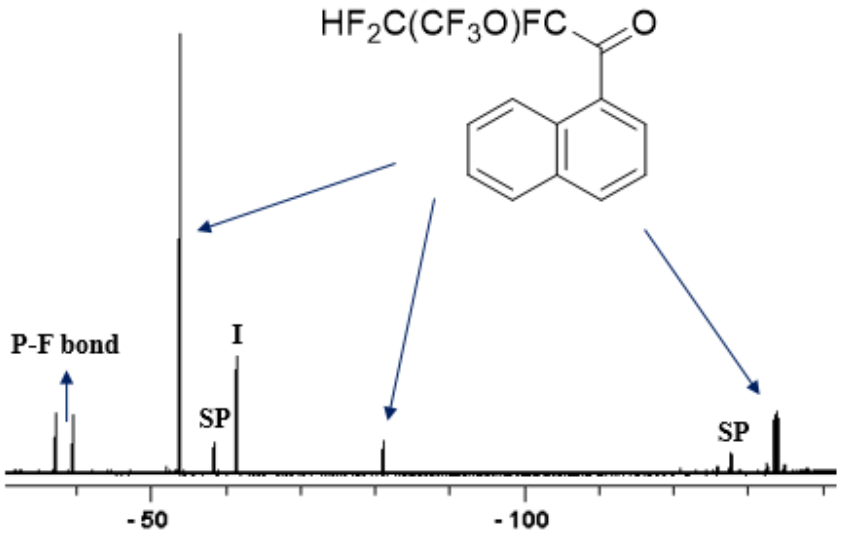

Figure A3.21 ^{19}F NMR spectrum (282 MHz, C_6D_6) of **3-3f**, after complex **3-1** reacted with 1 equiv of naphthoyl chloride in DMSO. SP = side products and I = Internal Standard ($PhCF_3$).

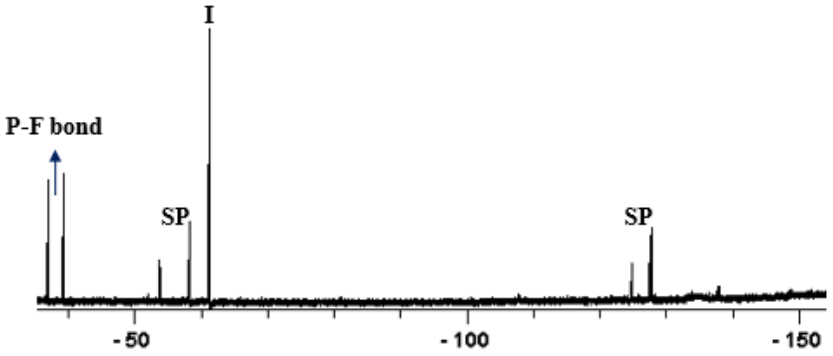

Figure A3.22 ^{19}F NMR spectrum (282 MHz, C_6D_6) of **3-3g**, after complex **3-1** reacted with 1 equiv of 2-nitrobenzoyl-chloride in DMSO. SP = side product and I = Internal Standard ($PhCF_3$).

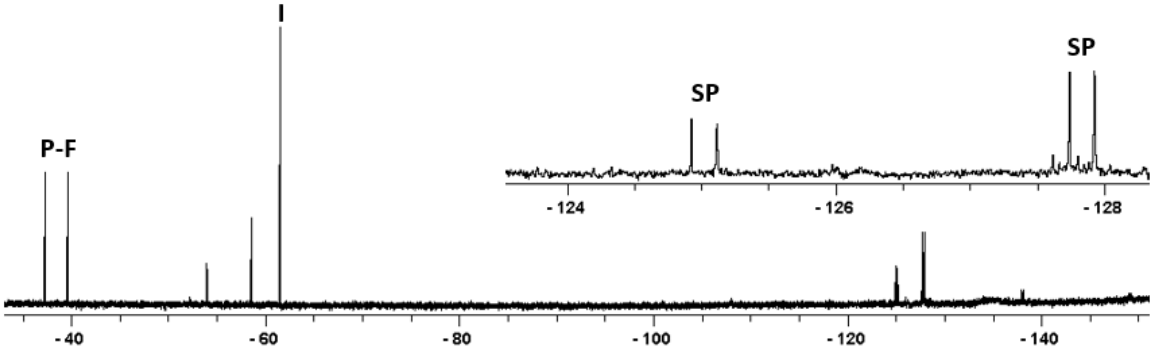

Figure A3.23 ^{19}F NMR spectrum (282 MHz, C_6D_6) of **3-3h**, after complex **3-1** reacted with 1 equiv of 4-nitrobenzoyl chloride in DMSO. SP = side product and I = Internal Standard ($PhCF_3$).

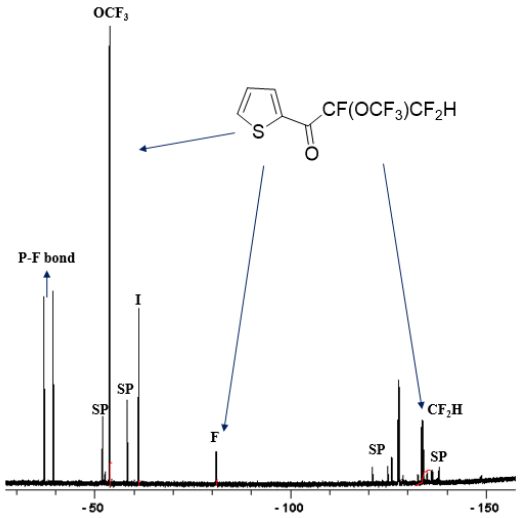

Figure A3.24 ^{19}F NMR spectrum (282 MHz, C_6D_6) of **3-3i**, after complex **3-1** reacted with 1 equiv of 2-thiophenylcarbonyl chloride in DMSO. SP = side product and I = Internal Standard ($PhCF_3$).

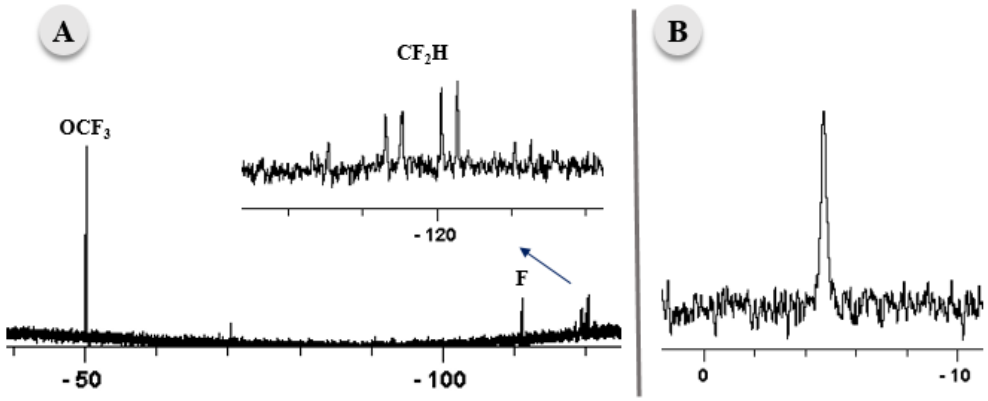

Figure A3.25 ^{19}F NMR (282 MHz, C_6D_6; **A**) and $^{31}P\{^1H\}$ NMR (121 MHz; **B**) spectra of complex **3-4a**.

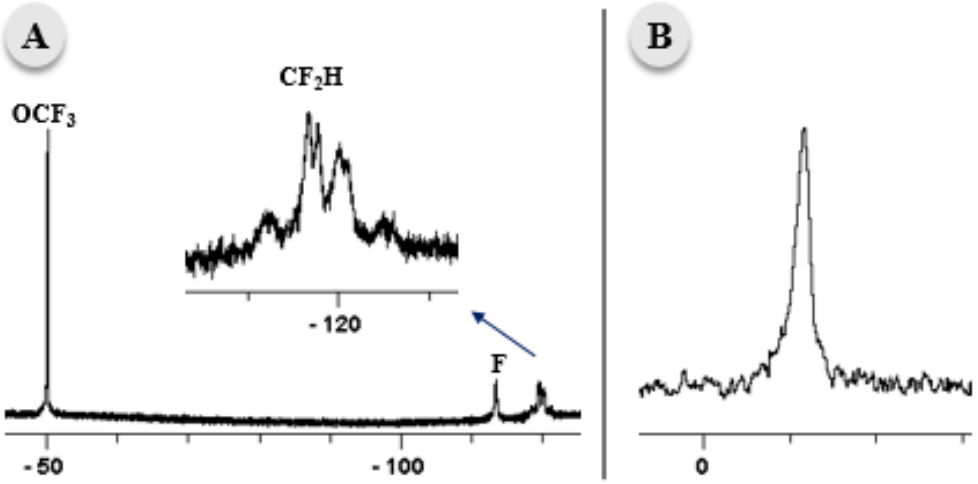

Figure A3.26 ^{19}F NMR (282 MHz, C_6D_6; **A**) and $^{31}P\{^1H\}$ NMR (121 MHz; **B**) of complex **3-4b.**

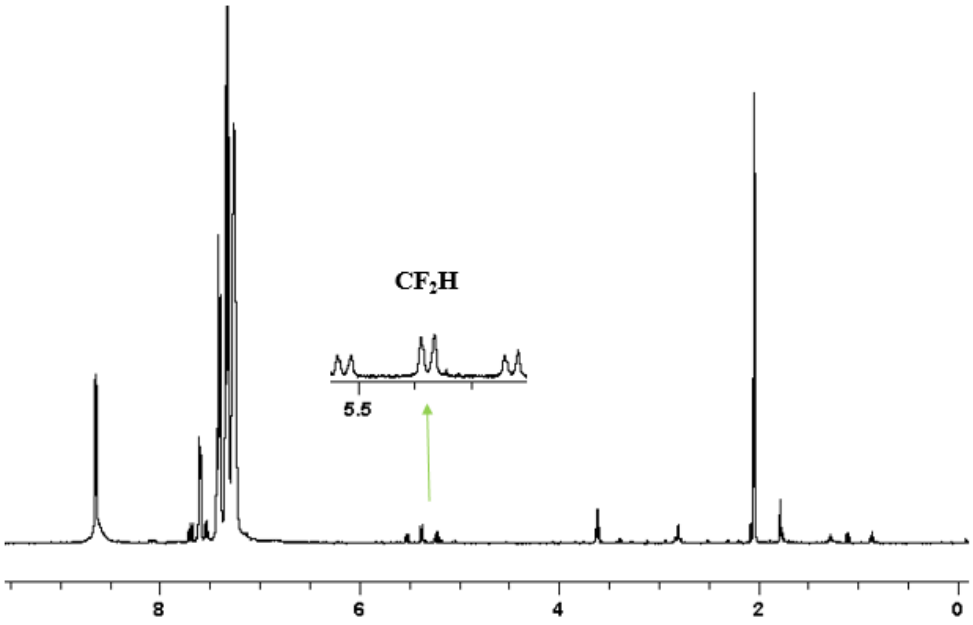

Figure A3.27 ^{1}H NMR spectrum (282 MHz, C_6D_6) of complex **3-4b.**

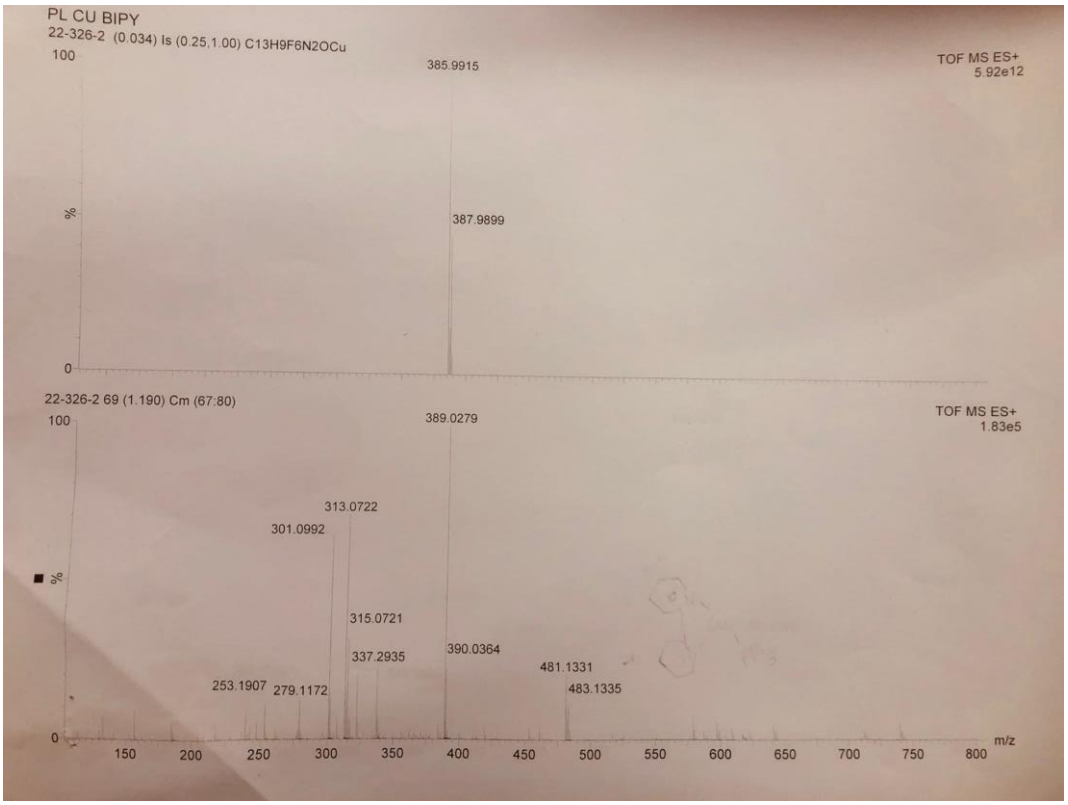

Figure A3.28 ESI-MS (positive mode) spectrum of complex **3-4b** showing $[Na\text{-}MR^{F}(Cl_2\text{-}bipy)]^{+}$

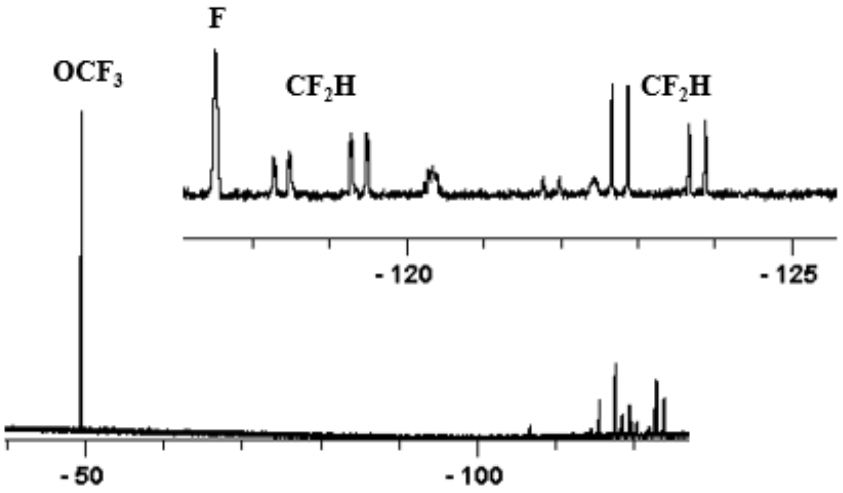

Figure A3.29 ^{19}F NMR spectrum (282 MHz, C_6D_6) of complex **3-5**.

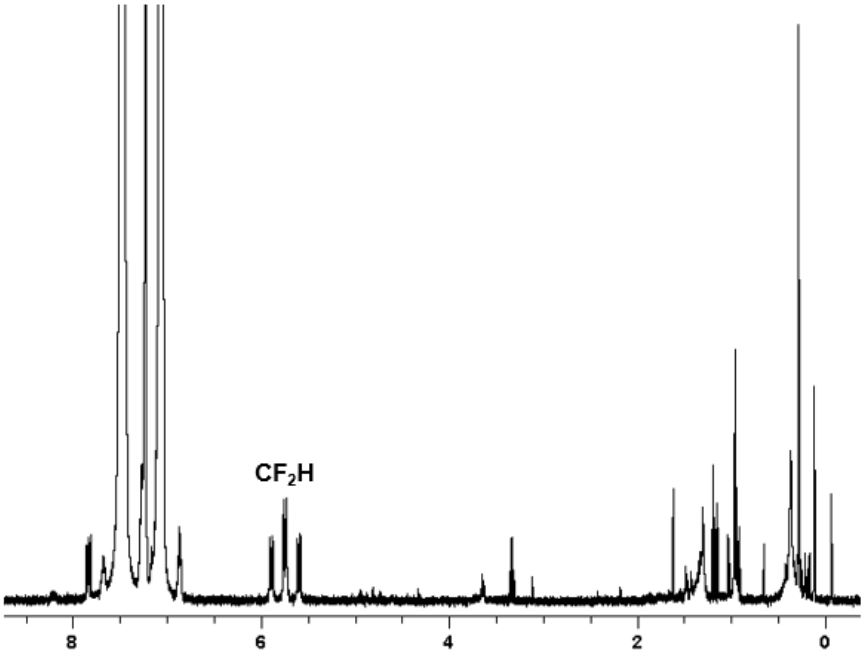

Figure A3.30 ^{1}H NMR spectrum (282 MHz, C_6D_6) of complex **3-5**.

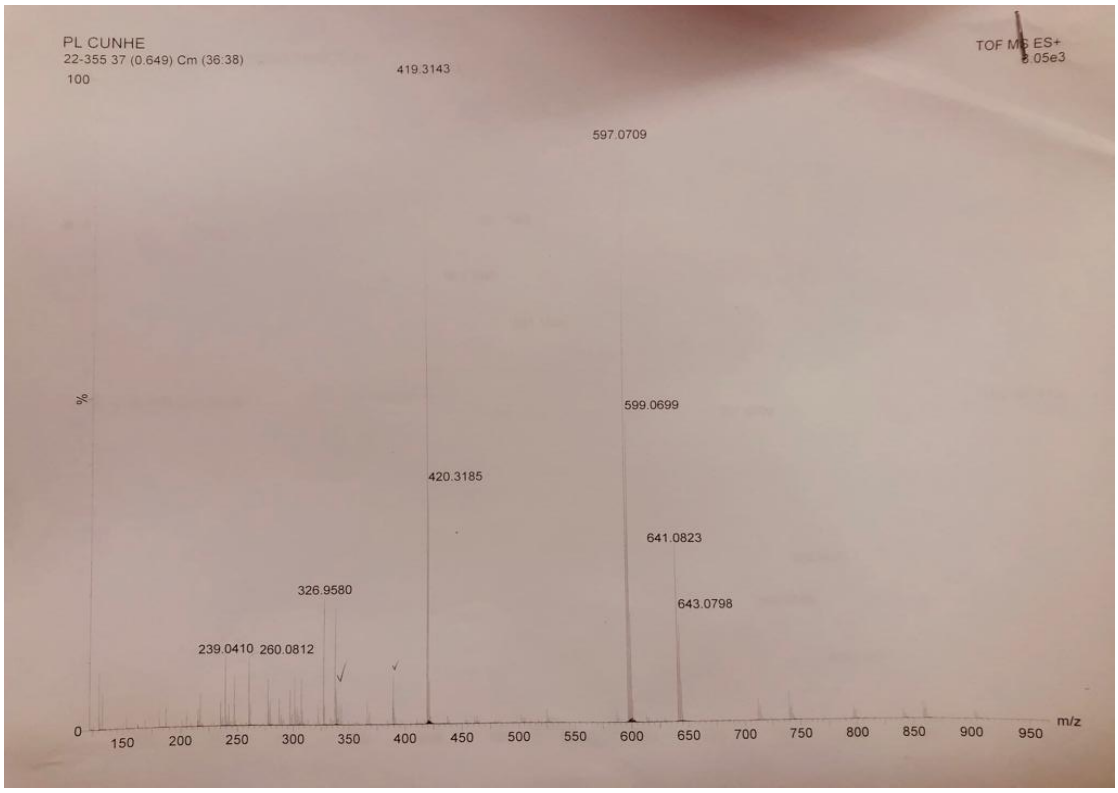

Figure A3.31 ESI-MS (positive mode) spectrum of complex **3-5**.

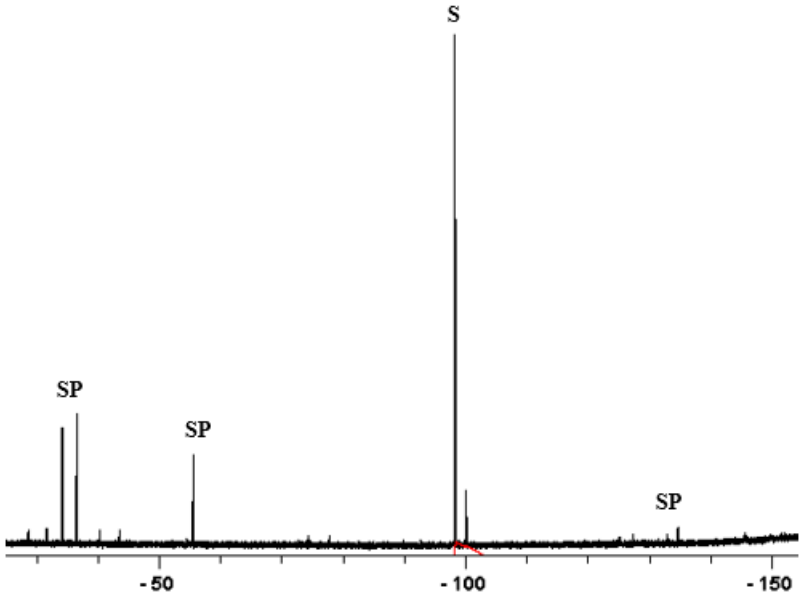

Figure A3.32 ^{19}F NMR spectrum (282 MHz, C_6D_6) after complex **3-4a** reacted with 1.5 equiv of 4-fluorobenzoyl chloride in benzene. SP = side product, SM = start material, S= substrate.

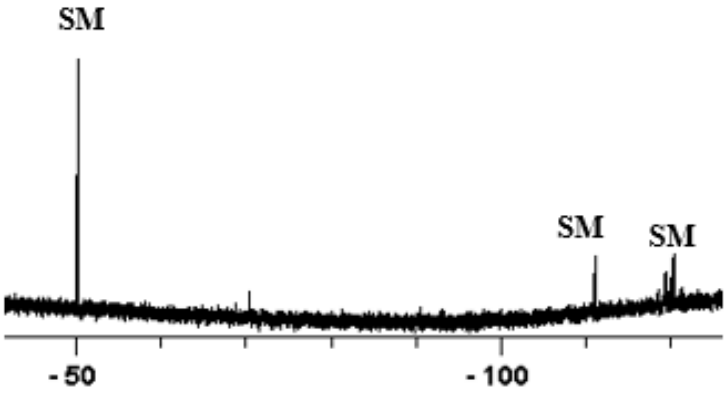

Figure A3.33 ^{19}F NMR spectrum (282 MHz, C_6D_6) after complex **3-4a** reacted with 1.5 equiv of benzoyl chloride in benzene. SM = starting material.

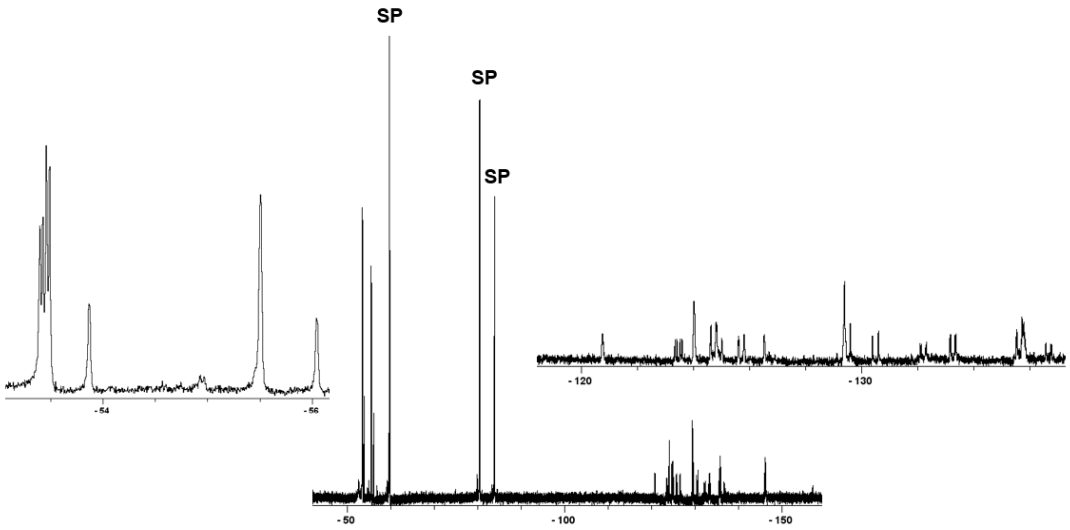

Figure A3.34 ^{19}F NMR spectrum (282 MHz, C_6D_6) after complex **3-5** reacted with 1.5 equiv of 4-benzoyl chloride in benzene. SP = side products, SM = starting material.

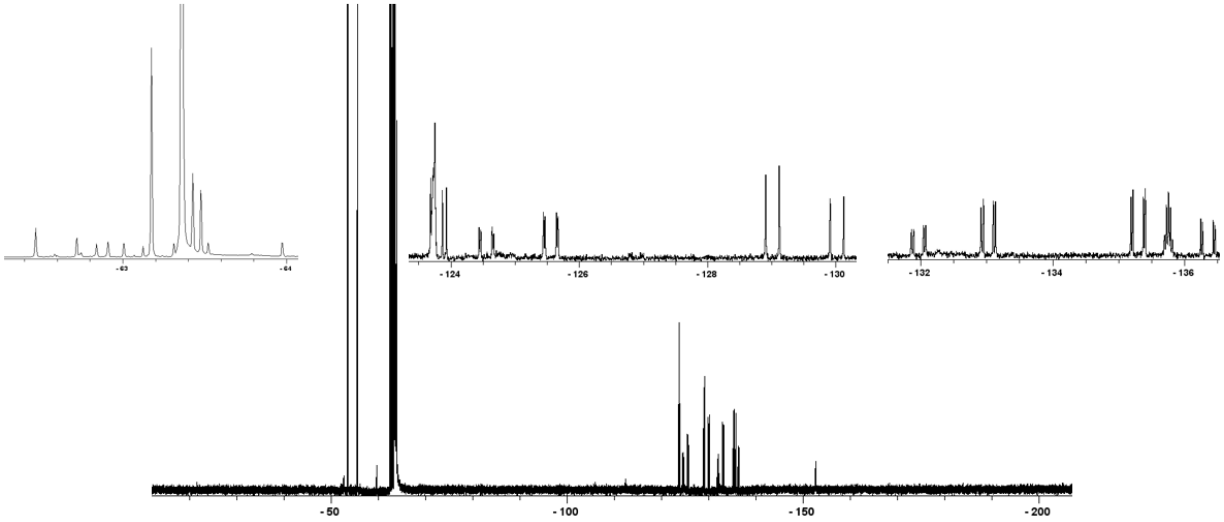

Figure A3.35 ^{19}F NMR spectrum (282 MHz, C_6D_6) after complex **3-5** reacted with 1.5 equiv of 4-CF_3-benzoyl chloride in benzene. SP = side products, SM = starting material.

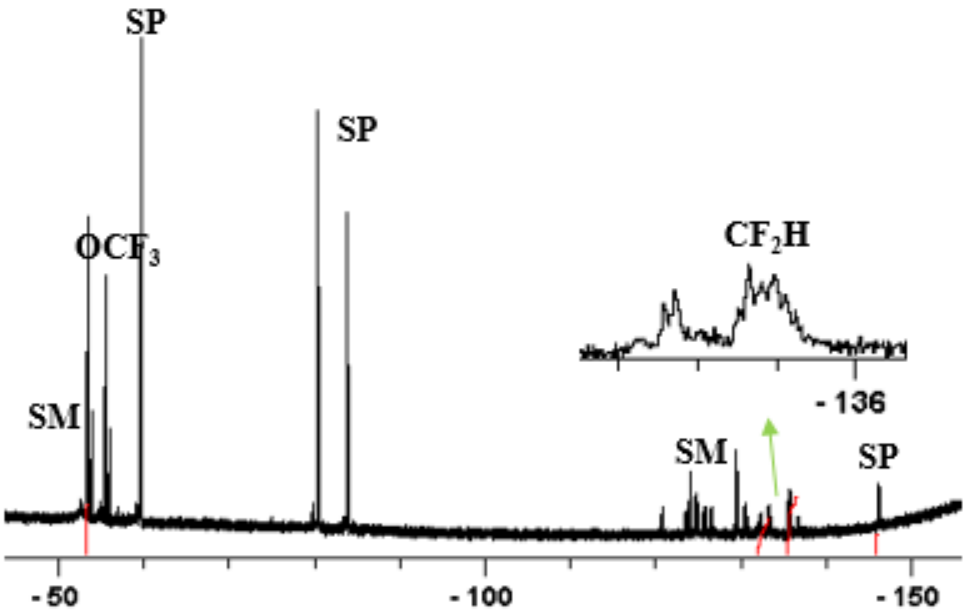

Figure A3.36 ^{19}F NMR spectrum (282 MHz, C_6D_6) after complex **3-5** reacted with 1.5 equiv of 4-fluorobenzoyl chloride in benzene. SP = side product, SM = starting material.

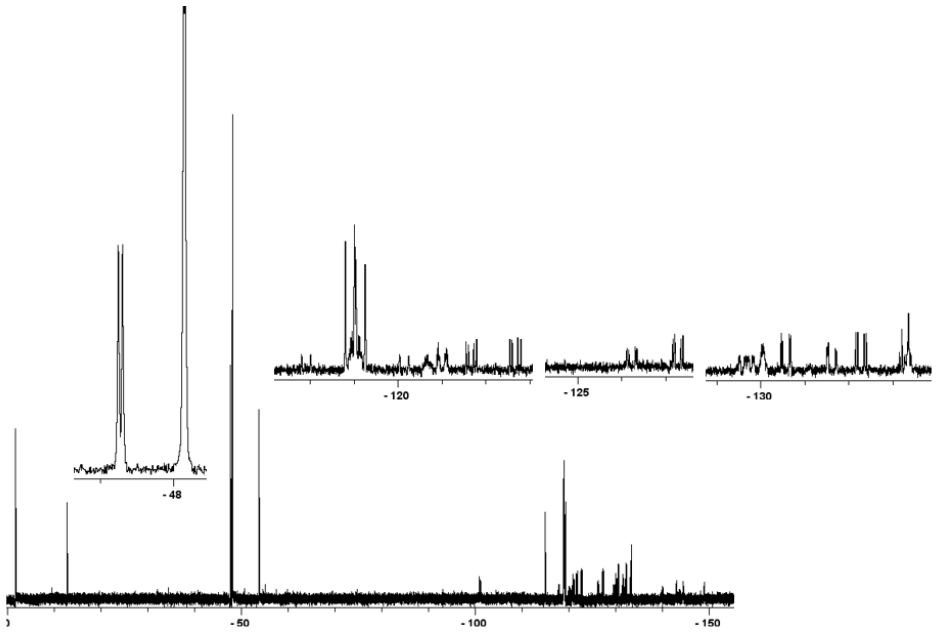

Figure A3.37 ^{19}F NMR spectrum (282 MHz, C_6D_6) after complex **3-5** reacted with 1.5 equiv of naphthoyl chloride in benzene. SP = side product, SM = starting material.

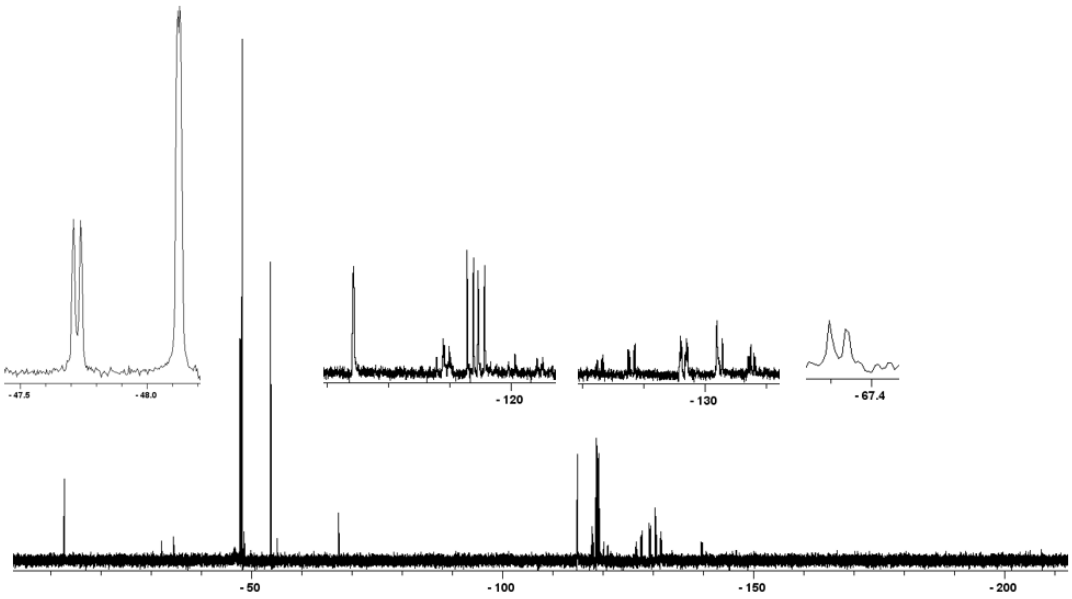

Figure A3.38 ^{19}F NMR spectrum (282 MHz, C_6D_6) after complex **3-5** reacted with 1.5 equiv of o-toluoyl chloride in benzene. P = product, SP = side product, SM = starting material.

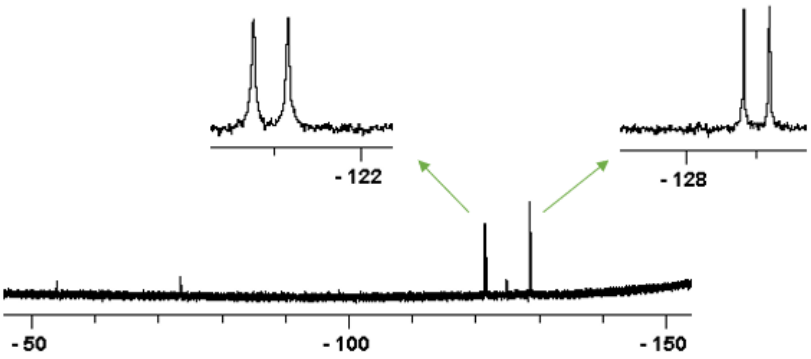

Figure A3.39 ^{19}F NMR spectrum (282 MHz) of complex **3-1** in DMSO-d_6.

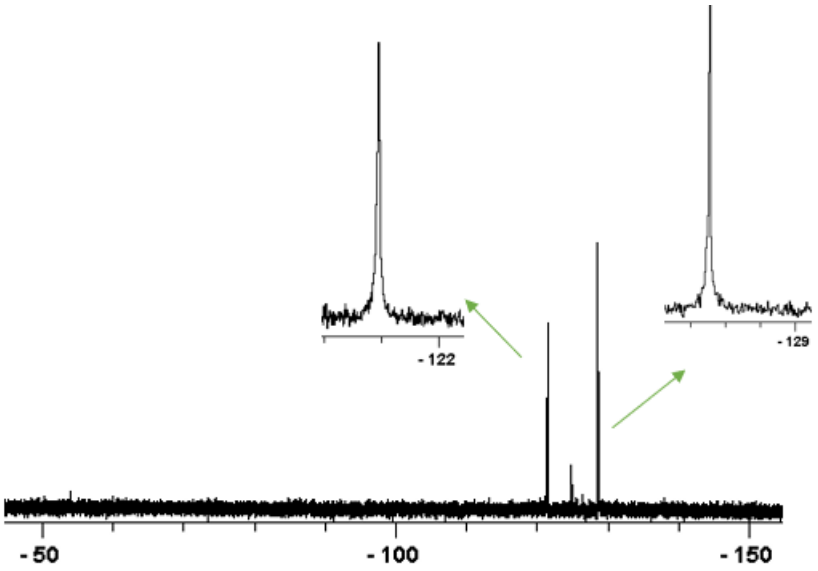

Figure A3.40 $^{19}F\{^{1}H\}$ NMR spectrum (282 MHz) of complex **3-1** in DMSO-d_6.

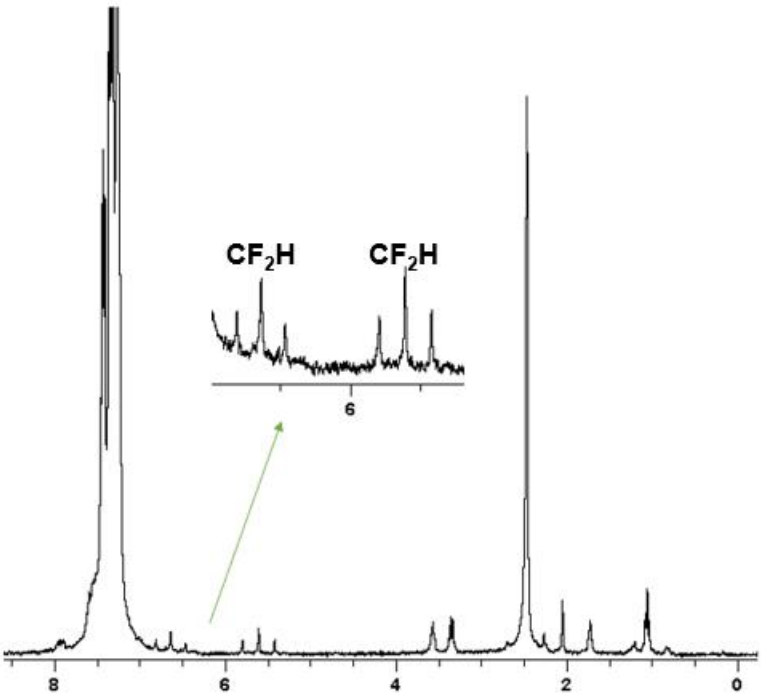

Figure A3.41 ^{1}H NMR spectrum (300 MHz) of complex **3-1** in DMSO-d_6.

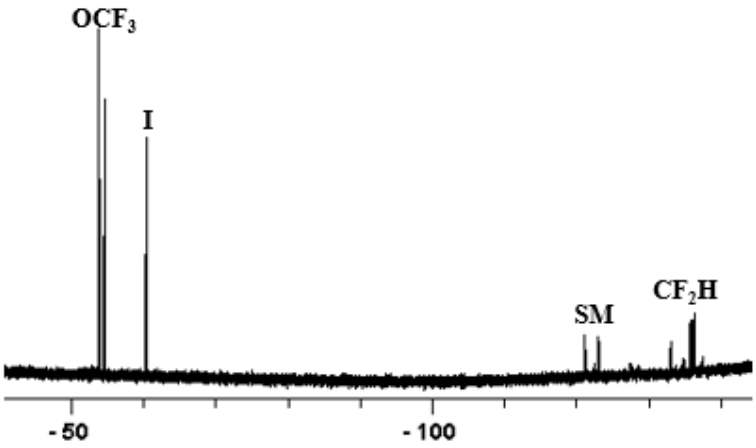

Figure A3.42 ^{19}F NMR spectrum (282 MHz, C_6D_6) after complex **3-1** reacted with DMSO (8 eq.) and methyl-2-iodobenzoate (1.5 eq.) in benzene at 50 °C. SM = starting material, I = internal standard ($PhCF_3$).

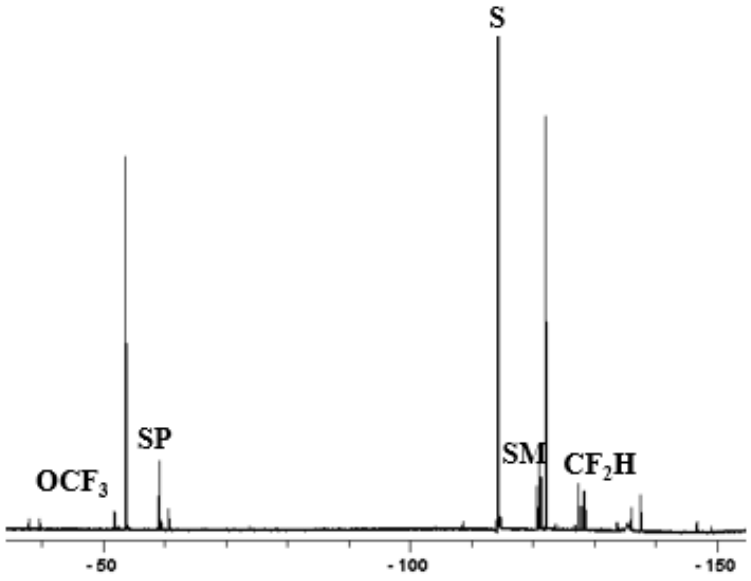

Figure A3.43 ^{19}F NMR spectrum (282 MHz, C_6D_6) after complex **3-1** reacted with DMSO (8 eq.) and 4-fluoroiodobenzene (1.5 eq.) in benzene at 50 °C. SM = starting material, S = substrate.

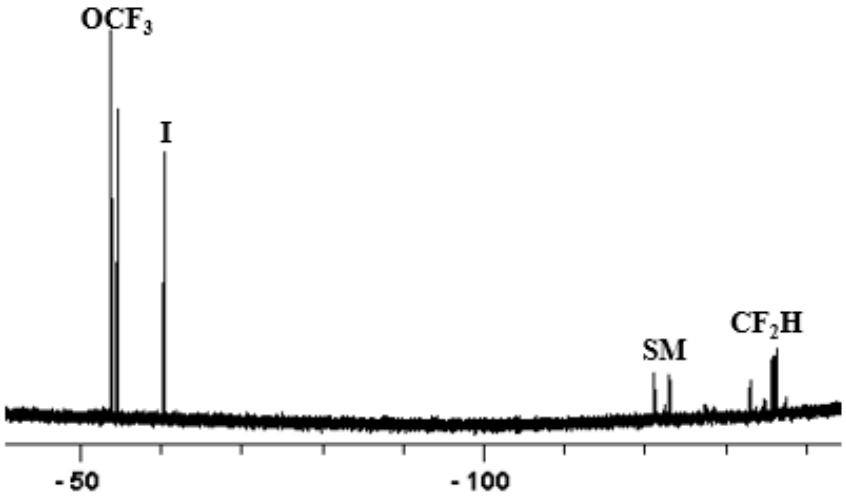

Figure A3.44 ^{19}F NMR spectrum (282 MHz, C_6D_6) after complex **3-1** reacted with DMSO (8 eq.) and 4-iodo-nitrobenzene (1.5 eq.) in benzene at 50 °C. SM = starting material, I = internal standard ($PhCF_3$).

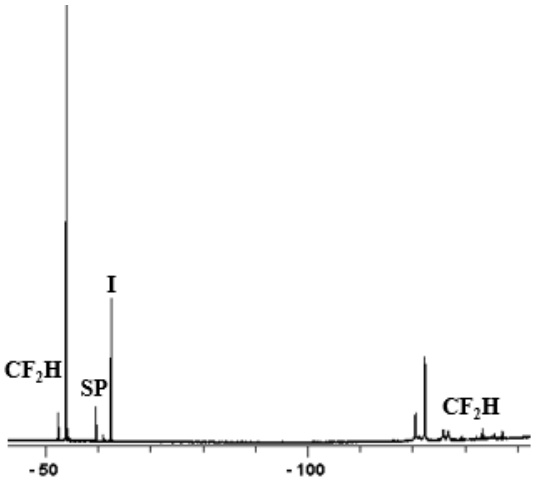

Figure A3.45 ^{19}F NMR spectrum (282 MHz, C_6D_6) after complex **3-1** reacted with DMSO (8 eq.) and 3-iodobenzonitrile (1.5 eq.) in benzene at 50 °C. SP = side product, I = internal standard ($PhCF_3$).

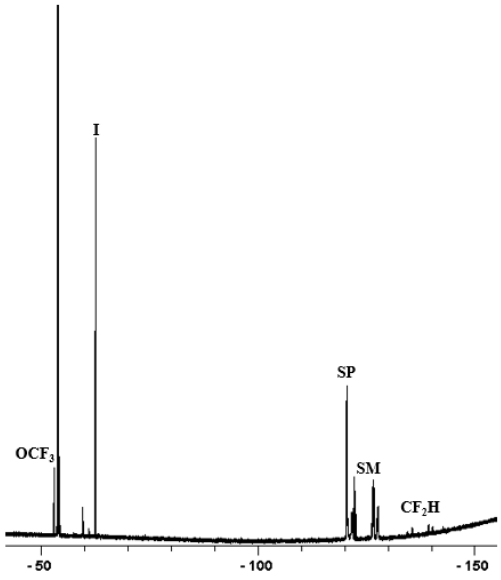

Figure A3. 46 ^{19}F NMR spectrum (282 MHz, C_6D_6) after complex **3-1** reacted with DMSO (8 eq.) and 2-iodo-pyridine (1.5 eq.) in benzene at 50 °C. SM = starting material, SP = side product, I = internal standard ($PhCF_3$).

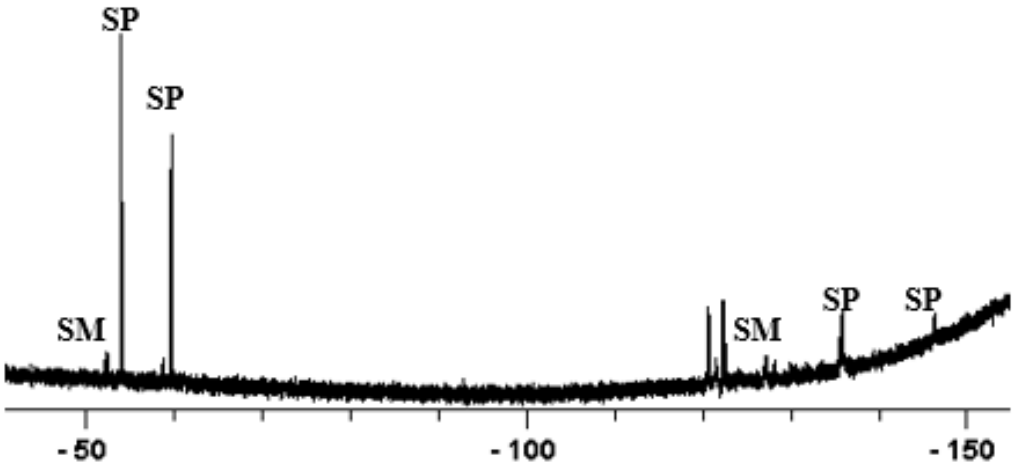

Figure A3. 47 ^{19}F NMR spectrum (282 MHz, C_6D_6) after complex **3-1** reacted with DMSO (10 eq.) and 4-iodo-nitrobenzene (1.5 eq.) in benzene at 50 ^{o}C. SM = starting material, SP = side product.

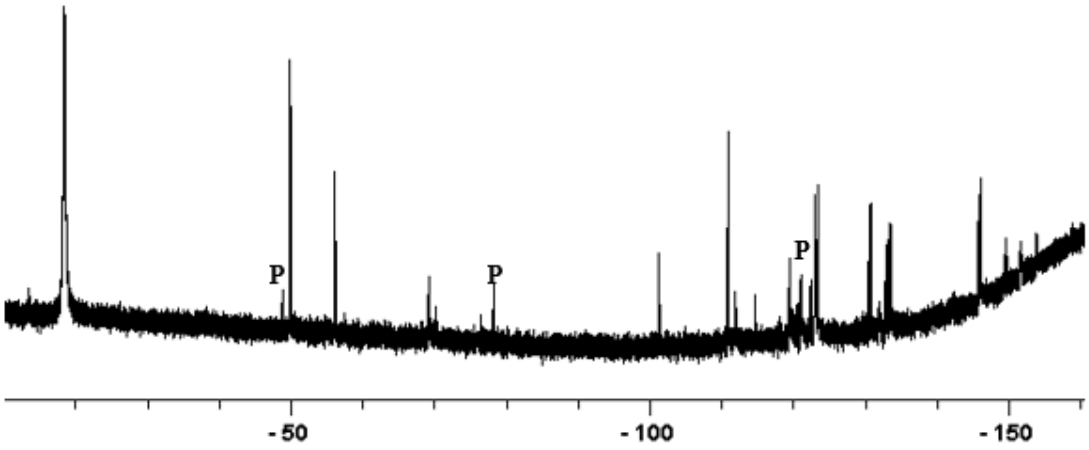

Figure A3.48 ^{19}F NMR spectrum (282 MHz, C_6D_6) after complex **3-4b** reacted with 1.5 equiv of iodobenzonitrile in benzene. P = product.

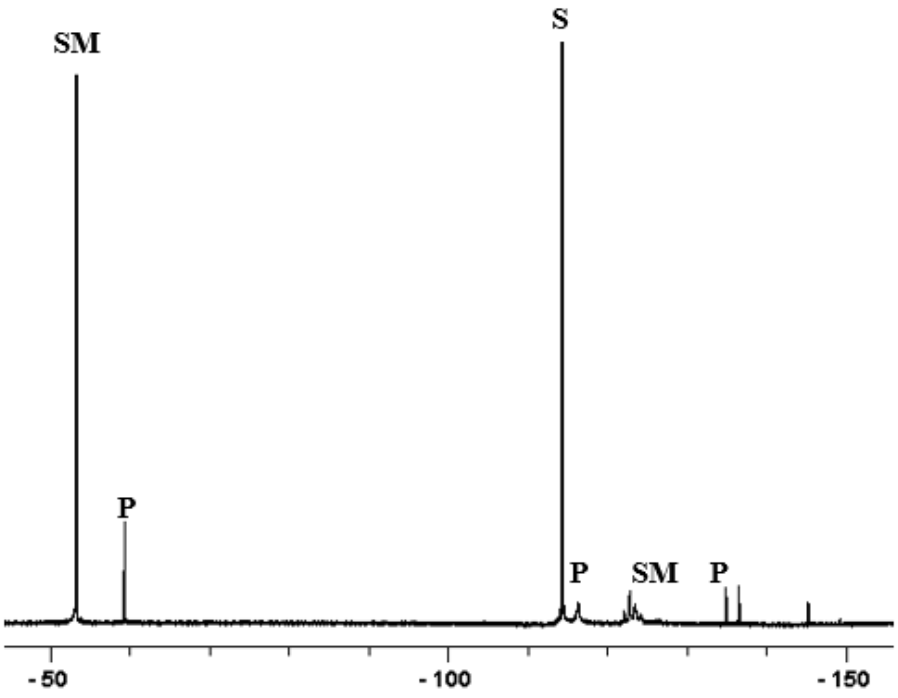

Figure A3.49 ^{19}F NMR spectrum (282 MHz, C_6D_6) after complex **3-4b** reacted with 1.5 equiv of 4-fluoro-iodobenzene in benzene. P = product, SM = starting material, S = substrate.

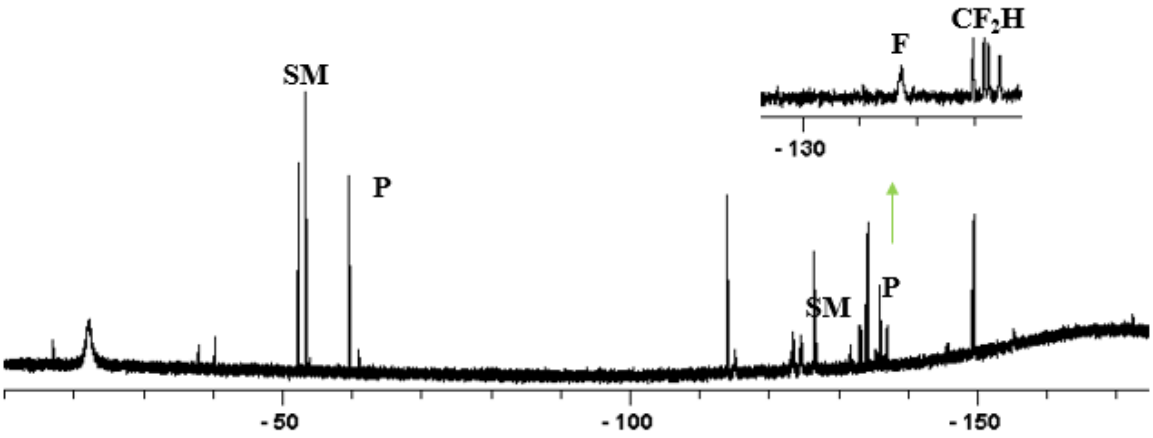

Figure A3.50 ^{19}F NMR spectrum (282 MHz, C_6D_6) after complex **3-4b** reacted with 1.5 equiv of 4-iodo-nitrobenzene in benzene. P = product, SM = starting material.

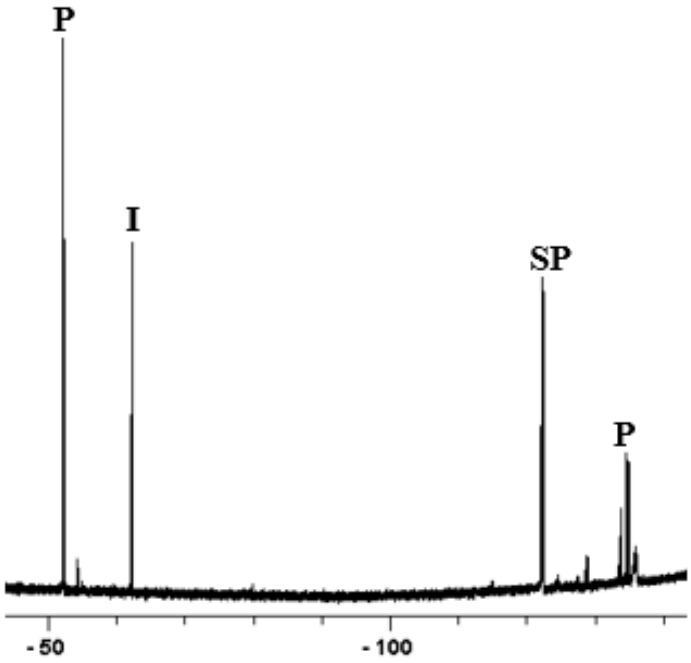

Figure A3.51 ^{19}F NMR spectrum (282 MHz, C_6D_6) after complex **3-1** reacted with CuCl/ DMSO (1.5 eq.) and 4-benzonitrile (1.5 eq) in benzene. P = product, SP = side product, I = internal standard ($PhCF_3$).

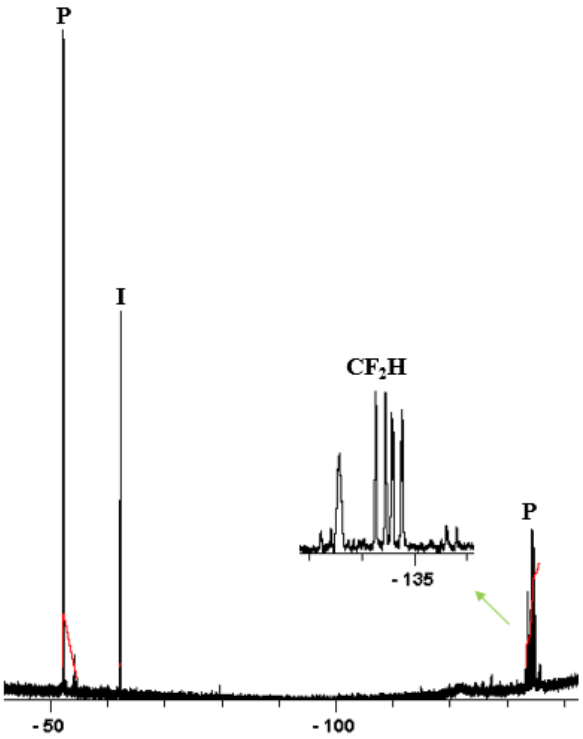

Figure A3.52 ^{19}F NMR spectrum (282 MHz, C_6D_6) after complex **3-1** reacted with CuCl/DMSO (2 eq.) and 4-benzonitrile (1.5 eq.) in benzene. P = product, I = internal standard ($PhCF_3$).

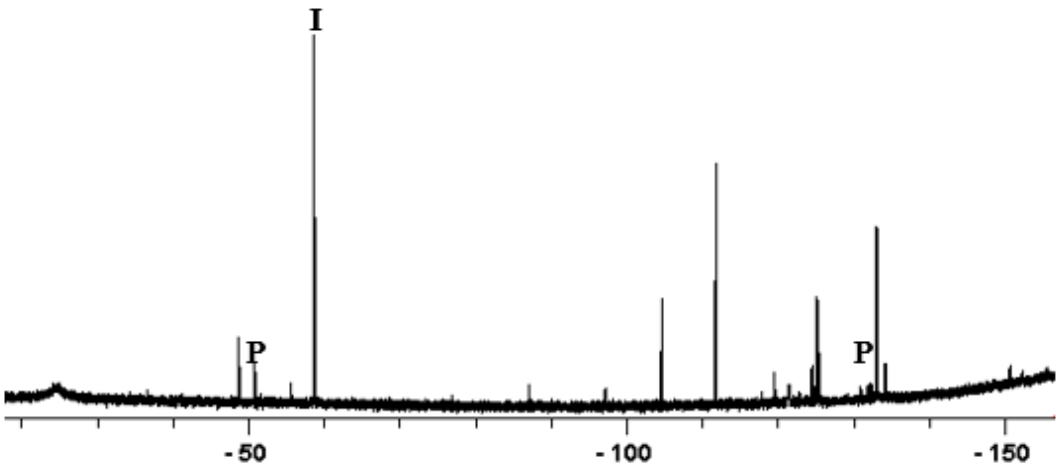

Figure A3.53 ^{19}F NMR spectrum (282 MHz, C_6D_6) after complex **3-1** reacted with CuCl/DMF (2 eq.) and 4-benzonitrile (1 eq.) in benzene. P = product, I = internal standard ($PhCF_3$).

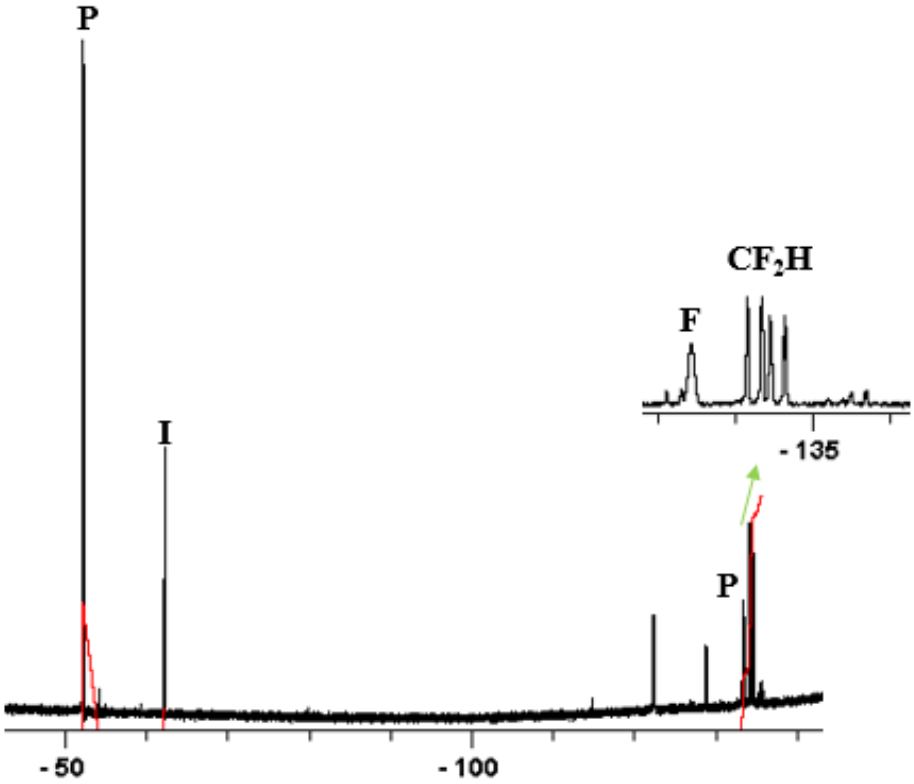

Figure A3.54 ^{19}F NMR spectrum (282 MHz, C_6D_6) after complex **3-1** reacted with CuCl/DMSO (2 eq.) and 4-benzonitrile (1 eq.) in benzene. P = product, I = internal standard ($PhCF_3$).

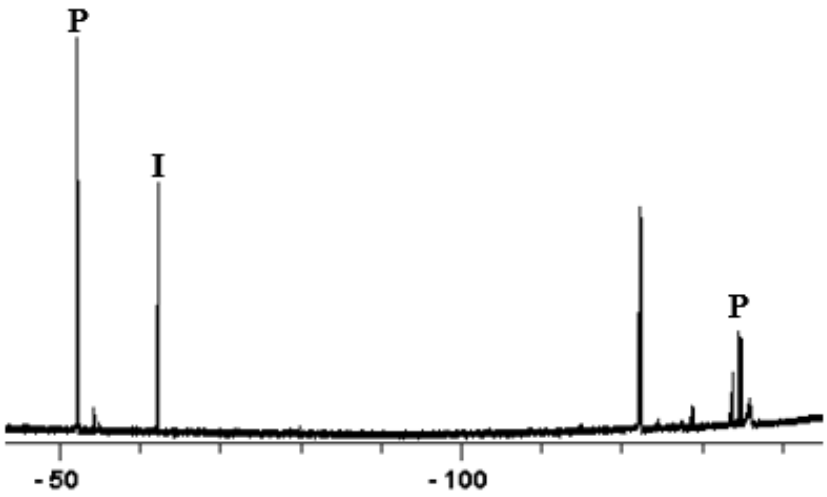

Figure A3.55 ^{19}F NMR spectrum (282 MHz, C_6D_6) after complex **3-1** reacted with CuI/DMSO (1.5 eq.) and 4-benzonitrile (1.5 eq.) in benzene. P = product, I = internal standard ($PhCF_3$).

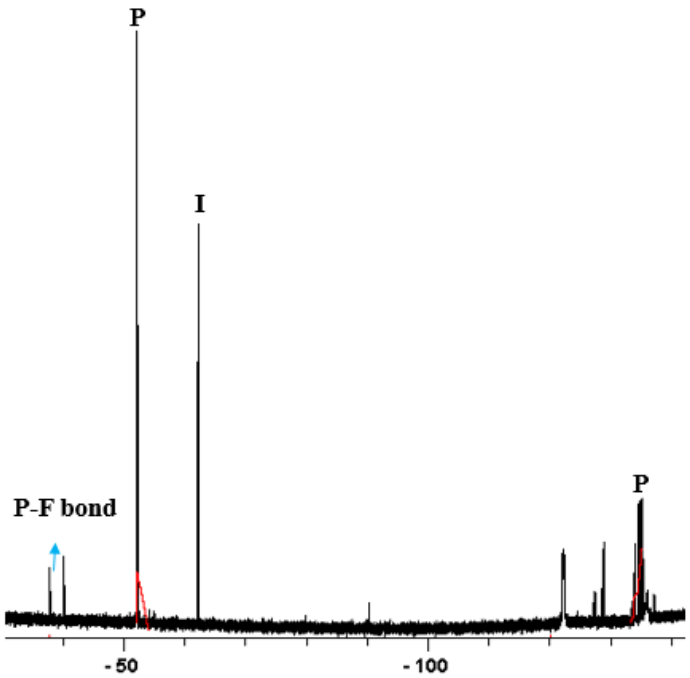

Figure A3.56 ^{19}F NMR spectrum (282 MHz, C_6D_6) after complex **3-1** reacted with CuI/DMSO (2 eq.) and 4-benzonitrile (1.5 eq.) in benzene. P = product, I = internal standard ($PhCF_3$).

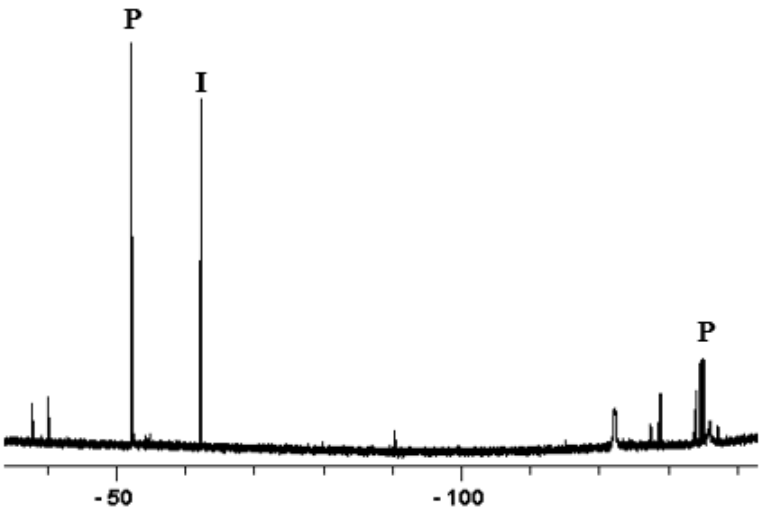

Figure A3.57 ^{19}F NMR spectrum (282 MHz, C_6D_6) after complex **3-1** reacted with CuI/DMSO (2 eq.) and 4-benzonitrile (1 eq.) in benzene. P = product, I = internal standard ($PhCF_3$).

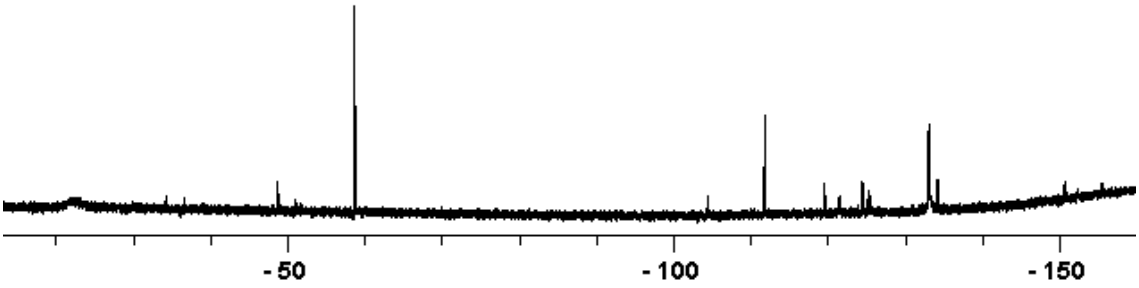

Figure A3.58 ^{19}F NMR spectrum (282 MHz, C_6D_6) after complex **3-1** reacted with CuI/DMF (2 eq.) and 4-benzonitrile (1 eq.) in benzene.

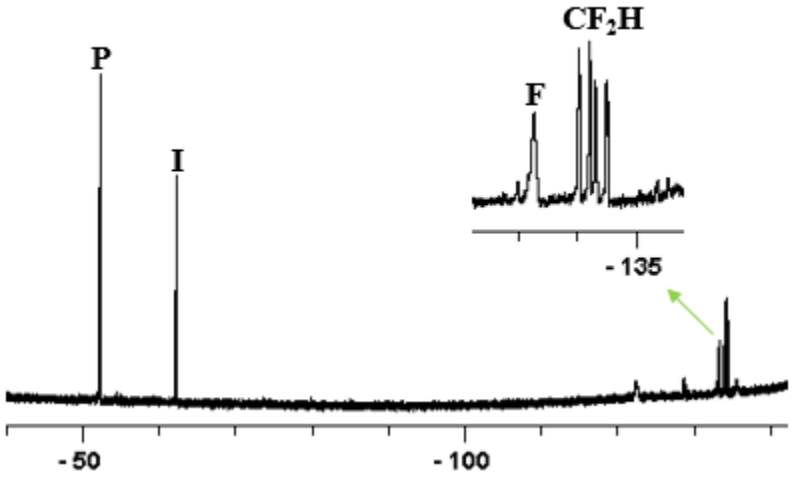

Figure A3.59 ^{19}F NMR spectrum (282 MHz, C_6D_6) after complex **3-1** reacted with CuBr/DMSO (1.5 eq.) and 4-iodo-benzonitrile (1.5 eq.) in benzene. P = product, I = internal standard ($PhCF_3$).

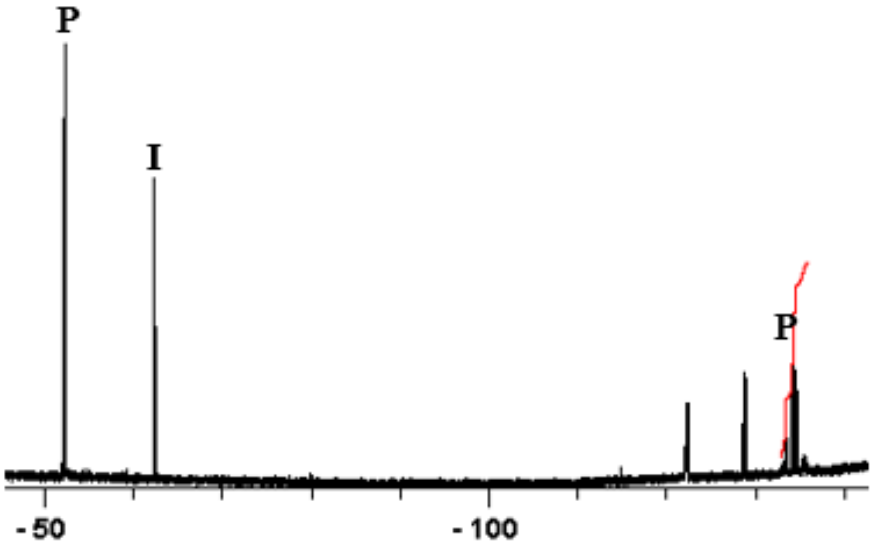

Figure A3.60 ^{19}F NMR spectrum (282 MHz, C_6D_6) after complex **3-1** reacted with CuBr/DMSO (2 eq.) and 4-iodobenzonitrile (1.5 eq.) in benzene. P = product, I = internal standard ($PhCF_3$).

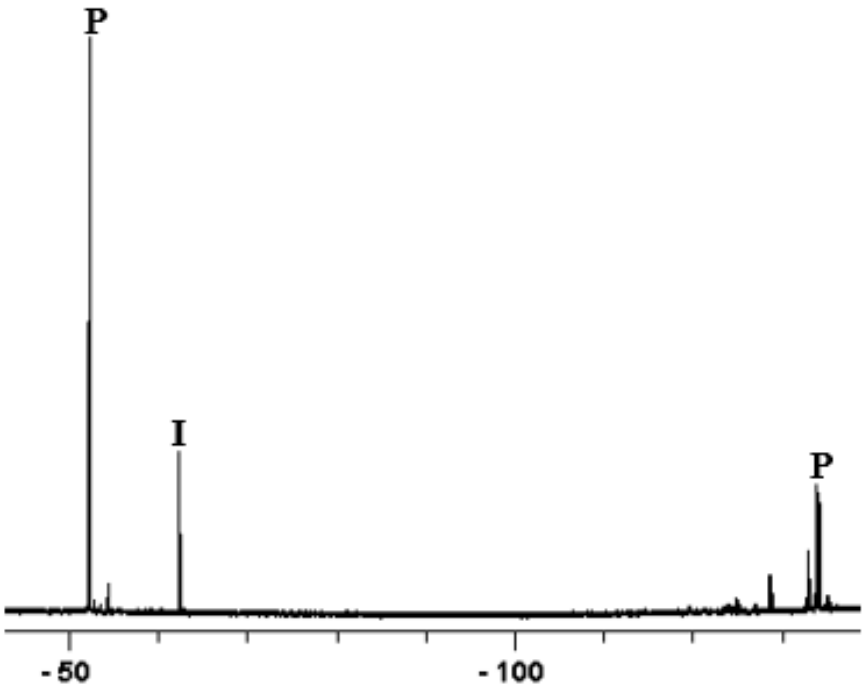

Figure A3.61 ^{19}F NMR spectrum (282 MHz, C_6D_6) after complex **3-1** reacted with CuBr/DMSO (2 eq.) and 4-iodobenzonitrile (1 eq.) in benzene. P = product, I = internal standard ($PhCF_3$).

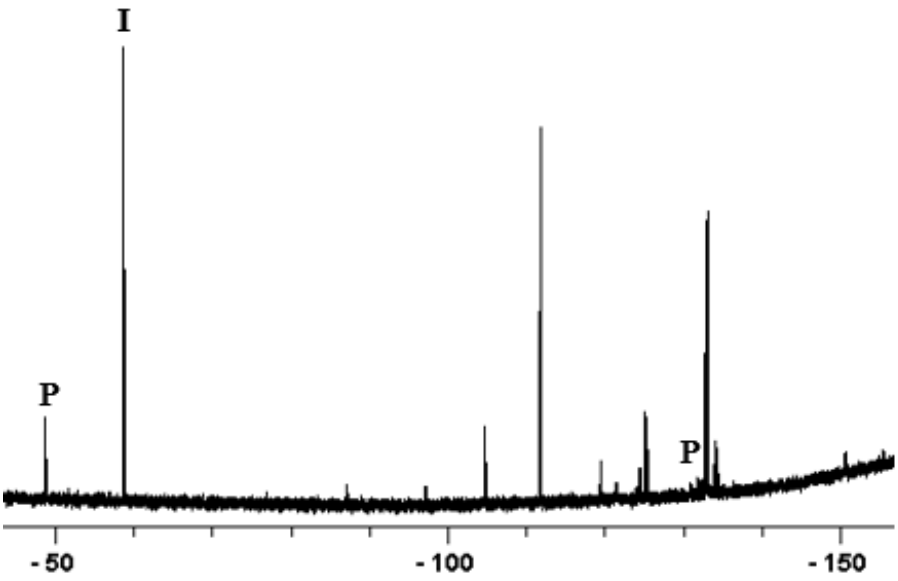

Figure A3.62 ^{19}F NMR spectrum (282 MHz, C_6D_6) after complex **3-1** reacted with CuBr/DMF (2 eq.) and 4-iodo-benzonitrile (1 eq.) in benzene. P = product, I = internal standard ($PhCF_3$).

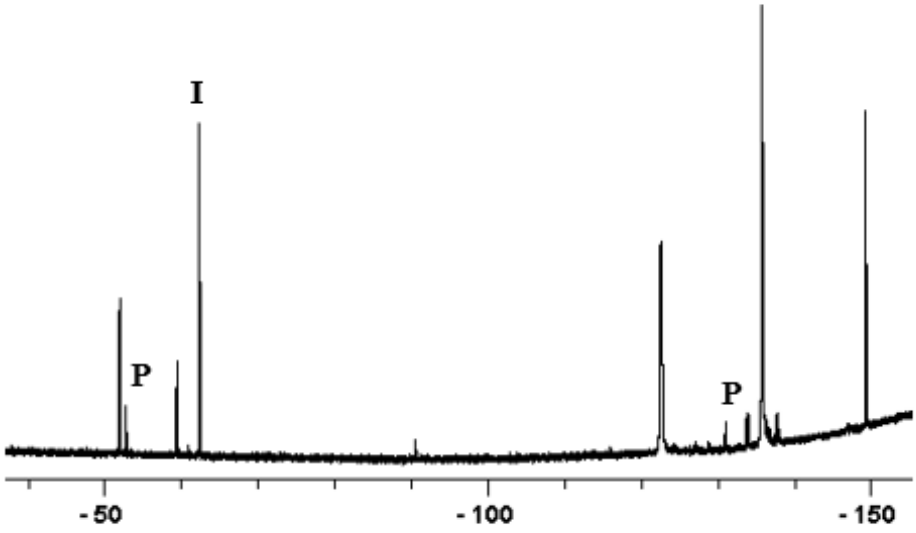

Figure A3.63 ^{19}F NMR spectrum (282 MHz, C_6D_6) after complex **3-1** reacted with CuBr/DMF (2 eq.) in 20 eq. of DMSO and 4-iodoanisole (1 eq.) in 0.5 mL of benzene at 50 ºC. P = product, I = internal standard ($PhCF_3$).

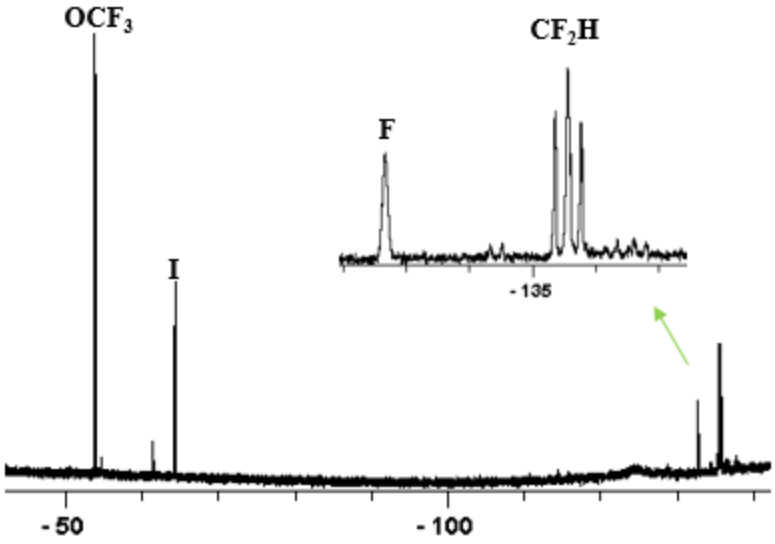

Figure A3.64 ^{19}F NMR spectrum (282 MHz, C_6D_6) after complex **3-1** reacted with CuBr/DMF (2 eq.) in 25 eq. of DMSO and 4-iodoanisole (1 eq.) in 0.5 mL of benzene at 50 ºC. I = internal standard ($PhCF_3$).

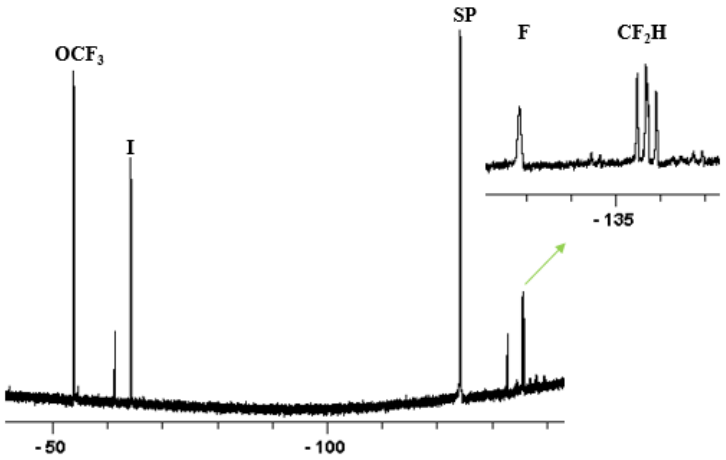

Figure A3.65 ^{19}F NMR spectrum (282 MHz, C_6D_6) after complex **3-1** reacted with CuBr/DMF (2 eq.) in 35 eq. of DMSO and 4-iodoanisole (1 eq.) in 0.5 mL of benzene at 50 ºC. I = internal standard ($PhCF_3$), SP = side product.

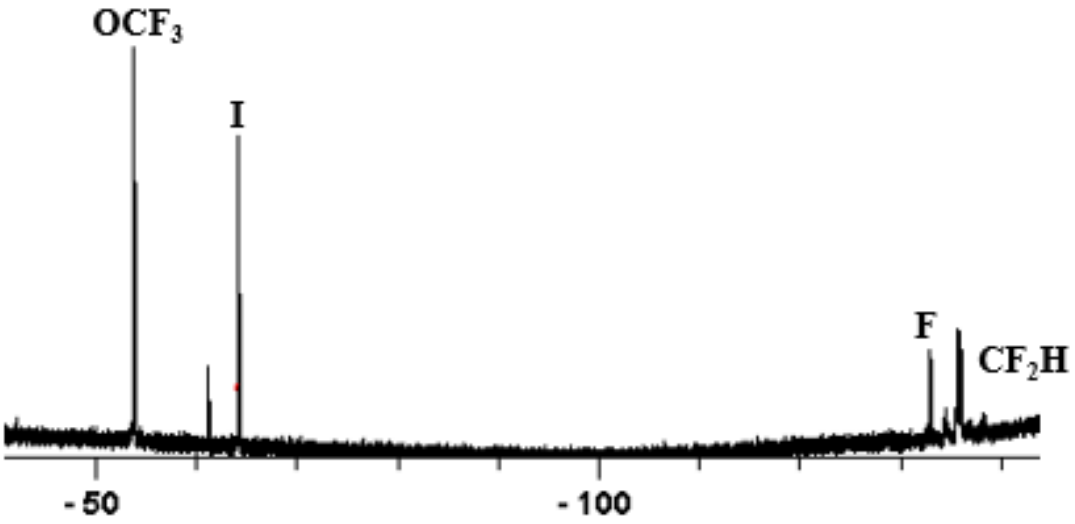

Figure A3.66 ^{19}F NMR spectrum (282 MHz, C_6D_6) after complex **3-1** reacted with CuBr/DMF (2 eq.) in 45 eq. of DMSO and 4-iodoanisole (1 eq.) in 0.5 mL of benzene at 50 °C. I = internal standard ($PhCF_3$).

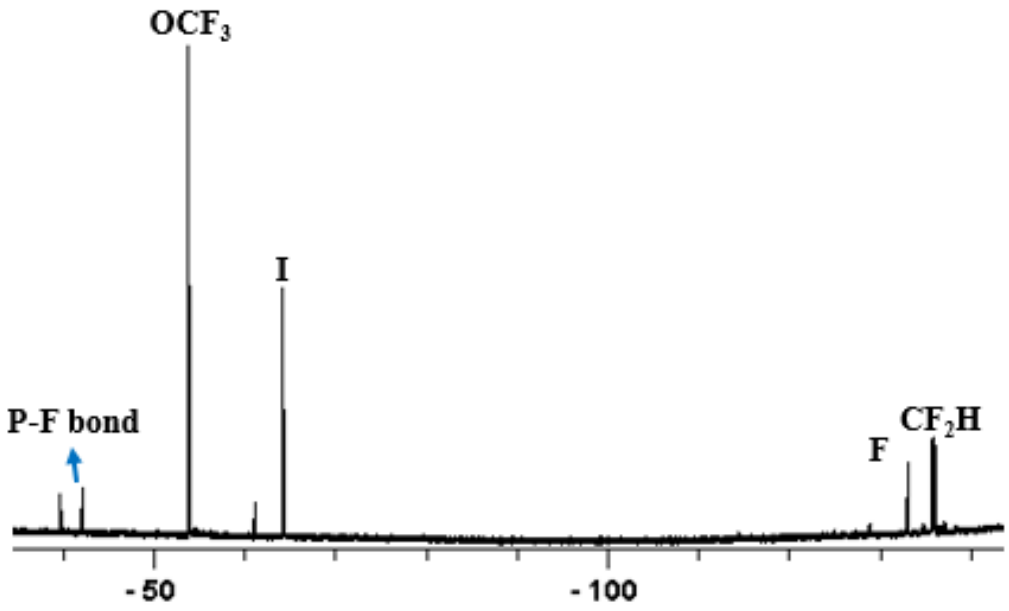

Figure A3.67 ^{19}F NMR spectrum (282 MHz, C_6D_6) after complex **3-** reacted with CuBr/DMF (2 eq.) in 55 eq. of DMSO and 4-iodoanisole (1 eq.) in 0.5 mL of benzene at 50 °C. I = internal standard ($PhCF_3$).

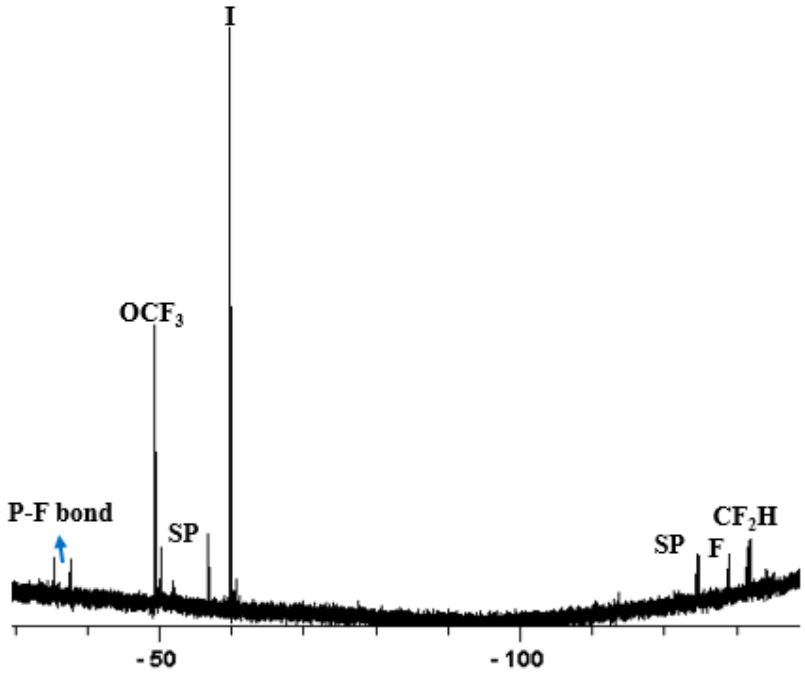

Figure A3.68 ^{19}F NMR spectrum (282 MHz, C_6D_6) after complex **3-1** reacted with CuBr/DMF (2 eq.) in 65 eq. of DMSO and 4-iodoanisole (1 eq.) in 0.5 mL of benzene at 50 °C. I = internal standard ($PhCF_3$), SP = side product.

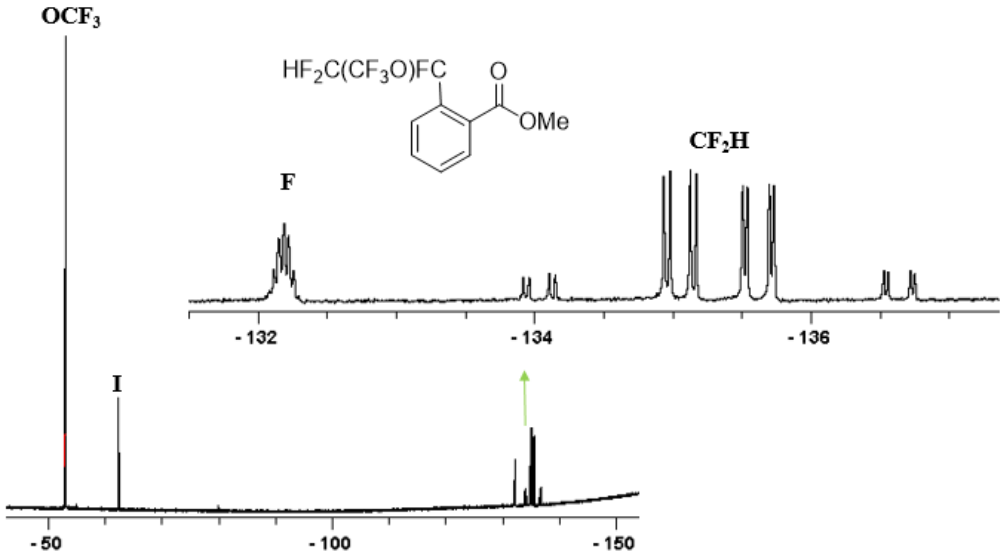

Figure A3.69 ^{19}F NMR spectrum (282 MHz, C_6D_6) of **3-7a**, after complex **3-1** reacted with CuBr (2 eq) DMSO (28 eq.) and methyl-2-iodobenzoate (1 eq.) in benzene at 50 °C. I = internal standard ($PhCF_3$).

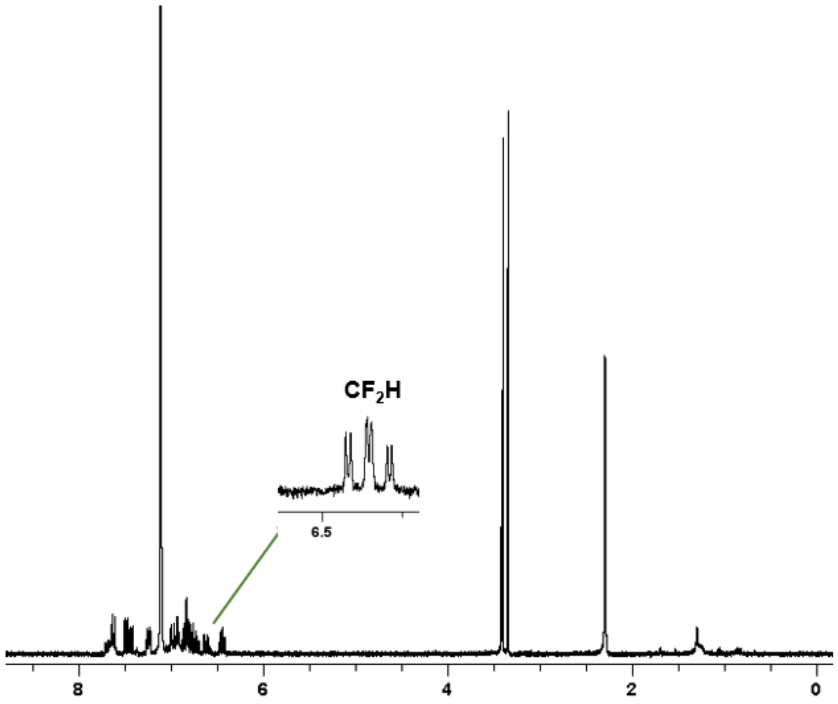

Figure A3.70 ^{1}H NMR spectrum (300 MHz, C_6D_6) of **3-7a**, after complex **3-1** reacted with CuBr (2 eq) DMSO (28 eq.) and methyl-2-iodobenzoate (1 eq.) in benzene at 50 ºC.

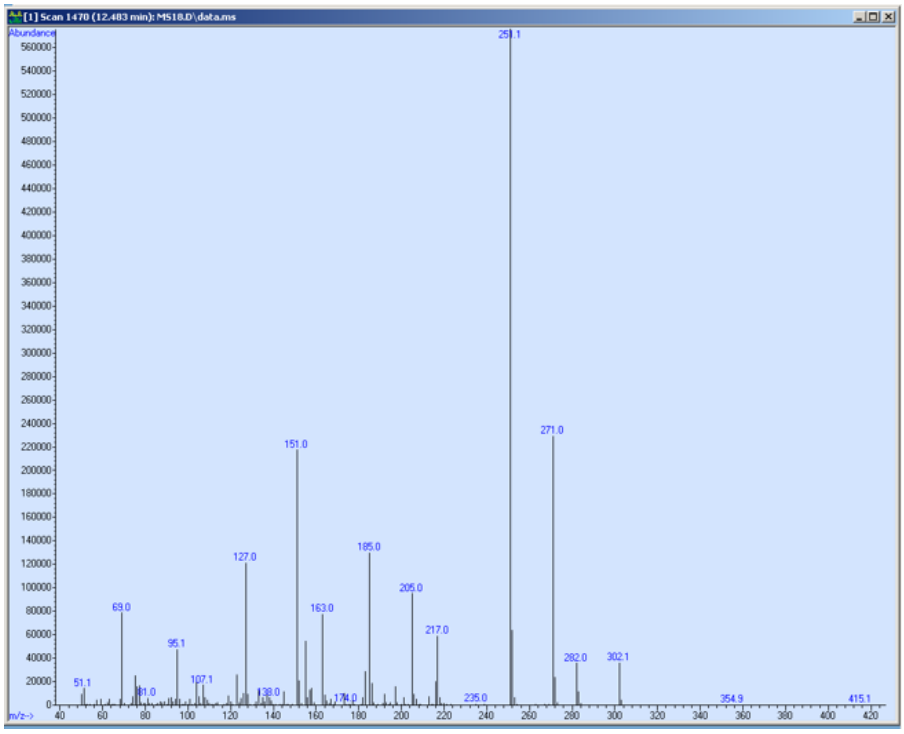

Figure A3.71 GC-MS of **3-7a**, after complex **3-1** reacted with CuBr (2 eq) DMSO (28 eq.) and 4-iodobenzonitrile (1 eq.) in benzene at 50 ºC. Retention time 12.483 min, expected 302.17 m/z (100%), found 302.1 m/z (20%) and 251 m/z (99%)

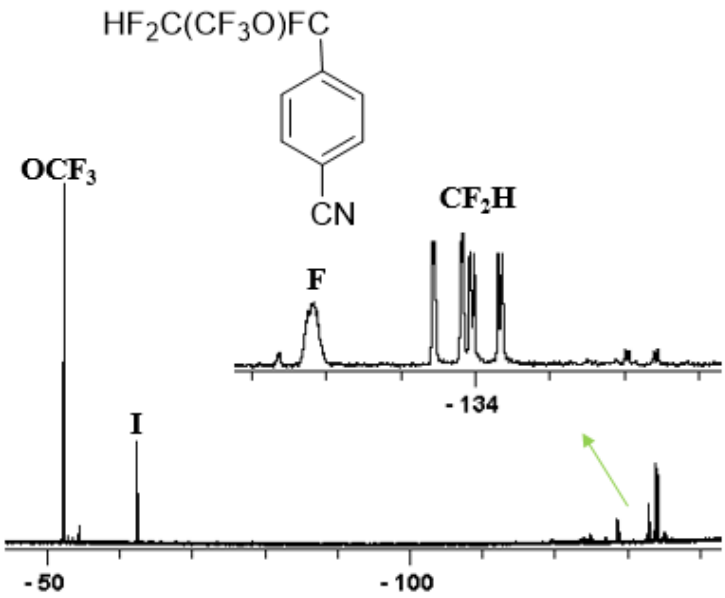

Figure A3.72 ^{19}F NMR spectrum (282 MHz, C_6D_6) of **3-7b**, after complex **3-1** reacted with CuBr (2 eq) DMSO (28 eq.) and 4-iodo-benzonitrile (1 eq.) in benzene at 50 °C. I = internal standard ($PhCF_3$).

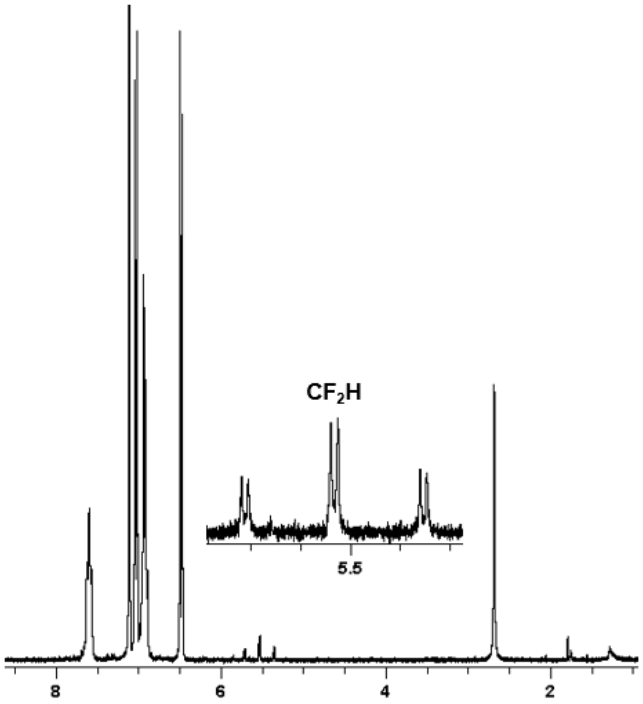

Figure A3.73 ^{1}H NMR spectrum (300 MHz, C_6D_6) of **3-7b**, after complex **3-1** reacted with CuBr (2 eq) DMSO (28 eq.) and 4-iodobenzonitrile (1 eq.) in benzene at 50 °C.

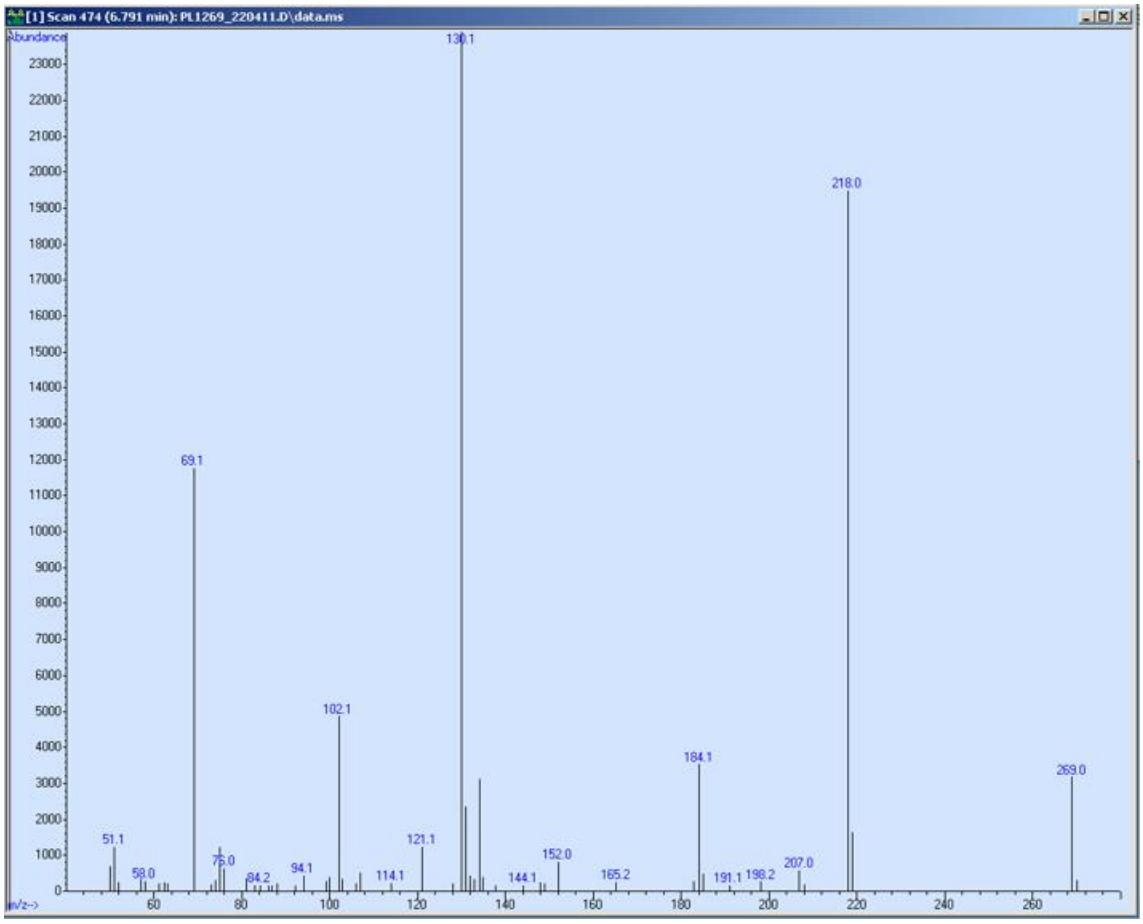

Figure A3.74 GC-MS of **3-7b**, after complex **3-1** reacted with CuBr (2 eq) DMSO (28 eq.) and 4-iodobenzonitrile (1 eq.) in benzene at 50 ºC. Retention time 6.791 min, expected 269.15 m/z and found 269 m/z.

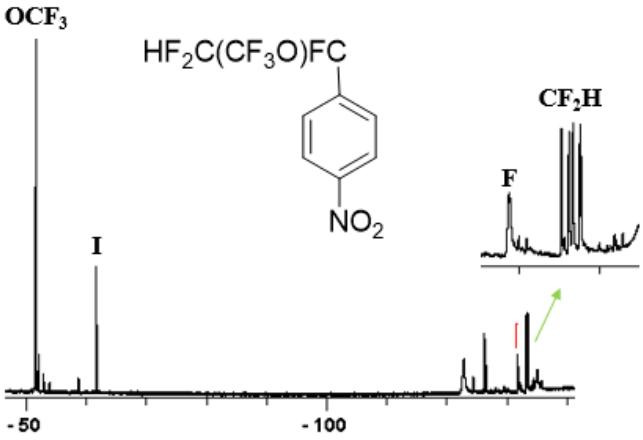

Figure A3.75 ^{19}F NMR spectrum (282 MHz, C_6D_6) of **3-7c**, after complex **3-1** reacted with CuBr (2 eq) DMSO (28 eq.) and 4-nitroiodobenzene (1 eq.) in benzene at 50 ºC. I = internal standard ($PhCF_3$).

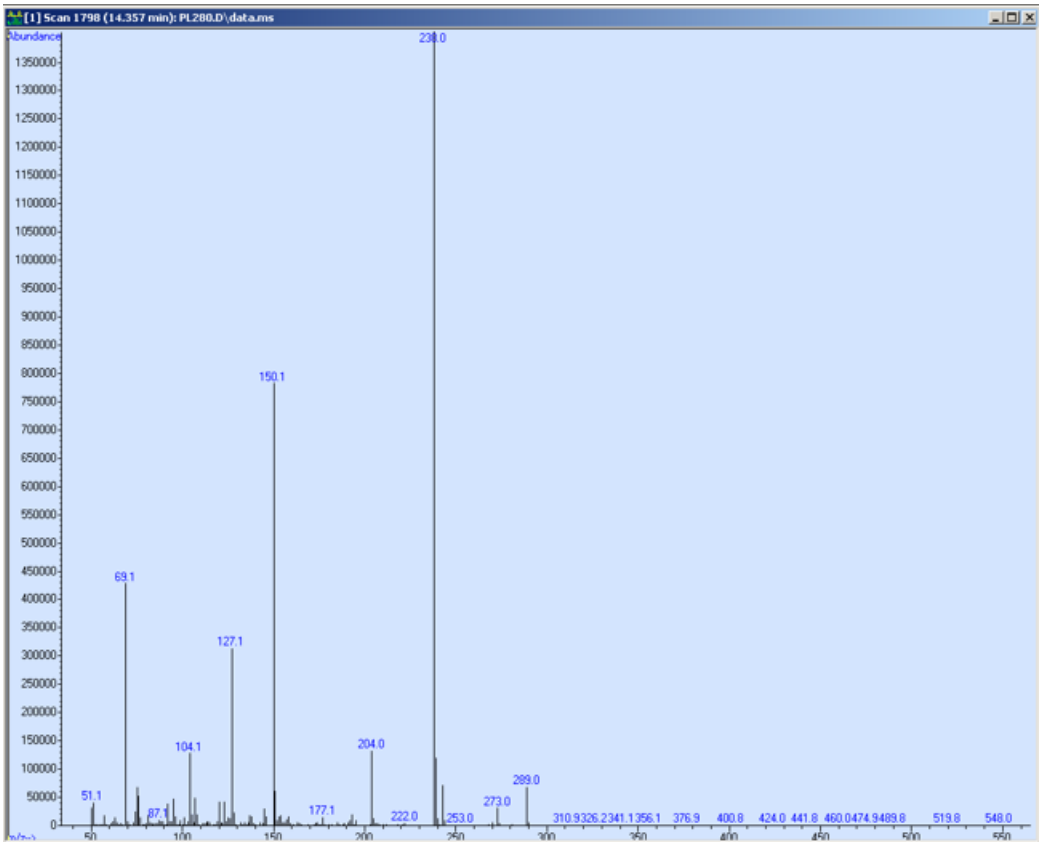

Figure A3.76 GC-MS of **3-7c**, after complex **3-1** reacted with CuBr (2 eq) DMSO (28 eq.) and 4-iodonitrobenzene (1 eq.) in benzene at 50 ºC. Retention time 12.357 min, expected 289.13 m/z (100%), found 289 m/z (20%) and 238 m/z (99%).

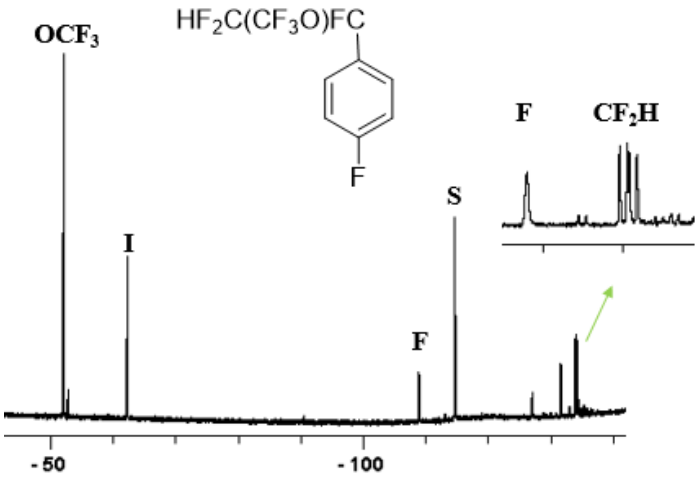

Figure A3.77 ^{19}F NMR spectrum (282 MHz, C_6D_6) of **3-7d**, after complex **3-1** reacted with CuBr (2 eq) DMSO (28 eq.) and 4-fluoroiodobenzene (1 eq.) in benzene at 50 ºC. S = substrate, I = internal standard ($PhCF_3$).

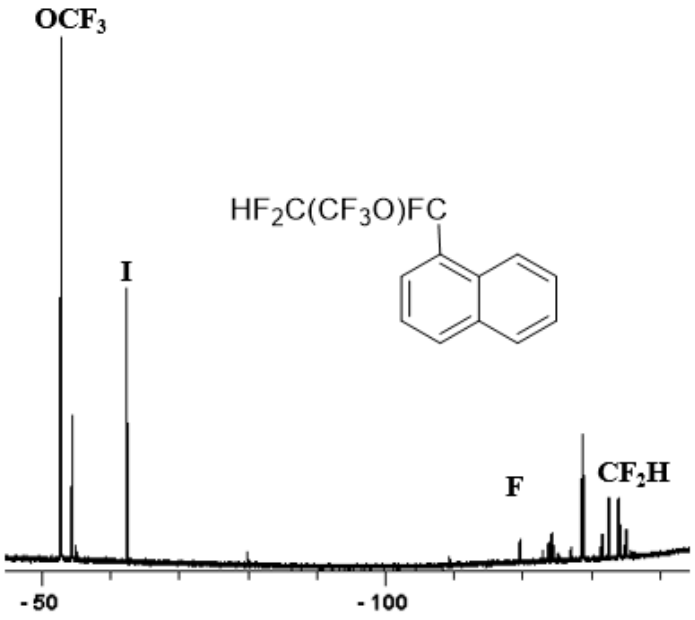

Figure A3.78 ^{19}F NMR spectrum (282 MHz, C_6D_6) of **3-7e**, after complex **3-1** reacted with CuBr (2 eq) DMSO (28 eq.) and 1-iodonaphthalene (1 eq.) in benzene at 50 °C. I = internal standard ($PhCF_3$).

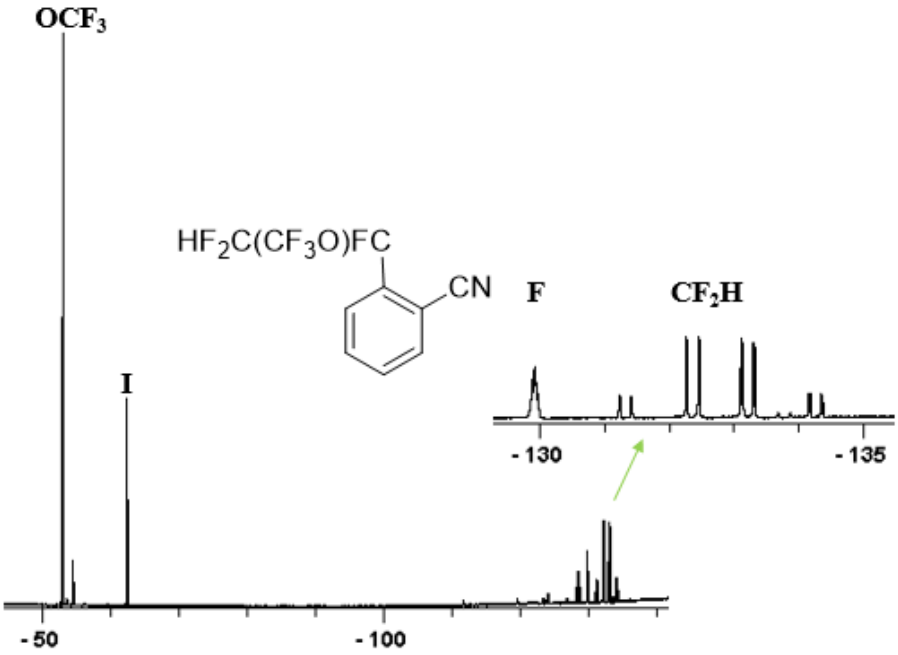

Figure A3.79 ^{19}F NMR spectrum (282 MHz, C_6D_6) of **3-7f**, after complex **3-1** reacted with CuBr (2 eq) DMSO (28 eq.) and 2-iodobenzonitrile (1 eq.) in benzene at 50 °C. I = internal standard ($PhCF_3$).

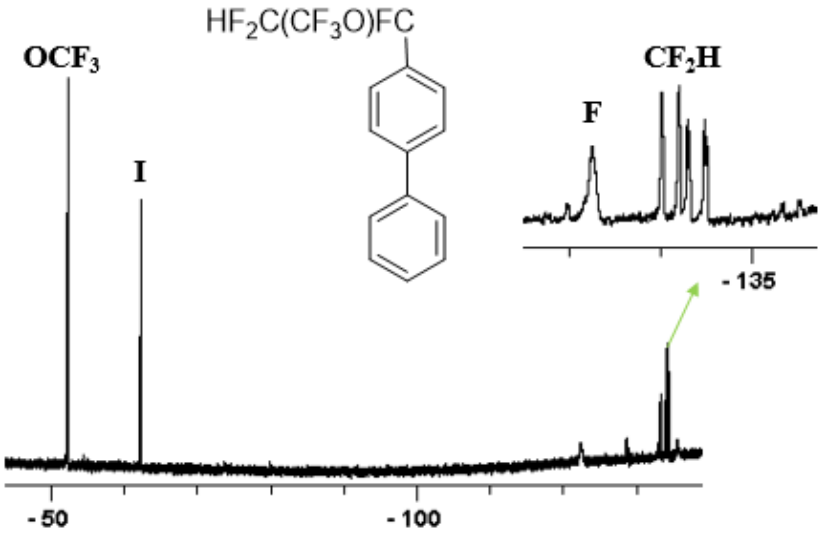

Figure A3.80 ^{19}F NMR spectrum (282 MHz, C_6D_6) of **3-7g**, after complex **3-1** reacted with CuBr (2 eq) DMSO (28 eq.) and (1 eq.) of biphenyl iodobenzene in benzene at 50 °C. I = internal standard ($PhCF_3$).

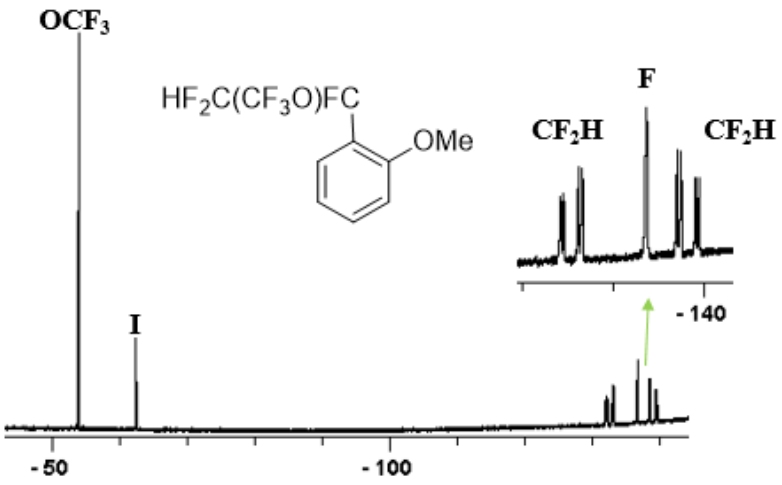

Figure A3.81 ^{19}F NMR spectrum (282 MHz, C_6D_6) of **3-7h**, after complex **3-1** reacted with CuBr (2 eq) DMSO (28 eq.) and 2-iodoanisole (1 eq.) in benzene at 50 °C. I = internal standard ($PhCF_3$).

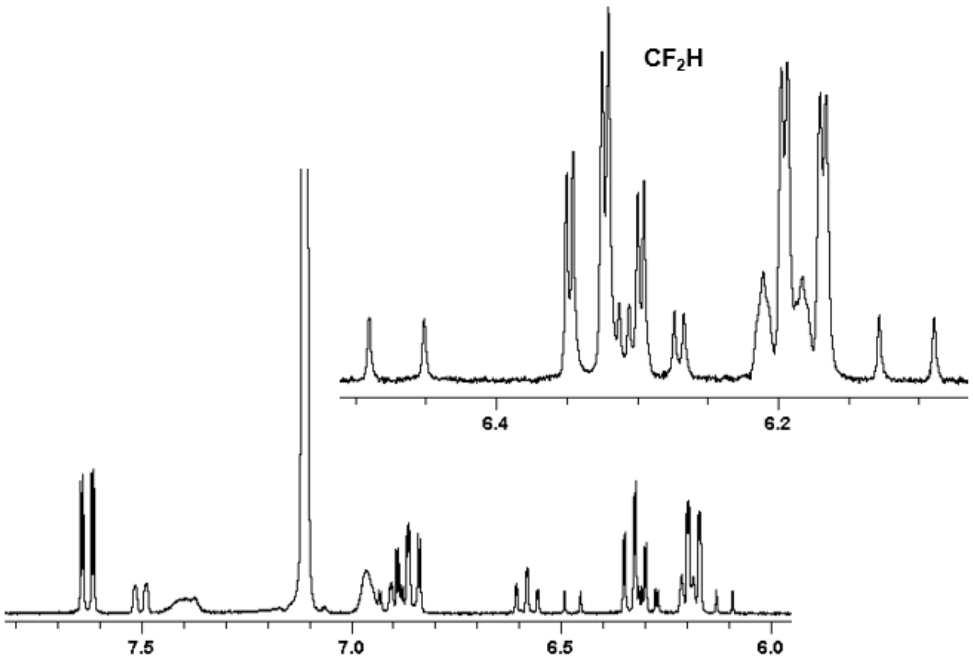

Figure A3.82 ^{1}H NMR spectrum (282 MHz, C_6D_6) of **3-7h**, after complex **3-1** reacted with CuBr (2 eq) DMSO (28 eq.) and 2-iodoanisole (1 eq.) in benzene at 50 ºC.

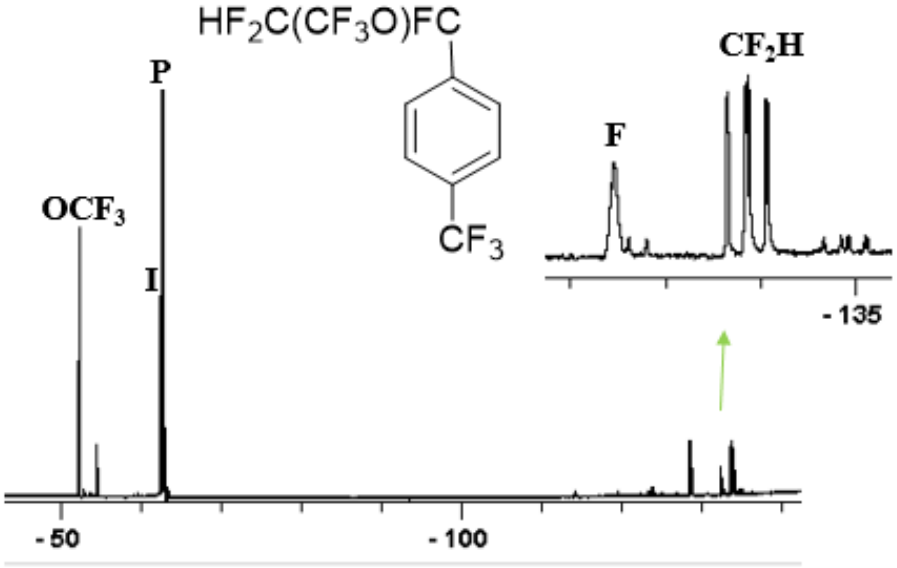

Figure A3.83 ^{19}F NMR spectrum (282 MHz, C_6D_6) of **3-7i**, after complex **3-1** reacted with CuBr (2 eq) DMSO (28 eq.) and 4-trifluoromethyliodobenzene (1 eq.) in benzene at 50 ºC. P = product, I = internal standard ($PhCF_3$).

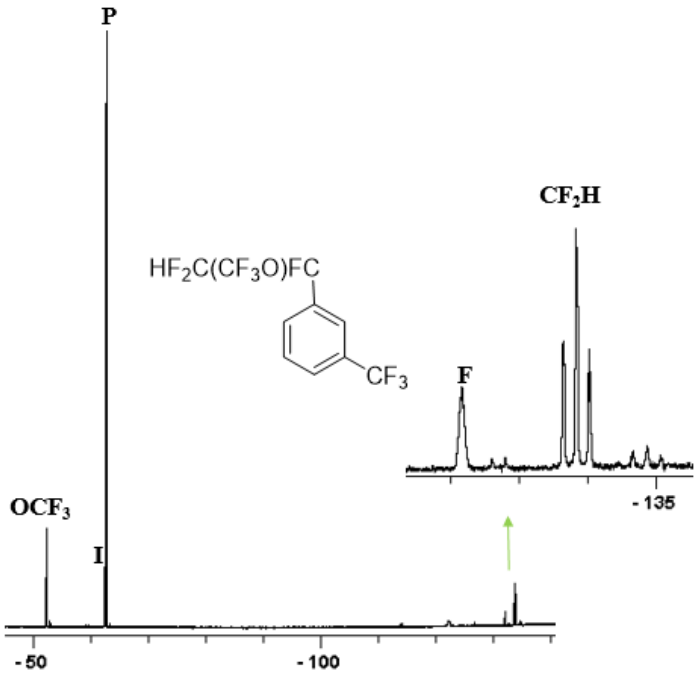

Figure A3.84 ^{19}F NMR spectrum (282 MHz, C_6D_6) of **3-7j**, after complex **3-1** reacted with CuBr (2 eq) DMSO (28 eq.) and 3-trifluoromethyl-iodobenzene (1 eq.) in benzene at 50 ^{o}C. I = internal standard ($PhCF_3$).

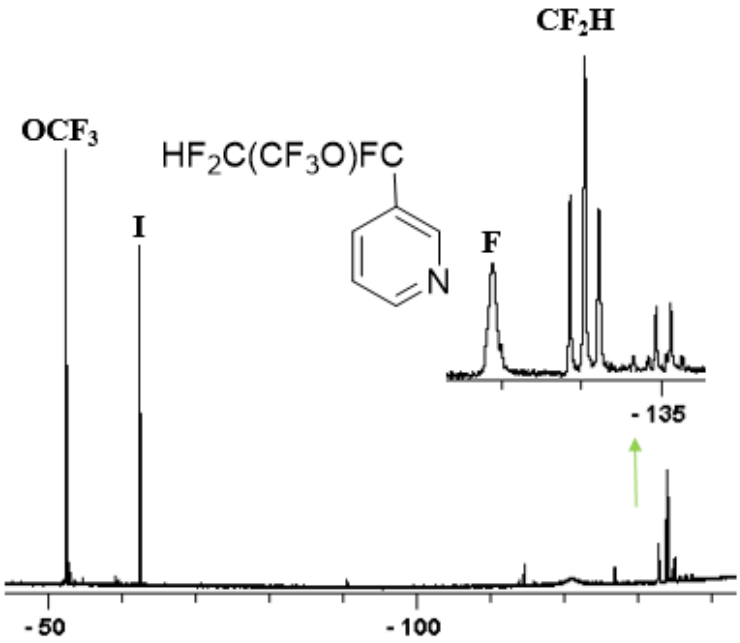

Figure A3.85 ^{19}F NMR spectrum (282 MHz, C_6D_6) of **3-7k**, after complex **3-1** reacted with CuBr (2 eq) DMSO (28 eq.) and 3-iodopyridine (1 eq.) in benzene at 50 ^{o}C. I = internal standard ($PhCF_3$).

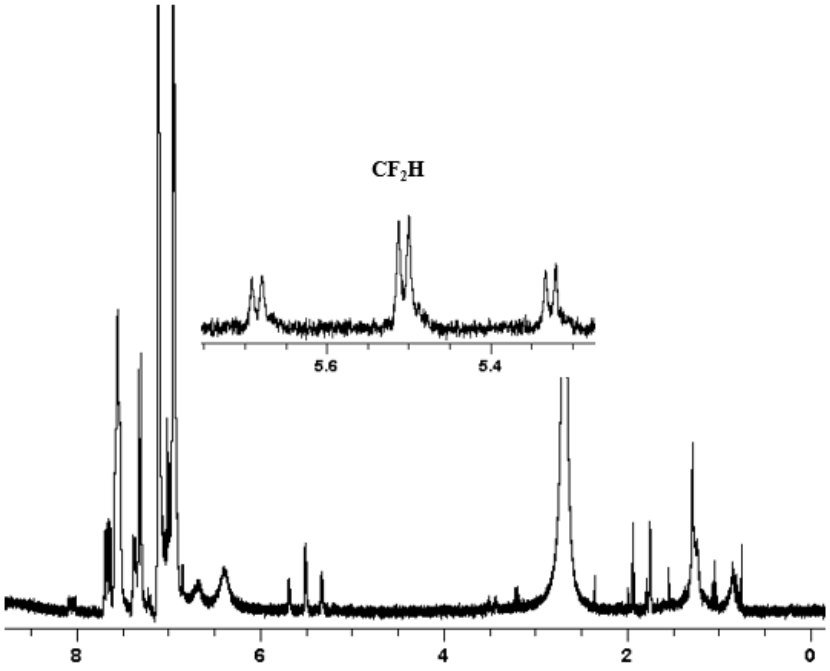

Figure A3.86 ^{1}H NMR spectrum (282 MHz, C_6D_6) of **3-7k**, after complex **3-1** reacted with CuBr (2 eq) DMSO (28 eq.) and 3-iodopyridine (1 eq.) in benzene at 50 ^{o}C.

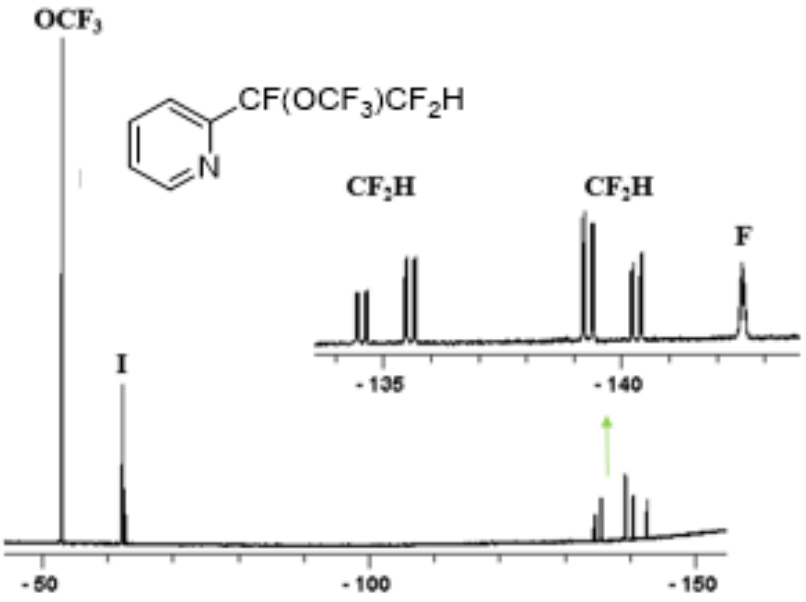

Figure A3.87 ^{19}F NMR spectrum (282 MHz, C_6D_6) of **3-7l**, after complex **3-1** reacted with CuBr (2 eq) DMSO (28 eq.) and 2-iodopyridine (1 eq.) in benzene at 50 ^{o}C. I = internal standard ($PhCF_3$).

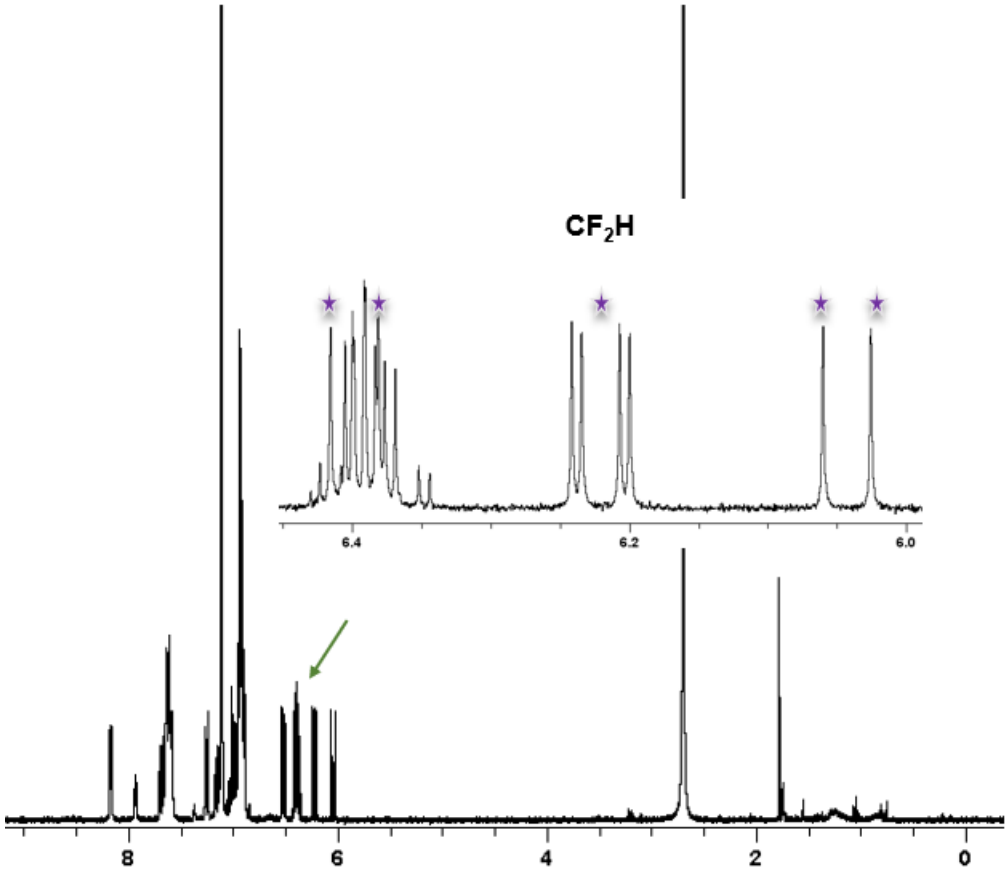

Figure A3.88 ^{1}H NMR spectrum (282 MHz, C_6D_6) of **3-7l**, after complex **3-1** reacted with CuBr (2 eq) DMSO (28 eq.) and 2-iodopyridine (1 eq.) in benzene at 50 ^{o}C.

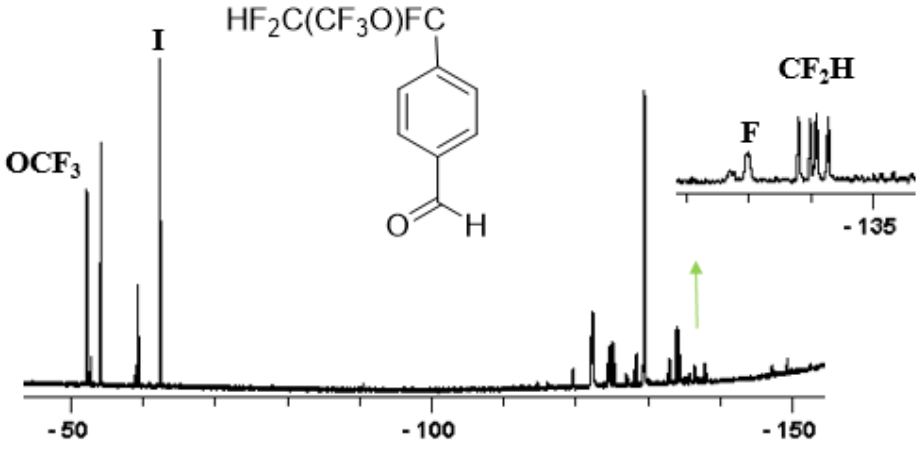

Figure A3.89 ^{19}F NMR spectrum (282 MHz, C_6D_6) of **3-7m**, after complex **3-1** reacted with CuBr (2 eq) DMSO (28 eq.) and 4-iodobenzaldehyde (1 eq.) in benzene at 50 ^{o}C. I = internal standard ($PhCF_3$).

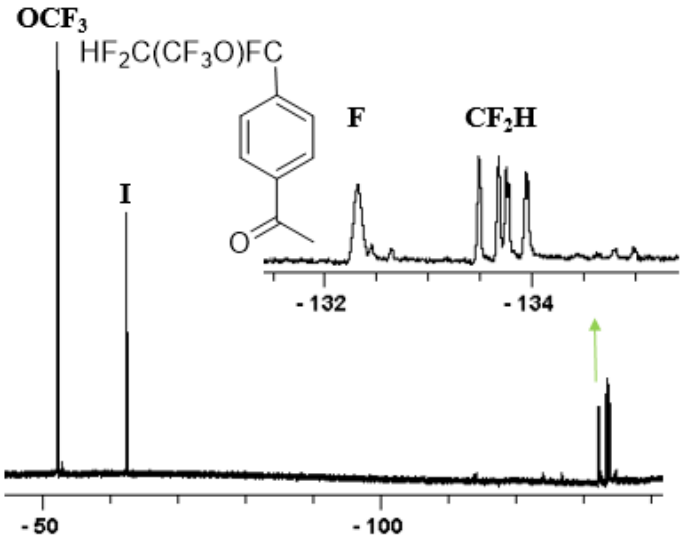

Figure A3.90 ^{19}F NMR spectrum (282 MHz, C_6D_6) of **3-7n**, after complex **3-1** reacted with CuBr (2 eq) DMSO (28 eq.) and 4-iodoacetophenone (1 eq.) in benzene at 50 °C. I = internal standard ($PhCF_3$).

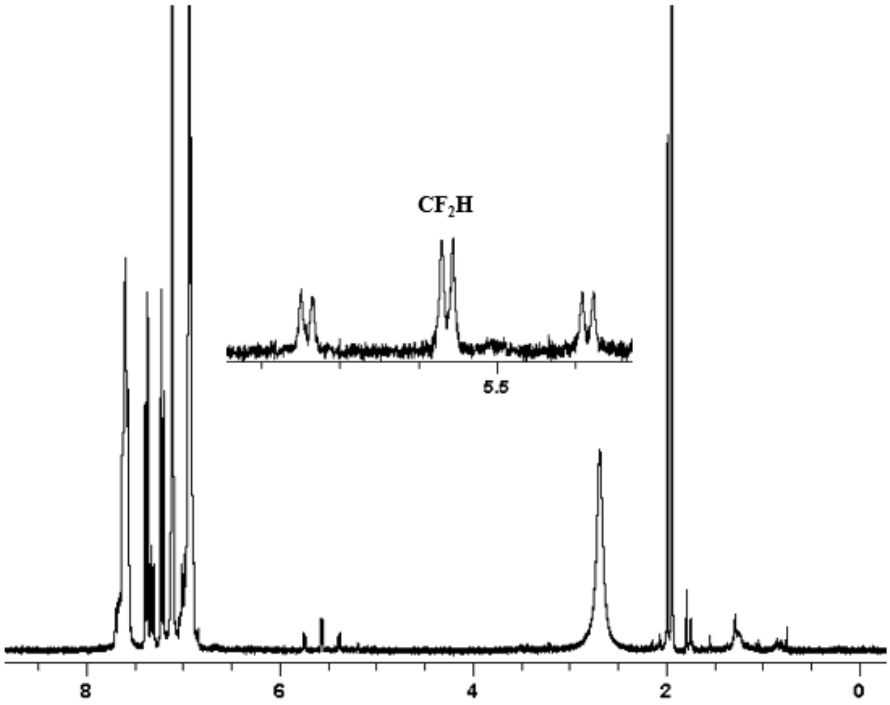

Figure A3.91 ^{19}F NMR spectrum (282 MHz, C_6D_6) of **3-7n**, after complex **3-1** reacted with CuBr (2 eq) DMSO (28 eq.) and 4-iodoacetophenone (1 eq.) in benzene at 50 ºC.

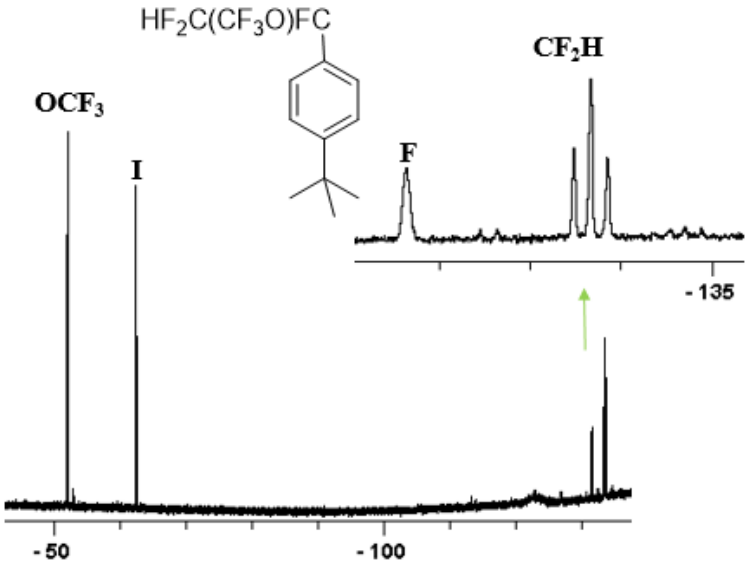

Figure A3.92 ^{19}F NMR spectrum (282 MHz, C_6D_6) of **3-7o**, after complex **3-1** reacted with CuBr (2 eq), DMSO (28 eq.) and t-butyl-4-iodobenzene (1 eq.) in benzene at 50 ºC. I = internal standard ($PhCF_3$).

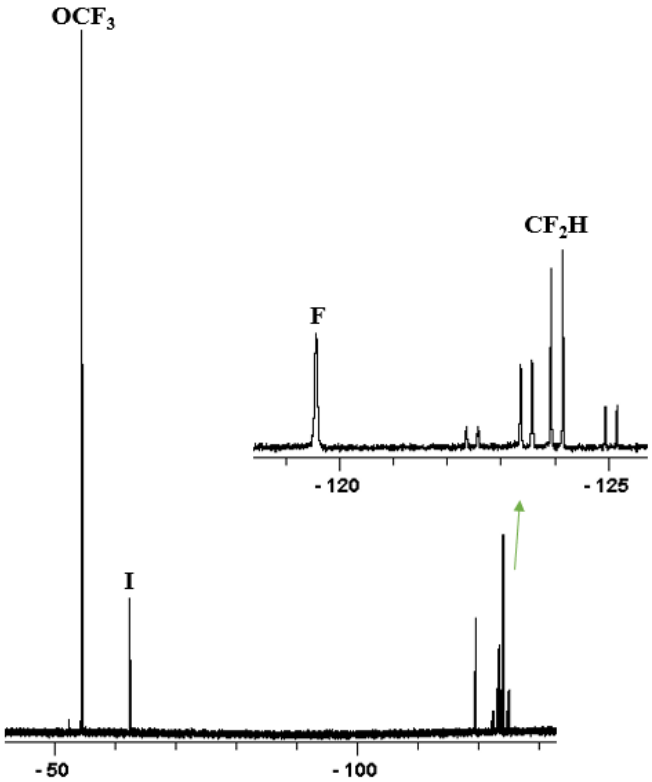

Figure A3.93 ^{19}F NMR spectrum (282 MHz, C_6D_6) of complex **3-1** reacted with CuBr (2 eq), DMSO (28 eq.) in benzene 5 min after addition of 4-benzonitrile at 50 ºC. I = internal standard ($PhCF_3$).

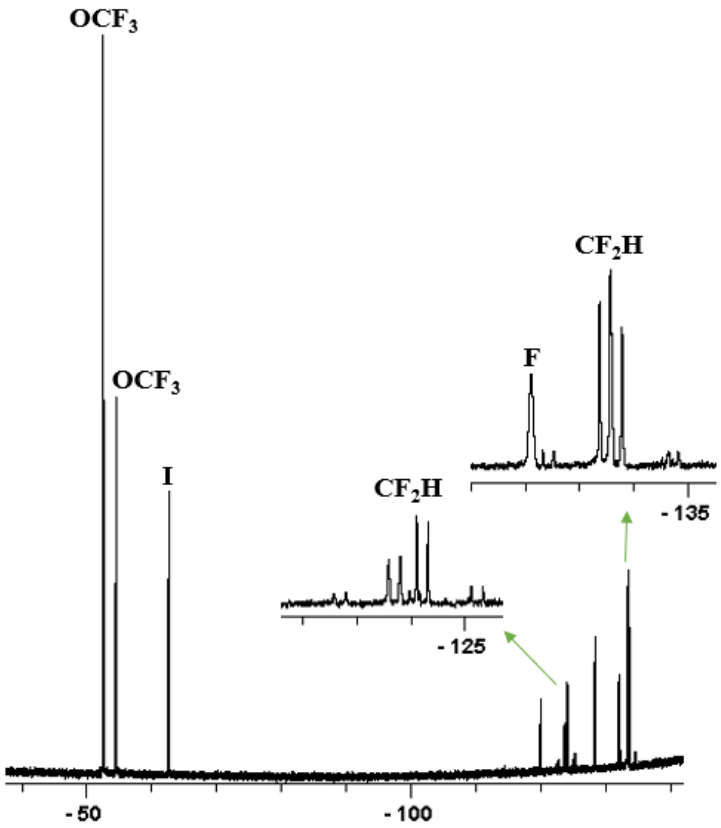

Figure A3.94 ^{19}F NMR spectrum (282 MHz, C_6D_6) of complex **3-1** reacted with CuBr (2 eq), DMSO (28 eq.) in benzene 10 min after addition of 4-benzonitrile at 50 °C. I = internal standard ($PhCF_3$).

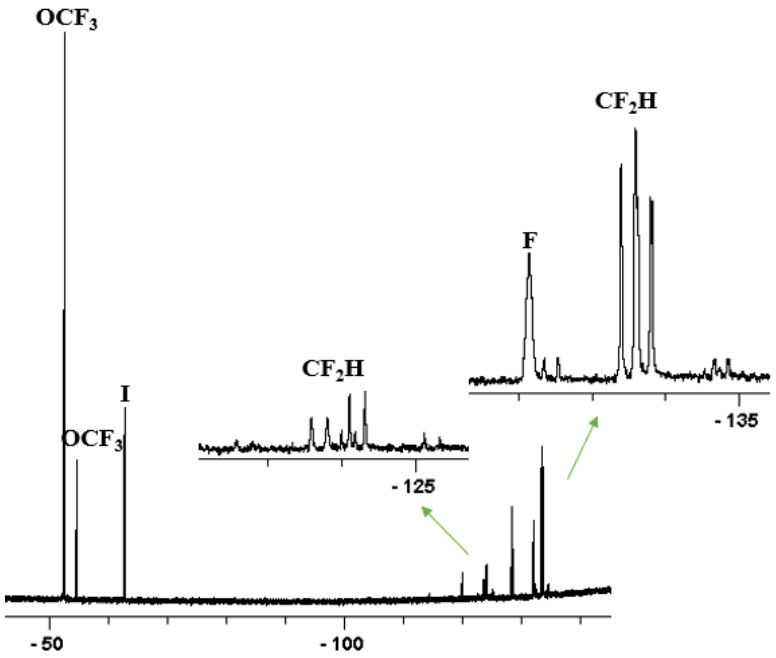

Figure A3.95 ^{19}F NMR spectrum (282 MHz, C_6D_6) of complex **3-1** reacted with CuBr (2 eq), DMSO (28 eq.) in benzene 20 min after addition of 4-benzonitrile at 50 °C. I = internal standard ($PhCF_3$).

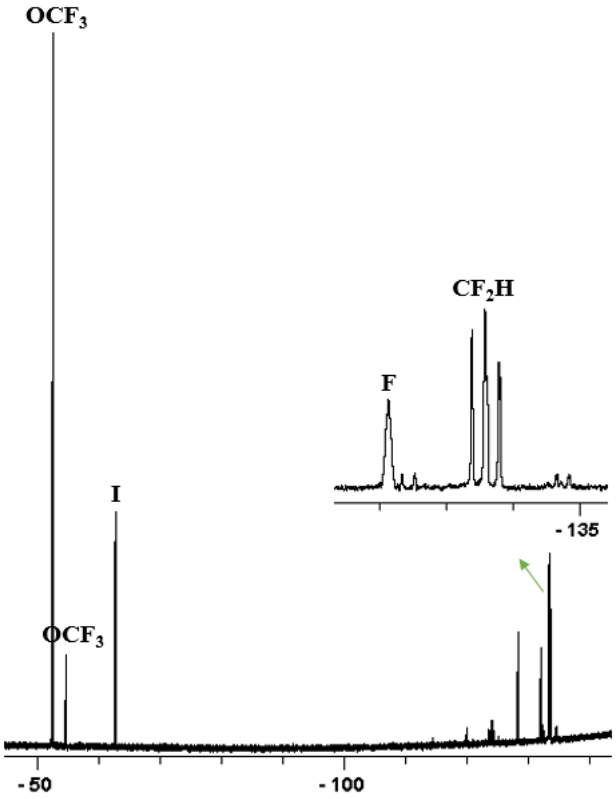

Figure A3.96 ^{19}F NMR spectrum (282 MHz, C_6D_6) of complex **3-1** reacted with CuBr (2 eq), DMSO (28 eq.) in benzene 30 min after addition of 4-benzonitrile at 50 ºC. I = internal standard ($PhCF_3$).

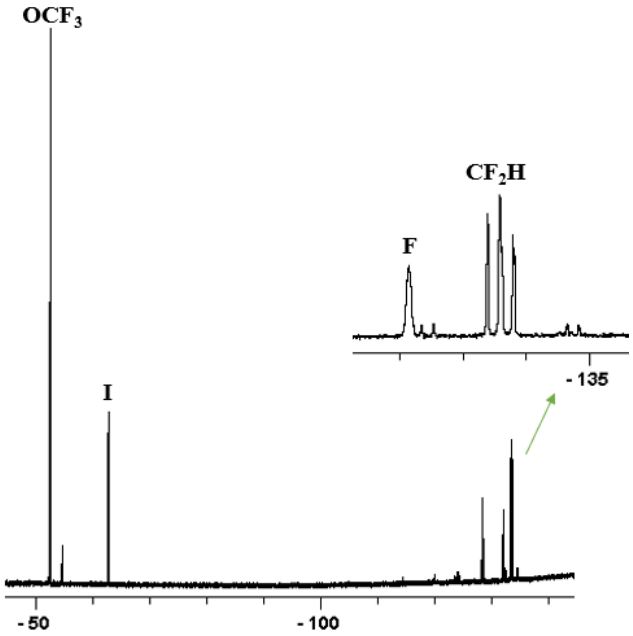

Figure A3.97 ^{19}F NMR spectrum (282 MHz, C_6D_6) of complex **3-1** reacted with CuBr (2 eq), DMSO (28 eq.) in benzene 40 min after addition of 4-benzonitrile at 50 ºC. I = internal standard ($PhCF_3$).

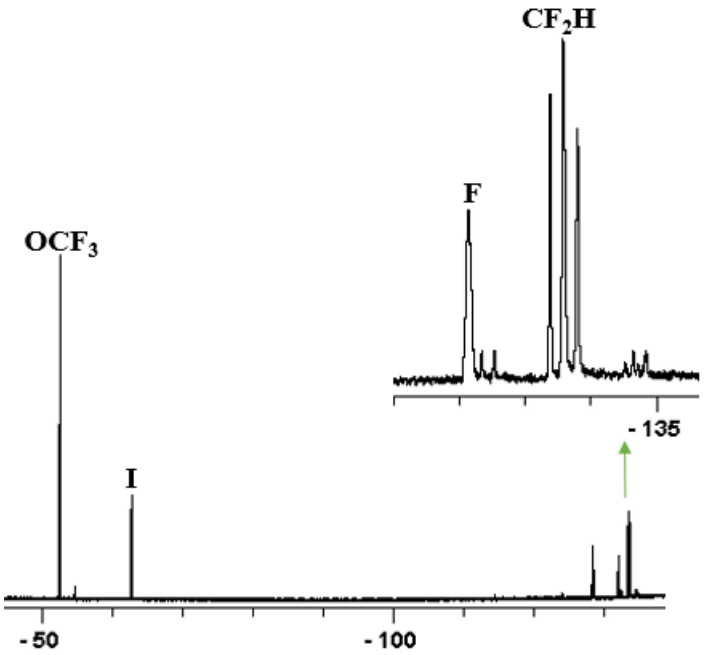

Figure A3.98 ^{19}F NMR spectrum (282 MHz, C_6D_6) of complex **3-1** reacted with CuBr (2 eq), DMSO (28 eq.) in benzene 50 min after addition of 4-benzonitrile at 50 °C. I = internal standard ($PhCF_3$).

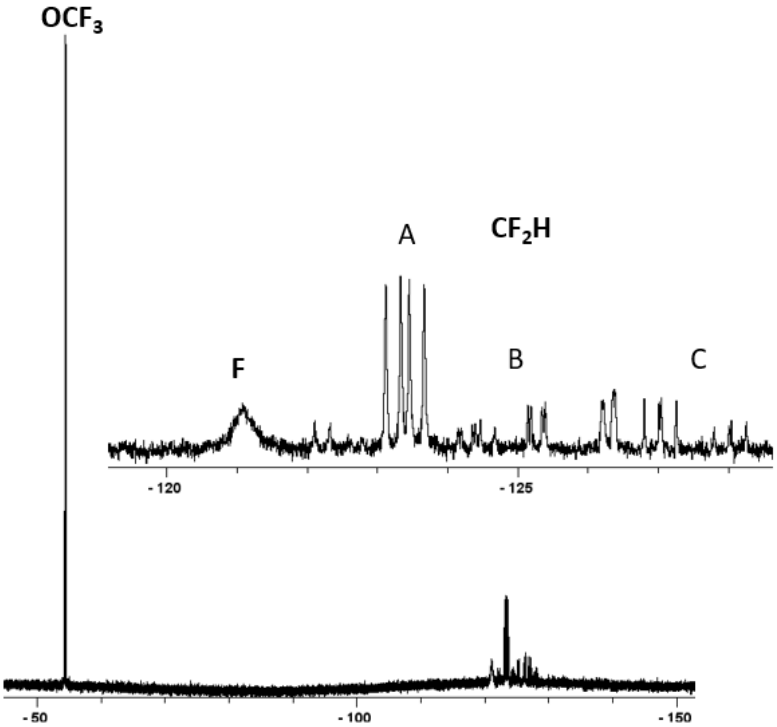

Figure A3.99 ^{19}F NMR spectrum (282 MHz, C_6D_6) of complex **3-1** reacted with CuBr (2 eq), DMSO (10 eq.) in benzene at 25 °C. A, B, and C are different species of CF_2H.

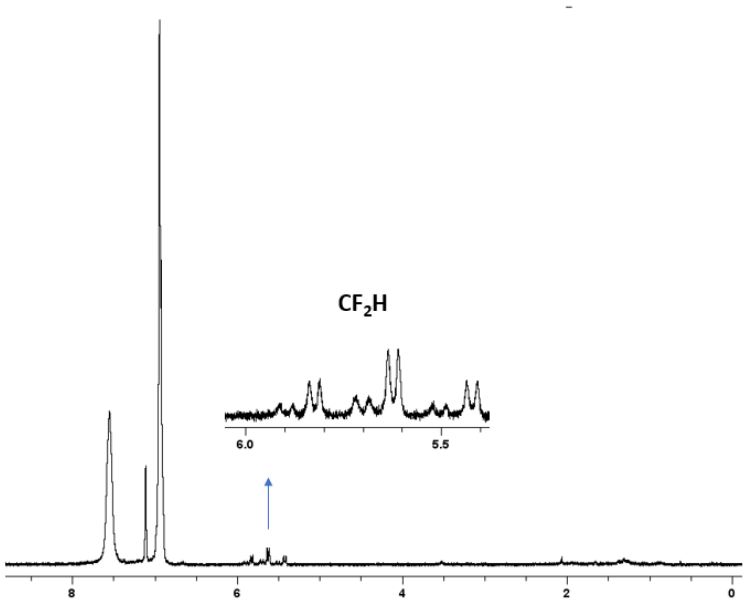

Figure A3.100 ^{1}H NMR spectrum (282 MHz, C_6D_6) of complex **3-1** reacted with CuBr (2 eq), DMSO (10 eq.) in benzene at 25 °C.

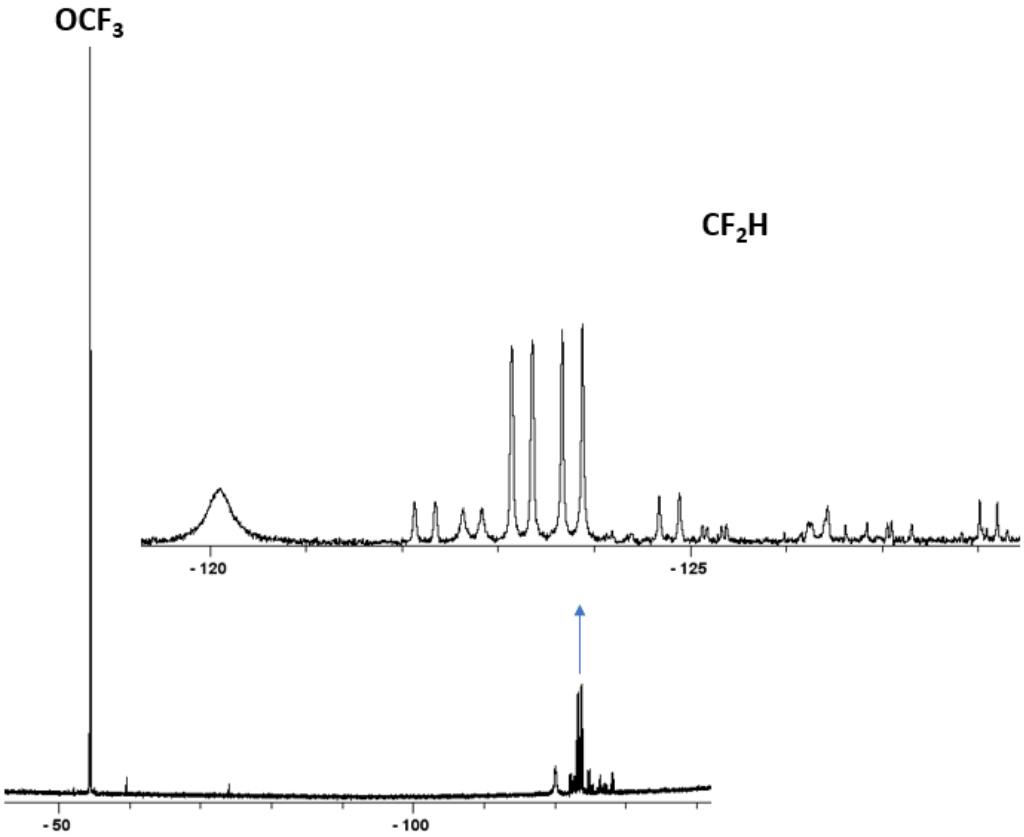

Figure A3.101 ^{19}F NMR spectrum (282 MHz, C_6D_6) of complex **3-1** reacted with CuBr (2 eq), DMSO (10 eq.) in benzene at 40 °C.

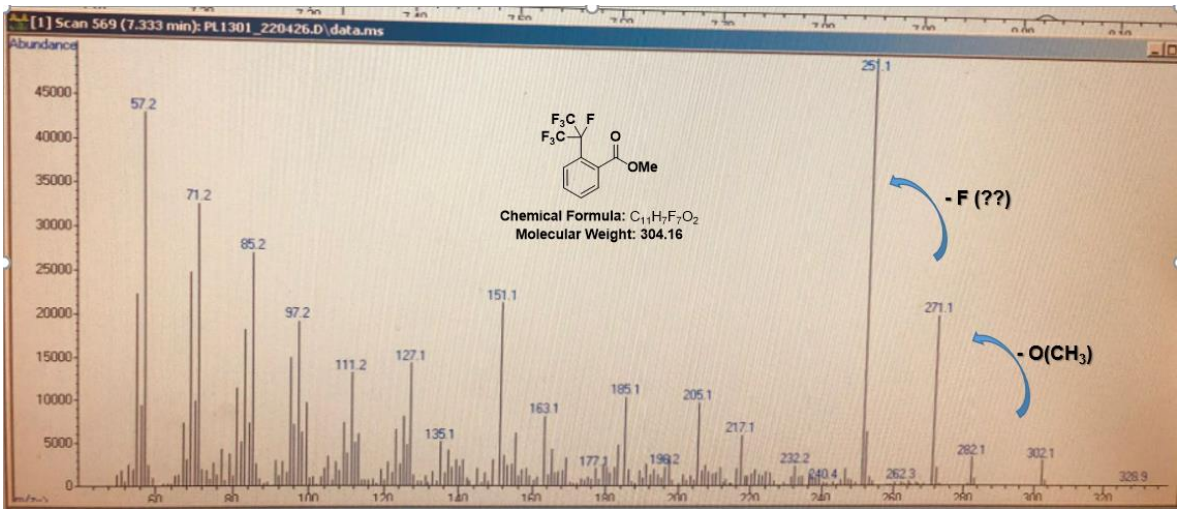

Figure A3.102 Selected peak (7.33 min) from GC-MS of Cu(hfip)$(PPh_3)_2$ after reacting with CuBr (2 eq) DMSO (28 eq.) and methyl-2-iodobenzoate (1 eq.) in benzene at 50 ºC. Expected 304.16 m/z (100%), found 302.1 m/z (20%) and 251 m/z (99%).

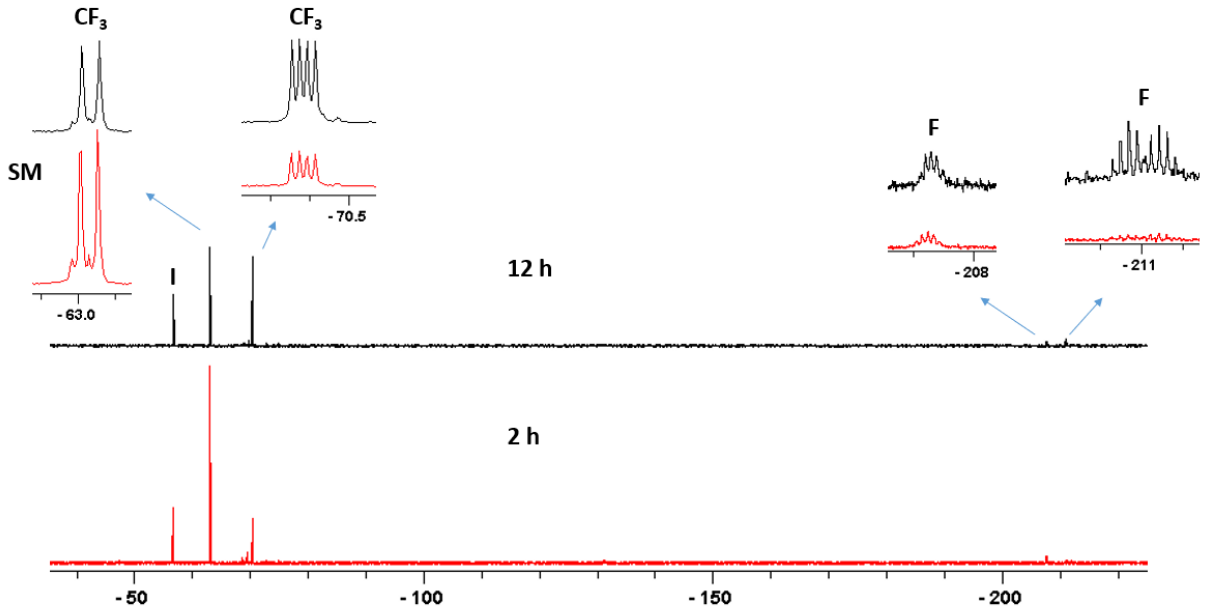

Figure A3.103 ^{19}F NMR of Cu(hfip)$(PPh_3)_2$ after reacting with CuBr (2 eq) DMSO (28 eq.) and methyl-2-iodobenzoate (1 eq.) in benzene at 50 ºC after 2 and 12 h. SM = starting material, I = internal standard ($PhCF_3$).

Table A3.2 Time course reaction of complex **3-1** with CuBr/DMSO and 4-iodo-benzonitrile monitored by ^{19}F NMR using the internal standard ($PhCF_3$) to calculate the concentration of product and starting material.

Time (min)	[Product] mmol/mL	[SM] mmol/mL
0	0	0.017
10	0.0078	0.0072
20	0.0091	0.0033
30	0.0109	0.0027
40	0.0125	0.0012
50	0.014	0.000906
60	0.0145	0.000331
70	0.0151	0

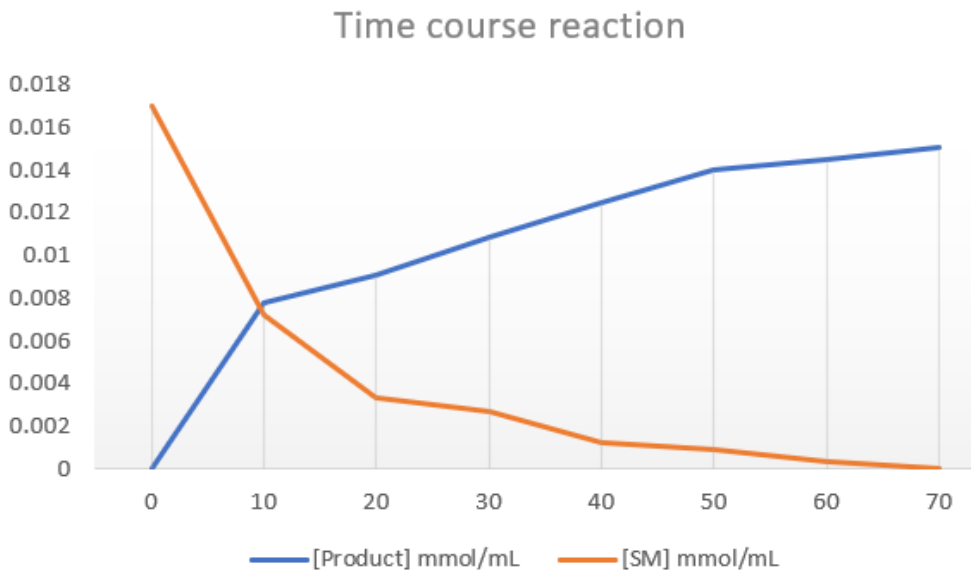

Figure A3.104 Time course reaction of complex **3-1** with CuBr/DMSO and 1 equiv. of 4-iodo-benzonitrile in benzene at 50 °C monitored by ^{19}F NMR using the internal standard ($PhCF_3$) to calculate the concentration of product and starting material.

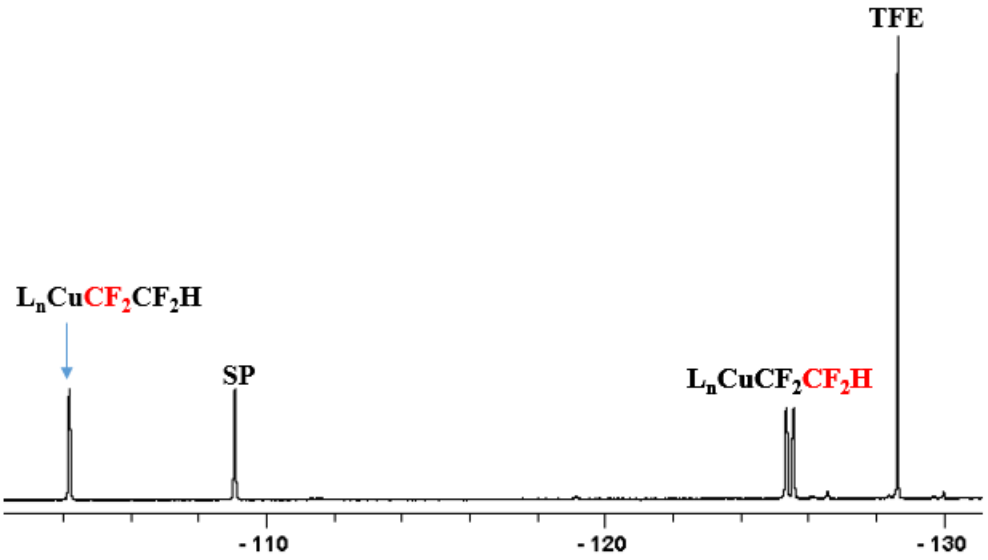

Figure A4.1 ^{19}F NMR spectrum (282 MHz) of [$CuH(PPh_3)$] + Xantphos + TMDSO + TFE:CO_2 in DMF after 7 h at RT.

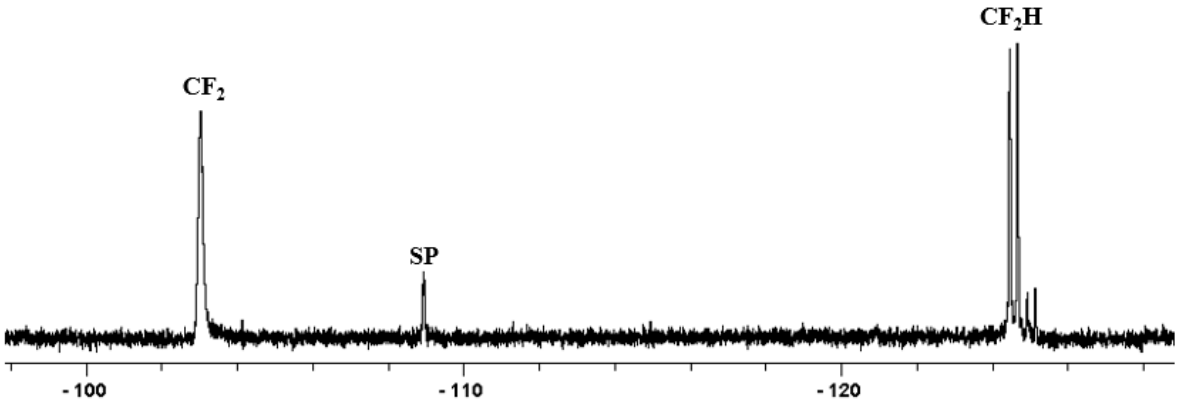

Figure A4.2 ^{19}F NMR spectrum (282 MHz) of Cu(CF_2CF_2H)(Xantphos) (**4-2**) in DMF.

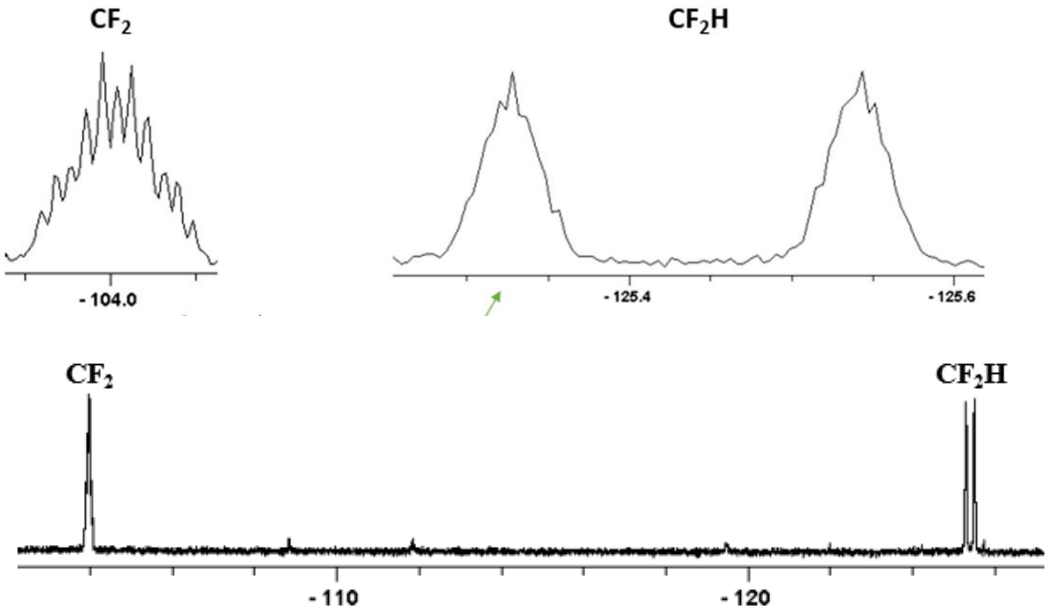

Figure A4.3 ^{19}F NMR spectrum (282 MHz) of $Cu(CF_2CF_2H)(Xantphos)$ (**4-2**) in C_6D_6.

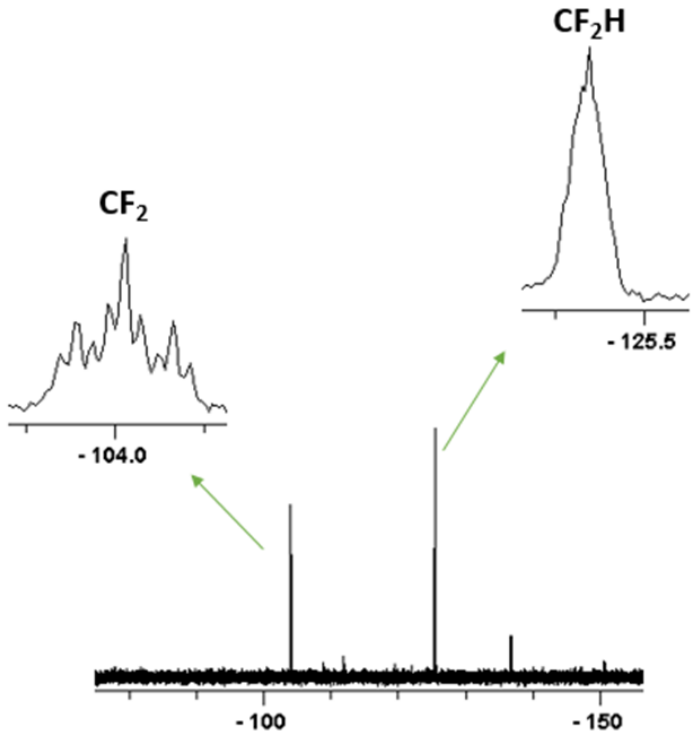

Figure A4.4 $^{19}F\{^1H\}$ NMR spectrum (282 MHz) of $Cu(CF_2CF_2H)(Xantphos)$ (**4-2**) in C_6D_6.

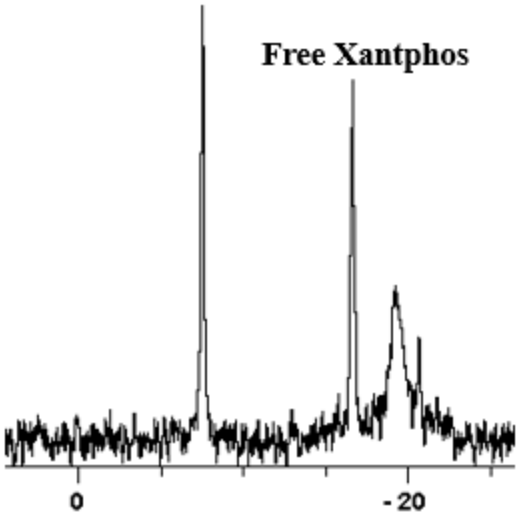

Figure A4.5 $^{31}P\{^{1}H\}$ NMR spectrum (121 MHz, C_6D_6) of Cu(CF_2CF_2H)(Xantphos) (**4-2**).

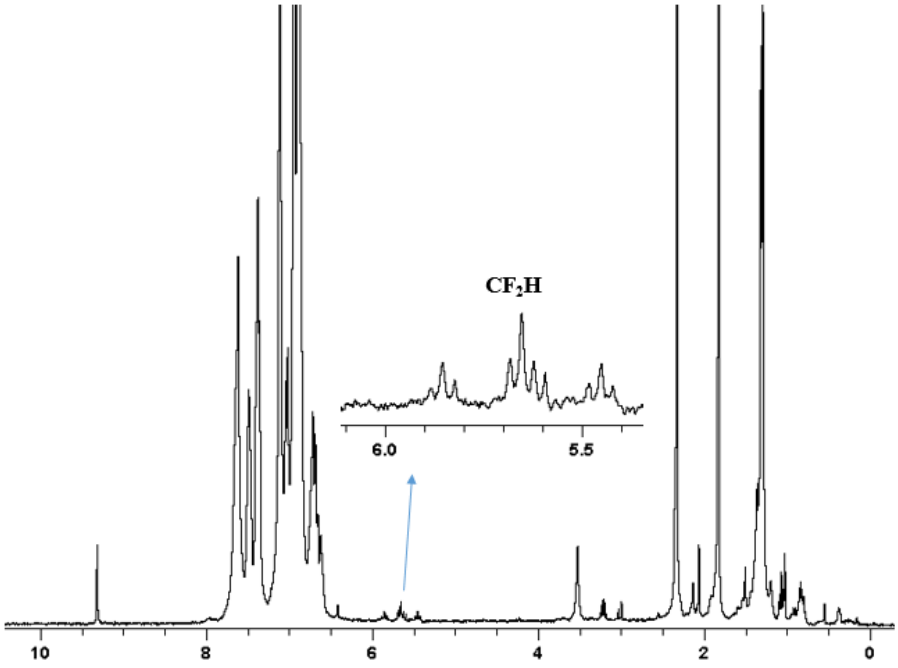

Figure A4. 6 ^{1}H NMR spectrum (300 MHz) of Cu(CF_2CF_2H)(Xantphos) **4-2**) in C_6D_6.

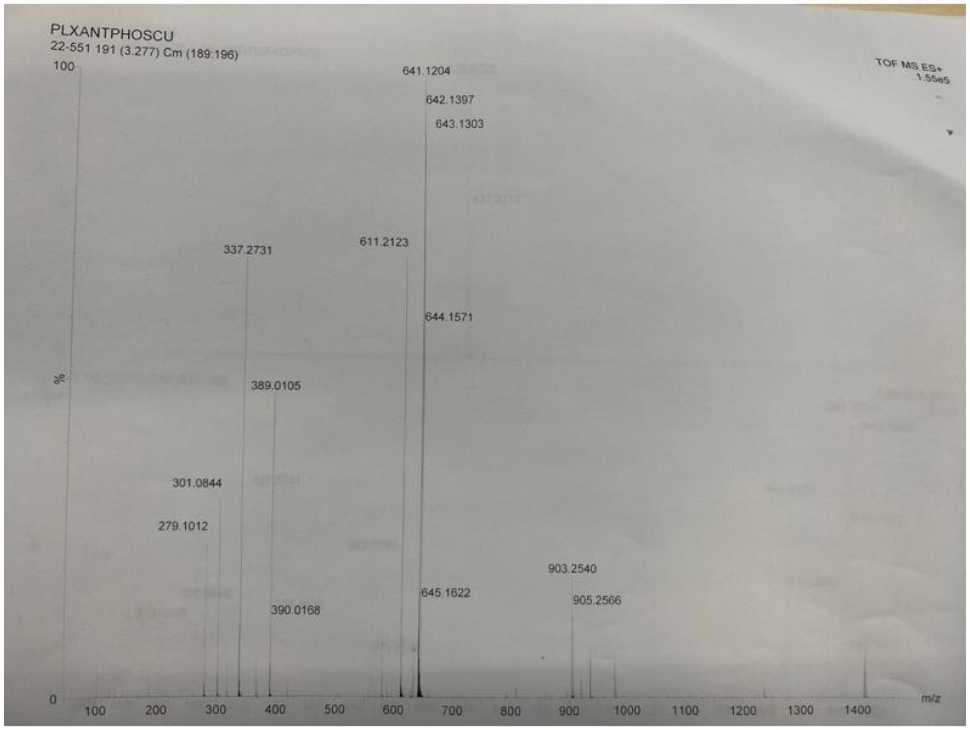

Figure A4.7 EI-MS of **4-2** showing $[Cu(Xantphos)]^+$ ion at m/s = 642.

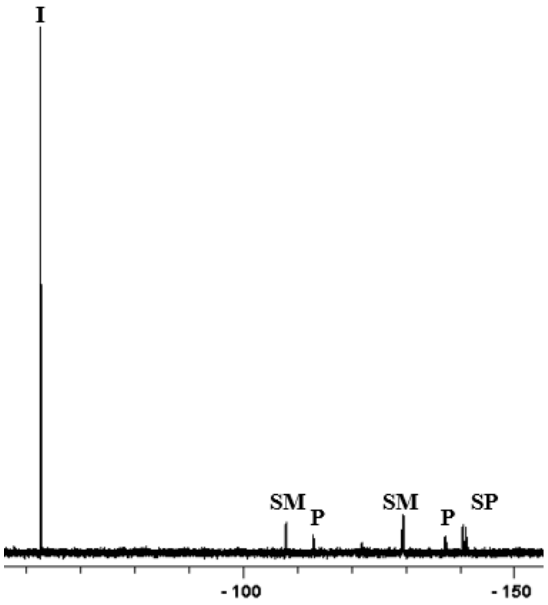

Figure A4.8 ^{19}F NMR spectrum (282 MHz) of **4-2** + 2-methyl-4-iodobenzoate in DMF at 50 ^{o}C after 16 h. SP = side product, SM = **4-2**, P = Product and I = Internal standard ($PhCF_3$).

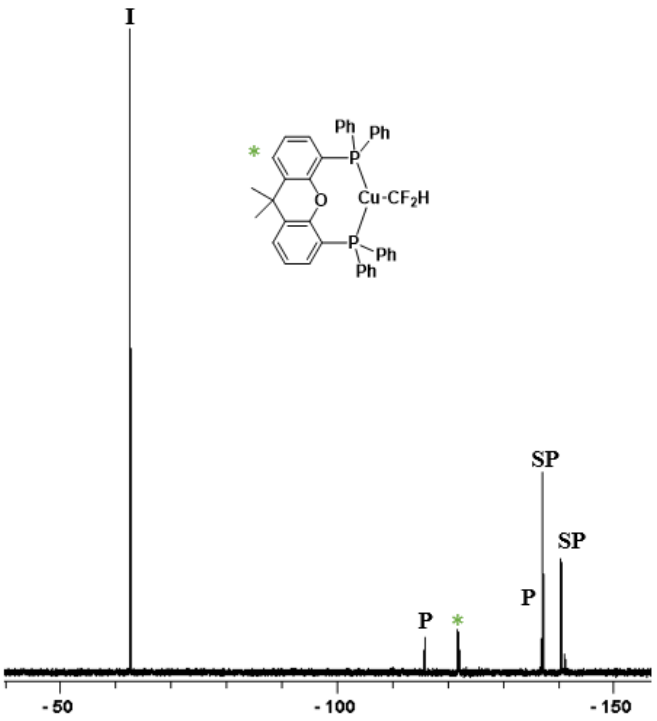

Figure A4.9 ^{19}F NMR spectrum (282 MHz) of **4-2** + 4-iodo-benzonitrile in DMF at 50 °C after 16. SP = side product, SM = **4-2**, P = Product and I = Internal standard ($PhCF_3$).

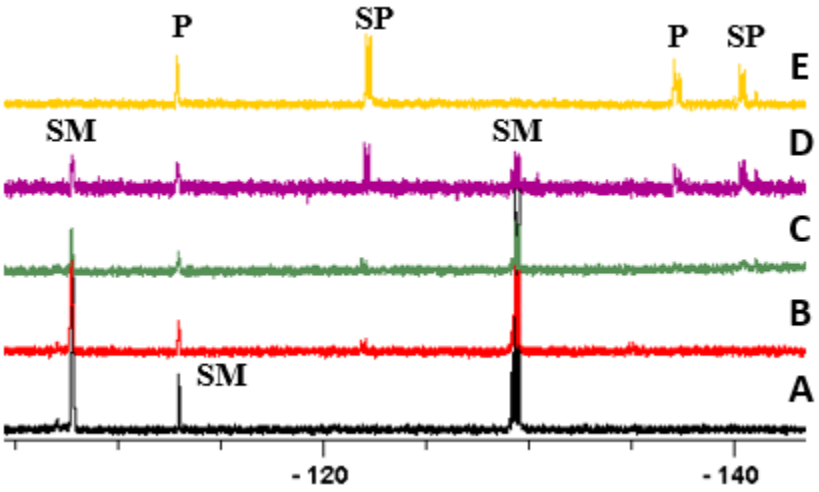

Figure A4.10 ^{19}F NMR spectrum (282 MHz) of **4-2** in DMF at 50 °C. After 15 min (**A**) and upon addition of 4-iodo-methyl-2-benzoate after 5 min (**B**), 2 h (**C**), 12 h (**D**) and 22 h (**E**).

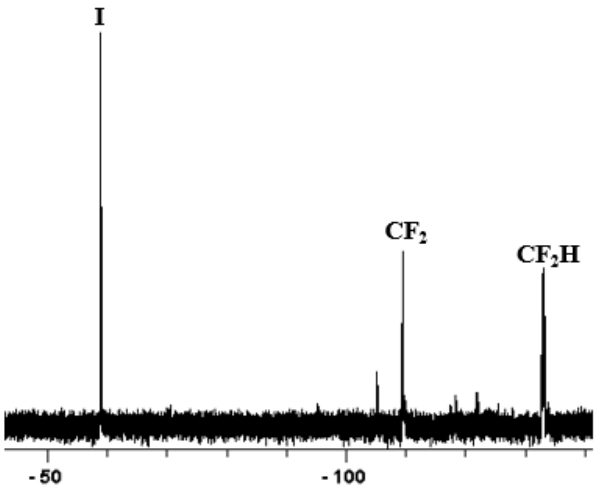

Figure A4.11 ^{19}F NMR spectrum (282 MHz) of **4-2** + 4-iodo-methyl-2-benzoate + 10 mol% CuCl(SIMes) in DMF at 90 ºC after 12 h.

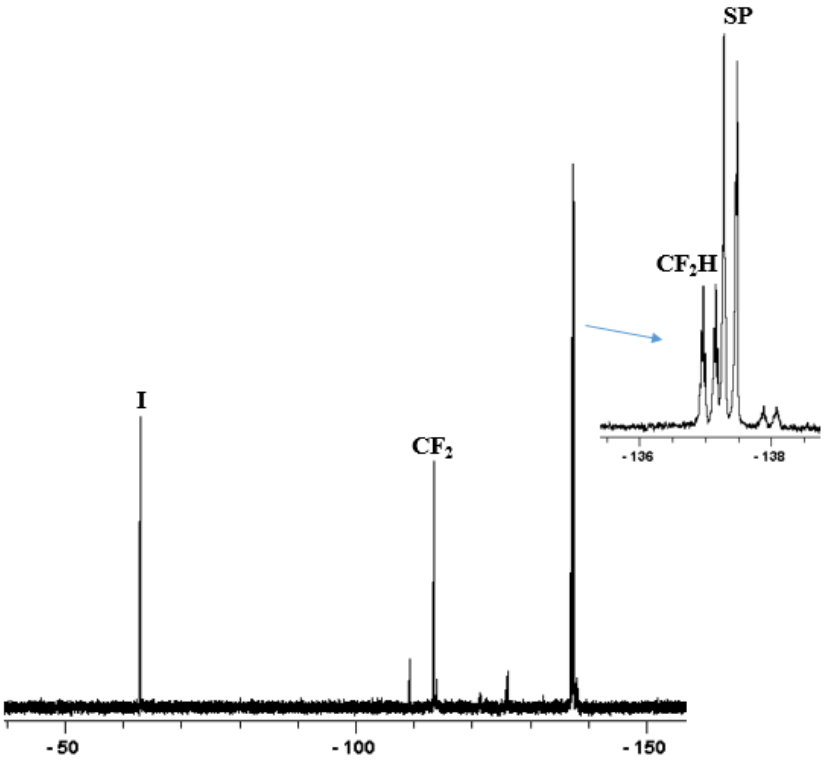

Figure A4.12 ^{19}F NMR $Cu(CF_2CF_2H)$(Xantphos) + 4-iodo-ethyl-2-benzoate + CuCl(SIMes) in DMF at 90 ºC after 12 h. ^{19}F NMR -113.4 ppm (m, CF_2), and – 137.0 ppm (dt, J^{FF} 10 Hz and J^{FH} 54 Hz).

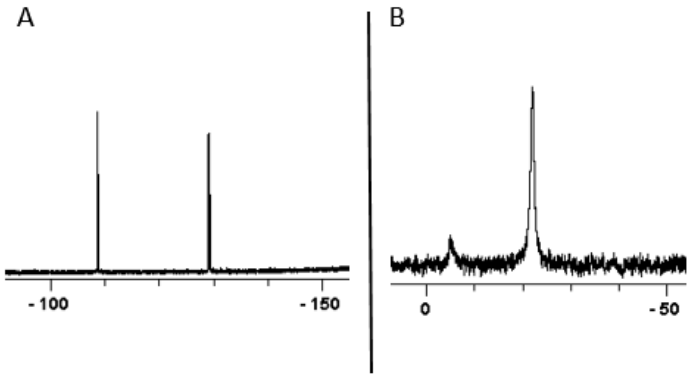

Figure A4.13 ^{19}F NMR (**A**) and $^{31}P\{^{1}H\}$ NMR (**B**) spectra of Complex **4-1** and 2 eq. of CuCl after 72 h in DMF.

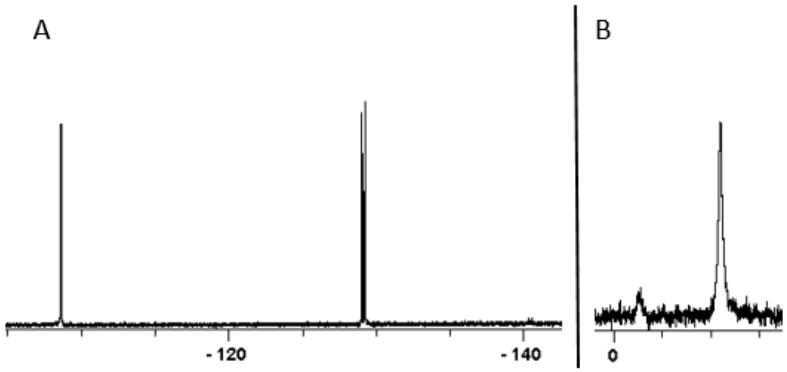

Figure A4.14 ^{19}F NMR (**A**) and $^{31}P\{^{1}H\}$ NMR (**B**) spectra of Complex **4-1** and 2 eq. of CuCl after 96 h in DMF.

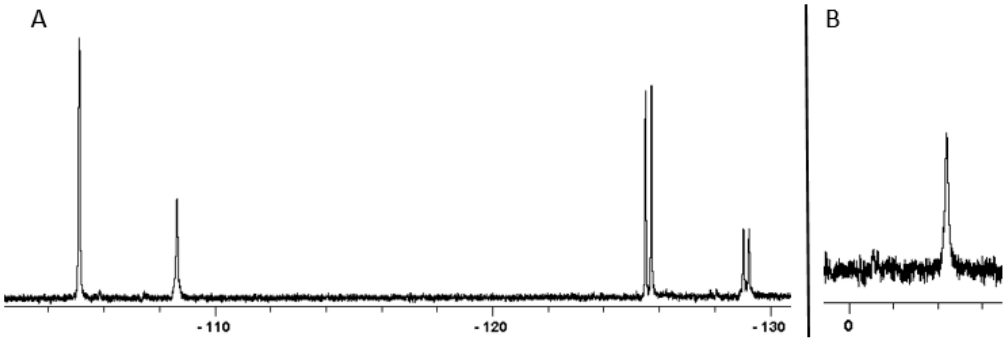

Figure A4.15 ^{19}F NMR (**A**) and $^{31}P\{^{1}H\}$ NMR (**B**) (spectra of Complex **4-1** and 2 eq. of CuCl after 2 weeks in DMF.

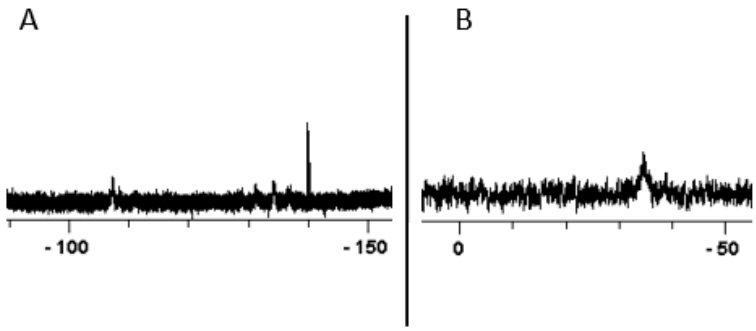

Figure A4.16 ^{19}F NMR (**A**) and $^{31}P\{^{1}H\}$ NMR (**B**) (spectra of Complex **4-1** and 2 eq. of CuCl after 4 months in DMF.

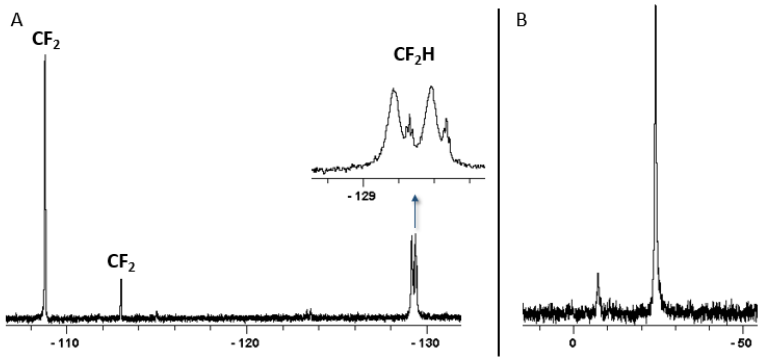

Figure A4.17 ^{19}F NMR (**A**) and $^{31}P\{^{1}H\}$ NMR (**B**) spectra of Complex **4-1** and 2 eq. of CuBr after 72 h in DMF.

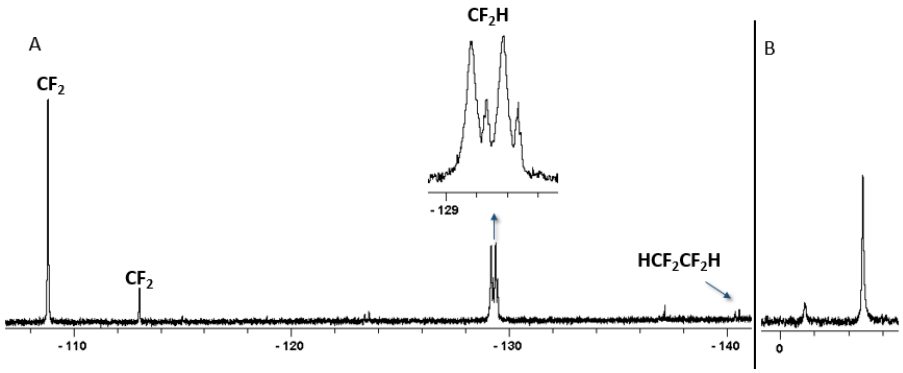

Figure A4.18 ^{19}F NMR (**A**) and $^{31}P\{^{1}H\}$ NMR (**B**) spectra of Complex **4-1** and 2 eq. of CuBr after 96 h in DMF.

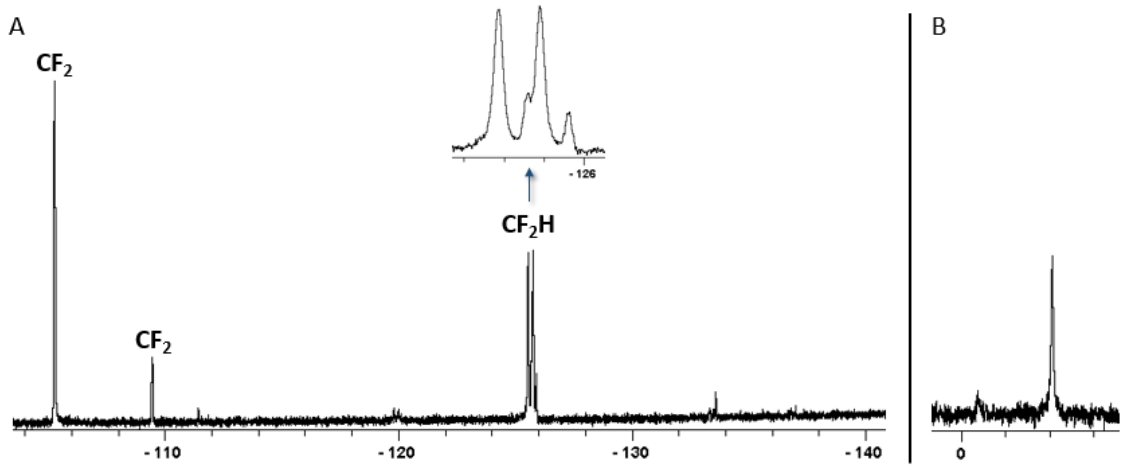

Figure A4.19 ^{19}F NMR (**A**) and $^{31}P\{^{1}H\}$ NMR (**B**) spectra of Complex **4-1** and 2 eq. of CuBr after 2 weeks in DMF.

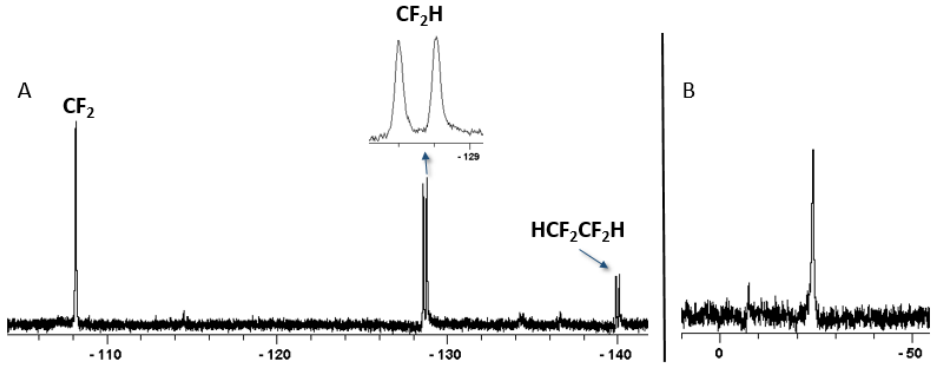

Figure A4.20 ^{19}F NMR (**A**) and $^{31}P\{^{1}H\}$ NMR (**B**) spectra of Complex **4-1** and 2 eq. of CuBr after 4 months in DMF.

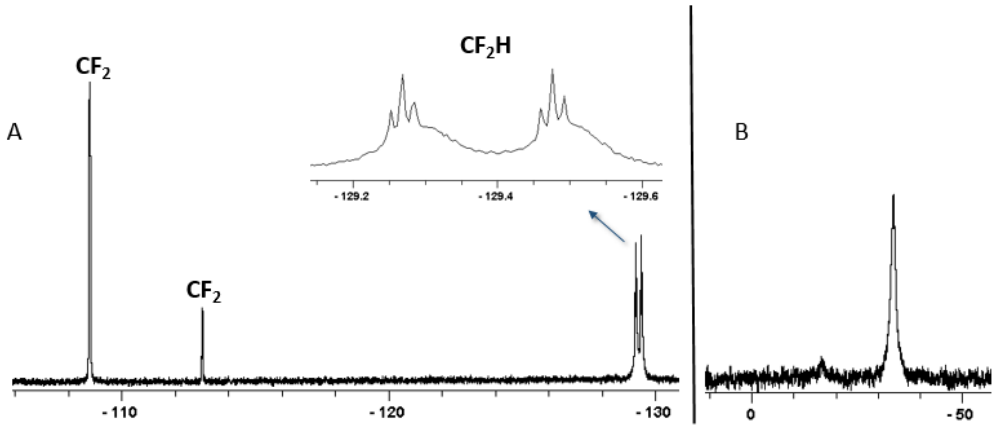

Figure A4.21 ^{19}F NMR (**A**) and $^{31}P\{^{1}H\}$ NMR (**B**) spectra of Complex **4-1** and 2 eq. of CuI after 72 h in DMF.

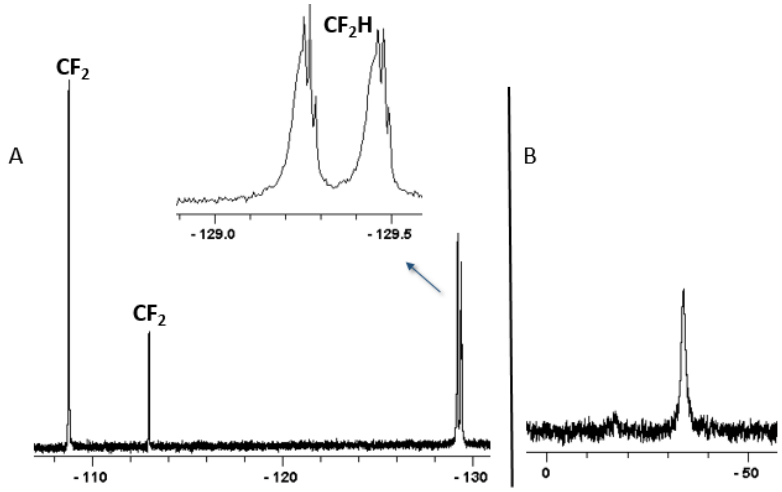

Figure A4.22 ^{19}F NMR (**A**) and ^{31}P NMR (**B**) spectra of Complex **4-1** and 2 eq. of CuI after 96 h in DMF.

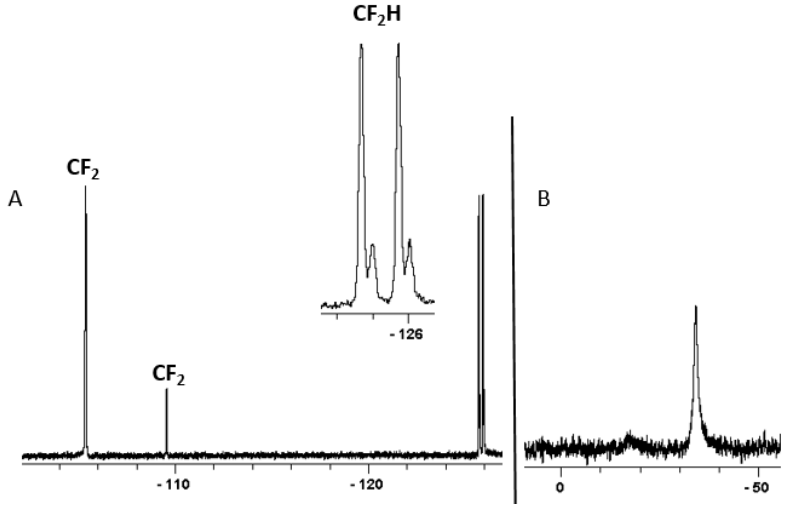

Figure A4.23 ^{19}F NMR (**A**) and ^{31}P NMR (**B**) spectra of Complex **4-1** and 2 eq. of CuI after 2 weeks in DMF.

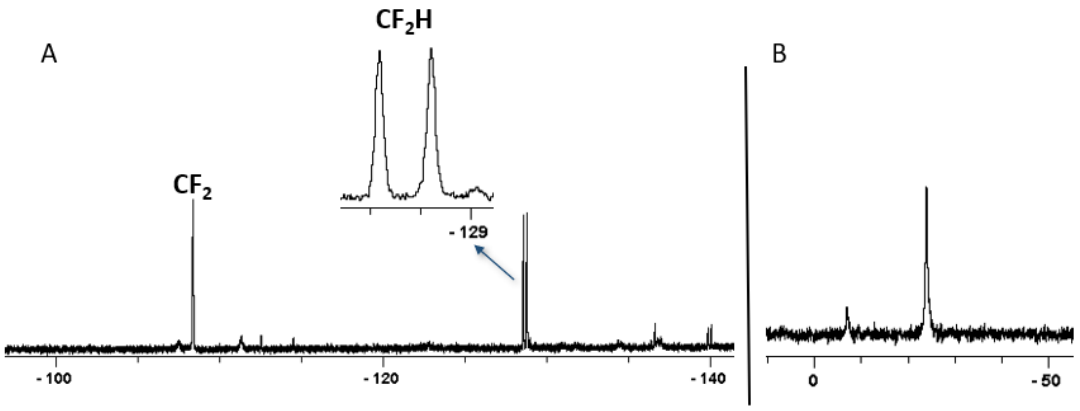

Figure A4.24 ^{19}F NMR (**A**) and ^{31}P NMR (**B**) spectra of Complex **4-1** and 2 eq. of CuI after 4 months in DMF.

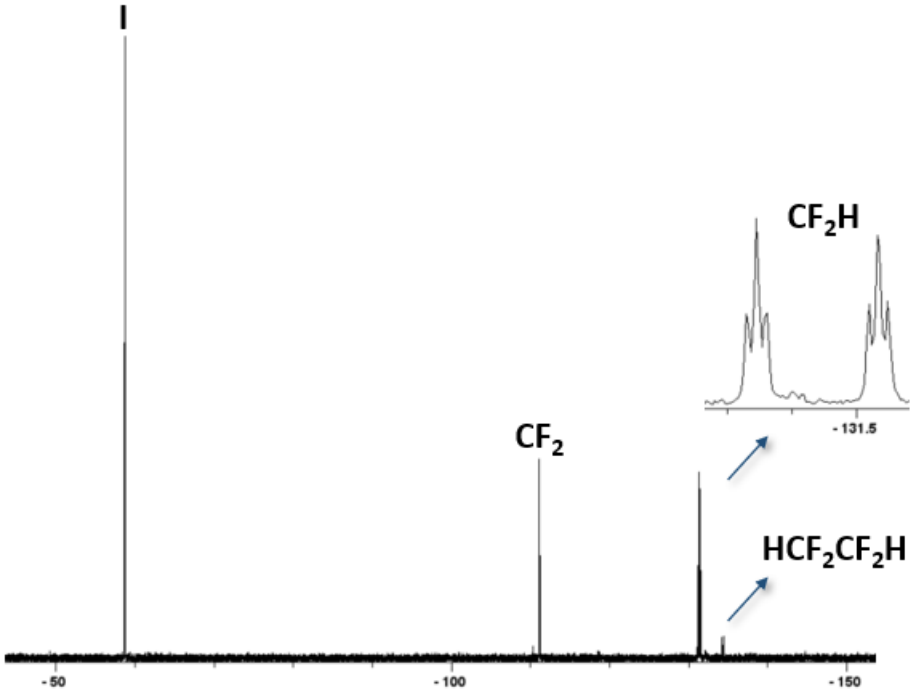

Figure A4.25 ^{19}F NMR (**A**) (282 MHz, C_6D_6) of Complex **4-1**, 1.5 eq. of CuI, 25 eq. of DMSO and 1 equiv. of 4-iodobenzonitrile after 7 h. I = internal standard ($PhCF_3$). 9% yield.

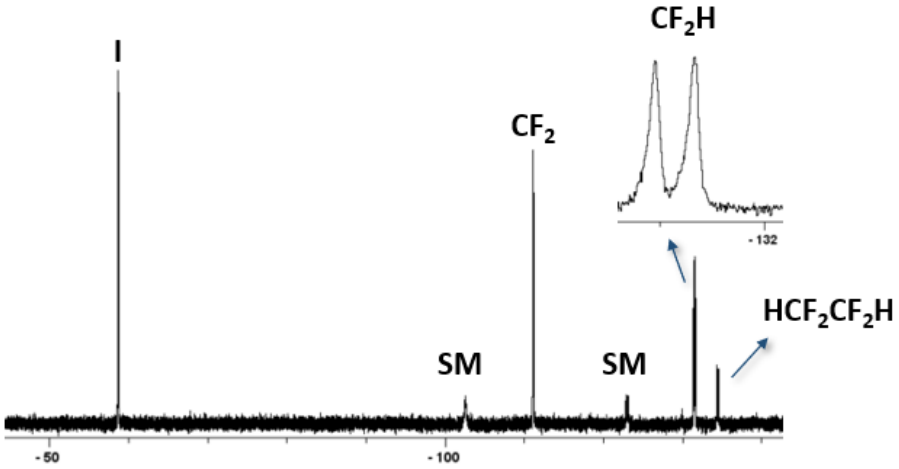

Figure A4.26 ^{19}F NMR (**A**) (282 MHz, C_6D_6) of Complex **4-1**, 1.5 eq. of CuBr, 25 eq. of DMSO and 1 equiv. of 4-iodo-benzonitrile after 7 h. I = internal standard ($PhCF_3$), SM = Starting material. 11% yield.

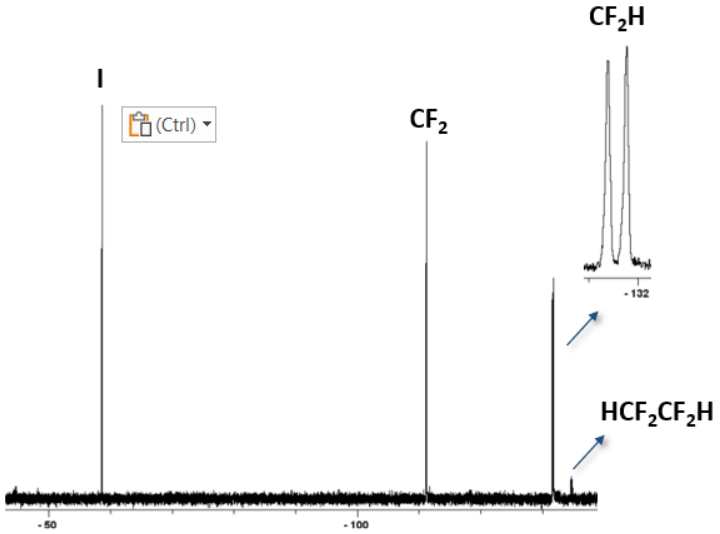

Figure A4.27 ^{19}F NMR (**A**) (282 MHz, C_6D_6) of Complex **4-1**, 1.5 eq. of CuCl, 25 eq. of DMSO and 1 equiv. of 4-iodobenzonitrile after 7 h. I = internal standard ($PhCF_3$). 16% yield.

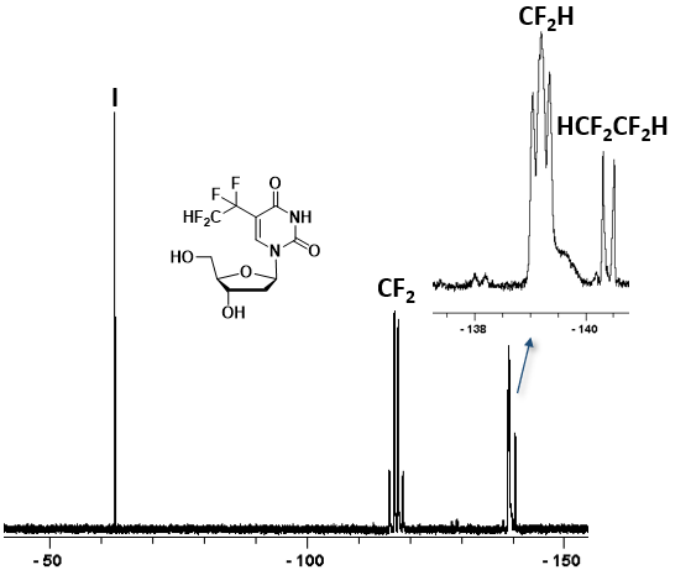

Figure A4.28 ^{19}F NMR (282 MHz, C_6D_6) of **4-3a**. The reaction of **4-1**, 2 eq. of CuBr, and 1 equiv. of 2'-deoxy-5-iodo-uridine in DMF after 12 h at 50 ^{o}C. I = internal standard ($PhCF_3$).

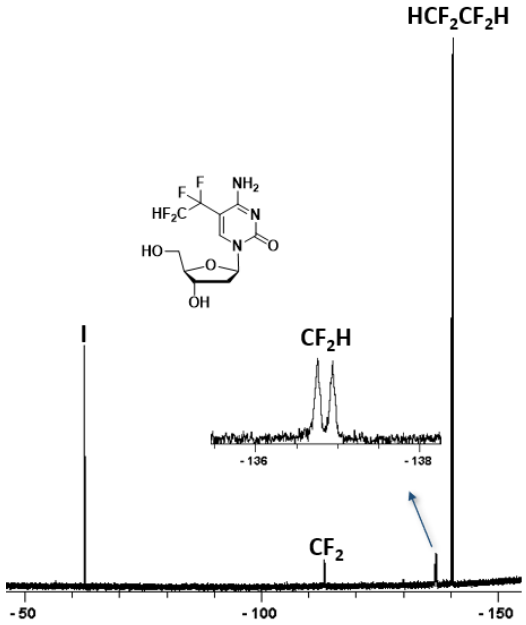

Figure A4.29 ^{19}F NMR (282 MHz, C_6D_6) of **4-3b**. The reaction of **4-1**, 2 eq. of CuBr, and 1 equiv. of 2'-deoxy-5-iodo-cytidine in DMF after 12 h at 50 ^{o}C. I = internal standard ($PhCF_3$).

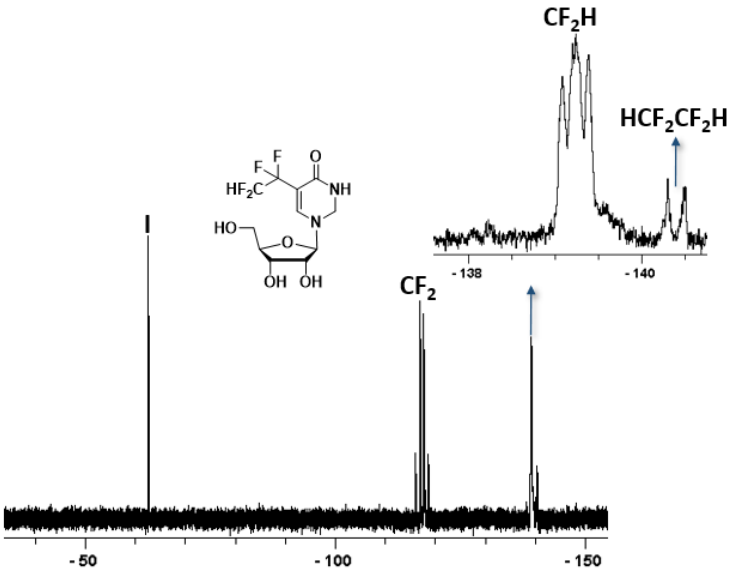

Figure A4.30 ^{19}F NMR (282 MHz, C_6D_6) of **4-3c**. The reaction of **4-1**, 2 eq. of CuBr, and 1 equiv. of 5-iodouridine in DMF after 12 h at 50 °C. I = internal standard ($PhCF_3$).

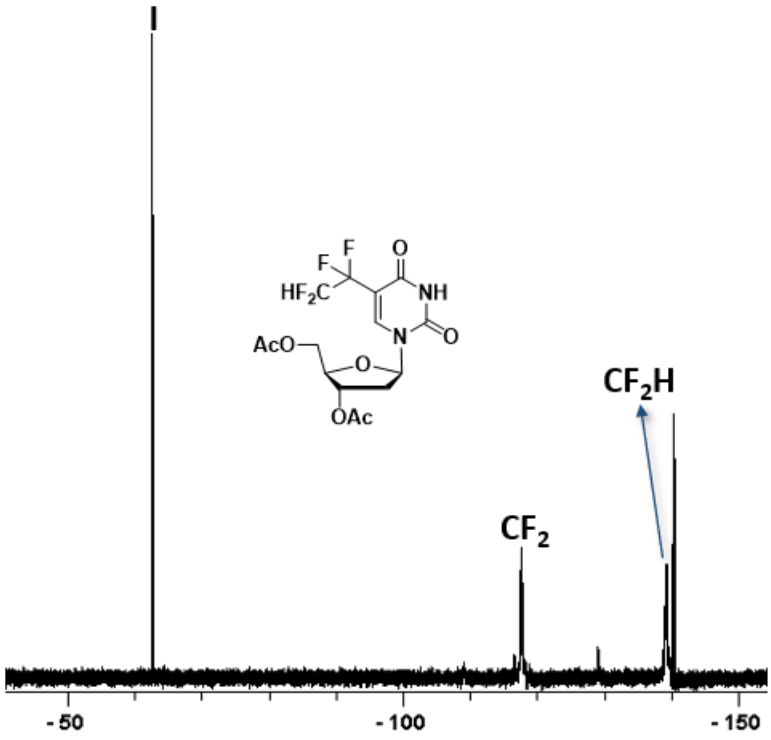

Figure A4.31 ^{19}F NMR (282 MHz, C_6D_6) of **4-3d**. The reaction of **4-1**, 2 eq. of CuBr, and 1 equiv. of 2'-5 o acetyl-5-iodo-uridine in DMF after 12 h at 50 °C. I = internal standard ($PhCF_3$).

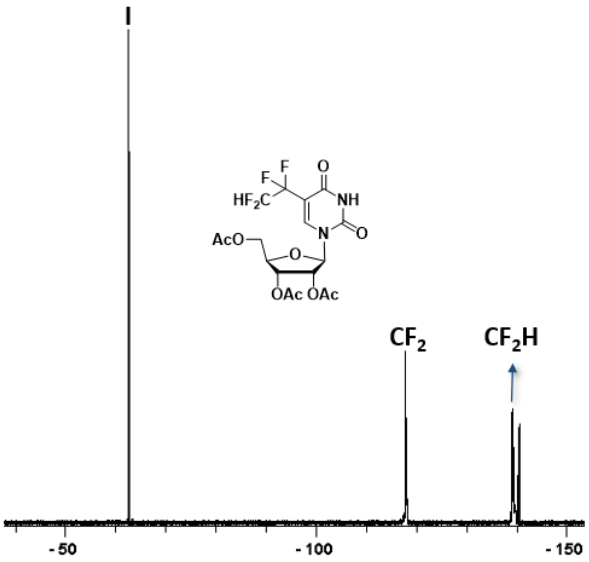

Figure A4.32 ^{19}F NMR (282 MHz, C_6D_6) of **4-3e**. The reaction of **4-1**, 2 eq. of CuBr, and 1 equiv. of 5-iodo-2',3',5'-triacetate uridine in DMF after 12 h at 50 ºC. I = internal standard ($PhCF_3$).

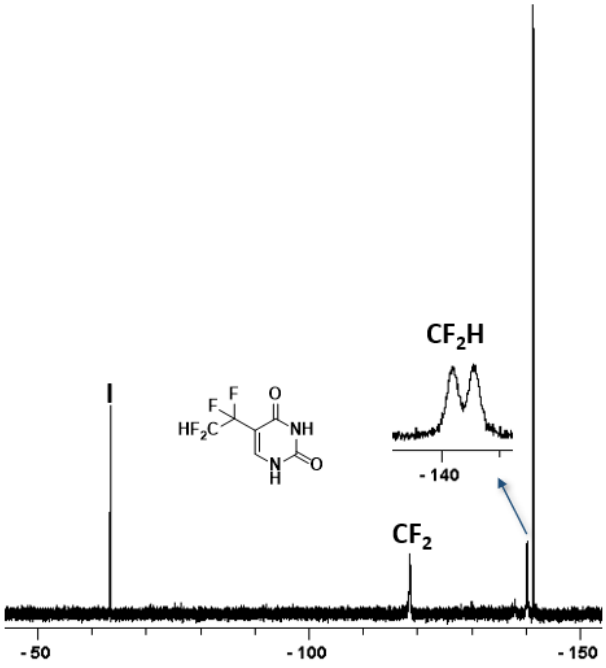

Figure A4.33 ^{19}F NMR (282 MHz, C_6D_6) of **4-3f**. The reaction of **4-1**, 2 eq. of CuBr, and 1 equiv. of 4-iodo uracil in DMF after 12 h at 50 ºC. I = internal standard ($PhCF_3$).

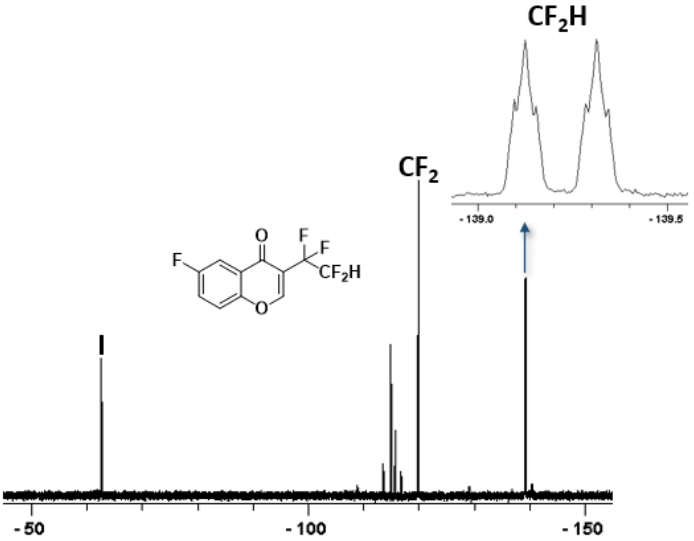

Figure A4.34 ^{19}F NMR (282 MHz, C_6D_6) of **4-3g**. The reaction of **4-1**, 2 eq. of CuBr, and 1 equiv. 6-Fluoro-3-iodochromone in DMF after 12 h at 50 °C. I = internal standard ($PhCF_3$).

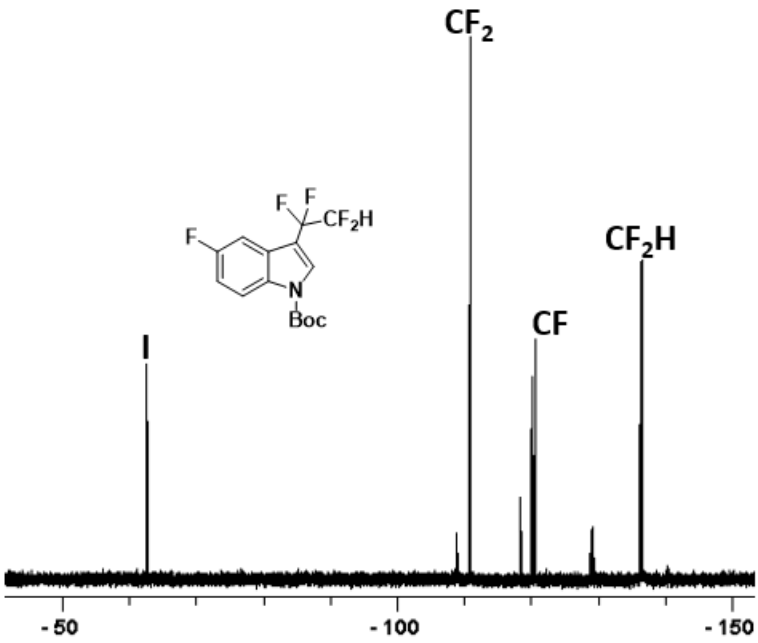

Figure A4.35 ^{19}F NMR (282 MHz, C_6D_6) of **4-3h**. The reaction of **4-1**, 2 eq. of CuBr, and 1 equiv. of t-butyl 5-fluoro-3-iodo-1H-indole-1-carboxylate in DMF after 12 h at 50 °C. I = internal standard ($PhCF_3$).

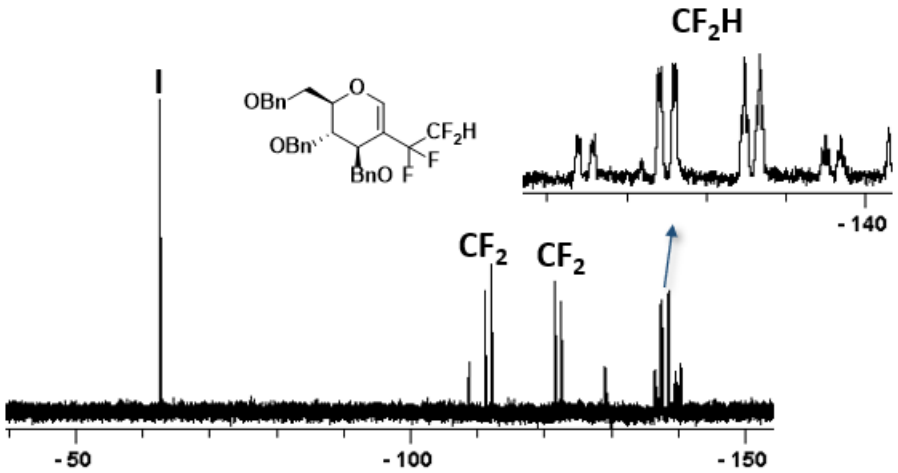

Figure A4.36 ^{19}F NMR (282 MHz, C_6D_6) of **4-3i**. The reaction of **4-1**, 2 eq. of CuBr, and 1 equiv. of 1,5-anhydro-3,4,6-tri-O-benzyl-2-deoxy-2-iodo-D- lyxo-hex-1-enitol in DMF after 12 h at 50 °C. I = internal standard ($PhCF_3$).

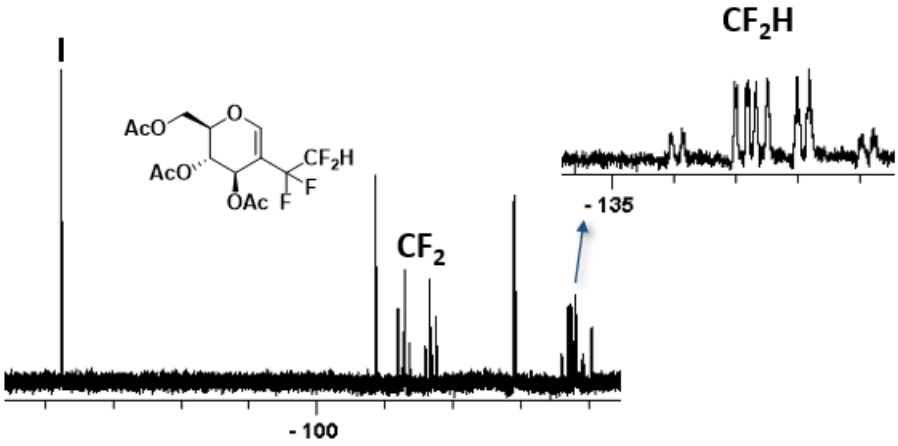

Figure A4.37 ^{19}F NMR (282 MHz, C_6D_6) of **4-3j**. The reaction of **4-1**, 2 eq. of CuBr, and 1 equiv. of 1,5-anhydro-3,4,6-tri-O-acetyl-2-deoxy-2-iodo-D- lyxo-hex-1-enitol in DMF after 12 h at 50 °C. I = internal standard ($PhCF_3$).

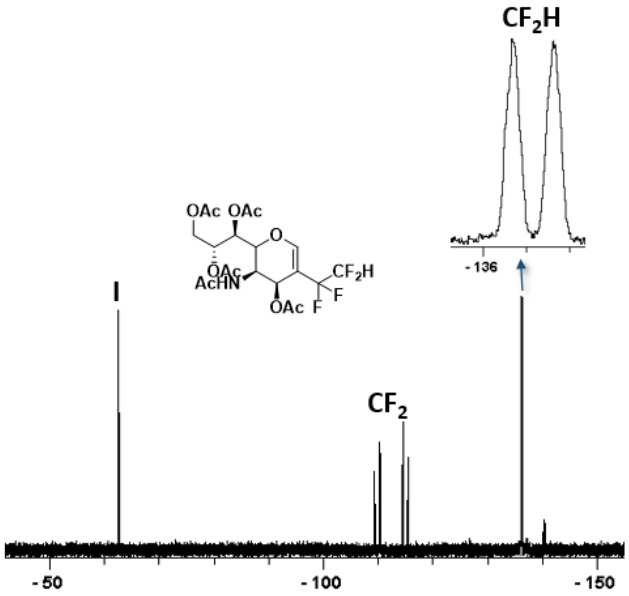

Figure A4.38 ^{19}F NMR (282 MHz, C_6D_6) of **4-3k**. The reaction of **4-1**, 2 eq. of CuBr, and 1 equiv. of methyl 5-acetamido-4,7,8,9-tetra-O-acetyl-2,6-anhydro-3,5-dideoxy-3-iodo-D-glycero-D-galacto-non-2-enonate in DMF after 12 h at 50 °C. I = internal standard ($PhCF_3$).

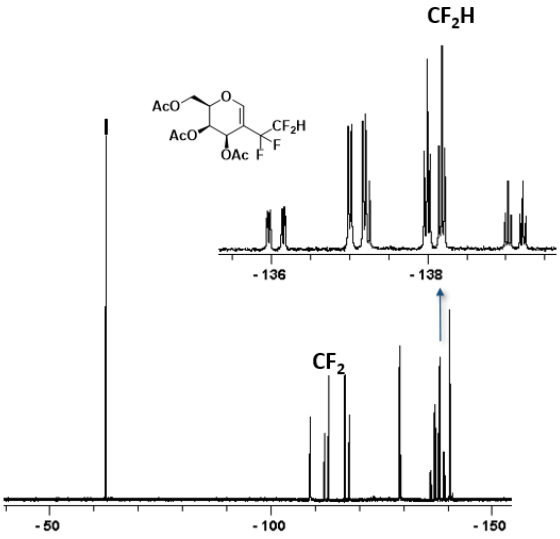

Figure A4.39 ^{19}F NMR (282 MHz, C_6D_6) of **4-3l**. The reaction of **4-1**, 2 eq. of CuBr, and 1 equiv. of methyl 5-acetamido-4,7,8,9-tetra-O-acetyl-2,6-anhydro-3,5-dideoxy-3-iodo-D-glycero-D-galacto-non-2-enonate in DMF after 12 h at 50 °C. I = internal standard ($PhCF_3$).

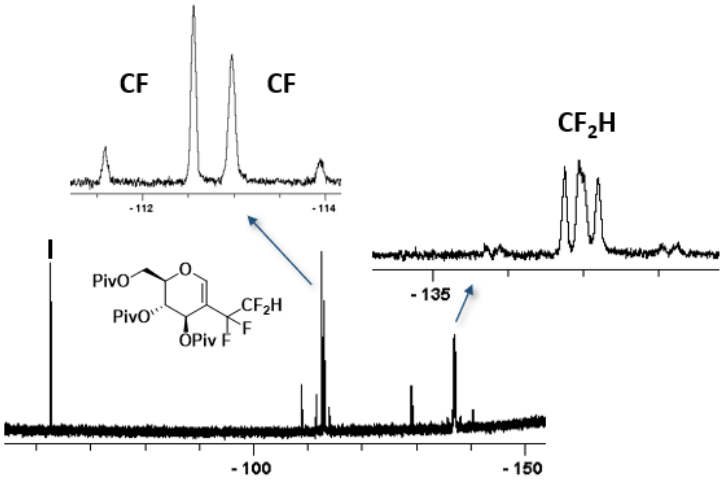

Figure A4.40 ^{19}F NMR (282 MHz, C_6D_6) of **4-3m**. The reaction of **4-1**, 2 eq. of CuBr, and 1 equiv. of 1,5-Anhydro-3,4,6-tri-O-pivaloyl-2-deoxy-2-iodo-Darabino-hex-1-enitol in DMF after 12 h at 50 ºC. I = internal standard ($PhCF_3$).

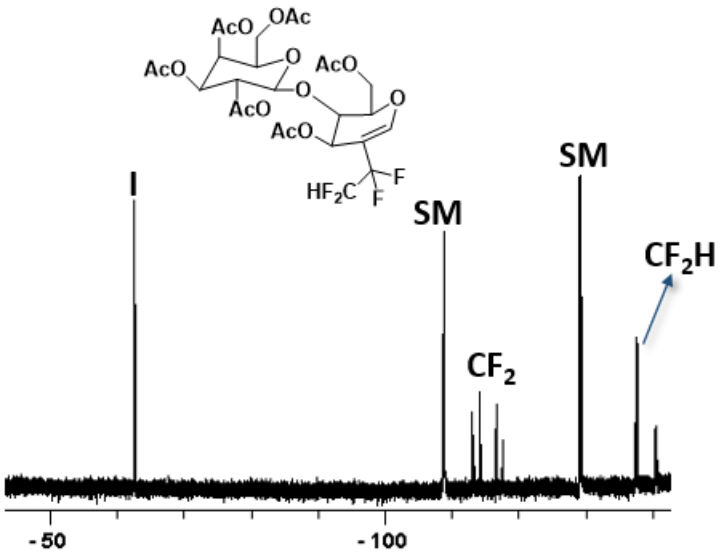

Figure A4.41 ^{19}F NMR (282 MHz, C_6D_6) of **4-3n**. The reaction of **4-1**, 2 eq. of CuBr, and 1 equiv. of 1,5-anhydro-3,6-di-O-acetyl-2-deoxy-4-O-(2,3,4,6-tetra-O-acetyl-β-D-galactopyranosyl)-2-iodo-D-arabino-hex-1-enitol in DMF after 12 h at 50 ºC. I = internal standard ($PhCF_3$).

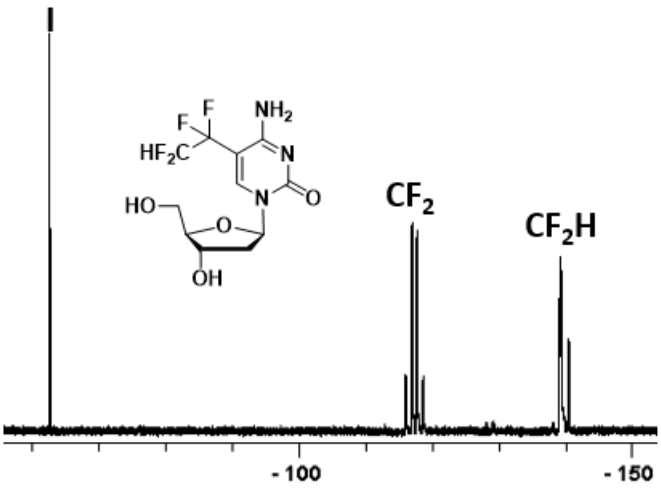

Figure A4.42 ^{19}F NMR (282 MHz, C_6D_6) of **4-3a**. The reaction of **4-1**, 2 eq. of CuBr, and 1.5 equiv. of 2'-deoxy-5-iodo-uridine in DMF after 12 h at 50 ^{o}C. I = internal standard ($PhCF_3$).

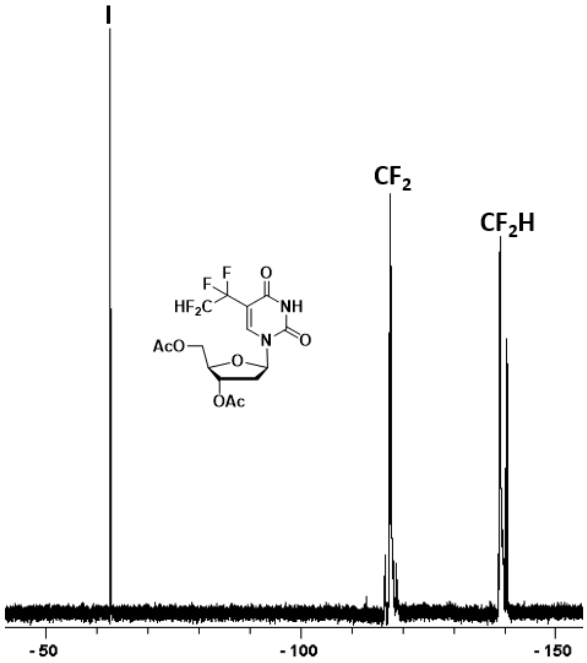

Figure A4.43 ^{19}F NMR (282 MHz, C_6D_6) of **4-3d**. The reaction of **4-1**, 2 eq. of CuBr, and 1.5 equiv. of 2'-5 o acetyl-5-iodo-uridine in DMF after 12 h at 50 ^{o}C. I = internal standard ($PhCF_3$).

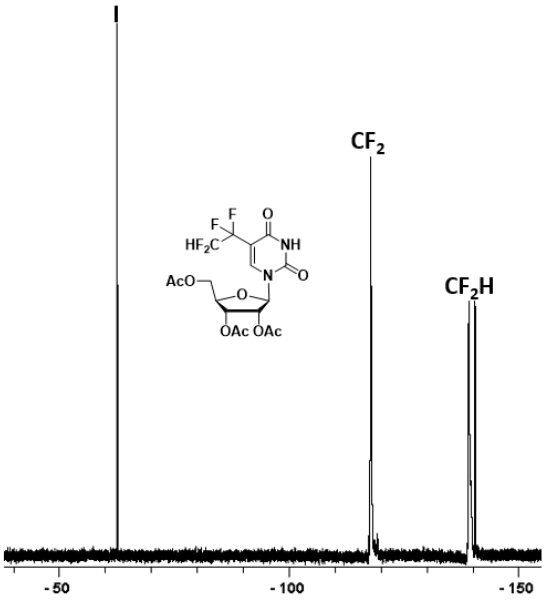

Figure A4.44 ^{19}F NMR (282 MHz, C_6D_6) of **4-3e**. The reaction of **4-1**, 2 eq. of CuBr, and 1 equiv. of 5-iodo-2',3',5'-triacetate uridine in DMF after 12 h at 50 °C. I = internal standard ($PhCF_3$).

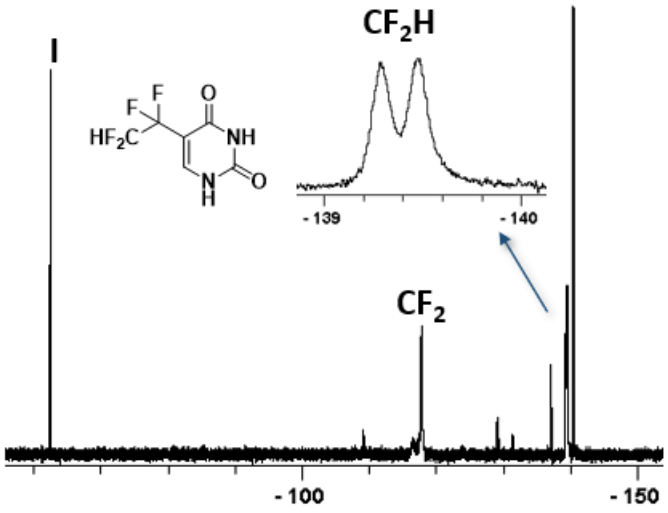

Figure A4.45 ^{19}F NMR (282 MHz, C_6D_6) of **4-3f**. The reaction of **4-1**, 2 eq. of CuBr, and 1 equiv. of 4-iodo uracil in DMF after 12 h at 50 °C. I = internal standard ($PhCF_3$).

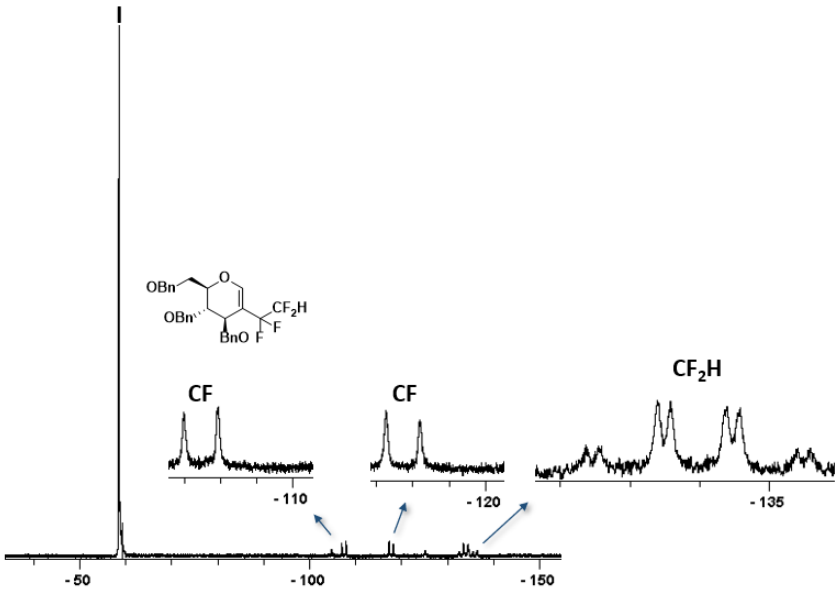

Figure A4.46 ^{19}F NMR (282 MHz, C_6D_6) of **4-3i**. The reaction of **4-1**, 2 eq. of CuBr, and 1.5 equiv. of 1,5-Anhydro-3,4,6-tri-O-benzyl-2-deoxy-2-iodo-D- lyxo-hex-1-enitol in DMF after 12 h at 50 °C. I = internal standard ($PhCF_3$).

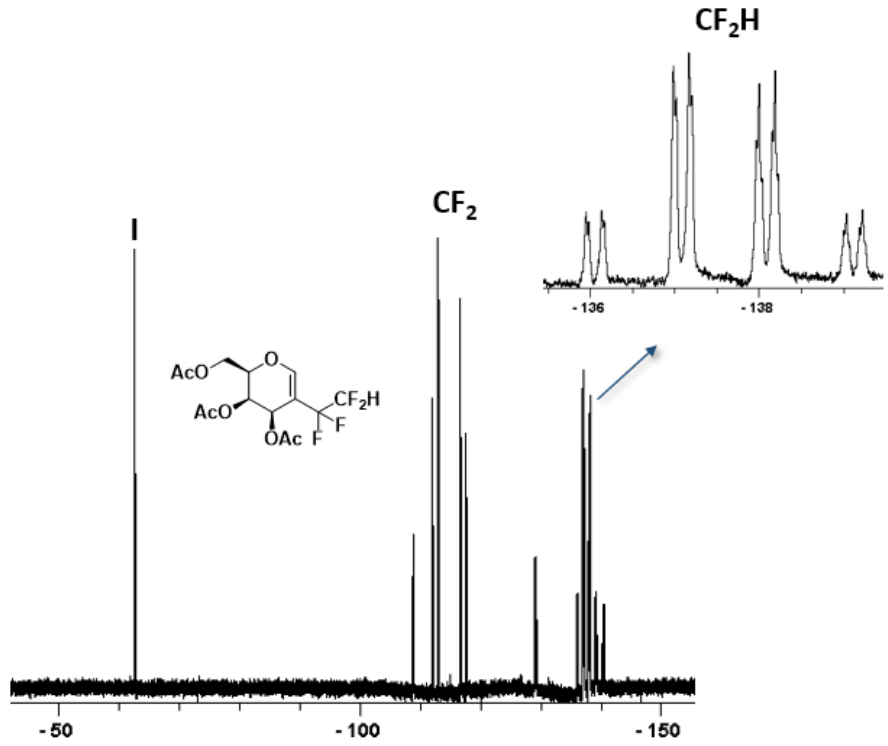

Figure A4.47 ^{19}F NMR (282 MHz, C_6D_6) of **4-3j**. The reaction of **4-1**, 2 eq. of CuBr, and 1 equiv. of 1,5-anhydro-3,4,6-tri-O-acetyl-2-deoxy-2-iodo-D-lyxo-hex-1-enitol in DMF after 12 h at 50 °C. I = internal standard ($PhCF_3$).

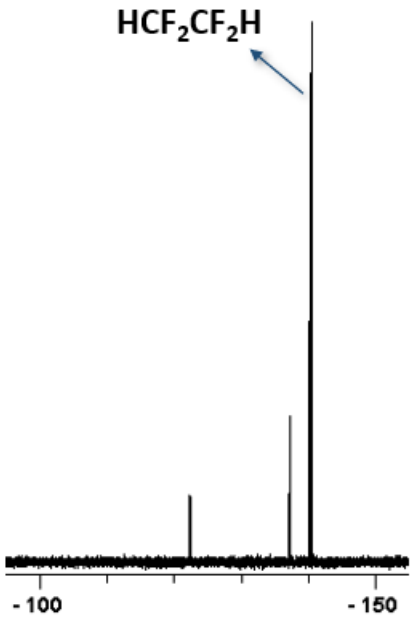

Figure A4.48 ^{19}F NMR (282 MHz, C_6D_6) of reaction 1.5 equiv. of **4-1**, 0.5 equiv. of CuBr, and 1 equiv. of 4-iodouracil in DMF after 12 h at 50 °C. I = internal standard ($PhCF_3$).

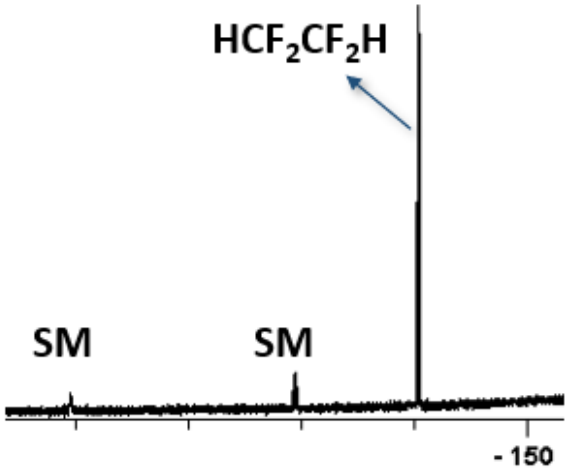

Figure A4.49 ^{19}F NMR (282 MHz, C_6D_6) of reaction 1 equiv. of **4-1**, 1 equiv. of CuBr, and 1 equiv. of 4-iodouracil in DMF after 12 h at 50 °C. I = internal standard ($PhCF_3$).

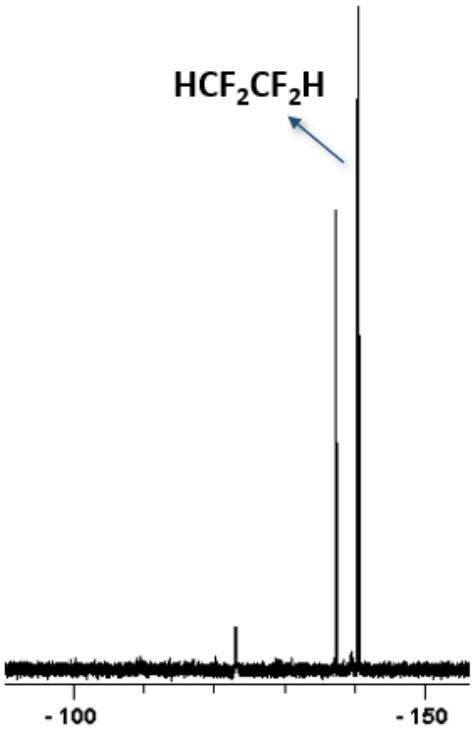

Figure A4.50 ^{19}F NMR (282 MHz, C_6D_6) of reaction 1 equiv. of **4-1**, 1 equiv. of CuBr, and 1.5 equiv. of 4-iodouracil in DMF after 12 h at 50 °C. I = internal standard ($PhCF_3$).

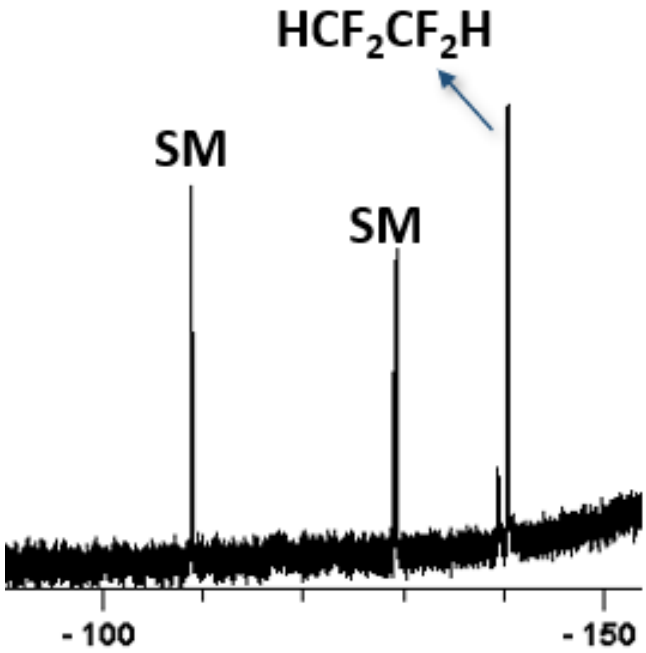

Figure A4.51 ^{19}F NMR (282 MHz, C_6D_6) of reaction 1 equiv. of **4-1**, 2 equiv. of CuCl, and 1.5 equiv. of 4-iodouracil in DMF after 12 h at 50 °C. I = internal standard ($PhCF_3$).

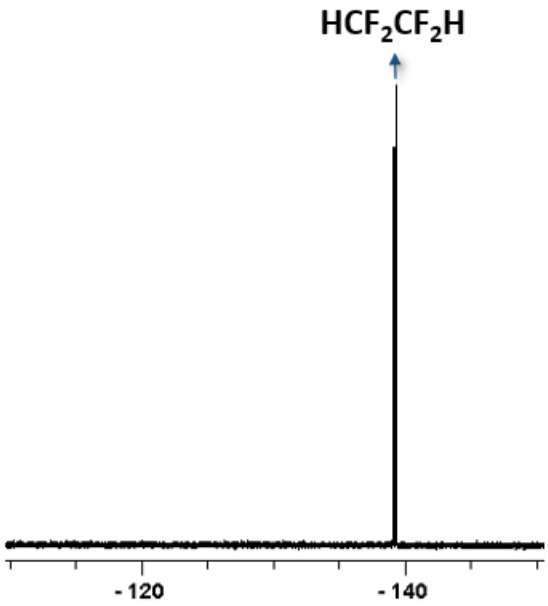

Figure A4.52 ^{19}F NMR (282 MHz, C_6D_6) of reaction 1 equiv. of **4-1**, 2 equiv. of CuBr, and 1.5 equiv. of 4-iodouracil in Et_2O/ DMF (1:0.005) after 12 h at 50 ºC. I = internal standard ($PhCF_3$).

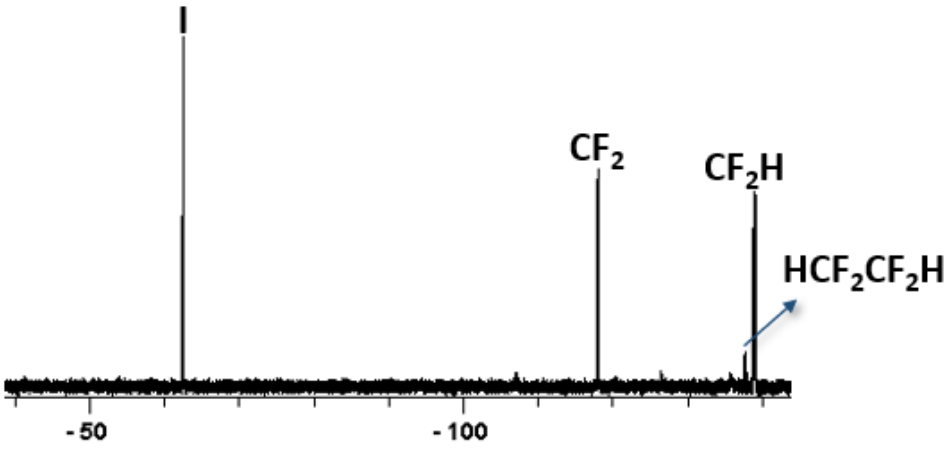

Figure A4.53 ^{19}F NMR (282 MHz, C_6D_6) of reaction 1 equiv. of **4-1**, 2 equiv. of CuBr, and 1 equiv. of 4-iodouracil in Toluene/DMF (1:0.005) after 12 h at 50 ºC. I = internal standard ($PhCF_3$).

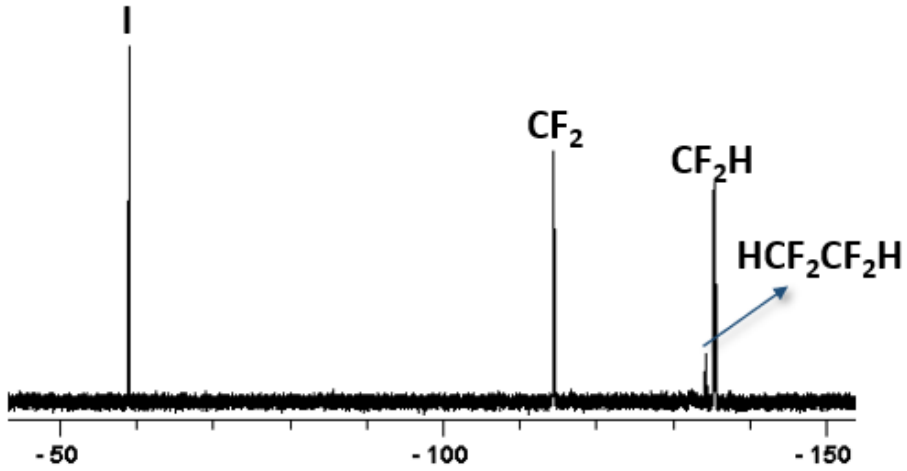

Figure A4.54 ^{19}F NMR (282 MHz, C_6D_6) of reaction 1 equiv. of **4-1**, 3 equiv. of CuBr, and 1 equiv. of 4-iodouracil in Toluene/DMF (1:0.005) after 12h at 50 ^{o}C. I = internal standard ($PhCF_3$).

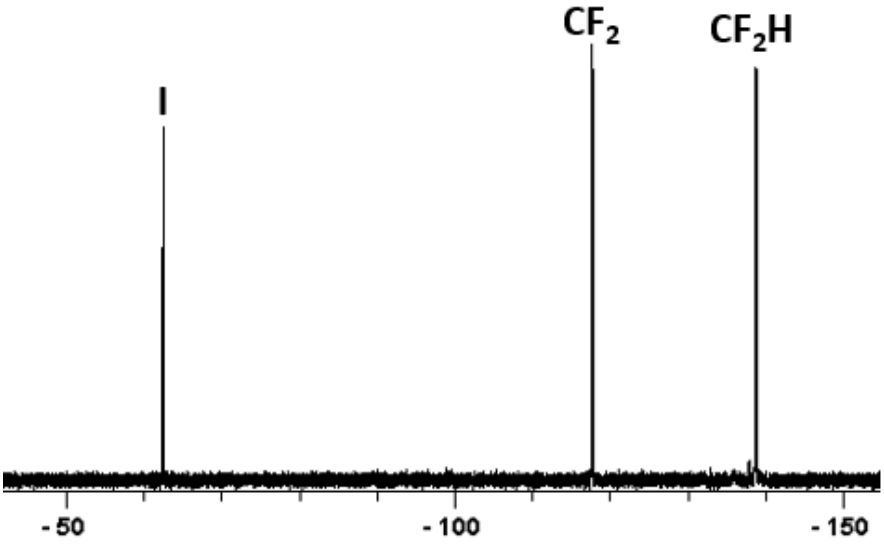

Figure A4.55 ^{19}F NMR (282 MHz, C_6D_6) of reaction 1 equiv. of **4-1**, 3 equiv. of CuBr, and 1 equiv. of 4-iodouracil in Toluene/DMF (1:0.005) after 12h at 50 ^{o}C. I = internal standard ($PhCF_3$).

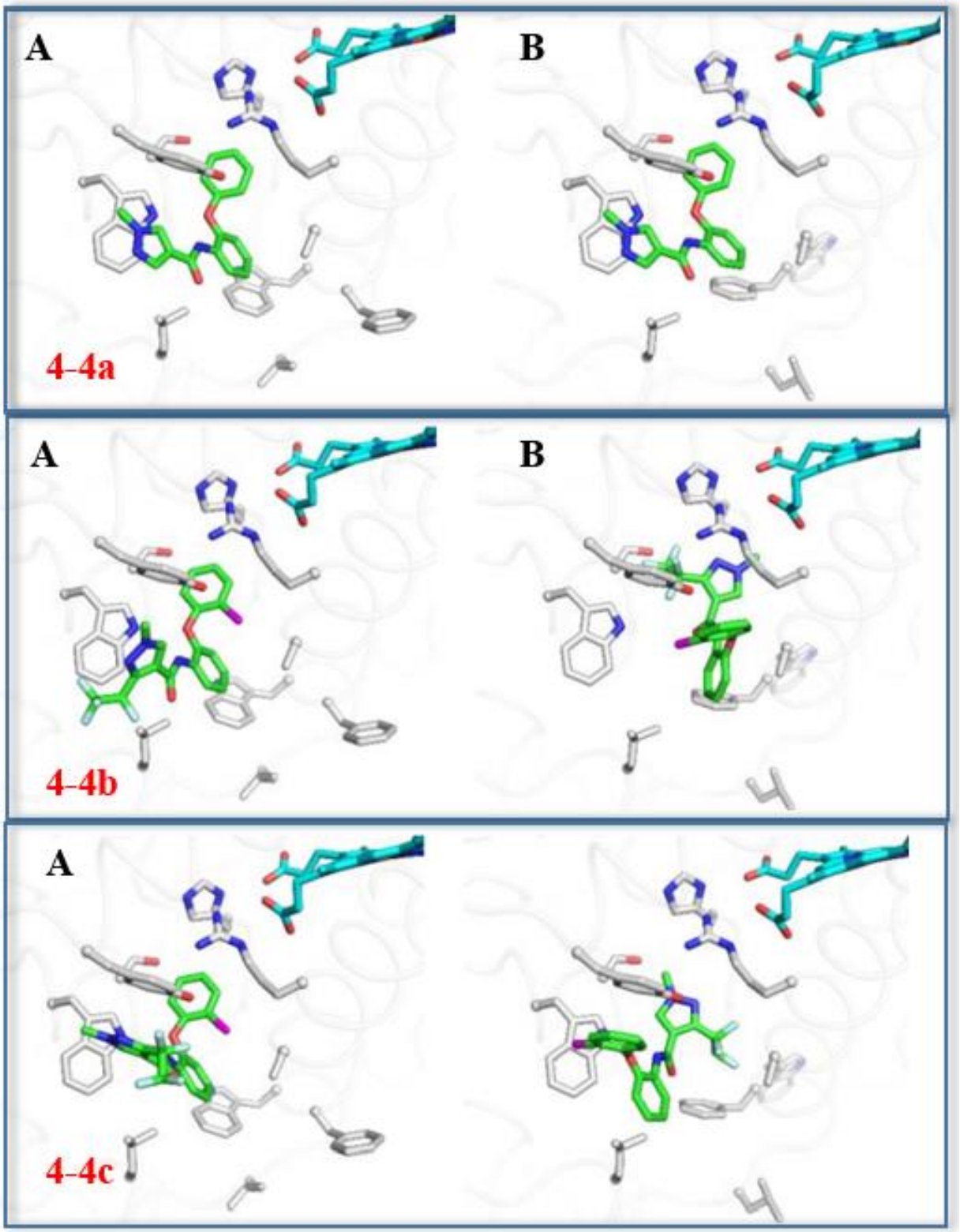

Figure A4.56 Binding modes of chemical analogues **4-4a-c.**

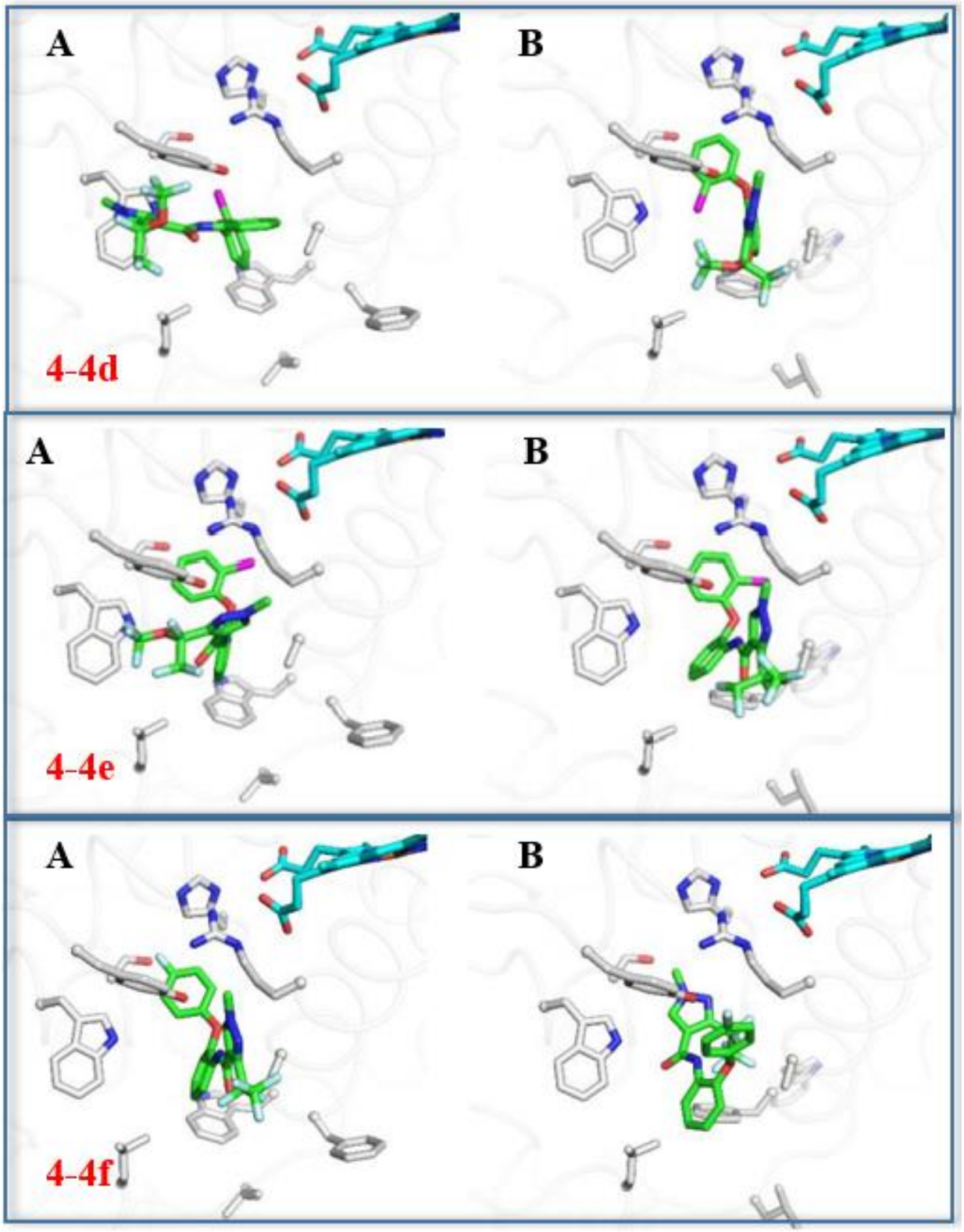

Figure A4.57 Binding modes of chemical analogues **4-4d-f.**

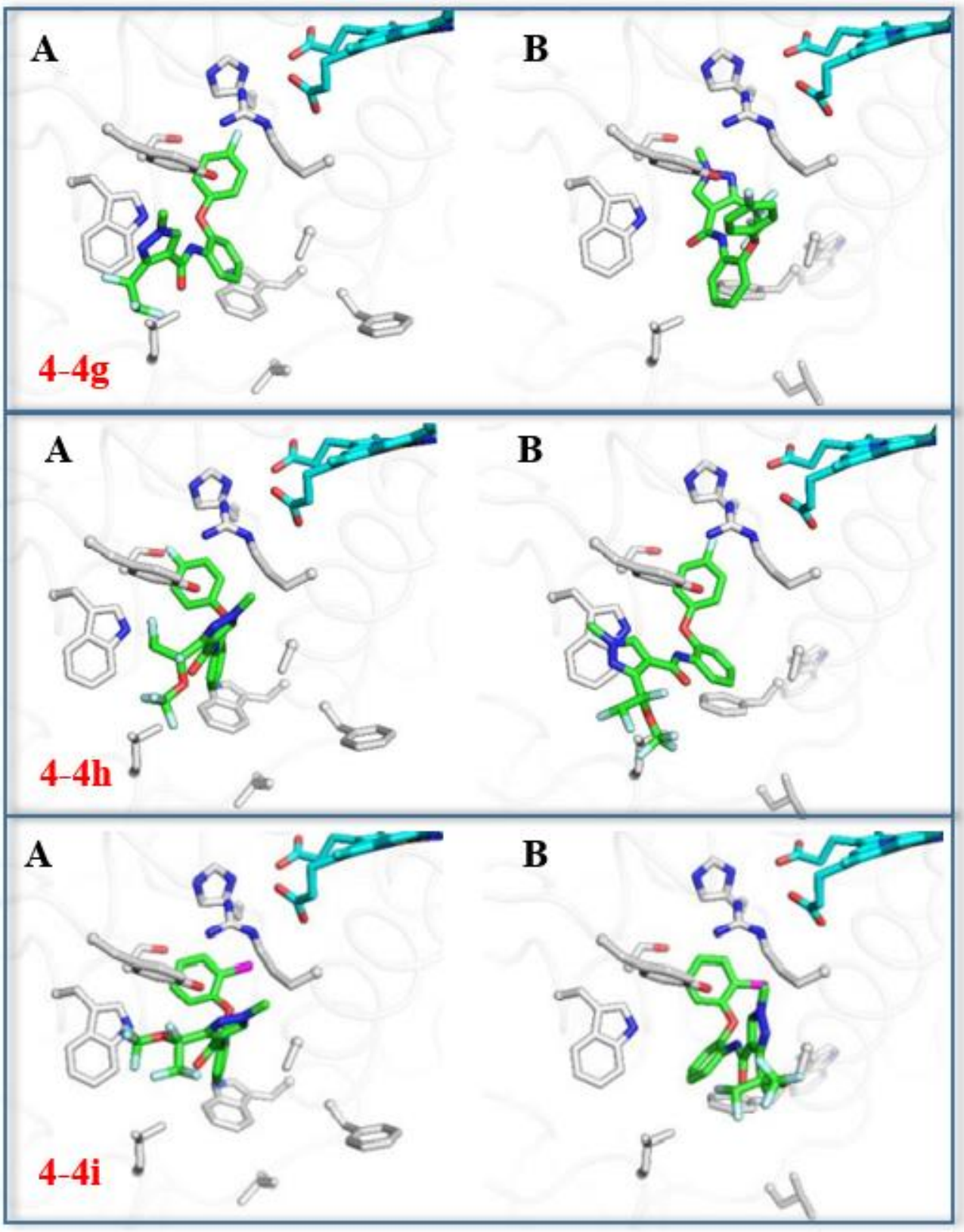

Figure A4.58 Binding modes of chemical analogues **4-4g-i.**

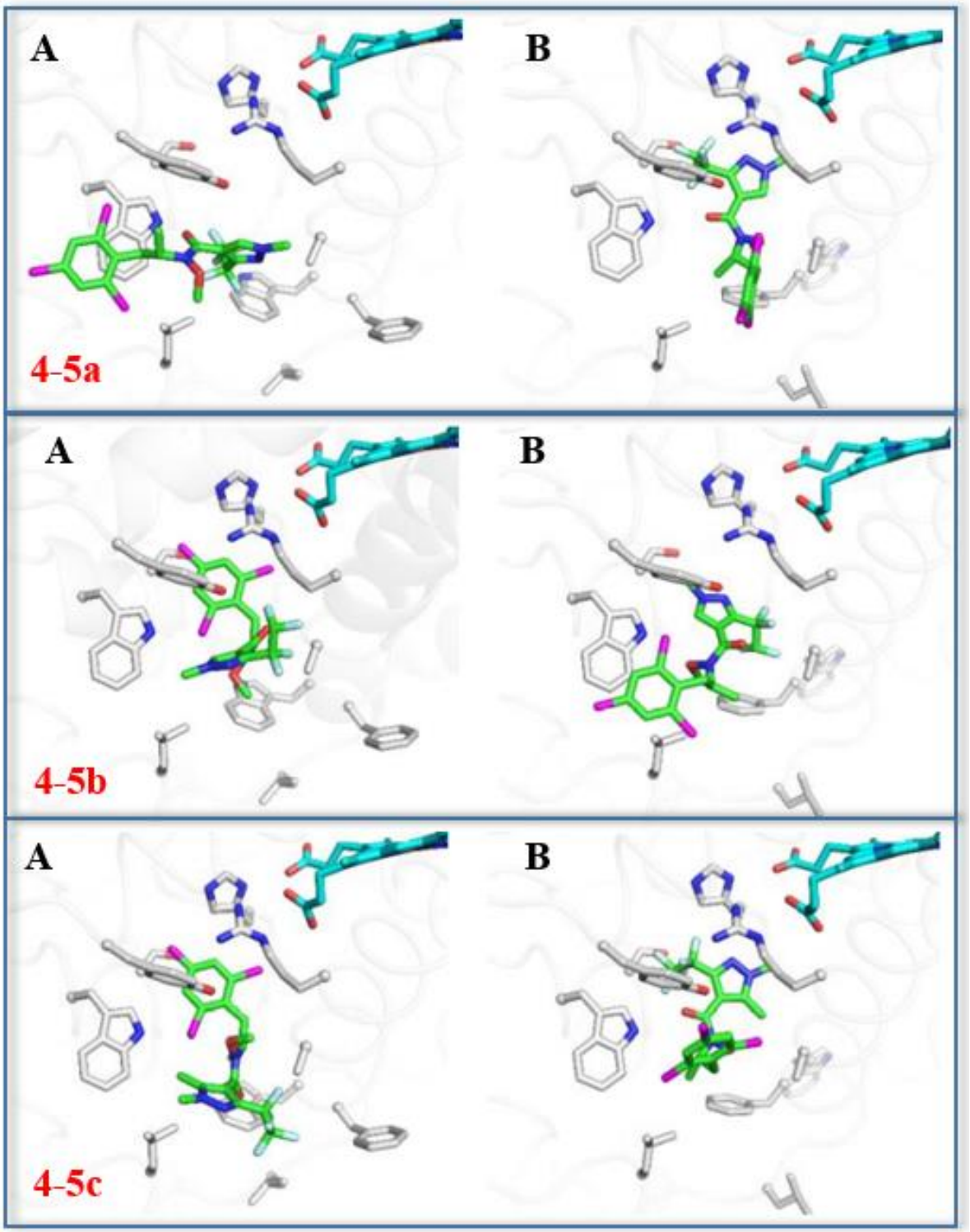

Figure A4.59 Binding modes of chemical analogues **4-5a-c**.

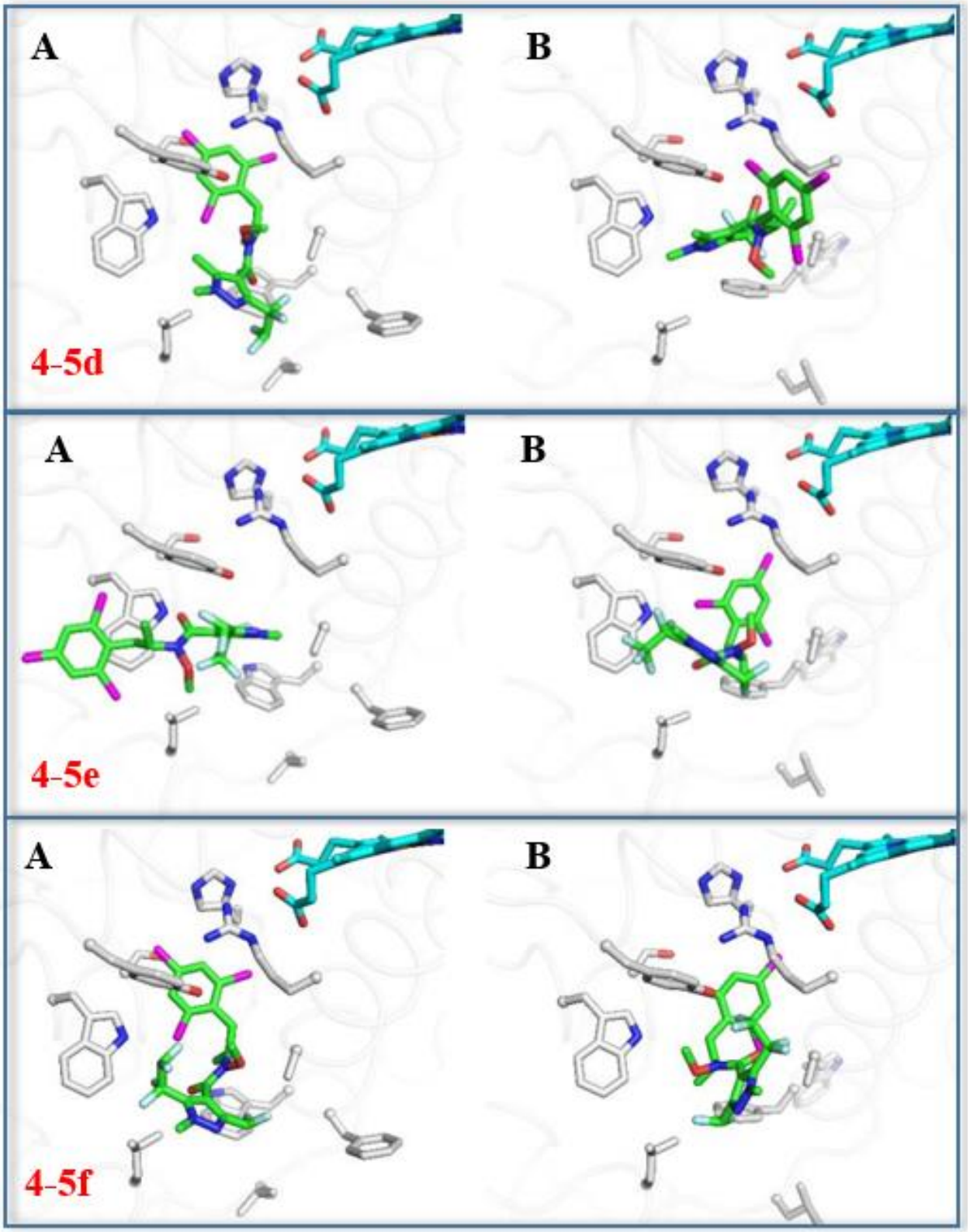

Figure A4.60 Binding modes of chemical analogues **4-5d-f**.

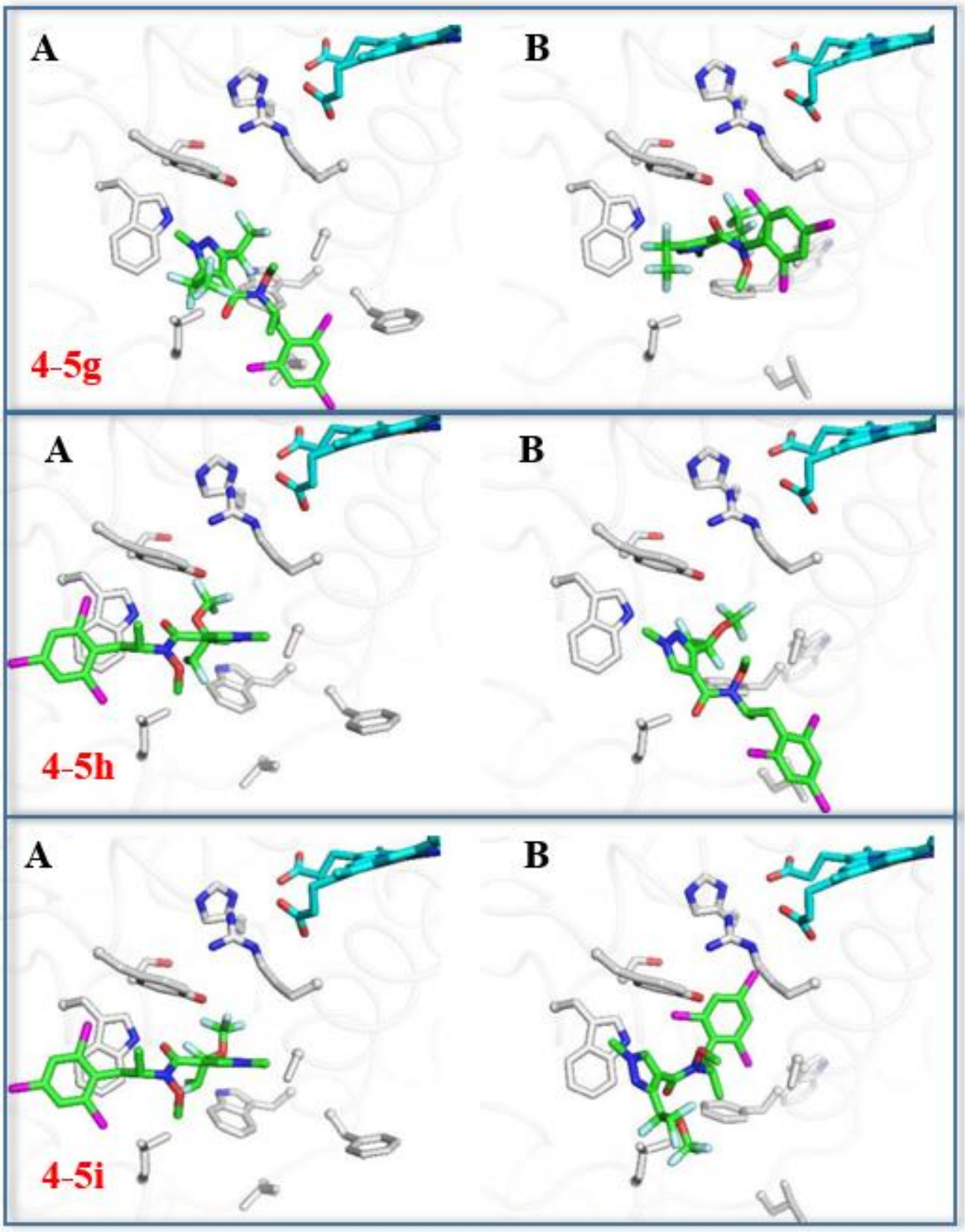

Figure A4.61 Binding modes of chemical analogues **4-5g-i.**

Chapter 5: Mechanism of Fluoronickelacyclopentane Formation from Fluoroalkenes

Table A5. 1 Details of X-ray diffraction data collection and refinement

Complex (code)	**5-1b** K0931	**5-2c** S0655	**5-5** K0888
empirical formula	$C_{42}H_{34}F_4FeNiP_2$	$C_{40}H_{28}F_8NiOP_2$	$C_{55}H_{44}F_{16}N_3Ni_2P_2$
formula weight, g/mol	791.19	797.27	1230.29
crystal system	monoclinic	monoclinic	triclinic
space group	*C* 2/*c*	*C* 2/*c*	$P\,\bar{1}$
a, Å	13.9752(4)	15.886(3)	9.6805(7)
b, Å	10.7858(2)	12.963(2)	17.1315(12)
c, Å	24.0777(6)	33.365(6)	17.2501(12)
α, °	90	90	74.283(1)
β, °	94.464(2)	92.840(2)	85.152(2)
γ, °	90	90	79.817(1)
V, Å^3	3618.29(15)	6862(2)	2708.4(3)
Z	4	8	2
T, K	213(2)	202(2)	213(2)
ρ_{calc}, g/cm^3	1.452	1.543	1.509
μ, mm^{-1}	1.060	0.736	0.849
$2\theta_{max}$, °	71.262	56.688	61.416
total/unique reflections	25170/8286	37718/8472	46884/16754
reflections [$I_o \geq 2\sigma(I_o)$]	5422	7128	8461
R_1, wR_2 [$I_o \geq 2\sigma(I_o)$]	0.0440, 0.919	0.0525, 0.1252	0.0562, 0.1155
goodness of fit	1.009	1.110	0.999

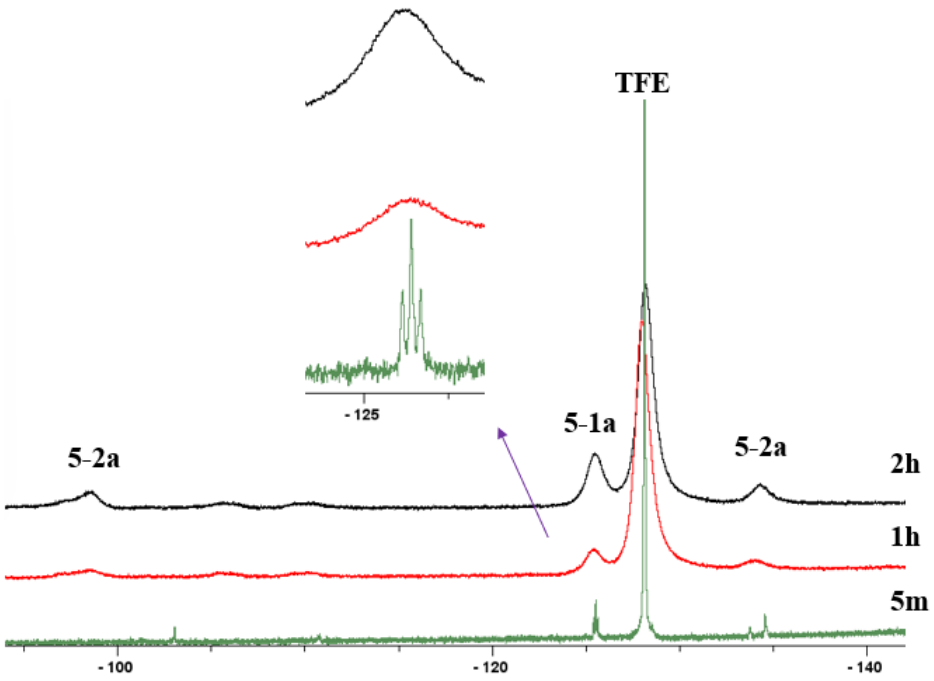

Figure A5.1 ^{19}F NMR spectra of $Ni(cod)_2$ + DPPE + 3 equiv of TFE in C_6D_6 after 5 min, 1 h and 2 h.

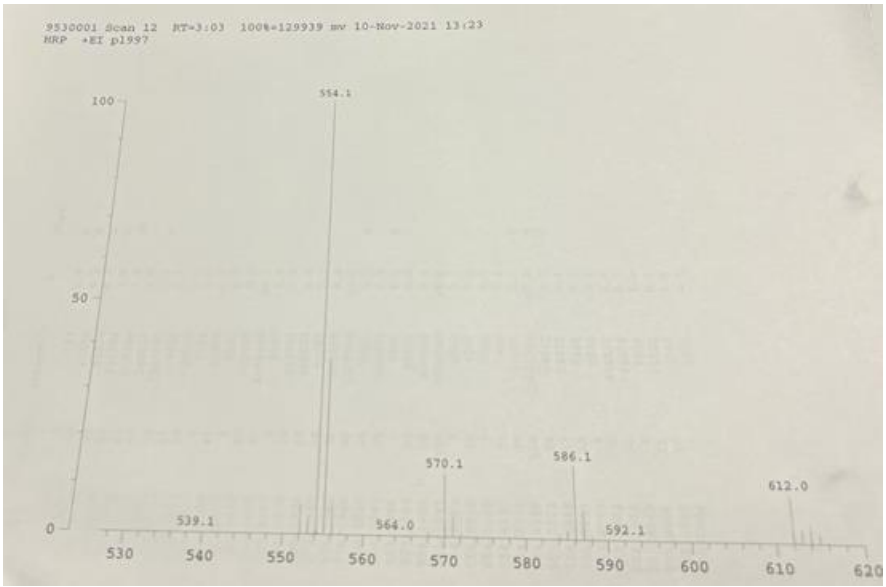

Figure A5.2 Selected peaks from the EI mass spectrum of complex **5-2a**.

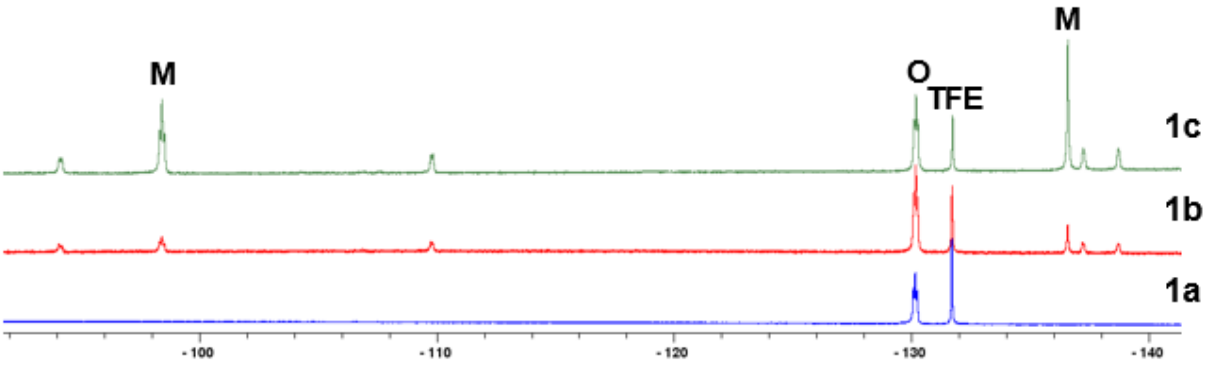

Figure A5.3 ^{19}F NMR of $Ni(cod)_2$ + dppf + TFE in benzene, 5 min (a), 2 h (b) and 12 h (c) after TFE addition. **M** = metallacyclopentane; **O** = olefin complex.

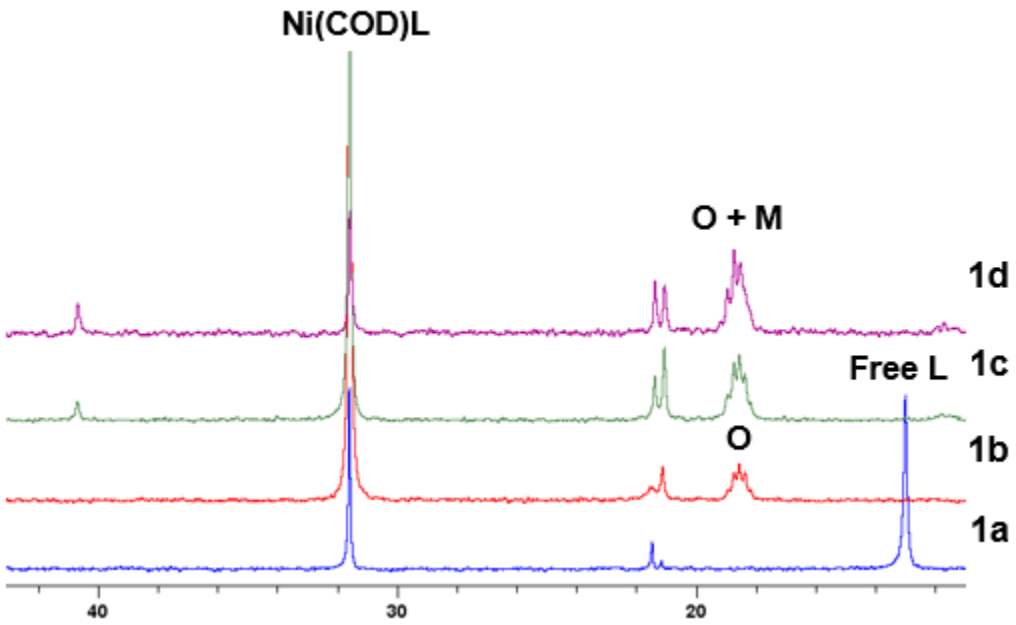

Figure A5.4 $^{31}P\{^{1}H\}$ NMR of $Ni(cod)_2$ + dppf + TFE in benzene, 5 min (a), 2 h (b) and 12 h (c) after TFE addition. **M** = metallacyclopentane; **O** = olefin complex.

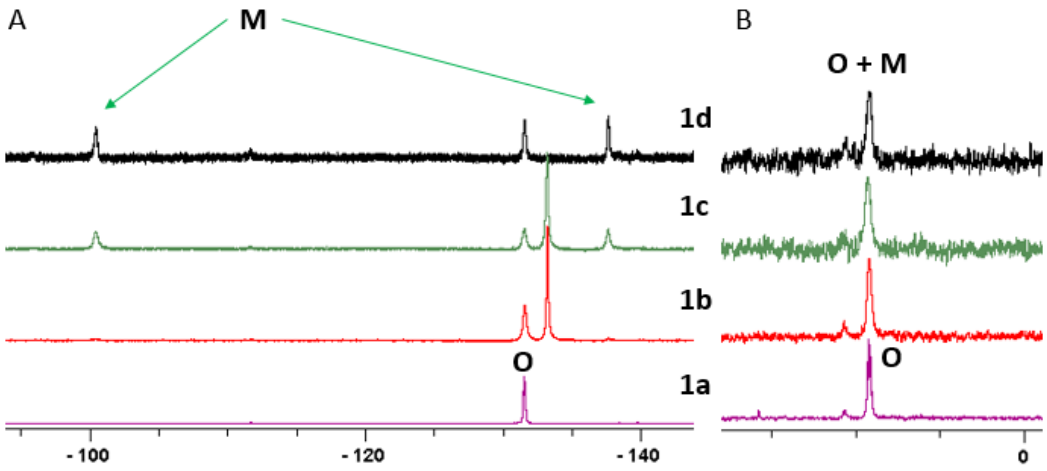

Figure A5.5 ^{19}F NMR (A) and $^{31}P\{^{1}H\}$ NMR (B) of Ni(η^2-C_2F_4)(dppf) (**5-1b**) in benzene (**a**), addition of TFE after 5 min (**b**), after 3 h (**c**) and after pumping off the solvent (**d**). **M** = metallacyclopentane; **O** = olefin complex.

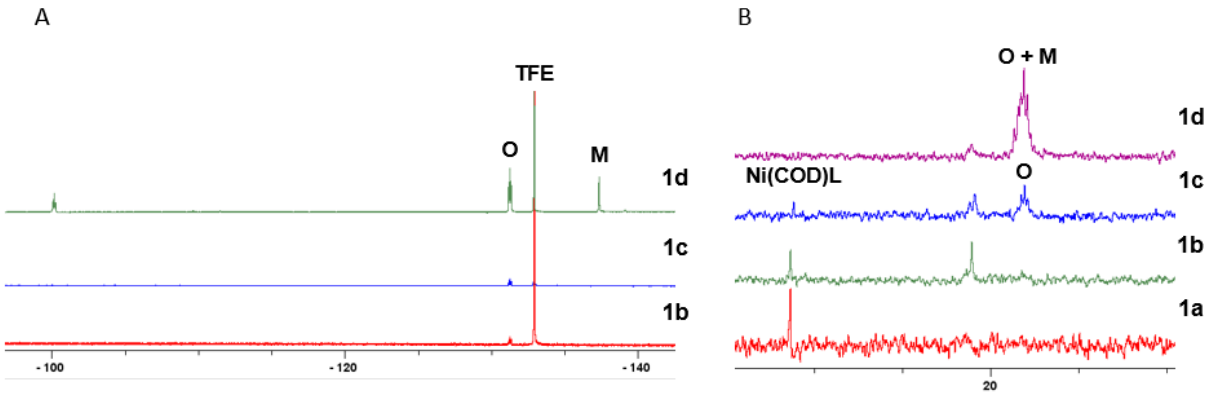

Figure A5.6 ^{19}F NMR (**A**) and $^{31}P\{^{1}H\}$ NMR (**B**) of Ni(cod)$_2$ + dppf + TFE in acetone, before TFE (a), 5 min (b), 2 h (c) and 12 h (d) after TFE addition. **M** = metallacyclopentane; **O** = olefin complex.

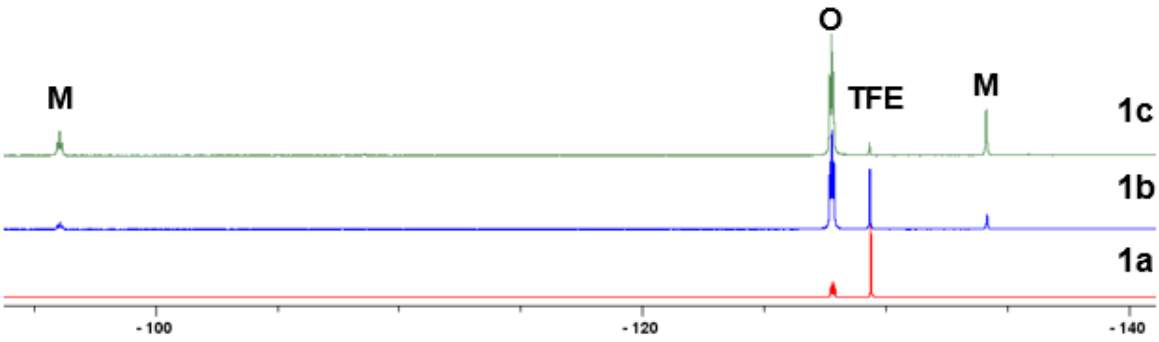

Figure A5.7 ^{19}F NMR of $Ni(cod)_2$ + dppf + TFE in THF, 5 min (a), 2 h (b) and 12 h (c) after TFE addition. **M** = metallacyclopentane; **O** = olefin complex.

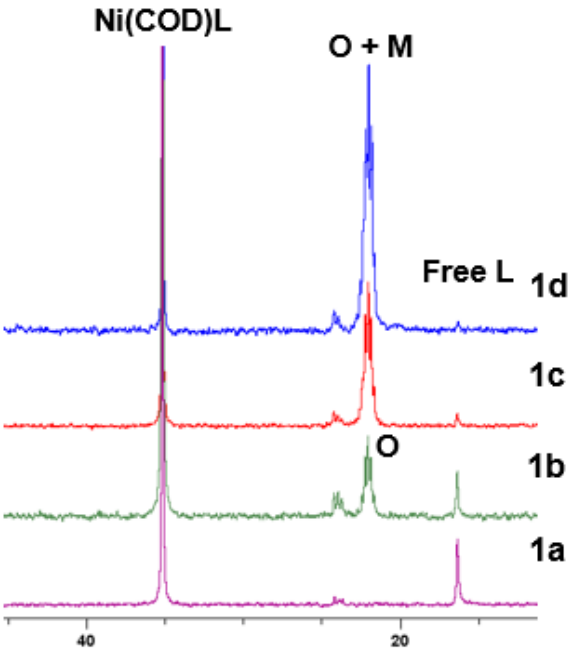

Figure A5.8 $^{31}P\{^1H\}$ NMR of $Ni(cod)_2$ + dppf + TFE in THF, 5 min (a), 2 h (b) and 12 h (c) after TFE addition. **M** = metallacyclopentane; **O** = olefin complex.

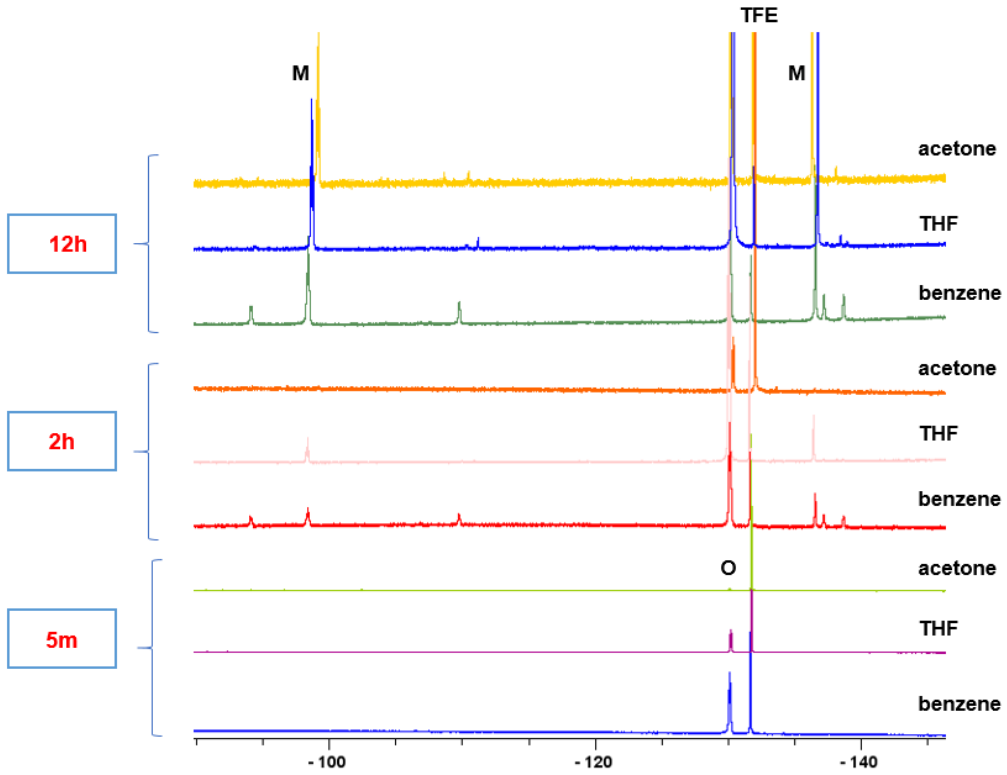

Figure A5.9 ^{19}F NMR of Ni(cod)$_2$ + dppf + TFE in benzene, acetone and THF after 5 min, 2 h and 12 h after TFE addition. Acetone line shifted to right for clarity.

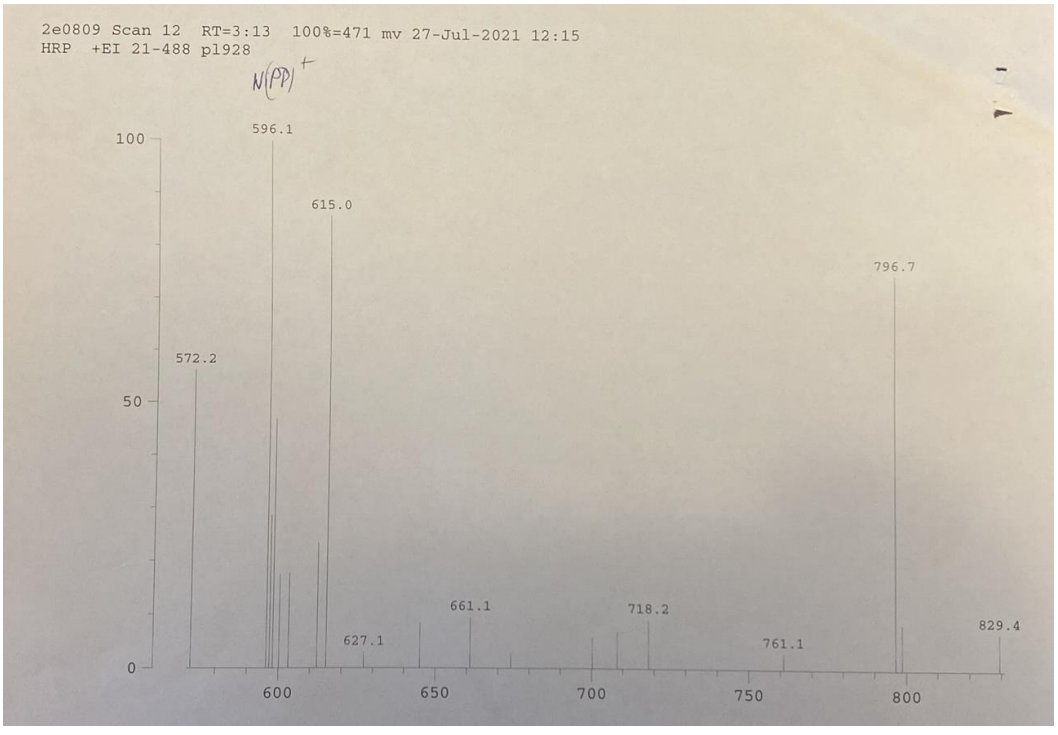

Figure A5.10 Selected peaks from the EI mass spectrum of complex **5-2c**.

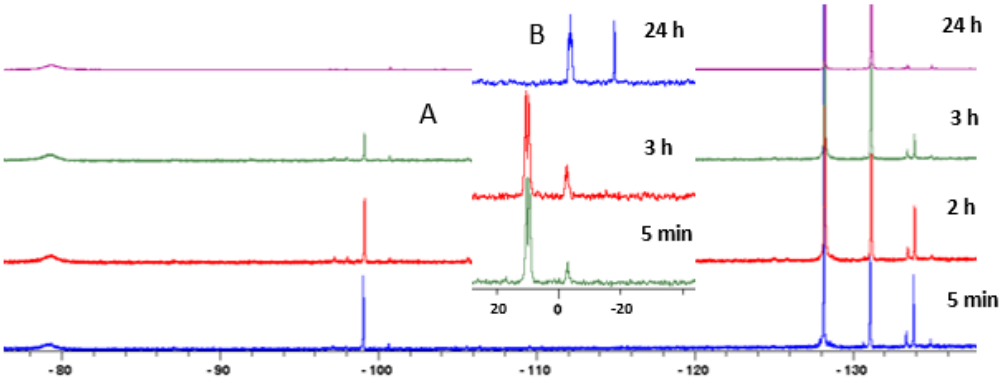

Figure A5.11 ^{19}F (**A**) and $^{31}P\{^{1}H\}$ (**B**) NMR spectra of $Ni(cod)_2$ + Xantphos + 3 equiv TFE in benzene C_6D_6

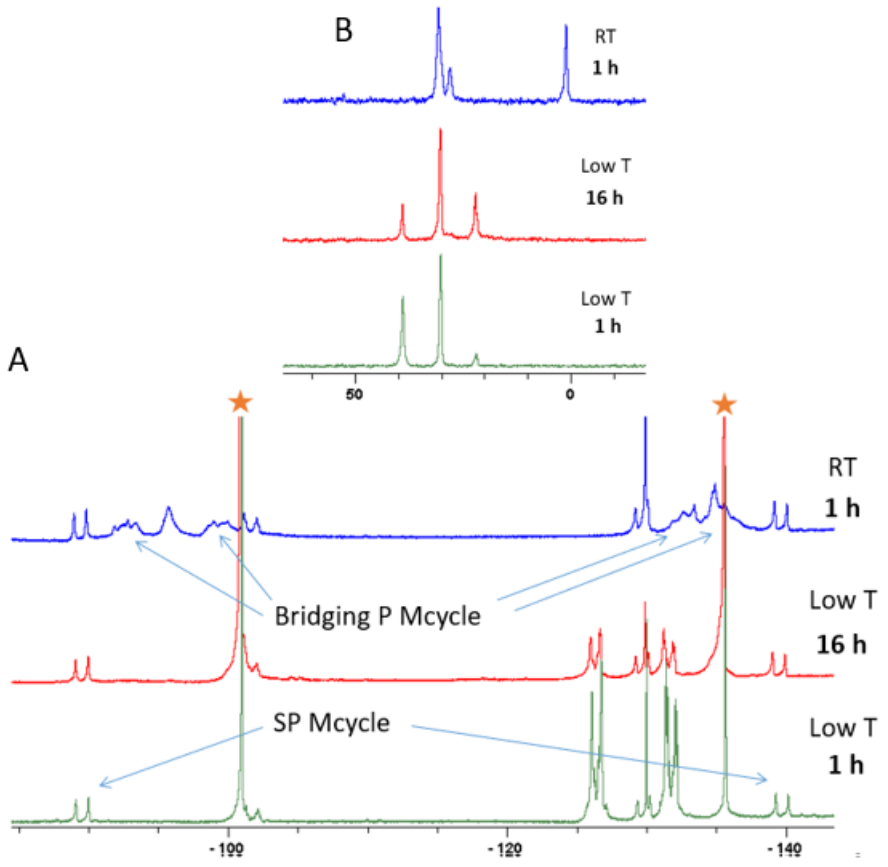

Figure A5.12 ^{19}F (**A**) and $^{31}P\{^{1}H\}$ (**B**) NMR spectra of $Ni(cod)_2$ + Bisbi + 3 equiv TFE in benzene C_6D_6. Star = $Ni(cod)(C_4F_8)$.

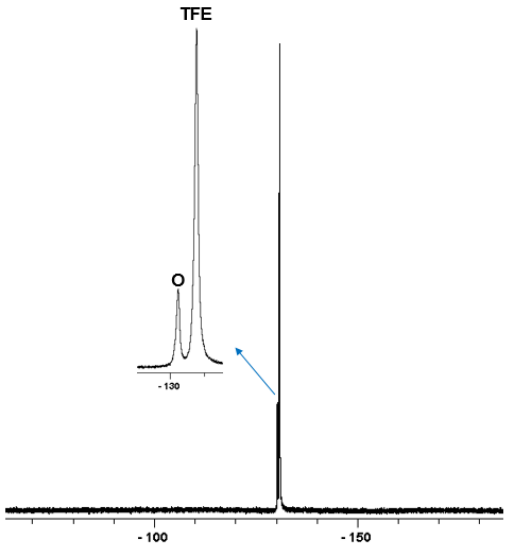

Figure A5.13 ^{19}F NMR of Ni(cod)$_2$ + TMEDA + TFE in THF, after 7 h at 50 °C.

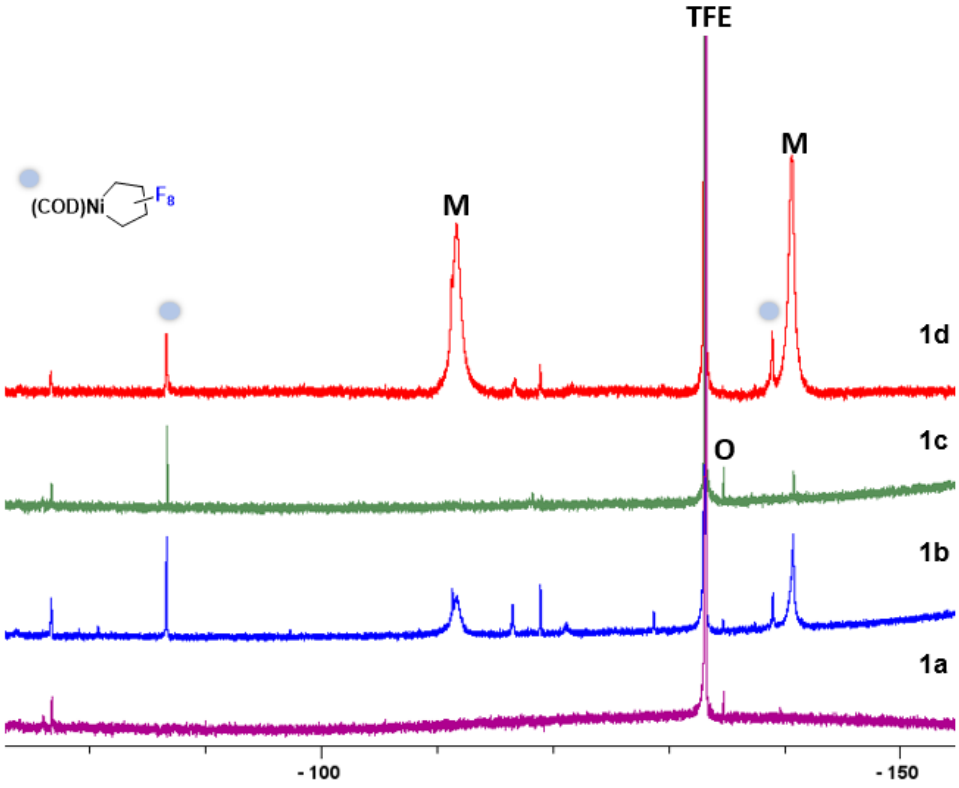

Figure A5.14 ^{19}F NMR of Ni(cod)$_2$ + TMEDA + TFE in acetone, after 30 min (**1a**), 7 h (**1c**) at 21 °C, 30 min (**1b**) and 7 h (**1d**) at 50 °C.

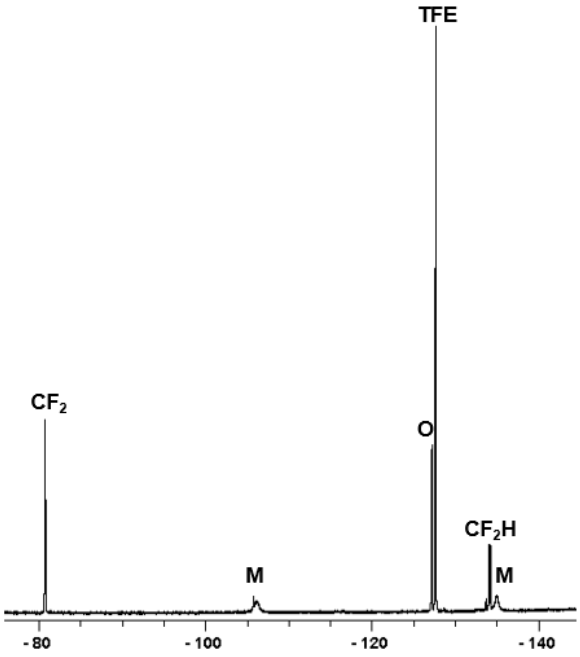

Figure A5.15 ^{19}F NMR of $Ni(cod)_2$ + TMEDA + TFE in acetonitrile, after 7 h at 50 °C.

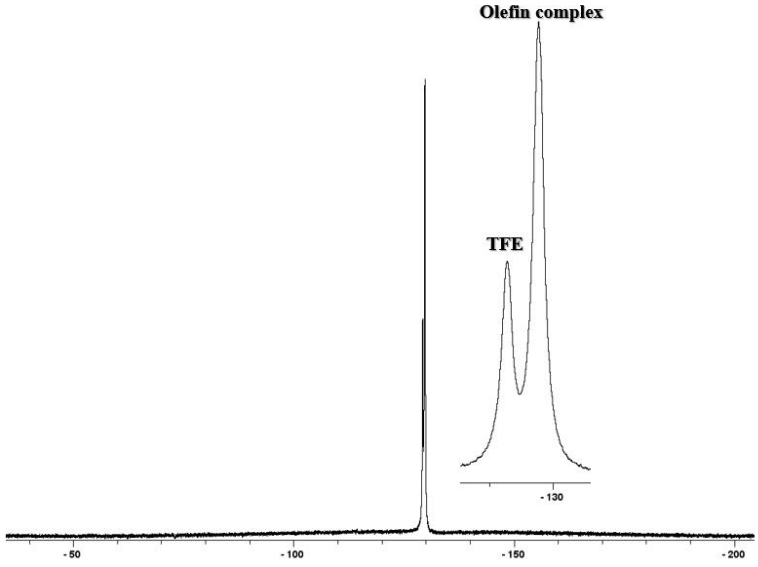

Figure A5.16 ^{19}F NMR spectrum of $Ni(cod)_2$ + TMEDA + TFE in 2,5-dimethyldihydrofuran, after 4 h at 25 °C.

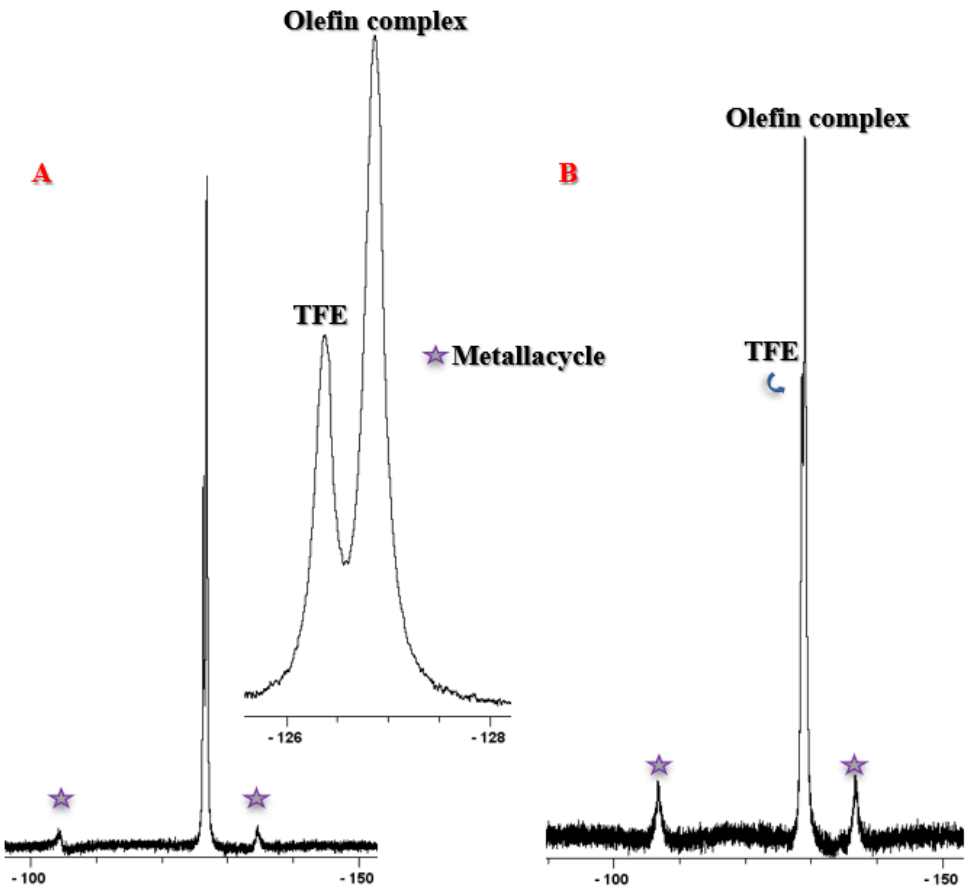

Figure A5.17 ^{19}F NMR spectra of $Ni(COD)_2$ + TMEDA + TFE in 2,5-dimethyldihydrofuran, after 21 h at 25 ºC (**A**) and 7 h at 50 ºC (**B**).

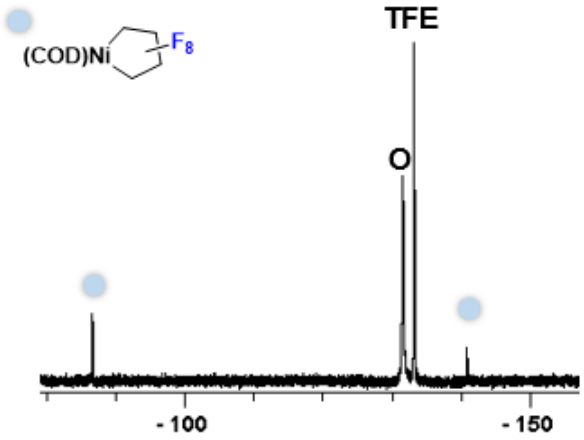

Figure A5.18 ^{19}F NMR spectrum of $Ni(cod)_2$ + bipyridine + TFE in acetone, after 7 h at 50 ºC.

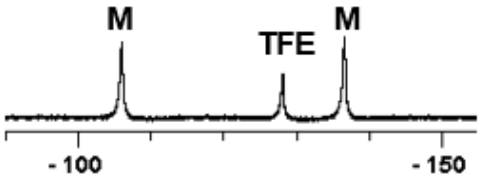

Figure A5.19 ^{19}F NMR spectrum of $Ni(cod)_2$ + bipyridine + TFE in THF, after 7 h at 50 ^{o}C.

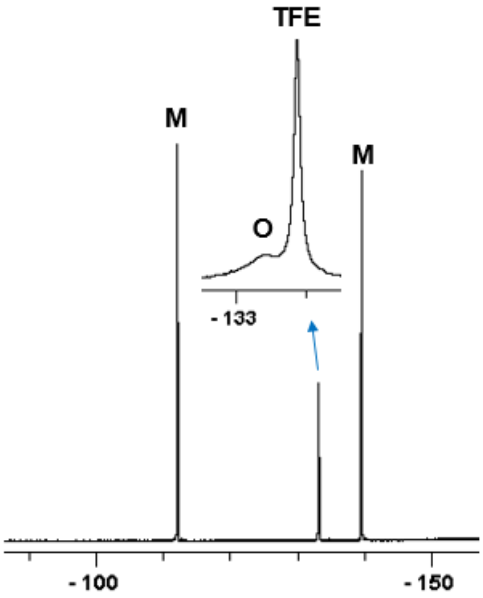

Figure A5.20 ^{19}F NMR of $Ni(cod)_2$ + 2 Pyridine + TFE in acetone, after 30 min at 50 ^{o}C.

Chapter 6: Designing and synthesis of stable perfluoronickelacyclopentane from PMVE and CTFE

Table A6. 1 Details of X-ray diffraction data collection and refinement

Identification code	6-2a	6-3a	S0944_FP
Empirical formula	$C_{24}H_{42}F_{12}NiO_8P_2$	$C_{38}H_{45}F_6NiO_4P_3$	$C_{37}H_{45}ClF_3O_3P_3Ni$
Formula weight	807.22	831.36	781.80
Temperature/K	213(2)	200.05	203(2)
Crystal system	triclinic	monoclinic	Triclinic
Space group	P-1	$P2_1/n$	P-1
a/Å	11.7240(9)	9.0838(3)	10.5209(8)
b/Å	12.4400(10)	20.9080(6)	11.8752(9)
c/Å	14.8795(12)	20.7027(6)	16.5843(12)
α/°	71.435(4)	90	95.082(2)
β/°	70.224(4)	90.410(2)	105.383(2)
γ/°	62.544(4)	90	104.984(2)
Volume/Å^3	1777.5(3)	3931.8(2)	1902.2(2)
Z	2	4	2
ρ_{calc}/g·cm^{-3}	1.508	1.404	1.365
μ/mm^{-1}	0.739	0.682	0.755
F(000)	832.0	1728.0	816.0
Crystal size/mm^3	0.813 × 0.254 × 0.23	0.41 × 0.36 × 0.35	0.471 × 0.278 × 0.082
Radiation	MoKα (λ = 0.71073)	MoKα (λ = 0.71073)	MoKα (λ = 0.71073)
2Θ range collection/°	3.762 to 66.66	2.768 to 61.092	2.584 to 67.244
Index ranges	-18 ≤ h ≤ 18 -19 ≤ k ≤ 19 -22 ≤ l ≤ 22	-12 ≤ h ≤ 12 -29 ≤ k ≤ 29 -29 ≤ l ≤ 29	-16 ≤ h ≤ 16 -18 ≤ k ≤ 18 -25 ≤ l ≤ 25
Reflections collected	45154	87245	110514
Independent reflections	13651 [R_{int} = 0.0213, R_{sigma} = 0.0247]	12004 [R_{int} = 0.0272, R_{sigma} = 0.0170]	14922 [R_{int} = 0.0512, R_{sigma} = 0.0320]
Data/restraints/parameters	13651/91/473	12004/535/621	14922/0/439
Goodness-of-fit on F^2	1.024	1.066	1.013
Final R indexes [I>=2σ (I)]	R_1 = 0.0448 wR_2 = 0.1190	R_1 = 0.0329 wR_2 = 0.0803	R_1 = 0.0385 wR_2 = 0.0927
Final R indexes [all data]	R_1 = 0.0654 wR_2 = 0.1329	R_1 = 0.0441 wR_2 = 0.0876	R_1 = 0.0608 wR_2 = 0.1052
Largest diff. peak/hole / e·Å^{-3}	0.87/-0.57	0.35/-0.30	1.16/-0.62

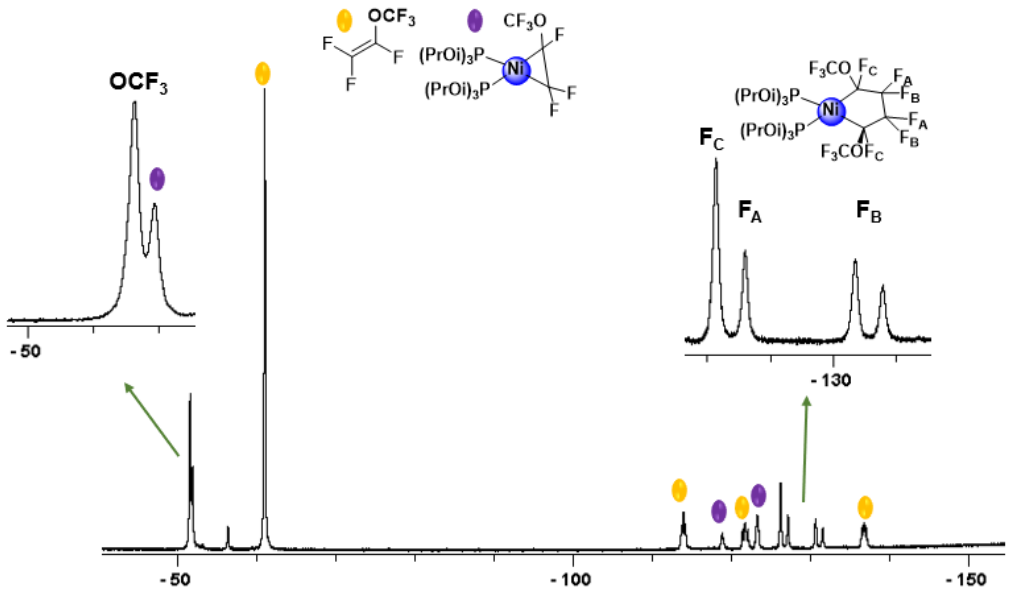

Figure A6.1 ^{19}F NMR spectrum (282 MHz, C_6D_6) of $Ni(cod)_2$, 2 equiv. of $P(OiPr)_3$ and PMVE.

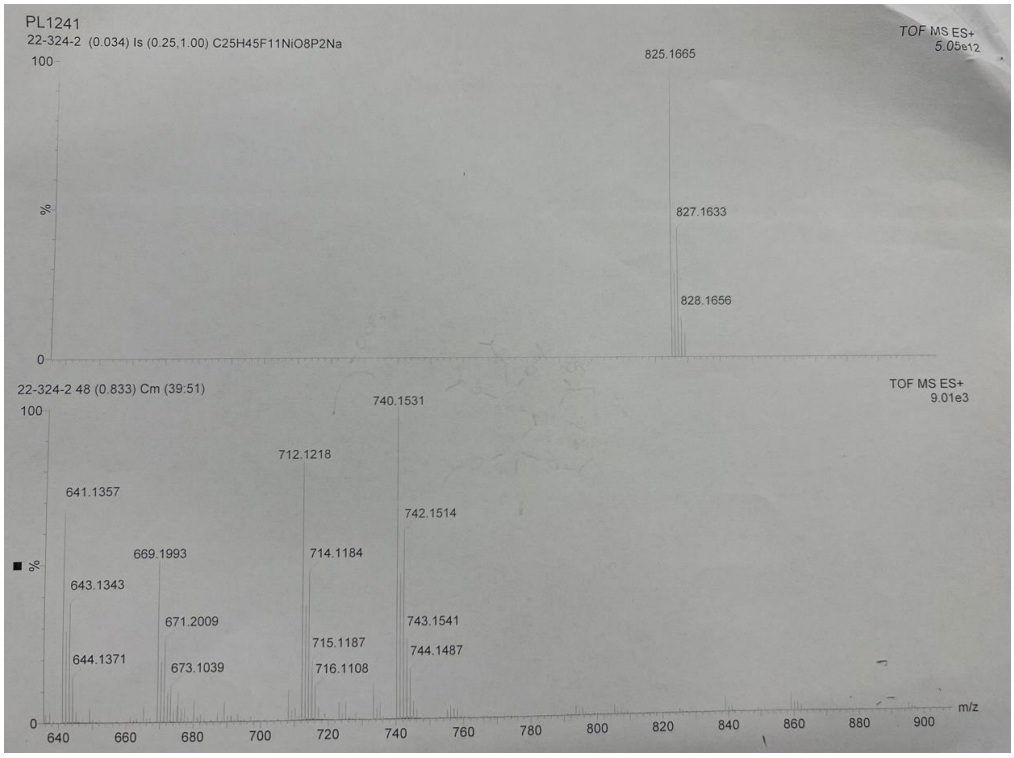

Figure A6.2 Selected peaks from the ESI mass spectrum (positive mode, CH_3CN) of complex **6-2a**.

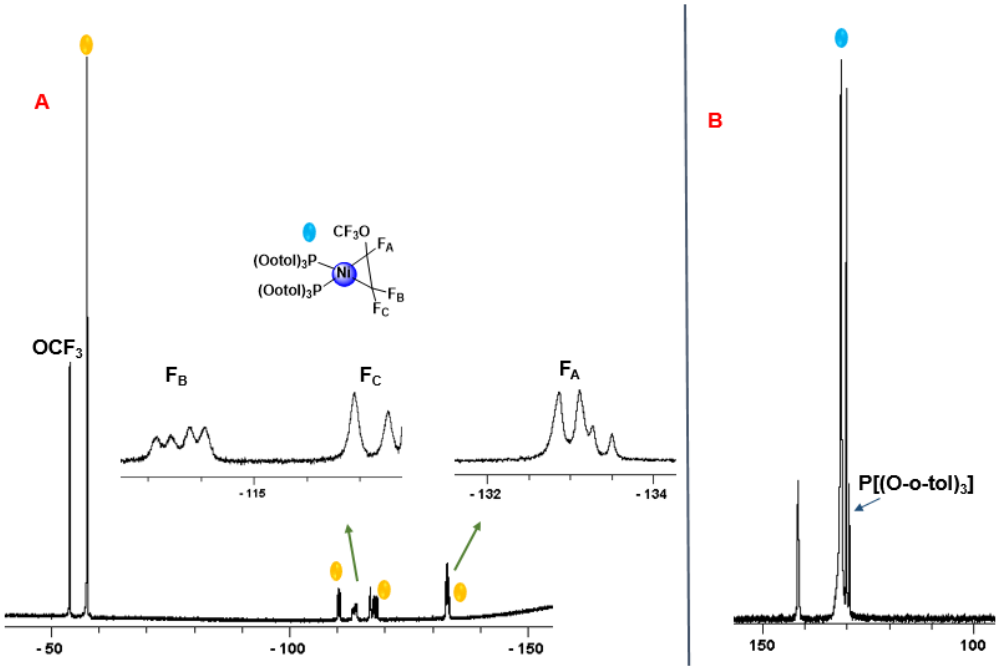

Figure A6.3 ^{19}F NMR (282 MHz, C_6D_6, **A**) and $^{31}P\{^1H\}$ NMR spectra (121 MHz, C_6D_6, **B**) of $Ni(cod)_2$, 2 equiv. of tri-o-tolylphosphite and PMVE.

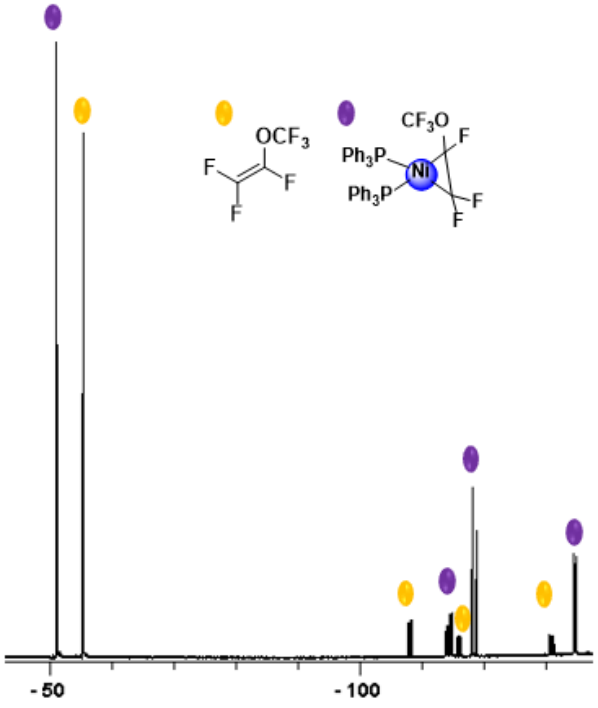

Figure A6.4 ^{19}F NMR spectrum (282 MHz, C_6D_6) of $Ni(cod)_2$, 2 equiv. of PPh_3 and PMVE.

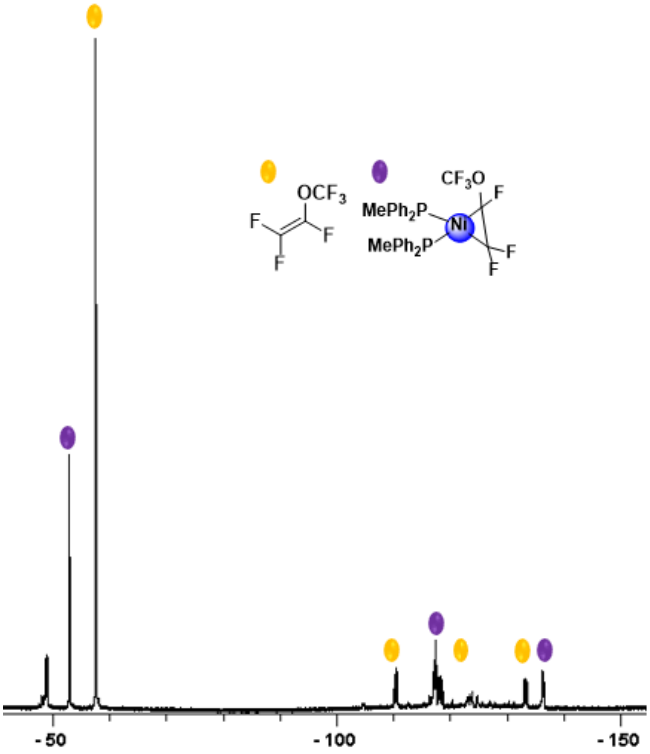

Figure A6.5 ^{19}F NMR spectrum (282 MHz, C_6D_6) of $Ni(cod)_2$, 2 equiv. of $PMePh_2$ and PMVE.

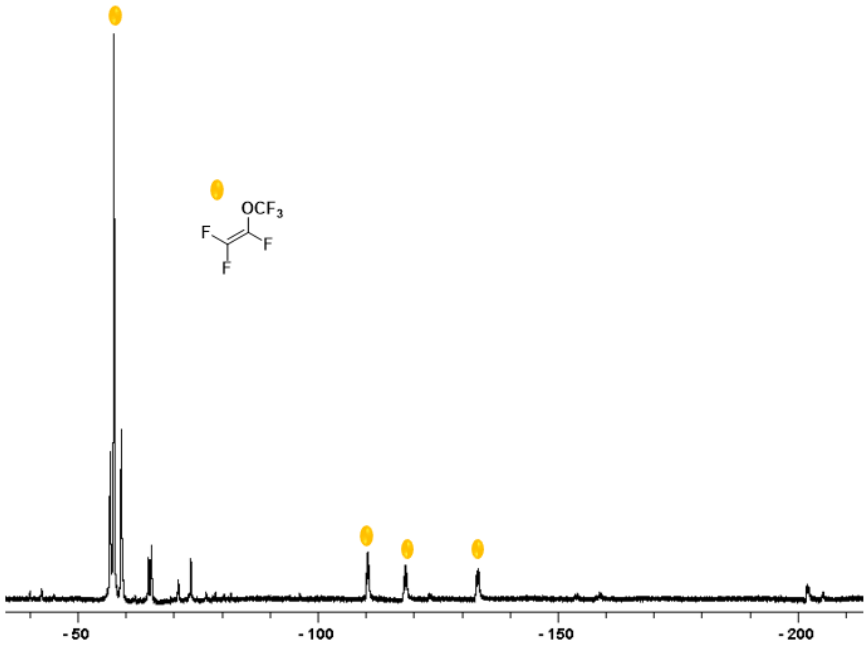

Figure A6.6 ^{19}F NMR (282 MHz, C_6D_6) spectrum of $Ni(cod)_2$, PCy_3 and PMVE.

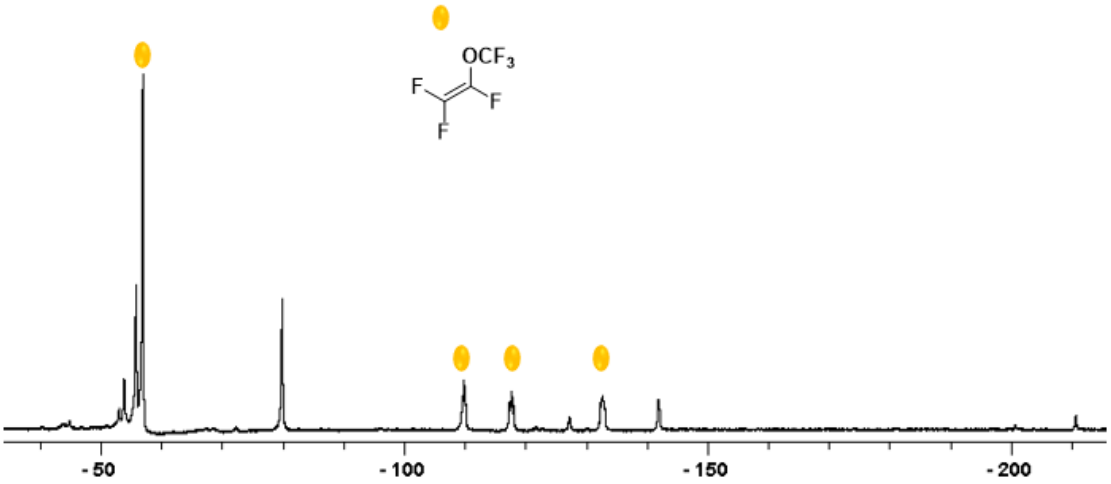

Figure A6.7 ^{19}F NMR (282 MHz, C_6D_6) spectrum of $Ni(cod)_2$, IPr and PMVE.

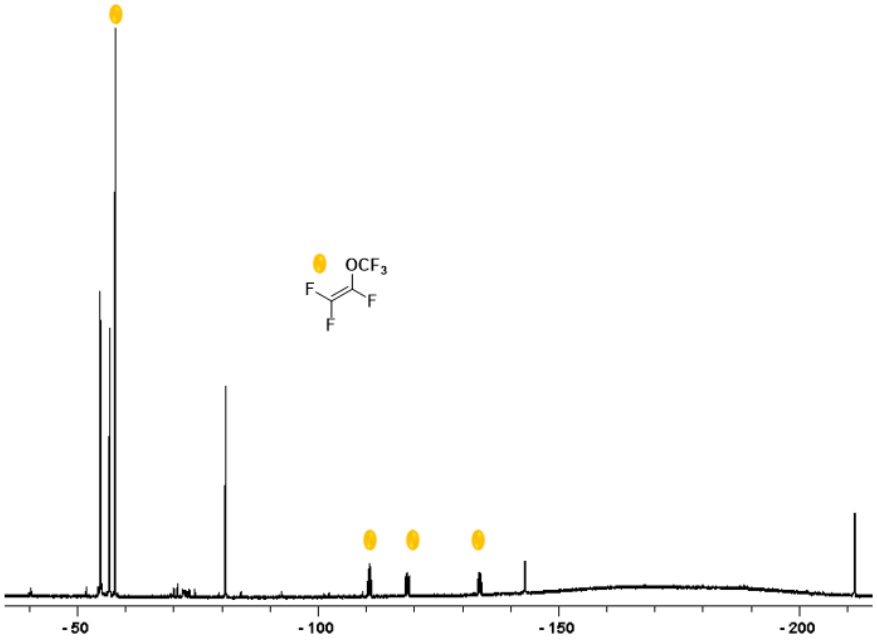

Figure A6.8 ^{19}F NMR (282 MHz, C_6D_6) spectrum of IPr and PMVE, without $Ni(cod)_2$.

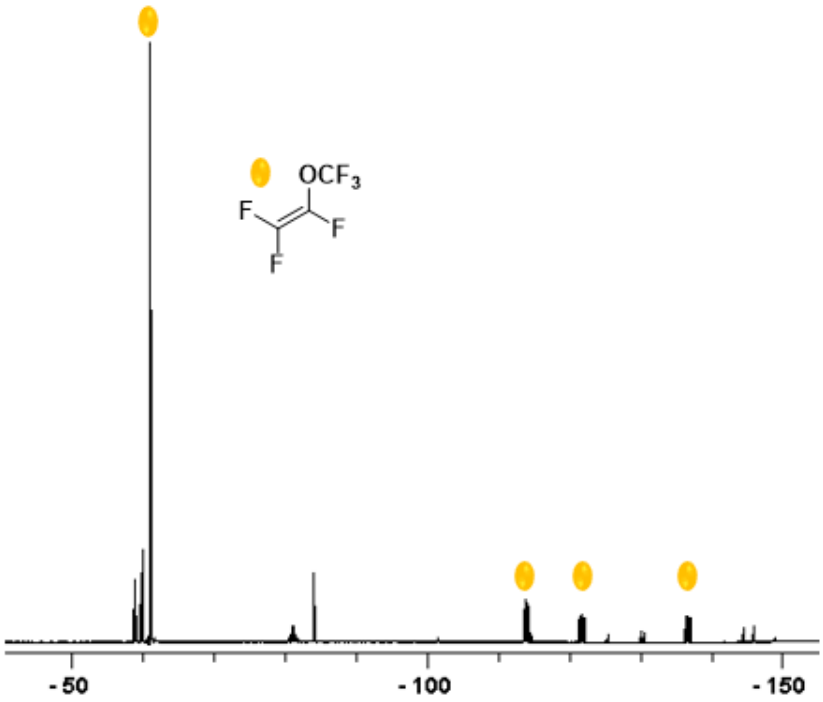

Figure A6.9 ^{19}F NMR (282 MHz, C_6D_6) of IAd and PMVE, without $Ni(cod)_2$.

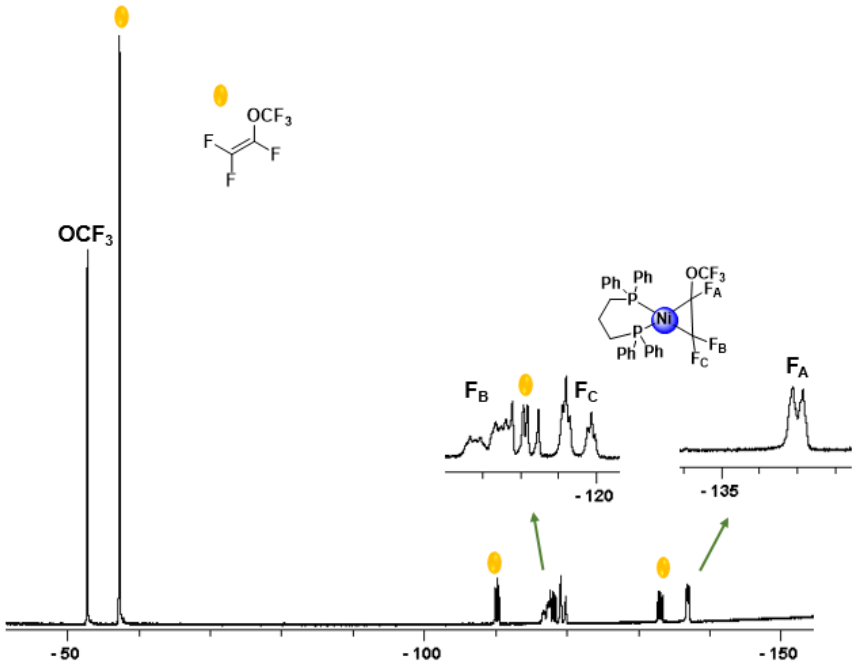

Figure A6.10 ^{19}F NMR spectrum (282 MHz, C_6D_6) of $Ni(cod)_2$, 1 equiv. of dppp and PMVE.

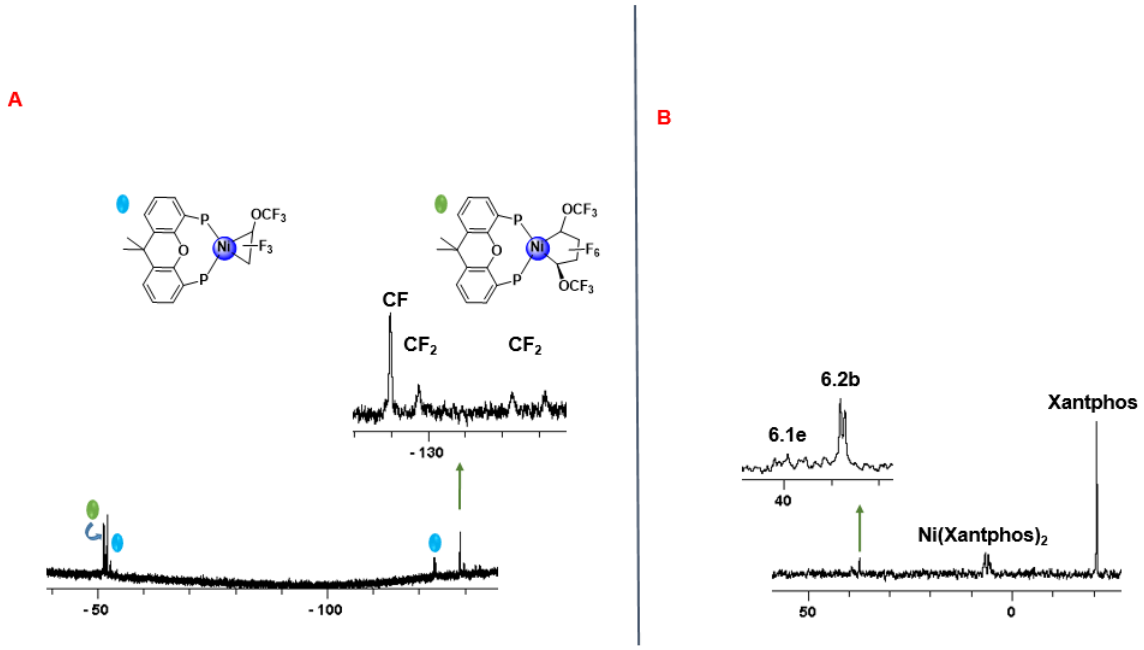

Figure A6.11 ^{19}F NMR (282 MHz, C_6D_6, **A**) and $^{31}P\{^1H\}$ NMR (121 MHz, C_6D_6, **B**) spectra of $Ni(Xantphos)_2$ and PMVE.

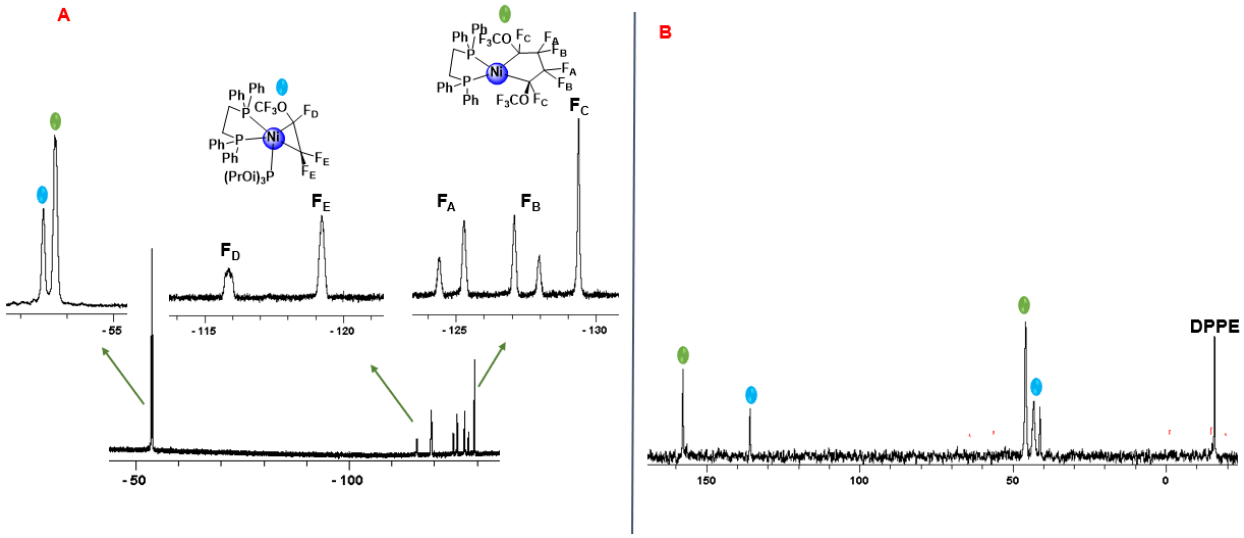

Figure A6.12 ^{19}F NMR (282 MHz, C_6D_6, **A**) and $^{31}P\{^1H\}$ NMR (121 MHz, C_6D_6, **B**) spectra of **6-2c** and **6-3** from addition of 1 equiv. of dppe to **6-1a,b.**

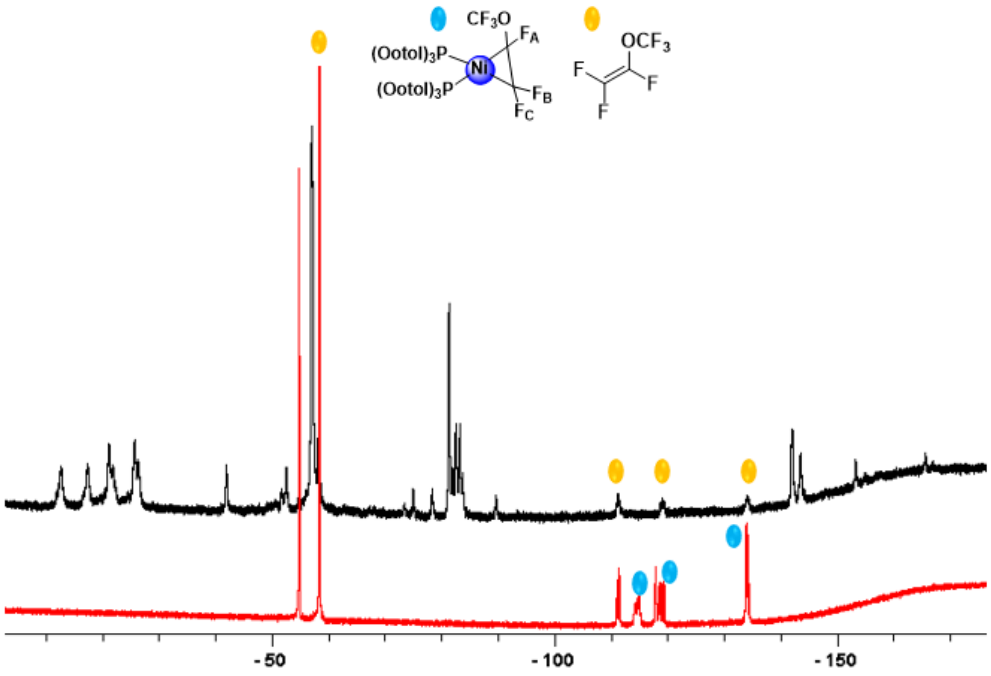

Figure A6.13 ^{19}F NMR (282 MHz, C_6D_6) spectrum of Ni[$C_2(OCF_3)F_3$][P(O-o-tolyl)$_3$] with IMes and excess PMVE.

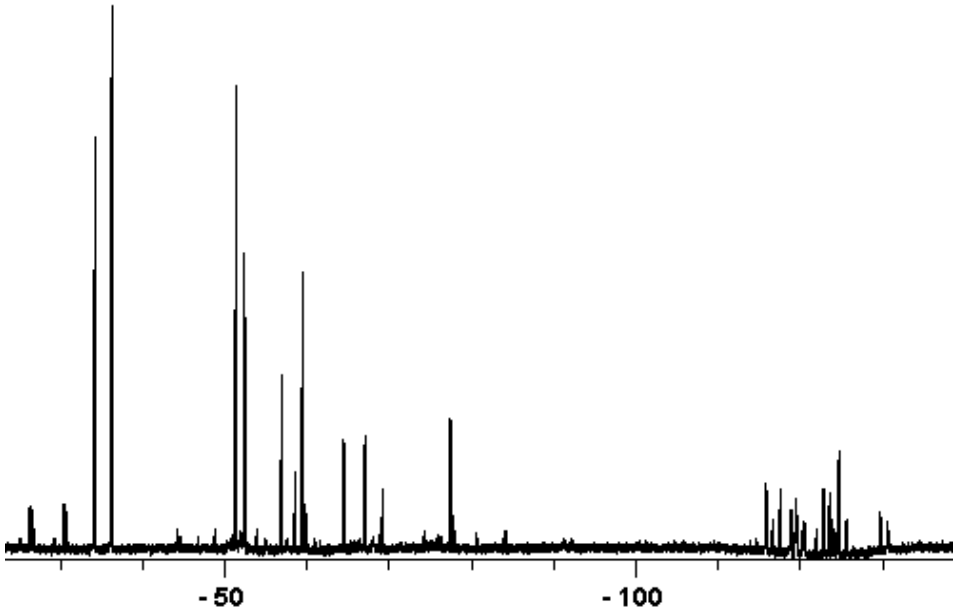

Figure A6.14 ^{19}F NMR (282 MHz, C_6D_6) spectrum of addition of 2 equiv. of P^{i}Pr$_3$ to the reaction containing Ni(cod)$_2$, 2 equiv. of tri-o-tolyl phosphite and PMVE.

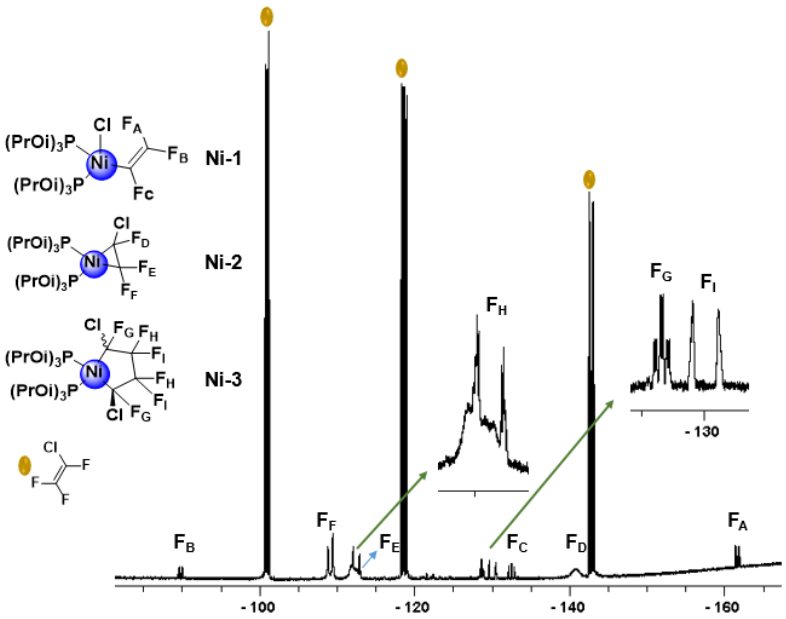

Figure A6.15 ^{19}F NMR (282 MHz, C_6D_6) spectrum of $Ni(cod)_2$, 2 equiv. of $P(OiPr)_3$ and CTFE.

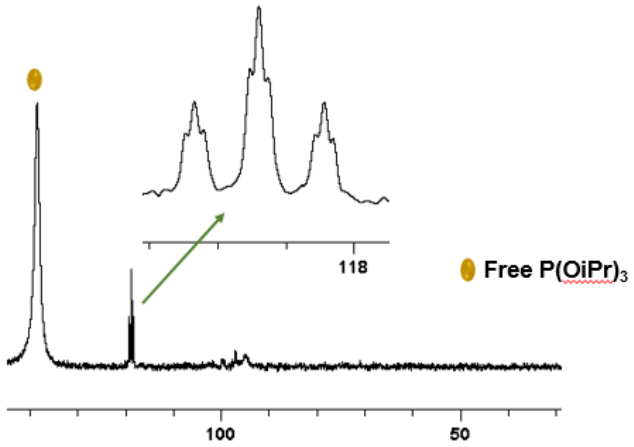

Figure A6.16 ^{31}P NMR (121 MHz, C_6D_6) of $Ni(COD)_2$, 2 equiv. of $P(OiPr)_3$ and CTFE.

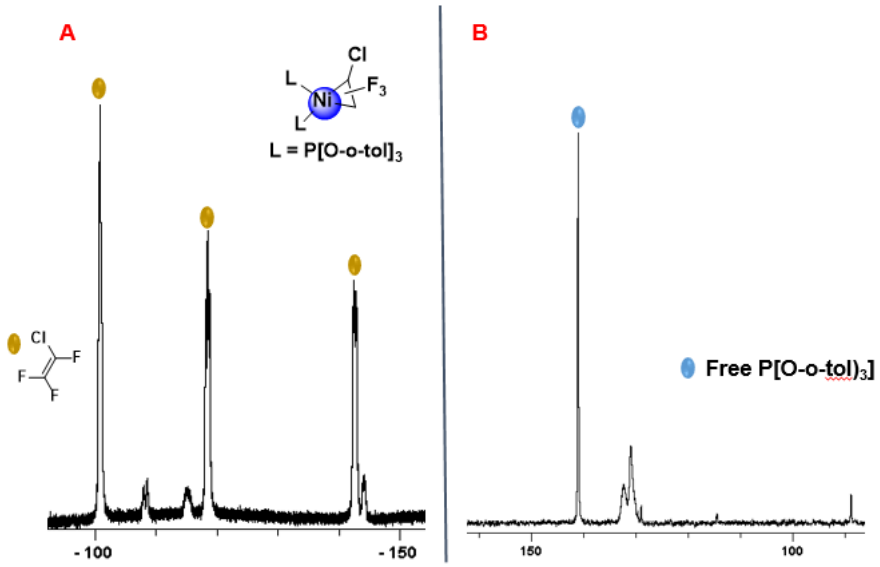

Figure A6.17 ^{19}F NMR (282 MHz, C_6D_6, **A**) and $^{31}P\{^1H\}$ NMR (121 MHz, C_6D_6, **B**) spectra of $Ni(cod)_2$, $P(O\text{-}o\text{-}tolyl)_3$ and CTFE after 4 h.

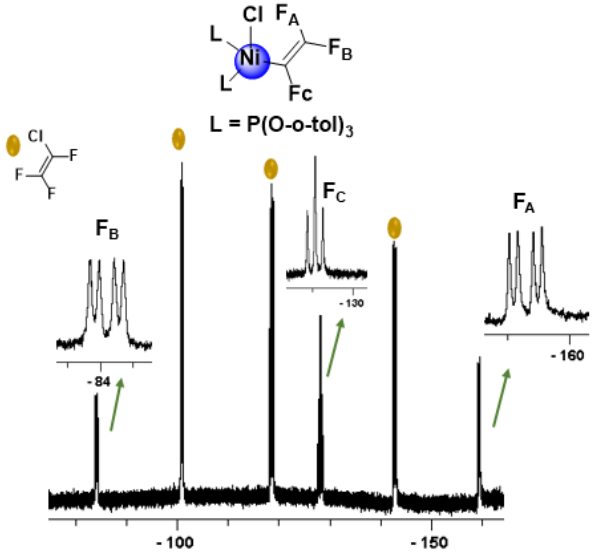

Figure A6.18 ^{19}F NMR (282 MHz, C_6D_6) spectrum of $Ni(cod)_2$, $P(O\text{-}o\text{-}tolyl)_3$ and CTFE after 12 h.

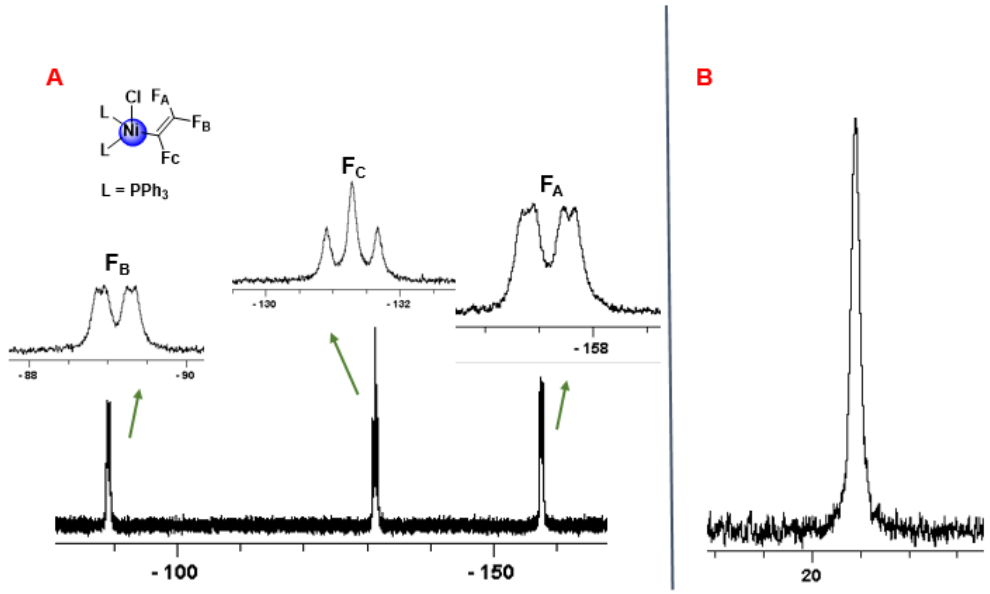

Figure A6.19 ^{19}F NMR (282 MHz, C_6D_6, **A**) and $^{31}P\{^1H\}$ NMR (121 MHz, C_6D_6, **B**) spectra of $Ni(cod)_2$, PPh_3 and CTFE.

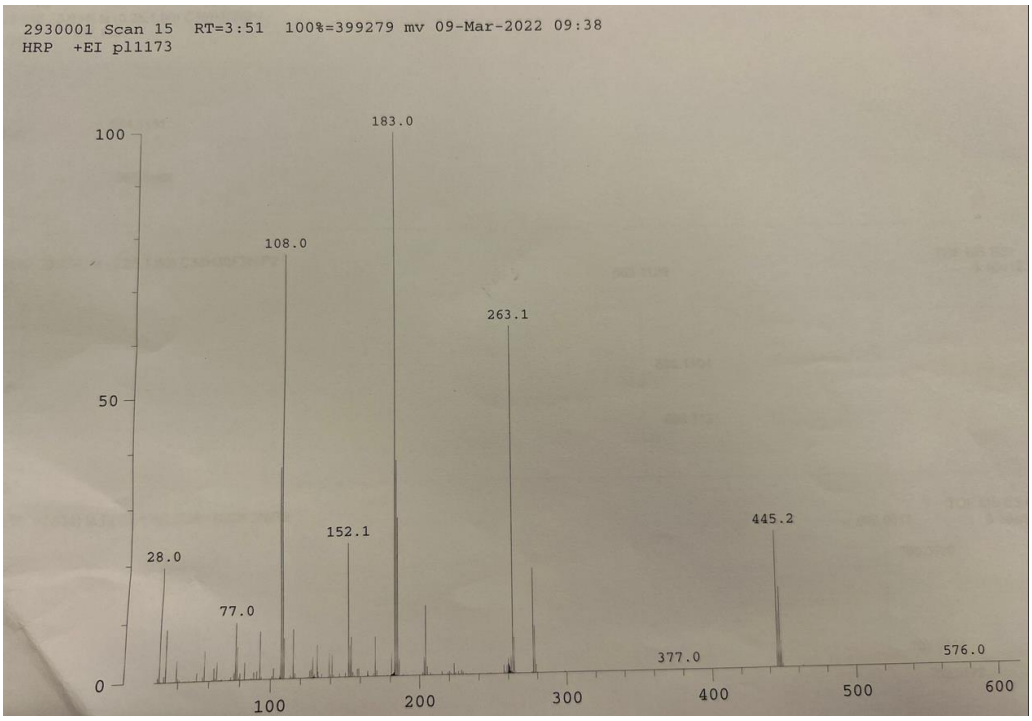

Figure A6.20 Selected peaks from the EI mass spectrum (positive mode, CH_3CN) of $NiCl(\eta^1\text{-}CF{=}CF_2)(PPh_3)_2$.

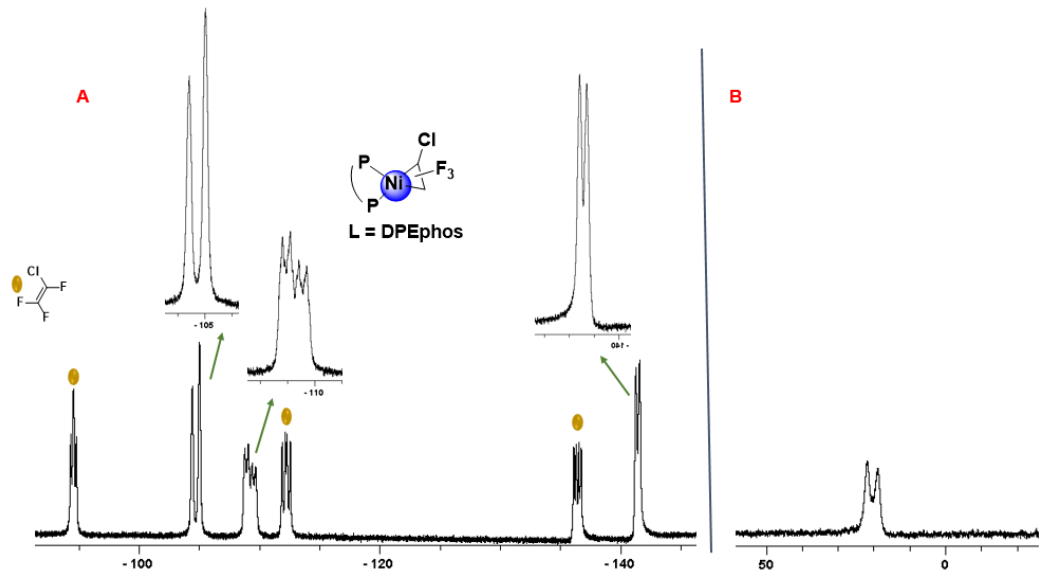

Figure A6.21 ^{19}F NMR (282 MHz, C_6D_6, **A**) and $^{31}P\{^1H\}$ NMR (121 MHz, C_6D_6, **B**) spectra of $Ni(cod)_2$, DPEphos and CTFE.

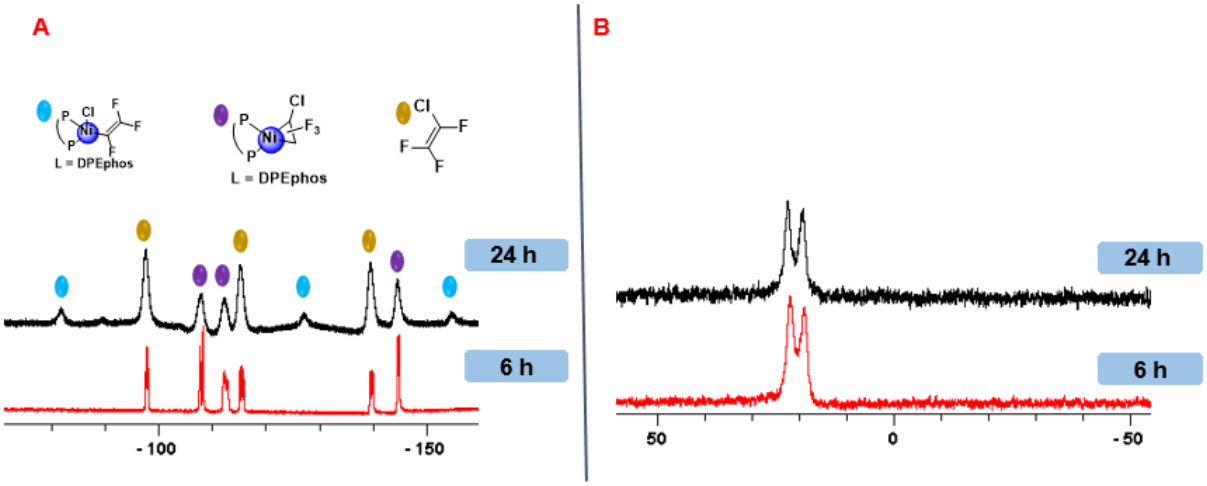

Figure A6.22 ^{19}F NMR (282 MHz, C_6D_6, **A**) and $^{31}P\{^1H\}$ NMR (121 MHz, C_6D_6, **B**) spectra of $Ni(cod)_2$, DPEphos and CTFE after 6 and 24 h, showing conversion of olefin into vinyl complex.

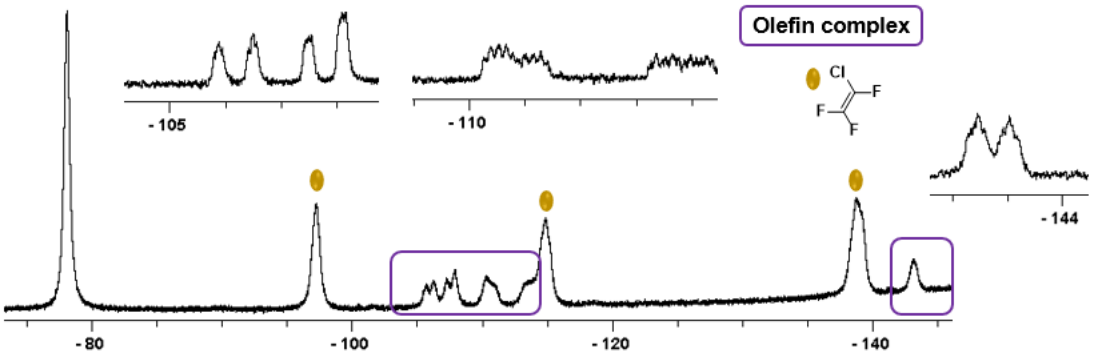

Figure A6.23 ^{19}F NMR (282 MHz, C_6D_6) spectrum of $Ni(cod)_2$, BINAP and CTFE after 7 h.

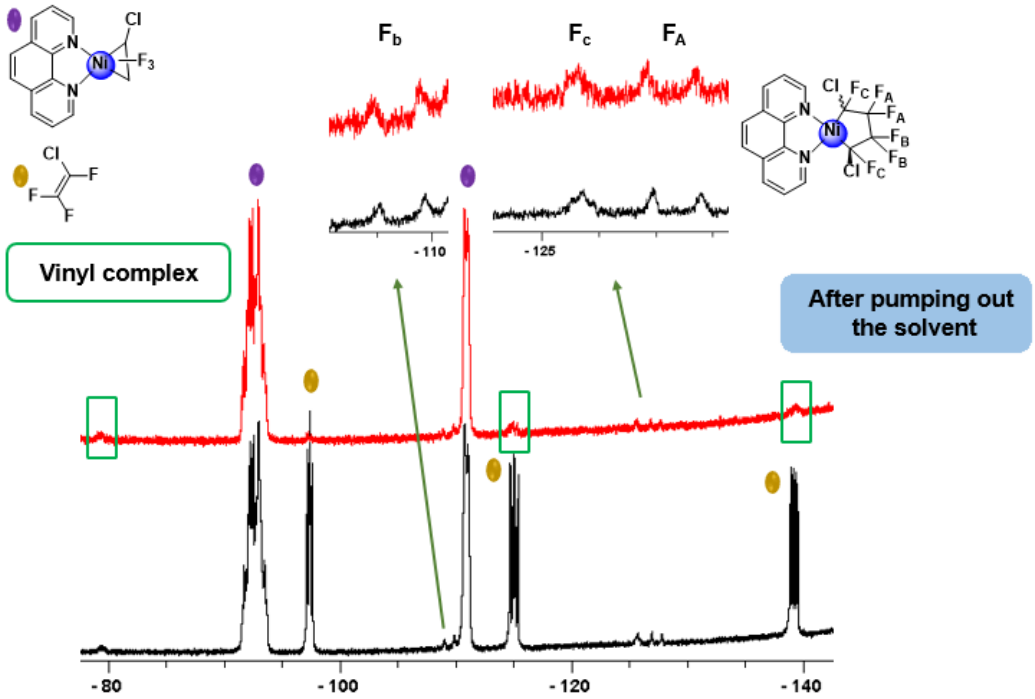

Figure A6.24 ^{19}F NMR (282 MHz, C_6D_6) spectrum after phen addition to the reaction of $Ni(cod)_2$, tri-isopropylphosphite and CTFE.

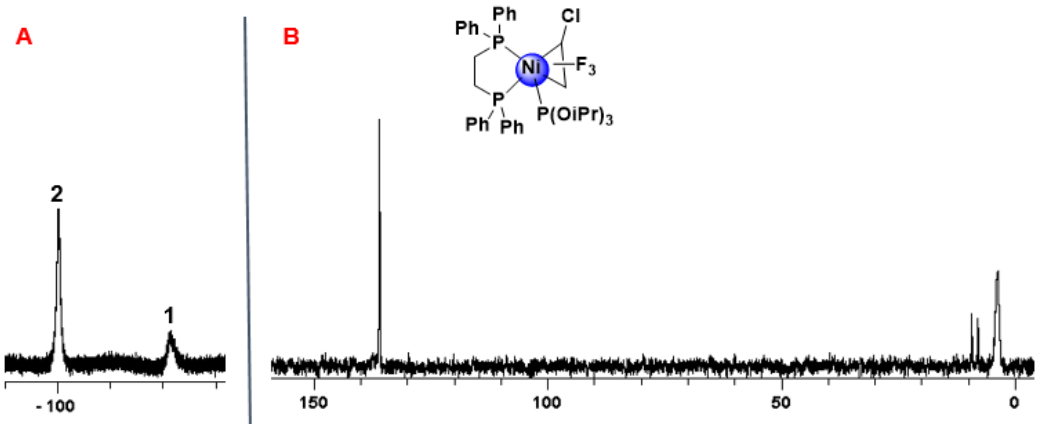

Figure A6.25 ^{19}F NMR (282 MHz, C_6D_6, **A**) and $^{31}P\{^1H\}$ NMR (121 MHz, C_6D_6, B) spectra of $Ni[C_2ClF_3](dppe)[(P(OiPr)_3]$.

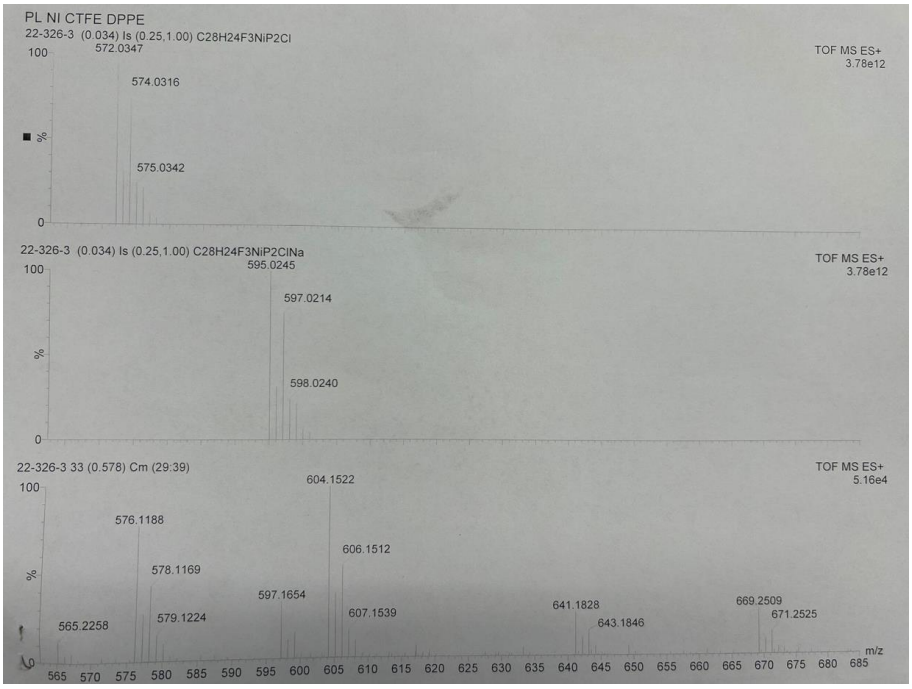

Figure A6.26 Selected peaks from the ESI mass spectrum (positive mode, CH_3CN) of complex $Ni(C_2ClF_3)(dppe)[(P(OiPr)]$.

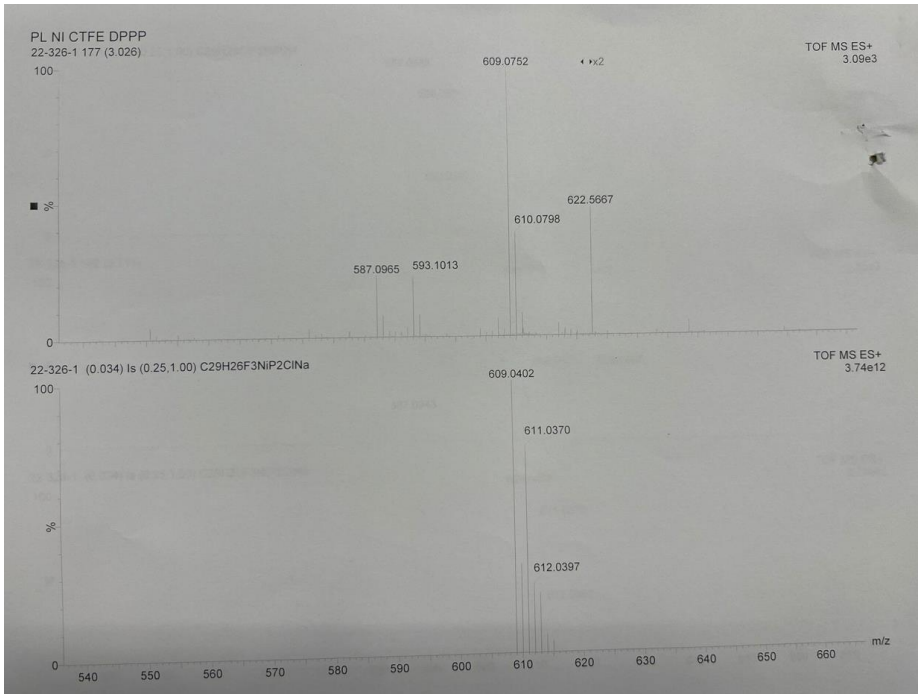

Figure A6.27 Selected peaks from the ESI mass spectrum (positive mode, CH_3CN) of complex $Ni(C_2ClF_3)(dppp)[(P(OiPr)]$.

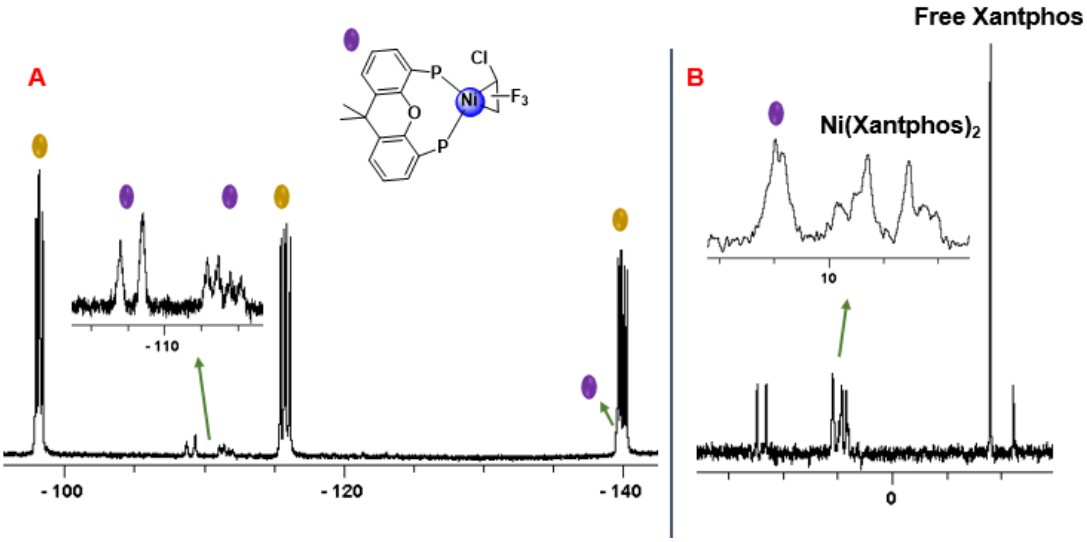

Figure A6.28 ^{19}F NMR (282 MHz, C_6D_6, **A**) and $^{31}P\{^1H\}$ NMR (121 MHz, C_6D_6, **B**) spectra of $Ni(Xantphos)_2$ + CTFE in benzene after 4 h.

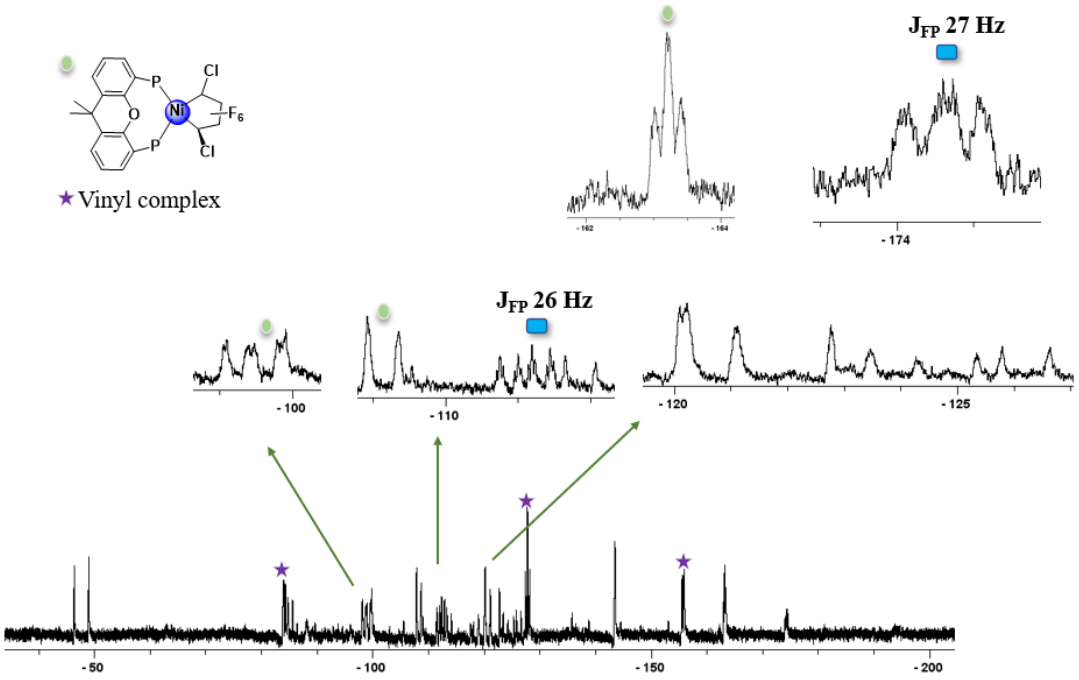

Figure A6.29 ^{19}F NMR (282 MHz, C_6D_6, **A**) spectra of Ni(Xantphos)$_2$ + CTFE in benzene after 12 h, then changed the solvent to DCM.

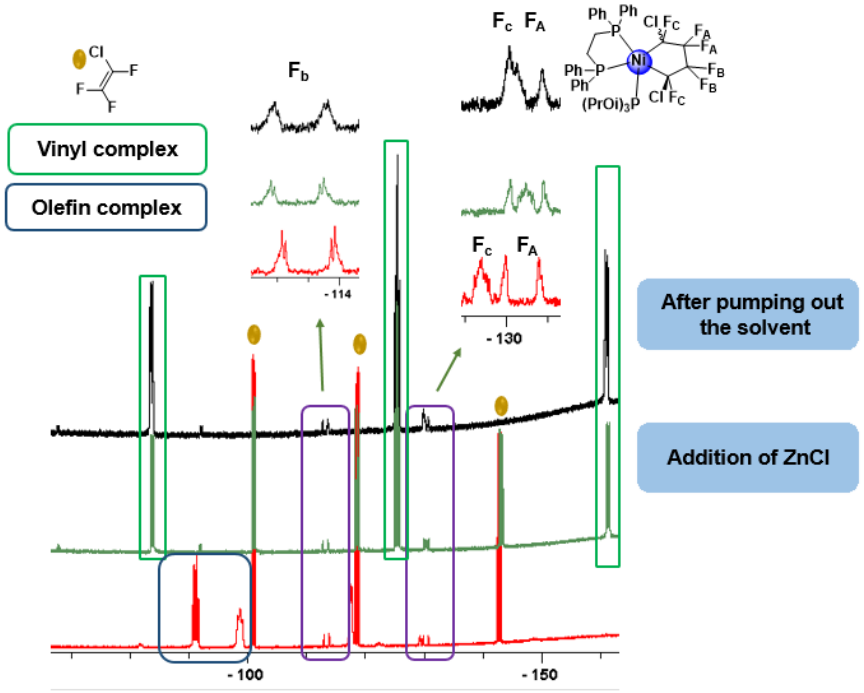

Figure A6.30 ^{19}F NMR (282 MHz, C_6D_6) spectrum of Ni($C_4Cl_2F_6$)(dppe) (**6-5c**) and Ni(C_2ClF_3)(dppe)[(P(O^{i}Pr)$_3$] (**6-7c**) plus $ZnCl_2$.

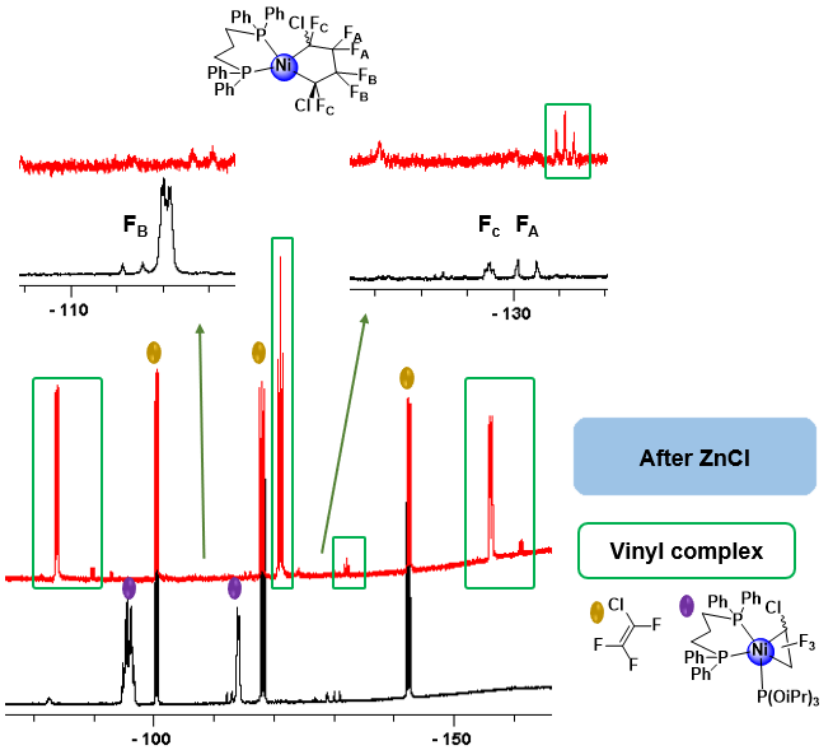

Figure A6.31 ^{19}F NMR (282 MHz, C_6D_6) spectrum of $Ni(C_4Cl_2F_6)(dppp)$ (**6-5b**) and $Ni(C_2ClF_3)(dppp)[(P(OiPr)_3]$ (**6-7b**) plus $ZnCl_2$.

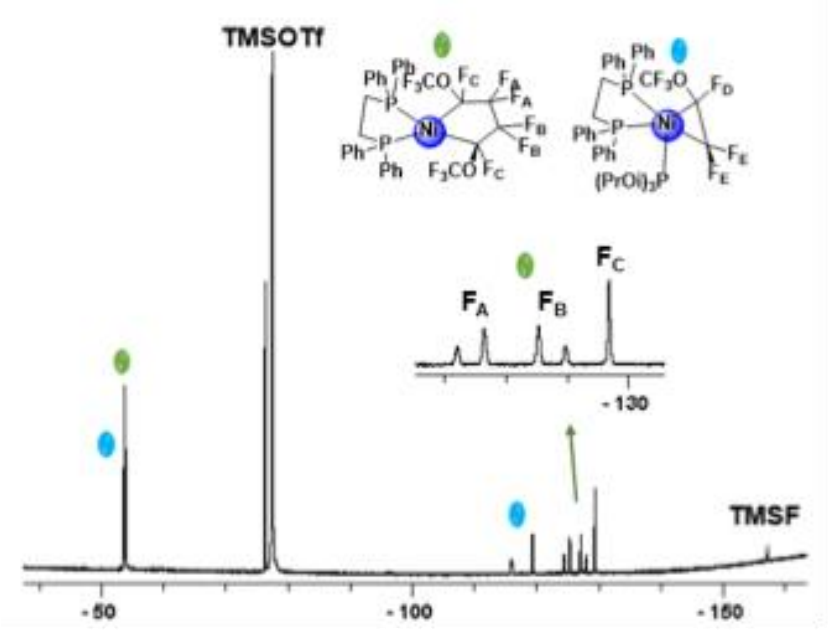

Figure A6.32 ^{19}F NMR (282 MHz, C_6D_6) spectrum of $Ni[C_4(OCF_3)_2F_6](dppe)$ (**6-2c**) and $Ni[C_2(OCF_3)F_3](dppe)[P(O^iPr)_3]$ (**6-3**) with TMSOTf.

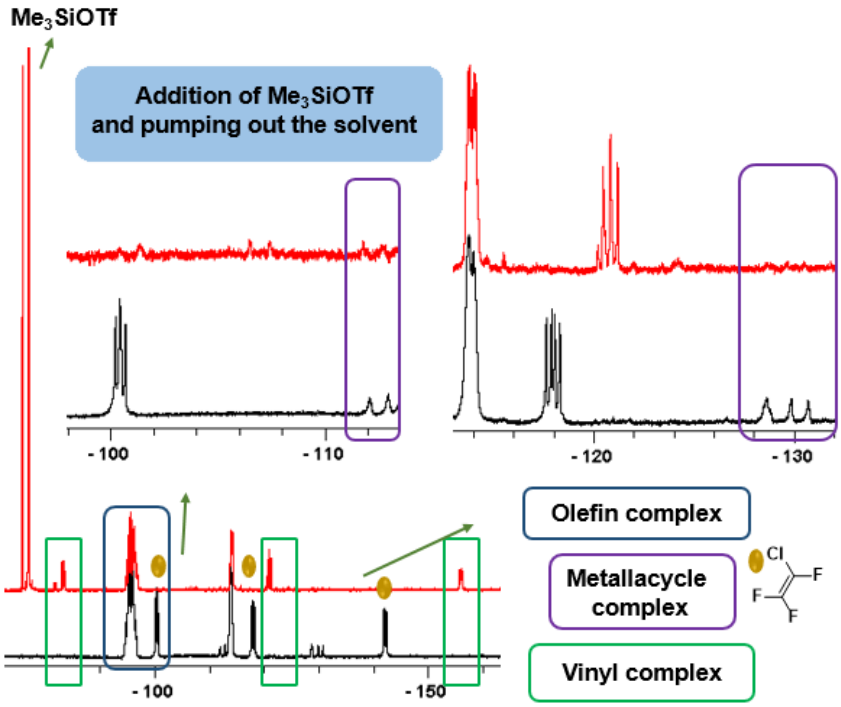

Figure A6.33 ^{19}F NMR (282 MHz, C_6D_6) spectrum of Ni[$C_4Cl_2F_6$][dppe][($P(O^iPr)_3$] (**6-5c**) and Ni[C_2ClF_3][dppe][($P(O^iPr)_3$] (**6-7c**) plus TMSOTf.

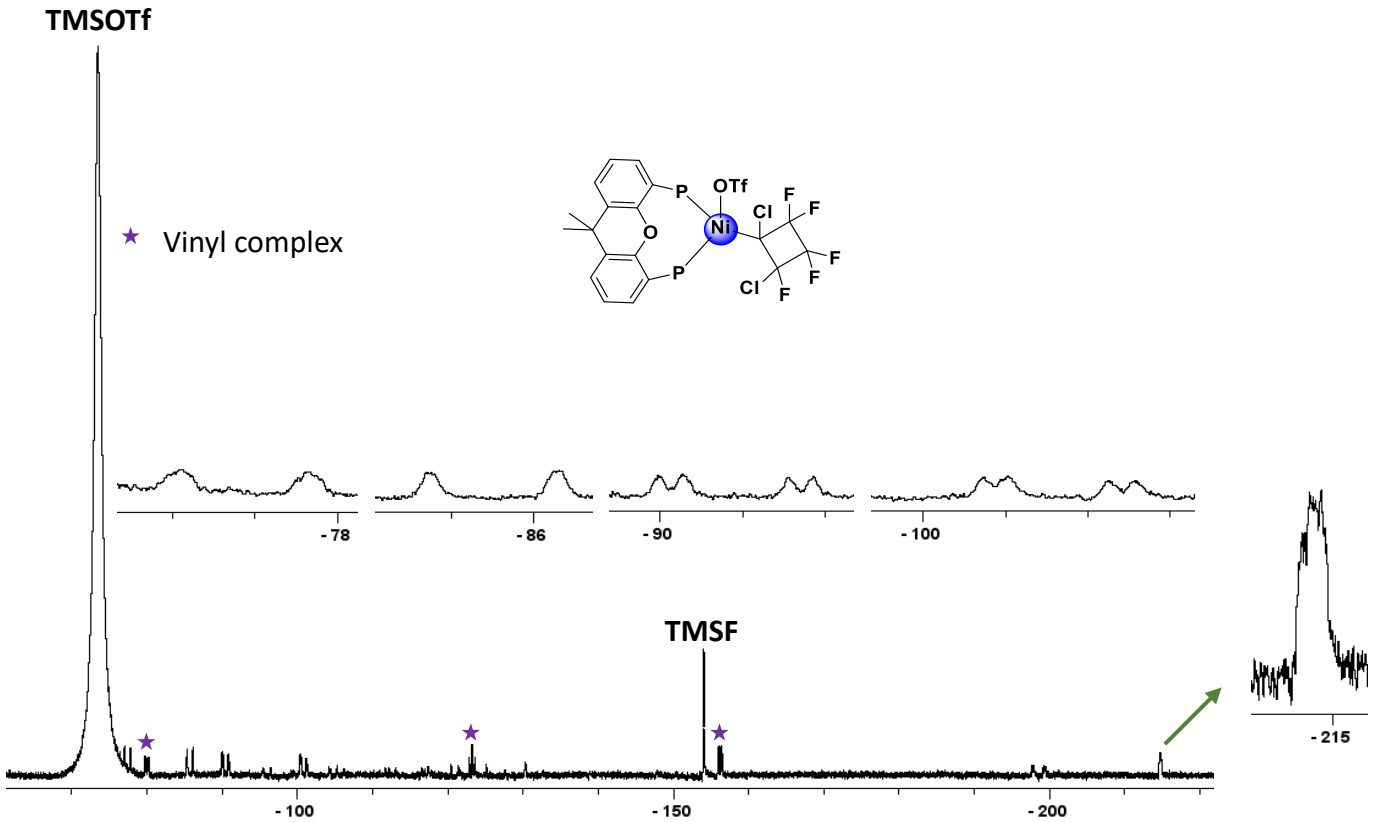

Figure A6.34 ^{19}F NMR (282 MHz, C_6D_6, **A**) spectra of Ni(Xantphos)$_2$ + CTFE in benzene, then changed the solvent to DCM and added TMSOTf.

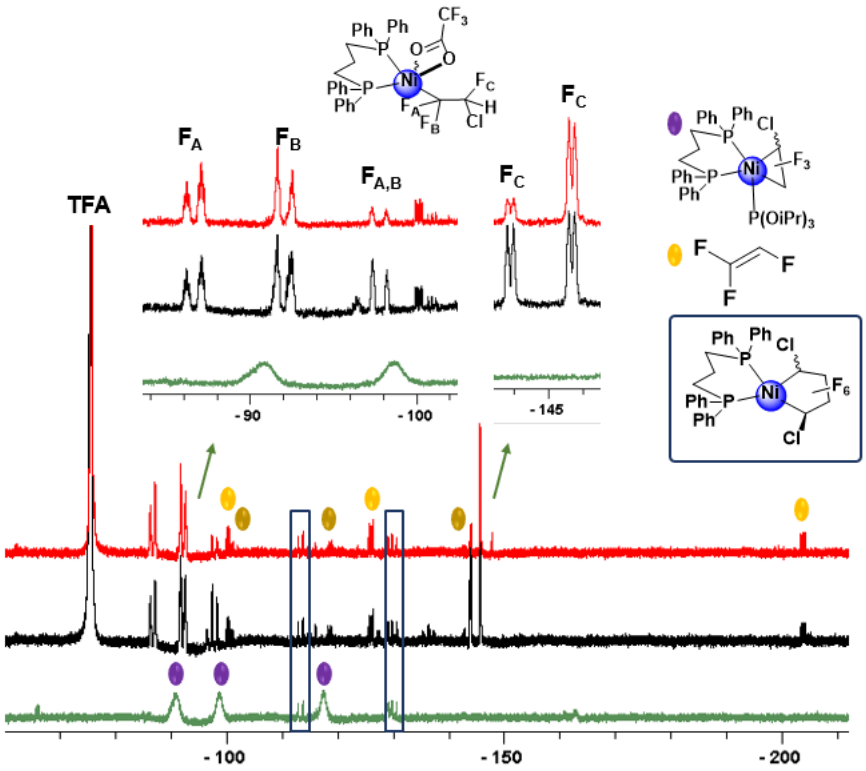

Figure A6.35 ^{19}F NMR (282 MHz, C_6D_6) spectrum of Ni[$C_4Cl_2F_6$](dppp) and Ni[C_2ClF_3](dppp)-[($P(O^iPr)_3$] (green line) plus trifluoroacetic acid after 7 h (black line) and 16 h (red line).